N67-32148

DESIGN GUIDE FOR PRESSURIZED GAS SYSTEMS

PREPARED FOR

NATIONAL AERONAUTICS AND SPACE ADMINISTRATION

CONTRACT NAS7-388

MARCH 1966

IIT RESEARCH INSTITUTE

CHICAGO, ILLINOIS

REPRODUCED BY
U.S. DEPARTMENT OF COMMERCE
NATIONAL TECHNICAL
INFORMATION SERVICE
SPRINGFIELD, VA 22161

U.S. DEPARTMENT OF COMMERCE
National Technical Information Service
N67-32148

DESIGN GUIDE FOR PRESSURIZED GAS SYSTEMS VOLUME I

NATIONAL AERONAUTICS AND SPACE ADMINISTRATION
WASHINGTON, DC

1966

FOREWORD

The revision of this guidebook was prepared by IIT Research Institute for the National Aeronautics and Space Administration, Western Operations Office, under Contract No. NAS7-388, IITRI Project C6070. The work was administered under the direction of the Jet Propulsion Laboratory, Liquid Propulsion Section, Propulsion Division. Mr. Richard N. Porter and Mr. James H. Kelley of JPL served as Technical Managers and Mr. Frank E. Compitello of NASA/Washington, Liquid Propulsion Systems, was Project Manager.

The program was administered by the Technical Information Research Section of IIT Research Institute under Miss Martha E. Williams, Manager. Miss Martha R. Miller, Associate Engineer, acted as Project Leader. She was responsible for the coordination of all contributions and for the technical and editorial content of the entire guidebook. Contributors are: Mr. Paul A. Bauer (Research Engineer, Fluid Systems and Lubrication), Mr. Robert I. Brabets (Research Engineer, Propellant Research), Mr. Kenneth E. Hofer, Jr. (Manager, Experimental Materials and Mechanics), Mr. Hugo J. Nielsen (Research Engineer, Heat and Mass Transfer), Mr. David T. Raske (Assistant Engineer, Experimental Materials and Mechanics), Mr. Z. Phil Saperstein (Manager, Welding Research), Mr. Harry Schwartzbart (Assistant Director, Metals), Dr. Richard H. Snow (Senior Research Engineer, Chemical Engineering Research) and Miss Audrone Valaitis (Technical Assistant, Technical Information Research).

The original guidebook was prepared by Stanford Research Institute under Contract No. NAS7-105, Project PSU-4000, entitled "Investigation of the Space Storability of Pressurizing Gases." The technical effort at Stanford Research Institute was directed by Dr. R. F. Muraca, Assistant General Manager, Physical Sciences Research Area.

TABLE OF CONTENTS

Section-Part	Title
I	INTRODUCTION AND CONVERSION TABLES
I-1	Introduction
I-2	Design Data Reference Units
I-3	Temperature Conversion Tables
I-4	Pressure Conversion Table
II	PRESSURIZATION SYSTEMS
II-1	Introduction
II-2	System Description
II-3	Comparison Factors and Selection Criteria
II-4	References
III	THE SPACE ENVIRONMENT
III-1	Introduction
III-2	Density, Pressure, Temperature
III-3	Meteoroids
III-4	Cosmic Radiation
III-5	Solar Emanations
III-6	Electromagnetic Radiation
III-7	Magnetic Fields
III-8	Effects of Space Environment on Materials
III-9	References
IV	ZERO GRAVITY CONSIDERATIONS
V	ATTITUDE CONTROL THEORY
V-1	Introduction
V-2	Torques Acting on Spacecrafts
V-3	Sensors
V-4	Hardware Design
V-5	References
VI	NOZZLE PERFORMANCE
VI-1	Introduction
VI-2	Nozzle Design Parameters
VI-3	Computation of Specific Impulse of Noncondensing Gases
VI-4	Performance of Nozzles with Condensing Fluids
VI-A	Appendix: Summary of Equations for Nozzle Performance Calculations
VII	PRESSURE VESSELS
VII-1	Introduction
VII-2	Design Criteria
VII-3	Construction Details and Support Structures
VII-4	Stress Analysis

CONTENTS (contd)

Section-Part	Title
VII-5	Material Behavior
VII-6	Materials Tracebility and Control
VII-7	Testing Procedures
VII-8	Design Example
VII-9	References
VIII	MATERIALS AND FABRICATION
VIII-1	Introduction
VIII-2	Properties of Base Materials
VIII-3	Joining
VIII-4	References
IX	PERMEABILITY THEORY
IX-1	Introduction
IX-2	Polymeric Materials
IX-3	Glasses
IX-4	Metals
IX-5	Laminates
IX-6	Distinction Between Permeation and Mass Flow
IX-7	References
X	SEALING AND LEAK DETECTION
X-1	Introduction
X-2	Static Seals
X-3	Dynamic Seals
X-4	Recommendation for Minimum Leakage
X-5	Leak Detection
X-6	Quantitative Leakage Measurements
X-7	Accuracy of Leakage Measurements
X-8	Sensitivity of Leakage Measuring Instrumentation
X-10	Leak Detection Recommendations
X-11	References
X-A	Appendix: Theoretical Leakage Consideration and Modes of Flow
X-B	Appendix: Calculations of Leakage Using Nomographs
XI	FLUID SYSTEM COMPONENTS
XI-1	Introduction
XI-2	Valves - General
XI-3	Factors Influencing Poppet Valve Design and Selection (Start Valves)
XI-4	Types of Valves
XI-5	Filters
XI-6	General Purpose Seals
XI-7	Seal Design and Selection Methods
XI-8	Expulsion Devices
XI-9	Fluid Connectors
XI-10	References

CONTENTS (contd)

Section-Page	Title
XII	STORAGE EFFICIENCY
XII-1	Introduction
XII-2	Storage Efficiency
XII-3	Thermodynamics of Pressure Vessel Blowdown
XII-4	More Exact Equations for Blowdown
XII-5	Work of Expansion
XII-6	References
XII-A	Nomenclature
XIII	HEAT BALANCE
XIV	RELIABILITY
XIV-1	Introduction
XIV-2	Reliability Models
XIV-3	Probability Distribution
XIV-4	Reliability Sampling
XIV-5	Design of Experiments
XIV-6	Tolerance Limits
XIV-7	References
XV	PROPERTIES OF GASES
XV-1	Introduction
XV-2	Properties of Nitrogen
XV-3	Properties of Hydrogen
XV-4	Properties of Helium
XV-5	Properties of Oxygen
XV-6	Properties of Carbon Dioxide
XV-7	Properties of Perchloryl Fluoride
XV-8	Properties of Chlorine Trifluoride
XV-9	Properties of Hydrazine
XV-10	Properties of Nitrogen Tetroxide
XV-11	Properties of UDHM (Unsymmetrical Dimethylhydrazine)
XV-12	Properties of Water
XV-13	Properties of Propane
XV-14	Properties of n-Butane
XV-15	Properties of Ammonia
XV-16	Properties of Hydrogen Peroxide
XV-17	Properties of Freon-11 (CCl_3F)
XV-18	Properties of Freon-12 (CCl_2F_2)
XV-19	Properties of Freon-13 ($CClF_3$)
XV-20	Properties of Freon-14 (CF_4)

DISTRIBUTION LIST

ORGANIZATION	NO. OF COPIES
NASA Headquarters Washington, D.C. 20546	
Contracting Officer, BCA	1
Patent Office, AGP	1
NASA Lewis Research Center 21000 Brookpark Road Cleveland, Ohio 44135	
Office of Technical Information	1
Contracting Officer	1
Patent Office	1
NASA Marshall Space Flight Center Huntsville, Alabama 35812	
Office of Technical Information, M-MS-IPC	1
Purchasing Office, PR-CH	1
Patent Office, M-PAT	1
Keith Chandler, R-P&VE-PA	1
NASA Western Operations Office 150 Pico Boulevard Santa Monica, California 90406	
Office of Technical Information	1
Contracts Management Division	1
General Counsel for Patent Matters	1
Chief, Liquid Propulsion Technology, RPL Office of Advanced Research and Technology NASA Headquarters Washington, D.C. 20546	4
NASA Scientific and Technical Information Facility P. O. Box 33 College Park, Maryland 20740	25
Mr. Vincent L. Johnson Director, Launch Vehicles and Propulsion, SV Office of Space Science and Applications NASA Headquarters, Washington, D.C. 20546	1
Mr. Edward L. Gray Director, Advanced Manned Missions, MT Office of Manned Space Flight NASA Headquarters, Washington, D.C. 20546	1
Mr. Clarence A. Syvertson Mission Analysis Division NASA Ames Research Center Moffett Field, California 24035	1
TECHNICAL MANAGER	1
Mr. J. H. Kelley Jet Propulsion Laboratory 4800 Oak Grove Drive Pasadena, California	

ORGANIZATION	NO. OF COPIES
NASA FIELD CENTERS	
Ames Research Center Moffett Field, California 94035 Harold Hornby Mission Analysis Div.	2
Goddard Space Flight Center Greenbelt, Maryland 20771 Merland L. Moseson Code 620	2
Jet Propulsion Laboratory California Institute of Technology 4800 Oak Grove Drive Pasadena, California 91103 Henry Burlage, Jr. Propulsion Div., 38	2
Langley Research Center Langley Station Hampton, Virginia 23365 Dr. Floyd L. Thompson Director	2
Lewis Research Center 21000 Brookpark Road Cleveland, Ohio 44135 Dr. Abe Silverstein Director	2
Marshall Space Flight Center Huntsville, Alabama 35812 Hans G. Paul Code R-P&VED	2
Manned Spacecraft Center Houston, Texas 77001 Dr. Robert R. Gilruth Director	2
Western Operations Office 150 Pico Boulevard Santa Monica, California 90406 Robert W. Kamm Director	2
John F. Kennedy Space Center, NASA Cocoa Beach, Florida 32931 Dr. Kurt H. Debus	2
GOVERNMENT INSTALLATIONS	
Aeronautical Systems Division Air Force Systems Command Wright-Patterson Air Force Base Dayton, Ohio 45433 D. L. Schmidt Code ASRCNC-2	1

DISTRIBUTION LIST

ORGANIZATION	NO. OF COPIES
Astropower Laboratory Douglas Aircraft Company 2121 Paularino Newport Beach, California 92663 Dr. George Moc Director, Research	1
Astrosystems International, Inc. 1275 Bloomfield Avenue Fairfield, New Jersey 07007 A. Mendenhall	1
Atlantic Research Corporation Edsall Road and Shirley Highway Alexandria, Virginia 22314 A. Scurlock	1
Beech Aircraft Corporation Boulder Division Box 631 Boulder, Colorado J.H. Rodgers	1
Beech Aircraft Corporation 9709 East Central Avenue Wichita, Kansas 67201 Mr. H.A. Schowalter Chief Equipment Engineer	1
Bell Aerosystems Company P.O. Box 1 Buffalo, New York 14240 W.M. Smith	1
Bendix Systems Division Bendix Corporation 3300 Plymouth Road Ann Arbor, Michigan John M. Brueger	1
Boeing Company P.O. Box 3707 Seattle, Washington 98124 J.D. Alexander	1
The Boeing Company - Michoud New Orleans, Louisiana 70129 Mr. W. Smith	1
Missile Division Chrysler Corporation P.O. Box 2628 Detroit, Michigan 48231 John Gates	1
Wright Aeronautical Division Curtiss-Wright Corporation Wood-Ridge, New Jersey 07075 G. Kelley	1

ORGANIZATION	NO. OF COPIES
Missile and Space Systems Division Douglas Aircraft Company, Inc. 3000 Ocean Park Boulevard Santa Monica, California 90406 R.W. Hallet Chief Engineer Advanced Space Tech.	1
Aircraft Missiles Division Fairchild Hiller Corporation Hagerstown, Maryland 10 J.S. Kerr	1
Garrett Corporation AiResearch Manufacturing 9851-9951 Sepulveda Boulevard Los Angeles, California 90009 Mr. Ken Miller Manager of Welding	1
General Dynamics/Astronautics Library & Information Services (128-00) P.O. Box 1128 San Diego, California 92112 Frank Dore	1
Re-Entry Systems Department General Electric Company 3198 Chestnut Street Philadelphia, Pennsylvania 19101 F.E. Schultz	1
Advanced Engine & Technology Dept. General Electric Company Cincinnati, Ohio 45215 D. Suichu	1
Grumman Aircraft Engineering Corp. Bethpage, Long Island, New York Joseph Gavin	1
Hughes Aircraft Company Centinela Avenue and Teale Street Culver City, California Dr. William Colner	1
IIT Research Institute 10 West 35 Street Chicago, Illinois 60616	
Main Files	1
Technical Information Research	4
Ling-Temco-Vought Corporation Astronautics P.O. Box 5907 Dallas, Texas 75222 Warren C. Trent	1

DISTRIBUTION LIST

ORGANIZATION	NO. OF COPIES
Air Force Missile Development Center Holloman Air Force Base, New Mexico Maj. R.E. Bracken Code MDGRT	1
Air Force Missile Test Center Patrick Air Force Base, Florida L.J. Ullian	1
Air Force Systems Division Air Force Unit Post Office Los Angeles 45, California Col. Clark Technical Data Center	1
Arnold Engineering Development Center Arnold Air Force Station Tullahoma, Tennessee Dr. H.K. Doetsch	1
Bureau of Naval Weapons Department of the Navy Washington, D.C. J. Kay RTMS-41	1
Defense Documentation Center Headquarters Cameron Station, Building 5 5010 Duke Street Alexandria, Virginia 22314 ATTN: TISIA	1
Headquarters, U.S. Air Force Washington 25, D.C. Col. C.K. Stambaugh AFRST	1
Picatinny Arsenal Dover, New Jersey 07801 I. Forsten, Chief Liquid Propulsion Laboratory SMUPA-DL	1
Air Force Rocket Propulsion Laboratory Research and Technology Division Air Force Systems Command Edwards, California 93523 RPRR/Mr. H. Main	1
U.S. Atomic Energy Commission Technical Information Services Box 62 Oak Ridge, Tennessee A.P. Huber Oak Ridge Gaseous Diffusion Plant (ORGDP) P.O.Box P	1
U.S. Army Missile Command Redstone Arsenal Alabama 35809 Dr. Walter Wharton	1

ORGANIZATION	NO. OF COPIES
U.S. Naval Ordnance Test Station China Lake California 93557 Chief, Missile Propulsion Div. Code 4562	1
CPIA	
Chemical Propulsion Information Agency Applied Physics Laboratory 8621 Georgia Avenue Silver Spring, Maryland 20910 Neil Safeer	1
INDUSTRY CONTRACTORS	
Aerojet-General Corporation P.O. Box 296 Azusa, California 91703 L.F. Kohrs	1
Aerojet-General Corporation P.O. Box 1947 Technical Library, Bldg 2015, Dept. 2410 Sacramento, California 95809 R. Stiff	1
Aerojet-General Corporation Von Karman Center Azusa, California 91703 Mr. W.J. Flaherty Manager, Pressurization Systems Product Engineering	1
Aeronautronic Philco Corporation Ford Road Newport Beach, California 92663 D.A. Carrison	1
Aerospace Corporation 2400 East El Segundo Boulevard P.O. Box 95085 Los Angeles, California 90045 John G. Wilder MS-2293 Propulsion Dept.	1
Allison Division General Motors Indianapolis, Indiana 46206 Mr. D.K. Haniuk Director of Materials Laboratories Mr. W.F. Egbert Assistant Chief Engineer, Rocket Products	1
Arde, Inc. 580 Winters Avenue Pramus, New Jersey 07652 Mr. George Hurley	1
Arthur D. Little, Inc. 20 Acorn Park Cambridge, Massachusetts 02140 E. Karl Bastress	1

DISTRIBUTION LIST

ORGANIZATION	NO. OF COPIES
Lockheed California Company 2555 North Hollywood Way Burbank, California 91503 G.D. Brewer	1
Lockheed Missiles and Space Co. ATTN: Technical Information Center P.O. Box 504 Sunnyvale, California 94088 Y.C. Lee	1
Lockheed Propulsion Company P.O. Box 111 Redlands, California 92374 H.L. Thackwell	1
The Marquardt Corporation 16555 Saticoy Street Van Nuys, California 91409 Warren P. Boardman, Jr.	1
Baltimore Division Martin Marietta Corporation Baltimore, Maryland 21203 John Calathes (3214)	1
Denver Division Martin Marietta Corporation P.O. Box 179 Denver, Colorado 80201 J.D. Goodlette (A-241)	1
McDonnell Aircraft Corporation P.O. Box 516 Municipal Airport St. Louis, Missouri 63166 R.A. Herzmark	1
McDonnell Aircraft Corporation P.O. Box 516 St. Louis, Missouri Mr. C. Fuqua Materials and Process Department	1
Menasco Manufacturing 805 South San Fernando Road Burbank, California	1
Space & Information Systems Division North American Aviation, Inc. 12214 Lakewood Boulevard Downey, California 90241 H. Storms	1
Parker Aircraft 5827 Century Boulevard Englewood, California Mr. P. Bradley	1
Rocketdyne (Library 586-306) North American Aviation, Inc. 6633 Canoga Avenue Canoga Park, California 91304 E.B. Monteath	1
Rocketdyne Division North American Aviation, Inc. 6633 Canoga Avenue Canoga Park, California 91304 Mr. G. Tellier	1
Northrop Space Laboratories 3401 West Broadway Hawthorne, California Dr. William Howard	1
Astro-Electronics Division Radio Corporation of America Princeton, New Jersey 08540 S. Fairweather	1
Reaction Motors Division Thiokol Chemical Corporation Denville, New Jersey 07832 Arthur Sherman	1
Republic Aviation Corporation Farmingdale Long Island, New York Dr. William O'Donnell	1
Solar Aircraft 2200 Pacific Highway San Diego, California Mr. John Long Director of Research	1
Space General Corporation 9200 East Flair Avenue El Monte, California 91734 C.E. Roth	1
Stanford Research Institute 333 Ravenswood Avenue Menlo Park, California 94025 Lionel Dickinson	1
TRW Systems Group TRW Incorporated One Space Park Redondo Beach, California 90278 G.W. Elverum	1
TRW Systems One Space Park Redondo Beach, California Mr. Glen Howell	1

DISTRIBUTION LIST

ORGANIZATION	NO. OF COPIES	ORGANIZATION	NO. OF COPIES
TAPCO Division TRW, Incorporated 23555 Euclid Avenue Cleveland, Ohio 44117 P.T. Angell	1		
Thiokol Chemical Corporation Huntsville Division Huntsville, Alabama John Goodloe	1		
Research Laboratories United Aircraft Corporation 400 Main Street East Hartford, Connecticut 06108 Erle Martin	1		
United Technology Center 587 Methilda Avenue P.O. Box 358 Sunnyvale, California 94088 B. Abelman	1		
Aerospace Operations Walter Kidde and Company, Inc. 567 Main Street Belleville, New Jersey 07109 R.J. Hanville Director of Research Engineering	1		
Florida Research and Development Pratt and Whitney Aircraft United Aircraft Corporation P.O. Box 2691 West Palm Beach, Florida 33402 R.J. Coar	1		
Rocket Research Corporation 520 South Portland Street Seattle, Washington 98108 Foy McCullough, Jr.	1		

I INTRODUCTION AND CONVERSION TABLES

Table of Contents

Section-Part	Title	Section-Part. Page
I-1	Introduction.....	I-1.1
I-2	Design Data Reference Units.....	I-2.1
	Universal Gas Constant.....	I-2.1
	Standard Gravity.....	I-2.1
	Absolute Zero.....	I-2.1
	Pressure Units.....	I-2.1
	Weight Units.....	I-2.1
	Density Units.....	I-2.1
	Volume Units.....	I-2.2
	Viscosity Units.....	I-2.2
	Thermal Units.....	I-2.3
	Work and Energy Units.....	I-2.3
I-3	Temperature Conversion Table.....	I-3.1
I-4	Pressure Conversion Chart.....	I-4.1

I-1 INTRODUCTION

The primary purpose of this book is to provide the preliminary design engineer a ready source of information to guide his selection of parameters in the design of pressurized gas systems for spacecraft. It is intended that the information contained in this guidebook be used in conjunction with the various methodologies currently employed to select component combinations and to establish the design details of suitable pressurized gas systems.

The sections of this revised edition have been rearranged to provide a more systematic development of the various parameters that must be considered in the design of any pressurized gas system for use in space.

Section I, "Introduction" includes conversion tables in both metric and English units and a listing of pertinent constants.

Section II, "Pressurization System," presents a general discussion of pressurized gas systems. This section was written by Mr. P. A. Bauer.

Section III, "The Space Environment," summarizes the available information on the composition of the atmosphere. It also includes data on the distribution of meteoroids and on the various types of radiation encountered by spacecraft. This section has been retained in its original form.

Section IV, "Zero Gravity Considerations," summarizes the behavior of liquids in an essentially gravitationally-free system (zero-g). Only those aspects related to pressurized gas systems are discussed. This section has been retained in its original form.

Section V, "Attitude Control Theory," presents the salient principles underlying the design of pressurized gas attitude control systems. This section has been retained in its original form.

Section VI, "Nozzle Performance," summarizes the computations of the performance of fluids expanding through nozzles. The discussion considers both condensable and noncondensable gases. This section has been retained in its original form.

Section VII, "Pressure Vessels," establishes vessel design criteria and discusses the various aspects of the problem of designing a pressure vessel. An outline of selection filters is presented to aid the engineer in selecting the best material, configuration, fabrication technique and support method for his particular vessel. The part on "Stress Analysis" presents methods of evaluating loads on pressure vessels of different geometries. The part on "Material Behavior" illustrates the use of fracture mechanics for design as well as for testing. Various testing procedures are discussed and an indication is given of the problems related to the selection of test criteria. An example problem and its detailed solution are presented as a direct guide to aid in the stress analysis of competing designs. This section was written by Mr. D.T. Raske and Mr. K.E. Hofer, Jr.

Section VIII, "Materials and Fabrication," discusses the various materials and fabrication methods currently used for pressure vessels. A discussion of base materials and their weldability and formability is presented. An outline is given to guide the engineer in establishing the criteria by which candidate materials and fabrication methods should be evaluated. The joining of tubing and components in the overall system is discussed. This section was prepared by Mr. H. Schwartzbart and Mr. Z. P. Saperstein.

Section IX, "Permability Theory," presents a discussion of the fundamental aspects of diffusion and permeability theory, and data on the permeability of various polymers and elastomers. This section has been retained in its original form.

Section X, "Sealing and Lead Detection," discusses static and dynamic seals, modes of leakage, and leak detection techniques. Recommendations are made for attaining minimum leakage and detecting leaks. The section was prepared by Mr. P. A. Bauer.

Appendix A, Section X, presents theoretical leakage consideration, and leakage equations for various modes of compressible and incompressible flow. Appendix B presents a method of calculating leakage using the depicted monographs.

Section XI, "Fluid System Components" presents discussions on the various components utilized in pressurized gas systems. Design and selection criteria are established to aid in the selection of the appropriate components to fulfill specified mission requirements. The components discussed include filters, valves, general purpose seals, connectors and fittings, and expulsion devices. This section was prepared by Mr. P. A. Bauer.

Section XII, "Storage Efficiency," presents definitions of storage and weight efficiency, and the theory of thermodynamic blowdown is discussed. General equations to estimate the heat flow are provided for various heat transfer modes and combinations thereof. A discussion of deviation from ideality and general equations for the calculation of the work of expansion are also presented. This section was prepared by Dr. R.H. Snow and Mr. H.J. Nielsen.

Section XIII, "Heat Balance," is a combination of Stanford Research Institute's original data and an expansion of information by IIT Research Institute. This section discusses various radiation sources and their effect on the spacecraft. It presents guide lines for calculating a heat balance and provides references to serve as a guide for detailed analysis of a spacecraft heat balance.

Section XIV, "Reliability," provides a brief review and summary of the principles of statistical relationships as applied to test programs and is intended to provide guidelines for the engineer. This section has been retained in its original form.

Section XV, "Properties of Gases," is a combined effort by IIT Research Institute and Stanford Research Institute. Mr. R. Brabets and Miss A. Valaitis conducted the search and prepared the data IIT Research Institute added, expanded, and converted. IIT Research Institute worked extensively on thirteen of the originally presented nineteen fluids. Those thirteen fluids are Nitrogen, Hydrogen, Helium, Oxygen, Carbon Dioxide, Water, Propane, n-Butane, Ammonia, Freon 11, Freon 12, Freon 13, and Freon 14. New and extensive density graphs, providing three-place readability, were prepared for these thirteen fluids. The existing tables

were expanded and new data added when necessary. Whenever feasible, the graphs were replotted in English units. The replotting of graphs applied also to the six fluids that were not otherwise revised or expanded: Perchloryl Fluoride, Chlorine Trifluoride, Hydrazine, Nitrogen Tetroxide, UDMH and Hydrogen Peroxide.

I-2 DESIGN DATA REFERENCE UNITS

UNIVERSAL GAS CONSTANT	
ergs/^{o}C/mole	8.3170×10^{7}
cal(15 ^{o}C)/^{o}C/mole	1.9869
cc-atm/^{o}C/g-mole	82.0567
liter-atm/^{o}C/g-mole	8.20544×10^{-2}
in^{3}-atm/^{o}F/lb-mole	1.260×10^{3}
in^{3}-psi/^{o}F/lb-mole	1.8510×10^{4}
ft^{3}-atm/^{o}F/lb-mole	7.30228×10^{-1}
ft-lb/^{o}F/lb-mole	1.5452×10^{3}
Btu/^{o}F/lb-mole	1.9869

STANDARD GRAVITY
980.665 cm/sec/sec
32.174 ft/sec/sec

ABSOLUTE ZERO
-273.15^{o}C = 0°K
-459.67^{o}F = 0°R

PRESSURE UNITS (FL^{-2}) ($ML^{-1}T^{-2}$)			
Unit / Equivalent	1 Std. Atmos.	1 mm of Hg at 0°C	1 dyne/cm^{2}
atmosphere	1	1.3158×10^{-3}	9.8692×10^{-7}
mm of Hg at 0°C	760	1	7.5006×10^{-4}
in of Hg at 32.0 ^{o}F	29.921	3.937×10^{-2}	2.953×10^{-5}
g/cm^{2}	1.033×10^{3}	1.3595	1.01971×10^{-3}
psia	14.696	1.9337×10^{-2}	1.4504×10^{-5}
lb/ft^{2}	2116.224	2.7845	2.0886×10^{-3}
dynes/cm^{2}	1.01325×10^{6}	1.33322×10^{3}	1

DENSITY UNITS (ML^{-3})			
Unit / Equivalent	1 g/cc	1 lb/in^{3}	1 lb/ft^{3}
g/cc	1	27.680	1.6018×10^{-2}
lb/in^{3}	3.613×10^{-2}	1	5.787×10^{-4}
lb/ft^{3}	62.43	1728.0	1

WEIGHT UNITS
1 lb = 453.5924 grams
1 g = 0.0022046 lb

VOLUME UNITS (L^3)

Unit / Equiv.	1 cm^3	1 in^3	1 ft^3	1 ml	1 liter	1 gal
cm^3	1	6.1023×10^{-2}	3.5314×10^{-5}	9.9997×10^{-1}	9.9997×10^{-4}	2.6417×10^{-4}
in^3	16.387	1	5.7870×10^{-4}	16.387	1.6387×10^{-2}	4.329×10^{-3}
ft^3	2.83×10^{4}	1.728×10^{3}	1	2.832×10^{4}	28.32	7.481
ml	1.000028	6.103×10^{-2}	3.532×10^{-5}	1	1×10^{-3}	2.642×10^{-4}
liter	1.000028×10^{3}	6.103×10^{1}	3.532×10^{-2}	1×10^{3}	1	2.642×10^{-1}
gal	3.785×10^{3}	2.31×10^{2}	1.337×10^{-1}	3.785×10^{3}	3.785	1

VISCOSITY UNITS ($ML^{-1}T^{-1}$) (FTL^{-2})

Unit / Equiv.	1 Poise	1 $\frac{lb\text{-}sec}{ft^2}$ (FTL^{-2})	1 $\frac{lb\text{-}hr}{ft^2}$ (FTL^{-2})	1 $\frac{slug}{ft\text{-}sec}$ ($ML^{-1}T^{-1}$)	1 $\frac{slug}{ft\text{-}hr}$ ($ML^{-1}T^{-1}$)
Poise	1	4.79×10^{2}	1.72×10^{6}	1.49×10^{1}	4.13×10^{-3}
$\frac{lb\text{-}sec}{ft^2}$	2.09×10^{-3}	1	3.60×10^{3}	3.11×10^{-2}	8.63×10^{-6}
$\frac{lb\text{-}hr}{ft^2}$	5.80×10^{-7}	2.78×10^{-4}	1	8.63×10^{-6}	2.40×10^{-9}
$\frac{slug}{ft\text{-}sec}$	6.72×10^{-2}	3.22×10^{1}	1.16×10^{5}	1	3.60×10^{3}
$\frac{slug}{ft\text{-}hr}$	2.42×10^{2}	8.95×10^{-3}	4.17×10^{8}	2.78×10^{-4}	1

DESIGN DATA REFERENCE UNITS (Cont'd)

THERMAL UNITS	
Heat capacity:	cal/g = Btu/lb
Heat of Vaporization:	cal/g × 1.79882 = Btu/lb
Heat of fusion:	cal/g × 1.79882 = Btu/lb
Thermal conductivity:	(cal/sec-cm-°C) × 242 = Btu/hr-ft°F

WORK AND ENERGY UNITS					
Unit / Equivalent	1 Btu (mean)	1 ft-lb	1 g-cal (mean)	1 ft^3-atm	1 liter-atm
kwh	2.930×10^{-4}	3.7662×10^{-7}	1.1628×10^{-6}	7.9705×10^{-4}	2.815×10^{-5}
cal (mean)	251.98	3.2389×10^{-4}	1.	680.74	24.2052
cal (15°C)	252.04	3.2381×10^{-4}	1.000238	680.58	24.1994
Btu (mean)	1.	0.0012854	0.0039685	2.7203	0.09607
ft^3-atm	0.3676	4.7253×10^{-4}	0.001459	1.	0.035319
liter-atm	10.409	0.013381	0.041311	28.313	1.
ft-lb	777.97	1.	3.0874	2116.3	74.735
joules (abs)	1054.8	1.35582	4.186	2869.4	101.328
ergs	1.0548×10^{10}	1.35582×10^{7}	4.186×10^{7}	2.8496×10^{10}	1.0132×10^{9}

I-3 TEMPERATURE CONVERSION

READING IN °F OR °C TO BE CONVERTED	°C	°K	°F	°R
-459.67	-273.15	0		0
-458	-272.22	0.93		1.67
-456	-271.11	2.04		3.67
-454	-270.00	3.15		5.67
-452	-268.89	4.26		7.67
-450	-267.78	5.37		9.67
-448	-266.67	6.48		11.67
-446	-265.56	7.59		13.67
-444	-264.44	8.71		15.67
-442	-263.33	9.82		17.67
-440	-262.22	10.93		19.67
-438	-261.11	12.04		21.67
-436	-260.00	13.15		23.67
-434	-258.89	14.26		25.67
-432	-257.78	15.37		27.67
-430	-256.67	16.48		29.67
-428	-255.56	17.59		31.67
-426	-254.44	18.71		33.67
-424	-253.33	19.82		35.67
-422	-252.22	20.93		37.67
-420	-251.11	22.04		39.67
-418	-250.00	23.15		41.67
-416	-248.89	24.26		43.67
-414	-247.78	25.37		45.67
-412	-246.67	26.48		47.67
-410	-245.56	27.59		49.67
-408	-244.44	28.71		51.67
-406	-243.33	29.82		53.67
-404	-242.22	30.93		55.67
-402	-241.11	32.04		57.67
-400	-240.00	33.15		59.67
-398	-238.89	34.26		61.67
-396	-237.78	35.37		63.67
-394	-236.67	36.48		65.67
-392	-235.56	37.59		67.67
-390	-234.44	38.71		69.67
-388	-233.33	39.82		71.67
-386	-232.22	40.93		73.67
-384	-231.11	42.04		75.67
-382	-230.00	43.15		77.67
-380	-228.89	44.26		79.67
-378	-227.78	45.37		81.67
-376	-226.67	46.48		83.67
-374	-225.56	47.59		85.67
-372	-224.44	48.71		87.67
-370	-223.33	49.82		89.67
-368	-222.22	50.93		91.67
-366	-221.11	52.04		93.67
-364	-220.00	53.15		95.67
-362	-218.89	54.26		97.67
-360	-217.78	55.37		99.67
-358	-216.67	56.48		101.67
-356	-215.56	57.59		103.67
-354	-214.44	58.71		105.67
-352	-213.33	59.82		107.67
-350	-212.22	60.93		109.67

TEMPERATURE CONVERSION (Cont'd)

READING IN °F OR °C TO BE CONVERTED	°C	°K	°F	°R
-348	-211.11	62.04		111.67
-346	-210.00	63.15		113.67
-344	-208.89	64.26		115.67
-342	-207.78	65.37		117.67
-340	-206.67	66.48		119.67
-338	-205.56	67.59		121.67
-336	-204.44	68.71		123.67
-334	-203.33	69.82		125.67
-332	-202.22	70.93		127.67
-330	-201.11	72.04		129.67
-328	-200.00	73.15		131.67
-326	-198.89	74.26		133.67
-324	-197.78	75.37		135.67
-322	-196.67	76.48		137.67
-320	-195.56	77.59		139.67
-318	-194.44	78.71		141.67
-316	-193.33	79.82		143.67
-314	-192.22	80.93		145.67
-312	-191.11	82.04		147.67
-310	-190.00	83.15		149.67
-308	-188.89	84.26		151.67
-306	-187.78	85.37		153.67
-304	-186.67	86.48		155.67
-302	-185.56	87.59		157.67
-300	-184.44	88.71		159.67
-298	-183.33	89.82		161.67
-296	-182.22	90.93		163.67
-294	-181.11	92.04		165.67
-292	-180.00	93.15		167.67
-290	-178.89	94.26		169.67
-288	-177.78	93.57		171.67
-286	-176.67	96.48		173.67
-284	-175.56	97.59		175.67
-282	-174.44	98.71		177.67
-280	-173.33	99.82		179.67
-278	-172.22	100.93		181.67
-276	-171.11	102.04		183.67
-274	-170.00	103.15		185.67
-273.15	-169.53	103.62		186.52
-273.15		0	-459.67	0
-272	-168.89	104.26	-457.6	2.07
-270	-167.78	105.37	-454.0	5.67
-268	-166.67	106.48	-450.4	9.27
-266	-165.56	107.59	-446.8	12.87
-264	-164.44	108.71	-443.2	16.47
-262	-163.33	109.82	-439.6	20.07
-260	-162.22	110.93	-436.0	23.67
-258	-161.11	112.04	-432.4	27.27
-256	-160.00	113.15	-428.8	30.87
-254	-158.89	114.26	-425.2	34.47
-252	-157.78	115.37	-421.6	38.07
-250	-156.67	116.48	-418.0	41.67

TEMPERATURE CONVERSION (Cont'd)

READING IN °F OR °C TO BE CONVERTED	°C	°K	°F	°R
-248	-155.56	117.59	-414.4	45.27
-246	-154.44	118.71	-410.8	48.87
-244	-153.33	119.62	-407.2	52.47
-242	-152.22	120.93	-403.6	56.07
-240	-151.11	122.04	-400.0	59.67
-238	-150.00	123.15	-396.4	63.27
-236	-148.89	124.26	-392.8	66.87
-234	-147.78	125.37	-389.2	70.47
-232	-146.67	126.48	-385.6	74.07
-230	-145.56	127.59	-382.0	77.67
-228	-144.44	128.71	-378.4	81.27
-226	-143.33	129.82	-374.8	84.87
-224	-142.22	130.93	-371.2	88.47
-222	-141.11	131.94	-367.6	92.07
-220	-140.00	133.15	-364.0	95.67
-218	-138.89	134.26	-360.4	99.27
-216	-137.78	135.37	-356.8	102.87
-214	-136.67	136.48	-353.2	106.47
-212	-135.56	137.59	-349.6	110.07
-210	-134.44	138.71	-346.0	113.67
-208	-133.33	139.82	-342.4	117.27
-206	-132.22	140.93	-338.8	120.87
-204	-131.11	142.04	-335.2	124.47
-202	-130.00	143.15	-331.6	128.07
-200	-128.89	144.26	-328.0	131.67
-198	-127.78	145.37	-324.4	135.27
-196	-126.67	146.48	-320.8	138.87
-194	-125.56	147.59	-317.2	142.47
-192	-124.44	148.71	-313.6	146.07
-190	-123.33	149.82	-310.0	149.67
-188	-122.22	150.93	-306.4	153.27
-186	-121.11	152.04	-302.8	156.87
-184	-120.00	153.15	-299.2	160.47
-182	-118.89	154.26	-295.6	164.07
-180	-117.78	155.37	-292.0	167.67
-178	-116.67	156.43	-288.4	171.27
-176	-115.56	157.59	-284.8	174.87
-174	-114.44	158.71	-281.2	178.47
-172	-113.33	159.82	-277.6	182.07
-170	-112.22	160.93	-274.0	185.67
-168	-111.11	162.04	-270.4	189.27
-166	-110.00	163.15	-266.8	192.87
-164	-108.89	164.26	-263.2	196.47
-162	-107.78	165.37	-259.6	200.07
-160	-106.67	166.48	-256.0	203.67
-158	-105.56	167.59	-252.4	207.27
-156	-104.44	168.71	-248.8	210.87
-154	-103.33	169.84	-245.2	214.47
-152	-102.22	170.93	-241.6	218.07
-150	-101.11	172.04	-238.0	221.67
-148	-100.00	173.15	-234.4	225.27
-146	- 98.89	174.26	-230.8	228.87
-144	- 97.78	175.37	-227.2	232.47
-142	- 96.67	176.48	-223.6	236.07
-140	- 95.56	177.59	-220.0	239.67

TEMPERATURE CONVERSION (Cont'd)

READING IN °F OR °C TO BE CONVERTED	°C	°K	°F	°R
-138	-94.44	178.71	-216.4	243.27
-136	-93.33	179.82	-212.8	246.87
-134	-92.22	180.93	-209.2	250.38
-132	-91.11	182.04	-205.6	254.07
-130	-90.00	183.15	-202.0	257.67
-128	-88.89	184.26	-198.4	261.27
-126	-87.78	185.37	-194.8	264.87
-124	-86.67	186.43	-191.2	268.47
-122	-85.56	187.59	-187.6	272.07
-120	-84.44	188.61	-184.0	275.67
-118	-83.33	189.82	-180.4	279.27
-116	-82.22	190.93	-176.8	282.87
-114	-81.11	192.04	-173.2	286.47
-112	-80.00	193.15	-169.6	290.07
-110	-78.89	194.26	-166.0	293.67
-108	-77.78	195.37	-162.4	297.27
-106	-76.67	196.48	-158.8	300.87
-104	-75.56	197.59	-155.2	304.47
-102	-74.44	198.71	-151.6	308.07
-100	-73.33	199.82	-148.0	311.67
-98	-72.22	200.93	-144.4	315.27
-96	-71.11	202.04	-140.8	318.87
-94	-70.00	203.15	-137.2	322.47
-92	-68.89	204.26	-133.6	326.07
-90	-67.78	205.37	-130.00	329.67
-88	-66.67	206.48	-126.4	333.27
-86	-65.56	207.59	-122.8	336.87
-84	-64.44	208.71	-119.2	340.47
-82	-63.33	209.82	-115.6	344.07
-80	-62.22	210.93	-112.0	347.67
-78	-61.11	212.04	-108.4	351.27
-76	-60.00	213.15	-104.8	354.87
-74	-58.89	214.26	-101.2	358.47
-72	-57.78	215.37	-97.6	362.07
-70	-56.67	216.48	-94.0	365.67
-68	-55.56	217.59	-90.4	369.27
-66	-54.44	218.71	-86.8	372.87
-64	-53.33	219.82	-83.2	376.47
-62	-52.22	220.93	-79.6	380.07
-60	-51.11	222.04	-76.0	383.67
-58	-50.00	223.15	-72.4	387.27
-56	-48.89	224.26	-68.88	390.87
-54	-47.78	225.37	-65.2	394.47
-52	-46.67	226.48	-61.6	398.07
-50	-45.56	227.59	-58.0	401.67
-48	-44.44	228.71	-54.4	405.27
-46	-43.33	229.82	-50.8	408.87
-44	-42.22	230.93	-47.20	412.47
-42	-41.11	232.04	-43.6	416.07
-40	-40.00	233.15	-40.0	419.67
-38	-38.89	234.26	-36.4	423.27
-36	-37.78	235.37	-32.8	426.87
-34	-36.67	236.48	-29.2	430.47
-32	-35.56	237.59	-25.6	434.07
-30	-34.44	238.71	-22.0	437.67

TEMPERATURE CONVERSION (Cont'd)

READING IN °F OR °C TO BE CONVERTED	°C	°K	°F	°R
-28	-33.33	239.82	-18.4	441.27
-26	-32.22	240.93	-14.8	444.87
-24	-31.11	242.04	-11.2	448.47
-22	-30.00	243.15	-7.6	452.07
-20	-28.89	244.26	-4.0	455.67
-18	-27.78	245.37	-0.4	459.27
-16	-26.67	246.48	+3.2	462.87
-14	-25.56	247.59	+6.8	466.07
-12	-24.44	248.71	+10.4	470.07
-10	-23.33	249.82	+14.0	473.67
-8	-22.22	250.93	+17.6	477.27
-6	-21.11	252.04	+21.2	480.87
-4	-20.00	253.15	+24.8	484.47
-2	-18.89	254.16	+28.4	488.07
0.00	-17.78	255.37	+32.0	491.67
+2	-16.67	256.48	+35.6	495.27
+4	-15.56	257.59	+39.2	498.87
+6	-14.44	258.71	+42.8	502.47
+8	-13.33	259.82	+46.4	506.07
+10	-12.22	260.93	+50.0	509.67
+12	-11.11	262.04	+53.6	513.27
+14	-10.00	263.15	+57.2	516.87
+16	-8.89	264.26	+60.8	520.47
+18	-7.78	265.37	+64.4	524.07
+20	-6.67	266.48	+68.0	527.67
+22	-5.56	267.59	+71.6	531.27
+24	-4.44	268.71	+75.2	534.87
+26	-3.33	269.82	+78.8	538.47
+28	-2.22	270.93	+82.4	542.07
+30	-1.11	272.04	+86.0	545.67
+32	0.00	273.15	+89.6	549.27
+34	+1.11	274.26	+93.2	552.87
+36	+2.22	275.37	+96.8	556.47
+38	+3.33	276.48	+100.4	560.07
+40	+4.44	277.59	+104.0	563.67
42	5.56	278.71	107.6	567.27
44	6.67	279.82	111.2	570.87
46	7.78	280.93	114.8	574.47
48	8.89	282.04	118.4	578.07
50	10.00	283.15	122.0	581.67
52	11.11	284.26	125.6	585.27
54	12.22	285.37	129.2	588.87
56	13.33	286.48	132.8	592.47
58	14.44	287.59	136.4	596.07
60	15.56	288.71	140.0	599.67
62	16.67	289.82	143.6	603.27
64	17.78	290.93	147.2	606.87
66	18.89	292.04	150.8	610.47
68	20.00	293.15	154.4	614.07
70	21.11	294.26	158.0	617.67
72	22.22	295.37	161.6	621.27
74	23.33	296.48	165.2	624.87
76	24.44	297.59	168.8	628.47
78	25.56	298.71	172.4	632.07
80	26.67	299.82	176.0	635.67

TEMPERATURE CONVERSION (Cont'd)

READING IN °F OR °C TO BE CONVERTED	°C	°K	°F	°R
82	27.78	300.93	179.6	639.27
84	28.89	302.04	183.2	642.87
36	30.00	303.15	186.8	646.47
88	31.11	304.26	190.4	650.07
90	32.22	305.37	194.0	653.67
92	33.33	306.48	197.6	651.27
94	34.44	307.59	201.2	660.87
96	35.56	308.71	204.8	664.47
98	36.67	309.82	208.4	668.07
100	37.78	310.93	212.0	671.67
102	38.89	312.04	215.6	675.27
104	40.00	313.15	219.2	678.87
106	41.11	314.26	222.8	682.47
108	42.22	315.37	226.4	686.07
110	43.33	316.48	230.0	689.67
112	44.44	317.59	233.6	693.27
114	45.56	318.71	237.2	696.87
116	46.67	319.82	240.8	700.47
118	47.78	320.93	244.4	704.07
120	48.89	322.04	248.0	707.67
122	50.00	323.15	251.6	711.27
124	51.11	324.26	255.2	714.87
126	52.22	325.37	258.8	718.47
128	53.33	326.48	262.4	722.07
130	54.44	327.59	266.0	725.67
132	55.56	328.66	269.6	729.27
134	56.67	329.82	273.2	732.87
136	57.78	330.93	276.8	736.47
138	58.89	332.04	280.4	770.07
140	60.00	333.15	284.0	743.67
142	61.11	334.26	287.6	747.27
144	62.22	335.36	291.2	750.87
146	63.33	336.48	294.8	754.47
148	64.44	337.59	298.4	758.07
150	65.66	338.71	302.0	761.67
152	66.67	339.82	305.6	765.27
154	67.78	340.93	309.2	768.87
156	68.89	341.64	312.8	772.47
158	70.00	343.15	316.4	776.07
160	71.11	344.26	320.0	779.67
162	72.22	345.37	323.6	783.27
164	73.33	346.48	327.2	786.87
166	74.44	347.59	330.8	790.47
168	75.56	348.71	334.4	794.07
170	76.67	349.82	338.0	797.67
172	77.78	350.93	341.6	801.27
174	78.89	352.04	345.2	804.87
176	80.00	353.15	348.8	808.47
178	81.11	354.26	352.4	812.07
180	82.22	355.37	356.0	815.67
182	83.33	356.48	359.6	819.27
184	84.44	357.59	363.2	822.87
186	85.56	358.71	366.8	826.47
188	86.67	359.82	370.4	830.07
190	87.78	360.93	374.0	833.67

TEMPERATURE CONVERSION (Concluded)

READING IN °F OR °C TO BE CONVERTED	°C	°K	°F	°R
192	88.89	362.04	377.6	837.27
194	90.00	363.15	381.2	840.87
196	91.11	364.26	384.8	844.47
198	92.22	365.37	388.4	848.07
200	93.33	366.48	392.0	851.67
202	94.44	367.59	395.6	855.27
204	95.56	368.71	399.2	858.87
206	96.67	369.82	402.8	862.47
208	97.78	370.93	406.4	866.07
210	98.89	372.04	410.0	869.67
212	100.00	373.15	413.6	873.27
214	101.11	374.26	417.2	876.87
216	102.22	375.37	420.8	880.47
218	103.33	376.48	424.4	884.07
220	104.44	377.59	428.0	887.67

I-4 PRESSURE CONVERSION

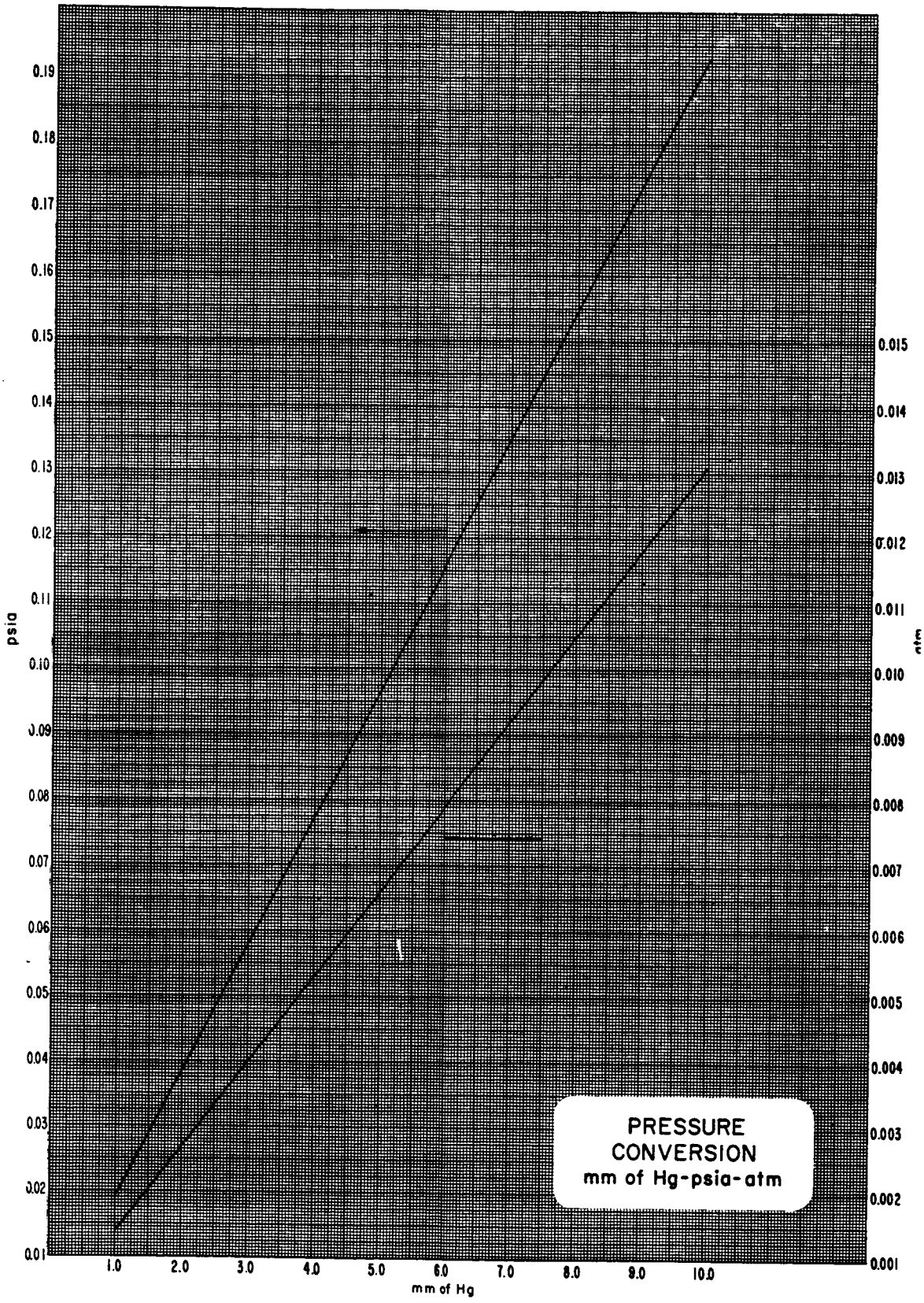

II PRESSURIZATION SYSTEMS

Table of Contents

Section-Part	Title	Section-Part.Page
II-0	List of Figures.....	II-0.2
II-1	Introduction.....	II-1.1
II-2	System Description.....	II-2.1
	General.....	II-2.1
	Construction Features.....	II-2.1
	Start Valves.....	II-2.7
	Fill Fitting.....	II-2.7
	Relief Valve.....	II-2.7
	Pressure Vessel.....	II-2.8
	System Thermodynamics.....	II-2.8
	Stored Gas.....	II-2.9
	Solid and Liquid Propellants.....	II-2.10
	Evaporated Propellants.....	II-2.12
	Evaporated Non-Propellants.....	II-2.13
II-3	Comparison Factors and Selection Criteria	II-3.1
II-4	References.....	II-4.1

II-0 LIST OF FIGURES

Section-Part-Figure	Title	Section-Part.Page
II-2-1	Typical Pressurized Gas Storage System.....	II-2.3
II-2-2	Integrated Pneumatic Components (Ref. 3).....	II-2.4
II-2-3	Semi-Integrated Sub-Assembly (Courtesy JPL).....	II-2.5
II-2-4	Composite Fill and Check Valve with Filter.....	II-2.6

II-1 INTRODUCTION

The purpose of a stored cold gas or cryogenic liquid system for spacecraft applications is to provide a storage of energy which (1) can be used directly as a propulsive or attitude control media or (2) can be employed in the blowdown of liquid propellant storage vessels. Typical spacecraft applications include:

(1) Rocket propellant turbopump feed systems - Booster and upper stage

(2) Spacecraft maneuvering

(3) Attitude control systems

(4) Fuel cell

(5) Personnel propulsion

Each of these systems utilizes the stored gas in a different manner. Additionally, within the same group of systems, wide variations in system concepts exist depending upon past performance, experience, designers preference, and mission requirements. There is no need to go into detail on individual systems because adequate information is readily available on operational systems plus a multiplicity of information on conceptual schemes. In each case, however, a stored gas is employed and the discussion can be limited to that portion of the spacecraft subsystem.

II-2 SYSTEM DESCRIPTION

General

The most general system consists of the following components:

(1) A gas storage vessel

(2) An electrically operated start valve

(3) Gas fill and vent valve

(4) Filters - often two where one precedes the storage vessel during fill and the other preceding the start valve

(5) A check valve to prevent back flushing of the fill valve filter

(6) A relief valve and possibly a burst disc

(7) Piping and associated connections

(8) Manifolds

(9) Pressure transducer

(10) Temperature transducer

Construction Features

There are several philosophies surrounding the construction of the fluid components. One philosophy suggests that all components (relief, fill, vent, start, and the regulator) be placed in one integrated assembly such as that shown in Figure II-2-2. This component development was conducted by Bell Aerosystems for the Air Force (Ref. 3). Another philosophy states that all components can be located within the pressure vessel. In both cases, the objective is to reduce component interconnections and, hence, leakage. Another less drastic concept suggests that the components be located on an integral frame as shown in Figure II-2-3. Coupled with this latter philosophy, is the integration of minor components such as the fill valve shown in Figure II-2-4. Fill and check valves and a filter are located in the same housing. A less desirable method is to use individual components connected together and scattered about the spacecraft. The advantage in modular construction is the ability to leak check complete packages before final assembly.

In addition, any integration of components reduces sources of contamination. The entire system, like the individual components, should be cleaned and assembled in a Class 10000 (or better) clean room. The classification of clean rooms is designated in Federal Standard 209. This standard states that a class 10000 room must contain less than 10000 particles per cubic foot of 0.5 micron size and larger. Continuous flushing of components with pressurant gas can also reduce contamination. The assembled integrated unit or sub-assembly should be pressurized with the pressurant or a more inert gas during storage.

The location of the center of gravity of the spacecraft is quite important. Consequently, the placement of components may be dictated by this factor.

Pressurization system components should have all external hermetic seals rather than general purpose seals. This reduces external leakage and improves reliability. All components should be provided with the necessary radiation and meteoroid protection depending upon the location within the spacecraft and its mission.

When selecting fluid conduits, the size of the tubing should be commensurate with tolerable pressure drop at maximum flow rates. The connections should preferably be brazed or welded using techniques which prevent any egress of contaminants. These connections should be made as far from individual components as possible. In the event close joining is necessary, adequate heat sinks should be provided.

Since it is often impossible to construct a completely welded system, a connector must be selected. For minimum leakage, the "O"-ring modified AN fitting is suggested, Section XI-9. When elastomers cannot be employed consideration should be given to the AFRPL or the "MC" connector.

The tubing should be resiliently mounted to compensate for thermal expansion. Simultaneously, the tube attachment points should be located such that minimum stresses are generated due to acceleration, vibration, and shock transients.

A schematic diagram of a typical subsystem is shown in Figure II-2-1.

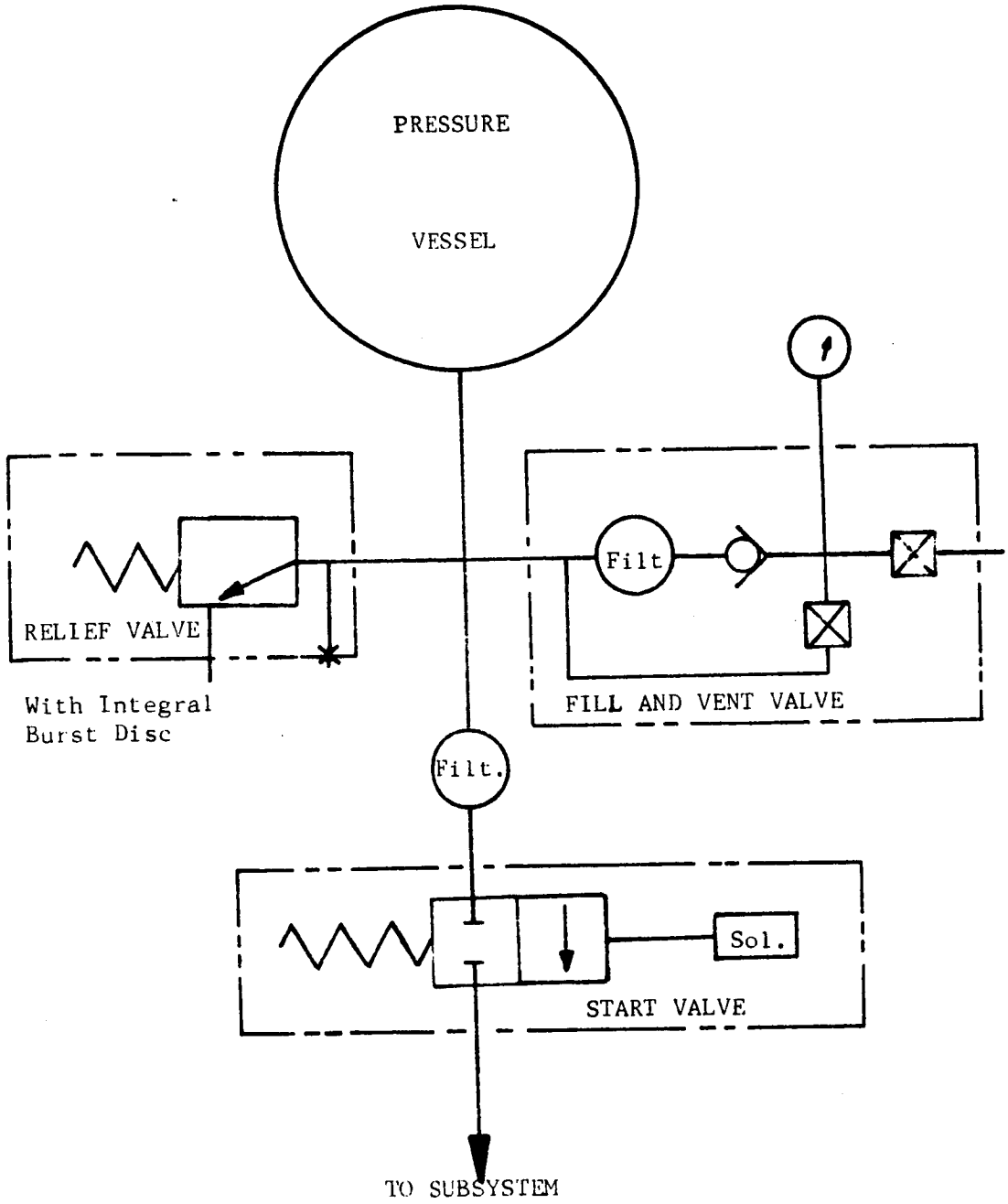

Fig. II-2-1 Typical Pressurized Gas Storage System

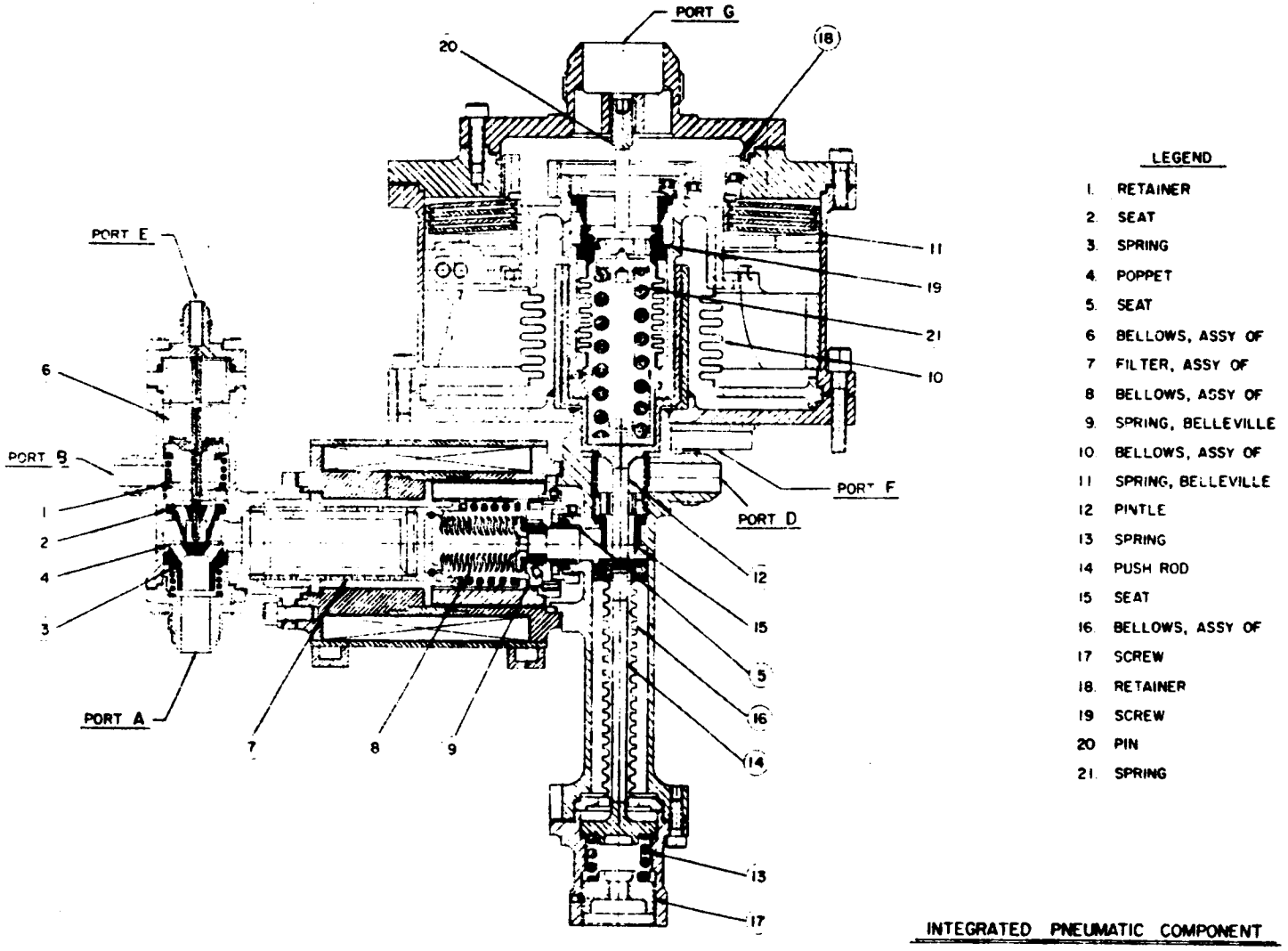

Fig. II-2-2 Integrated Pneumatic Components (Ref. 3)

ORIGINAL PAGE
BLACK AND WHITE PHOTOGRAPH

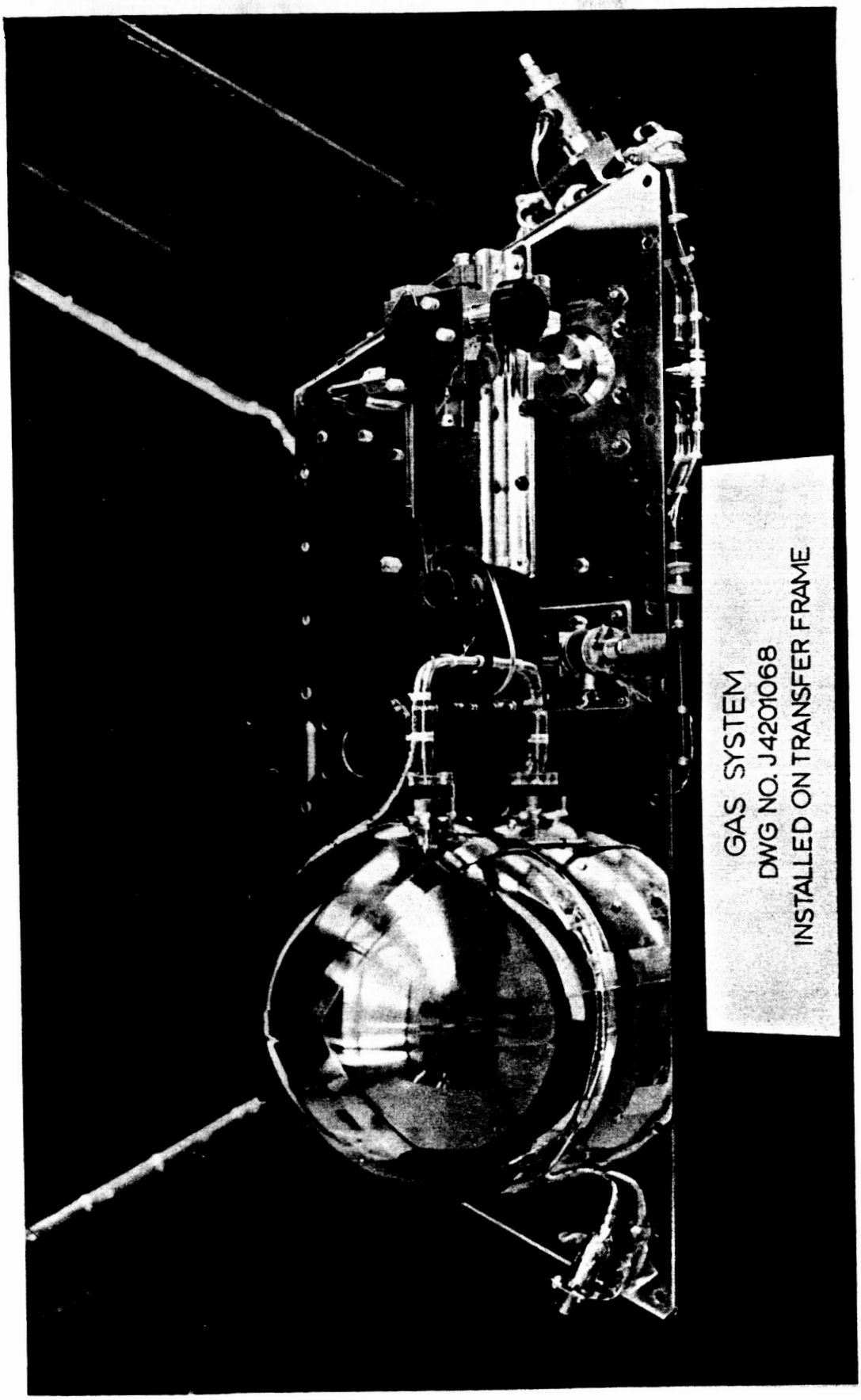

Fig. II-2-3 Semi-Integrated Sub-Assembly
(Courtesy JPL)

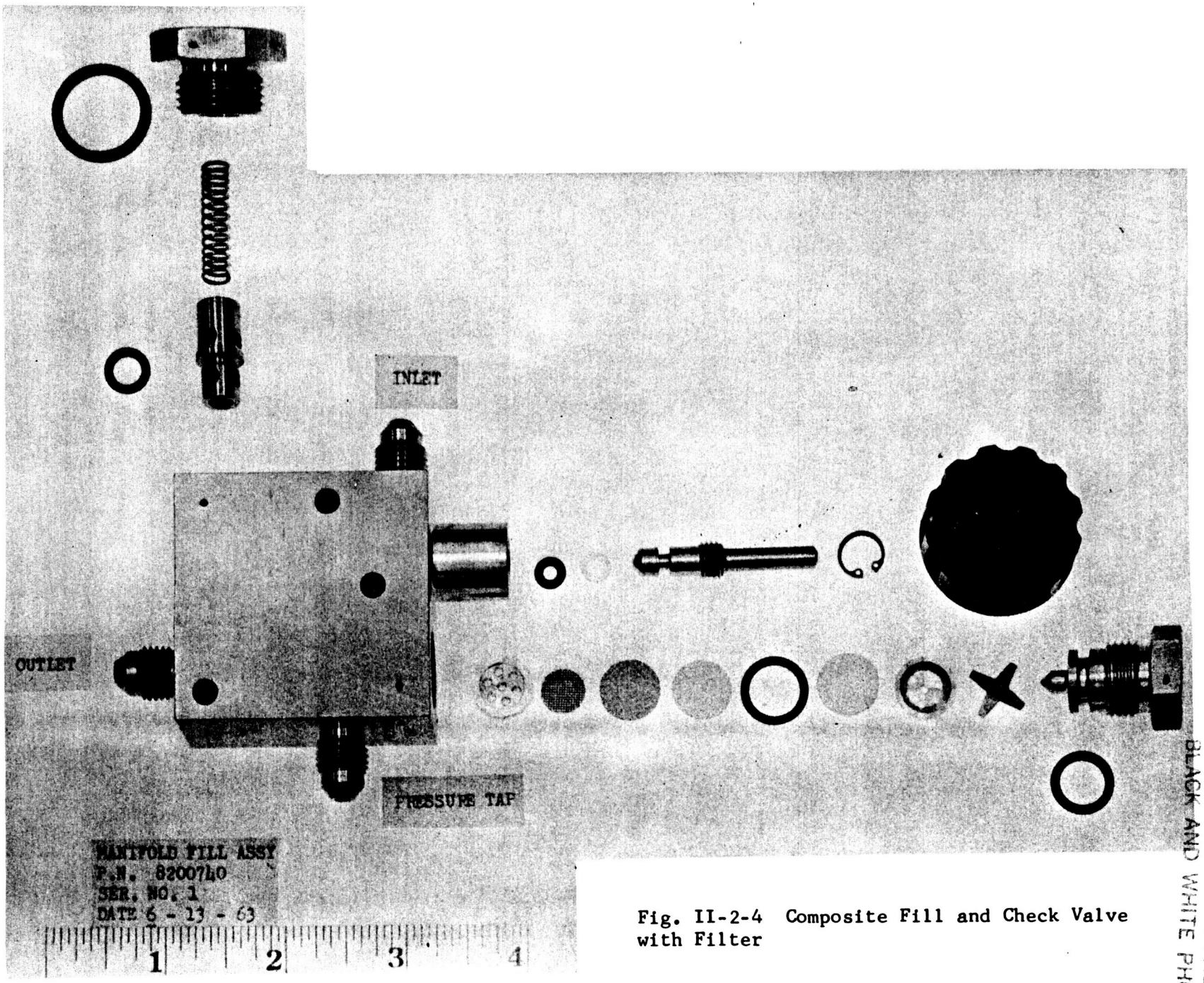

Fig. II-2-4 Composite Fill and Check Valve with Filter

ORIGINAL PAGE
BLACK AND WHITE PHOTOGRAPH

Start Valves

Solenoid start valves should be capable of continuous actuation with minimum power requirements. Squib and other methods of actuation should not introduce contaminants into the system. Leakage past the valve seat should be minimized commensurate with the size of the valve. For small valves, it is preferable to use soft seats with hard poppets. The orientation of the valve on the spacecraft should be such that acceleration forces do not tend to open the valve.

Fill Fitting

The subsystem must include a fill fitting which in a dual role can serve as a vent. In some cases, a separate vent fitting or a combination fill and vent can be used. A filter capable of removing one hundred percent of the contaminant particles (three microns or larger in size) should be placed immediately upstream of the fitting and should impose minimum flow restriction. The contaminants collected by the filter should be minimal when similar prefiltering techniques are employed on the gas issuing from ground storage.

A charging line should be readily attachable to a fill valve. This may be achieved through the use of a quick disconnect coupling or a slip on an elastomeric sealed, threaded connector. The use of tools should be avoided. A separate vent connection may be useful in the event an abort or disassembly is required. The rate of outflow should be determined by limitations of thermal changes within the vessel and vent valve. This is particularly significant when a cryogenic liquid is also stored in the vessel. A remote vent can also be operated as part of the ground fill system. This is a preferable method in that only one fill valve fitting is required. A check valve is required with this arrangement as shown in Figure II-2-1.

Relief Valve

The relief valve should protect the system from pressures exceeding the proof pressure rating. The response should be sufficiently fast so

that a minimum of fluid is lost and simultaneously protect the system from overpressures. The vented fluid from the relief valve should be jettsoned with a low velocity and in some predetermined mode with respect to the spacecraft. The relief valve should be oriented in such a manner, so that acceleration forces do not tend to open the valve.

Pressure Vessel

System requirements should be established prior to the selection of a location for the pressure vessel since the design process optimizes the relationships between such variables as configuration, volume, weight, and mounting techniques. Any subsequent changes will therefore necessitate a re-evaluation of this entire system. The pressure vessel itself should be considered as a simple geometric shape with a maximum degree of symmetry. Connections or parts should be located at extremities and their number should be a minimum. The pressure vessel should be mounted in a resilient manner so that dimensional changes due to heating or changing gas pressure do not adversely affect the vessel structure or the location and alignment of the fluid conduits and other components.

If the pressure vessel is to contain internal or nearby external parts which have reliabilities less than that of the vessel itself it should be located in a readily accessible area. However, the weight of the pressure vessel is usually significant compared to the rest of the systems. Its effect upon the center of gravity of the spacecraft must be considered.

Finally it should be remembered that the pressure vessel's reliability is directly related to its simplicity. Section VII provides an extensive discussion of pressure vessel design. Section VIII presents a discussion of pressure vessel fabrication, joining techniques, and material selection.

System Thermodynamics

The thermodynamic state of the pressurant in the storage vessel can be determined with difficulty if the initial conditions are known and the thermal characteristics of the vessel (i.e., heat leakage, insulation, etc.) are available. The conditions of the fluid in the storage tank will

depend not only on the initial thermodynamic conditions of the fluid and the thermal properties of the vessel, but also on the time involved to determine the degree of thermodynamic equilibrium of the fluid. For the same amount of work or static pressurization done the pressurant requirement will vary according with the regime governing the process. In other words the amount of pressurant required for an operation will vary depending on whether the operation is performed under adiabatic, isothermal, or diabatic conditions. The methods of analysis used in each case are discussed in Section XII.

Stored Gas

In the stored gas pressurization system the pressurant is stored at high pressure and released to flow upon demand through a pressure or flow control device. This system is shown in Figure XI-2-1.

Although the system is simple from a construction and functioning viewpoint, the estimating of pressurant required for a given mission can be a complex exercise resulting in an accuracy to within 10%.

Appreciable gas temperature changes occur for a stored gas system where the gas is not purposely heated, stemming from the expansion of the gas within a very short time period from the considerably higher pressure in the storage bottle to the pressure of the propellant tank. Usually when a major fraction of the pressurization process occurs in a short time span (up to 500 sec), the transfer of heat occurs almost entirely under transient temperature conditions. In most applications, the stored gas pressurizing process cannot be considered to be isothermal, although two special cases can be treated as approximating an isothermal expansion: (a) very low flows for long times (greater than 500 sec), and (b) single, widely spaced, very short expansions where the drop in pressure of the gas storage bottle is less than 5%. Precise solution of the heat transfer and energy equations for the majority of stored gas systems that pressurize in a transient temperature manner are best made in incremental steps using graphical or computer programs, which are the methods used in exact final design. However, it has been found to be considerably less time consuming and sufficiently accurate for preliminary design purposes to use approximate methods in estimating the gas temperature in the propellant tank.

Approximate methods for the calculation of weight and volume of stored gas are contained in Section XII and Reference 1.

Solid and Liquid Propellants

Gas generation can be achieved by combustion of gases outside or within the storage vessel. Each method imposes different boundary conditions on the analysis of the system capacity. Reference 1 should be referred to for details of analysis. As with any system or component, a system utilizing combustion products as its pressurant has special problems and areas that merit primary consideration. The following should be examined before extensive calculations are undertaken.

For missions with multiple restarts and sufficiently long coast periods, the equilibrium temperature of the ullage that will be reached during the first few coast periods will be near the original bulk propellant temperature, particularly if the firings are small. If a large fraction of combustion products have condensation temperatures above the initial bulk temperature of the propellant, another method of pressurization should be considered for these systems. The condensation of a large portion of the combustion products during coast results in (a) the requirement for an unusually large amount of combustion products for the succeeding pressure makeup, and (b) the possibility of foreign material contained within the propellant interfering with the operation of the propellant feed system or engine, unless such foreign material is filtered out. In the latter case, the nature of the condensate should also be considered. A fine powder might be flushed through the feed system with the main propellant while another constituent might form a glutinous mass that would interfere with component operation or degrade engine performance.

Excessive condensation may be discovered easily by examining the curve for effective molecular weight of the combustion products as a function of temperature for the constant density cases. A large increase in effective molecular weight as the temperature approaches the original bulk temperature of the propellant indicates that a large fraction of the combustion products is passing from the gaseous to liquid or solid phases.

The foregoing consideration is not important when the subject mission consists of a single firing since the temperature of the combustion products will remain relatively high throughout operation of the system.

Although the inlet temperature of gas generator combustion products should be as high as possible to take advantage of the large specific volume (low density), such high temperatures require heavy, durable propellant tanks and components. The designer should select the inlet temperature that best fulfills the requirements of the system as a whole. The inlet temperature may be controlled by changing the gas generator mixture ratio or propellant composition (which also varies the molecular weight of the combustion products) or by transferring some of the generated heat to other systems by means of heat exchangers.

For propellants insulated from, and stored at a temperature below the vehicle skin temperature, the limiting factor is the amount of heat that can be absorbed by the propellant. This heat can come from the combustion products, engine assemblies or other shipboard systems, and external sources (solar radiation, earth albedo). The heat input can affect propellant vapor pressure, cause decomposition, or raise the bulk temperature of the propellant to the critical value. The designer should consider the weight tradeoff between the hot gas pressurization system with additional insulation and the cold gas systems with minimal amounts of insulation.

Systems with propellants stored at the equilibrium skin temperature of the vehicle offer the best areas for application of combustion product pressurization. Since the bulk propellant temperature tends to return to the equilibrium skin temperature by radiating excess heat into space, the tank can never become overpressurized during coast periods as can those storing cryogenic liquids. At the same time, the ullage temperature will never fall below this equilibrium temperature however long the coast period.

Most systems using combustion products as the pressurizing medium can be adapted to restart conditions. The primary considerations, such as bringing the propellant tank back up to pressure at the end of coast and the possible contamination of the propellant by condensed reaction products are discussed in Reference 1.

It should be mentioned that for bipropellant gas generator systems utilizing diergolic propellants, some reliable form of ignition system will be required for restarts.

Evaporated Propellant

The Vapak pressurization concept is based on utilization of the internal energy of liquid propellant stored in a closed container to perform the work required to expel the liquid from the container. Before such a system is started, the entire bulk of the propellant is conditioned to the temperature at which its vapor pressure is equal to the desired propellant tank pressure. When a temperature other than ambient must be used, electric heaters and/or insulation may provide the required temperature, but will add to the system weight unless they can be made a part of the ground support equipment. The liquid propellant is therefore in thermal equilibrium with the saturated propellant vapors present in the ullage. As the propellant tank valve is opened, the liquid propellant flows from the bottom of the tank. The boiling, which takes place within the liquid remaining in the tank, produces vapor to fill the volume of the liquid being discharged. The heat of vaporization of the vapor being generated is obtained from the liquid; therefore, the temperature of the liquid decreases. Since the vapor pressure of a liquid is a function of temperature, there is a progressive decrease in tank pressure as the liquid propellant is expelled. The rate at which the tank pressure decreases is a function of the thermodynamic properties of the propellant and the relative volume of propellant remaining in the tank.

The concept of liquid propellant expulsion through vaporization of either the propellant itself (primary vaporization) or of a second fluid (secondary vaporization) is attractive because of its simplicity and associated high reliability. Combinations of primary and secondary vaporization systems may be attractive with certain propellant combinations.

In general, it is best to use as low an expulsion pressure as possible with Vapak systems. Higher pressures require higher temperatures. This increases the weight of the system by (1) increasing the size and weight of the propellant tanks due to lower initial propellant density, (2) increasing

the weight of residual propellant vapor left in the tank at the completion of the liquid expulsion, and (3) adding to possible heating requirements.

Sizing methods for vapor pressurization systems are outlined in Reference 1.

Evaporated Non-Propellants

A properly designed evaporated non-propellant system can, for certain applications, offer significant weight ahd volume reductions over other pressurization schemes, e.g., stored gas. For ambient temperature applications where the storage time before use may be weeks or months, the pressurant may be stored in liquid form under its own vapor pressure and then be vaporized to be used in the gaseous phase when required.

This type of storage, two phase or "subcritical", is superior to high pressure stored gas in at least two respects: (1) the specific volume of the pressurant during storage is much less, resulting in a smaller, lighter storage bottle; (2) the storage pressure is much lower (being equal to the vapor pressure of the liquid at the ambient storage temperature), which decreases the wall thickness of the pressurant storage bottle, and thus offers a second design method for decreasing its weight. In exchange for this weight saving, however, the system complexity usually is greater than the stored gas system as will be seen. There are also other disadvantages of liquid pressurant storage: (1) the system is not self starting, i.e., some method of furnishing energy to vaporize the pressurant must be available; (2) a liquid-gas orientation or positive expulsion device must be fitted to those systems operating in a zero-g environment; (3) those pressurants which may be stored conveniently in the liquid phase (i.e., at earth storable or space vehicle storable temperature with low vapor pressure) have high molecular weights relative to helium (e.g., NH_3, etc.); (4) the heat exchanger-vaporizer and associated control system must be relatively sophisticated to ensure proper operation of the system, particularly in variable flow-rate applications, compared, for example, to a high-pressure stored gas type of system which usually can be designed to operate satisfactorily with only a pressure regulator.

The second type of evaporated non-propellant system is the supercritical cryogenic storage system. In this system, the pressurant (He, N_2, etc.) is loaded as a liquid but is converted within the sealed storage vessel to a gaseous state by addition of heat and pressure before withdrawal. As is explained more fully in Reference 1, this method has the primary advantage of storing the fluid in such a manner that the density achieved is greater even than the normal liquid density. Significant decreases in system volume and weight result from this storage method. In addition, supercritical cryogenic storage places no constraints on zero-g operation as long as the fluid is maintained in the supercritical state by addition of heat during withdrawal.

Coupled with these advantageous features, however, are several problem areas. Supercritical cryogenic storage systems such as that proposed for the Lunar Excursion Module (Ref. 1) must be insulated from their surroundings. Because the storage temperature of the helium pressurant in such a system is so very low, only an extremely effective type of insulation system can be used, such as evacuated annular jackets with multiple radiation shields and vapor refrigerated shrouding or "super insulation". Even with sophisticated methods the heat sink of the bottle and its fluid pressurant is relatively small so that the heat transferred into the system will ultimately raise the pressure and require the beginning of withdrawal or venting some of the fluid overboard if it cannot be gainfully used by this time.

Another area requiring careful attention is the internal and external heat exchangers system and control of the heat so inducted into the storage vessel. If the internal heat exchanger transfers too much heat to the stored fluid during operation, over-pressurization and subsequent venting of pressurant will result. Conversely, if insufficient heat is transferred, excessive pressure decay will occur. If the deficiency in energy supply continues to the end of the duty cycle, a large outage of pressurant will result which could cause mission failure.

The external heat exchangers and their controls also require knowledgeable design. They must operate over a wide temperature range (-430° to about $0^{\circ}F$), be lightweight, and must be carefully designed to avoid excessive

Δp loss in the warm (propellant) loop. This last constraint can be especially serious if overlooked since injector performance may be quite sensitive to adverse pressure changes, particularly if the system has variable thrust capability.

The last problem area of supercritical cryogenic storage systems to be pointed out here is that of ground support equipment. Due to its low heat capacity and low temperature, liquid helium cannot be pumped over long distances without refrigeration. Portable dewars and a specially designed filling system will have to be employed for loading the storage vessel. The system must be charged just before lift-off because of the standby time constraint. The most advantageous location for the GSE would be at the same level as the storage vessel. For upper stage vehicles, this will introduce considerations of both weight and space on the arming tower.

Helium and other non-propellant pressurants are sometimes loaded and stored in the gaseous state in a container which can be submerged in the available liquid propellant at cryogenic temperatures. This type of storage may also be termed supercritical since the pressurant is maintained above its critical temperature and pressure. There is, however, an important difference between this type of supercritical storage and the one previously discussed. The pressurant in the previous system is loaded as a liquid, which becomes a gas through addition of heat and pressure from outside the system. Because the system is thermally insulated, it may be maintained for a period of time in an external environment of much higher temperature. The cryogenic gas storage systems as used on Titan and Saturn depend upon the surrounding propellant for temperature control. These systems, therefore, are actually stored gas systems maintained at low available ambient temperatures. Their chief advantages over stored-gas systems at normal temperature, of course, lies in the fact that the increased storage density of the pressurant at the cryogenic temperatures permits the use of smaller, and hence lighter, pressure spheres. The thermodynamic analysis of such systems is virtually identical with that of other stored gas systems although the non-insulated design is much simpler.

The subcritical storage of non-propellants will not be extensively treated in this Section either. In applications requiring handling zero

gravity conditions subcritical storage is not operationally as feasible at this time as single phase supercritical systems.

The basic thermodynamic analysis for these systems are outlined in Reference 1.

II-3 COMPARISON FACTORS AND SELECTION CRITERIA

A pressurant may be initially stored in the gaseous, solid or liquid phase. If stored in the gaseous state, the system is called simply a stored gas or cold gas pressurization system. Storage in the solid or liquid state can be in the form of propellants where combustion converts the materials to a gas at launch, just preceding subsystem operations or upon periodic demand. The liquids used in these systems can be mono or bi-propellants.

Liquid pressurants can also be propellants where the mode of gas generation is the production of vapor through heating rather than combustion. They are commonly called Vapak or evaporated propellant systems. Additionally, cryogenic liquids can be used as pressurants where the mode of gas generation is also the production of vapor. These systems are commonly called non-propellant vapor systems. In the following discussion only the briefest details are considered. The reader can obtain additional details on most pressurization system concepts in Reference 1 and 2.

The selection of a pressurization systems is based generally on compatibility requirements between the pressurant and the subsystem. For instance, propellant systems utilizing liquid hydrogen as fuel will tolerate only helium as a pressurant, and in view of the difficulties associated with the storage and handling of liquid helium, the choice must necessarily fall to gaseous storage systems.

When the pressurized systems will tolerate a number of pressurants, then the selection must be made on the basis of weight, volume, reliability, availability, shelf life or any other initial requirement characteristic of particular spacecraft or missions in question.

Factors such as reliability, availability, shelf life, etc., are difficult to evaluate in concrete terms since they vary from application to application and are dependent on many different variables impossible to consider in their entirety. Therefore the designer must consider individual cases and decide the merits of each system as it applies to his particular

situation. Only the most general recommendations and guidelines can be expected here on these highly individual and intangible factors.

However, other characteristics, such as weight and volume are more amenable to calculations and therefore a serious attempt at predicting these variables can be made in order to help in the selections and designs of the systems. Before any estimate of the volume and weight required by the pressurizations systems can be made, it is necessary to determine the amount of pressurant needed for a mission. For instance, if the system supplies an attitude control nozzle it is necessary first to determine the mass of gas required per actuation, the mass rate of flow and the total number of actuations. For the case of a propellant expulsion system, as for ullage pressurizations for instance, the number of actuations will be one (an actuation consisting of the operation as operations taking place from the time the system is activated until the propellant is exhausted). The amount of pressurant required will depend on the ullage, the volume of propellant displaced, the thermodynamic properties of the pressurant and propellant, and other variables considered in greater detail in Reference 1.

The amount of pressurant required per actuation cannot be easily obtained analytically. This information is usually obtained by experimentation or through complex computer programming. The duty cycle, again, may be calculated from the character of the missions or determined by experimentations.

II-4 REFERENCES

1. Anon. (Aerojet - General Corp., Von Karman Center, Azusa, Calif.) Pressurization Systems Design Guide. NAS7-169, Rept. no. 2736, Sept. 1964, Revised Dec. 1965.

2. Bauer, P. (IIT Research Institute) Investigation of Leakage and Sealing Parameters. AF04(611)-9704, AFRPL-TR-65-153, AF Systems Command, Rocket Propulsion Lab., Res. and Technol. Div., Edwards AFB, Calif., Aug. 1965.

3. Anon. (Bell Aerosystems Co., Buffalo, N.Y.) Study, Design and Test of Functionally Integrated Pneumatic Components for Rocket Propulsion Systems. AF04(611)-9077, AFRPL-TR-65-93, AF Systems Command, Rocket Propulsion Lab., Res. and Technol. Div., Edwards AFB, Calif., June 1965.

III THE SPACE ENVIRONMENT

Table of Contents

Section-Part	Title	Section-Part.Page
III-0	List of Tables	III-0.2
III-0	List of Figures	III-0.3
III-1	Introduction	III-1.1
III-2	Density, Pressure, Temperature	III-2.1
III-3	Meteoroids	III-3.1
III-4	Cosmic Radiation	III-4.1
III-5	Solar Emanations	III-5.1
III-6	Electromagnetic Radiation	III-6.1
III-7	Magnetic Fields	III-7.1
III-8	Effects of Space Environment on Materials	III-8.1
III-9	References	III-9.1

III-0 LIST OF TABLES

Section-Part-Table	Title	Section-Part.Page
III-2-1	Atmospheric Parameters *versus* Altitude	III-2.4
III-2-2	Properties of the Atmosphere (English Units)	III-2.5
III-2-3	Properties of the Atmosphere (Metric Units)	III-2.6
III-2-4	Variation of Gaseous Composition with Altitude	III-2.7
III-3-1	Meteoroid Bumper Materials for Equivalent Protection . .	III-3.3
III-8-1	Estimated Sublimation Losses of Metals in Space at 150°C	III-8.6
III-8-2	Typical Outgassing Rate for Materials	III-8.6
III-8-3	Estimated Maximum Radiation Dosages for Various Orbits	III-8.8

III-0 LIST OF FIGURES

Section-Part-Figure	Title	Section-Part.Page
III-2-1	Density of the Atmosphere *vs.* Altitude	III-2.8
III-2-2	Pressure of the Atmosphere *vs.* Altitude	III-2.9
III-2-3	Mean Free Path *vs.* Altitude	III-2.10
III-2-4	U.S. Standard Atmosphere, 1962 (1)	III-2.11
III-2-5	U.S. Standard Atmosphere, 1962 (2)	III-2.12
III-3-1	Probability of No Meteoroid Penetration in 100 Square Feet of Surface Area	III-3.4
III-3-2	Estimates of Meteoroid Flux in the Vicinity of the Earth	III-3.5
III-3-3	Distribution of Meteor Flux about the Plane of the Ecliptic at the Earth's Distance from the Sun.	III-3.6
III-4-1	Integral Number-Energy Spectrum of Primary Cosmic Rays	III-4.3
III-4-2	Vertical Flux of Particles Near the Top of the Earth's Atmosphere as a Function of Geomagnetic Latitude	III-4.4
III-5-1	Normal Daytime Ion Distribution During Sunspot Maximum	III-5.4
III-5-2	Idealized Distribution of Radiation	III-5.5
III-5-3	Distribution of Protons	III-5.6
III-6-1	Spectral Energy Curves Related to the Sun	III-6.3
III-6-2	A Typical Spectral Emissive Power Curve for the Thermal Radiation Leaving the Earth	III-6.4
III-8-1	Atmospheric Pressure *vs.* Altitude	III-8.10

III-1. INTRODUCTION

The purpose of this section is to provide a summary of the physical properties of the upper atmosphere and the space environment. Environmental parameters, such as pressure and density, the acceleration of gravity, temperature, ionization, radiation, magnetism, etc., must be considered in the design of storage systems for pressurizing gases. The discussion in this section is based upon a survey of unclassified literature and in many instances the data, particularly at high altitudes, may be altered significantly as more satellite and space-probe data are accumulated.

The most common method of deriving the atmospheric properties of pressure, density, gravity, etc. is based upon the perfect gas law and the hydrostatic equation, but results obtained for altitudes above 300 miles are questionable largely because these relationships do not take into account differences in the molecular composition of the atmosphere in the upper regions. Kallman and Juncosa[5] derived the variation of pressure with height from the variation of density with height by numerical integration of data obtained from rocket and satellite observations without assuming a scale height or temperature gradient. The Satellite Environment Handbook[7] contains a comprehensive review of the data available through 1960 regarding the physical properties of the upper atmosphere, radiation, micrometeorites, etc.

Since the atmosphere is not heated uniformly by the sun, its physical properties at a given altitude at any time can vary greatly from a particular value derived from a "model atmosphere" based on the gas law and the hydrostatic equation. It has been estimated from satellite data that the density can vary by a factor of 10 at an altitude of 435 miles within a 24-hour period.

III-2 DENSITY, PRESSURE, TEMPERATURE

The density of the atmosphere versus altitude is shown in Figure III-2-1, and Figure III-2-2 illustrates the pressure of the atmosphere versus altitude. Table III-2-1, which summarizes atmospheric parameters as a function of altitude, is derived from the models of Kallman and Juncosa[5] and those of the Satellite Environment Handbook.[7] The data in columns titled "Solar Max." and "Solar Min." are from the Satellite Environment Handbook; the columns titled "K & J Model A" are from Kallman and Juncosa. The drop in mean molecular weight at 1600 and 800 km at solar maximum and minimum, respectively, is attributed to the presence of atomic hydrogen in the atmosphere, but the particle-concentration data are tentative. The variation of gaseous compositions from the earth's atmosphere to outer space is indicated in Table III-2-4 (Jaffe and Rittenhouse[6]).

By definition, free molecular flow occurs whenever the mean free path of the molecules is larger than the linear dimension of the body under consideration. The ratio of the length of the mean free path to the linear dimension of the body is known as the Knudsen number (K) and free molecular flow is assumed for large values of K. Because of the low density and long mean free path in outer space, atmospheric drag and heat transfer to a spacecraft are to be computed from the theory of free molecular flow.

Figure III-2-3 shows the mean free path in feet versus the altitude in km, assuming that the mean molecular weight of the atmosphere is 15. At 90 km, the mean free path is about 6.5×10^{-2} ft; at 240 km, about 1000 ft. Thus above 240 km, the heating effect of drag is negligible, and solar radiation is the main influence in determining the shell temperature of a spacecraft as it moves into and out of the earth's shadow. The temperature of the spacecraft in this region depends upon the absorptivity and the emissivity of its surface and the heat capacity of the outer shell. If the absorptivity is high, the temperature may vary by 100°C or more per revolution; for example, the shell temperature of Explorer I ranged from −25°C to 75°C, although most observations indicated a temperature of 0 ± 25°C at a perigee distance of 270 km, and an apogee distance of 1800-2250 km.

Recently, three new model atmospheres have been established, by ARDC, COSPAR, AND COESA respectively. The COSPAR atmosphere is published in [14], and the (COESA) U.S. Standard Atmosphere 1962, Figure III-2-4 and Figure III-2-5, is discussed in [15]. In the latter reference, seasonal and latitudinal variations are explained, and basic temperature profiles are given.

A few derived densities are plotted by Sissenwine *et al.*[15], for altitudes 80-700 km. They seem to be higher than those of the curves in Figure III-2-1 by a factor of 10. The ranges indicated in Figure III-2-1 at 400 km are the data quoted in Kallman-Bijl, *et al*,[14] and also lie mostly above the curves. Densities at great altitudes are inferred from satellite observations. It is known that there is a strong correlation between density and 10-cm (or 20-cm) solar electromagnetic radiation; semi-annual and diurnal variations are well-documented. It is now customary to normalize density measurements against these effects; for example, it is assumed that density is proportional to the energy of 10-cm solar radiation, and the normalized value of the latter is taken to be 220×10^{-22} watts m^{-2} $cycle^{-1}$ sec^{-1} by H. K. Paetzold [14, p. 81].

Experimental Methods

The temperature of a satellite in space is not determined by the kinetic temperature of the environment, but by the radiative heat gains and losses. (See p. III-6.2.)

Atmospheric parameters are based on the following measurements.

(a) The drag of the atmosphere on a satellite has been measured at great altitudes. The drag is not uniform in time (even at a fixed altitude), and its nature is uncertain; some workers claim that at very great altitudes a metallic satellite becomes electrically charged and attracts a cloud of ions around itself. This cloud increases the effective area the satellite presents to the braking effect of the atmosphere through which it passes.

There is fairly uniform agreement among physicists as to the drag mechanism and the importance of the ion-cloud effect. It is fair to note that this agreement amounts to a (probably correct) physical assumption, which has not been confirmed experimentally. Existence of charged particles (ions) at great altitudes has been confirmed in satellite experiments, which have also measured the proportion of some molecular species.

(b) At very low altitudes (less than 30 miles), sensors in balloons have established molecular composition, pressure, density, and temperature by direct measurement.

(c) At intermediate altitudes (20-200 miles), rocket-borne equipment has taken soundings of pressure, and sampled the environment in bottles. In general, it has been rather difficult to correlate these soundings with the perturbations of satellite orbits at the same altitude. A satellite must fly above about 62 mi. to remain in orbit for any length of time.

(d) Direct measurement of temperature at altitudes above 30-50 miles with a temperature sensor is difficult because of the long response time and weight of most sensors.

Finally, it should be remarked that values of density derived from drag measurements are most useful for estimating expected drag, and probably somewhat less useful for estimating totally unrelated phenomena, such as rate of diffusion. The reason for this is that a certain amount of analysis involving physical assumptions necessarily intervenes in any data reduction process. (In using observed drag to compute density, the assumption is made that density in the neighborhood of perigee is orders of magnitude greater than density at apogee. Moreover, the density gradient is assumed to be exponential. On the other hand, rate of diffusion is governed by number of particles, *i.e.* by degree of dissociation of the molecules, which is difficult to estimate from drag observations.)

Besides pressure, density, molecular weight, acceleration of gravity, and temperature, certain other properties of the space environment must be considered in designing pressurized gas systems.

Table III-2-1
ATMOSPHERIC PARAMETERS VERSUS ALTITUDE

Height Km	Density-gm., cm.$^{-3}$ Solar Max.	Density-gm., cm.$^{-3}$ Solar Min.	Density-gm., cm.$^{-3}$ K. & J. Model A	Pressure-dyne, cm.$^{-2}$ Solar Max.	Pressure-dyne, cm.$^{-2}$ Solar Min.	Pressure-dyne, cm.$^{-2}$ K. & J. Model A	Molecular Wgt. Solar Max.	Molecular Wgt. Solar Min.	Log_{10} Particles per cm.^{3} Solar Max.	Log_{10} Particles per cm.^{3} Solar Min.	Accel. of Gravity g.cm.,sec.$^{-2}$ K. & J. Model A	Temperature °K Solar Max.	Temperature °K Solar Min.
100	2.82×10^{-10}	2.82×10^{-10}	6.93×10^{-10}	1.74×10^{-1}	1.74×10^{-1}	5.34×10^{-1}	27.8	27.8	12.78	12.78	950.5	208	208
120	2.88×10^{-11}	1.95×10^{-11}	6.34×10^{-11}	3.39×10^{-2}	2.09×10^{-2}	7.67×10^{-2}	26.1	26.1	11.80	11.65	944.7	390	340
140	4.68×10^{-12}	2.88×10^{-12}	1.24×10^{-11}	1.05×10^{-2}	4.57×10^{-3}	1.98×10^{-2}	24.5	24.3	11.06	10.82	938.9	662	500
160	1.51×10^{-12}	7.76×10^{-13}	3.24×10^{-12}	5.13×10^{-3}	1.86×10^{-3}	7.38×10^{-3}	23.7	22.9	10.60	10.33	933.1	926	628
180	7.76×10^{-13}	3.02×10^{-13}	1.21×10^{-12}	3.09×10^{-3}	9.12×10^{-4}	3.64×10^{-3}	22.8	21.5	10.30	9.98	927.4	1115	732
200	4.17×10^{-13}	1.48×10^{-13}	5.91×10^{-13}	1.85×10^{-3}	5.01×10^{-4}	2.06×10^{-3}	22.0	20.5	10.06	9.65	921.8	1230	807
220	2.69×10^{-13}	7.76×10^{-14}	3.22×10^{-13}	1.20×10^{-3}	2.82×10^{-4}	1.25×10^{-3}	21.2	19.5	9.82	9.37	916.2	1305	865
240	1.70×10^{-13}	4.27×10^{-14}	1.89×10^{-13}	8.51×10^{-4}	1.78×10^{-4}	7.98×10^{-4}	20.6	18.9	9.66	9.15	910.6	1356	906
260	1.12×10^{-13}	2.63×10^{-14}	1.16×10^{-13}	6.46×10^{-4}	1.15×10^{-4}	5.27×10^{-4}	20.0	18.3	9.52	8.95	905.1	1400	937
280	7.94×10^{-14}	1.62×10^{-14}	7.38×10^{-14}	4.68×10^{-4}	7.59×10^{-5}	3.59×10^{-4}	19.5	17.9	9.37	8.76	899.7	1430	959
300	5.75×10^{-14}	1.05×10^{-14}	4.84×10^{-14}	3.63×10^{-4}	5.13×10^{-5}	2.51×10^{-4}	19.1	17.5	9.26	8.58	894.3	1455	973
320	4.27×10^{-14}	6.92×10^{-15}	3.27×10^{-14}	2.69×10^{-4}	3.47×10^{-5}	1.80×10^{-4}	18.7	17.2	9.12	8.41	888.9	1472	984
340	3.09×10^{-14}	4.79×10^{-15}	2.26×10^{-14}	2.04×10^{-4}	2.35×10^{-5}	1.32×10^{-4}	18.4	16.9	9.00	8.23	883.6	1485	991
360	2.29×10^{-14}	3.31×10^{-15}	1.61×10^{-14}	1.55×10^{-4}	1.66×10^{-5}	9.82×10^{-5}	18.0	16.7	8.88	8.08	878.4	1491	996
380	1.78×10^{-14}	2.24×10^{-15}	1.17×10^{-14}	1.23×10^{-4}	1.15×10^{-5}	7.40×10^{-5}	17.8	16.5	8.77	7.92	873.2	1496	998
400	1.38×10^{-14}	1.58×10^{-15}	8.74×10^{-15}	9.77×10^{-5}	8.32×10^{-6}	5.63×10^{-5}	17.5	16.3	8.67	7.78	868.0	1500	1000
450	7.25×10^{-15}	6.76×10^{-16}	4.35×10^{-15}	5.25×10^{-5}	3.63×10^{-6}	2.94×10^{-5}	17.0	16.0	8.40	7.42	855.3	1500	1000
500	4.07×10^{-15}	3.09×10^{-16}	2.28×10^{-15}	2.88×10^{-5}	1.66×10^{-6}	1.58×10^{-5}	16.6	15.9	8.16	7.08	842.9	1500	1000
600	1.32×10^{-15}	6.31×10^{-17}	6.68×10^{-16}	9.99×10^{-5}	3.39×10^{-7}	4.97×10^{-6}	16.3	15.6	7.68	6.39	818.8	1500	1000
700	4.57×10^{-16}	1.29×10^{-17}	2.04×10^{-16}	3.55×10^{-6}	7.94×10^{-8}	1.79×10^{-6}	16.1	14.7	7.23	5.76	795.8	1500	1000
800	1.66×10^{-16}	2.88×10^{-18}	6.63×10^{-17}	1.32×10^{-6}	2.40×10^{-8}	8.63×10^{-7}	16.0	10.2	6.80	5.24	773.7	1500	1000
900	6.03×10^{-17}	7.25×10^{-19}		4.90×10^{-7}	1.26×10^{-8}		15.8	5.1	6.37	4.96		1500	1000
1000	2.40×10^{-17}	2.69×10^{-19}		1.91×10^{-7}	9.77×10^{-9}		15.7	2.3	5.96	4.85		1500	1000
1200	3.80×10^{-18}	1.07×10^{-19}		3.16×10^{-8}	7.24×10^{-9}		15.2	1.3	5.18	4.72		1500	1000
1400	6.61×10^{-19}	7.59×10^{-20}		6.76×10^{-9}	6.17×10^{-9}		13.0	1.0	4.51	4.65		1500	1000
1600	1.35×10^{-19}	6.31×10^{-20}		2.09×10^{-9}	5.13×10^{-9}		8.3	1.0	4.00	4.57		1500	1000
1800	3.55×10^{-20}	5.62×10^{-20}		1.15×10^{-9}	4.27×10^{-9}		3.5	1.0	3.76	4.49		1500	1000
2000	1.45×10^{-20}	4.79×10^{-12}		9.55×10^{-10}	3.80×10^{-9}		1.8	1.0	3.66	4.44		1500	1000
2500	6.03×10^{-21}	3.39×10^{-20}		7.24×10^{-10}	2.82×10^{-9}		1.0	1.0	3.54	4.31		1500	1000

Table III-2-2

PROPERTIES OF THE ATMOSPHERE (ENGLISH UNITS)
(Ref. 16)

ALTITUDE		TEMPERATURE °R	PRESSURE lb/ft^2	SPEED OF SOUND, ft/sec
Ft x 10^3	Miles			
0	0	518.69	2.1162×10^3	1116.4
5	0.95	500.86	1.7609×10^3	1097.1
25	4.73	429.64	7.8633×10^2	1016.1
50	9.47	390.00	2.4361×10^2	968.08
100	18.94	418.79	2.3085×10	1003.2
150	28.41	500.11	3.0597×10	1096.3
200	37.88	449.00	4.715×10^{-1}	1038.7
250	47.30	328.20	4.364×10^{-2}	888.1
300	56.82	299.2	2.118×10^{-3}	846.5
400	75.76	923.9	3.762×10^{-5}	
500	94.70	1933.	1.036×10^{-5}	
600	113.64	2478.	4.908×10^{-6}	
700	132.58	2545.	2.592×10^{-6}	
800	151.52	2547.	1.438×10^{-6}	
900	170.45	2551.	8.294×10^{-7}	
1000	189	2564.	4.949×10^{-7}	
1200	227	2619	1.923×10^{-7}	
1400	267	2706	8.246×10^{-8}	
1500	284	2758	5.571×10^{-8}	
1700	322	2873	2.684×10^{-8}	
1900	341	2999	1.376×10^{-9}	
2100	397	3130	7.442×10^{-9}	
2300	435	3265	4.215×10^{-9}	

Table III-2-3

PROPERTIES OF THE ATMOSPHERE (METRIC UNITS)
(Ref. 16)

ALTITUDE, Km	TEMP., °K	PRESSURE, mm Hg	SOUND SPEED, $m\text{-}sec^{-1}$
0	288.16	7.6000×10^{2}	340.29
1	281.66	6.7413×10^{2}	336.43
5	255.69	4.0539×10^{2}	320.54
10	223.26	1.9876×10^{2}	299.53
20	216.66	4.1473×10	295.07
50	282.66	6.5899×10^{-1}	337.03
70	209.59	4.5160×10^{-2}	290.22
90	165.7	1.015×10^{-3}	258.00
100	199.0	1.604×10^{-4}	
110	286.7	3.680×10^{-5}	
120	477.0	1.533×10^{-5}	
130	664.9	8.632×10^{-6}	
140	849.9	5.627×10^{-6}	
150	1031.	4.001×10^{-6}	
175	1359	2.102×10^{-6}	
200	1404.	1.222×10^{-6}	
250	1415.	4.608×10^{-7}	
300	1423.	1.924×10^{-7}	
350	1445.	8.729×10^{-8}	
400	1480.	4.246×10^{-8}	
450	1525.	2.191×10^{-8}	
500	1576.	1.190×10^{-8}	
550	1632.	6.751×10^{-9}	
600	1691.	3.981×10^{-9}	
650	1751.	2.429×10^{-9}	
700	1812	1.528×10^{-9}	

Table III-2-4

VARIATION OF GASEOUS COMPOSITION WITH ALTITUDE
(Ref. 6)

ALTITUDE	GASEOUS COMPOSITION
Sea level	78% N_2, 21% O_2, 0.94% A
30 km	N_2, O_2, A
200 km	N_2, O, O_2, O^+
800 km	O, O^+, H
6500 km	H^+, H
Above 22,000 km	85% H^+, 15% He^{++}

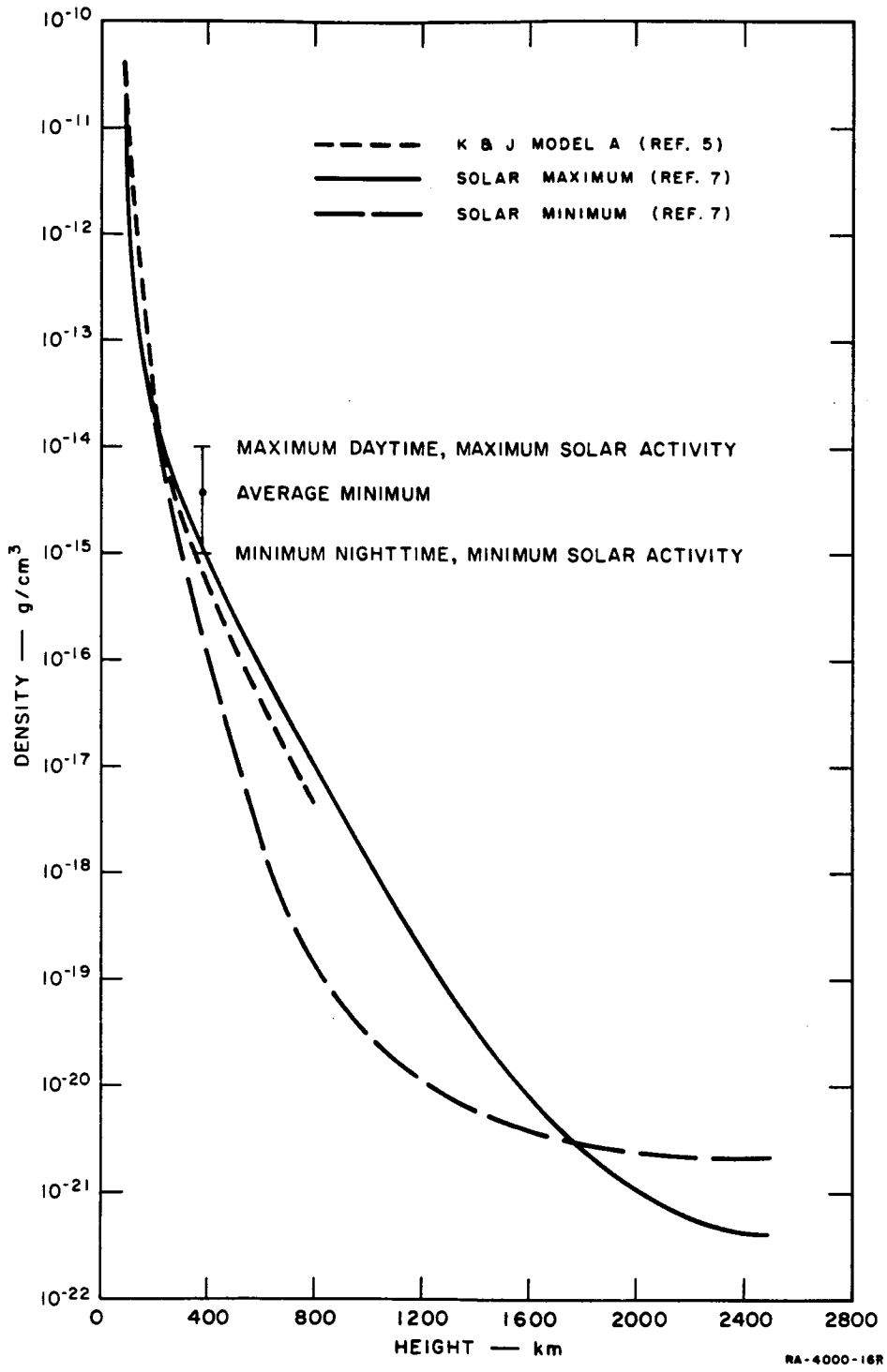

Fig. III-2-1 DENSITY OF THE ATMOSPHERE vs. ALTITUDE

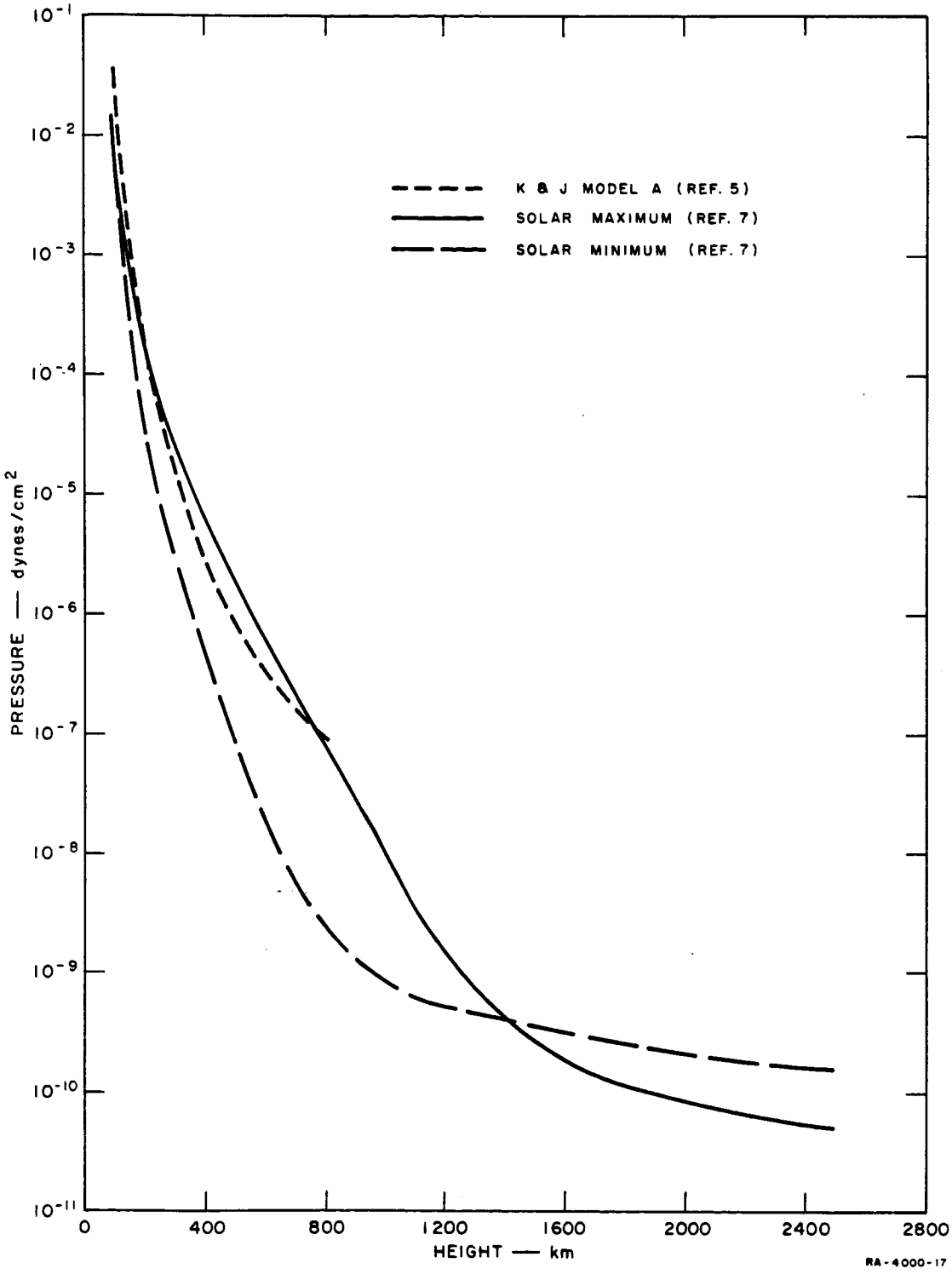

Fig. III-2-2 PRESSURE OF THE ATMOSPHERE vs. ALTITUDE

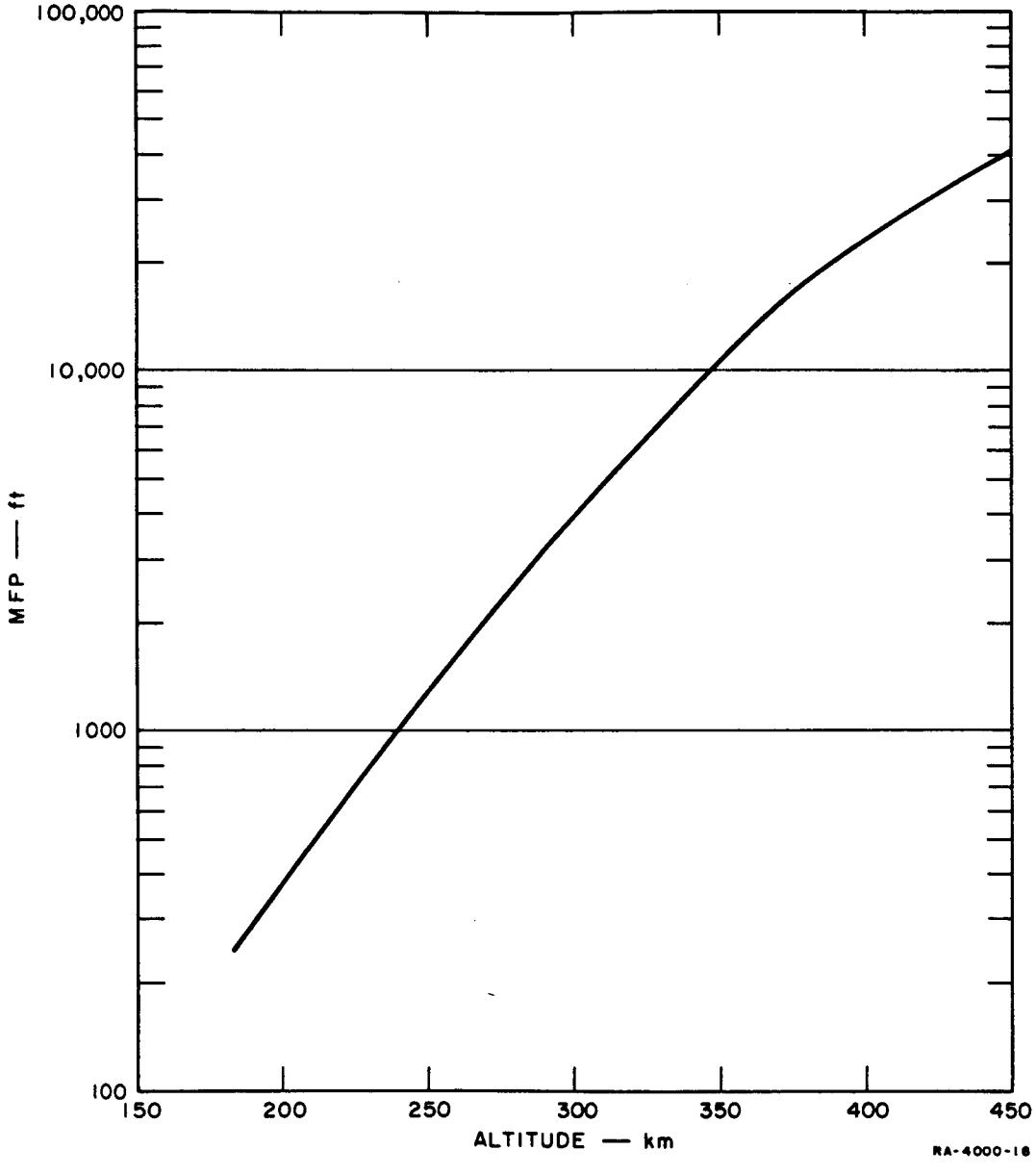

Fig. III-2-3 MEAN FREE PATH vs. ALTITUDE

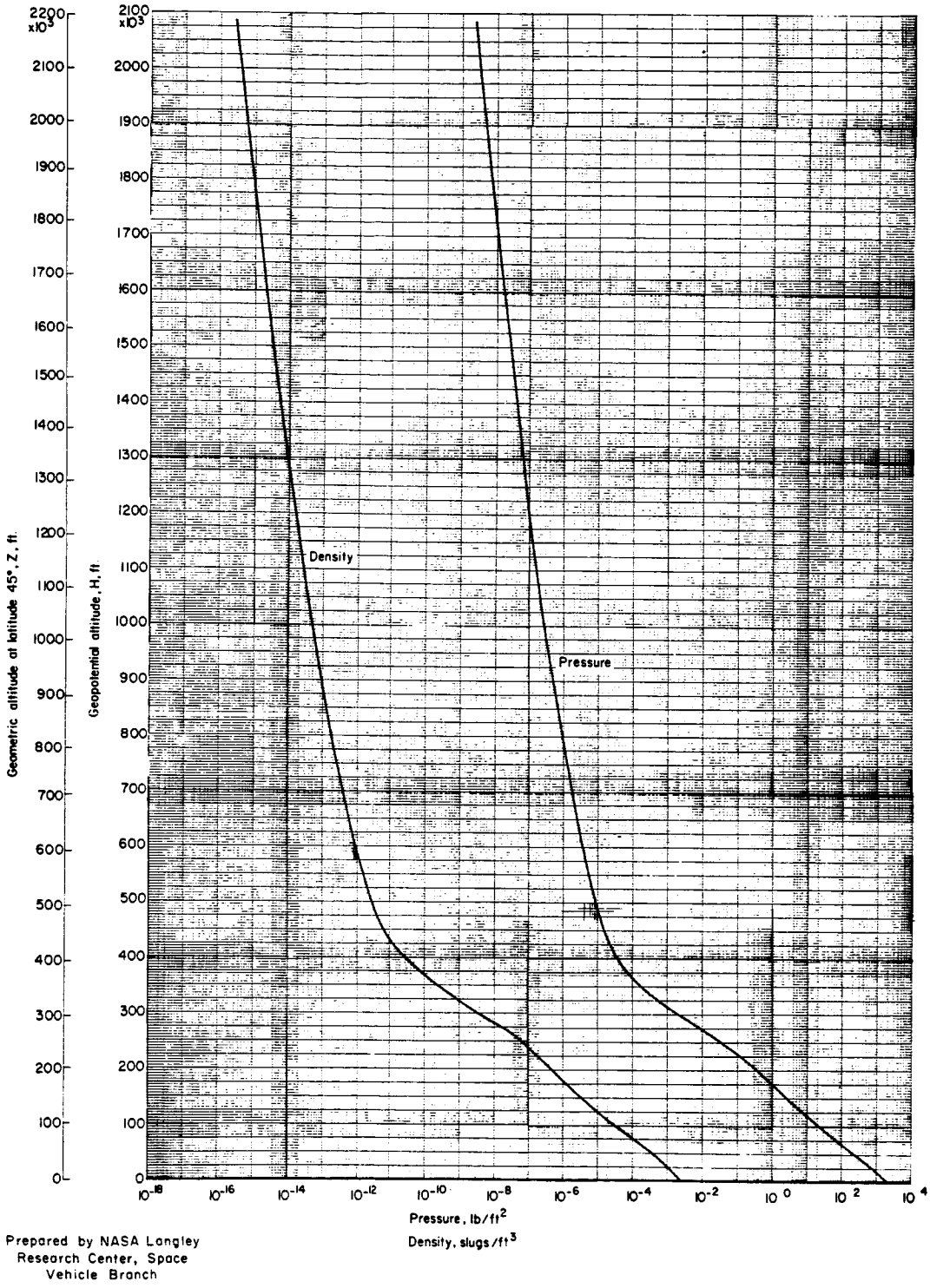

Fig. III-2-4 U.S. STANDARD ATMOSPHERE, 1962 (1)

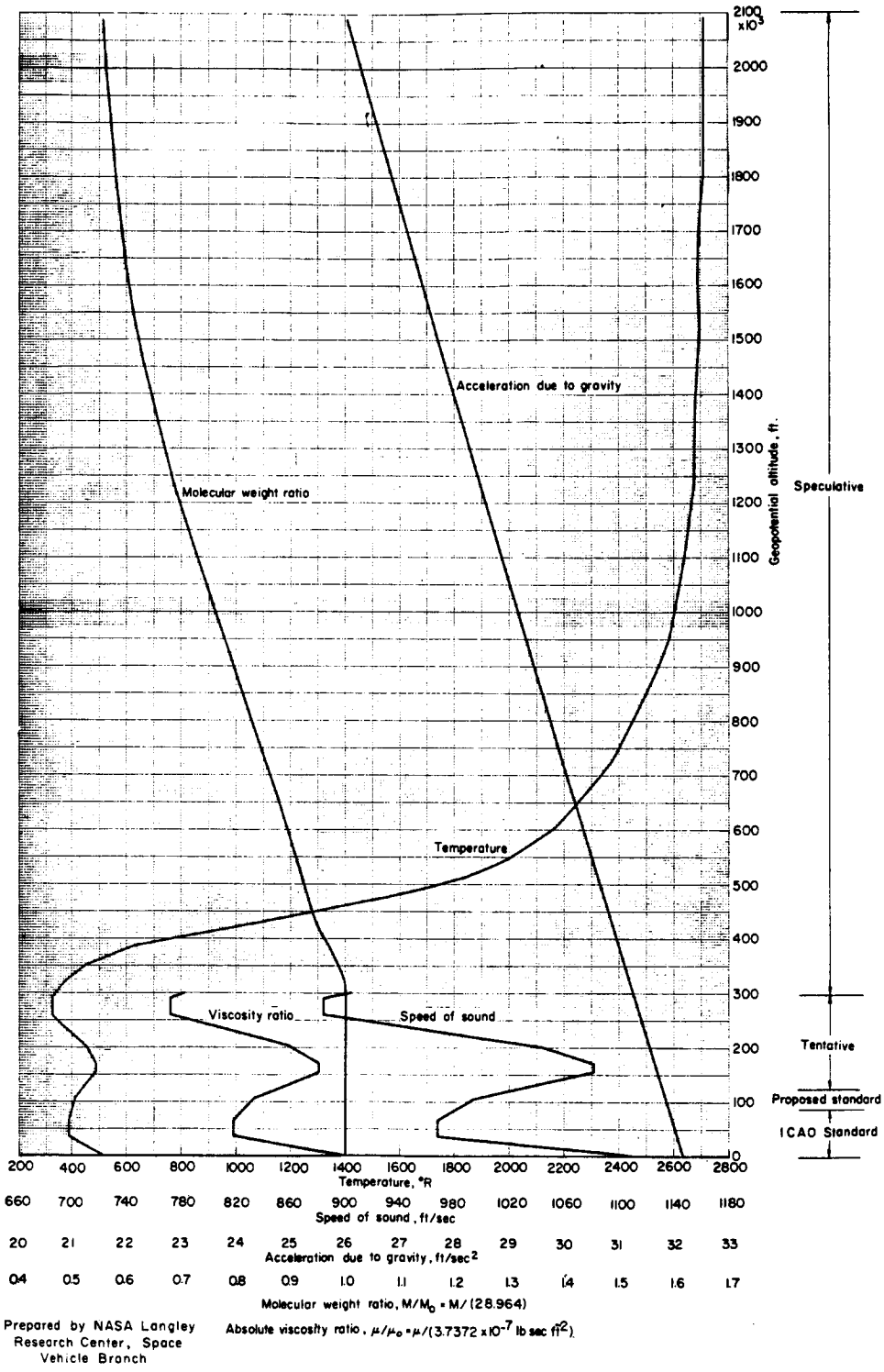

Fig. III-2-5 .S. STANDARD ATMOSPHERE, 1962 (2)

III-3 METEOROIDS

Meteoroids are solid particles in the solar system which range in size from 0.1 micron to several feet in diameter, and in weight from 10^{-15} grams to many tons with the small meteoroids being more prevalent than the larger ones. It is believed that the total meteoric accretion by earth is 1000 metric tons per day. The velocity of meteoroids is 28×10^3 m/sec (Whipple); for magnitudes 7 to 20, the average velocity decreases linearly from 28×10^3 to 15×10^3 m/sec. Meteoritic particles smaller than magnitude 30 are presumed to be swept out of the solar system by radiation pressure. The mass of individual meteoroids decreases by a factor of $10^{-0.4}$ for each apparent visual magnitude step and the number increases at the rate of $10^{+0.4}$ for each magnitude step. Thus, the mass of a meteoroid of magnitude $M + 1$ is 1/2.512 times the mass of magnitude M and the number of magnitude $M + 1$ is 2.512 times the number of magnitude M.* Although considerable information regarding meteoroids near or within the earth's atmosphere has been gathered, little information is currently available regarding size-density distributions in outer space. It is believed, however, that meteoroids are not randomly distributed in space (results of Mariner-II Venus flight) but that they are concentrated in orbits around the sun that intersect the earth's orbit.

The observed velocities of meteoroids on collision with the earth's atmosphere range from 10 to 80 km/sec. Space vehicles are also subjected to meteoroid bombardment; from 4 to 11×10^{-4} impacts/sec/cm^2 to less than 10^{-8} impacts/sec/cm^2 have been registered by meteoroid sensors on satellites. A meteoroid with a diameter as large or larger than the thickness of a space vehicle's shell, or with a mass equal to or greater than the mass of the shell, will penetrate with a clean hole, and the greater part of the initial momentum will be retained by the meteoroid as it passes through the shell. Meteoroids with diameters of from 10 to 20 percent of the shell thickness will just penetrate, or nearly penetrate; a crater will be formed on the impact site and the opposite side of the shell will show spalling.

* A zero magnitude meteoroid is approximately 25 grams (Whipple).

The impact of micrometeoroids on the shell of a space craft will cause surface craters of microscopic size which gradually erode the surface. It is estimated that about one percent of the total surface area of a satellite reasonably close to the earth will be cratered at the end of one year,[12,13] thus gradually affecting the vehicle's equilibrium temperature by changing the absorptivity (or emissivity) of the outer surface.

Calculation of the frequency of penetration of a space vehicle by meteoroids is, at best, uncertain. Wiederhorn,[13] on the basis of Bjork's penetration theory, Whipple's frequency estimates, and an average meteoroid velocity of 70,000 ft/sec, constructed the graph shown in Figure III-3-1 which indicates the probability of no penetrations per 100 square feet of surface area versus time and wall thickness. The graph shows that for a propellant storage tank of reasonable volume, mounted outside a space vehicle, the required wall thickness for a high probability of no penetration over a relatively long time period would be too great to be practical. Hence, various systems of "meteor bumpers" are being considered as an approach to a light-weight protection system.

When a "bumper" or a double skin is used to afford protection from meteoroid penetration, incident particles are shattered as they penetrate the outer skin and then stopped completely by the inner skin. Tests have shown that a bumper skin at least ¾-in. away from the inner skin is effective; either skin may be the load-carrying structure of the spacecraft. The two skins may be proportioned:

$$T_1 = \frac{T_0}{12} \qquad T_2 = \frac{T_0}{4}$$

where T_1 and T_2 are the thicknesses of the outer and inner skins, respectively, and T_0 is the total thickness required to give the desired degree of protection (Figure III-3-1). Although aluminum is generally considered adequate for protective skins, other materials may be substituted; data given in Table III-3-1 indicates thickness and weight trade-offs which result from use of materials other than aluminum.

Table III-3-1

METEOROID BUMPER MATERIALS FOR EQUIVALENT PROTECTION

MATERIAL	DENSITY	RELATIVE THICKNESS	RELATIVE WEIGHT
Aluminum	0.098	1.00	1.00
Magnesium	0.065	1.32	0.88
Beryllium	0.066	0.72	0.48
Filament wound plastic	0.077	1.61	1.24
Fused silica	0.079	1.05	0.85
6Al-4V titanium	0.160	0.72	1.18
17-7PH steel	0.276	0.49	1.38

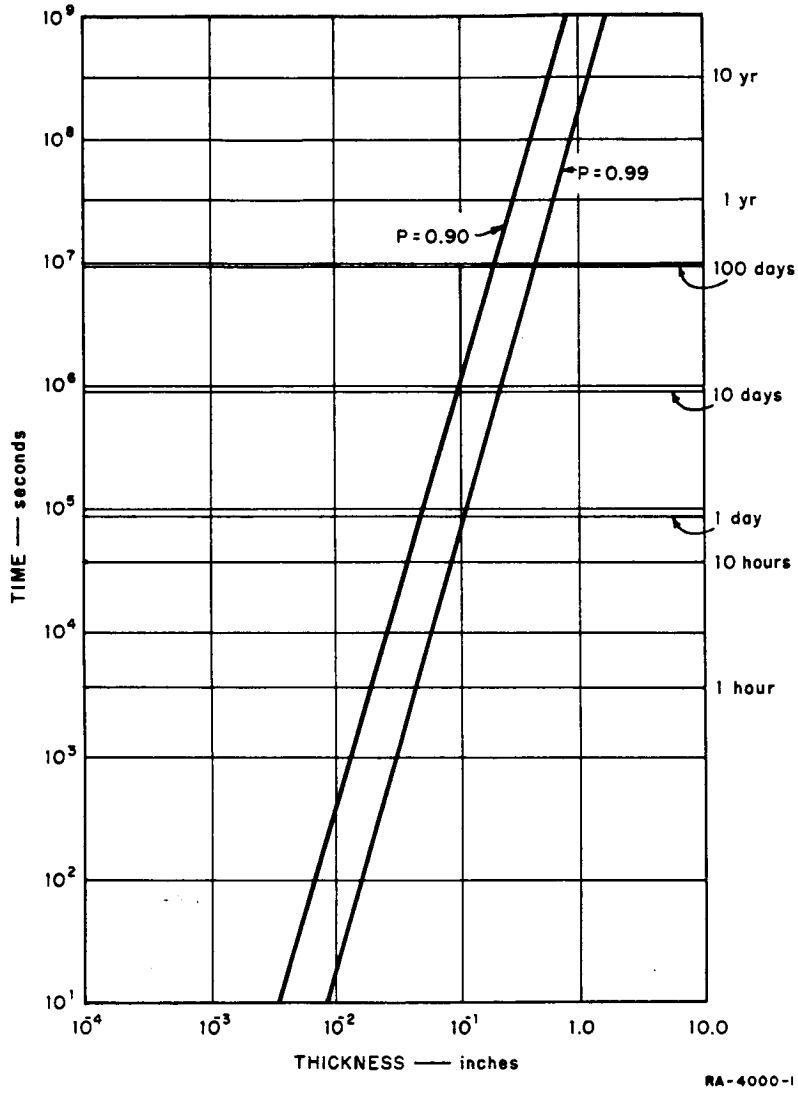

Fig. III-3-1 PROBABILITY OF NO METEOROID PENETRATION IN 100 SQUARE FEET OF SURFACE AREA

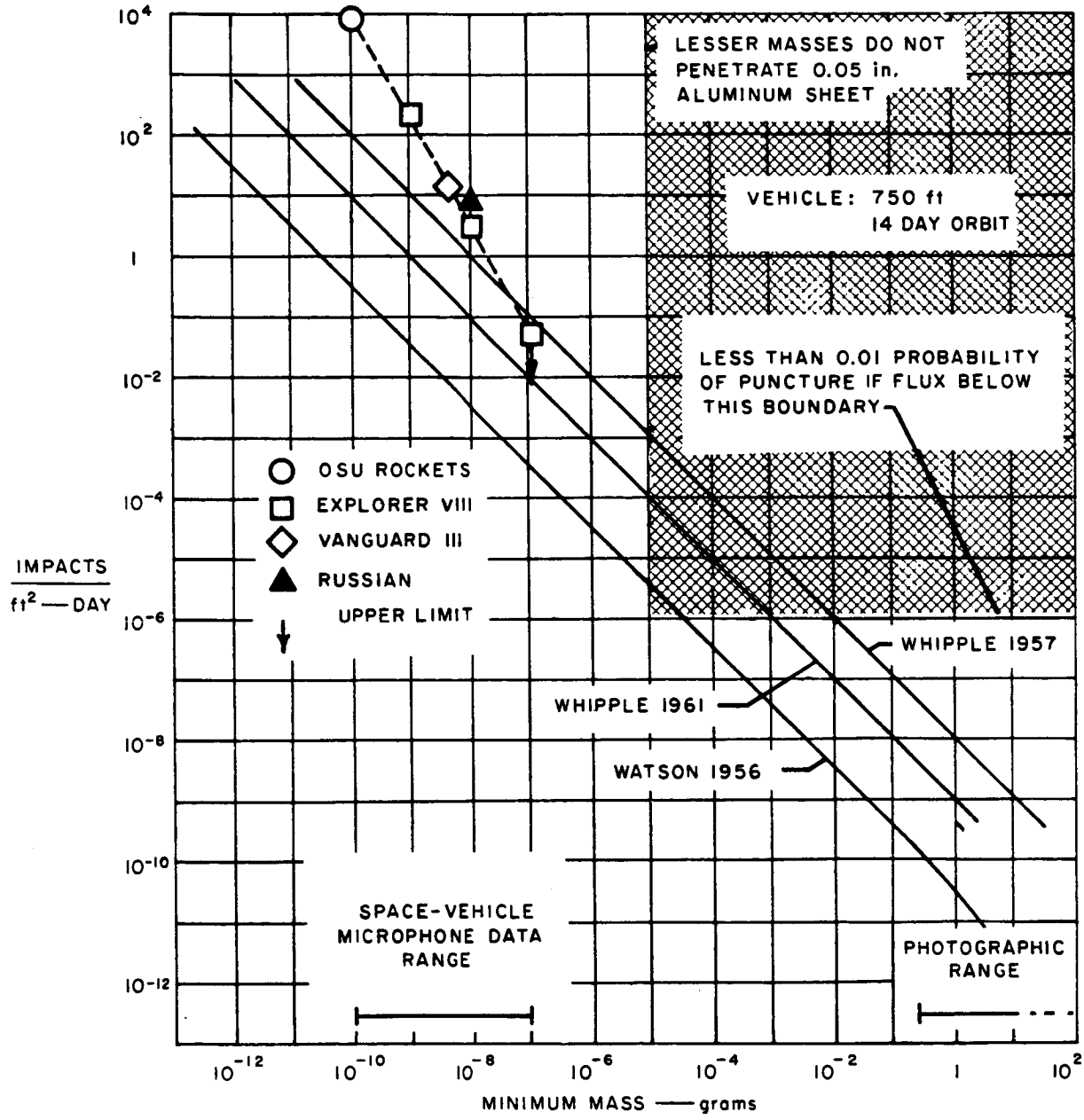

Fig. III-3-2 ESTIMATES OF METEOROID FLUX IN THE VICINITY OF THE EARTH (Ref. 21)

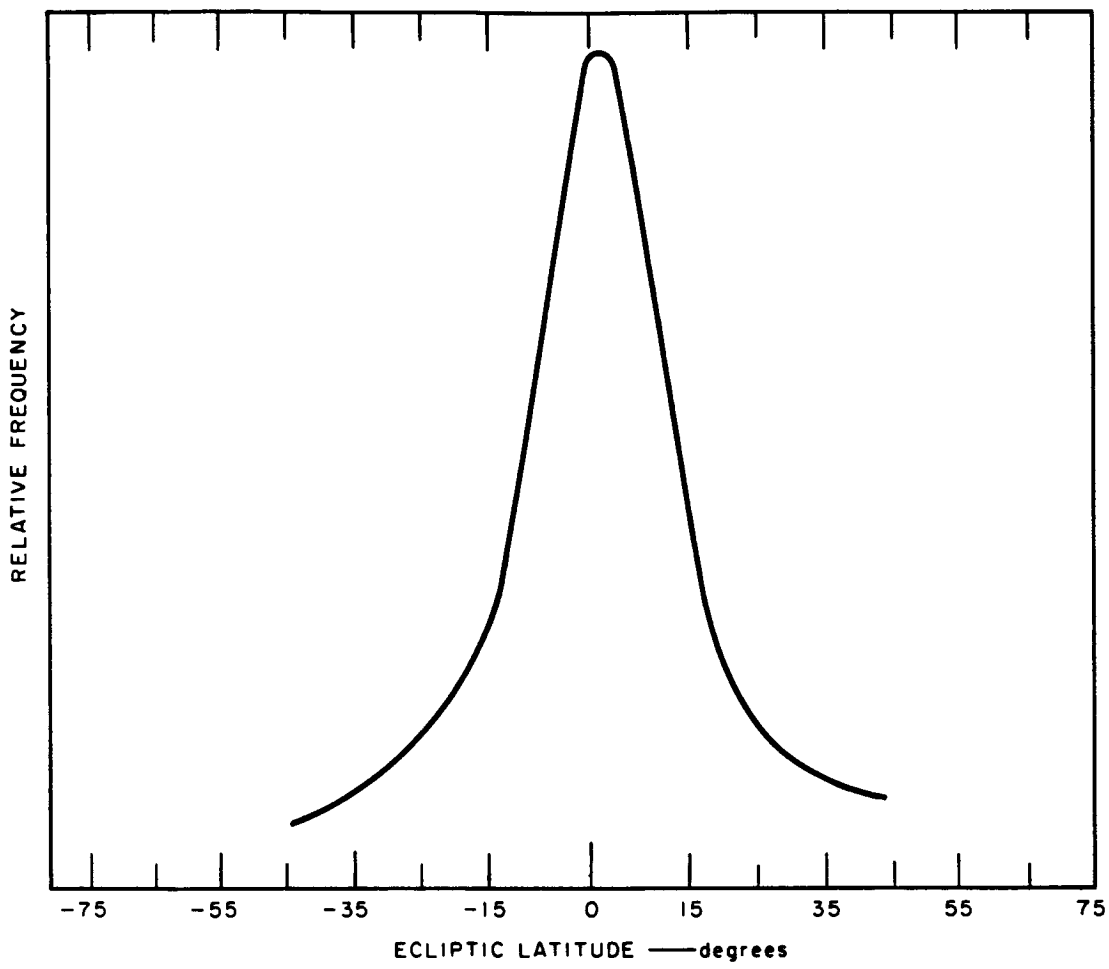

Fig. III-3-3 DISTRIBUTION OF THE METEOR FLUX ABOUT THE PLANE OF THE ECLIPTIC AT THE EARTH'S DISTANCE FROM THE SUN (Ref. 21)

III-4 COSMIC RADIATION

Cosmic radiation is the flux of highly energetic particles existing outside the earth's atmosphere and assumed to permeate interplanetary and intergalactic space. The nature of the cosmic radiation immediately outside the earth's atmosphere depends appreciably upon the geographical location and direction of observation relative to a vertical on the earth's surface. The geographical and directional dependence of the cosmic radiation has been shown to be governed by the interaction of the earth's magnetic field and the charged particles of the cosmic radiation. The primary cosmic radiation is extraterrestrial in origin.

Upon arrival of the primary radiation in the vicinity of the earth, but well outside of its atmosphere, the primary particles follow curved paths in the terrestrial magnetic field without interacting in any way with their surroundings. Primary particles which fall closer to the earth follow practically rectilinear paths and generally interact with the atoms or ions of the outer fringes of the earth's atmosphere to produce less energetic secondary cosmic radiation. Thus, the outer atmosphere of the earth contains a mixture of primary and secondary radiation of a composition governed chiefly by ambient pressure.

Secondary cosmic radiation is composed of diverse elementary particles and some nuclei which are heavier than protons. The most common elementary particles found in secondary cosmic radiation are: electrons, positrons, photons, mu-mesons, pi-mesons, protons, neutrons, and neutrinos.

Showers of cosmic radiations are readily observed on the earth's surface whenever surges of primary cosmic radiations interact with the upper atmosphere at altitudes between 9 and 22 mi, and the resulting highly energetic secondary cosmic rays react further to yield extraordinary amounts of additional secondary radiation.

Galactic cosmic radiation consists primarily of protons and alpha particles with smaller quantities of heavier elements; the composition of galactic cosmic radiation reflects heavily the distribution of atoms in the universe as indicated in the following table:

APPROXIMATE COMPOSITION OF THE UNIVERSE
AND OF COSMIC RADIATION

ELEMENT	% OF ATOMS IN UNIVERSE	% OF ATOMS IN COSMIC RAYS
H	90	90
He	9.0	9.0
C, N, O	0.9	0.5
Other	0.1	0.1

The energy spectrum of cosmic rays is indicated in Figure III-4-1; it can be seen that the free-space flux of cosmic ray particles is quite small and of concern only for very long missions in space. Shielding for particles of these very high energies is impractical and there is likelihood that secondary x-rays and particles produced by shielding may actually increase damage.

The vertical flux of cosmic particles is a function of the geomagnetic latitude (see Figure III-4-2).

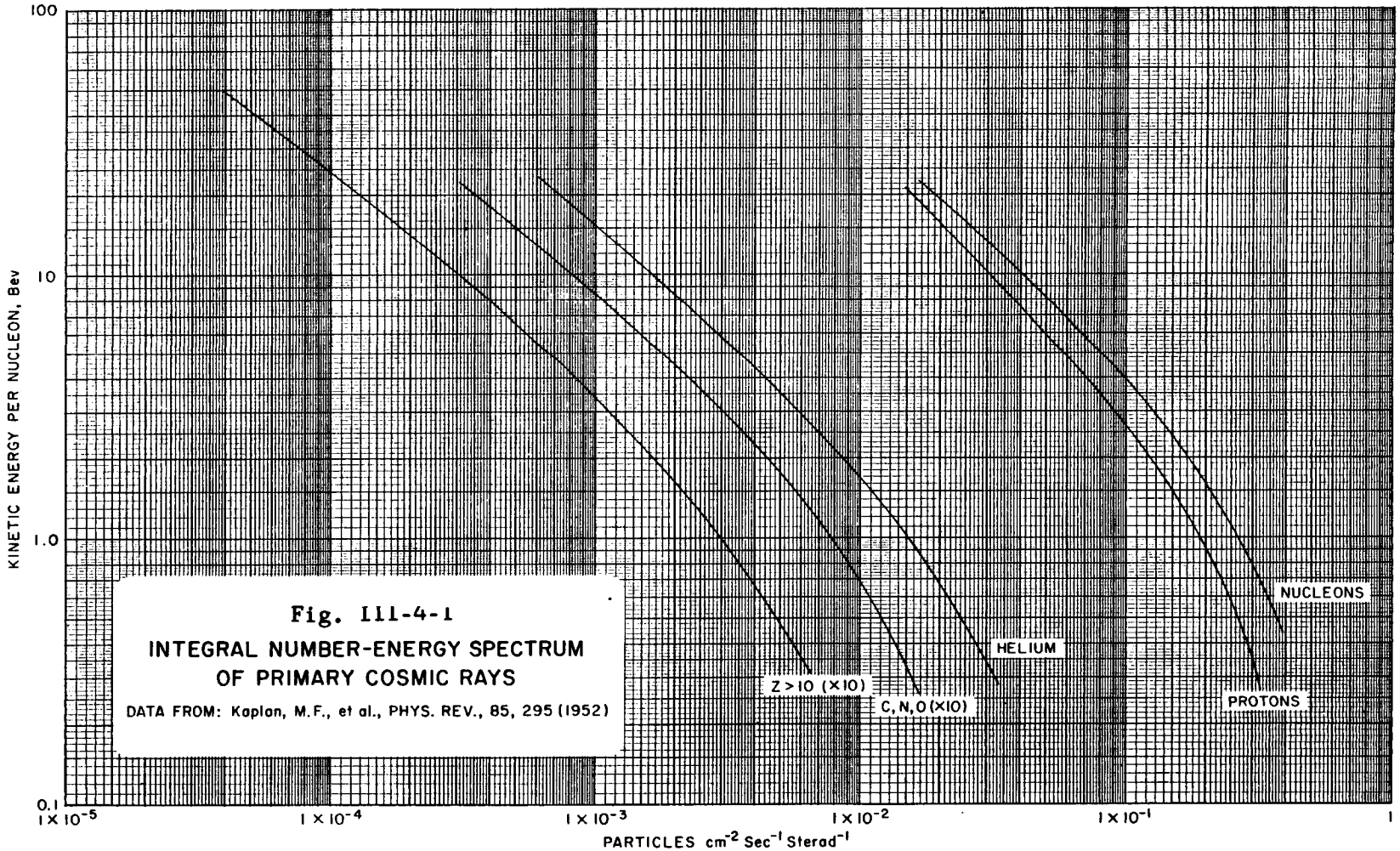

Fig. III-4-1

INTEGRAL NUMBER-ENERGY SPECTRUM OF PRIMARY COSMIC RAYS

DATA FROM: Kaplan, M.F., et al., PHYS. REV., 85, 295 (1952)

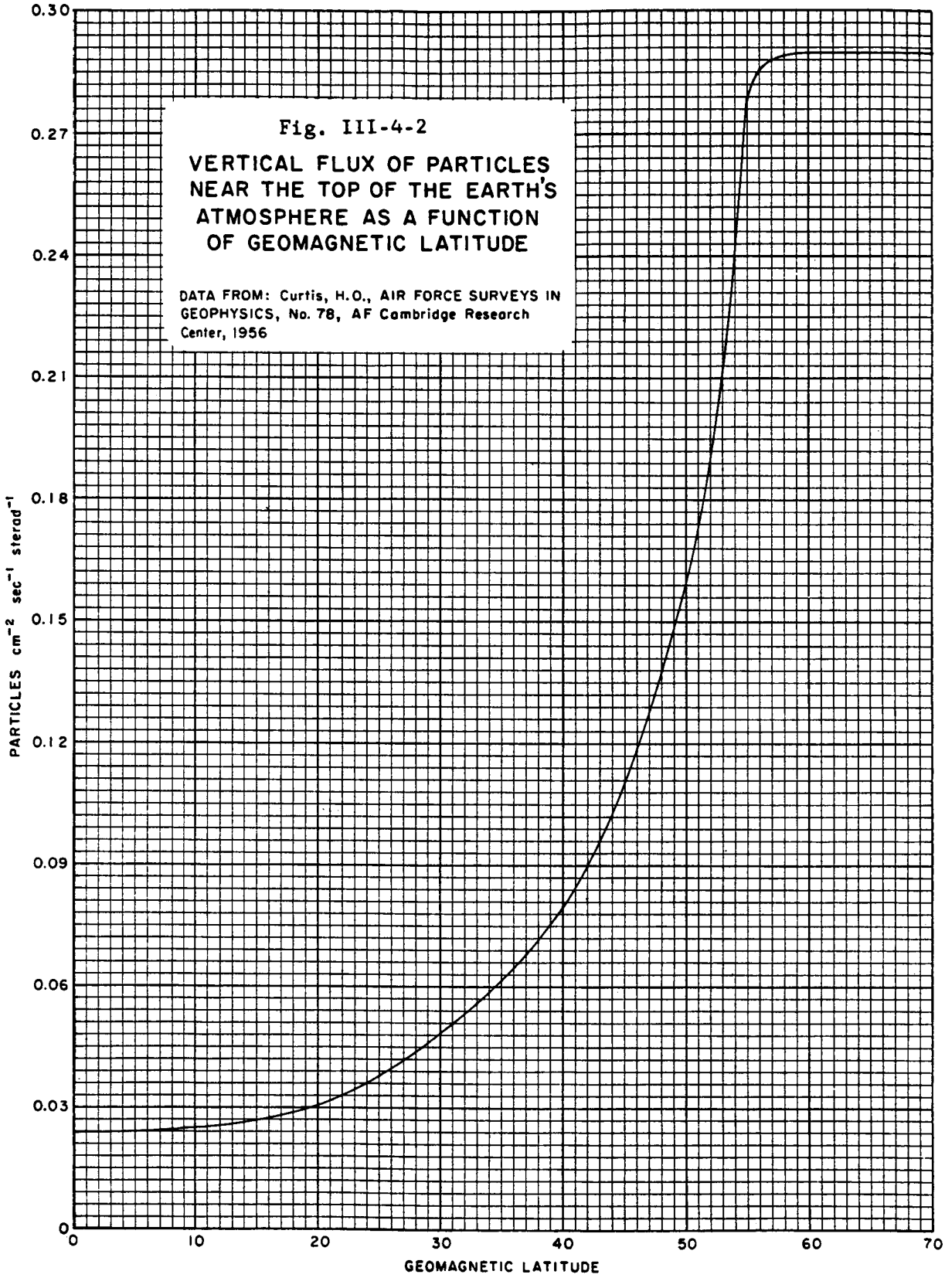

Fig. III-4-2

VERTICAL FLUX OF PARTICLES NEAR THE TOP OF THE EARTH'S ATMOSPHERE AS A FUNCTION OF GEOMAGNETIC LATITUDE

DATA FROM: Curtis, H.O., AIR FORCE SURVEYS IN GEOPHYSICS, No. 78, AF Cambridge Research Center, 1956

III-5 SOLAR EMANATIONS

Solar Winds

The sun issues a continuous stream of particles from its surface which extends far beyond the earth. These particles have an average velocity of 500 km/sec and an equivalent kinetic temperature of the order of 2×10^6°K. The concentration of particles at 1 earth distance from the sun varies widely as a function of solar activity; generally, however, the concentration is of the order of 10-100 particles/cc.

Solar Flares

When great storms erupt on the surface of the sun, solar winds increase dramatically. A solar flare can create an average energy and particle density many times greater than the normal, continuous radiation from the sun's corona and photosphere. The highest energy particles released by a flare (greater than 10^4 Mev) begin to arrive at the earth almost instantaneously, followed by particles of lower energy; the particles continue to arrive at the earth for many hours, and, in extreme cases, for days after the disappearance of the flare. During large flares, average fluxes are as high as 10^4-10^5 particles/cm^2/sec and, in general, the energy spectrum ranges from 30 to 300 Mev. The frequency of solar flares tends to follow sun-spot activity, and during periods of high activity, 10-12 flares may occur each year.

Interplanetary Zone

Radiation in the interplanetary zone consists of primary cosmic radiation from outside our solar system and the primary cosmic radiation indigenous to solar winds and solar flares. The primary cosmic radiation originating outside of our solar system is extremely stable and of exceptionally high energy; the cosmic radiation with solar phenomena is temporally erratic and of relatively smaller energy. On the other hand, very large solar flares have occurred in which enormous quantities of energy are released in the form of highly relativistic protons; energetic flares such as these are relatively rare, and only nine have occurred in the last 20 years. Smaller solar flares may occur as often as 8 times a day.

Effect of Solar Emanations

Radiation from the sun causes appreciable ionization of the earth's atmosphere at high altitudes. Because of the low atmospheric density which exists at high altitudes, recombination of ions and electrons proceeds so slowly that concentrations of electrons persist even throughout the night. The electron density varies with the eleven-year solar cycle, and is generally higher during sunspot maximum.

During the day, five distinct layers are recognized, the *D, E, F,* F_2, and protonosphere. The graph shown in Figure III-5-1 (from Johnson[7]) identifies the regions and shows a typical daytime distribution of electrons as a function of altitude.

The shape and strength of the earth's magnetic field determines the extent to which charged particles from solar eminences (or from interaction of cosmic rays with the very outer fringes of the earth's atmosphere) are trapped and maintained in the earth's vicinity. The earth's geomagnetic axis is tilted about 11.5 degrees with respect to the axis of rotation of the earth, and it is therefore necessary to make allowances for this difference when making estimations of the radiation encountered in a trajectory or orbit. The general shape of the envelope of trapped particles around the earth is indicated in Figure III-5-2, where it can be seen that the particles are concentrated in an inner and an outer belt (Van Allen belts). The inner belt has a maximum intensity about 2000 miles above the ground at low latitudes; the maximum for the outer belt is at about 10,000 miles and extends to much lower heights at high altitudes.

The Inner Belt

Prior to the high altitude nuclear test bomb blast of July 9, 1962 above Johnston Island (Pacific Ocean), the inner belt was characterized as being composed essentially of protons; at present, there exist a large number of fission electrons of a peak omnidirectional intensity of the order of 10^9 $cm^{-2}sec^{-1}$ at an altitude of 1300 to 5500 km. The electrons have energies of the order of 5 to 7 Mev and approximately half have energies below one Mev. Measurements of the temporal decay of the fission electrons indicate a surprisingly low decay rate and it is expected that the artificial belt may last as long as 10 years.

Isointensity contours of the artificial electron belt are shown in Figure III-5-3.

Proton isointensity contours for particles of energy greater than 40 Mev are also shown in Figure III-5-3. The intensity contours in the inner radiation zone show small variations, generally less than about 3%, owing to arrivals of particles from solar storms. On the other hand, the earth's geomagnetic field acts as an excellent shield, for it excludes protons of energies less than about 6.8 Bev from the equatorial plane at altitudes below about 1.25 earth radii. A typical distribution in the heart of the inner belt may be:

10^4 protons/cm^2/sec	$E > 40$ Mev
10^{10} electrons/cm^2/sec	$E > 20$ Kev
10^8 electrons/cm^2/sec	$E > 200$ Kev
10^7 electrons/cm^2/sec	$E > 600$ Kev

The Outer Belt

The trapped particles in this belt consist principally (*i.e.*, greater than 100 particles cm^{-2}sec^{-1}) of electrons and protons of energy less than 10 Mev. The outer zone begins at about 2.25 earth radii and extends to about 10 R_e, with the heart located at about 3.6 R_e. The particle fluxes in the outer belt is influenced by solar storms, it not being uncommon to being increased by 10- to 20-fold or more. Magnetic storms and variations also may cause diurnal variations of two- or three-fold. Average values for particle fluxes in the heart of the belt are:

protons	more than 140 Kev	about 1×10^8 cm^{-2}sec^{-1}
protons	more than 100 Mev	about 10 cm^{-2}sec^{-1}
electrons	more than 500 Kev	about 2×10^7 cm^{-2}sec^{-1}

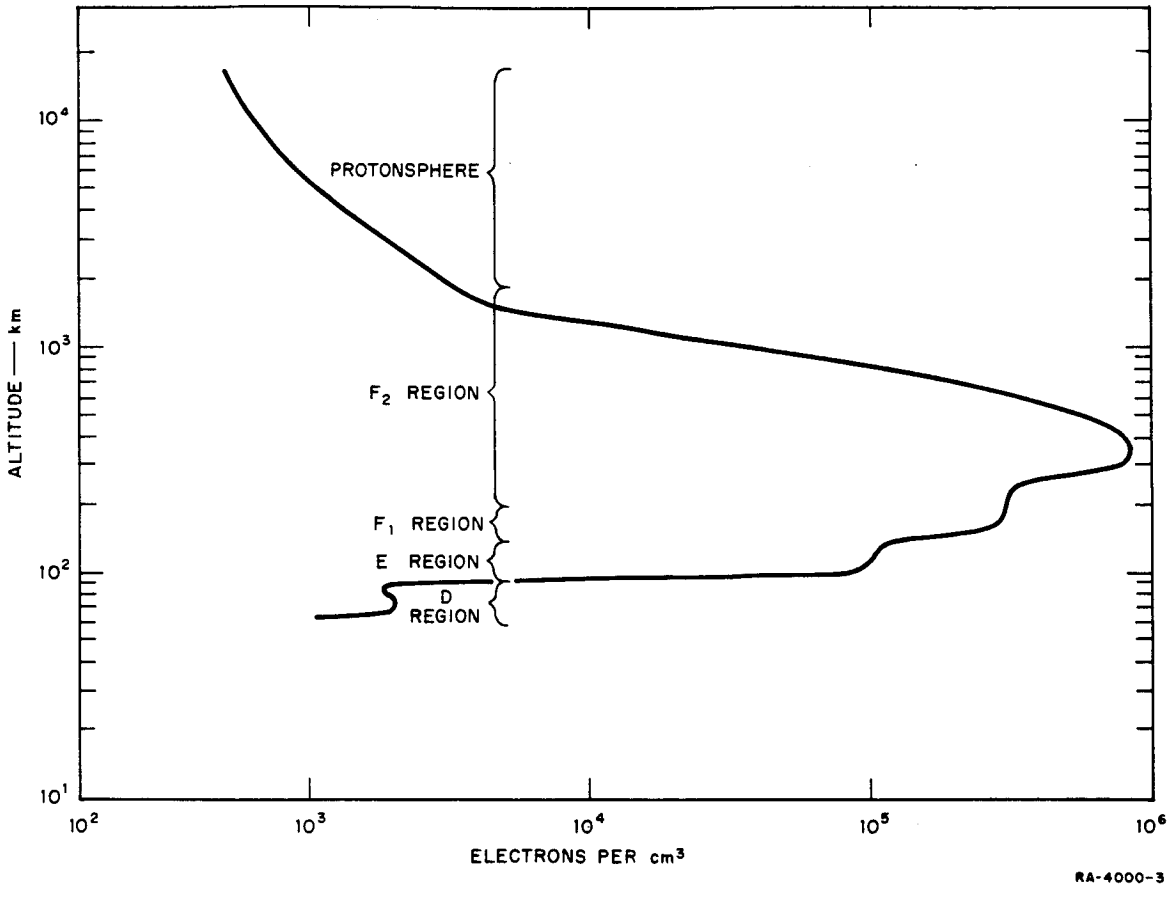

Fig. III-5-1 NORMAL DAYTIME ION DISTRIBUTION DURING SUNSPOT MAXIMUM

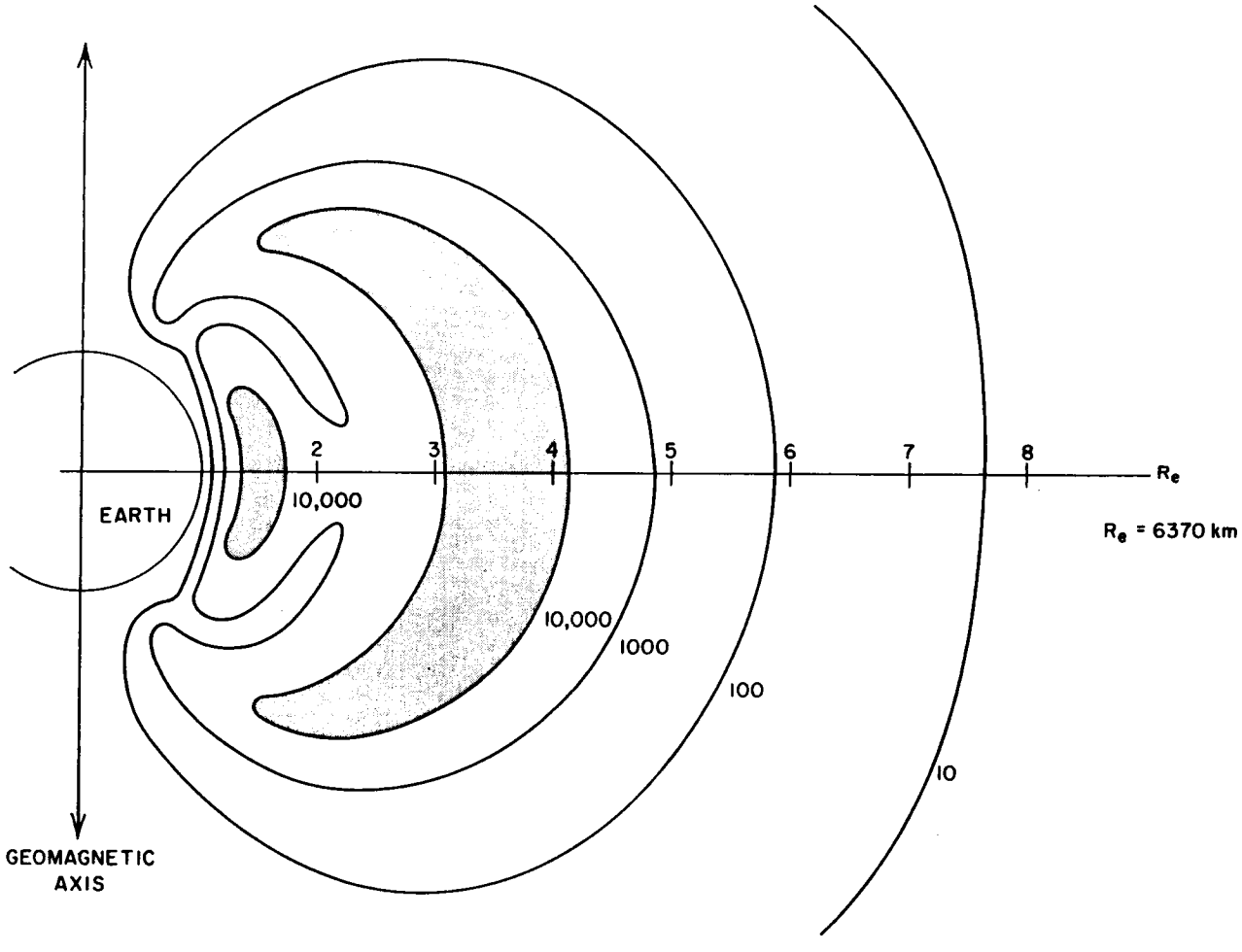

Fig. III-5-2 IDEALIZED DISTRIBUTION OF RADIATION
The contour lines indicate the counting rates of Geiger counters carried in Explorer IV and Pioneer III, and the shaded areas define the position of the two belts of intense radiation.

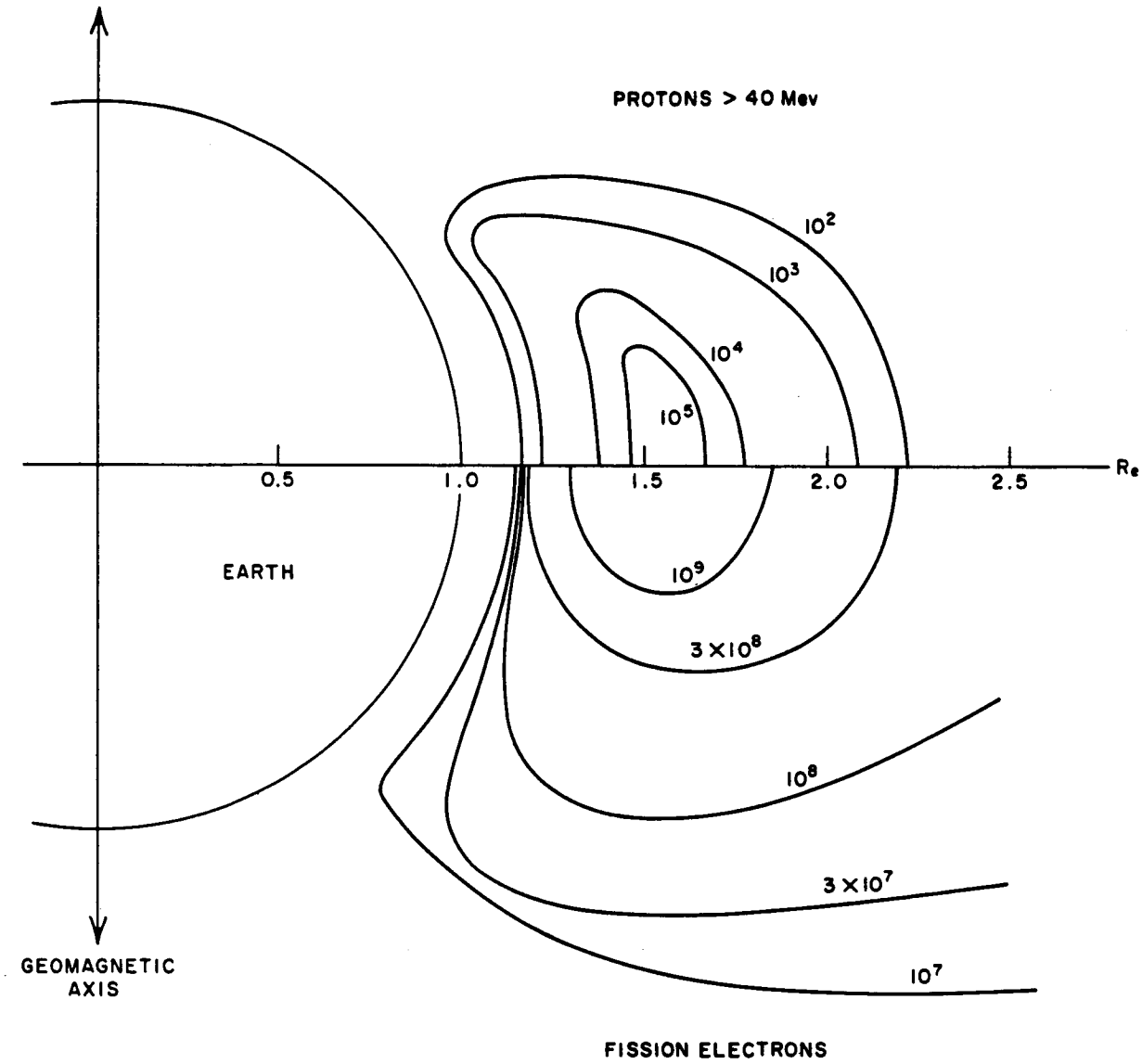

Fig. III-5-3 DISTRIBUTION OF PROTONS

The distribution of protons in the inner radiation belt is given in the upper part; the isocontour lines indicate protons cm^{-2} sec^{-1}. The approximate distribution of electrons in the artificial belt created by the high altitude nuclear blast of July 9, 1962 is indicated in the lower part of the diagram; the isointensity lines are electrons cm^{-2} sec^{-1}.

III-6 ELECTROMAGNETIC RADIATION

The spectrum of radiation emanating from the sun ranges from long radio waves (>1 cm), through infrared, visible and ultraviolet light, to x-rays (<100 Angstroms). Approximately 99% of the total energy flux lies within the wavelength region of 0.3 to 4 microns, but only the energy in the range of about 0.3 to 3 microns can penetrate the earth's atmosphere. The solar constant (irradiation per unit area normal to the direction of the sun) above the earth's atmosphere is generally accepted as being about 0.14 watts-cm^{-2}-min^{-1}; Figure III-6-1 illustrates the difference in the solar constant at sea level and outside the atmosphere, and also illustrates the attenuation of radiation by the earth's atmosphere. The unit of radiation, measured in g-calories per square centimeter is the langley (ly). Hence, 1 g-cal/cm^2/unit time equals 1 ly/unit time; in engineering units, 1 ly/min = 1 cal/cm^2/min = 221.2 Btu/ft^2/hr = 698 watts/m^2. The solar constant is 1.95 ly/min.

The amount of solar radiation reflected from a planet's surface and atmosphere (albedo) must be considered in computations of radiation incident on spacecraft. The albedo figures can only be considered as average figures, and estimates have ranged from 0.30 to 0.40 for the earth; for most heat balance computations, the figure of 0.34 has been used. The most recent average albedo figures for some other planets and the moon are as follows: Moon, 0.07; Mars, 0.26; Venus, 0.73; Jupiter, 0.44.

The amount of thermal radiation emitted from the earth (wave-lengths longer than 4 microns) also enters into computations for heat balance of a spacecraft in near-earth orbit. Figure III-6-2 illustrates a typical spectral-radiance curve for thermal radiation leaving the earth (from Johnson, Ref. 8); it is emphasized that this curve is only illustrative, since many variables enter into the problem.

The major effect of the electromagnetic radiation upon a propellant and its storage system is produced by the absorption of radiation which is transmitted as a heat input to the propellant. In the case of cryogenic propellants, heavy insulation and a venting system are required to minimize evaporation of the propellant and tank rupture.

In the case of storable propellants in unvented tanks, an equilibrium temperature will be reached where the rate of heat absorption will equal the rate of energy emitted from the surface of the storage tank.

For a tank that is tumbling in space and exposed to direct radiation, this temperature is equal to:

$$T = 3.3 \times 10^2 \, [A_r \cdot \alpha \cdot S/e]^{1/4}$$

where

A_r = ratio of average cross-sectional area to total surface area.

α = the average absorptivity of the surface of solar radiation.

S = solar constant in calories/cm^2/min

e = emissivity of the surface corresponding to the temperature of the surface.

For a tank that is oriented in space, a complex temperature gradient would be established throughout the tank's surface and its content. However, it has been pointed out[13] that in either case the equilibrium temperature is sensibly determined by the ratio of d/e, and this ratio can be controlled within reasonable limits, *i.e.*, within the range of α/e from 0.15 to 20, through selection of the surface coatings.

Since α/e is determined solely by the properties of the surface, the stability of the surface to space environment is of importance. For example, radiation in the ultraviolet region will degrade organic paints and discolor inorganic material thus changing the ratio of α/e with time. It has also been observed that for materials with low values of α/e, the ratio tends to increase with time when exposed to an ultraviolet source. Thus one could expect the average temperature of a tank and its propellant to increase with time.

Additional information on the equilibrium temperatures of spacecrafts is given in Section XIII, Heat Balance.

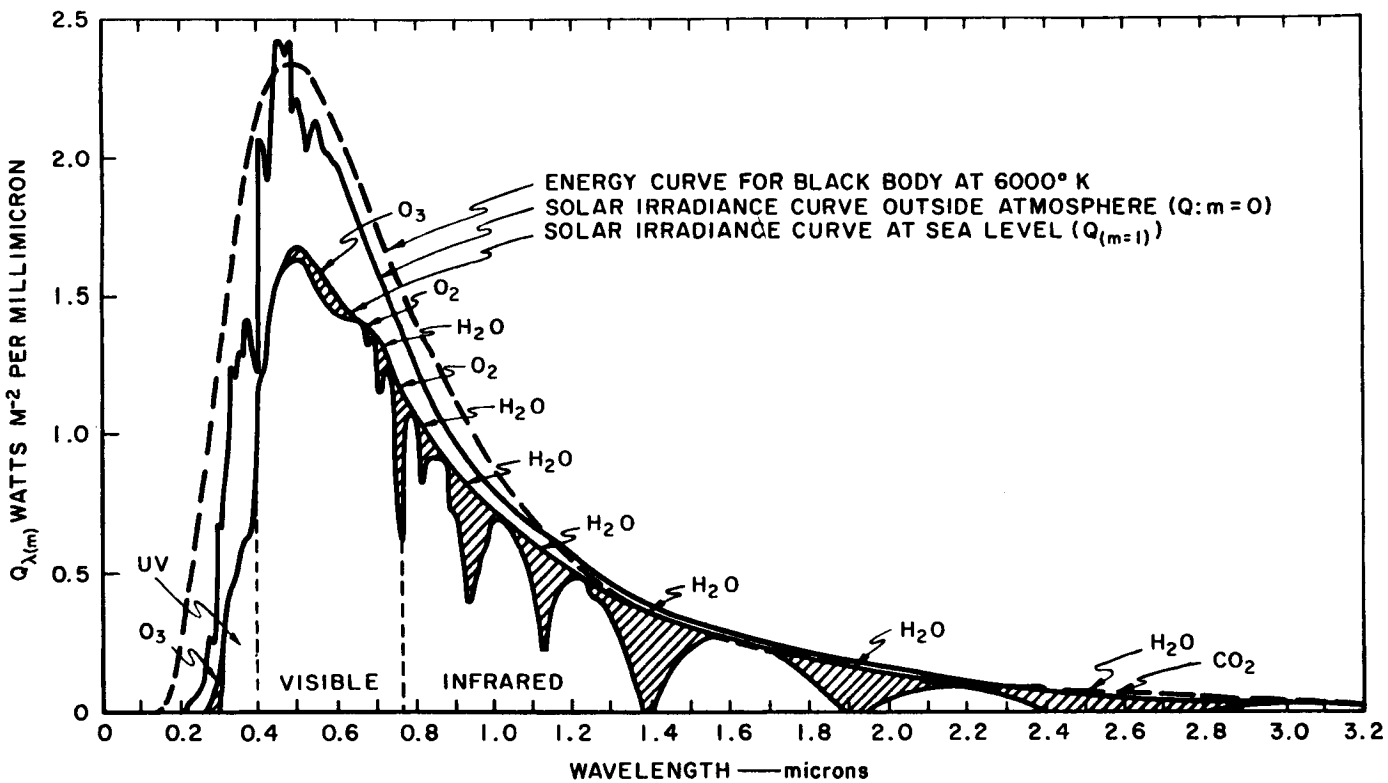

Fig. III-6-1 SPECTRAL ENERGY CURVES RELATED TO THE SUN

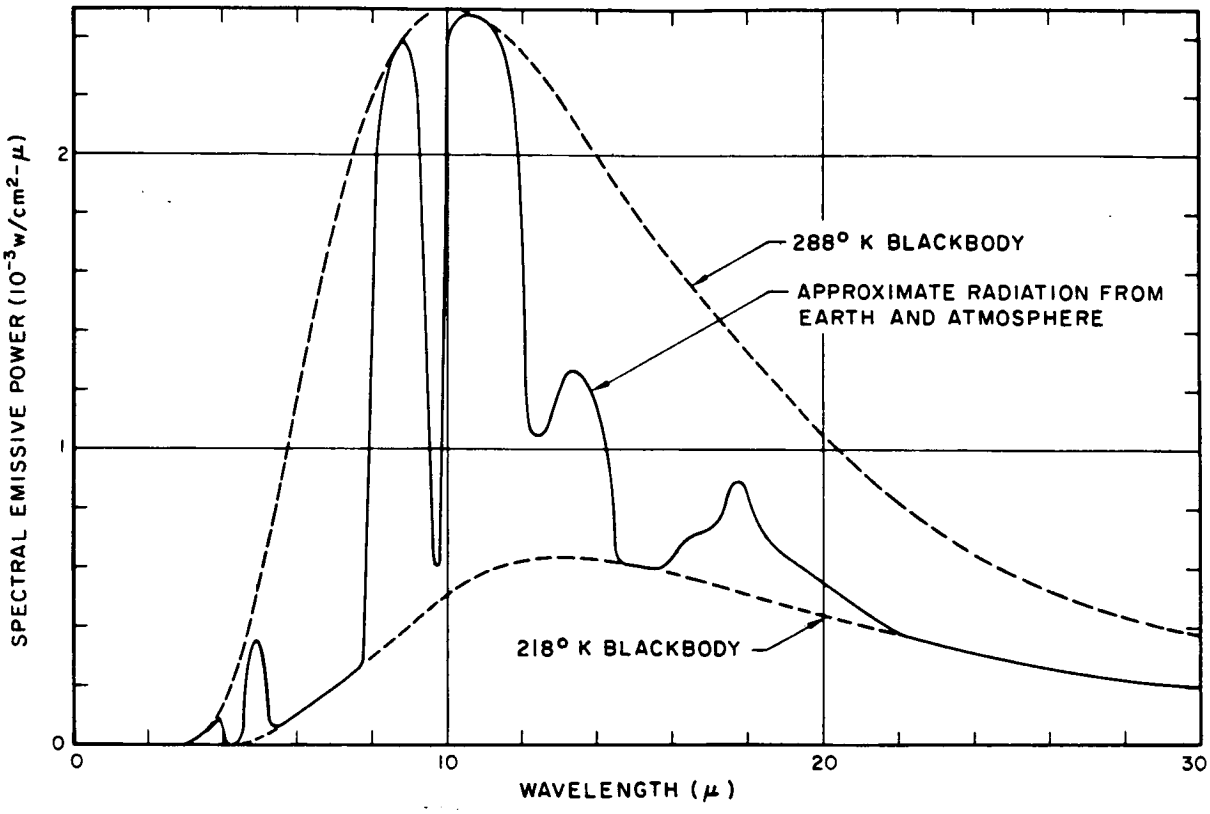

Fig. III-6-2 A TYPICAL SPECTRAL EMISSIVE POWER CURVE FOR THE THERMAL RADIATION LEAVING THE EARTH
(The 288°K blackbody curve approximates the radiation from the earth's surface, and the 218°K blackbody curve approximates the radiation from the atmosphere in those spectral regions where the atmosphere is opaque.) (Ref. 8)

III-7 MAGNETIC FIELDS

Like the earth, the sun is known to have a magnetic field, and it is speculated that the sun's magnetic field is dipolar similar to the earth's. The origin of these magnetic fields is unknown although it is commonly thought that the earth's field is the result of the dynamic action of its molten metallic core. The fact that Venus apparently has no magnetic field and is probably not rotating lends support to this hypothesis; Venus should have an appreciable core. With the exception of Jupiter, nothing is known concerning the existence of magnetic fields around the other planets. Recent observations of radio emissions from Jupiter suggest that it has an ionosphere and a field with an intensity of about 2 gauss; the intensity of the earth's field ranges from 0.5 to 0.7 gauss at its surface. The best judgment at the present time is that the superior planets have magnetic fields of intermediate intensity.

Magnetic fields do not directly affect the storage of propellants in space. However, they do affect the collection and motion of charged particles; a planet without a magnetic field can not have a Van Allen radiation belt, since cosmic particles would not be bound in quasi-periodic orbits. Also, a metallic satellite orbiting a planet that possesses a magnetic field would be subject to attitude perturbing torques, and thus might need an elaborate attitude control system.

III-8 EFFECTS OF SPACE ENVIRONMENT ON MATERIALS

One of the major problems in the design of spacecraft systems is the requirement that the materials of construction withstand and perform in the space environment, *i.e.*, at zero gravity in a high vacuum simultaneously with ultraviolet and penetrating charged-particle radiations. Much experimental and theoretical work has been performed in an effort to determine the effects of the space environment because it is impossible, at this time, to simulate accurately the combination of conditions known to exist in space.

It is particularly difficult to simulate the charged-particle radiation of the space environment first because the particle distribution is not accurately known, and second because the energy spectrum (ranging from a few electron volts to as much as 10 billion electron volts) is not easily accessible. Thus, all laboratory values relating to the behavior of materials in a space environment can only be regarded as approximate at this time; it is anticipated that future space stations will provide facilities for testing of materials in the true environment.

Vacuum

The low pressure encountered in space is conducive to the loss of materials of construction by sublimation (or evaporation) because molecules which leave the surface of materials are not returned by collisions with ambient gas molecules. Thus, above altitudes of about 100 miles, the mean free path of a molecule at ambient temperatures is so long in comparison with the size of the spacecraft that any molecule which leaves the surface will not return. Loss of material by sublimation in the vacuum of space is intuitively obvious, but the effect of very high vacuum on the rupture and fatigue properties of materials is unexpected; however, experiments have indicated[17,18] that the density of the gas surrounding a material is an important parameter defining its behavior under stress. Apparently, the character of the gas layer adsorbed on materials influences certain mechanical properties. Thus, prolonged exposure of materials to a space environment will alter or remove adsorbed

gas layers and some of the physical properties of the materials in space will be different than on earth.

The removal of material from a spacecraft structure will obviously lead to an over-all weakening of members. The weakening of a member can be simply computed by knowledge of the mass-strength relationship. Where gross sublimation of a material is involved, tests made before and after exposure of specimens to a vacuum will furnish experimental values. Ideally, the tests should be performed in an atmosphere closely resembling the space environment; however, for practical evaluation of the effects of sublimation, the most important condition to be met is that a molecule leaving the surface of the test piece has a negligible chance of returning.

The test chamber for evaluating the effects of sublimations on a material must provide the following:

(1) A residual pressure low enough so that the mean free path of molecules is long with respect to chamber dimensions. For the residual-gas molecules in the chamber, the mean free path at 1×10^{-5} mm of Hg is of the order of several meters and thus, by maintaining a vacuum of at least this order of magnitude, the motion of molecules leaving the surface of the test piece is governed essentially by their collisions with the walls of the chamber and not by collisions with residual-gas molecules.

A high probability that molecules leaving the test piece will be removed from the chamber rather than returned to the surface of the test piece. This can be accomplished when the cross-sectional area of the pumping duct is large in comparison with the exposed area of the test piece and when both the test piece and the pumping duct can be freely exposed to the chamber. For testing materials, such as metal, which condense readily at ambient temperature, this condition is easily met because molecules leaving the test piece will condense on the chamber walls; however, when polymeric materials are to be tested, elaborate precautions must be taken to ensure removal of released substances. Baffles maintained as liquid nitrogen temperatures are ofen employed to condense organic matter and cooled baffles must always be employed in pump throats to prevent back-streaming of pump-fluid vapors.

The rate of evaporation of an ideal, pure substance is given by Langmuir's equation[19]:

$$E = \frac{P}{17.14}\sqrt{\frac{M}{T}}$$

where

E is rate in g-sec^{-1}-cm^{-2} of exposed surface,

M is the molecular weight of the material,

P is the equilibrium vapor pressure in mm of Hg,

and

T is the absolute temperature, °K.

Comparison of predictions from the above equation with experimental data indicate that the Langmuir equation is conservative; thus, the equation must be employed cautiously. Further, it is necessary to recognize that its use to predict vacuum volatility is limited by the following:

(1) The vapor pressure, P, in the equation is the equilibrium pressure. In the space environment, molecules which leave the surface of the liquid or solid phase do not return, and thus equilibrium is not established.

(2) The molecular weight of the evaporating molecules must be known; for most materials, this molecular weight is frequently different than assumed (association).

(3) Oxide films or thin coatings may act as barriers to the escape of molecules.

(4) In practice, most materials are complex mixtures (alloys or polymers) which defy simple treatment. The average, assumed molecular weight of a system can not be used in the equation.

(5) The process of evaporation for systems of practical interest is very different from the purely random process assigned to ideal systems. For example, evaporation from localized planes of high surface energy is much greater than from planes of low energy; this leads to uneven evaporation, and etching of the surface becomes evident.

As is evident from the above discussion, the Langmuir equation is limited to approximations of evaporation rates in a space environment; it is useful in that it assists in the selection of appropriate materials of construction for spacecraft. For example, the equation indicates that every substance has a rate of evaporation in free space as long as the absolute temperature is not zero. Thus, at a given temperature, say 25°C, one should select materials which exhibit very low vapor pressures;

obviously, the usual metals of construction (iron, copper, etc.) can qualify, but there is some question about the lighter metals such as cadmium, magnesium, aluminum, etc. Table III-8-1 illustrates the estimated sublimation losses suffered by metals in a space environment at a temperature of 150°C; it is evident that cadmium and zinc do not appear to be useful metals for the construction of spacecrafts or components which are exposed to the high vacuum of space. Pure magnesium metal barely qualifies for the construction of spacecrafts; however, the alloys of magnesium which are currently used show considerably lower losses because the surface presented to the space environment acts as a barrier for sublimation (oxide-chromate conversion coatings, etc.). It is of interest to note that thin films of lead (as in soldered joints) may be weakened by prolonged exposure to the space environment. On the other hand, a thin coating of pure tin will act as an efficient barrier for sublimation of other materials.

The sublimation of materials from polymers or resinous matter is a complex phenomenon not expressible in the ideal case by a simple formula such as the Langmuir equation. This comes about because these materials contain a variety of ingredients; the basic polymer structure is usually composed of a distribution of nonvolatile molecules composed of a range of numbers of repetitive units but there are generally present various substances of relatively low vapor pressure which are added deliberately to modify properties (*e.g.*, plasticizers).

Since the composition of plastic or polymeric materials of the type used in the construction of spacecrafts are not divulged in detail by commercial suppliers, and since it is impractical to approximate sublimation rates from theoretical considerations, experiments are necessary to determine the effect of exposure to the simulated vacuum of space. As a consequence there appear interspersed throughout the available literature results of various tests performed largely to determine the sublimation losses of typical polymeric material and, in some instances, the effect of these losses on physical properties.

For the most part, the sublimation loss suffered by polymeric materials is found by determining the loss in weight incurred over a period of time after exposure at a given temperature to a vacuum of at least 1×10^{-6} mm of Hg. The results obtained are thus largely determined by factors such as the geometry of the test specimen, the temperature,

the mobility of the easily volatile components within the specimen, the pressure of residual gas in the test system, etc. Furthermore, since the generic structure of most polymeric materials has a very low vapor pressure, only low-molecular weight material is removed by sublimation (especially if the polymer is cross-linked). Thus, it is meaningless to extrapolate the observed weight loss to make estimates of the "life" of a polymeric substance in space (as can be done for pure metals). On the other hand, if a material suffers a loss of 5-10% after exposure for 100 hours at a temperature of not more than 125°C, it may be assumed that the physical properties are so altered by this loss that the material should not be used for construction of spacecrafts. But even in these instances, an actual check on the physical properties is necessary before the material is summarily rejected. The irregular behavior of polymers and the necessity for long exposure time indicates that published results must be examined carefully for validity.

Numerous tables of values for the outgassing rates of various polymeric substances are available and are useful for determining the type of materials to be used for construction of vacuum systems. It is to be emphasized, however, that a high outgassing rate should not be used as a criterion for rejecting materials for use in spacecrafts (see Table III-8-2).

The physical properties of most polymeric materials suitable for space use seldom change more than 10% on exposure to vacuum at temperatures less than 125°C. For the most part, physical property tests have been performed on samples "before" and "after" exposure; it is only recently that a limited number of results have been obtained for tests performed *in vacuo*. The results obtained *in situ* supposedly reveal the effect of an adsorbed gas layer on the mechanical properties of the material. It is not possible at this time to predict what kind of gas film will form on a material in space, and it is probably even more difficult to provide a synthetic environment on earth that will deposit the required gas film. As a consequence, and largely because all of the test equipment employed thus far for *in situ* polymer testing are notoriously poor in design (from the viewpoint of control of adherent gas films) it is recommended that published results be regarded with skepticism.

Table III-8-1

ESTIMATED SUBLIMATION LOSSES OF METALS IN SPACE AT 150°C

METAL	RATE OF EVAPORATION ($g/cm^{-2}-sec^{-1}$)	PERCENT LOSS IN ONE YEAR FOR INITIAL THICKNESS OF METAL IN INCHES			
		0.2	0.1	0.05	0.01
Aluminum	1×10^{-14}	2×10^{-5}	5×10^{-5}	1×10^{-4}	5×10^{-4}
Cadmium	1×10^{-6}	←	100%		→
Copper	1×10^{-19}	←	negligible		→
Iron	1×10^{-20}	←	negligible		→
Lead	1×10^{-10}	0.055	0.10	0.20	1.0
Magnesium	5×10^{-10}	1.8	3.5	7.0	35
Tin	5×10^{-13}	4.3×10^{-4}	8.5×10^{-4}	1.7×10^{-3}	8.5×10^{-3}
Zinc	1×10^{-7}	←	100%		→

Table III-8-2

TYPICAL OUTGASSING RATES FOR MATERIALS

MATERIAL	OUTGASSING RATE, $liter-mm-sec^{-1}-cm^{-2}$ AFTER INITIAL EVACUATION	
	1 Hour	8 Hours
Aluminum	10^{-6}	10^{-8}
Stainless steel	10^{-6}	10^{-8}
Silver	10^{-6}	10^{-8}
Steatite	10^{-7}	10^{-8}
High vacuum waxes	10^{-7}	10^{-8}
Polyethylene	10^{-6}	10^{-7}
Nylon	10^{-5}	10^{-6}
Methacrylates	10^{-5}	10^{-6}
Teflon	10^{-6}	10^{-8}

Radiation

Intense nuclear radiations alter properties of solid materials so profoundly that extensive studies have been required to establish the behavior of engineering materials in piles or in the vicinity of reactors. The interaction of radiation with matter leads to the production of ionization effects, vacancies and interstitial atoms, thermal spikes, displacement spikes, impurity atoms, etc. Depending on the type of material subjected to radiation, any or several of these interactions will define the response of the material. Metals are very sensitive to vacancies, interstitial atoms, etc., while the behavior of organic materials can best be explained as the results of ionization effects.

The ionization and electronic excitation produced by passage of charged particles through organic matter generally results in the rupture of bonds, formation of free radical, luminescence, and even coloration. The greater part of the energy of the incident radiation is discharged in organic material by ionization mechanisms; thus, as a general rule, the gross radiation damage produced in an organic substance is proportional to the energy absorbed. The semiconductor properties of organic substances are extremely sensitive to radiation-induced displaced atoms, and it is incorrect in these (or similar) instances to assess damage by total energy absorption.

When radiation damage can be assessed by energy absorption, the radiation tolerance is expressed in energy units, typically as ergs per gram, although it is also common to indicate the radiation environment in *r* units (Roentgens). The relationship is, approximately, 1 *r* = 87 ergs/g in air. Most tests of the radiation resistance of polymers have been performed in air; consequently, the values imply that the degradation mechanisms include the reaction of ionized air molecules with the basic organic structure. Some tests have been performed in vacuum; in these instances, it is necessary to examine the experimental technique in order to ascertain that the specimens were thoroughly outgassed (very difficult to achieve in thick sections).

Various estimates have been made of the radiation dose rates encountered by spacecrafts in various types of near-earth orbits established in the hearts of the inner or outer zones of radiation[20]. The following table summarizes the typical dosages:

Table III-8-3

ESTIMATED MAXIMUM RADIATION DOSAGES FOR VARIOUS ORBITS

ORBIT	APPROX. PERIOD	MAX. PARTICLES/cm^2/DAY		MAX. DOSAGE, rad/day		
		Electrons	Protons	Electrons	Protons	Total
Polar	3 hr	10^{13}	10^{9}	10^{5}	10^{2}	10^{5}
Polar	12 hr	10^{13}	--	10^{5}	--	10^{5}
Equatorial	3 hr	10^{14}	10^{10}	10^{6}	10^{3}	10^{6}
Equatorial	12 hr	10^{13}	--	10^{5}	--	10^{5}

The values given in Table III-8-3 can easily be converted to more realistic values for orbits outside the radiation belts by comparisons with expected particle densities as indicated in Figures III-5-2 and III-5-3. However, since most of the polymers used in spacecrafts begin to degrade at total radiation dosages of the order of 10^8, the data given in Table III-8-3 indicate that spacecraft performance may be affected in 4 to 12 months if orbits are established in the radiation belts (provided the polymers are exposed). Fortunately, the mere interposition of a thin metal shield significantly decreases the deleterious effects of the particles of the radiation belts. For example, the total dosage of a maximum of 10^6 rad per day indicated in Table III-8-3 can be reduced about a thousand-fold with 50-mil aluminum shielding.

The various elements of the ionizing radiation environment can have a number of reactions with a propellant and its storage system. Liquid propellant losses during space flights may occur because of the following possible effects:[13]

A change in absorptivity and emissivity of outer metallic or metal oxide surfaces due to sputtering.

Radiation embrittlement of metals due to dislocations.

Embrittlement of structural materials due to radiation-induced dissociation of hydrogen and diffusion of the hydrogen atoms into metals with the formation of hydrides.

Desorption of gases absorbed in multi-layer radiation shielding thereby changing the gas pressure within the shielding.

Formation of ozone in liquid oxygen, or oxides on the inside tank walls.

Decomposition of hydrazine and UDMH.

On the basis of the best estimates available regarding the flux and energy spectrum of radiation in space, including an average input of solar flares, Wiederhorn[13] states that the total dosage received by a propellant in a stainless steel tank with a wall thickness of 50 mils would be of the order of a few rads per hour in the center of the inner Van Allen belt; it is stated that this dosage rate is so low that the effects listed above are all negligible.

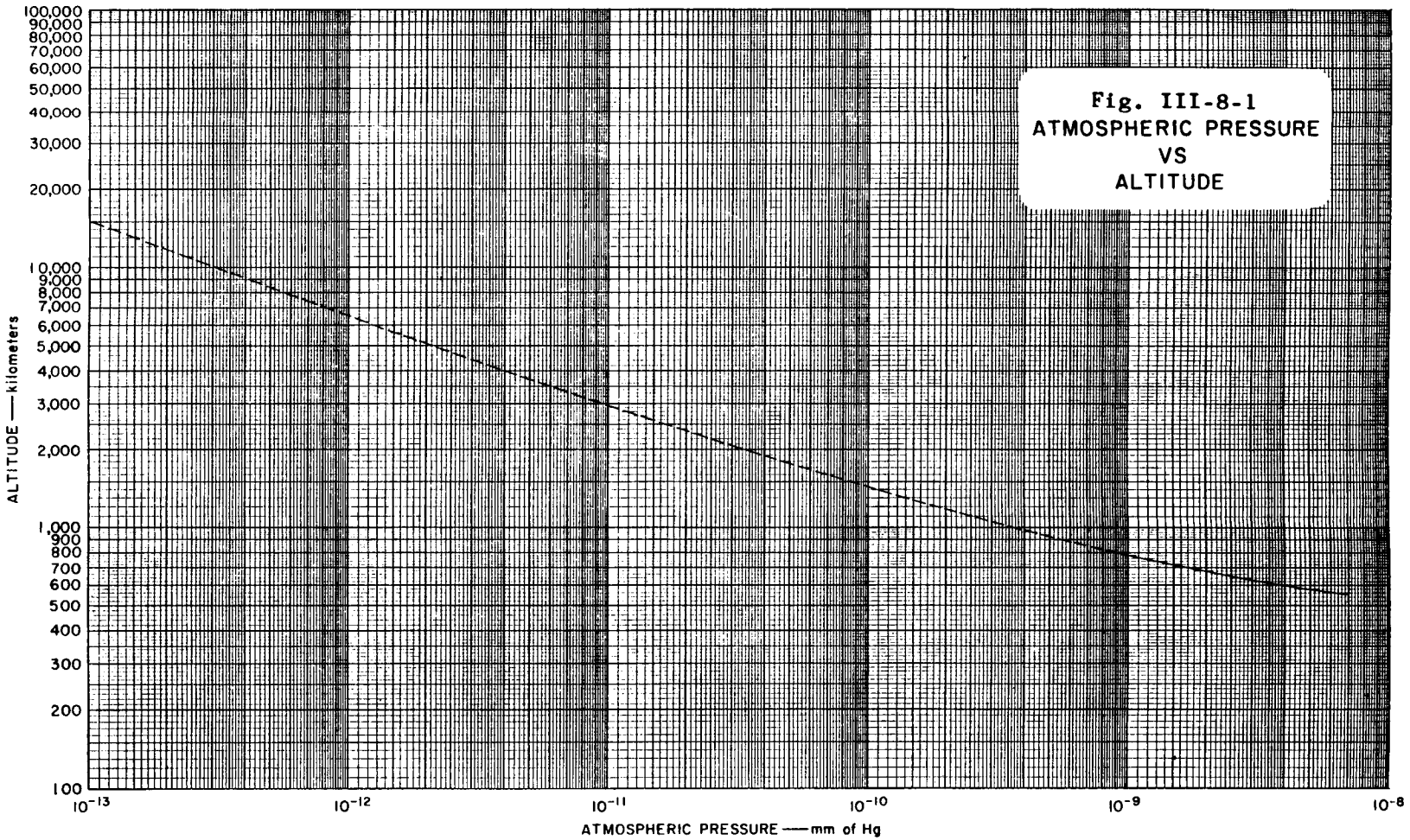

Fig. III-8-1
ATMOSPHERIC PRESSURE
VS
ALTITUDE

III-9 SPACE ENVIRONMENT REFERENCES

1. Anon., *NACA TN-1235,* 1955.
2. Batrakov, Yu., B., and Proskurin, V. F., *NASA TT F-46,* November 1960.
3. Cook, G. E., Roy. Aircraft Establ., *TN-GW531,* September 1959.
4. Gazley, C., Jr., Kellogg, W. W., and Vestine, E. H., *J. Aerospace Sci.*, **26**, No. 12, 770 (1959).
5. Kallman, H. K., and Juncosa, M. L., RAND, *Rept. No. RM-2286,* October 1958.
6. Jaffe, L. D., and Rittenhouse, J. B., Jet Propulsion Laboratory, *Tech Rept. No. 32-150,* November 1, 1961.
7. Johnson, F. S., *LMSD-895006,* December 1960.
8. Johnson, F. S., "Satellite Environment Handbook," Stanford University Press, 1961, p. 115.
9. McCoy, T. M., "R&D Handbook 1960-1961," *Space/Aeronautics*, p 8-5.
10. Mooney, D. A., "Mechanical Engineering Thermodynamics," Prentice-Hall, New York, 1953.
11. Sears, F. W., "Mechanics, Heat, and Sound," Addison-Wesley Publishing Co.,, Reading, Mass.,1950.
12. Shaw, J. H., Ohio State Univ. Research Foundation, *RF Project 847,* January 1960.
13. Wiederhorn, N., A. D. Little, Inc., *Rept. No. 63270-02-1,* September 1961.
14. Kallman-Bijl, H., *et al.*, *CIRA 1961,* North Holland Publishing Co., Amsterdam, 1961.
15. Sissenwine, N., Wexler, H., and Dubin, M., "The U.S. Standard Atmosphere, 1962," *ARS Preprint No. 2678-62,* November 13-18, 1962.
16. United States Air Force, "Handbook of Geophysics," Revised Edition, The Macmillan Company, New York, 1961, p. 16-15.
17. Shahinian, P., and Achter, M. R., *Trans. Met. Soc. of AIME,* **215**, 37 (1959).
18. Wadsworth, N. J., and Hutchings, J., *Phil. Mag.*, **3**, 1154 (1958).
19. Dushman, S., *Vacuum Technique*, John Wiley & Sons, Inc., New York, 1949.
20. Brady, B. P., and Salvinski, R. J., Space Technology Laboratories, Inc., *Report 8651-6016-RU-000,* March 1963.
21. Davidson, J. R., and Sandorff, P. E. *NASA TN D-1493,* January 1963.

IV ZERO GRAVITY CONSIDERATIONS

TABLE OF CONTENTS

Section	Title	Section-Part. Page
IV-0	List of Figures	IV-0.2
IV-1	Zero Gravity Considerations	IV-1.1
	Introduction	IV-1.1
	Forces on Liquids at Zero-G	IV-1.2
	The Central Vapor Bubble	IV-1.5
	Vapor Pressure Relationships	IV-1.6
	Film Thickness	IV-1.8
	Equilibrium Configuration	IV-1.9
	Separation of Liquid and Vapor Phases ...	IV-1.10
IV-2	References	IV-2.1

IV LIST OF FIGURES

TABLE OF CONTENTS

Section-Figure	Title	Section-Page
IV-1	Diagram of Change of Liquid from a Central Drop to a Wall-Wetting Configuration	IV-1.12
IV-2	Pressures Across Capillary Membranes	IV-1.12
IV-3	Equilibrium Conditions at Zero-G for a Vapor Bubble	IV-1.12

IV-1 ZERO GRAVITY CONSIDERATIONS

Introduction

The state of apparent weightlessness, called zero-gravity, is experienced by matter within space vehicles when moving solely under action of gravitation as in "free fall" or in orbit around Earth. Actually, the term "zero gravity" is a misnomer because the effects attributed to weightlessness are due to the vehicle and its contents experiencing the same gravitational acceleration, which varies widely but is never zero; it is the acceleration of the contents that is zero with respect to the confining vehicle. Hence, it is more appropriate to use the term "zero-g" to describe the state of weightlessness commonly associated with space flight.

In zero-g state, the vehicle and its contents both "fall" at the same rate. Thus, there is no "up" or "down" even though every body within the spacecraft and the craft itself has mass but does not exert any weight forces on its environment. As a consequence, fluids exert no hydrostatic head; buoyancy, convection, and other "natural" phenomena depending on weight or density differences are not observable.

Of the many engineering problems associated with the handling of fluids in zero-g, the only ones of major interest to the engineer concerned with pressurized gas systems are:

(1) The location of the bulk of the liquid contained in a tank.

(2) Methods for separating liquid and gaseous phases.

(3) Effects of temperature gradients.

(4) Liquid behavior in capillary or permeable-membrane systems.

The spatial configuration of loosely-contained liquids at a given time in zero-g is a function of many things, among which are: the shape of the container, liquid-to-volume ratio, interfacial energies, mechanical disturbances, heat transfer, and minor residual forces such as atmospheric drag or even thrusts from the attitude-control system.

ORIGINAL PAGE IS
OF POOR QUALITY

Forces on Liquids at Zero-G

The orienting forces on a liquid in an orbiting tank include the following:

(a) Gravitational force between liquid and tank-vehicle system

(b) Aerodynamic drag forces

(c) Centrifugal forces due to vehicle spin

(d) Electric field forces

(e) Magnetic field forces

(f) Inertial forces due to mass and motion of the liquid

(g) Viscous forces within the liquid

(h) Cohesive forces; wetting at liquid-solid interfaces

Most of these forces can be combined as ratios to express recognizable, nondimensional parameters:[1]

$$\frac{\text{inertial force}}{\text{viscous force}} = \frac{\rho V L}{\mu} \text{ (Reynolds number, } R_e) \tag{1}$$

$$\frac{\text{inertial force}}{\text{compressibility force}} = \frac{\rho V^2}{E} \text{ (Cauchy number, } C_a = M_a^2) \tag{2}$$

$$(M_a = \text{mach number})$$

$$\frac{\text{inertial force}}{\text{cohesive force}} = \frac{\rho V^2 L}{\sigma} \text{ (Weber number, } W_e) \tag{3}$$

$$\frac{\text{inertial force}}{\text{gravitational force}} = \frac{V^2}{gL} \text{ (Froude number, } F_r) \tag{4}$$

$$\frac{\text{gravitational force}}{\text{cohesive force}} = \frac{\rho L^2 g}{\sigma} \text{ (Bond number, } B_0) \tag{5}$$

$$\frac{\text{viscous force}}{\text{cohesive force}} = \frac{V\mu}{\sigma} = \frac{W_e}{R_e} \tag{6}$$

$$\frac{\text{viscous force}}{\text{gravitational force}} = \frac{V\mu}{g\rho L^2} = \frac{F_r}{R_e} \tag{7}$$

$$\frac{\text{centrifugal force}}{\text{gravitational force}} = \frac{V^2}{Rg} \tag{8}$$

where

L = characteristic length

R = radius of curvature

V = velocity of flow

g = gravitational acceleration

ρ = density

μ = viscosity

E = bulk elasticity

σ = liquid-gas interfacial tension.

It is of interest to ascertain the value of these nondimensional ratios as gravity is reduced to zero; obviously the Froude number increases to infinity and the Bond number to zero. Fluid motion is defined by the Reynolds number, Weber number, Mach number, and cohesive forces at all values of g. Wetting at all values of g is determined by the interaction of cohesive and adhesive forces, and since they do not act in the same direction, their net effect is the result of their vectorial combination. Under zero-g, cohesion and adhesion vectors are to be combined with inertial, viscous, and compressibility vectors. When a liquid is at rest or moving at very low velocities, the adhesive and cohesive forces predominate; inertial forces predominate at reasonably high values of Reynolds and Weber numbers.

The predominant external force acting on a liquid in zero-g is the vector force resulting from aerodynamic drag. Even at altitudes as high as 300 miles, the force is sufficient to insure that the liquid (at equilibrium) will gather at the forward end of the tank; the gas-liquid interfaces will, in general, be highly curved as demanded by surface tension forces.[2] At higher altitudes, centripetal acceleration forces the liquid to opposite ends of the confining vessel.

ORIGINAL PAGE IS
OF POOR QUALITY

Although not a force, heat input, such as may arise from the absorption of solar energy, leads to thermal gradients within a liquid bulk at zero-g and inevitably causes transfer of liquid from warmer to colder sections of the container by successive vaporization and condensation. The net effect is thus a mass and heat transfer which upsets equilibrium tendencies that are established by balancing of the forces described above.

Convection is absent in zero-g; hence, a significant heat transfer mechanism is not active. As a result, and because vapor bubbles tend to cling to heated surfaces at zero-g, burnout of heating elements is possible. Furthermore, there is a finite possibility that cohesive forces which normally tend to make wetting liquids at zero-g gather in some symmetrical shape about the walls of their containers (*vide infra*) are prevented from coming into play by an interceding vapor barrier generated by a heated container wall.

The equilibrium spatial configuration of liquids loosely confined in tanks at zero-g is essentially the result of the interplay of adhesive and cohesive forces, and requires time for establishment. When a fluid is displaced from equilibrium, the surface tension forces tend to restore the equilibrium spatial configuration, but an overshooting usually occurs and the configuration cannot be restored until the surface free energy in excess of that energy existing at equilibrium is dissipated (generally by conversion to heat). The time required for attainment of equilibrium is not only a function of fluid parameters (like viscosity) and the magnitude of the disturbance but also the size of the container and the mass of the fluid. The mass of the fluid to be placed in the equilibrium position increases as the cube of the tank radius while the surface free energy increases only as the square of the radius.

The spreading coefficient governs the wetting of a solid by a liquid:

$$S = \gamma_{SV} - \gamma_{SL} - \gamma_{LV} = -\Delta F \quad . \tag{9}$$

The above equation also indicates that the spreading coefficient is actually the negative value of the free energy change for the process of spreading liquid over the solid, and that it is positive for liquid-solid systems in which spreading is spontaneous. When S is negative,

ORIGINAL PAGE IS
OF POOR QUALITY

Young's equation defines the contact angle:

$$\gamma_{SV} = \gamma_{SL} + \gamma_{LV} \cos \theta \tag{10}$$

Liquids in contact with solids which have relatively high surface free energies generally exhibit small or zero contact angles; *i.e.*, for these systems Young's equation becomes:

$$\gamma_{SV} \geqq \gamma_{SL} + \gamma_{LV} \tag{11}$$

and it follows that spreading occurs readily. Most liquid propellants used in rocketry exhibit zero contact angles on all metals[3] and ceramic or inorganic glassy solids, and it follows that propellants will wet tank walls in zero-g and that adhesive forces will take part in the establishment of an equilibrium spatial configuration.

The Central Vapor Bubble[4]

Consider a tank containing a mass of liquid located at its center and not in contact with the sides. The liquid will have a convex surface; actually, the liquid mass will be contained in the form of a sphere, its shape entirely independent of the shape of the tank. Under these conditions, the inside area of the tank will be greater than the area of the surface of the centrally-located mass of liquid (see Figure IV-1):

$$A_t > A_d \tag{12}$$

Now, consider a tank in which the same mass of liquid is distributed uniformly over its internal surface area and that the layer of liquid is thick enough so that the liquid-vapor interface is not influenced by the wall material. The change in the interfacial free energy in going from the free-floating mass of liquid surrounded by vapor to a volume of vapor surrounded by liquid is:

$$\Delta F = -\gamma_{SV} A_t + \gamma_{LS} A_t + \gamma_{LV}(A_t - A_d) \tag{13}$$

If ΔF is negative, then the configuration in which the liquid in contact with the tank walls is favored. Rearranging the above equation to give:

ORIGINAL PAGE IS
OF POOR QUALITY

$$\Delta F + \gamma_{SV}A_t - \gamma_{LS}A_t = \gamma_{LV}(A_b - A_d) \tag{14}$$

and recognizing (Figure IV-1) that

$$A_t > A_b - A_d \tag{15}$$

it follows that

$$\Delta F + \gamma_{SV}A_t - \gamma_{LS}A_t < \gamma_{LV}A_t \tag{16}$$

or that

$$\Delta F < A_t(-\gamma_{SV} + \gamma_{LS} + \gamma_{LV}) \quad . \tag{17}$$

Now, referring to Young's equation [Equation (11)], if the equal sign is assumed, then the quantity in parentheses in Equation (17) is zero and the free energy is less than zero or negative. If the inequality is assumed in Young's equation, then the free energy is again less than the negative quantity in the parentheses. Thus, the wet-wall configuration is preferred over the centrally-located liquid mass.

Vapor Pressure Relationships

The pressure of vapor in equilibrium with a liquid which has a flat surface (ordinary definition of vapor pressure) is different from that in equilibrium with a curved surface. For curvatures of radius of the order of millimeters or larger, the differences in pressure are very small but significant. The equilibrium pressure of a curved liquid surface in comparison with a flat surface is given by the relationship:

$$RT \ ln \ P/P_0 = \gamma V(r_1^{-1} + r_2^{-1}) \tag{18}$$

where V is the molar volume of the liquid and P_0 is the vapor pressure over the flat surface. The pressures on the two sides of a curved surface are related by the equation of capillarity:

$$P_1 - P_2 = \gamma(r_1^{-1} + r_2^{-1}) \tag{19}$$

ORIGINAL PAGE IS
OF POOR QUALITY

where P_1 is the pressure of the liquid and P_2 is the pressure in the vapor. As a consequence, a drop of liquid will have a higher internal hydrostatic pressure than the gas surrounding it and a vapor bubble will have a higher pressure than the liquid surrounding it.

Figure IV-2 depicts capillary action in a gravitational field for liquids which wet (contact angle = 0°) and for liquids which do not wet (contact angle → 180°) the material from which the capillary tube is constructed; only the liquid and its vapor are present. According to Equation (19) the qualitative relationships of the pressures across the menisci are:

$$P_6 > P_5 \tag{20}$$

$$P_3 = P_4 \tag{21}$$

$$P_2 > P_1 \tag{22}$$

and according to Equation (18) the relative vapor pressures are:

$$P_5 > P_3 > P_2 \tag{23}$$

Since only the liquid and its vapor are present, P_3 is the ordinary vapor pressure of the liquid. Hence, the pressures may be arranged in decreasing order:

$$P_6 > P_5 > P_4 (= P_3) > P_2 > P_1 \tag{24}$$

If the vapor phase is interspersed with other gases (such as air or pressurizing gases), the pressures in the system depicted in Figure IV-2 would be increased in an almost uniform increment and the relative order of the pressures indicated above would remain unchanged. Also, the system shown in this figure is in equilibrium even though the pressure (P_5) is greater over the left meniscus than over the right; the pressure exists because of meniscus curvature and is consistent with the gravity pressure gradient.

In zero-g, the conditions depicted in Figure IV-2 are the same and the pressure relationships given by Equation (24) also hold. Capillarity

ORIGINAL PAGE IS
OF POOR QUALITY

and effects due to adhesive or cohesive forces will occur in zero-g and can be used to advantage in spacecraft design.

Film Thickness

Physical adsorption on flat surfaces when more than three or four monolayers are involved is defined by the Frenkel-Halsey-Hill equation[5]

$$ln\ P/P_0 = -k/n^S \tag{25}$$

where n is the thickness in monolayers, k is theoretically of the order of magnitude of unity,[6] and S is a constant (approximately 3).

For a system in which a flat surface covered by an adsorbed film of liquid is in equilibrium with a concave surface of bulk liquid of equal radii of curvature, Equation (25) can be combined with Equation (18) to give:

$$-\frac{k}{n^S} = \gamma(V/RT)(r_1^{-1} + r_2^{-1}) \tag{26}$$

and since $r_1 = r_2$,

$$n = (-kRTr/2\gamma V)^{1/S} \tag{27}$$

When adsorption takes place on a strongly concave surface, the adsorbed film will be much thicker than given by Equation (27) because, by derivation of Equation (25), on a concave surface there will be more of the solid close enough to a given molecule in the film to exert an appreciable attractive force. However, the radii of curvature in propellant tanks of the kinds used in pressurized systems generally are large enough to be considered as flat surfaces, but some error may be incurred for smaller radii. Nevertheless, the wet film thickness is small, as indicated by the following examples:

For water at 273°K in a tank of 2 cm radius, the number of molecule layers in the wet film is found by Equation (27):

$$n = \left(\frac{-4(8.317 \times 10^7)(273)(-2)}{2(75.6)(18.02)}\right)^{1/3} = 406$$

using $k = 4$, $S = 3$, $\gamma = 75.6$ dyne/cm, $V = 18.02$ cc/mole, and $R = 8.317 \times 10^7$ erg/°K/mole.

The thickness of the wet film is computed from the molecular diameter, 4.68 Å, and is, thus,

$$n \cdot d = 406 \cdot 4.68 = 1900 \text{ Å} \quad \text{or} \quad 190 \text{m}\mu \quad .$$

If the water were contained in a tank of about 10 feet in diameter, then the tank radius is essentially 150 cm, and the thickness of the wet film would be about 800mμ. Hence, the wet film thickness is very small and the bulk of the liquid (see Figure IV-3) is for all practical purposes contained on both sides of the hemispherical boundaries.

Equilibrium Configuration

In a previous section, it was established that the wet-wall configuration for the equilibrium figure of a mass of liquid within a tank is preferred over a centrally-located mass. The following considerations indicate some additional details about the nature of the configuration.

The equilibrium configuration of the centrally-located vapor pocket is of such shape that the interfacial free energy will be a minimum, *i.e.*, there will be no ripples or bumps on the liquid surface and the surface area will be a minimum. If the tank is spherical or if its configuration and size will accommodate a sphere, the vapor pocket will be a sphere.[7]

Returning to Equation (18), since V, P_0, and γ are constant, the curvature represented by $r_1^{-1} + r_2^{-1}$ determines the vapor pressure over the surface (radii are positive in the liquid and negative in the vapor). Thus, for equilibrium to be established, the pressure must be uniform throughout the vapor volume and the curvature must be constant for all surfaces at equilibrium.

The first three diagrams of Figure IV-3 are consistent with the above statements, but as the amount of liquid in the tank of Figure IV-3 is reduced, the vapor pocket increases in size and its volume becomes such that a sphere of the minimum tank diameter cannot suffice. Hence, the configuration must become a cylinder with hemispherical ends. If

ORIGINAL PAGE IS
OF POOR QUALITY

the ends have a radius r', then the curvature will impose a particular vapor pressure on the system:

$$RT \ ln \ P/P_0 = \gamma V[(-r')^{-1} + (-r')^{-1}] = -2/r'\gamma V \quad . \qquad (28)$$

If the cylindrical section were backed by bulk liquid, the vapor pressure over this surface would be greater than that over the hemispherical ends

$$-\frac{1}{r'} > -\frac{2}{r'}$$

but this can not exist at equilibrium. Thus, it is necessary to assume that the cylindrical section is not backed by bulk liquid but by a film of such thinness that the attractive force of the tank material on the surface molecules of the liquid film reduces the vapor pressure to the same level as in equilibrium with the hemispherical surfaces. The thickness of the film may be computed with the aid of Equation (27).

In a tank of the configuration indicated in Figure IV-3, as more liquid is removed, the hemispherical confining surfaces will recede toward the ends of the tank. At any time, however, the central cylindrical section will have a very thin film-wet surface, and bulk liquid must define the hemispherical ends of the vapor envelope; this means that if the envelope migrates towards one end of the tank, the liquid thickness between the tank wall and the envelope will adjust itself to any irregularities in the tank wall in such a way as to maintain an hemispherical surface.

For most liquids, $d\gamma/dT$ is negative. Thus, if there were a higher rate of heat flow through one wall of a tank, the surface tension would be lower on the warm side. The reduced surface tension would allow the warm surface to be drawn toward the colder areas. The over-all effect is a movement of the envelope.

Separation of Liquid and Vapor Phases

Maintaining a discrete liquid phase in a tank at zero-g is a difficult task. For tanks containing propellants used in high-level thrust units (such as rocket engines), the problem is of little concern because the moment the thrust units are activated by the propellants remaining in feed lines, sufficient accelerative forces are brought into

play to position the liquid masses in their tanks. Alternatively, small thrust units may be employed to provide forces for positioning propellants before the large thrust units are activated. For specialized applications, such as dumping propellant, special systems have been devised and successfully applied.[2]

The use of bladders, diaphragms, pistons, and other artifacts for maintaining intact a mass of liquid in zero-g while permitting pressurization has been employed extensively. The most common of these systems involve use of diaphragms or bags, but the biggest problems encountered are the permeability of materials and the extremely corrosive nature of most rocket propellants. For short-time missions, diaphragms can be made which are flexible and quite impermeable; however, for extended missions, permeability must be taken into consideration.

The problem of withdrawing gas or reducing the vapor or gas pressure in a pressurized system containing a liquid phase at zero-g is exceedingly complex and has been solved only in limited instances, for example the rapid-dump system for blowdown or venting of the Agena vehicle.[2] This problem is particularly vexing in the case of systems for supplying pressure from liquefied gas; in instances where the systems are to perform effectively for extremely long periods of time (such as satellite attitude control systems), it is especially important to insure clean separation of the phases. Since most pressurizing systems utilizing a liquefied gas include diaphragm-type pressure regulators, separation of phases can be conveniently effected by use of bags or diaphgrams to contain the liquefied gas, and the liquid phase is bled through the regulator into an expansion chamber; however, for long missions, the permeability of the bag to both the pressurizing gas and the contained liquid will eventually lead to diffusion of the pressurizing gas into the bag. If piston-and-seal-type systems can be utilized, the greatly reduced area for permeability (*e.g.*, an O-ring) will insure a longer period of performance.

ORIGINAL PAGE IS
OF POOR QUALITY

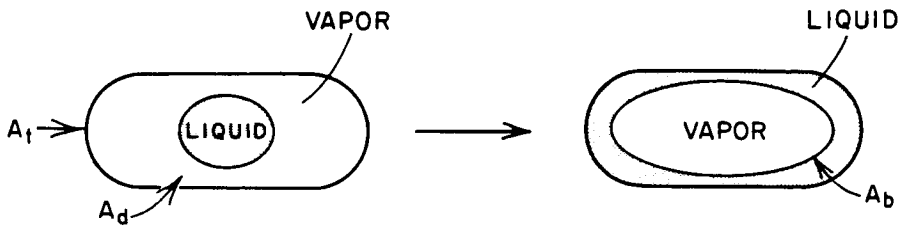

A_t = AREA OF INNER TANK SURFACE

A_d = AREA OF SURFACE OF DROP

A_b = AREA OF INNER BUBBLE SURFACE

FIG. IV-1 DIAGRAM OF CHANGE OF LIQUID FROM A CENTRAL DROP TO A WALL-WETTING CONFIGURATION

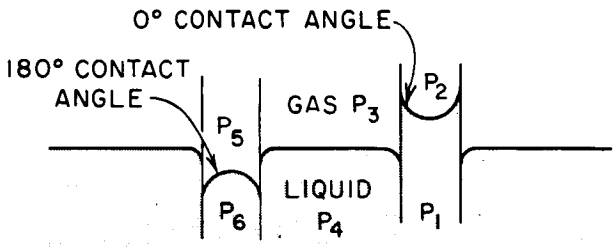

P_1, P_4, P_6 : PRESSURES BELOW MEMBRANE

P_2, P_3, P_5 : PRESSURES ABOVE MEMBRANE

FIG. IV-2 PRESSURES ACROSS CAPILLARY MEMBRANES

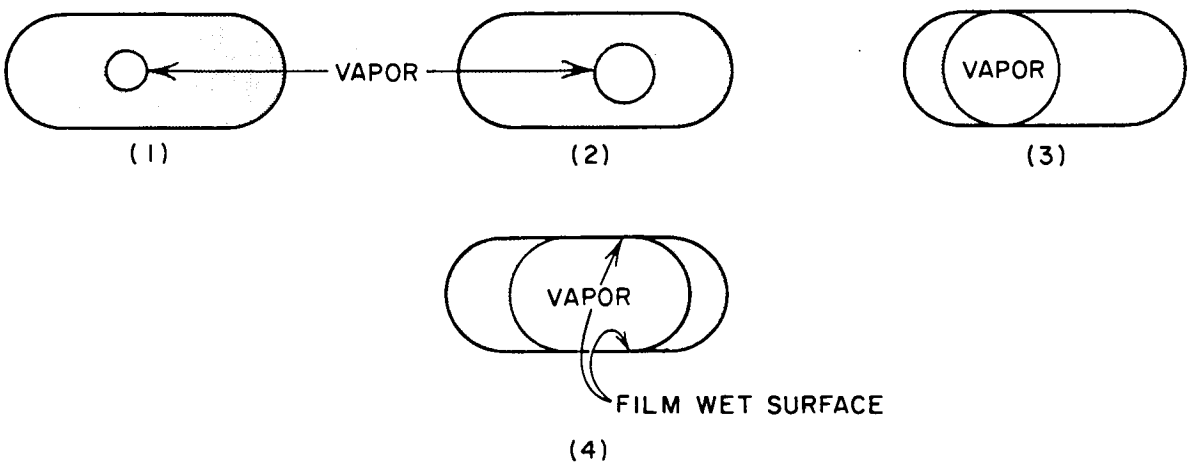

FIG. IV-3 EQUILIBRIUM CONDITIONS AT ZERO-G FOR A VAPOR BUBBLE

IV-2 ZERO GRAVITY CONSIDERATIONS REFERENCES

1. Unterberg, W., and Congelliere, J., *ARS J.*, **32**, 862 (1962).
2. Satterlee, H. M., *Space/Aeronautics*, **38**, July 1962, p. 72.
3. "Studies of the Contact Angles of Storable Liquid Propellants," Stanford Research Institute, Final Report, Project PD-3462, 1961; Muraca, R. F., Longwell, A. P., and Burns, E. A., *Rev. Sci. Inst.*, **34**, 479 (1963).
4. Neu, J. T., and Good, R. G., *AIAA J.*, **1**, 814 (1963).
5. Hill, T. L., "Theory of Physical Adsorption" in *Advances in Catalysis*, edited by Frankenburg, Komarensky, and Rideal, Academic Press, New York, 1952, Vol. IV, Ch. 5.
6. MacMillan, W. G., and Teller, E., *J. Chem. Phys.*, **19**, 25 (1951).
7. Li, T. C. H., *J. Chem. Phys.*, **36**, 2369 (1962).

V ATTITUDE CONTROL THEORY

TABLE OF CONTENTS

Section-Part	Title	Section-Part. Page
V-0	List of Tables	V-0.2
V-0	List of Figures	V-0.2
V-1	Introduction	V-1.1
V-2	Torques Acting on Spacecrafts	V-2.1
V-3	Sensors	V-3.1
V-4	Hardware Design	V-4.1
V-5	References	V-5.1

V-O LIST OF TABLES

Section-Part-Table	Title	Section-Part. Page
V-3-1	Typical Attitude Sensors	V-3.3
V-4-1	Time Delays in Gas Attitude-Control Systems	V-4.2

V-O LIST OF FIGURES

Section-Part-Figure	Title	Section-Part. Page
V-4-1	Cold Gas System Hardware Implementation	V-4.3

V-1 INTRODUCTION

Attitude control is used to stabilize a space vehicle or portions of the vehicle about a tracking line from a reference on the vehicle to an external reference. An external reference may be a vertical to a planet, the sun or a star, a gravitational or magnetic field, or an imaginary line between any two bodies in space.

The accuracy of attitude control depends on the mission of the vehicle, and for most purposes a limit of ±1 degree is sufficient. On the other hand, special experiments may require accuracies of 10-20 seconds, and in the case of vehicles bearing telescopes (OAO), about ±0.1 sec of arc is the minimum acceptable. In general, the over-all system performance is the result of compromises in design limitations, available accuracy within weight allowances, average power available on board, the vehicle's moment of inertia, and the nature and magnitude of disturbing torques. The last two factors greatly influence the performance of an attitude control system, but, unfortunately, they are outside the responsibility of the control system's designer and depend upon factors such as the vehicle's configuration and materials of construction.

There are seven primary sources of torque which must be counteracted by the attitude-control system; these are: atmospheric drag; gravitational gradient; solar radiation pressure; magnetic fields; micrometeoroid impact; movements internal to the vehicle; apparent torques arising from rotation of reference axes.

The methodology utilized in the design of a space-vehicle attitude-control system generally involves the following:

(a) The operational requirements of the attitude-control system are determined by the operational specifications of the mission the vehicle is to perform. These specifications will determine system characteristics such as how accurate a control is required, whether the whole vehicle or only a part must be stabilized, the portion of the trajectory or orbit over which control must be exercised, the lifetime of the control system, and even whether any control at all is required. The operational

ORIGINAL PAGE IS
OF POOR QUALITY

requirements will also determine some of the restrictions to be imposed on the control system, such as size, weight, and consumption of power.

(b) The co-ordinate reference system and the vehicle reference axes are then selected; suitable deviation angles between the two are then established, and these determine the differential equations of motion for the control system.

(c) The actual design and constructional features are tentatively determined after solution of the differential equations of motion. At this point, factors to be taken into consideration include: limitations of size, weight, and power consumption; internal and external torques which need to be counteracted by the control system; magnitude of the control torques available within size and weight limitations, etc. Whenever possible, the system is designed or programmed to utilize ambient field torques (such as the earth's magnetic field or solar radiation) to accomplish or aid in the control function. At this stage of the design, the control-torque mechanisms and the sensors and control-system computer scheme are determined.

(d) Once the general design and constructional features of the control system are determined, analytical studies of the performance of the system are made. However, the analysis tends to be complicated because of the nonlinear characteristics of the control system and because there is generally three-axis coupling. Often, simplifying assumptions are made in order to avoid intractable mathematics; techniques developed for nonlinear control theory are often applied.

V-2 TORQUES ACTING ON SPACECRAFTS

The sources of torque which act on spacecrafts act as disturbances, but they may be used as sources of energy for control. The determination of the magnitude of torques acting on a spacecraft and the anticipated time over which they will act establishes the total impulse required to maintain attitude control. For example, if a 1000-lb satellite in a synchronous orbit is subjected to a continuous force of 10^{-5} lb over two years because of gravitational gradient (*vide infra*), about 630 lb-sec of impulse will be required to maintain a geographically-fixed position; thus the minimum total impulse of the attitude control system (one axis) is established. For the other axes, assuming that nearly static positioning is required (no spin), the natural frequency of oscillation about an axis must be computed and the on-off time for each attitude-control thrust generator must be determined as a function of the sensitivity of the attitude sensors, thrust levels, etc., in order to obtain the total impulse required for the mission. The following sections summarize the nature and magnitude of the torques which affect spacecrafts.

Atmospheric Drag

Aerodynamic drag predominates below 500 miles and is often used for control by moving surfaces in the slip stream. At 500 miles, typical drag corresponds to a dynamic pressure of about 6×10^{-5} dyne/cm^2 (1.25×10^{-9} lb-ft^{-2}); at 80 miles, it is about 5 dynes/cm^2 (10^{-2} lb-ft^{-2}). The drag can be calculated on the basis of free molecular flow, but the computations are quite complex. If the molecular speed ratio is at least 10, good approximations (±10% for altitudes below 375 miles) can be made by assuming Newtonian flow with a drag coefficient of 2. When aerodynamic drag is used for control, some form of damping must also be employed.

Internal Motions

These torques are unpredictable; they can, however, be held to low values by system design. Typical torques result from moving vanes, extensible booms, mechanisms for winding film, scanning devices, etc.

ORIGINAL PAGE IS
OF POOR QUALITY

Gravity Gradient

In general, a spacecraft is accelerated in the direction of the mass-attraction vertical at its center, but the attraction is essentially in equilibrium with the centrifugal force resulting from the orbital velocity of the vehicle. However, since the earth is not a body of revolution about its poles, it does not have a truly radial and uniform gravitational vector ; moreover, for vehicles not in an equatorial plane, a gradient exists which is attributable to a slight dipole distribution of the earth's mass relative to the equatorial plane. As a consequence, a space vehicle tends to be rotated about its center of mass by the gravity gradient across it, and the tendency is to cause an alignment of the long axis of an unsymmetrical vehicle with the gradient. The earth's oblateness also causes rotation of the vehicle's orbit plane about the earth's polar axis and oscillation about the line of nodes; it also leads to an aperiodic rotation of the orbit's major axis and a periodic variation of its semi-major axis.

The horizontal component of gravitational acceleration that is attributable to the slight dipole distribution of the earth's mass relative to the equatorial plane may be expressed[1] as follows:

$$g = -\frac{3G(I_2 - I_1)}{2r^4} \sin 2\theta$$

where

g = horizontal component, ft/sec^2

G = universal gravitational constant, 1.068×10^{-9} ft^3/lb-sec^2

$I_2 - I_1$ = difference of principal moments of inertia in the equatorial plane, lb-ft^2

r = orbital radius, ft

θ = angular position relative to the earth's major axis in the equatorial plane.

As an example of the magnitude of this disturbance, a 1000-lb satellite in a 24-hour orbit ($r = 1.38 \times 10^8$ ft) at an angular position $\theta = 70°$ and for which $I_2 - I_1 = 1.22 \times 10^{35}$ lb-ft^2 is influenced by a component g of about 3.4×10^{-7} ft/sec^2; the force on the satellite is eastward and about 10^{-5} lb (5 dynes). Hence, the satellite will drift 20° longitudinally

to the west in about 200 days; since this drift represents the limit of the western boundary of a typical communication satellite system, this example gives an idea of the minimum frequency with which adjustments must be made.

Gravitational accelerations of the sun and moon are much larger (several magnitudes) than the horizontal component of the earth's field but they tend to average out (except for a small residual). However, solar and lunar gravitational perturbations eventually tilt the orbital plane of a synchronous-orbit satellite relative to the equatorial plane; the average tilt rate corresponds to about 1 degree per year.

Magnetic Fields

A magnetic field generates a torque which is perpendicular to the field; thus, if one of a vehicle's control axes is parallel to the field, torques are produced about only two of the axes. The earth's magnetic field sensibly extends beyond 10,000 miles; it is cyclic in position and time, and is affected by solar storms. The earth's field is warped and, thus, the effect on a spacecraft is difficult to predict with any degree of accuracy. The sun's magnetic field predominates at distances beyond 10,000 miles from the earth; it is extremely random in strength and orientation. Fortunately, disturbing effects from magnetic fields can be reduced by using nonmagnetic materials for construction of spacecrafts, avoiding closed conductive loops as much as possible, and eliminating spin. Magnetic torques as little as 10 dyne-cm can be realized by appropriate vehicle design.

Solar Radiation

The photon stream from the sun can also produce torques on the axes of a spacecraft, and these torques are particularly significant on asymmetrical vehicles, or vehicles with surface materials of different reflectivities, because the center of pressure will not be aligned with the center of mass at all angles of incidence. For example, if the center of pressure is six inches away from the center of mass of a medium reflectivity surface 100 ft^2 in area, a solar pressure of 1.4×10^{-7} lb-ft^{-2} will exert a torque of about 7×10^{-6} lb-ft. The solar radiation pressure in the vicinity of earth is at most 2×10^{-7} lb-ft^{-2} at normal incidence on a specularly reflecting surface; it should be possible to design a space vehicle so that the torque attributable to solar radiation is below about 10^{-5} lb-ft.

Meteoroids

Impacts from meteoroids produce the largest impulsive forces on space vehicles. There is available very little tangible information on the density of meteoroids in space, but estimates may be used to provide an idea of the demands on an attitude control system. Mariner II data obtained in the region between earth and Venus seems to indicate that the concentration of tiny cosmic particles in deep space is about a ten-thousandth of the concentration near earth. For example, only one dust particle impact occurred during a 129-day period of the Mariner II mission in deep space, while as many as 3700 impacts are registered in periods of 500 hours by satellites in the vicinity of earth.

The impact of meteoroids (especially as a shower or as exceptionally heavy particles) may produce torque which can not be offset by the attitude control system (saturation). A meteoroid may be large enough to penetrate the vehicle's skin and damage internal equipment as well as produce an overturning moment.

If it is assumed that the total meteoric accretion by earth is 10^6 kg per day and that the mass accretion in each magnitude is equal[2] for each of 30 magnitudes (see Section III-3), the total accretion may be expressed by

$$\sum_{m=0}^{m=30} M_m^E N_m^E = 31 M_0^E N_0^E = 10^6 \text{ kg} \qquad (1)$$

Since the mass M_0^E of a zero magnitude meteoroid is assumed to be 25×10^{-3} kg, the number, N_0^E, meteorites falling on earth per day is found by solving the above equation:

$$N_0^E = 1.3 \times 10^6 \qquad (2)$$

Now, the number of meteorites of magnitude $M + 1$ is 2.512 times the number of magnitude M (see Section III-3); thus, the average number of meteorites falling on the earth in t hours is

$$N_m^+ = \frac{N_0 10^{0.4m} t}{24} \qquad (3)$$

The number, N_m, of meteoroids of magnitude m impinging on a vehicle in the time interval t hours is:

$$N_m = \frac{N_0^E 10^{0.4m} t}{24} \left(\frac{A_S}{A_E}\right) \tag{4}$$

where

A_S = effective surface area of the vehicle,

A_E = surface area of the earth,

and

N_0^E = 1.3×10^6 impacts per day (zero magnitude).

The effective area of the vehicle can be expressed as

$$A_S = A\left[1 - \left(\frac{R_0}{2R}\right)^2\right] \tag{5}$$

where A is the actual area of the vehicle, R_0 is the radius of the earth, and R is the altitude of the vehicle from the center of the earth. Thus, the number of meteoroids striking a vehicle is a function of the altitude; at low altitudes, the earth shields the underside of a vehicle from meteoroid impacts.

The angular velocity change in degrees per second, θ, imparted to a vehicle by a meteoroid impact of magnitude and mass M_m is:

$$\theta = \frac{57.3 M_m V L}{I} \tag{6}$$

where V is the average velocity of a meteoroid (28×10^3 m/sec), L is the moment arm to the center of mass (m), and I is the vehicle's inertia, kg/m^2. This equation may be written as

$$\theta = \frac{57.3 M_0 V 10^{-0.4m} L}{I} \tag{7}$$

by substitution of $M_m = M_0 10^{-0.4m}$ and then transformed to:

$$N_m = \frac{KA_S tL}{\theta I} \tag{8}$$

by solving it for $10^{0.4m}$, substituting into Equation (4), and recognizing the constant term $(57.3M_0N_0V)/(24A_E) = K$.

In order to express the angular disturbance as a function of probability, the meteoroid distribution is assumed to be a Poisson function; thus, taking N_m as the mean, the probability of h hits on a vehicle in t time is

$$P = N_m^h \exp(-N_m)/h! \tag{9}$$

and the probability of no hits is

$$P_d = \exp(-N_m) \tag{10}$$

while the probability of the vehicle being hit one or more times, P_{1+}, plus the probability of no hit is obviously:

$$P_{1+} + P_0 = 1 \tag{11}$$

Hence,

$$P_{1+} = 1 - \exp(-N_m) \tag{12}$$

represents the probability of one or more hits in an interval of time t. Substituting Equation (8) into (12), yields the probability for one or more hits on the vehicle:

$$P_{1+} = 1 - \exp(KA_S tL/\theta I) \tag{13}$$

or,

$$\theta = -\frac{KA_S tL}{I \ln(1 - P_{1+})} = -\frac{KA_S tL}{I \ln P_0} \tag{14}$$

Equation (14) permits computation of the angular disturbance of any vehicle configuration from one impact of each visual magnitude, but nothing has been said about disturbances resulting from multiple hits of combinations of meteoroids of the same or various magnitudes. The most probable disturbance is, however, the result of a single impact, as shown below.

The disturbance resulting from h impacts of magnitude m is found from Equation (7):

$$\theta = h \frac{57.3\ M_0 V 10^{-0.4m} L}{I} \quad . \tag{15}$$

Substituting Equation (4) into (15) and recognizing the constant K:

$$N_m = \frac{K A_S t L h}{\theta I} \quad . \tag{16}$$

On the other hand, the probability of h hits on the vehicle is given by Equation (9); hence,

$$P = (Zh)^h \exp\ (-Zh)/h! \tag{17}$$

where

$$Z = K A_S t L / \theta I .$$

Since P is a maximum when $Z = 1$ for any value of h, the maximum probability occurs when

$$\theta = K A_S t L / I \tag{18}$$

Further, since P is a maximum for $Z = 1$ when $h = 1$, it follows that the most probable disturbance occurs from only one impact.

The number of impacts of magnitude m per second per square meter is

$$N_{m,s} = \frac{N_0 10^{0.4m}}{(24)(3600) A_E}$$

and the total number of impacts per second per square meter is

$$N_T = \frac{N_0 10^{12}}{(24)(3600)A_E} \sum_{n=0}^{n=30} \left(\frac{1}{2.512}\right)^n$$

V-3 SENSORS

The two basic operational functions of an attitude-control system are sensing and actuation; in some instances, these functions can be combined in a single device. Additionally, the system must provide some form of damping, usually a feed-back loop. Thus, for each control axis, a control system is composed of a sensor, electronics for processing the sensor's signals and issuing control signals, an actuator, and a damping device. The electronic system requirements for attitude control are well within the state of the art, although some improvement is desirable in reliability and life of components. The greatest room for improvement is in the field of sensors and actuators. Specifically, actuators (valves) and sensors are needed which will provide greater accuracy and reliability than currently available.

Table V-3-1 indicates the types of sensors currently used, the accuracies they provide, and the accuracies which it is hoped future developments may provide. However, some of the accuracies hoped for may not be achievable; indeed, a study of the Ranger vehicle indicates that it is highly unlikely that control accuracies of the order of 0.005 degree will be possible in any spacecraft because of flexing of one part of the vehicle with respect to another. On the other hand, the flimsy vehicles currently launched into space may be replaced with sturdy craft when larger boosters are available.

The major problem encountered in the design and use of sensors is that the phenomena they utilize to derive information are either poorly defined or swamped by spurious signals. Thus far, practical sensors have relied on only a few phenomena: direction of the sun; gravity fields; magnetic fields; stellar radiation; horizons or infrared interfaces.

Earth and planet horizon sensors detect infrared differences which are easily obscured by clouds or large temperature gradients on the planet surface. Thus, to increase sensor accuracy, considerable improvement in signal-to-noise ratio must be realized. Similarly, solar trackers lose accuracy when they are required to track within magnitudes approaching the sun's subtended angle. The sun itself presents a disc which subtends an

ORIGINAL PAGE IS
OF POOR QUALITY

arc of about ½ degree as viewed from earth, but the aten is surrounded by concentric rings of ionized gases (which also radiate infrared energy) and subtend as much as several degrees of arc. During solar eruptions the rings may have temperatures approaching the central core.

When a star is used to activate a sensor, a bright star against a black background obviously gives an optimum signal-to-noise ratio. However, this ideal case can seldom be realized, for the portion of the sky to be used for reference is determined by the mission of the vehicle and, as is often the case, the selected star is but one in the midst of others of nearly equal magnitude. Hence, discrimination is based on spectral radiation and brightness, and since the sensor must have high selectivity to track dimmer images, its signal-to-noise ratio will tend to be low.

Gyroscopes perform well in spacecraft (*e.g.*, Mariner II) and are often used to sense deviations from orbit planes. However, the limited life of bearings and the inevitable accumulation of drift errors appears to dampen enthusiasm for their continued employ. The drift rate of free gyroscopes is far too great for long missions (0.1 to 0.5 deg/min), but single-degree-of-freedom, rate-integrating gyroscopes of high quality offer drift rates of the order of 0.001 deg/hr and may even sense angular velocities of the order of small fractions of the earth's rate. Life expectancies can be improved by turning off the gyroscopes during coast periods (Mariner II).

The most widely used sensor is the horizon scanner. In principle, the scanner uses a thermistor bolometer to detect the high temperature gradient which exists between the earth and empty space at the horizon. However, accuracies are limited to 0.2 to 0.5 degree because, at altitudes below 1000 miles, uneven distribution of water vapor and the earth's oblateness limit the sensing of the horizon to no better than ±0.1 degree.

Table V-3-1

TYPICAL ATTITUDE SENSORS

TYPE	SENSED	ACCURACY (RMS deg)	
		Present	Future
Solar	any plane	0.1	0.01
Planet	any plane	0.2	0.01
Stellar	any plane	1	0.01
Horizon	local vertical	0.2-0.5	0.1
Rate Gyro	rate of deviation from any plane	0.2/hr	0.001/hr

V-4 HARDWARE DESIGN

Hardware implementation of the block diagram of Figure V-4-1 illustrates the essentials of a cold gas system. The operation of this idealized control system is as follows: There are three sets of controls, one for each axis (pitch, yaw, roll). In each of the three controls, the desired attitude is either set in a gyro before flight, acquired by a sensing device, or telemetered from an outboard master control. This desired attitude may be constant, or may vary according to a preset program. In the latter case, the desired attitude may require a combination of a memory device and a timed cam-operated read-off mechanism.

The current attitude signal is fed back to a synthesizer which computes attitude error θ. Usually the attitude error is differentiated to give rate of change of attitude $\dot{\theta}$. Finally, the signal $\theta + K\dot{\theta}$ is relayed to a switch. (K is a positive number, typically 0.1 sec). If this signal exceeds a threshold value $\pm\epsilon$, it activates a switch for right (if positive) or left (if negative) rudder.

In this case a "rudder" is a pair of reaction jets which produces a torque. Activation of the right rudder switch automatically inactivates the left rudder switch, and vice versa. However, complications can occur because of delayed response on the one hand, and difference between the pull-in- and release-voltage (both nominally $+\epsilon$) on the other hand (see Table V-4-1). These complications can even cause the switch to chatter. On-off periods, levels of thrust, and the natural oscillation period about an axis must be closely matched in order to minimize nutations.

The number of on-off cycles contemplated has some influence on the choice of the fuel. Because of its high reliability, a cold gas system has been preferred when the expected number of on-off cycles is large (>1000).

Table V-4-1

TIME DELAYS IN GAS ATTITUDE-CONTROL SYSTEMS
(Ref. 3)

SYSTEM TYPE	THRUST PER JET	TIME DELAY
Cold gas-high thrust jet	20 lb	5-10 milliseconds
Cold gas-low thrust jet	5 lb	<5-10 milliseconds
Hot gas-hydrogen peroxide (high thrust)	44 lb	no thrust for 48 msec; then decreasing substantially, and returning to full thrust 108 msec after valves are activated.

V-5 ATTITUDE CONTROL THEORY REFERENCES

1. Olds, R. H., *AIAA J.*, **1**, 852 (1963).
2. White, J. B., *ARS J.*, **31**, 75 (1961).
3. Traynelis, K. A., and Ryan, D. L., *Control Eng.*, **8**, 109 (1961).

VI-0 LIST OF TABLES

Section-Table	Title	Section-Part-Page
VI-1	Values of Functions of the Specific Heat Ratio, k	VI-4.5
VI-2	Values of the Function $\left[1-\left(\frac{p_e}{p_i}\right)^{\frac{k-1}{k}}\right]$	VI-4.6
VI-3	Values of the Function $\sqrt{1-\left(\frac{p_e}{p_i}\right)^{\frac{k-1}{k}}}$	VI-4.7
VI-4	Summary of Computations for Performance of Nozzles with Water Vapor	VI-4.8

VI NOZZLE PERFORMANCE

Table of Contents

Section-Part	Title	Section-Part.Page
VI-0	List of Tables	VI-0.2
VI-0	List of Figures	VI-0.3
VI-1	Introduction	VI-1.1
VI-2	Nozzle Design Parameters	VI-2.1
VI-3	Computation of Specific Impulse of Noncondensing Gases . . .	VI-3.1
VI-4	Performance of Nozzles with Condensing Fluids	VI-4.1
VI-A	*APPENDIX*--Summary of Equations for Nozzle Performance Calculations	VI-A.1

~~PRECEDING PAGE BLANK NOT FILMED~~

VI-0 LIST OF FIGURES

Section-Figure	Title
VI-1	Values of Functions of Specific Heat Ratio, k $\left(\frac{k-1}{k} \text{ and } \sqrt{\frac{2gk}{g(k-1)}}\right)$
VI-2	Values of the Functions of Specific Heat Ratio, k $\left(\frac{k}{k-1} \text{ and } \sqrt{\frac{k}{k-1}}\right)$
VI-3 (a,b)	Values of the Function $\eta = \left[1 - \left(\frac{P_e}{P_i}\right)^{\frac{k-1}{k}}\right]$
VI-4 (a,b)	Values of the Function $\sqrt{\eta} = \sqrt{1 - \left(\frac{P_e}{P_i}\right)^{\frac{k-1}{k}}}$
VI-5	Value of $\left(\frac{P_{exit}}{P_{inlet}}\right)^{\frac{k-1}{k}}$; Pressure Ratio = 1-100.
VI-6	Value of $\left(\frac{P_{exit}}{P_{inlet}}\right)^{\frac{k-1}{k}}$; Pressure Ratio = $10-10^6$.
VI-7	Calculated Performance of Saturated Water Vapor

VI-1 INTRODUCTION

The optimization of a pressurized gas system which is to be used in conjunction with attitude-control systems may involve calculation of the efficiency of performance of working fluids and an evaluation of nozzle design parameters.

The gases which are generally used as working fluids for pressurization or in attitude-control systems are employed at temperatures greatly in excess of their saturation or critical temperatures, and are seldom expanded to the point where they are cooled sufficiently to cause condensation; these gases will be referred to as "noncondensing" gases in this section of the Handbook. On the other hand, certain working fluids may be used which are expanded in operating cycles to the point where condensation occurs; these gases will be referred to as "condensing" gases.

Computation of nozzle performances with noncondensing working fluids is outlined in this section and details of the computations of nozzle performance with a condensing gas (water vapor) are presented.

VI-2 NOZZLE DESIGN PARAMETERS

The designs of cold-gas attitude-control nozzles is based on the general principles of design of nozzles for use in rockets. The major difference is, of course, that the cold-gas attitude-control nozzles are very small and, consequently, little effort is made to control the exact shape of the exit bell or the throat A characteristic design for cold-gas attitude-control nozzles is given in the sketch below:

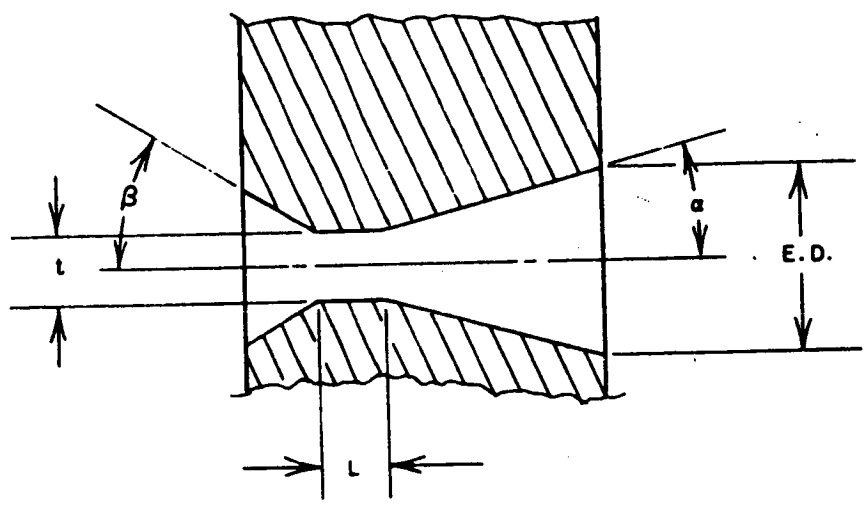

α = nozzle cone divergence half-angle

β = nozzle cone convergence half-angle

t = throat diameter

E.D. = exit diameter

L = throat length.

The throat diameter of a cold-gas nozzle may be as small as 0.006 inch, but generally is of the order of 0.025 inch for vernier controls. The length of the throat section, L, generally is 1 to 4 throat diameters; the longer throats are relatively difficult to produce with smooth bores. Discontinuities in the contour of the throat wall may cause shock waves and thus reduce nozzle performance.

The convergence half-angle, β, is not very critical and is usually 15 to 30 degrees. On the other hand, the divergence half-angle, of the nozzle is important in that it affects the energy recovery from the exhaust. Highly divergent exhausts have large radial velocity components which are not useful in producing thrust. Correction for the nonaxial component of the gas velocity factor can be made with the aid of the following table:

NOZZLE ANGLE CORRECTION FACTOR

HALF-ANGLE, DEGREES	CORRECTION FACTOR
0	1.0000
2	0.9997
4	0.9988
6	0.9972
8	0.9951
10	0.9924
12	0.9890
14	0.9851
16	0.9806
18	0.9755
20	0.9698
22	0.9636
24	0.9567

Thus, for a rocket nozzle with a divergence half-angle of 20°, the exhaust velocity would be 96.98% of the theoretical exit velocity. It is of interest to note that the theoretical computation of nozzle performance is based on the spherical area obtained from the assumption of radial flow in the expansion cone and not on the plane area in the exit cone normal to the axis; however, this error is quite small.*

Most nozzles for cold-gas attitude-control systems are relatively short in length and seldom offer expansion ratios of more than 100, that is, the area of the throat is seldom less than 1% of the area of the exit plane. As a result, because of their operation in space, the nozzles are always *underexpanding* and they discharge working fluid at a pressure greater than the external or ambient pressure.

Nozzles for cold-gas attitude-control systems are usually constructed of metals and very little attention is given to selection of material because there is no need to provide great strength or resistance to high temperatures as for rocket nozzles. Little effort is made to fabricate nozzles of minimum weight.

* Landsbaum, Ellis M., *ARS J.*, **29**, 212 (1959).

VI-3 COMPUTATION OF SPECIFIC IMPULSE OF NONCONDENSING GASES

The method for the computation of the specific impulse of "noncondensing" gases is based on the consideration of the working fluid as an ideal gas and is patterned after the usual methods for computing the performance of rocket nozzles.

Theoretical Specific Impulse

The computation of the theoretical specific impulse of a working fluid gas flowing through a properly-shaped and constructed nozzle is based on the following assumptions:

(a) The working fluid is a perfect gas and obeys the ideal gas laws; condensation does not occur in the nozzle.

(b) The working fluid is a singular substance undergoing no decomposition or dissociation.

(c) Flow through the nozzle is adiabatic; there is no heat transfer to the nozzle wall.

(d) The flow of the working fluid through the nozzle is constant.

(e) The velocity of the working fluid is uniform across any section normal to the axis of the nozzle.

(f) The flow of the exhaust fluid has an axially-directed velocity.

(g) There is no resistance to the flow of fluid at any point within the nozzle.

The noncondensing gases generally used for working fluids for pressurization or in attitude-control systems are operating at relatively low pressures and at temperatures well above saturation and thus follow the perfect gas laws close enough to permit evaluation of their performance in nozzles by the classical treatment of adiabatic ideal gases. A summary of the important relationships between nozzle performance and the thermodynamics of ideal gases is presented as an Appendix to this section. The specific impulse obtainable from a working fluid is given by the relation:

$$I_s = \sqrt{\frac{2R'k}{g(k-1)}\frac{T_i}{M}\left[1-\left(\frac{P_e}{P_i}\right)^{(k-1)/k}\right]} + \left(\frac{P_e - P_a}{\dot{W}}\right)A_e \qquad (13^*)$$

where

R' = universal gas constant (1545.2 ft-lb/R°/lb-mole)

k = specific heat ratio

T_i = temperature of the working fluid at the inlet, R°

M = molecular weight of the working fluid,

P_e = pressure of the working fluid at the nozzle exit plane

P_i = pressure of the working fluid at the inlet

P_a = ambient pressure into which the nozzle exhausts

A_e = area of the exhaust jet

$\dot{W}$ = flow rate of the working fluid.

When the pressure in the exit plane of the nozzle is equal to the ambient pressure, the second term in the above equation becomes 0 and the expression for the specific impulse is independent of flow rate; therefore, the expression permits computation of the optimum impulse:

$$\text{optimum } I_s = \sqrt{\frac{2R'k}{g(k-1)}\frac{T_i}{M}\left[1-\left(\frac{P_e}{P_i}\right)\right]^{(k-1)/k}} = \sqrt{\frac{2R'k}{g(k-1)}}\sqrt{\eta}\sqrt{\frac{T_i}{M}} \qquad (12)$$

where η is the *ideal cycle* efficiency of an engine operating between the pressure P_e and P_i. As the exit pressure approaches 0, the cycle efficiency approaches 1, and the maximum specific impulse obtainable from a working fluid is given by the expression:

$$\text{max. } I_s = \sqrt{\frac{2R'k}{g(k-1)}}\sqrt{\frac{T_i}{M}}$$

Computation of the theoretical optimum impulse and the maximum theoretical impulse for a noncondensing working fluid is a simple matter with the aid of tables and graphs for the square root of the ideal cycle efficiency and other functions of the specific heat ratio (see Tables VI-1

* The equation numbers refer to the numerical sequence in the Appendix.

ORIGINAL PAGE IS
OF POOR QUALITY

to VI-3 and Figures VI-1 to VI-6). The temperature of the exhaust working fluid is computed from the relation for isentropic flow:

$$T_e = T_i \left(\frac{P_e}{P_i} \right)^{(k-1)/k} \tag{24}$$

As was indicated before, most working fluids do not condense during expansion through nozzles; however, the above equation should be used to compute the exit temperature and assist in selection of an expansion ratio which will prevent occurrence of condensation. If condensation occurs, the computation of impulse by any of the above equations is invalid.

Actual Specific Impulse

The estimation of the actual specific impulse provided by a working fluid in small attitude-control nozzles is severely influenced by the design and construction of the nozzle and gas supply system and only relatively minorly influenced by deviation of the working fluid from an ideal gas. The following factors largely determine the actual specific impulse obtainable from attitude-control nozzles:

(a) The smoothness of the nozzle throat and bell. Resistance to flow and the formation of shock waves from discontinuities may lead to losses in performance.

(b) Underexpanding nozzles. Loss due to underexpansion can be computed from the thrust coefficient [Equation (19) in the Appendix]. Losses computed in this way generally are in accurate agreement with observed results.

(c) Nozzle exit angle. In order to achieve large expansion ratios in short distances, nozzle exit angles generally are greater than 20° (half-angle). Correction of the theoretical exit velocity by use of nozzle angle correction factors permits estimation of loss in performance with a fairly high degree of accuracy.

(d) Specific heat ratios. The values for the specific heat ratios of many of the gases used as working fluids in cold-gas attitude-control systems are quite constant at high temperatures and pressures. However, at the temperatures and pressures commonly encountered in attitude-control systems, specific heat ratios of fluids may change considerably during flow through a nozzle.

The effect of shifting specific heat ratios may be estimated by computing performances with an iterative process in which a preliminary estimation of the exit temperature and pressure is used to approximate the final specific heat ratio and then using an average of the initial and final specific heat ratios in successive computations.* Graphs showing the value of specific heat ratios as a function of temperature and pressure are given for various working fluids in Section XV.

(e) Heat transfer. The working fluid may gain or lose heat in the inlet section between the control valve and the nozzle throat; additional heat transfer may occur in the bell of the nozzle itself. This exchange of heat may lead to deviation from computed performances, especially when the inlet section is much colder than the entering working fluid. It is exceedingly difficult, if at all possible, to estimate changes in expected performance when heat exchange is possible, and especially for the occasional pulses of short duration characteristic of attitude-control systems. It should be recognized that evaluations of nozzle performances in the laboratory are generally performed under the steady-state conditions obtained when all working parts have achieved equilibrium temperatures; thus, the results of these tests are not indicative of the actual performance obtained during occasional short-duration operation periods.

* Iberall, A. S., *J. Appl. Phys.*, **19**, 997 (1948).

VI-4 PERFORMANCE OF NOZZLES WITH CONDENSING FLUIDS

The performance of nozzles with condensing fluids cannot be calculated with the same formulas that are used for "noncondensing" fluids. Condensation releases the latent heat of vaporization (or sublimation) and thus tends to relieve adiabatic cooling effects; the additional heat also provides more energy for thrust than is available from the expansion of "noncondensing" working fluids.

The theoretical maximum impulse obtained from condensing working fluids may be computed by the following formula:

$$I_{sp} = 6.954 \sqrt{\Delta h}$$

where Δh is the enthalpy change in Btu per lb undergone by the fluid in its reversible expansion through the nozzle. When the working fluid is a saturated vapor in equilibrium with its condensed phase, condensation occurs immediately as the vapor expands; the thrust obtained from expansion through a nozzle will be a maximum if equilibrium between the phases can be maintained at all times.

At any instance during an expansion, conservation of mass requires

$$M_c + M_v = M_i$$

where the subscript c refers to the mass of the condensed phase, v the mass of the vapor phase, and i the mass of the original volume of vapor undergoing expansion. Similarly, conservation of energy requires

$$M_c h_c + M_v h_v = M_i h_i - \Delta(pv)$$

where h is the total enthalpy (over absolute zero) per unit mass of the respective phases and $\Delta(pv)$ is the work done by the system.

Consider one pound of saturated vapor entering the throat section of a nozzle at P_i = initial pressure in atmospheres, T_i = initial saturation temperature in Rankine degrees, V_i = initial volume in ft^3/lb (specific

volume), and h_i = initial total enthalpy in Btu/lb. After expansion to a new volume in the nozzle, the remaining vapor will occupy the new volume at equilibrium with the condensed phase; the following equation relates the temperature, the total enthalpy of the system, and the specific volume of the vapor:

$$\frac{V_f}{V_{spv}^{T_f}} h_v^{T_f} + \left(1 - \frac{V_f}{V_{spv}^{T_f}}\right) h_c^{T_f} = h_i - \Delta(PV)$$

where V_f = final volume, and $V_{spv}^{T_f}$ = specific volume of the vapor at the final temperature. (It is assumed that the volume of the condensed phase is negligible in comparison to the volume of the vapor phase.)

The specific volume of the vapor at large expansions may be computed from ideal gas relationships (actual values of specific volumes seldom are available at low temperatures and low pressures); consequently,

$$V_{spv} = \frac{0.7302}{M} \frac{T_f}{P_f}$$

where T_f is the final temperature, P_f is the final pressure in atmospheres, and M is the molecular weight of the gas.

The work expended by an expanding *undersaturated* working fluid is obtained by consideration of the cycle in the following figure:

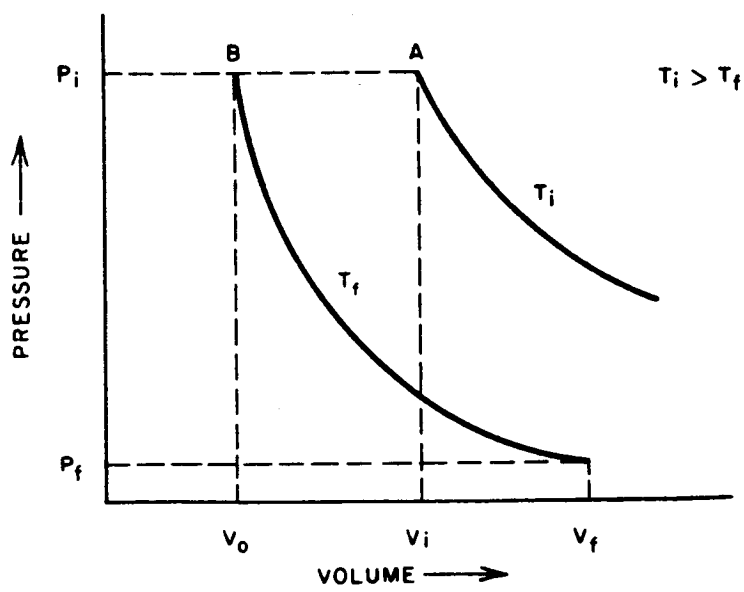

Starting at point A with the fluid at temperature T_i and pressure P_i at the initial volume V_i, reduce the temperature to T_f at constant P_i. The work done on the fluid is the area ABV_oV_i and is equal to $P_i(V_i - V_o)$ for an ideal gas. The work expended during isothermal expansion of the fluid from point $B(P_i, T_f, V_o)$ to the final conditions, P_f, V_f, T_f is the area under the T_f curve between V_o and V_f; for an ideal gas the work for one mole is: $RT_f \ ln \ V_f/V_o$. Hence, the net work is

$$\Delta(PV) = RT_f \ ln \frac{V_f}{V_o} - P_iV_i + P_iV_o$$

For an ideal gas at constant pressure, $V_o = V_iT_f/T_i$, and the net work is given by the expression,

$$\Delta(PV) = P_iV_i\left(\frac{T_f}{T_i} - 1\right) + RT \ ln \frac{V_fT_i}{V_iT_f}$$

Thus, the maximum work available from an initial mass of one pound of working fluid at T_i and P_i (equal to saturation temperature and pressure, respectively) which has a volume V_i and a total enthalpy of h_i, and is expanded reversibly to V_f final volume is:

$$\max \Delta(PV) = 2.7203 \ P_iV_i\left(\frac{T_f}{T_i} - 1\right) + \frac{X}{M}(2.303)(1.9869) \ T_f \ \log \frac{V_fT_i}{V_iT_f}$$

where X is the weight (pounds) of vapor in the final volume (ft^3), P_i is the initial pressure in atmospheres, T_f is the final temperature ($^\circ R$), and $\Delta(PV)$ is in Btu's. Introducing the above expression for maximum work in the earlier expression relating the distribution of total enthalpy, and recognizing that the weight of the vapor (X) in the final volume is $V_f/V_{spv}^{T_f}$, the conditions at any point downstream of the throat must fulfill the equation:

$$X h_v^{T_f} + (1 - X) \ h_c^{T_f} = h_i - \left[2.7203 \ P_iV_i\left(\frac{T_f}{T_i} - 1\right) + 4.5758 \frac{X}{M} T_f \ \log \frac{V_fT_i}{V_iT_f}\right]$$

Solution of this equation is simplified by use of tables or graphs of total enthalpies and specific volumes versus temperature. An estimate of the final temperature is made, and then the left-hand and right-hand members of the above equation are computed for two temperatures in the vicinity of the estimated final temperature. The values for each member of the equation are straight-line functions over narrow temperature ranges (several degrees); hence, the intersection of the plotted line of the left-hand member with the plotted line of the right-hand member closely represents the actual final temperature, and the corresponding work term of the right-hand member is used to compute the maximum specific impulse $[I_{sp} = 6.954 \sqrt{\Delta(PV)}]$.

Specific impulse values computed in this way are based on the following assumptions:

(a) The unsaturated working fluid performs as an ideal gas at low pressures and temperatures.

(b) The condensed and uncondensed phases are at all times in reversible equilibrium.

(c) The condensed phase is of such a small particle size that its axial velocity in the nozzle is at all times equal to the velocity of the uncondensed phase.

(d) The enthalpy difference between the total enthalpy available in the throat section and the vapor at the nozzle exit plane is completely available for production of thrust.

(e) The condensed phase is a negligible fraction of the uncondensed phase.

(f) There is no heat transfer to the nozzle.

A summary of computations for the performance of water vapor is given in Table VI-4 and Figure VI-5. It is interesting to note that there is very little difference in specific impulse when supercooled water is formed as the condensed phase rather than ice. Moreover, variations in the initial temperature and pressure do not influence performance significantly, especially at the relatively low expansion ratios usually available in attitude-control nozzles. This is due to the fact that L_e, the latent heat of vaporization of water is so large that dL_e/dT is a relatively small number.

Table VI-1

VALUES OF FUNCTIONS OF THE SPECIFIC HEAT RATIO, K

(g = 32.1740 ft/sec^2; R = 1545.0 ft-lb/°R/mole)

K	$\frac{K-1}{K}$	$\frac{K}{K-1}$	$\sqrt{\frac{K}{K-1}}$	$\sqrt{\frac{2gK}{K-1}}$	$\sqrt{\frac{2RK}{g(K-1)}}$	$\left(\frac{2}{K+1}\right)^{K/K-1}$	$K\sqrt{\left(\frac{2}{K+1}\right)^{K+1/K-1}}$
1.10	0.0909	11.000	3.317	26.608	32.51	0.5846	0.6590
1.11	0.0991	10.091	3.177	25.485	31.14	0.5826	0.6642
1.12	0.1071	9.333	3.055	24.506	29.94	0.5806	0.6694
1.13	0.1150	8.692	2.948	23.648	28.89	0.5787	0.6748
1.14	0.1228	8.143	2.854	22.894	28.80	0.5763	0.6798
1.15	0.1304	7.667	2.769	22.212	27.14	0.5744	0.6848
1.16	0.1379	7.250	2.699	21.651	26.45	0.5723	0.6900
1.17	0.1452	6.882	2.623	21.041	25.71	0.5704	0.6951
1.18	0.1525	6.556	2.560	20.536	25.09	0.5683	0.7002
1.19	0.1597	6.263	2.506	20.102	24.56	0.5665	0.7054
1.20	0.1667	6.000	2.450	19.653	24.01	0.5645	0.7104
1.21	0.1736	5.762	2.400	19.252	23.52	0.5626	0.7155
1.22	0.1803	5.545	2.355	18.891	23.08	0.5606	0.7207
1.23	0.1870	5.348	2.312	18.546	22.66	0.5587	0.7256
1.24	0.1936	5.167	2.273	18.233	22.28	0.5567	0.7306
1.25	0.2000	5.000	2.236	17.937	21.91	0.5549	0.7356
1.26	0.2064	4.846	2.201	17.656	21.57	0.5530	0.7408
1.27	0.2126	4.704	2.169	17.399	21.26	0.5512	0.7457
1.28	0.2188	4.571	2.138	17.150	20.95	0.5494	0.7507
1.29	0.2248	4.448	2.109	16.918	20.67	0.5475	0.7558
1.30	0.2308	4.333	2.082	16.701	20.40	0.5457	0.7608
1.31	0.2366	4.226	2.055	16.485	20.14	0.5439	0.7658
1.32	0.2424	4.125	2.031	16.292	19.90	0.5422	0.7707
1.33	0.2481	4.030	2.008	16.108	19.68	0.5404	0.7758
1.34	0.2537	3.941	1.985	15.923	19.45	0.5386	0.7807
1.35	0.2593	3.857	1.964	15.755	19.25	0.5368	0.7856
1.36	0.2647	3.778	1.944	15.594	19.05	0.5351	0.7906
1.37	0.2701	3.703	1.924	15.434	18.85	0.5334	0.7954
1.38	0.2754	3.632	1.906	15.289	18.68	0.5316	0.8004
1.39	0.2806	3.564	1.888	15.145	18.50	0.5300	0.8054
1.40	0.2857	3.500	1.871	15.009	18.36	0.5282	0.8102
1.41	0.2908	3.439	1.855	14.880	18.18	0.5266	0.8151
1.42	0.2958	3.381	1.839	14.752	18.02	0.5250	0.8199
1.43	0.3007	3.326	1.824	14.632	17.88	0.5232	0.8248
1.44	0.3056	3.273	1.809	14.511	17.73	0.5216	0.8297
1.45	0.3103	3.222	1.795	14.399	17.59	0.5202	0.8348
1.46	0.3151	3.174	1.782	14.295	17.46	0.5184	0.8394
1.47	0.3197	3.128	1.769	14.190	17.34	0.5167	0.8442
1.48	0.3243	3.083	1.756	14.086	17.21	0.5152	0.8491
1.49	0.3289	3.041	1.744	13.990	17.09	0.5135	0.8538
1.50	0.3333	3.000	1.732	13.894	16.97	0.5120	0.8586
1.51	0.3377	2.961	1.721	13.805	16.87	0.5104	0.8634
1.52	0.3421	2.923	1.710	13.717	16.76	0.5089	0.8682
1.53	0.3464	2.887	1.699	13.629	16.65	0.5073	0.8729
1.54	0.3506	2.852	1.689	13.549	16.55	0.5057	0.8778
1.55	0.3548	2.818	1.679	13.468	16.45	0.5042	0.8826
1.56	0.3590	2.786	1.669	13.388	16.36	0.5026	0.8873
1.57	0.3630	2.754	1.660	13.316	16.27	0.5013	0.8919
1.58	0.3670	2.724	1.651	13.244	16.18	0.4997	0.8968
1.59	0.3710	2.695	1.642	13.172	16.09	0.4982	0.9015
1.60	0.3750	2.667	1.633	13.099	16.00	0.4973	0.9062
1.61	0.3789	2.639	1.625	13.035	15.92	0.4953	0.9109
1.62	0.3826	2.613	1.616	12.963	15.84	0.4939	0.9156
1.63	0.3865	2.587	1.608	12.899	15.76	0.4924	0.9203
1.64	0.3903	2.562	1.600	12.835	15.68	0.4910	0.9250
1.65	0.3940	2.538	1.593	12.786	15.61	0.4894	0.9294
1.66	0.3976	2.515	1.586	12.722	15.54	0.4881	0.9344
1.67	0.4013	2.492	1.579	12.666	15.47	0.4867	0.9390
1.68	0.4048	2.470	1.572	12.610	15.40	0.4853	0.9437
1.69	0.4083	2.449	1.565	12.554	15.34	0.4839	0.9483
1.70	0.4119	2.428	1.558	12.498	15.27	0.4825	0.9530

Table VI-2

VALUE OF THE FUNCTION $\left[1-\left(\frac{P_e}{P_i}\right)^{\frac{k-1}{k}}\right]$

$\frac{P_i}{P_e}$	k												
	1.10	1.15	1.20	1.25	1.30	1.35	1.40	1.45	1.50	1.55	1.60	1.65	1.70
1													
5	0.136	0.189	0.235	0.275	0.310	0.341	0.369	0.393	0.415	0.435	0.453	0.470	0.485
10	0.189	0.260	0.319	0.369	0.412	0.450	0.482	0.511	0.536	0.558	0.578	0.596	0.612
50	0.299	0.400	0.479	0.542	0.595	0.637	0.673	0.703	0.729	0.750	0.769	0.785	0.800
100	0.342	0.452	0.536	0.602	0,655	0.697	0.732	0.760	0.785	0.805	0.822	0.836	0.850
500	0.432	0.555	0.645	0.711	0.762	0.801	0.830	0.854	0.874	0.890	0.903	0.914	0.923
1 000	0.466	0.594	0.684	0.749	0.787	0.833	0.861	0.883	0.900	0.914	0.925	0.934	0.942
5 000	0.539	0.671	0.785	0.818	0.860	0.890	0.912	0.929	0.942	0.951	0.959	0.965	0.970
10 000	0.567	0.699	0.785	0.842	0.880	0.908	0.928	0.943	0.954	0.962	0.968	0.973	0.978
50 000	0.626	0.756	0.835	0.885	0.918	0.939	0.955	0.965	0.973	0.979	0.983	0.987	0.988
100 000	0.649	0.777	0.853	0.900	0.930	0.950	0.963	0.972	0.979	0.983	0.987	0.989	0.991
500 000	0.697	0.819	0.888	0.928	0.951	0.967	0.977	0.983	0.987	0.990	0.992	0.994	0.996
1 000 000	0.715	0.835	0.900	0.937	0.959	0.972	0.981	0.986	0.990	0.993	0.994	0.996	0.997

Table VI-3

VALUE OF THE FUNCTION $\sqrt{1 - \left(\frac{P_e}{P_i}\right)^{\frac{k-1}{k}}}$

$\frac{P_i}{P_e}$	k												
	1.10	1.15	1.20	1.25	1.30	1.35	1.40	1.45	1.50	1.55	1.60	1.65	1.70
1													
5	0.369	0.435	0.485	0.524	0.557	0.584	0.607	0.627	0.644	0.660	0.673	0.686	0.696
10	0.435	0.510	0.565	0.607	0.642	0.671	0.694	0.715	0.732	0.747	0.760	0.772	0.782
50	0.547	0.632	0.692	0.736	0.771	0.798	0.820	0.838	0.854	0.866	0.877	0.886	0.894
100	0.585	0.672	0.732	0.776	0.809	0.835	0.856	0.872	0.886	0.897	0.907	0.914	0.922
500	0.657	0.745	0.803	0.843	0.873	0.895	0.911	0.924	0.935	0.943	0.950	0.956	0.961
1 000	0.683	0.771	0.827	0.866	0.893	0.913	0.928	0.940	0.949	0.956	0.962	0.966	0.971
5 000	0.734	0.819	0.871	0.904	0.928	0.943	0.955	0.964	0.971	0.975	0.979	0.982	0.985
10 000	0.753	0.836	0.886	0.918	0.938	0.953	0.963	0.971	0.977	0.981	0.984	0.987	0.989
50 000	0.791	0.870	0.914	0.941	0.958	0.969	0.977	0.982	0.987	0.989	0.991	0.994	0.994
100 000	0.806	0.881	0.924	0.949	0.965	0.975	0.981	0.986	0.989	0.991	0.993	0.995	0.996
500 000	0.835	0.905	0.942	0.963	0.975	0.983	0.989	0.991	0.994	0.995	0.996	0.997	0.998
1 000 000	0.846	0.914	0.949	0.968	0.979	0.986	0.990	0.993	0.995	0.996	0.997	0.998	0.998

Table VI-4

SUMMARY OF COMPUTATIONS FOR PERFORMANCE OF NOZZLES WITH WATER VAPOR

EXPANSION RATIO	$^{o}R_{exit}$	% CONDENSED	CONDENSED PHASE	P_{exit}, atm	ENTHALPY DIFFERENCE	SPECIFIC IMPULSE
Saturated water vapor at 585°R (about 52°C) P_{sat} = 0.13329 atm. Specific volume = V_i = 177.78 ft^3/lb h_i = 1389.7 btu/lb						
2	558.3	2.8	water	0.062	41.4	44.7
5	527.2	6.1	water	0.0227	87.2	65.0
10	506.4	7.8	water	0.0111	117.3	75.0
20	487.9	9.4	water	0.00507	144.3	83.5
20	488.2	8.3	ice	0.00513	146.1	84.1
40	472.4	11.0	water	0.00241	168.7	90.3
40	472.6	10.2	ice	0.00242	170.6	90.8
100	453.5	12.4	water	0.00091	198.4	98.0
100	453.8	11.2	ice	0.00092	201.5	98.7
1 000	412.3	16.2	water	0.00008	256.9	111.5
1 000	412.4	15.3	ice	0.00008	260.1	112.2
10 000	378.4	14.1	ice	0.000007	307.2	121.8
Saturated water vapor at 530°R (about 21°C) P_{sat} = 0.02497 Specific volume = V_i = 859.69 ft^3/lb h_i = 1365.7 btu/lb						
2	508.8	2.6	water	0.0117	37.3	42.5
5	484.4	5.6	water	0.00431	80.7	62.5
5	484.7	4.3	ice	0.00436	81.9	62.9
40	441.4	11.4	water	0.00046	158.4	87.5
40	441.7	10.0	ice	0.00047	160.0	88.0
100	424.9	12.7	water	0.00018	186.0	94.8
100	425.0	11.8	ice	0.00018	188.0	95.4
1 000	391.9	12.3	ice	0.00002	256.6	109.6
10 000	358.4	18.3	ice	0.000001	291.1	118.7

VI-A *APPENDIX*

SUMMARY OF EQUATIONS FOR NOZZLE PERFORMANCE CALCULATIONS

Specific Impulse is defined as the thrust obtained from unity flow rate of propellant, *i.e.*,

$$I_s = \frac{F}{\dot{W}} = \frac{C}{g} \tag{1}$$

where C is the effective exhaust velocity, g is the gravitational constant, $\dot{W}$ is the weight flow rate of the propellants, and F is the thrust.

Total Impulse is the integral of the thrust, F, over the duration of operation, t:

$$I_t = \int_0^t F dt = \int_0^t I_s \dot{W} dt \tag{2}$$

Effective Exhaust Velocity

$$C = \frac{Fg}{\dot{W}} = V_2 + \frac{(P_2 - P_3)A_e g}{\dot{W}} \tag{3}$$

where

A_e = exhaust jet area

P_2 = exhaust jet pressure

P_3 = pressure behind exhaust jet

V_2 = exhaust velocity

Nozzle Exhaust Velocity

$$V_2 = \sqrt{\frac{2gk}{k-1}\frac{R'T_1}{M}\left[1 - \left(\frac{P_2}{P_1}\right)^{\frac{k-1}{k}}\right]} + V_1 \tag{4}$$

where

subscripts 1 are inlet conditions,

subscripts 2 are outlet conditions,

$k = c_p/c_v$,

M = molecular weight,

R' = universal gas constant = 1545.2 ft-lb per °R-lb-mole

Generally $V_2 >> V_1$, and hence V_1 can be neglected. T_1 is the nozzle inlet temperature, and for isentropic flow is also equal to the stagnation temperature. At infinite pressure ratio, *i.e.*, when the nozzle exhausts into a vacuum,

$$V_2 = \sqrt{\frac{2gk}{k-1}\frac{R'T_0}{M}} \tag{5}$$

where

T_0 is the stagnation temperature.

From equations (1) and (3), the external force or thrust exerted by a nozzle is given by

$$F = \frac{\dot{W}}{g} V_2 + (P_e - P_a)A_e \tag{6}$$

where

P_a is the ambient pressure.

P_e is the exit pressure

A_e is the exhaust jet area.

But, the nozzle exhaust velocity is:

$$V = \sqrt{\frac{2gk}{k-1}\frac{R'T_i}{M}\left[1-\left(\frac{P_e}{P_i}\right)^{\frac{k-1}{k}}\right]} + V_i \tag{7}$$

where the i subscripts refer to inlet conditions.

Hence,

$$F = \frac{\dot{W}}{g}\sqrt{\frac{2gk}{k-1}\frac{R'T_i}{M}\left[1-\left(\frac{P_e}{P_i}\right)^{\frac{k-1}{k}}\right]} + V_i + (P_e - P_a)A_e \qquad (8)$$

where V_i can be ignored because it is much less than the exhaust veolcity.

Now, in order to carry a minimum of fuel weight, the thrust must be maximized. Thus, since P_i can easily be fixed (as also T_i), only A_e and P_e need be considered. We need find conditions for which

$$\left(\frac{\partial F}{\partial A_e}\right)_{P_e} = P_e - P_a = 0$$

and

$$\left(\frac{\partial F}{\partial P_e}\right)_{A_e} = 0 \quad .$$

From the first, the equation is maximized when $P_e = P_a$ and $P_e \neq 0$; from the second,

$$\left(\frac{\partial F}{\partial P_e}\right)_{A_e} = -\frac{\dot{W}}{2g}\left[\frac{\frac{k-1}{k}\left(\frac{2gk}{k-1}\frac{R'T_i}{M}\right)P_e^{\frac{k-1}{k}-1}}{\sqrt{\frac{2gk}{k-1}\frac{R'T_i}{M}\left[1-\left(\frac{P_e}{P_i}\right)^{\frac{k-1}{k}}\right]}\,P_i^{\frac{k-1}{k}}}\right] + A_e$$

$$= A_e - \dot{W}\left[\frac{R'T_i}{M\sqrt{\frac{2gk}{k-1}\frac{R'T_i}{M}\left[1-\left(\frac{P_e}{P_i}\right)^{\frac{k-1}{k}}\right]}}\right]\frac{P_e^{-\frac{1}{k}}}{P_i^{\frac{k-1}{k}}}$$

$$= A_e - \left[\frac{\dot{W}R'T_i}{M\sqrt{\frac{2gk}{k-1}\frac{R'T_i}{M}\left[1-\left(\frac{P_e}{P_i}\right)^{\frac{k-1}{k}}\right]}}\right]\frac{P_e^{-\frac{1}{k}}}{P_i^{\frac{k-1}{k}}} \qquad (9)$$

In other words, for $(\partial F/\partial P_e)_{A_e} = 0$, it is necessary for A_e to be equal to the right term; alternatively, there exists for each A_e an unique P_e for which the thrust is maximum. Since calculations with random selections of P_e are unwieldy, it is preferable to select the first condition, *i.e.*,,

$$\left(\frac{\partial F}{\partial A_e}\right)_{P_e} = 0$$

and the equation is:

$$F_{\text{optimum}} = \frac{\dot{W}}{g}\sqrt{\frac{2gk}{k-1}\,\frac{R'T_i}{M}}\sqrt{1-\left(\frac{P_e}{P_i}\right)^{\frac{k-1}{k}}} \tag{10}$$

This equation can be rewritten as:

$$F_{\text{optimum}} = \sqrt{\frac{2gk}{k-1}\,\frac{R'T_i}{M}}\left[\left(\frac{\dot{W}}{g}\right)\eta^{1/2}\right] \tag{11}$$

where η is the *ideal cycle* efficiency of an engine operating between the pressures P_e and P_i.

In view of equations (1) and (11), the optimum impulse is

$$\text{optimum } I_s = \sqrt{\frac{2R'k}{g(k-1)}\,\frac{T_i}{M}}\left(\eta^{1/2}\right) \tag{12}$$

where $\eta^{1/2} \to 1$ when $P_e \to 0$.

The equation for the actual impulse, however, is found by combining equation (1) with equation (8):

$$I_s = \sqrt{\frac{2\,k}{k-1}\,\frac{R'T_i}{gM}\left[1-\left(\frac{P_e}{P_i}\right)^{\frac{k-1}{k}}\right]} + \left(\frac{P_e - P_a}{\dot{W}}\right)A_e$$

$$= \sqrt{\frac{2R'k}{g(k-1)}\,\frac{T_i}{M}}\,(\eta^{1/2}) + \left(\frac{P_e - P_a}{\dot{W}}\right)A_e \tag{13}$$

Returning to equation (8) and introducing the expressions for critical velocity or throat velocity [equation (29)]

$$V_{tc} = \sqrt{\frac{2gk}{k+1}\frac{R'T_1}{M}} \tag{14}$$

specific volume,

$$v_{tc} = v_1\left(\frac{k+1}{2}\right)^{\frac{1}{k-1}} \tag{15}$$

weight flow in the critical section, equation (30),

$$\dot{W} = \frac{A_t V_{tc}}{v_{tc}} \tag{16}$$

and the perfect gas relationship,

$$P_1 v_1 = \frac{R'T_1}{M} \tag{17}$$

there results a new equation for the thrust:

$$F = A_t P_i \sqrt{\frac{2k^2}{k-1}\left(\frac{2}{k+1}\right)^{\frac{k+1}{k-1}}\left[1-\left(\frac{P_e}{P_i}\right)^{\frac{k-1}{k}}\right]} + (P_e - P_a)A_e \tag{18}$$

where A_t = throat area.

Now, we define a thrust coefficient by:

$$C_F = \sqrt{\frac{2k^2}{k-1}\left(\frac{2}{k+1}\right)^{\frac{k+1}{k-1}}\left[1-\left(\frac{P_e}{P_i}\right)^{\frac{k-1}{k}}\right]} + \frac{P_e - P_a}{P_i}\frac{A_e}{A_t} \tag{19}$$

For optimum expansion, $P_e = P_a$, and the last term becomes zero. Then, the *ideal thrust equation* becomes;

$$F = C_F A_t P_i \tag{20}$$

Hence, in view of equation (1),

$$I_s = \frac{C_F A_t P_i}{\dot{W}} \tag{21}$$

$$I_s = \frac{A_t P_i}{\dot{W}} \sqrt{\frac{2k^2}{k-1} \left(\frac{2}{k+1}\right)^{\frac{k+1}{k-1}} \eta} + \frac{P_e - P_a}{P_i} \epsilon \tag{22}$$

where $\epsilon = A_e/A_t$ = area ratio.

Equation (19) is the more useful because there are available tabulated values of C_F where P_a = vacuum.

When $P_e = P_a$, the optimum area ration ϵ and the pressure ratio P_e/P_i are related by the equation:

$$\epsilon = \frac{\left(\frac{2}{k+1}\right)^{\frac{k+1}{2(k-1)}}}{\left(\frac{P_e}{P_i}\right)^{\frac{1}{k}} \sqrt{\frac{2}{k-1} \left(1 - \left[\frac{P_e}{P_i}\right]^{\frac{k-1}{k}}\right)}} \tag{23}$$

An additional useful relation for isentropic flow of ideal gases through a nozzle is:

$$\left(\frac{V_i}{V_e}\right)^{k-1} = \frac{T_e}{T_i} = \left(\frac{P_e}{P_i}\right)^{\frac{k-1}{k}} \tag{24}$$

Weight Flow. For an isentropic, steady flow process, the general equation for the weight flow in a nozzle between any section x and the nozzle inlet section is given by:

$$\dot{W} = \frac{A_x P_1 M}{R'} \sqrt{2gJ} \sqrt{\frac{c_p}{T_1}\left[\left(\frac{P_x}{P_1}\right)^{\frac{2}{k}} - \left(\frac{P_x}{P_1}\right)^{\frac{k+1}{k}}\right]} \tag{25}$$

where J = mechanical equivalent of heat. (777.97 ft-lb per btu.)

Throat Conditions. The throat pressure for which the isentropic weight flow is a maximum is called the *critical pressure* and is obtained from (23):

$$P_{tc} = P_1 \left(\frac{2}{k+1}\right)^{\frac{k}{k-1}} \quad . \tag{26}$$

The specific volume in the throat at critical pressure is:

$$v_{tc} = v_1 \left(\frac{k+1}{2}\right)^{\frac{1}{k-1}} \tag{27}$$

The temperature in the throat at critical pressure is:

$$T_{tc} = T_1 \left(\frac{2}{k+1}\right) \quad . \tag{28}$$

The *critical velocity* is:

$$V_{tc} = \sqrt{\frac{2gk}{k+1}\,\frac{R'T_1}{M}} = \sqrt{\frac{gkR'T_{tc}}{M}} \tag{29}$$

The weight flow in the critical section is:

$$\dot{W} = \frac{A_t V_{tc}}{v_{tc}} = A_t P_1 g \frac{k\sqrt{\frac{2}{k+1}^{\frac{k+1}{k-1}}}}{\sqrt{\frac{gkR'T_1}{M}}} \tag{30}$$

Specific Impulse from Enthalpy Change

When the enthalpy change which a fluid undergoes in an isentropic expansion through a nozzle is known, the exhaust velocity is given by the equation:

$$V = \frac{\sqrt{2gJ\Delta h}}{\sqrt{1 - \left(\frac{A_2}{A_1}\right)^2 \left(\frac{V_1}{V_2}\right)^2}} \qquad (31)$$

V_1 is often small compared to V_2 and under these conditions, the denominator in equation (31) becomes approximately equal to unity so that,

$$V = \sqrt{2gJ\Delta h} \qquad (32)$$

where

J = mechanical equivalent of heat (777.97 ft-lb/Btu)

g = 32.174 ft-sec^2

Δh = enthalpy change, Btu per lb

Since $I_s = V/g$, equation (31) may be converted to:

$$I_s = 6.954\sqrt{\Delta h} \qquad (33)$$

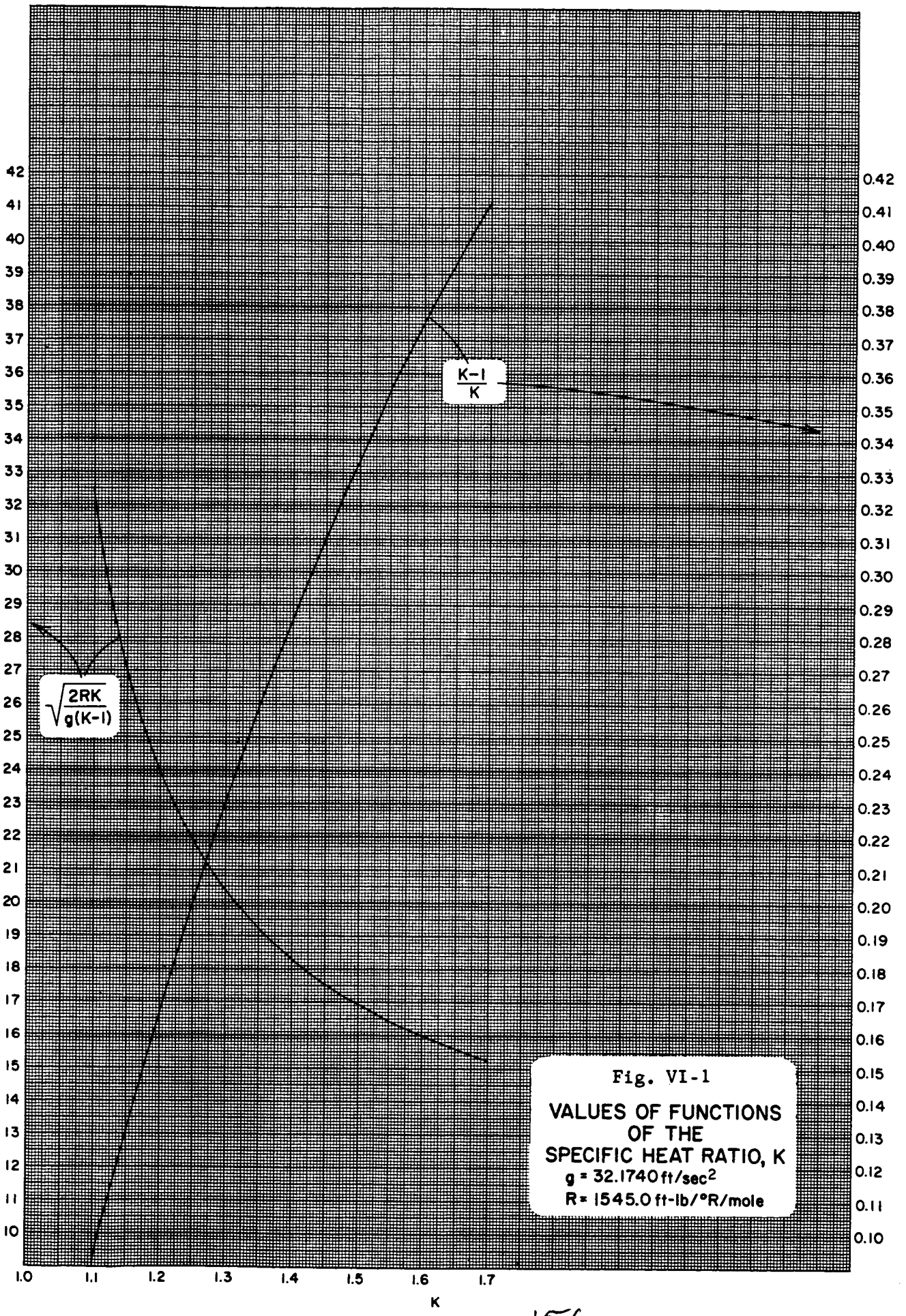

Fig. VI-1

VALUES OF FUNCTIONS OF THE SPECIFIC HEAT RATIO, K

$g = 32.1740$ ft/sec^2

$R = 1545.0$ ft-lb/°R/mole

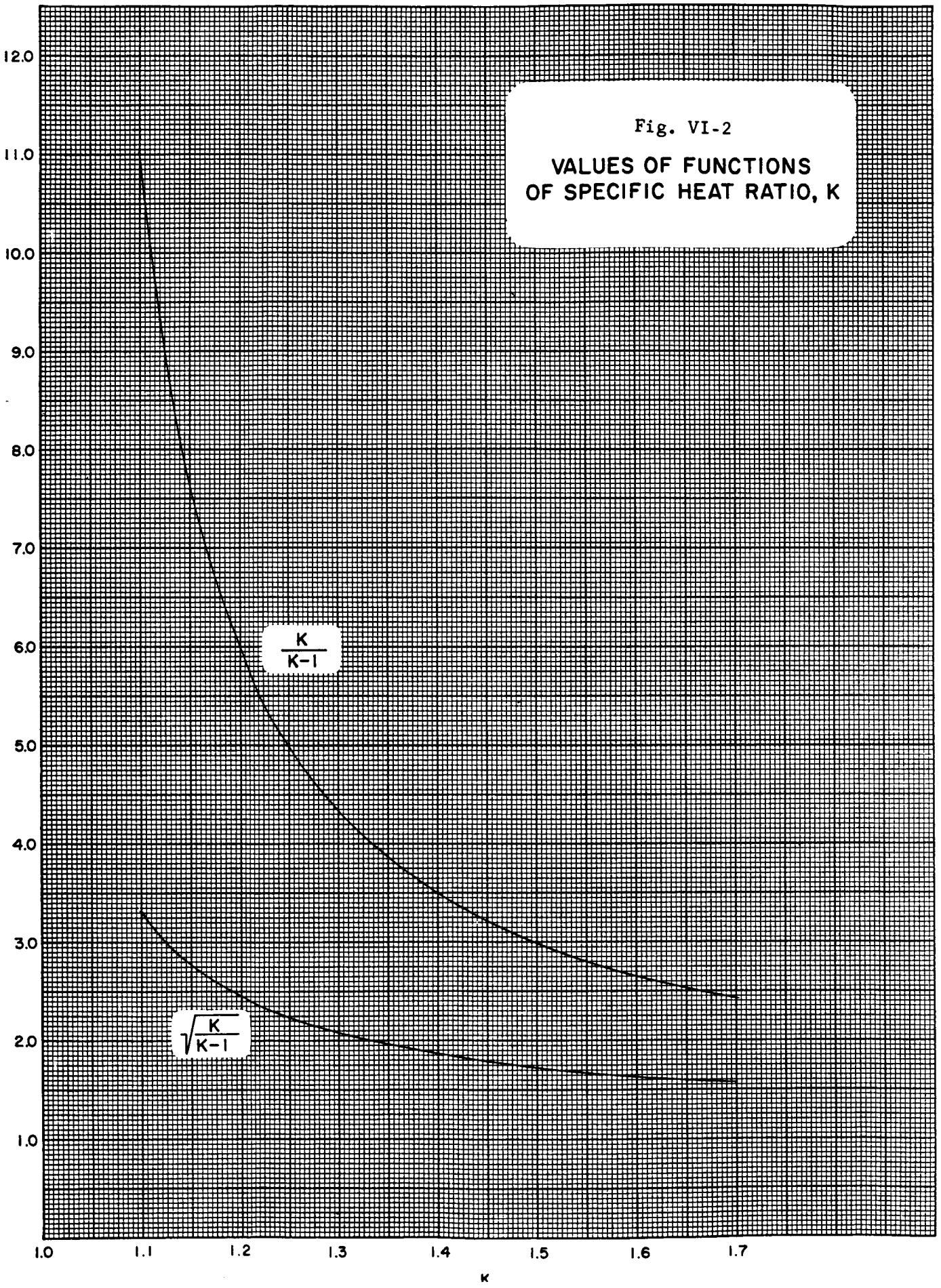

Fig. VI-2

VALUES OF FUNCTIONS OF SPECIFIC HEAT RATIO, K

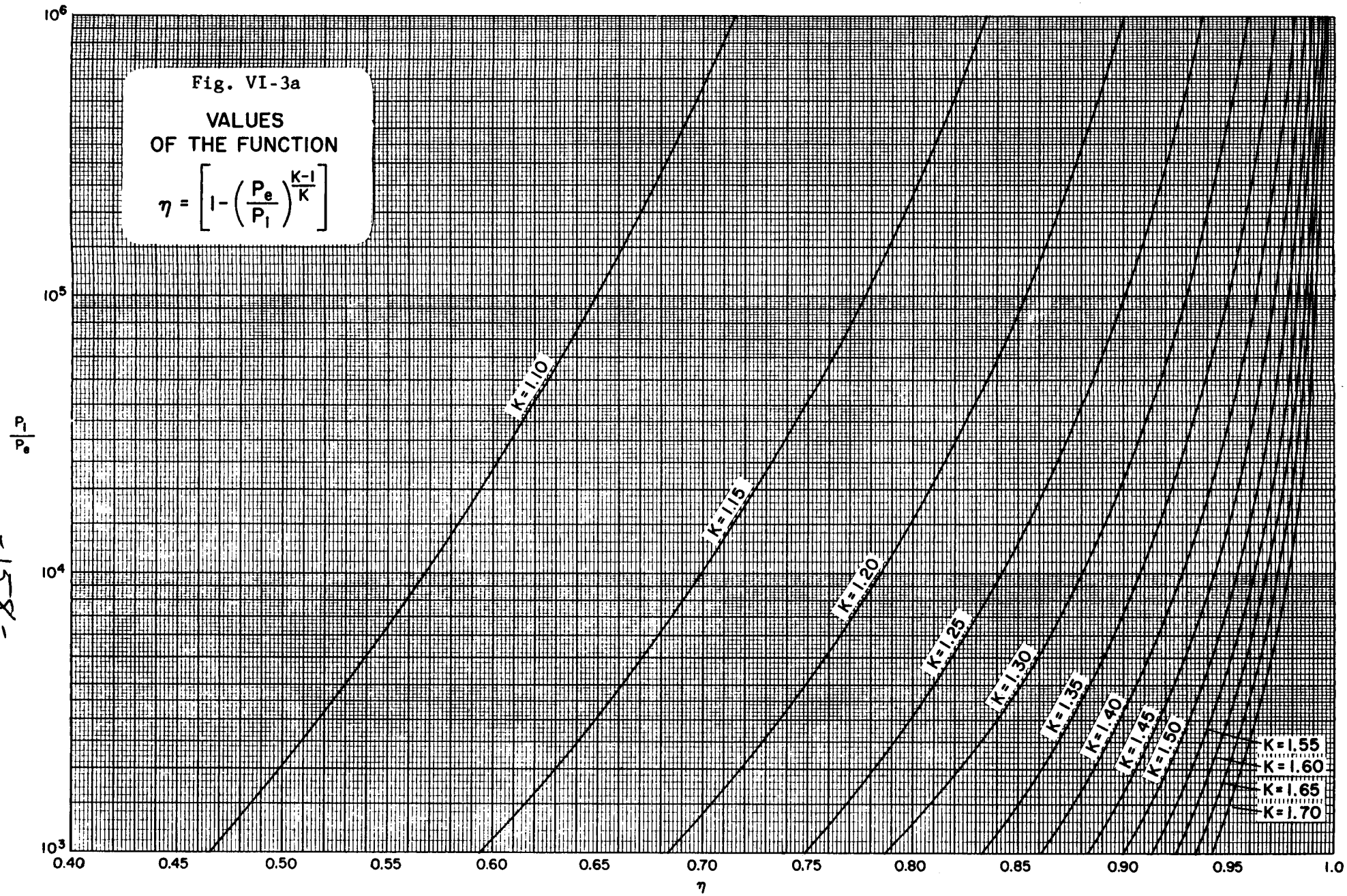
Fig. VI-3a
VALUES
OF THE FUNCTION
$\eta = \left[1-\left(\frac{P_e}{P_1}\right)^{\frac{K-1}{K}}\right]$
$\frac{P_1}{P_e}$
10^6
10^5
10^4
10^3
0.40
0.45
0.50
0.55
0.60
0.65
0.70
0.75
0.80
0.85
0.90
0.95
1.0
η
K=1.10
K=1.15
K=1.20
K=1.25
K=1.30
K=1.35
K=1.40
K=1.45
K=1.50
K=1.55
K=1.60
K=1.65
K=1.70

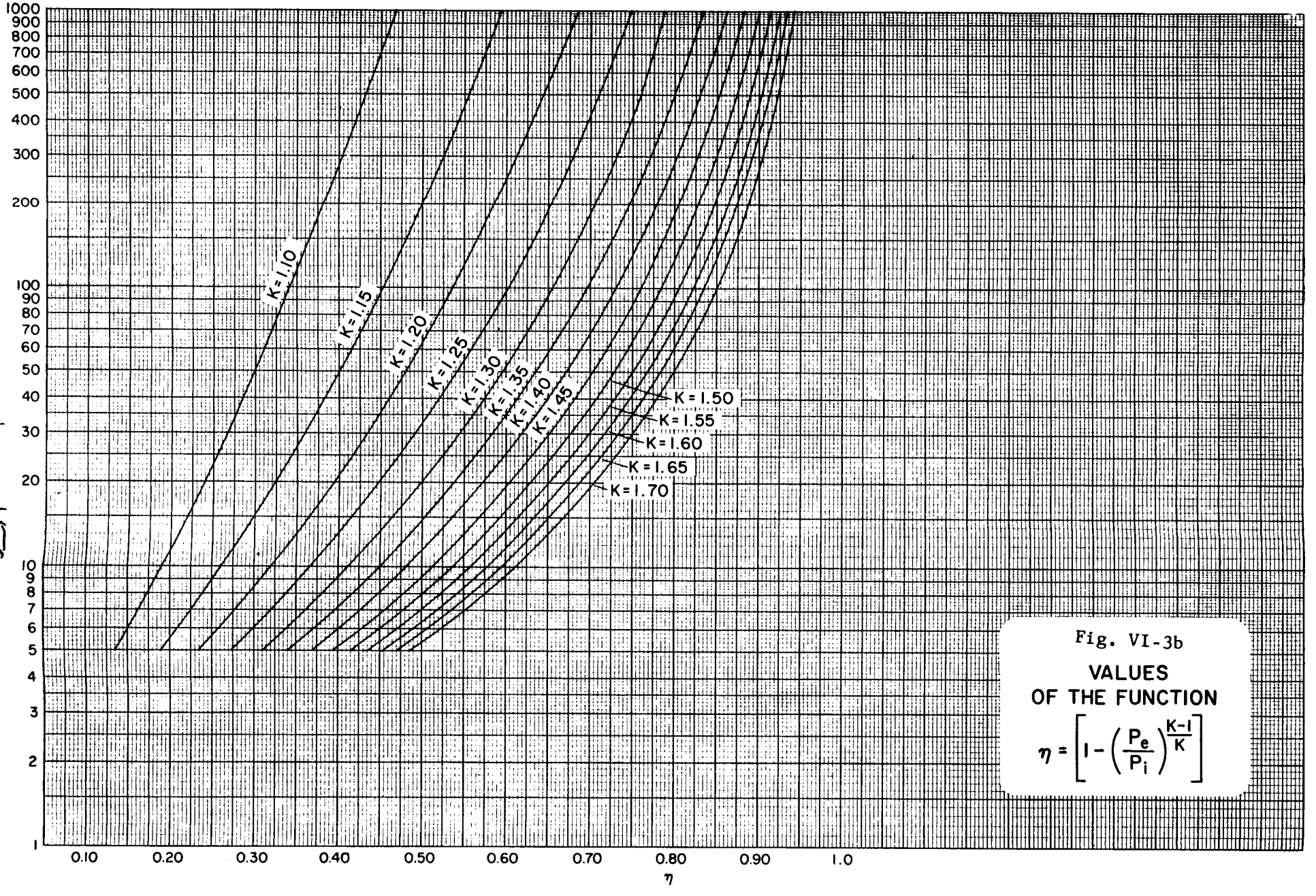

Fig. VI-3b

VALUES OF THE FUNCTION

$$\eta = \left[1 - \left(\frac{P_e}{P_i}\right)^{\frac{K-1}{K}}\right]$$

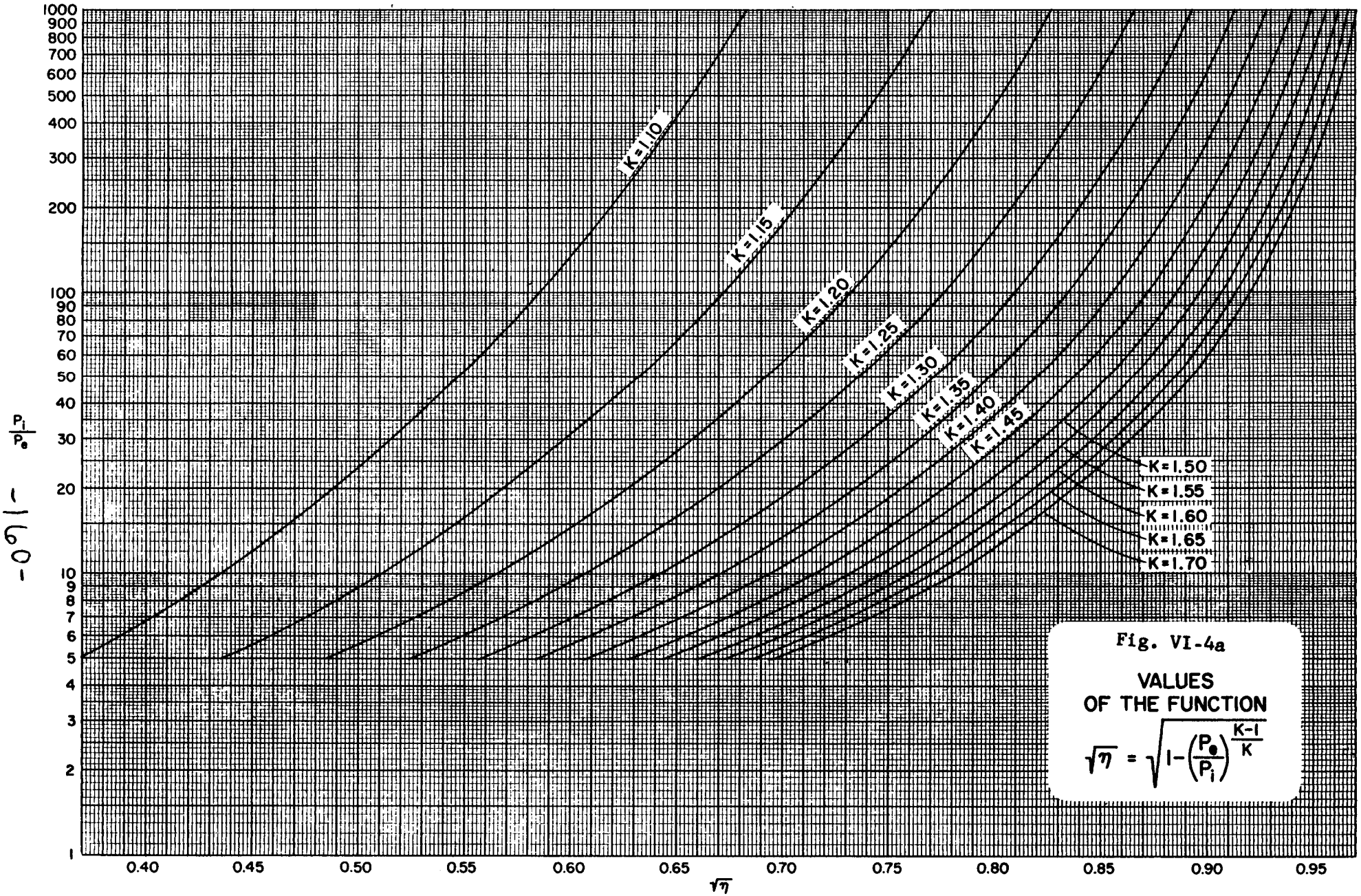

Fig. VI-4a

VALUES OF THE FUNCTION

$$\sqrt{\eta} = \sqrt{1-\left(\frac{P_e}{P_i}\right)^{\frac{K-1}{K}}}$$

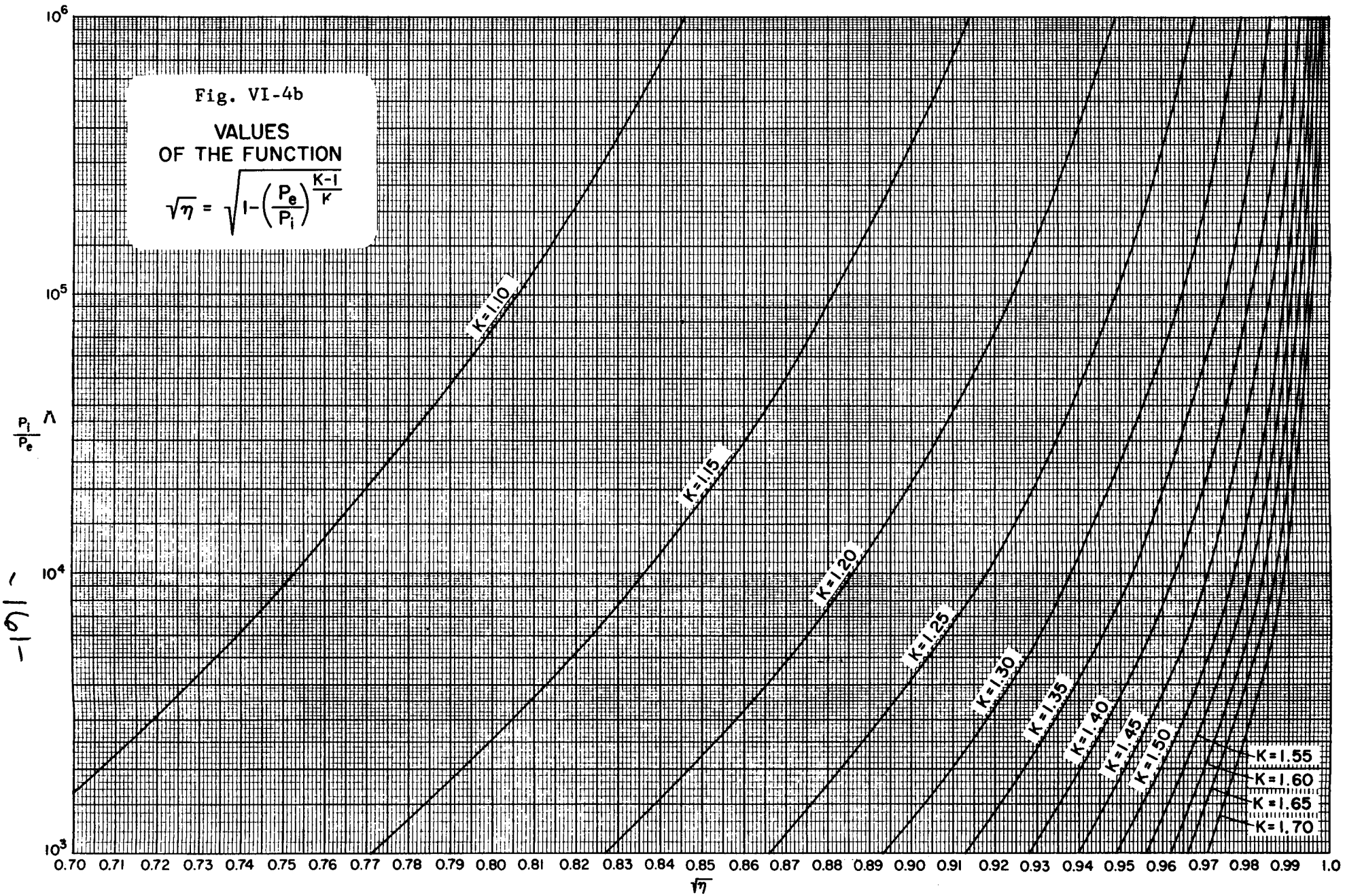
Fig. VI-4b
VALUES
OF THE FUNCTION
$\sqrt{\eta} = \sqrt{1-\left(\frac{P_e}{P_i}\right)^{\frac{K-1}{K}}}$
$\frac{P_i}{P_e}$
$\sqrt{\eta}$
10^6
10^5
10^4
10^3
0.70 0.71 0.72 0.73 0.74 0.75 0.76 0.77 0.78 0.79 0.80 0.81 0.82 0.83 0.84 0.85 0.86 0.87 0.88 0.89 0.90 0.91 0.92 0.93 0.94 0.95 0.96 0.97 0.98 0.99 1.0
K=1.10
K=1.15
K=1.20
K=1.25
K=1.30
K=1.35
K=1.40
K=1.45
K=1.50
K=1.55
K=1.60
K=1.65
K=1.70

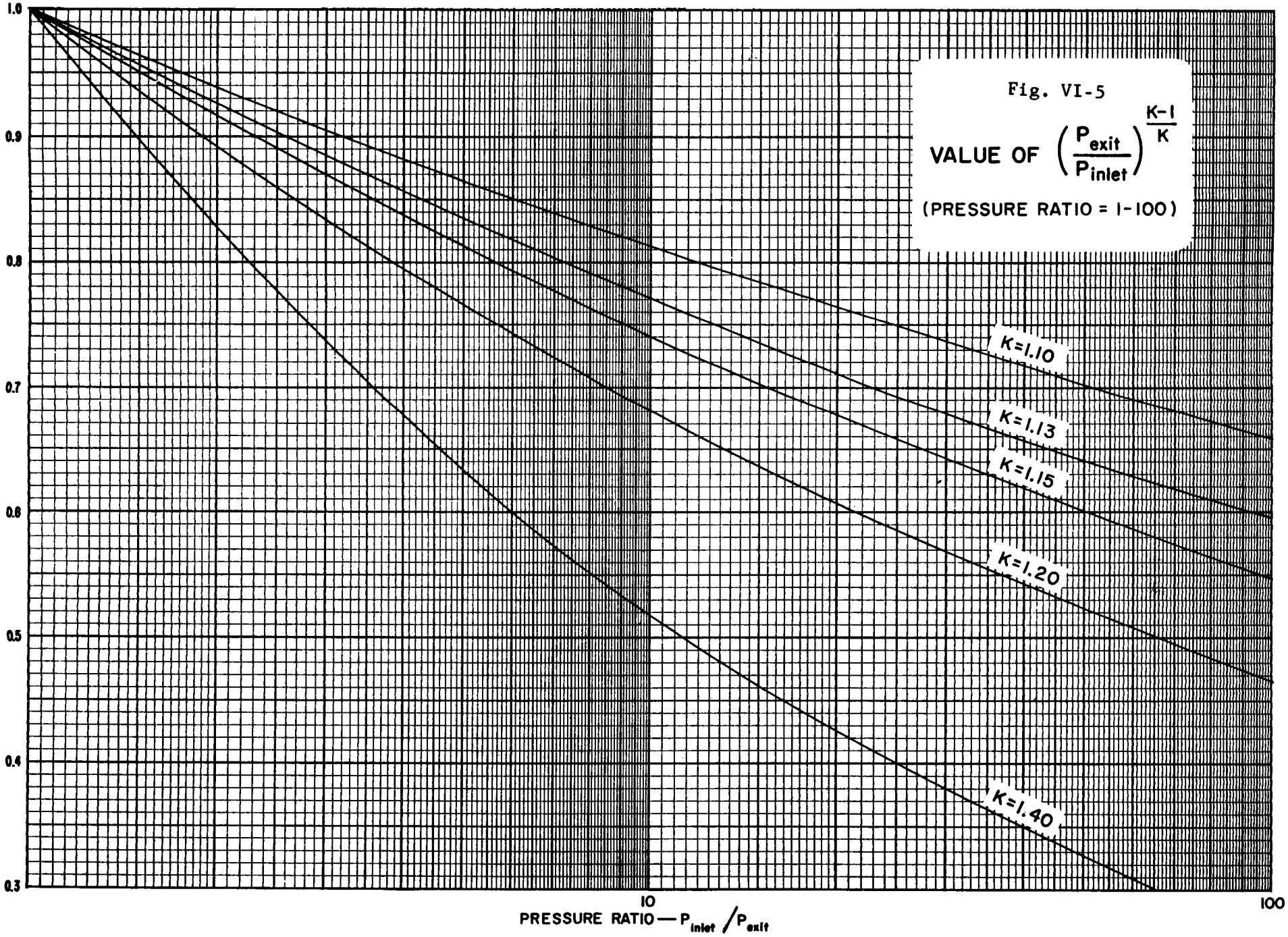
Fig. VI-5
VALUE OF $\left(\frac{P_{exit}}{P_{inlet}}\right)^{\frac{K-1}{K}}$
(PRESSURE RATIO = 1-100)
K=1.10
K=1.13
K=1.15
K=1.20
K=1.40
1.0
0.9
0.8
0.7
0.6
0.5
0.4
0.3
10
100
PRESSURE RATIO — P_{inlet}/P_{exit}

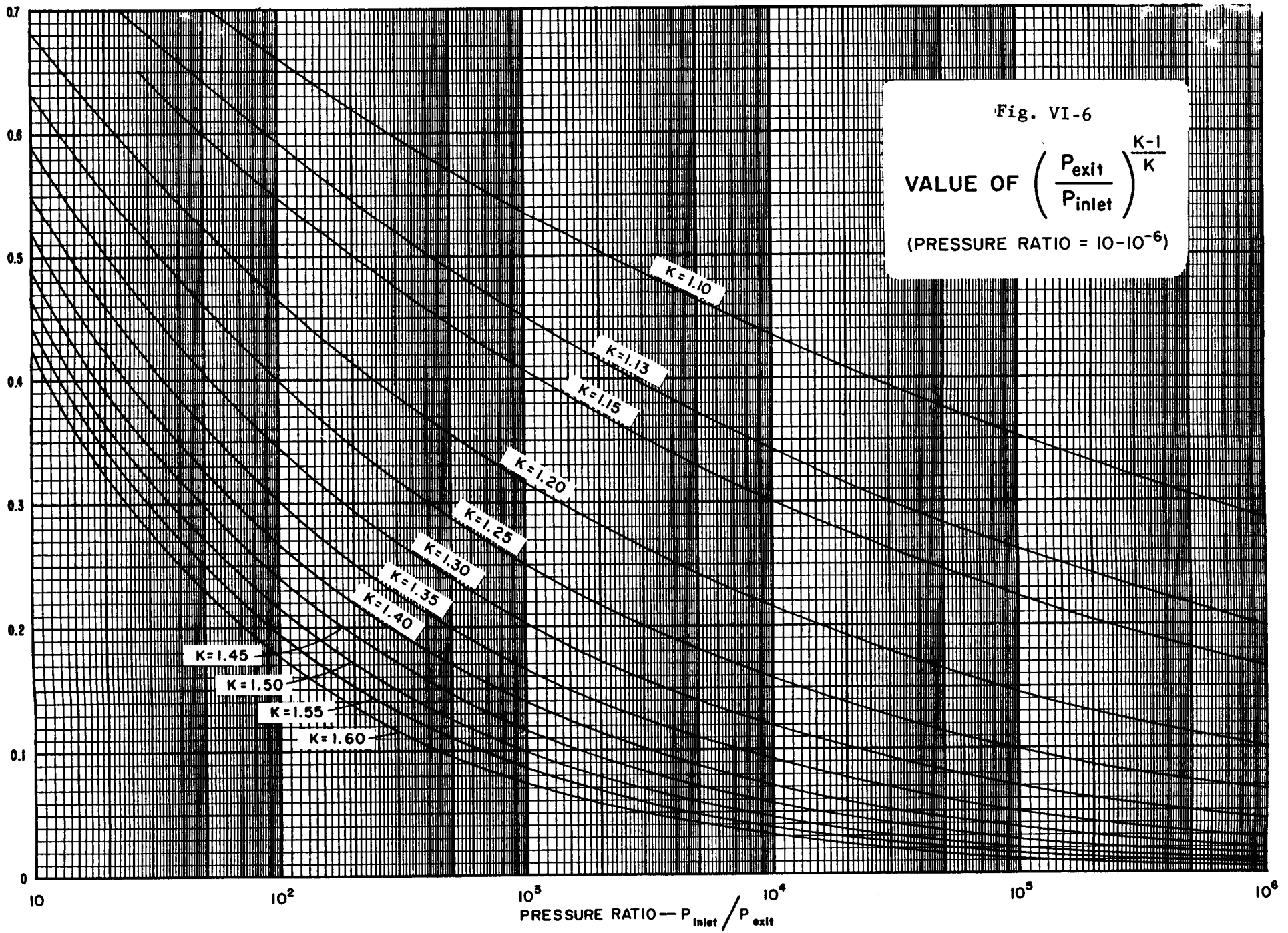
Fig. VI-6
VALUE OF $\left(\frac{P_{exit}}{P_{inlet}}\right)^{\frac{K-1}{K}}$
(PRESSURE RATIO = 10-10^{-6})
K=1.10
K=1.13
K=1.15
K=1.20
K=1.25
K=1.30
K=1.35
K=1.40
K=1.45
K=1.50
K=1.55
K=1.60
0.7
0.6
0.5
0.4
0.3
0.2
0.1
0
10
10^2
10^3
10^4
10^5
10^6
PRESSURE RATIO — P_{inlet}/P_{exit}

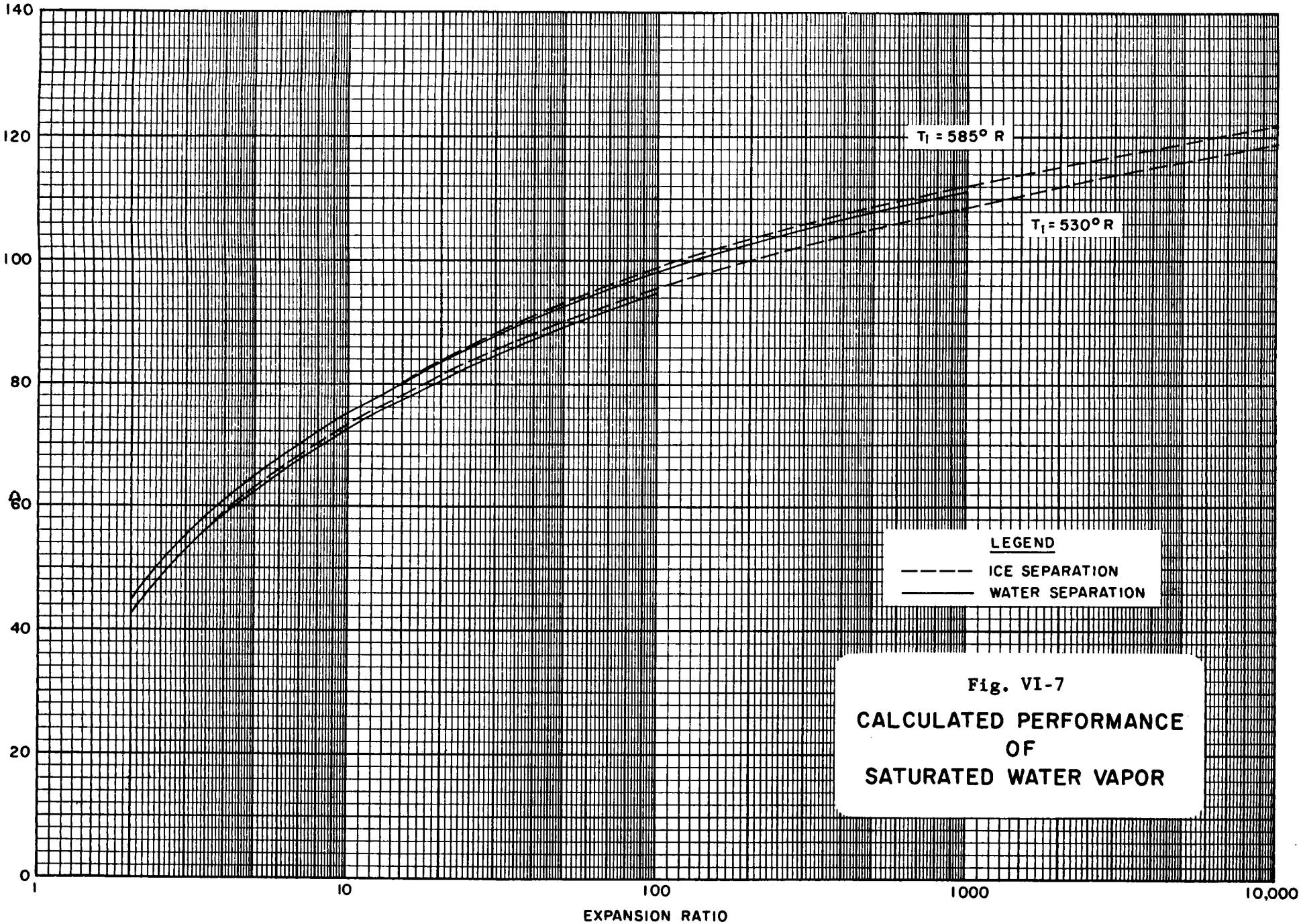

Fig. VI-7

CALCULATED PERFORMANCE OF SATURATED WATER VAPOR

VII PRESSURE VESSELS

Table of Contents

Section-Part	Title	Section-Part.Page
VII-0	List of Tables	VII-0.3
VII-0	List of Figures	VII-0.4
VII-1	Introduction	VII-1.1
VII-2	Design Criteria	VII-2.1
	Vessel Construction	VII-2.1
	Stresses Due to Steady State Temperature and Internal Pressure	VII-2.3
	Shape, Configuration Requirements . .	VII-2.4
	Spherical Vessels	VII-2.5
	Cylindrical Shells	VII-2.6
	Elliptical Ends	VII-2.6
	Membrane Stresses	VII-2.7
	Materials Selection	VII-2.12
	Development of Criteria for Material Compatibility	VII-2.13
	Development of Criteria for Weldability	VII-2.15
	Workability and Machinability	VII-2.15
	Cyclic Material Behavior	VII-2.15
	Sustained Load Properties	VII-2.16
	Development of Criteria for Corrosion Properties	VII-2.16
	Inspectability	VII-2.16
	Optimum Design Considerations and Processing Variables	VII-2.19
VII-3	Construction Details and Support Structures	VII-3.1
VII-4	Stress Analysis	VII-4.1
	Introduction	VII-4.1
	Membrane Analysis	VII-4.2
	Displacements	VII-4.6
	Discontinuity Stress	VII-4.7
	Influence Coefficients for Long Cylinders	VII-4.18

Table of Contents (contd)

Section-Part	Title	Section-Part.Page
VII-4 (contd)	Influence Coefficients for Short Cylinders	VII-4.20
	Heads	VII-4.20
	Openings in Shells	VII-4.25
	Hemispherical Heads	VII-4.32
	Concentrated Loads	VII-4.45
	Cylinders	VII-4.47
	Spherical Membrane	VII-4.50
	Thick-Walled Pressure Vessels	VII-4.51
VII-5	Material Behavior	VII-5.1
	Phenomenological Theories	VII-5.1
	Fracture Mechanics	VII-5.3
	Statistical Fracture Techniques	VII-5.17
	Temperature and Fracture Transition	VII-5.20
VII-6	Materials Traceability and Control	VII-6.1
VII-7	Testing Procedures	VII-7.1
VII-8	Design Example	VII-8.1
	Introduction	VII-8.1
	Membrane Analysis	VII-8.1
	Section I (Hemisphere)	VII-8.4
	Section II (Cylinder)	VII-8.5
	Section III (Reverse Knuckle)	VII-8.6
	Section IV (Knuckle)	VII-8.7
	Section V (Elliptical Head)	VII-8.12
	Section VI (Upper Opening, Cylinder)	VII-8.17
	Discontinuity Stresses	VII-8.19
	Section I to Section II (Hemisphere to Cylinder)	VII-8.19
VII-9	References	VII-9.1
VII-A	Appendix	VII-A.0

VII-O LIST OF TABLES

Section-Part-Table	Title	Section-Part.Page
VII-4-1	S_1, S_2 and δ for Common Shells of Revolution	VII-4.7
VII-4-2	Functions A_χ, B_χ, C_χ, and D_χ (Ref. 14)	VII-4.11
VII-4-3	Influence coefficients for Long Cylinders (Ref. 36)	VII-4.18
VII-4-4	Formulas for Deflections and Rotations	VII-4.34
VII-5-1	Phenomenological Failure Theories.....	VII-5.2
VII-5-2	Stress Intensity Factors for Various Shapes and Loads	VII-5.8
VII-5-3	Fracture Toughness for Several Materials Employed in Pressurized Tankage . . .	VII-5.19
VII-A-1	Properties of Various Head Shapes . .	VII-A.1
VII-A-2	R_1 and R_2 for Shells of Revolution .	VII-A.2
VII-A-3	Shock and Vibration Loading Factors .	VII-A.3

VII-0 LIST OF FIGURES

Section-Part-Figure	Title	Section-Part.Page
VII-2-1	Membrane Free Body Diagram	VII-2.7
VII-2-2	Sphere with Internal Pressure, P. . . .	VII-2.8
VII-2-3	Free Body Diagram at Section AA . .	VII-2.9
VII-2-4	Cylindrical Vessel with Elliptical Heads	VII-2.10
VII-2-5	Free Body Diagram at Section AA . .	VII-2.11
VII-2-6	Establishing P_p by Considering Fracture Mechanics	VII-2.18
VII-2-7	Notch Strength versus Crack Area for Material Selection Filter	VII-2.18
VII-4-1	Free Body Diagram of General Shell of Revolution	VII-4.2
VII-4-2	Shell of Revolution Showing Relationship of T_1 and T_2	VII-4.3
VII-4-3	Shell of Revolution where $R_1 > 2R_2$ . .	VII-4.4
VII-4-4	Shell of Revolution with R_2 Negative in the Shaded Area	VII-4.5
VII-4-5	Torus with Associated Membrane Forces (Ref. 36)	VII-4.5
VII-4-6	Discontinuity Stresses for a Steel (ν = 1/3) Cylindrical Pressure Vessel with a Hemispherical Head (Ref. 36)	VII-4.7
VII-4-7	Discontinuity Stresses for a Cylinder with a Skirt and a Hemispherical Head (Ref. 36)	VII-4.8
VII-4-8	Beam on an Elastic Foundation (Ref. 36)	VII-4.9
VII-4-9	Loading, Deflection, Slope, Moment and Shear in a Beam on an Elastic Foundation (Ref. 14)	VII-4.10
VII-4-10	Uniformly Distributed Load over a Portion of a Beam on an Elastic Foundation (Ref. 14)	VII-4.12
VII-4-11	Single Moment Acting on a Beam on an Elastic Foundation (Ref. 14)	VII-4.13

Figures (contd)

Section-Part-Figure	Title	Section-Part.Page
VII-4-12	Semi-infinite Beam on an Elastic Foundation (Ref. 14)	VII-4.13
VII-4-13	Discontinuity at Cylinder to Hemispherical Head Junction with Internal Pressure P	VII-4.14
VII-4-14	Stress Concentration Factors in Cylinders Connected to Elliptical Heads (Ref. 36)	VII-4.16
VII-4-15	Stress Distribution Near Elliptical Head to Cylinder Joint (Ref. 36) . .	VII-4.17
VII-4-16	Influence Coefficients for Short Cylindrical Shells (Ref. 36)	VII-4.19
VII-4-17	Elliptical Head (Ref. 36)	VII-4.20
VII-4-18	Membrane Forces for a Typical Elliptical Head (b/a = 0.6) (Ref. 36)	VII-4.21
VII-4-19	Membrane Forces in Elliptical Heads versus b/a (Ref. 36)	VII-4.22
VII-4-20	Tensile and Compressive Forces in Cassinian Heads (Ref. 36)	VII-4.23
VII-4-21	Zero Hoop Stress Head (Ref. 36) . .	VII-4.23
VII-4-22	Comparison of Head Shapes (Ref. 36)	VII-4.24
VII-4-23	Unreinforced Opening in a Membrane with Internal Pressure P	VII-4.25
VII-4-24	Variation in Stress in the Region of a Circular Hole in (a) Cylinder, (b) Sphere Subjected to Internal Pressure (Ref. 14)	VII-4.26
VII-4-25	Reinforcement Boundaries for Circular Openings in Cylindrical and Spherical Vessels (Ref. 14)	VII-4.27
VII-4-26	Equilibrium Forces Around a Reinforced Hole (Ref. 36)	VII-4.27
VII-4-27	Diagrammatic Location of Nozzle Opening Reinforcement, (a) Balanced, (b) Unbalanced Inside, (c) Unbalanced Outside (Ref. 14)	VII-4.28
VII-4-28	Comparison of Symmetrical versus Unsymmetrical Reinforcing Rings (Ref. 36)	VII-4.29

Figures (contd)

Section-Part-Figure	Title	Section-Part.Page
VII-4-29	Spherical Shell with a Reinforced Opening (Ref. 36)	VII-4.30
VII-4-30	Discontinuity Moments and Forces (Ref. 36)	VII-4.30
VII-4-31	Influenced Coefficients for a Small Opening ($0^{o} < \phi_{o} \leq 10^{o}$) (Ref. 36) .	VII-4.36
VII-4-32	Longitudinal Bending Moment M_2 for a Symmetric Ring (Ref. 36)	VII-4.37
VII-4-33	Longitudinal and Hoop Forces for a Symmetrical Ring (Ref. 36)	VII-4.38
VII-4-34	Resultant Stresses Due to Moment, Horizontal Forces V, and Membrane Forces for a Symmetrical Ring (Ref. 36)	VII-4.39
VII-4-35	Stresses at the Ring-Membrane Junction for a Symmetrical Ring (Ref. 36) . .	VII-4.40
VII-4-36	Stresses at the Ring-Membrane Junction for an Unsymmetrical Ring (Ref. 36)	VII-4.41
VII-4-37	Comparison of the Maximum Stresses at the Ring-Membrane Junction (Ref. 36)	VII-4.42
VII-4-38	Stresses at the Ring-Membrane Junction versus Eccentricity (Ref. 36) . . .	VII-4.43
VII-4-39	Off-Apex Opening in a Head of Arbitrary Shape (Ref. 36)	VII-4.44
VII-4-40	Stress Concentration in a Membrane Reinforced with a Rigid Insert	VII-4.46
VII-4-41	Cylinder with Radial Load P (lb) Concentrated on Area of Radius b at a Distance ℓ from an End	VII-4.47
VII-4-42	Uniform Radial Pressure (P lb/in of Circumference)	VII-4.48
VII-4-43	Cylinder with Reinforcing Ring of Cross Sectional Area A	VII-4.49
VII-4-44	Spherical Membrane with Load P (lb) Concentrated over a Circular Area with Radius r_o (Edges Fixed and Held) . .	VII-4.50

Figures (contd)

Section-Part-Figure	Title	Section-Part.Page
VII-5-1	Three Possible Fracture Modes . . .	VII-5.4
VII-5-2	Example of Practical Application of Fracture Mechanics	VII-5.7
VII-5-3	Distribution Curve of Fracture Stresses for 1/4 in X 1/4 in X 4 in Bend Specimens of Three Gypsum Cements	VII-5.18
VII-8-1	Vessel Configuration and Specification for the Design Example	VII-8.2
VII-8-2	Reduction of Vessel to Individual Geometric Elements	VII-8.3
VII-8-3	Free Body Diagram of Section I, Hemisphere	VII-8.4
VII-8-4	Free Body Diagram of Section II, Cylinder	VII-8.5
VII-8-5	Free Body Diagram of Section III, Reverse Knuckle	VII-8.6
VII-8-6	Free Body Diagram of Section IV, Knuckle	VII-8.7
VII-8-7	Reduction of Membrane to Cylinder for Buckling Analysis	VII-8.8
VII-8-8	Equivalent Axially Loaded Cylinder with End Stress S' Equal to the Maximum Value of the Negative Hoop Stress on the Membrane	VII-8.10
VII-8-9	Free Body Diagram of Section V, Elliptical Head	VII-8.12
VII-8-10	Membrane Junction with Rigid Ring .	VII-8.13
VII-8-11	Coordinate System for Elliptical Head	VII-8.14
VII-8-12	Reduction of Membrane to Cylinder for Buckling Analysis	VII-8.15
VII-8-13	Free Body Diagram of Section VI, Lower Opening, Rigid Ring	VII-8.17
VII-8-14	Wall Thickness of Pressure Vessel from Membrane Analysis	VII-8.18

Figures (contd)

Section-Part-Figure	Title	Section-Part.Page
VII-8-15	Membrane Displacements when Pressurized	VII-8.19
VII-8-16	Final Shape of Joint A	VII-8.22
VII-A-1	Properties of 2014 Aluminum (Ref. 17)	VII-A.4
VII-A-2	Properties of 2017 Aluminum (Ref. 17)	VII-A.5
VII-A-3	Properties of 2018 and 2218 Aluminum (Ref. 17)	VII-A.6
VII-A-4	Strength of 2024 Aluminum (Ref. 17)	VII-A.7
VII-A-5	Properties of 2024 Aluminum (Ref. 17)	VII-A.8
VII-A-6	Properties of 2025 Aluminum (Ref. 17)	VII-A.9
VII-A-7	Strength of AISI 304 Stainless Steel (Ref. 17)	VII-A.10
VII-A-8	Properties of AISI 304 Stainless Steel (Ref. 17)	VII-A.11
VII-A-9	Properties of AISI 321 Stainless Steel (Ref. 17)	VII-A.12
VII-A-10	Strength of AISI 347 Stainless Steel (Ref. 17)	VII-A.13
VII-A-11	Properties of AISI 347 Stainless Steel (Ref. 17)	VII-A.14
VII-A-12	Strength of Titanium Alloys (Ref. 17)	VII-A.15
VII-A-13	Properties of Titanium Alloys (Ref. 17)	VII-A.16
VII-A-14	Strength of 4Al-4Mn Titanium (Ref. 17)	VII-A.17
VII-A-15	Strength of 5Al-2.5Sn Titanium (Ref. 17)	VII-A.18
VII-A-16	Strength of 6Al-4V Titanium (Ref. 17)	VII-A.19
VII-A-17	Properties of Titanium Alloys (Ref. 35)	VII-A.20
VII-A-18	Properties of Various Alloys (Ref. 35)	VII-A.21
VII-A-19	Properties of Nickel Base Alloys (Ref. 35)	VII-A.22

Figures (contd)

Section-Part-Figure	Title	Section-Part.Page
VII-A-20	Yield Strength Density Ratios vs. Temperature for Various Alloys (Ref. 35)	VII-A.23
VII-A-21	Tensile Strength Density Ratios vs. Temperature for Various Alloys (Ref. 35)	VII-A.24
VII-A-22	Surface Area of Spherical Tanks . .	VII-A.25
VII-A-23	Surface Area of Oblate Spheroidal Tanks	VII-A.26
VII-A-24	Volume of Spherical Tanks	VII-A.27
VII-A-25	Volume of Oblate Spheroidal Tanks .	VII-A.28
VII-A-26	Spherical Tank Weights for Various Pressures	VII-A.29

VII-1 INTRODUCTION

The design of flight-weight pressurized gas systems may be typified as primarily a problem of controls. The function of these controls is to provide structural reliability of the pressure vessel. These controls are imposed in two broad areas, material control and process control. The sources of these controls are varied and they include input from personnel in materials, welding, stress analysis, nondestructive testing, and manufacturing.

It is the task of the project engineer to correlate and implement these controls. This, however, is no small task as a working knowledge of all of these disciplines is required by the project engineer to prevent what may be described as chaos.

It is the aim of this Section, therefore, to bring forth as many of the potential problem areas as possible and to provide adequate references so that the project engineer may use this as a guide for his programs.

Vessel Construction

that the complete operating cycle of the proposed vessel is known so that each potential problem may be considered prior to its occurrence. This history plus the anticipated fabrication problems, which will be covered in a later section, will allow a design engineer to predict the ramifications of any decision he may make during the construction of a spacecraft pressure vessel.

First there is the establishment of the primary design parameters of a pressure vessel. These are as follows: 1) the gas to be stored, 2) the anticipated pressure history of the gas, 3) the anticipated temperature history of the gas, 4) the amount or volume of gas to be stored, 5) the space envelope available for the pressure vessel, and 6) the maximum weight of the pressurized gas system. It is not enough to know the limits of these parameters, but the time relationships should be established. In doing this the designer may tell at what stress level the pressure vessel is at any time. To accomplish this a simple time versus pressure and time versus temperature plot is constructed. The time base should begin at the start of the testing cycle and be carried through to the end of the mission. Each of these primary design parameters will influence the selection of a candidate material, and therefore the proposed cycle history should be established as completely as possible.

Obviously the first primary design parameter (the gas to be stored) will be established from system requirements. These requirements will usually include the anticipated shock and vibration loads reduced to simple pressure loads (see Table VII-A-3 in the Appendix) and added to the working pressure of the gas which has been established, to a degree, from the same analysis. This will serve to fix P_{op} (operating pressure), but the proof and burst pressures remain unknown. The selection of P_p (proof pressure) and P_b (burst pressure) are a function of two parameters: a) contractural requirements and b) the state of the gas stored, i.e., the temperature of the gas.[4]

The contractural requirements may be further subdivided for man-rated and non-man-rated application. In a man-rated application the pressure vessel is designed so that its reliability (certainty against premature failure) is as high as possible. This is usually done by increasing the controls so that the chances are small that a sub-specification material or a manufacturing error will go undetected. Another way of promoting a high reliability is to increase the design safety factors. The amount of increase is however, a function of system weight and cost and is therefore usually considered at the contractural level.

In a cryogenic application a larger amount of gas may be stored in a smaller volume, but besides the additional complexity of the system a pressure gradient exists (in the absence of zero-g loading) due to the weight of the fluid in the vessel. This gradient must not only be considered as changing P_{op} with respect to location, but the choice of P_p may be influenced due to a change in the mechanical properties of the material at low temperatures.[17,23] This will influence P_p if, in addition to anticipated over-pressurization, a no-yield test condition is imposed.[4] Briefly this implies that at no time is the pressure vessel allowed to be stressed such that any part of the structure will exhibit stresses which are beyond the yield point of the material. At the test temperature this condition has the tendency to introduce strain gradients into the structure which are unaccounted for and unknown unless a complex reanalysis of the stresses is performed.[4] Figures 1 through 21 (Appendix) illustrate the temperature dependence of the mechanical properties of some typical pressure vessel materials.[2] These figures, however, emphasize the low temperature properties whereas the pressure vessel may be operating at a considerably higher temperature. In cases where the gas temperature is high, a usual source for material properties is MIL-HDBK-5. Paragraph 3 of this part describes another approach to the establishment of P_p.

Burst pressure (P_b) is usually selected as an ultimate pressure beyond which the pressurized gas system function is no longer a factor in the functioning of the spacecraft and is usually determined by contractural agreement.[4,6] Burst pressure is used in the preliminary qualification testing of the pressure vessel.[4] The usual techniques of this test series is outlined in Part VII-7 of this Section. Realistically the burst test serves to give the designers of a pressure vessel some knowledge of the nature of the vessel

failure.[9] These results should be compared with the failure criteria assumed in the design of the vessel (Part VII-5) to ensure compliance of the assumed failure mechanism with the observed mode of failure.

Generally speaking then, the proof and burst pressures are functions of the design pressure and can be designated as follows:

$P_p = \alpha P_{op}$ where $\alpha > 1$, $P_b = \beta P_{op}$ where $\beta > 1$, $\beta > \alpha$

and α is such that no yielding will occur. It might be pointed out here that a no-yield proof test criterion implies that the state of stress in all parts of the pressurized gas system must be known. This is difficult to anticipate with conventional gross effects associated with the $\frac{P}{kt}$ approach to vessel design and should be used only when a more sophisticated approach to the analysis of stresses is used. One such approach which has gained wide acceptance[4,10,32] is the use of a computer as a means to solve a set of generalized shell equations.

The duty cycle of the pressure vessel requires that the temperature of the gas be known at all times. Specifically, the periodic withdrawal of a gas stored at cryogenic temperatures is implemented by means of a heater or a positive-expulsion device. This withdrawal process results in an increased fluid temperature, which, in turn, may degrade the properties of the material enough to cause local yielding or elastic over-stressing of the vessel. This could be disastrous if the design considers the effect of fatigue damage[12] in the vessel life. While thermal shock is not generally a design consideration because the vessels considered here are usually enclosed or otherwise thermally protected during the ascent and descent stages of a mission, its effect should be considered if inadequate insulation is indicated.[14]

Thermal stresses, however, should be considered even during manufacture of the pressure vessel. The case here is that a pressure vessel with a defective weld may sometimes be discarded because repairing the weld could introduce unknown thermal stresses, which, in turn, could deform the vessel.[12]

Stresses Due to Steady-State Temperature and Internal Pressure[40]

Vessels, to withstand high pressures, are usually designed on the basis that the internal pressure leads to elastic failure at the inside surface.

However, thermal gradients cause stresses which may easily achieve levels comparable to or greater than the pressurization stresses. Thus, it is important to take into account thermal and pressurization stresses simultaneously in the design of pressure vessels.

The behavior of spherical and cylindrical vessels stressed by pressure and temperature when the stresses are everywhere below the elastic limit is well known,[44] but it is not always possible to maintain stresses below the elastic limit. The behavior of vessels subjected to both pressure and temperature stresses when the elastic limit has been exceeded was studied by Whalley.[45]

The equations presented are based on the following assumptions:[45]

(1) A brittle material is perfectly elastic up to its ultimate strength. When it fractures, according to the maximum principal stress theory, it does so without appreciable yielding.

(2) A ductile material is perfectly elastic up to the yield point; thereafter it yields at constant maximum shear stress (Tresca theory); no strain hardening occurs.

(3) The temperature is low enough so that creep is negligible.

(4) Temperature and stress have no effect on elastic moduli and the yield point; the coefficient of thermal expansion is negligible.

(5) The Bauschinger effect does not occur (reduction in yield point due to previous plastic flow in the reverse direction).

(6) The strains are small compared with the dimensions of the vessel.

(7) Important stress raisers are absent.

Shape, Configuration Requirements

As stated previously, a gas can be stored as a liquid or in its gaseous form depending on such factors as cost, weight, volume necessary versus space available, and use. This decision, however, is one made during the systems analysis, and only the design problems associated with each case will be treated in this section.

Usually the space envelope is fixed prior to the design of the pressure vessel[6,8] and the designer then must choose the best shape for the vessel which fits into the available space. In cases such as these any vessel configuration other than spherical imposes weight penalties because of the particular stress distribution encountered.

In arriving at a weight estimate for a particular vessel shape the simple technique of membrane stress may be used to compute the shell thickness. This, however, does not account for bosses, weld reinforcing areas, or support brackets which could increase the weight considerably. To account for all of these additional components without at least a simplified analysis would be merely guesswork. But if the candidate vessel (or vessels if various shapes are being considered) is being considered for some trade-off, such as different strength levels for a given material or pressure-versus-mission requirements, it may be advantageous to ignore these additional components since they will, in these cases, remain approximately constant. The following may serve to aid the designer in establishing the preliminary weight of a pressure vessel prior to the formal stress analysis.

"The minimum weight of a pressure vessel depends upon the permissible level of stress in which the material of construction is to operate. In general, the stress level at proof pressure is used for development of equations and formulae for computing minimum weight. The actual weight of a vessel is determined by the number and thickness of bosses, the required thickness at butt-welded joints to maintain strength, and, among other such considerations, safety factors and available techniques for fabrication."[40]

Spherical Vessels[40]

The thickness of the vessel walls is given by:

$$t = \frac{Pd}{4\sigma - P}$$

where d = inside diameter and σ is the maximum stress level for the material; the weight-to-volume ratio is:

$$\frac{W}{V} = \frac{96 \rho P \sigma^2}{(4\sigma - P)^3}$$

where ρ is the density of the material.

Cylindrical Shells[40]

The wall thickness of the shell of a cylindrical pressure vessel at some distance away from the ends must be:

$$t = \frac{Pd}{2\sigma - P}$$

and the weight-to-volume ratio is

$$\frac{W}{V} = 4(d + t)Pt/d^2$$

Elliptical Ends[40]

The maximum stresses in the knuckle region and the dome region are given by:

(1) Knuckle region

The maximum stress is

$$\sigma = KPa/t_1$$

where K is a stress factor for an elliptical ratio, e; P = differential pressure; and a = inside radius.

(2) Dome region

The maximum stress in this region is

$$\sigma = \frac{PR}{2t} = \frac{ePa}{2t_2}$$

Solving for $t_1 + t_2$ and taking an average value, there is found an effective end thickness:

$$t_e = \frac{Pa}{2\sigma}\left(K + \frac{e}{2}\right)$$

and the weight-to-volume ratio is:

$$\frac{W}{V} = \frac{3}{8}\frac{\rho P}{\sigma}\left(K + \frac{e}{2}\right)L$$

where

$$L = 2e + \frac{1}{\sqrt{e^2-1}} \ln\left(\frac{e + \sqrt{e^2 - 1}}{e - \sqrt{e^2 - 1}}\right)$$

Figures VII-A-22 thru VII-A-26 in the Appendix also provide data for volume/weight calculations.

The effect of vessel shape on the stresses may also be established by a simple membrane analysis of the pressure vessel in the manner described in the following section.

Membrane Stresses

For shells of revolution a free-body diagram may be taken of any section where the membrane stresses, S_1 and S_2 (Eq. 7), are required to be known.

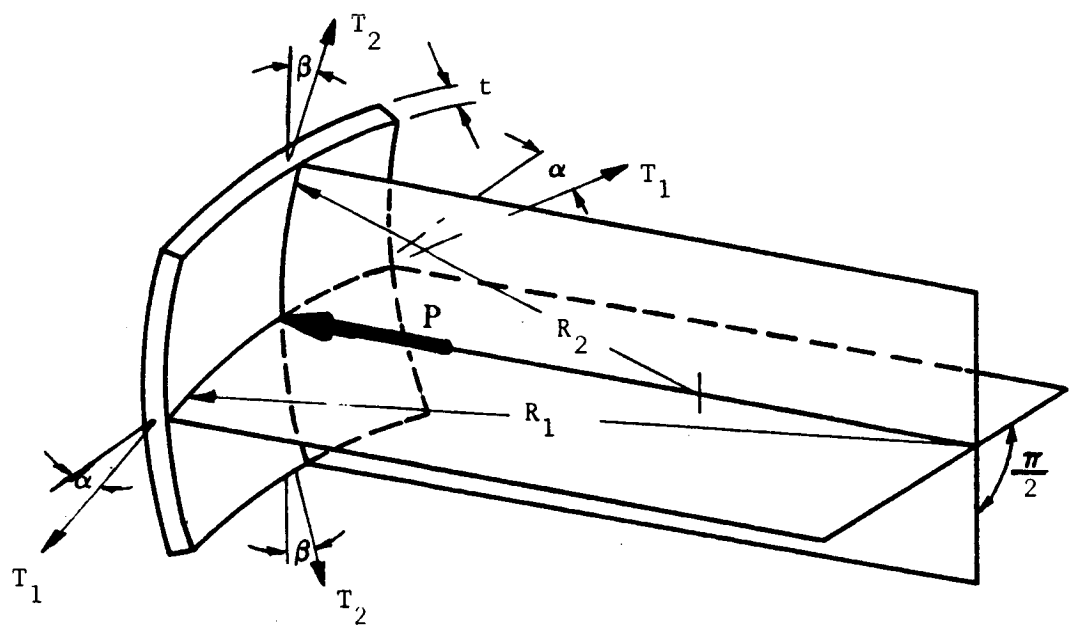

Fig. VII-2-1 Membrane Free Body Diagram

The solution for the membrane stresses may be obtained through the following steps.

T_1 = The hoop stress (latitudinal stress), lb/in

T_2 = The longitudinal stress (meridian stress), lb/in

R_1 = The radius of curvature in the vertical planes, in

R_2 = The radius of curvature in normal planes, in

t = The membrane thickness, in

Then, since the sum of the forces must balance for equilibrium, one arrives at the general form:

$$P = \frac{T_1}{R_1} + \frac{T_2}{R_2} \tag{1}$$

where P is the applied load in lb/in^2.

Applying equation (1) to some common shapes, the stresses are computed as follows. First consider the case of a sphere that has a material density, ρ (lb/in^3) and a gas stored at pressure, P.

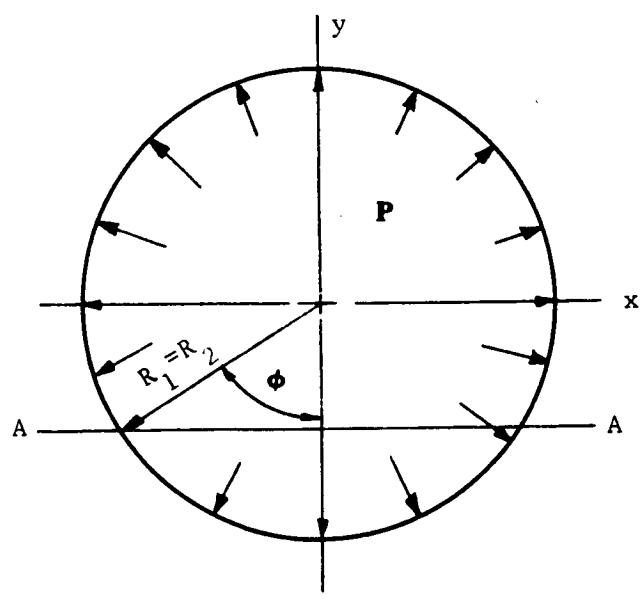

Fig. VII-2-2 Sphere with Internal Pressure, P

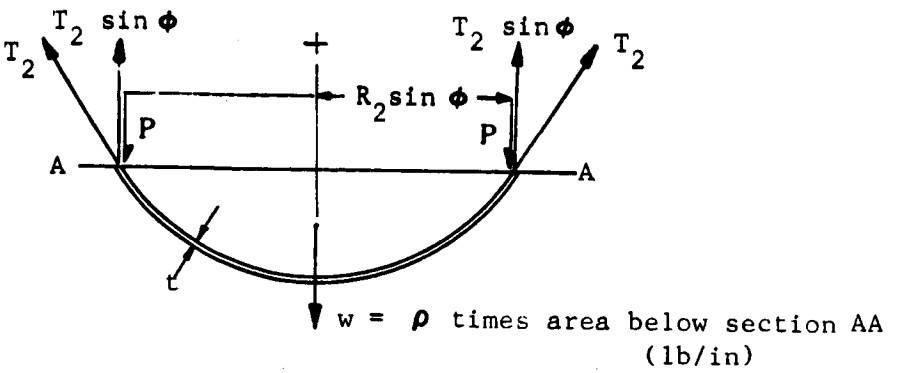

Fig. VII-2-3 Free-Body Diagram at Section AA

$\Sigma F_y = 0$ gives:

$$2\pi T_2 \sin\phi R_2 \sin\phi = \pi P (R_2 \sin\phi)^2 + wt \tag{2}$$

$$\therefore T_2 = \frac{R_2}{2}\left(P + \frac{wt}{\pi (R_2 \sin\phi)^2}\right) \tag{3}$$

and since $R_1 = R_2 = R$ (4)

equation (1) gives $RP = T_1 + T_2$ (5)

then $T_1 = \frac{R}{2}\left(P - \frac{wt}{\pi (R \sin\phi)^2}\right)$ (6)

It is obvious from equations (3) and (6) that $T_2 > T_1$. Therefore, the membrane thickness, t, would be computed from equation (3). The relationship between stresses is given by

$$S_i = \frac{T_i}{t}, \qquad i = 1, 2 \tag{7}$$

and S_1 is the allowable working stress selected by applying some factor of safety to the yield point of the material. The selection of safety factors

will be discussed more fully in Part VII-3. Combining equations (3) and (7) gives finally:

$$t = \frac{PR}{2}\left[\frac{1}{S_2 - \frac{w}{\pi R^2 \sin^2\phi}}\right] \tag{8}$$

which reduces to the usual form for a hemisphere with $\phi = \pi/2$ and w assumed negligible.

$$t = \frac{PR}{2S_2} \tag{9}$$

(b) Cylindrical vessel with elliptical heads and a cryogenically stored gas at density ρ_g (lb/in^3) and pressure P.

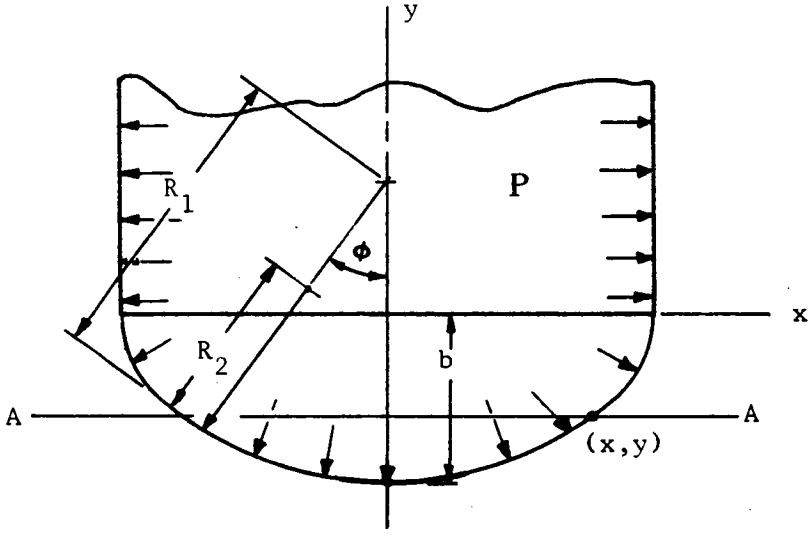

Fig. VII-2-4 Cylindrical Vessel with Elliptical Heads

Again for stresses at section AA a free-body diagram is as follows:

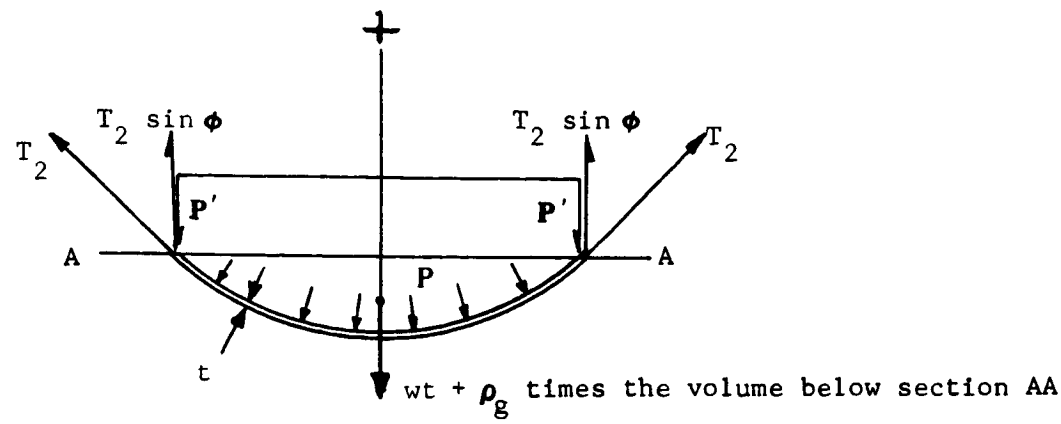

Fig. VII-2-5 Free-Body Diagram at Section AA

where P' is the pressure due to the liquid above section AA plus P. Again $\Sigma F_y = 0$ gives:

$$T_2 \sin\phi \, 2\pi R_1 \sin\phi = P' \pi R_1^2 \sin^2\phi + \rho V + wt \tag{10}$$

Therefore:

$$T_2 = \frac{R_1}{2}\left[P' + \frac{(\rho V + wt)}{R_1^2 \pi \sin^2\phi}\right] \tag{11}$$

and, from Equation (1):

$$T_1 = R_1\left(P' - \frac{T_2}{R_2}\right)$$

with

$$R_1 = \frac{R}{k}\sqrt{1-K^2(1-k^2)} \tag{12}$$

and

$$R_2 = \left(\frac{k}{R}\right)^2 R_1^{\,3} \qquad \text{(Ref. 29)} \tag{13}$$

where R is the radius of the cylinder, $k = \frac{b}{R}$, and $K = \frac{X}{R}$; b is from the equation of the ellipse, which is:

$$\frac{X^2}{R^2} + \frac{Y^2}{b^2} = 1 \qquad (14)$$

Table VII-A-1 in the Appendix lists the values of R_1 and R_2 for the usual shells of revolution used in pressurized gas systems.

Another approach to membrane stress analysis of shells of revolution, which uses a geometrical approximation, may be found under Reference 28 in the bibliography. It should be understood that the preceeding analysis is for shells of revolution only, and if nonaxisymmetric vessels are considered, an approach similar to that described in Part VII-4 must be used.

Materials Selection

After the establishment of the primary design parameters, a material must be selected for use in the pressure vessel. This is usually somewhat more subjective than other aspects of the design because an "experience factor" enters the picture when a manufacturer of pressure vessels selects a material for a new design.[2,3,12] The implication here is that because a pressure vessel manufacturer has used only aluminum in his previous designs, he may wish to do so again even at the expense of an optimum weight because he can offer reliability born from experience as an acceptable substitute. The "experience factor" therefore must not be discounted[3,4] during the establishment of the primary design criteria. Some manufacturers base their materials selection upon an inspectability criterion such as minimum detectable flaw size,[3] whereas others may favor the weldability of the material as paramount. This makes the task of the design engineer extremely difficult, especially if the fabrication will be done by a competitive vendor. What this also implies is that there can be no fixed set of values for screening or ranking factors for selecting an optimum material unless the capabilities of the potential vendors are also considered. The following outlines the design implications of the nine (9) most important qualities other than strength-to-weight ratio.

Candidate or admissible materials should be chosen by a "filtering or screening" process. A set of "filters (selectors)" are established to

provide a sound base upon which to select a group of candidate materials from the full spectrum of materials. These filters are used to screen out all but a select group of materials, which possess the desired qualities for flight-weight pressure vessels. If the design input requires a prior selection of materials for each quality except a minimum weight, then the following properties of the candidate materials must be screened: (1) material compatibility,(2) weldability,(3) workability,(4) machinability, (5) cycle (fatigue) properties,(6) sustained load (creep) properties,(7) corrosion properties, and(8) inspectability.[30]

Development of Criteria for Material Compatibility

Compatibility as discussed here will deal only with the compatibility of materials in the sense that they behave well with each other. Material compatibility in the broader sense is discussed in Section VIII.

Material compatibility may be divided into seven major subgroups: (1) pressure vessel material compatibility with the stored fluid, (2) pressure vessel material compatibility with the insulation, (3) pressure vessel material compatibility with the external piping, (4) outer shell material compatibility with the insulation, (5) outer shell material compatibility with its external environment, (6) outer shell material compatibility with its support structure, and (7) pressure vessel and outer shell material compatibility with their connecting supports. This assumes that the compatibility of the joining techniques is established.

A material selection filter for compatibility must account for each of the above seven items. The following briefly describes the effect of compatibility for these items.

(1) If the stored fluid in contact with the pressure vessel material causes a corrosive condition, this may not only contaminate the fluid, but it will alter the mechanical and physical properties of the material such that design input becomes an unreliable factor. If it is established that the conditions of contact will produce a corrosive situation, then a suitable coating must be selected. This poses additional problems in the

parent material since a coating must then be able to withstand the thermal stresses imposed and yet remain an integral part of the structure.

If the fluid causes a corrosive coating, which is an integral part of the structure such as an anodized finish, then this surface effect must be considered on the design allowables, specifically, tensile strength, fatigue life, and noted sensitivity, to name a few of the usually affected material properties. Stress corrosion is another factor in design which, if not accounted for, can cause catastrophic failures due to production-produced microcrack propagation from an embrittlement of the material at the crack tip. Along with the effect of stress corrosion is hydrogen embrittlement, which produces similar phenomenogical effects. This implies that certain materials such as some titanium alloys may not be used for the cryogenic storage of hydrogen. It also implies that the test fluid must be compatible with the vessel. Many times it is desirable to select as a test fluid something other than the working fluid because of safety considerations, etc. However, Section VIII discusses this in greater detail.

(2) Basically the same problems described above may be anticipated with the bonding or resting of the insulation against the pressure vessel whether the insulation is in solid or gaseous form.

(3) External piping, if not made of the same material as the pressure vessel, may cause thermal discontinuity stresses in service or from welding or the use of a mechanical joint. The piping must therefore be related to the pressure vessel material to avoid the need for extensive and elaborate devices to overcome this effect.

(4) As with the discussion of the corrosion effects encountered in the pressure vessel itself, the outer shell material cannot tolerate any unaccounted-for changes in its properties since it too must resist buckling.

(5) The outer shell's resistance to buckling could be altered by the possibility of corrosion and/or thermal changes resulting from an incompatible external environment.

(6) and (7) Joining the components together and to some supporting structures requires consideration of localized centers of high thermal

ORIGINAL PAGE IS
OF POOR QUALITY

stresses and possible corrosive centers. Joining technology in these areas is generally directed at maintaining alignment and producing low concentrations of stresses. However, even a purely mechanical joint requires some corrosion-oriented consideration because of the difficulty in sealing closely fitting components against corrosive elements.

Development of Criteria for Weldability

A metallic candidate material must meet some basic requirements for fabricability. Of these requirements, welding is one of the most critical since the usual techniques require the joining to be such that structural integrity, leak tightness, etc. are unimpaired. Further, some materials are welding-process sensitive, which could imply some minimum thickness limits for design input. Finally, where mechanical joints are unacceptable or otherwise prohibitive, the candidate material must be weldable. Section VIII describes the weldability of current candidate materials in detail.

Generally speaking then, a candidate material will be selected on the basis of its fabricated behavior.[2] Where various welding processes exist for the same material, that material will be classified for each process. This will provide the greatest possible choice in a particular material. Also, each process for a particular material should be examined by the other selection filters and ranked for ability to satisfy the requirements of each selection filter passed.

Workability and Machinability

The development of these filter criteria would consider the individual capabilities of the manufacturer. Some pertinent input here could include weld tooling (Section VIII), personnel, and professional experience[4,8,9,10]

Cyclic Material Behavior

Cumulative fatigue damage criteria for use as a fatigue filter may be found in References 32,33.

Sustained Load Properties

Creep and relaxation properties are important in many phases of pressure vessel design. For long-term storage, compatibility may influence the selection of a candidate material because of the possibility of stress corrosion.[12] Some pressure vessel manufacturers will degrade the selected material in terms of mechanical properties if high-temperature storage is anticipated even for a short time.[12] Others[10] will age-test to insure against creep failures. Reference 31 in the bibliography provides a readable and informative source for the mechanisms of creep and its design implications.

Development of Criteria for Corrosion Properties

Basically, the corrosive properties of a candidate material are in either one of two forms. It either corrodes or contaminates the material surrounding it, or it is corroded or contaminated by the surrounding material. If either one of these conditions exists, some means of protection must be considered. This can affect the service life, fabricability, weight, or compatibility of the storage system. This may be done by oxide formation on the material surface, which will alter the mechanical and physical properties of the material. A solution would be to coat the surface or, as an alternative, to account for these effects in the design input. It must also be kept in mind that if a corrosion preventative is used, its compatibility with the materials on either side of it must also be considered. For example, a coating may be selected which is somewhat permeable to the stored fluid, but if the mission is short enough a trade-off may be considered if the permeability is low. The aforementioned serves to illustrate in very general terms the effect corrosion has on the selection of a candidate material.

Inspectability

This selection criterion has probably caused more problems in the selection of a candidate material than any other filter here listed. This is because the current state of the art of nondestructive testing has not kept

pace with the designer's ability to predict a realistic failure criterion for a given material under some load profile.

It has been established that a material containing flaws (i.e., cracks) of some critical length will exhibit a far lower strength than the same material with these flaws removed.[32,33] With this principle, manufacturers have developed many schemes to overcome this disparity. All of these schemes rely, to some degree, on fracture mechanics to screen candidate materials for pressure vessel applications. See Part 5 of this section for a discussion of how fracture mechanics may be applied directly to design. The simplest scheme is to limit the ultimate tensile strength to some maximum value since it is assumed that higher ultimate strengths imply a reduction in the fracture toughness of a material.[3,9] Another approach is to plot stress versus the crack area of a material and to use this to establish a proof-test pressure. Figure VII-2-6 illustrates how this is done. First, the curve shown is plotted for a candidate material; then from the stress analysis of the vessel the operating stress is located. Now from the nondestructive testing capabilities a minimum detectable crack size is established, and its intersection with the curve will establish the stress at which the proof test should be done. This will automatically eliminate any vessel during proof testing which has a flaw greater than the detectable size. From the curve one also has the range of potential crack growth which, when used in the design, can predict the service life of the vessel.

Another approach[3] is to plot the notched strength versus the crack area (for part through surface cracks) for various strength levels of a material and then to select the material which has the highest strength at the smallest crack area detectable by the nondestructive testing. This is illustrated in Figure VII-2-7.

Some manufacturers prefer to check their material against fracture by performing a proof test which includes cycling to eliminate the possibility of a precritically cracked vessel escaping detection by their nondestructive testing techniques.[6,11] And finally, the notched-to-unnotched strength

ratio of a candidate material can be compared with the rejection of all those materials with a ratio lower than some arbitrary number.[7]

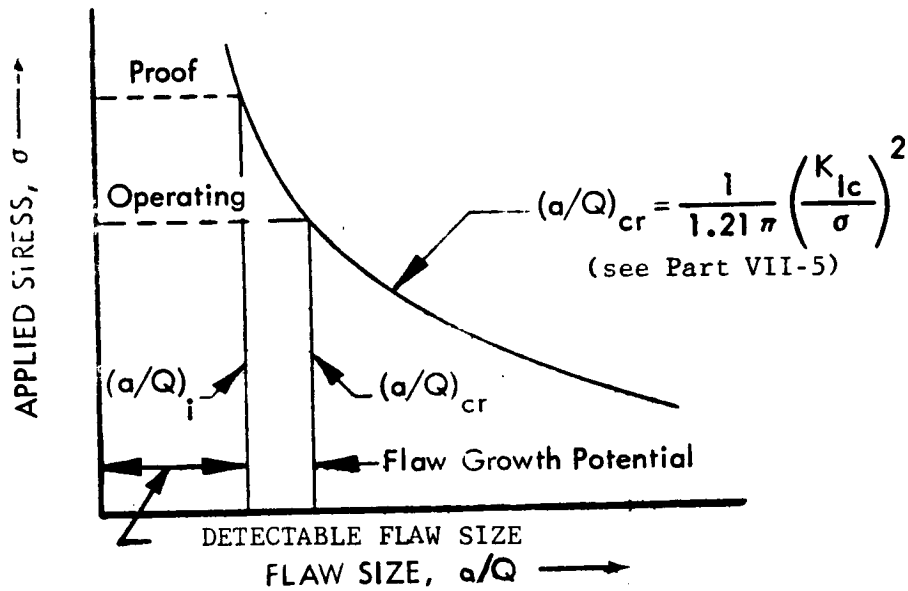

Fig. VII-2-6 Establishing P_p by Considering Fracture Mechanics[4,86]

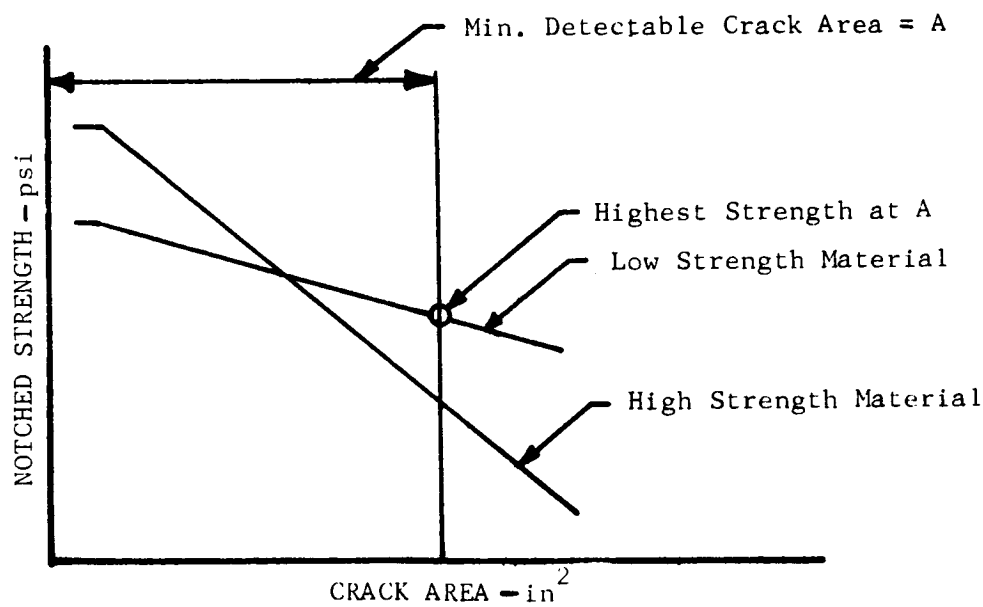

Fig. VII-2-7 Notched Strength Versus Crack Area for Material Selection Filter

The completed set of candidate materials which pass every selection filter should then be tabulated in order of rank. This rank will be the sum of the material's ability to satisfy all of the requirements of the selection filters. Rank in this sense need not mean that the material with the best performance in each category will be the material selected. What will result is the reduction of all possible materials to a select set, which will possess tabulated differences in their abilities to satisfy the selection filters. The presentation of these differences will consequently establish a means by which a material may be selected once the design is completed.

Optimum Design Considerations and Processing Variables

As discussed earlier, weight is usually the primary concern for designers of flight-weight pressurized gas systems. One approach in saving weight has also been previously mentioned, that of using a computer with weight as the only optimizing objective in a set of generalized shell equations similar to those described in Part VII-4. Another approach is that of configuration efficiency coefficients,[1] and yet another is in the use of a mass fraction, which is defined as the ratio of the weight of the complete pressurized gas system to the weight of the gas to be carried.[22] In the latter approach the idea is to increase the mass fraction to some maximum value. This is done by analyzing a number of configurations and selecting the one with the largest mass fraction. A large number of configurations may be studied if a computer is used to perform the computations.

However, it is not always possible to build an optimumly designed pressure vessel because of various subtleties, which are not apparent during the design stage. One of these is handling. It is not always possible to physically move or manipulate a large, thin shell without denting or otherwise damaging the membrane surface.[10,12,13] It then becomes necessary to either provide expensive, delicate handling devices and instructions to the manufacturing personnel or to increase the membrane thickness to a degree at which it becomes insensitive to existing handling procedures. A second problem area may be the weld tooling. If the designed joint can develop

sufficient strength with little or no reinforcement, the design program will indicate this However, it may not be possible to join pieces of the vessel together in this state. What would be required here is to increase the weld reinforcement in thickness or extent or both until sufficient stiffness is attained to be joined using existing tooling techniques without distortion.[6,7] A third problem would be in the location of bosses and brackets for support structures, etc. If the design program locates a bracket, which is, for example, on the cylindrical section of a pressure vessel, then special machining procedures must be expected. Since most pressure vessels are constructed from forgings and then machined to size, any obstruction to a complete machining cycle naturally requires individual attention to overcome. Most manufacturers prefer to provide bosses at either end of a pressure vessel for piping connections and structural supports to overcome this problem.[6,7,9] The junction of hemispheres or a hemisphere to a cylinder is also a likely place to provide support arrangements since there is usually an area of low stress; however, high-stress risers due to the bending moment are transferred to the adjacent membrane.[37,38,39]

VII-3 CONSTRUCTION DETAILS AND SUPPORT STRUCTURES

As mentioned earlier, joining pieces of a pressure vessel together has additional design implications, which are not easy to account for. This is due to the additional bending moment in the membrane adjacent to a junction. The cause of this moment is easy to understand as it is essentially due to a change in stiffness at that point. When the vessel is loaded, one section will tend to deform more than another, at the junction of a hemispherical head and a cylindrical section. The usual approach is to consider the membrane as a beam on an elastic foundation and add an additional stress to the stresses computed by the membrane analysis. Reference 14 may be used to establish the rough magnitudes of these stresses for preliminary weight computations, but a more sophisticated approach should be considered when the exact contour of the junction is required. One such approach is the use of nonlinear terms in the equilibrium equations. This is illustrated in Reference 38.

The design of bosses and other connections may also be done using Reference 14 but again only for rough dimensions. For the final design a technique such as that described in Part VII-4 should be used in conjunction with the nonlinear theory of shell design.

Seals and sealing techniques are also discussed in detail in Section X and will not be considered here.

Little attention is usually given to support structures as they are usually designed with the main structure of the spacecraft.[5] It is, however, important that provision for some flexability in support design be allowed because of changing design concepts while the pressure vessel is in the premanufacturing stage.[13] More important than this is the fact that between pressure cycles there may be a considerable difference in the size of the vessel and its associated piping. This pressure growth must be absorbed by the supports, and therefore an additional load or flexibility will be required as a design input for the supports. Often the piping from the vessel to the first rigid connection is purposely made as long as

possible to overcome the possibility of overstressing a valve or the support structure. In cryogenic vessels the thermal gradient which exists between the inner and outer vessels is large enough to cause extreme changes in the stress state of a connecting pipe. Therefore, a long curved pipe is often used to compensate for these stresses, while the supports for the inner vessel have provision for mechanical movement.

A consideration which the project engineer must not overlook, especially during the testing of a pressurized gas system, is safety. One must be intimately informed about all potential hazards associated with the system so that adequate devices and techniques can be established to prevent an accident. There are four primary categories of hazards for any pressurized gas system: 1) hazards due to flamability, 2) hazards due to high pressure gases, 3) hazards due to materials of construction, and 4) hazards associated with inexperienced personnel.[26]

VII-4 STRESS ANALYSIS

Introduction

The preliminary stages of pressure vessel design usually require the study of various vessel configurations so that later system requirements will be met. This entails the use of an accurate but simple design technique. As described in Part 3 of this Section, a simple membrane analysis is sufficient to determine the rough weight of a pressure vessel. As it turns out, this, along with some additional simple techniques of analysis, is also sufficient for the initial design of a pressure vessel. This part will provide enough basic ideas and equations so that an adequate design of a pressure vessel may be performed.

A design technique of this sort necessarily ignores many effects associated with the containment of a gas or fluid under pressure. To do this requires that some restrictions be imposed on the physical aspects of the vessel and that the final design is followed by a rigorous analysis, usually with the aid of a digital computer. Some of the more significant physical restrictions are that this treatment covers only pressure vessels which are described by shells of revolution, and that the pressure vessel wall thickness, t, is small compared to the inside radius.

From Fig. VII-2-1 in Part 2, Equation (1) was developed by equilibrium and is as follows:

$$\frac{T_1}{R_1} + \frac{T_2}{R_2} = P \qquad (1)$$

And as before, the definition of terms are as follows:

T_1 = hoop stress (latitudinal stress) (lb/in)
T_2 = longitudinal stress (meridian stress) (lb/in)
R_1 = radius of curvature in vertical plane (in)
R_2 = radius of curvature in normal plane (in)
t = membrane thickness (in)
P = applied load (pressure + dynamic + static loads) (lb/in^2)
ϵ_1 = hoop strain (in/in)

ϵ_2 = longitudinal strain (in/in)

ν = Poisson's ratio

E = Modulus of Elasticity (lb/in^2) (values may be found in MIL-HDBK-5)

ρ = density (lb/in^3)

w $= \rho A$ = weight of membrane divided by t (lb/in)

δ = hoop displacement (in)

y = deflection (in)

k = spring constant (lb/in)

I = moment of inertia (in^4)

M = ring or membrane edge moment (in-lb)

V = axial force (lb)

ln = logarithms to the base e, (Naperian)

Membrane Analysis

For a membrane under internal pressure P, the following free-body diagram may be drawn:

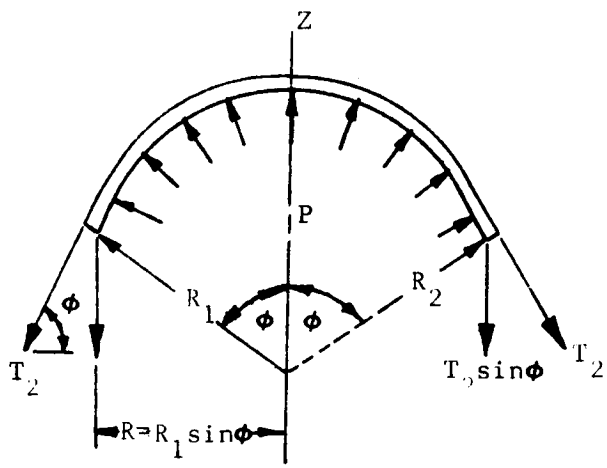

Fig. VII-4-1 Free-Body Diagram of General Shell of Revolution

Where $\sum F_z = 0$ for equilibrium gives:

$$2\pi T_2 R_1 \sin^2\phi = \pi P (R_1 \sin\phi)^2 \qquad (15)$$

or

$$T_2 = \frac{PR_1}{2} \tag{16}$$

And Equation (9) along with (1) may be solved for T_1 as follows:

$$T_1 = PR_1\left(1 - \frac{R_1}{2R_2}\right) \tag{17}$$

And from Equation (10), if $2R_2 \leq R_1$, then the hoop stresses will be compressive. Notice also that for a cylinder $R_2 \rightarrow \infty$ and $T_1 = PR_1$ or from Equation (7), $S_1 = \frac{T_1}{t}$, therefore, $t = \frac{PR_1}{S_1}$, which is the familiar form for cylindrical hoop stress. To see how T_1 and T_2 are related consider the following figure.

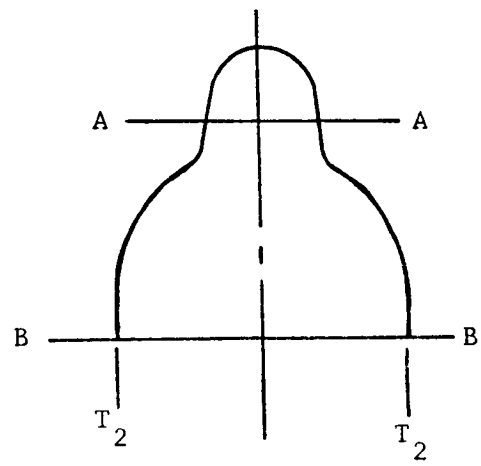

Fig. VII-4-2 Shell of Revolution
Showing Relationship of T_1 and T_2
(Ref. 36)

Here, T_2 at section B•B depends upon the area at BB whereas T_2 at A•A depends upon the area at AA. But since A•A is obviously smaller than B•B how does T_2 change? Between AA and BB, the change in T_1 is enough to compensate for the changes in T_2.

As mentioned before if $2R_2 < R_1$, compressive hoop stresses will result and buckling may follow. The following will illustrate how this may occur.

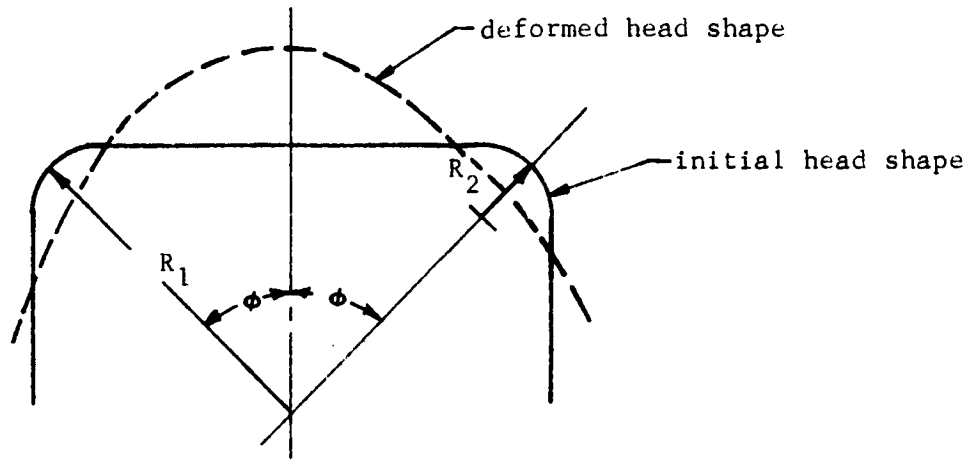

Fig. VII-4-3 Shell of Revolution where $R_1 > 2\ R_2$

As r_2 increases the flat portion of the head tends to assume a spherical shape which, since there is extra material in the sharp knuckle region, will cause a series of shock waves around the circumference[36]. If the ratio of T_1 and T_2 is taken the result is:

$$\frac{T_1}{T_2} = 2 - \frac{R_1}{R_2} \tag{18}$$

so if a head is designed such that $\frac{R_1}{R_2} = 2$, then $T_1 = 0$ everywhere on the head. However, this is not as desirable as is first thought since $R_1 = R_2 = \infty$ at the apex of a head. This will cause T_2 to be extremely large.

For shells of revolution with negative curvature, R_2 is replaced by $-R_2$ and the same analysis follows. (See Fig. VII-4-4)

One special case that exists is the torus. Fig. VII-4-5 shows how the forces are distributed and the following equations are developed by the same equilibrium requirements as before.

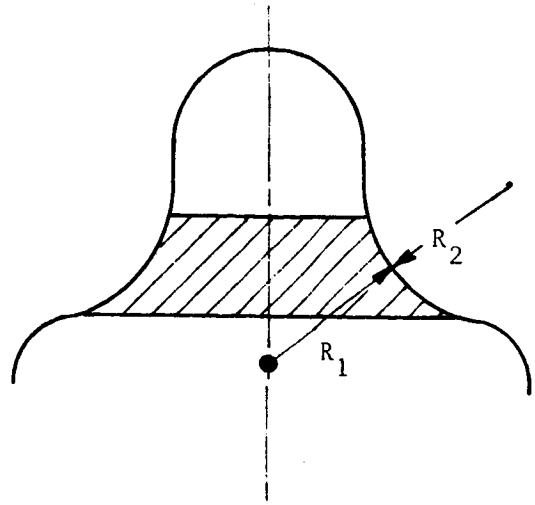

Fig. VII-4-4 Shell of Revolution with R_2 Negative in the Shaded Area

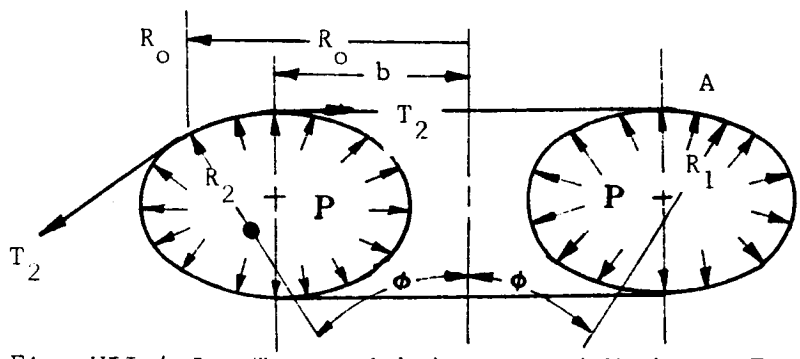

Fig. VII-4-5 Torus with Associated Membrane Forces (Ref. 36)

$\Sigma F_z = 0$ gives:

$$2\pi T_2 R_o \sin\phi = \pi P\left(R_o^2 - b^2\right), \quad \sin\phi = \frac{R_o}{R_1}$$

$$\therefore\ T_2 = \frac{PR_1}{2}\left[1 - \left(\frac{b}{R_o}\right)^2\right] \tag{19}$$

And using Equation (1):

$$T_1 = PR_1 \left[1 - \frac{R_1}{2R_2} \left(1 - \frac{b^2}{R_o^2} \right) \right] \tag{20}$$

And the hoop forces become negative if :

$$2 \frac{R_2}{R_1} \leq 1 - \left(\frac{b}{R_o} \right)^2 \tag{21}$$

If the cross-section of the torus is circular then Equations (19) and (20) become :

$$\left. \begin{aligned} T_1 &= \frac{Pa}{2} \\ T_2 &= \frac{P\varepsilon}{2} \left(1 + \frac{b}{R_o} \right) \end{aligned} \right\} \tag{22}$$

where :

$$R_2 = 0 \text{ and } \sin \Phi = \frac{R_o - b}{a} \quad \text{(Ref. 36)}$$

Displacements

Many occasions arise where the hoop displacements of a membrane are required to be known. For the usual biaxial stress state encountered in pressure vessels, Hooke's law is :

$$\epsilon_1 = \frac{1}{E} (S_1 - \nu S_2) \tag{23}$$

And the hoop strain ϵ_1 is defined by .

$$\epsilon_1 = \frac{\Delta \ell}{\ell} = \frac{2\pi(R + \delta) - 2\pi R}{2\pi R} = \frac{\delta}{R} \tag{24}$$

therefore :

$$\delta = \epsilon_1 R$$

Combining Equations (7), (23) and (24) gives an expression for the displacement, δ, in terms of T_1 and T_2:

$$\delta = \frac{R}{Et} (T_1 - \nu T_2) \tag{25}$$

Table VII-4-1 lists the values of S_1, S_2, and δ for some common shells of revolution[36].

Table VII-4-1

S_1, S_2 AND δ FOR COMMON SHELLS OF REVOLUTION

SHELL	S_1	S_2	δ
Cylinder - hoop stress only	$\frac{Pa}{t}$	0	$\frac{Pa^2}{Et}$
Cylinder - hoop and longitudinal stress	$\frac{Pa}{t}$	$\frac{Pa}{2t}$	$\frac{Pa^2}{Et}\left(1 - \frac{\nu}{2}\right)$
Sphere	$\frac{Pa}{2t}$	$\frac{Pa}{2t}$	$\frac{Pa^2}{2Et}(1 - \nu)$
Ellipse - at equator	$\frac{Pa}{t}\left(1 - \frac{a^2}{2b^2}\right)$	$\frac{Pa}{2t}$	$\frac{Pa^2}{2Et}\left(2 - \nu - \frac{a^2}{b^2}\right)$

Discontinuity Stresses

Because of the differing stiffnesses between a membrane and a head or between a membrane and a part, discontinuity stresses develop and must be considered in design. Figures VII-4-6 and VII-4-7 illustrate some typical discontinuity problems encountered.

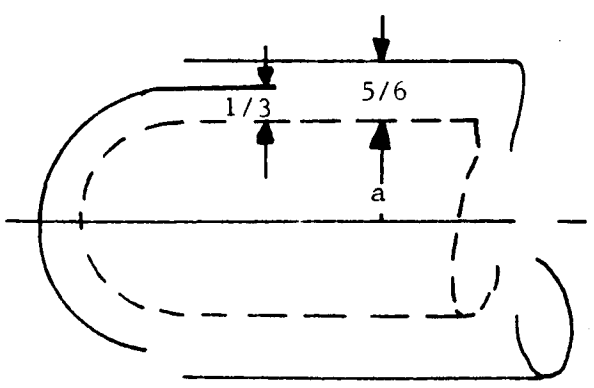

$$\delta_{Sphere} = \frac{(I)}{3}\frac{Pa^2}{Et}$$

$$\delta_{Cylinder} = \frac{5}{6}\frac{Pa^2}{Et}$$

Fig. VII-4-6 Discontinuity Stresses for a Steel (ν = 1/3) Cylindrical Pressure Vessel with a Hemispherical Head (Ref. 36)

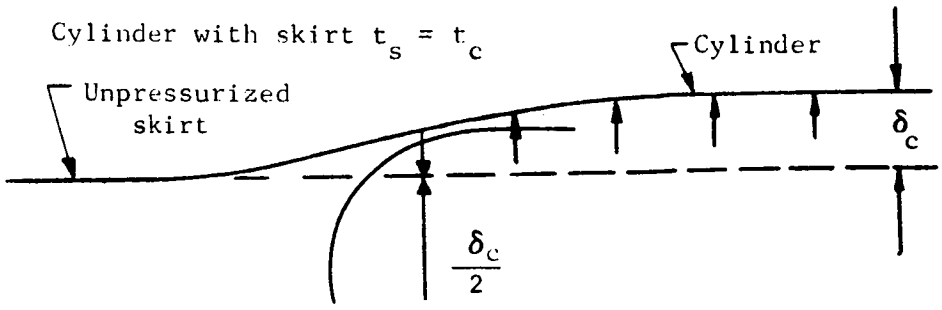

Fig. VII-4-7 Discontinuity Stresses
for a Cylinder with a Skirt and A Hemispherical Head (Ref. 36)

From continuity, the radial displacement of the cylinder must match that of the head. These discontinuities produce bending and compressive stresses in the membrane which must be added to the membrane stresses as computed by Equation (1). These stresses are included in the hoop stress by the addition of the compressive (or tensile) stress S_c, acting on the radius, and the bending stress, S_b acting around the circumference. Therefore, the total circumferential (hoop) stresses become :

$$S_1' = S_1 \pm S_c \pm S_b \tag{26}$$

where, as usual, $S_b = \frac{Mc}{I}$. However, because of the lateral restrictions of a plate,

$$I = \frac{t^3}{12(1 - \nu^2)}$$

and

$$c = t/2$$

therefore,

$$S_b = \frac{6M}{t^2(1 - \nu^2)} .$$

The longitudinal stress contains the membrane stress plus the discontinuity stress found by using the elastic foundation beam formulas. (Ref. 14)

A beam on an elastic foundation may be thought of as a beam held in equilibrium under a load by an infinite number of springs, each with the spring constant k. Figure VII-4-8 roughly shows this analogy.

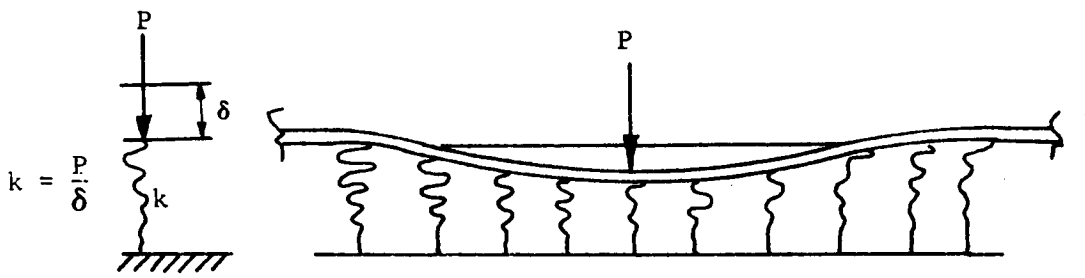

Fig. VII-4-8 Beam on an Elastic Foundation (Ref. 36)

The development of the equations will not be given here but may be found in References 14 or 23. The solution to the differential equation for various loading conditions usually encountered in pressure vessel design is as follows:

Case 1. Infinitely long beam, single concentrated load deflection:

$$y = \frac{P\beta}{2k} A_{\beta x} \tag{27}$$

where:

$$\left.\begin{aligned} \beta &\equiv \sqrt[4]{\frac{k}{4EI}} = \frac{\sqrt[4]{3(1-\nu^2)}}{\sqrt{RT}} \\ k &= \frac{Et}{R^2} \end{aligned}\right\} \tag{28}$$

and the slope is:

$$\theta = -\frac{P\beta^2}{k} B_{\beta x} \tag{29}$$

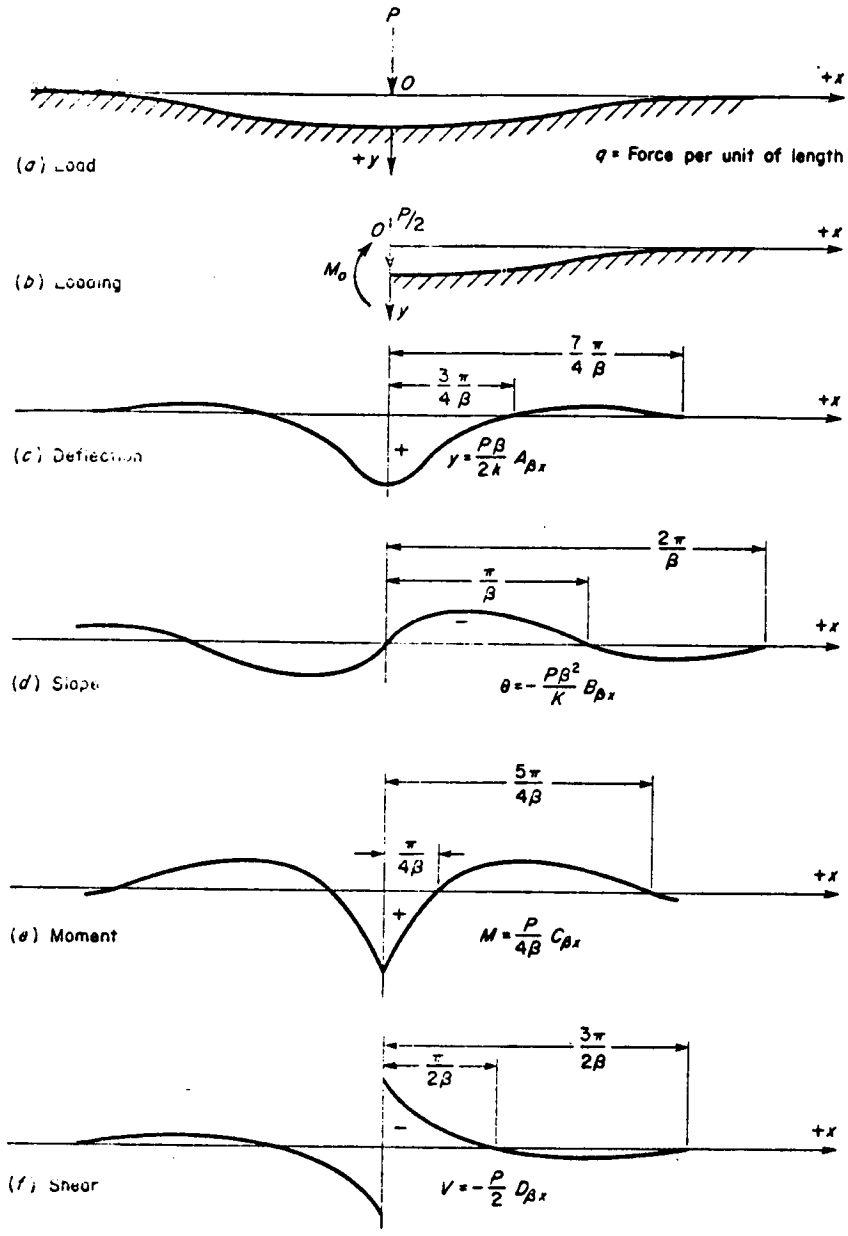

Fig. VII-4-9 Loading, Deflection, Slope, Moment and Shear in a Beam on an Elastic Foundation (Ref. 14)

Table VII-4-2

FUNCTIONS A_x, B_x, C_x, AND D_x (Ref. 14)

βx	$A_{\beta x}$	$B_{\beta x}$	$C_{\beta x}$	$D_{\beta x}$	βx	$A_{\beta x}$	$B_{\beta x}$	$C_{\beta x}$	$D_{\beta x}$
0	1.0000	0	1.0000	1.0000	3.6	−0.0366	−0.0121	−0.0124	−0.0245
0.1	0.9907	0.0903	0.8100	0.9003	3.7	−0.0341	−0.0131	−0.0079	−0.0210
0.2	0.9651	0.1627	0.6398	0.8024	3.8	−0.0314	−0.0137	−0.0040	−0.0177
0.3	0.9267	0.2189	0.4888	0.7077	3.9	−0.0286	−0.0140	−0.0008	−0.0147
0.4	0.8784	0.2610	0.3564	0.6174	$5\pi/4$	−0.0278	−0.0140	0	−0.0139
0.5	0.8231	0.2908	0.2415	0.5323	4.0	−0.0258	−0.0139	0.0019	−0.0120
0.6	0.7628	0.3099	0.1431	0.4530	4.1	−0.0231	−0.0136	0.0040	−0.0095
0.7	0.6997	0.3199	0.0599	0.3798	4.2	−0.0204	−0.0131	0.0057	−0.0074
$\pi/4$	0.6448	0.3224	0	0.3224	4.3	−0.0179	−0.0125	0.0070	−0.0054
0.8	0.6354	0.3223	−0.0093	0.3131	4.4	−0.0155	−0.0117	0.0079	−0.0038
0.9	0.5712	0.3185	−0.0657	0.2527	4.5	−0.0132	−0.0108	0.0085	−0.0023
1.0	0.5083	0.3096	−0.1108	0.1988	4.6	−0.0111	−0.0100	0.0089	−0.0011
1.1	0.4476	0.2967	−0.1457	0.1510	4.7	−0.0092	−0.0091	0.0090	0.0001
1.2	0.3899	0.2807	−0.1716	0.1091	$3\pi/2$	−0.0090	−0.0090	0.0090	0
1.3	0.3355	0.2626	−0.1897	0.0729	4.8	−0.0075	−0.0082	0.0089	0.0007
1.4	0.2849	0.2430	−0.2011	0.0419	4.9	−0.0059	−0.0073	0.0087	0.0014
1.5	0.2384	0.2226	−0.2068	0.0158	5.0	−0.0046	−0.0065	0.0084	0.0019
$\pi/2$	0.2709	0.2709	−0.2709	0	5.1	−0.0033	−0.0057	0.0080	0.0023
1.6	0.1959	0.2018	−0.2077	−0.0059	5.2	−0.0023	−0.0049	0.0075	0.0026
1.7	0.1576	0.1812	−0.2047	−0.0235	5.3	−0.0014	−0.0042	0.0069	0.0028
1.8	0.1234	0.1610	−0.1985	−0.0376	5.4	−0.0006	−0.0035	0.0064	0.0029
1.9	0.0932	0.1415	−0.1899	−0.0484	$7\pi/4$	0	−0.0029	0.0058	0.0029
2.0	0.0667	0.1230	−0.1794	−0.0563	5.5	0.0000	−0.0029	0.0058	0.0029
2.1	0.0439	0.1057	−0.1675	−0.0618	5.6	0.0005	−0.0023	0.0052	0.0029
2.2	0.0244	0.0895	−0.1548	−0.0652	5.7	0.0010	−0.0018	0.0046	0.0028
2.3	0.0080	0.0748	−0.1416	−0.0668	5.8	0.0013	−0.0014	0.0041	0.0027
$3\pi/4$	0	0.0671	−0.1342	−0.0671	5.9	0.0015	−0.0010	0.0036	0.0026
2.4	−0.0056	0.0613	−0.1282	−0.0669	6.0	0.0017	−0.0007	0.0031	0.0024
2.5	−0.0166	0.0492	−0.1149	−0.0658	6.1	0.0018	−0.0004	0.0026	0.0022
2.6	−0.0254	0.0383	−0.1019	−0.0636	6.2	0.0019	−0.0002	0.0022	0.0020
2.7	−0.0320	0.0287	−0.0895	−0.0608	2π	0.0019	0	0.0019	0.0019
2.8	−0.0369	0.0204	−0.0777	−0.0573	6.3	0.0019	+0.0001	0.0018	0.0018
2.9	−0.0403	0.0132	−0.0666	−0.0534	6.4	0.0018	0.0003	0.0015	0.0017
3.0	−0.0423	0.0070	−0.0563	−0.0493	6.5	0.0018	0.0004	0.0012	0.0015
3.1	−0.0431	0.0019	−0.0469	−0.0450	6.6	0.0017	0.0005	0.0009	0.0013
π	−0.0432	0	−0.0432	−0.0432	6.7	0.0016	0.0006	0.0006	0.0011
3.2	−0.0431	−0.0024	−0.0383	−0.0407	6.8	0.0015	0.0006	0.0004	0.0010
3.3	−0.0422	−0.0058	−0.0306	−0.0364	6.9	0.0014	0.0006	0.0002	0.0008
3.4	−0.0408	−0.0085	−0.0237	−0.0323	7.0	0.0013	0.0006	0.0001	0.0007
3.5	−0.0389	−0.0106	−0.0177	−0.0283	$9\pi/4$	0.0012	0.0006	0	0.0006

moment: $M = \frac{P}{4\beta} C_{\beta x}$ (30)

and shear: $V = -\frac{P}{2} D_{\beta x}$. (31)

and at x = 0 the maximum values become:

$$\left.\begin{aligned} y_{max} &= \frac{P\beta}{2k} \\ M_{max} &= M_o = \frac{P}{4\beta} \\ V_{max} &= -\frac{P}{2} \end{aligned}\right\} \quad (32)$$

These results are summarized in Figure VII-4- 9 and the coefficients for βx are listed in Table VII-4-2.

Case 2. Infinitely long beam, uniformly distributed load. This form of loading is shown in Fig. VII-4-10.

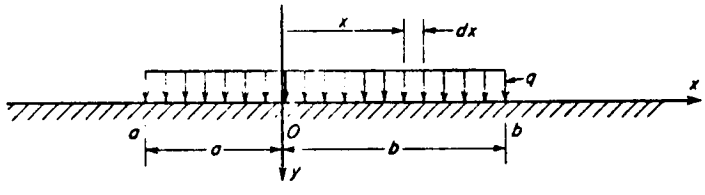

Fig. VII-4-10 Uniformly Distributed Load Over a Portion of a Beam on an Elastic Foundation (Ref. 14)

$$\left.\begin{aligned} &\text{deflection:} && y_o = \frac{q}{2k}(2 - D_{\beta a} - D_{\beta b}) \\ &\text{slope:} && \theta = \frac{q\beta}{2k}(A_{\beta a} - A_{\beta b}) \\ &\text{moment:} && M = \frac{q}{4\beta^2}(B_{\beta a} + B_{\beta b}) \\ &\text{shear:} && V = \frac{q}{4\beta}(C_{\beta a} - C_{\beta b}) \end{aligned}\right\} \quad (33)$$

Case 3. Infinitely long beam, single moment or couple. Figure VII-4-11

describes this loading.

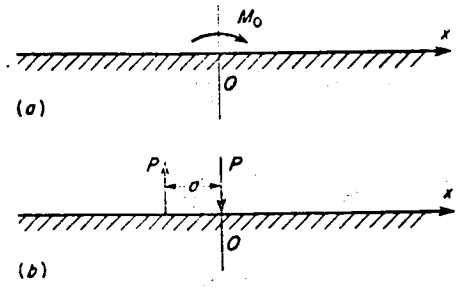

Fig. VII-4-11. Single Moment Acting on a Beam on an Elastic Foundation (Ref. 14)

$$\left.\begin{aligned}
&\text{deflection: } y = \frac{M_o\beta^2}{k} B_{\beta x} \\
&\text{slope: } \theta = \frac{M_o\beta^2}{k} C_{\beta x} \\
&\text{moment: } M = \frac{M_o}{2} D_{\beta x} \\
&\text{shear: } V = \frac{M_o\beta}{2} A_{\beta x}
\end{aligned}\right\} \quad (34)$$

Case 4. Semi-infinite beam. Figure VII-4-12 describes this loading.

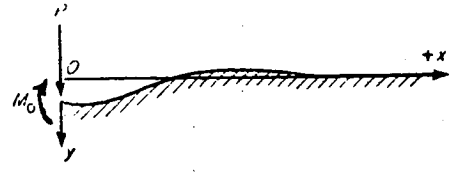

Fig. VII-4-12 Semi-infinite Beam on an Elastic Foundation (Ref. 14)

$$\left.\begin{aligned}
&\text{deflection:}\quad y = \frac{2P\beta}{k} D_{\beta x} - \frac{2M_o\beta^2}{k} C_{\beta x} \\
&\text{slope:}\quad \theta = \frac{2P\beta^2}{k} A_{\beta x} + \frac{4M_o\beta^3}{k} D_{\beta x} \\
&\text{moment:}\quad M = -\frac{P}{\beta} B_{\beta x} + M_o A_{\beta x} \\
&\text{shear:}\quad V = -PC_{\beta x} - 2M_o B_{\beta x}
\end{aligned}\right\} \qquad (35)$$

and at x = 0 the maximum values become:

$$\left.\begin{aligned}
y_{max} &= \frac{2P\beta}{k} - \frac{2M_o\beta^2}{k} \\
\theta_{max} &= -\frac{2P\beta^2}{k} + \frac{4M_o\beta^3}{k}
\end{aligned}\right\} \qquad (36)$$

Now with the above equations and superposition, discontinuity problems may be considered. Also, the examination of these equations lead to the following results for local loads on a cylindrical shell[36].

a) the load is distributed as hoop stresses from deflection and by longitudinal bending.

b) the load may be considered negligible beyond the distance $x \doteq 2.45\sqrt{Rt}$

As an example of the application of the previous development, consider the problem of a cylindrical vessel with a hemispherical head.

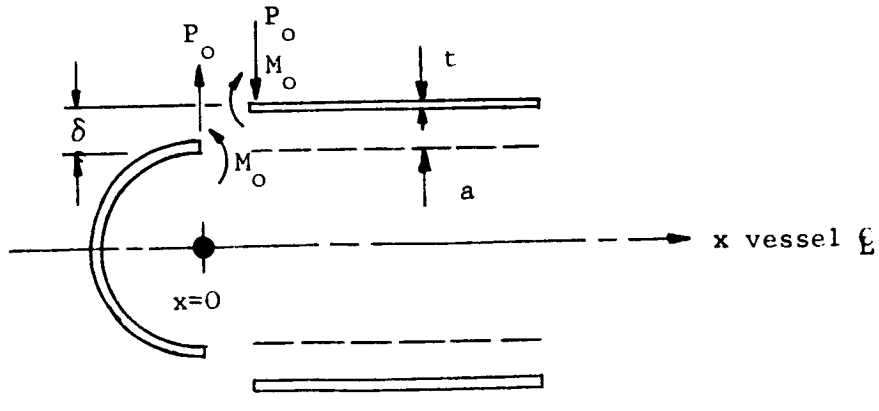

Fig. VII-4-13 Discontinuity at Cylinder to Hemispherical Head Junction with Internal Pressure P

From Table VII-4-1, stresses and deflections are as follows:

cylinder:

$$\left.\begin{aligned} S_{1c} &= \frac{Pa}{t} \\ S_{2c} &= \frac{Pa}{2t} \\ \delta_c &= \frac{Pa^2}{2tE}(2 - \nu) \end{aligned}\right\} \quad (37)$$

hemisphere:

$$\left.\begin{aligned} S_{1s} &= \frac{Pa}{2t} \\ S_{2s} &= \frac{Pa}{2t} \\ \delta_s &= \frac{Pa^2}{2Et}(1 - \nu) \end{aligned}\right\} \quad (38)$$

The difference in displacement is $\delta = \delta_c - \delta_s = \frac{Pa^2}{2Et}$. If the thickness of the cylinder and hemisphere are equal ($t_c = t_s$) then the deflections caused by the shear load V_o are equal and therefore continuity is satisfied if the edge moment $M_o = 0$ and $V_o = \delta/2$ (Ref. 14). Substituting these values for M_o and y into Equation (35), the following results:

$$\frac{\delta}{2} = \frac{2V_o\beta}{k} D_{\beta x} \quad (39)$$

From Table VII-4-2, $D_{\beta x} = 1$ at $x = 0$, and using the value of k from Equation (28), a solution for V_o is:

$$V_o = \frac{P}{8\beta} \quad (40)$$

Consequently the total hoop and longitudinal stress for the cylinder at any x becomes:

$$\left.\begin{aligned} S_1^* &= \frac{Pa}{t} - \frac{Pa}{4t} D_{\beta x} \pm \frac{3\nu P}{4t^2\beta^2} B_{\beta x} \\ S_2^* &= \frac{Pa}{2t} \pm \frac{3P}{t^2 4\beta^2} B_{\beta x} \end{aligned}\right\} \quad (41)$$

If the ratio of the stresses with discontinuity versus the stresses without discontinuity is considered as a stress concentration factor, equations may be developed and plotted for differing geometries[36]. One such plot is for the junction between a cylinder and an elliptical head and is summarized in Figures VII-4-14 and VII-4-15.

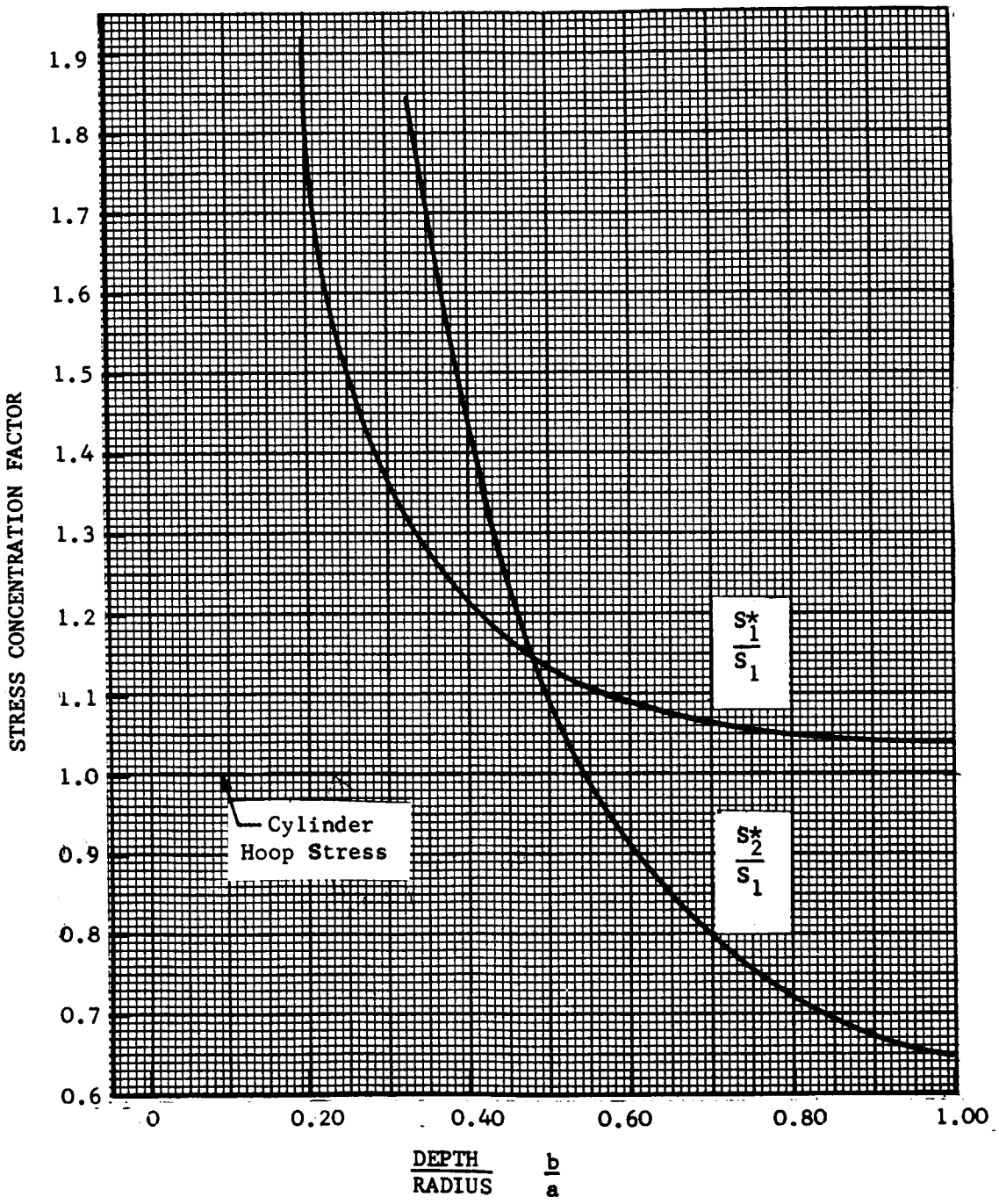

Fig. VII-4-14 Stress Concentration Factors in Cylinders Connected to Elliptical Heads (Ref. 36)

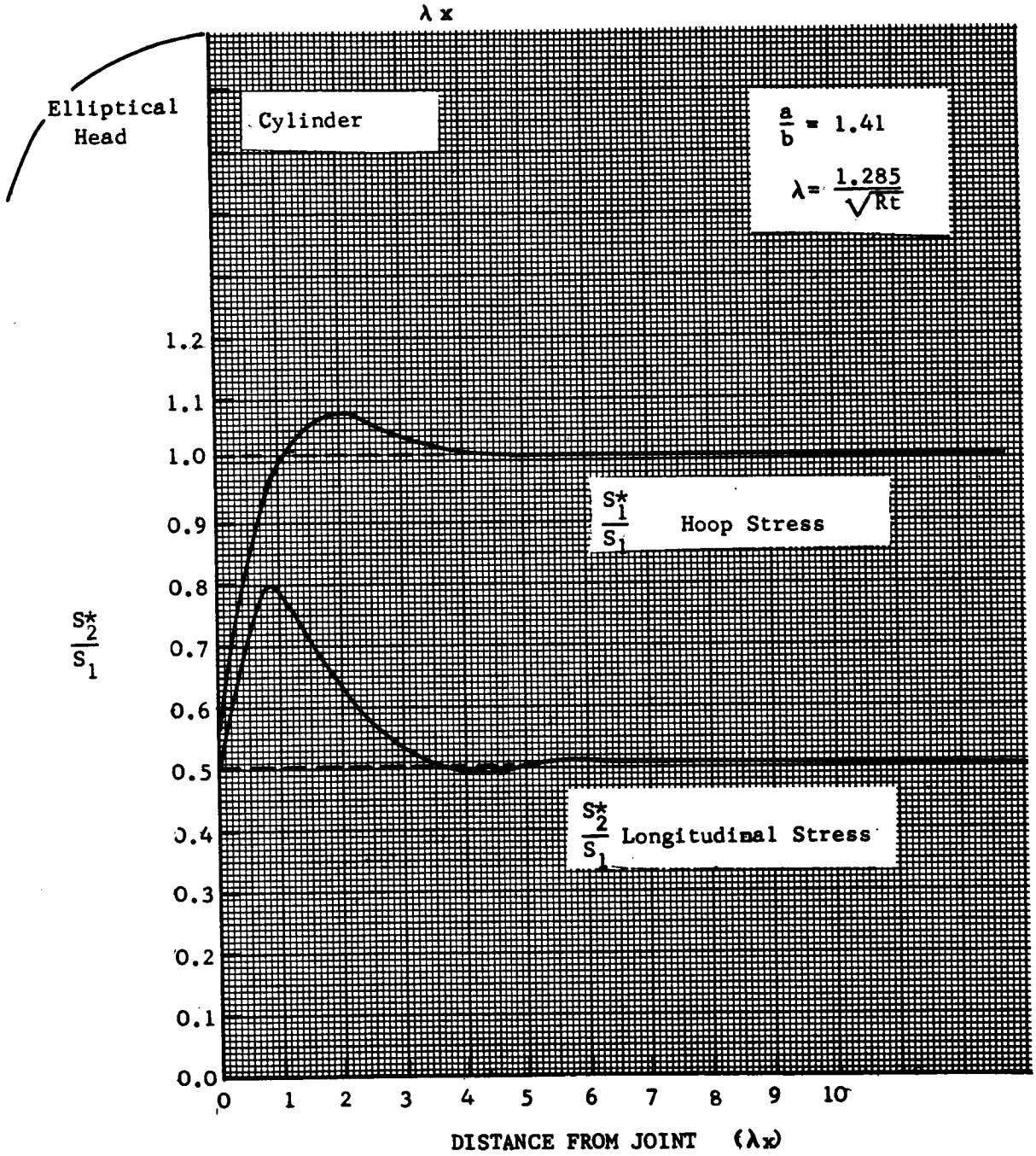

Fig. VII-4-15 Stress Distribution Near Elliptical Head to Cylinder Joint (Ref. 36)

Influence Coefficients for Long Cylinders

Solutions to various basic problems of the type just considered have been tabulated as influence coefficients and are shown in Table VII-4-3.

Table VII-4-3

INFLUENCE COEFFICIENTS FOR LONG CYLINDERS (Ref. 36)

	DEFORMATIONS		MAXIMUM STRESSES	
	RADIAL DISPLACEMENT	ROTATIONS (Radians)	HOOP STRESS, S_1	LONGITUDINAL STRESS, S_2
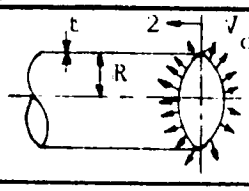	$y = \frac{2.57V_o}{E}\left(\frac{R}{t}\right)^{\frac{3}{2}}$	$\theta = \frac{3.30RV_o}{Et^2}$	$S_1 = \frac{2.57V_o}{t}\left(\frac{R}{t}\right)^{\frac{1}{2}}$	$S_2 = \frac{1.504V_o}{t}\left(\frac{R}{t}\right)^{\frac{1}{2}}$ at $x = 0.611(Rt)^{\frac{1}{2}}$
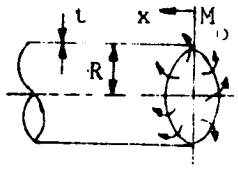	$y = \frac{3.30RM_o}{Et^2}$	$\theta = \frac{8.50}{Et^2}\left(\frac{R}{t}\right)^{\frac{1}{2}} M_o$	$S_1 = \frac{5.104M_o}{t^2}$ at $x = 0$	$S_2 = \frac{6M_o}{t^2}$ at $x = 0$
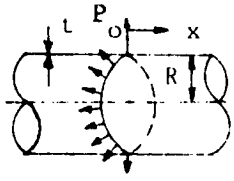	$y = \frac{0.643P_o}{E}\left(\frac{R}{t}\right)^{\frac{3}{2}}$	$\theta = 0$	$S_1 = \frac{0.993P_o}{t}\left(\frac{R}{t}\right)^{\frac{1}{2}}$ at $x = 0$	$S_2 = \frac{1.167P_o}{t}\left(\frac{R}{t}\right)^{\frac{1}{2}}$ at $x = 0$
	STRESSES AT $x = 0$		MAXIMUM STRESSES	
	HOOP STRESS, S_1	LONGITUDINAL STRESS, S_2	HOOP STRESS, S_1	LONGITUDINAL STRESS, S_2
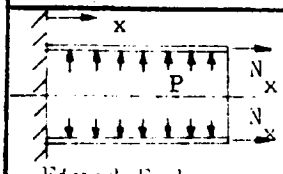 Fixed End	$S_1 = 0.546\frac{PR}{t}$	$S_2 = 2.32\frac{PR}{t}$	$S_1 = \frac{PR}{t}$	$S_2 = 2.32\frac{PR}{t}$
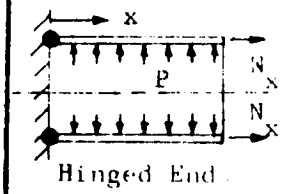 Hinged End	$S_1 = 0$	$S_2 = 0.5\frac{PR}{t}$	$S_1 = \frac{PR}{t}$	$S_2 = 1.086\frac{PR}{t}$
Free End	$S_1 = \frac{PR}{t}$	$S_2 = 0.5\frac{PR}{t}$	$S_1 = \frac{PR}{t}$	$S_2 = 0.5\frac{PR}{t}$

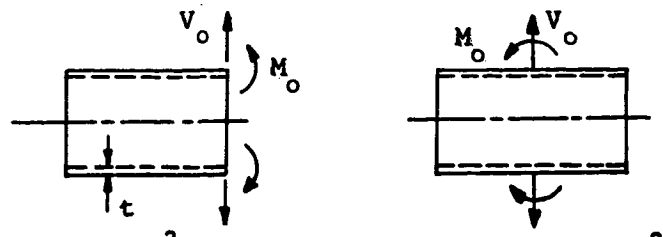

$$Y_{RV_o} = \frac{2.57}{E}\left(\frac{R}{t}\right)^{\frac{3}{2}} X_3 \qquad Y_{RV_o} = \frac{0.643}{E}\left(\frac{R}{t}\right)^{\frac{3}{2}} X_5$$

$$\theta_{RM} = \frac{8.50}{Et^2}\left(\frac{R}{t}\right)^{\frac{1}{2}} X_1 \qquad \theta_{RM} = \frac{2.12(R)^{\frac{1}{2}}}{E\,(t)^{\frac{5}{2}}} X_4$$

$$\theta_{RV_o} = Y_{RM} = \frac{3.30R}{Et^2} X_2$$

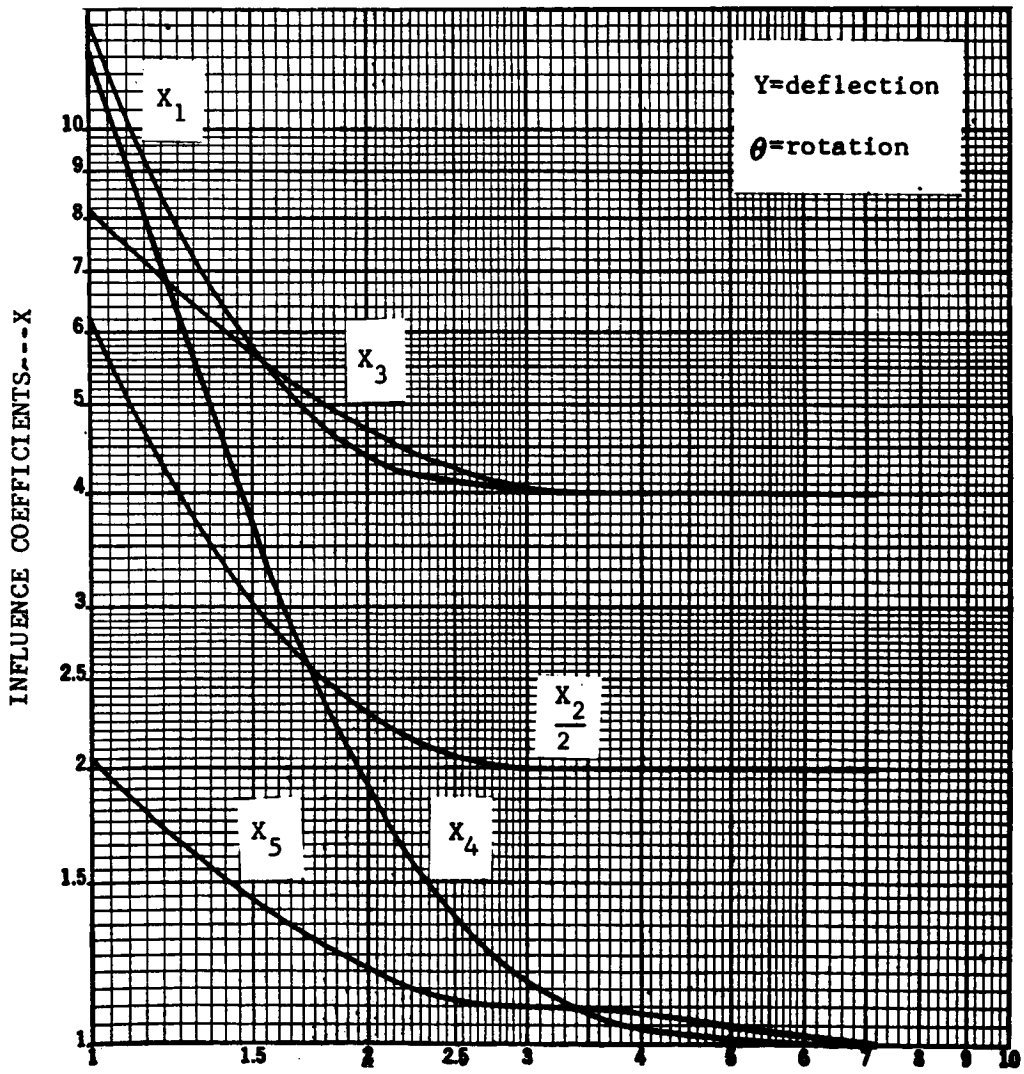

$$\lambda\ell = \frac{1.285}{\sqrt{Rt}}\,\ell$$

Fig. VII-4.16 Influence Coefficients for Short Cylindrical Shells (Ref. 36)

Influence Coefficients for Short Cylinders

If the cylinder is short, a load at one end will produce an influence at the other end which cannot be ignored. This effectively entails adding a correction factor to the solution of the differential equation for the infinitely long cylinder[36]. As it turns out, if the length of a cylinder, ℓ, is less than $\frac{2\pi}{\beta}$, i.e.

$$\ell < \frac{2\pi}{\beta} \tag{42}$$

this effect must be considered[36]. Figure VII-4-16 summarizes these corrections.

Heads

So far the various head shapes have been ignored, however this paragraph will outline some properties of interest of the more common head shapes.

1. Elliptical Heads. Figure VII-4-17 describes an elliptical head in terms of the stresses and deflections.

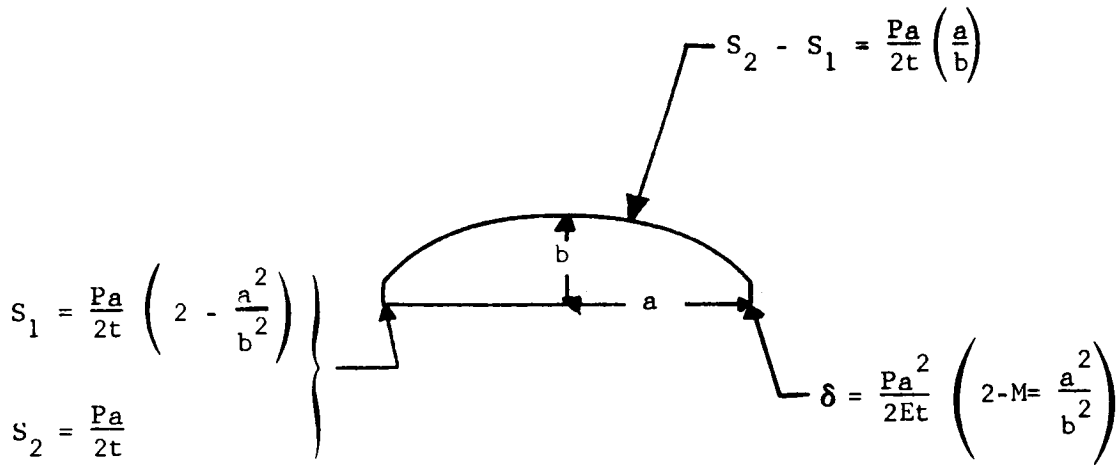

Fig. VII-4-17 Elliptical Head (Ref. 36)

One disadvantage of an elliptical head is that once the depth, b, is selected the edge displacement, δ, is fixed and if $b/a < 0.707$ the edge will move

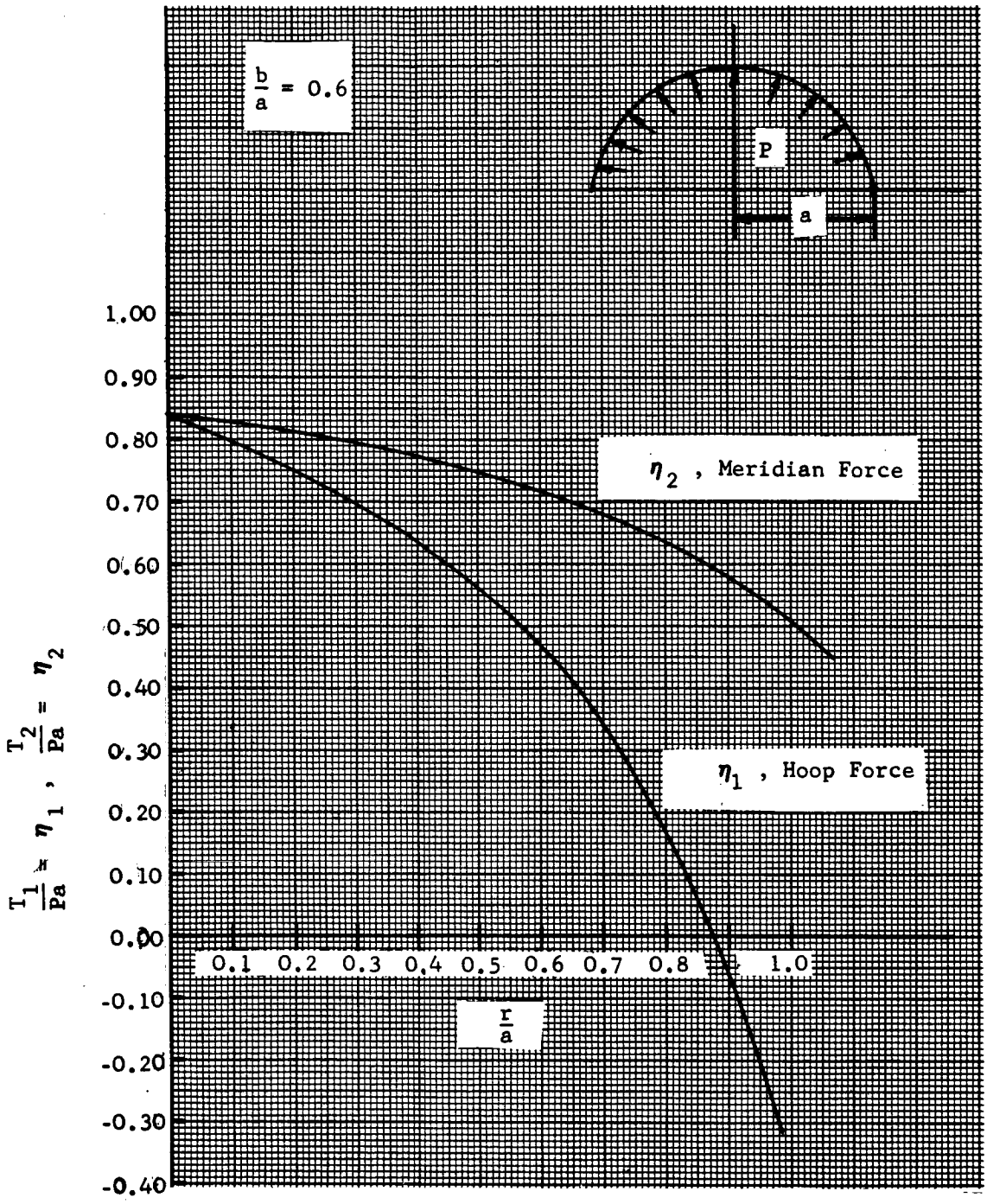

Fig. VII-4-18 Membrane Forces for a Typical Elliptical Head (b/a = 0.6) (Ref. 36)

inward under pressure causing an increase in the discontinuity stresses[36]. Figures VII-4-18 and VII-4-19 show the distribution of forces for a typical elliptical head.

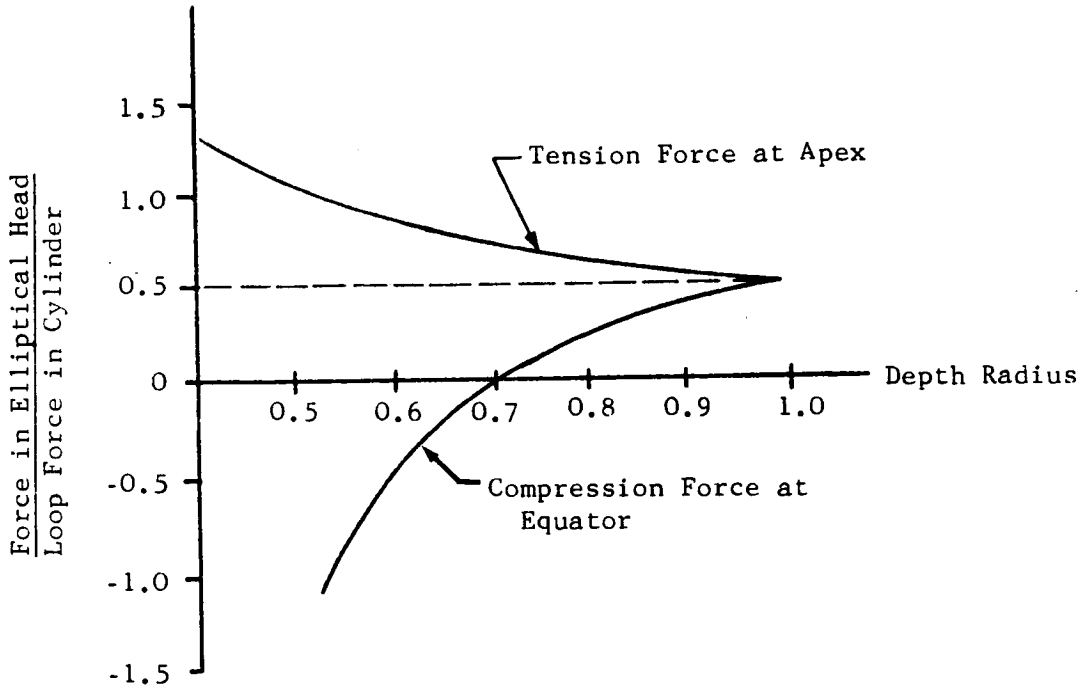

Fig. VII-4-19 Membrane Forces in Elliptical Heads Versus b/a (Ref. 36)

2. Cassinian Heads. An advantage of the Cassinian head is that the dome and edge displacements may be chosen as required which gives the designer a greater flexibility than with conventional shapes[36]. Figure VII-4-20 describes some properties of Cassinian heads. Reference 27 describes the Cassinian curves in detail and will not be recounted here except to point out that the hemisphere and ellipse are special cases of these curves.

3. Zero Hoop Stress Head. From Equation (18), if the hoop stress is set to zero, the following relationship exists between R_1 and R_2.

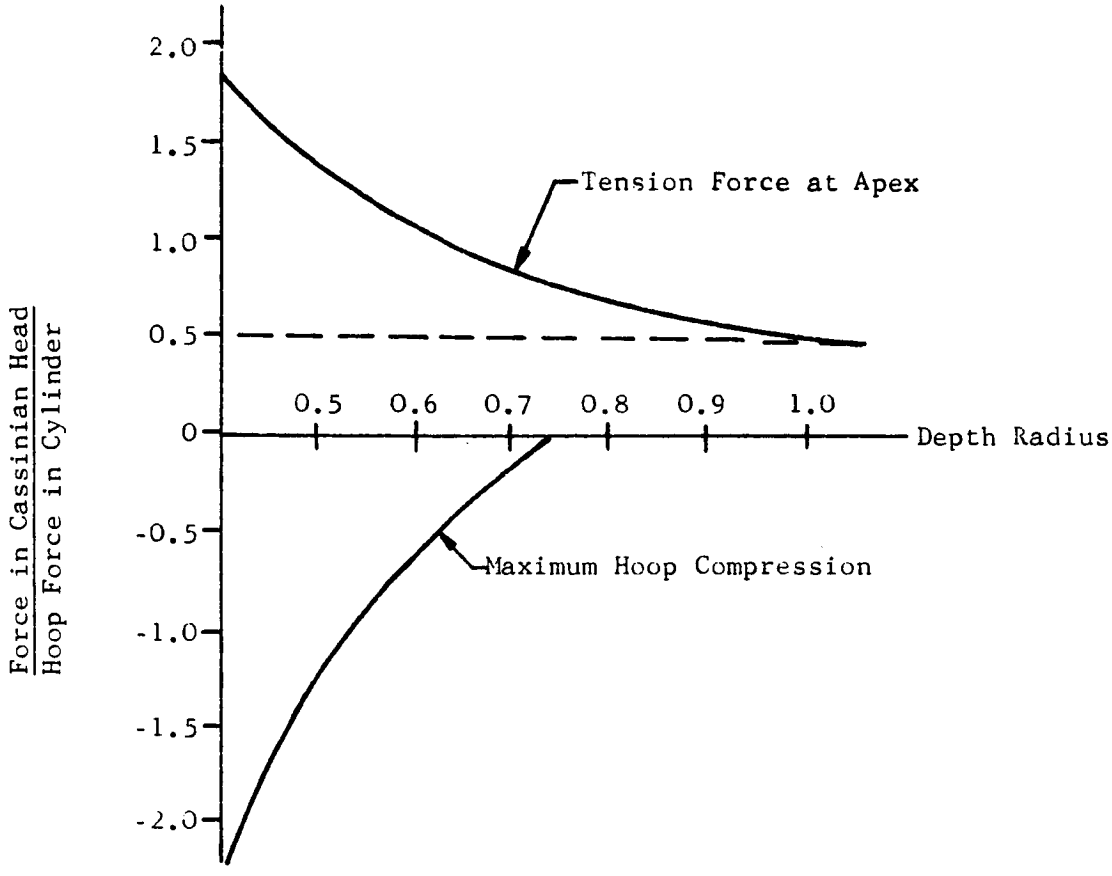

Fig. VII-4-20 Tensile and Compressive Forces in Cassinian Heads (Ref. 36)

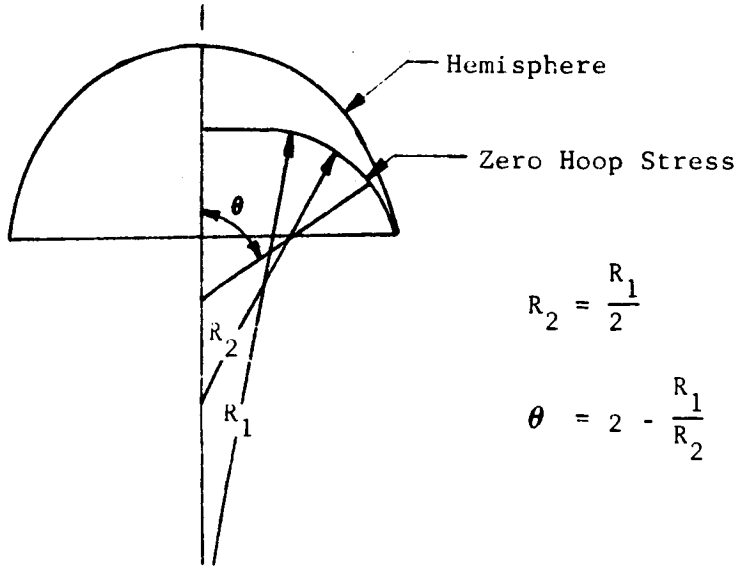

Fig. VII-4-21 Zero Hoop Stress Head (Ref. 36)

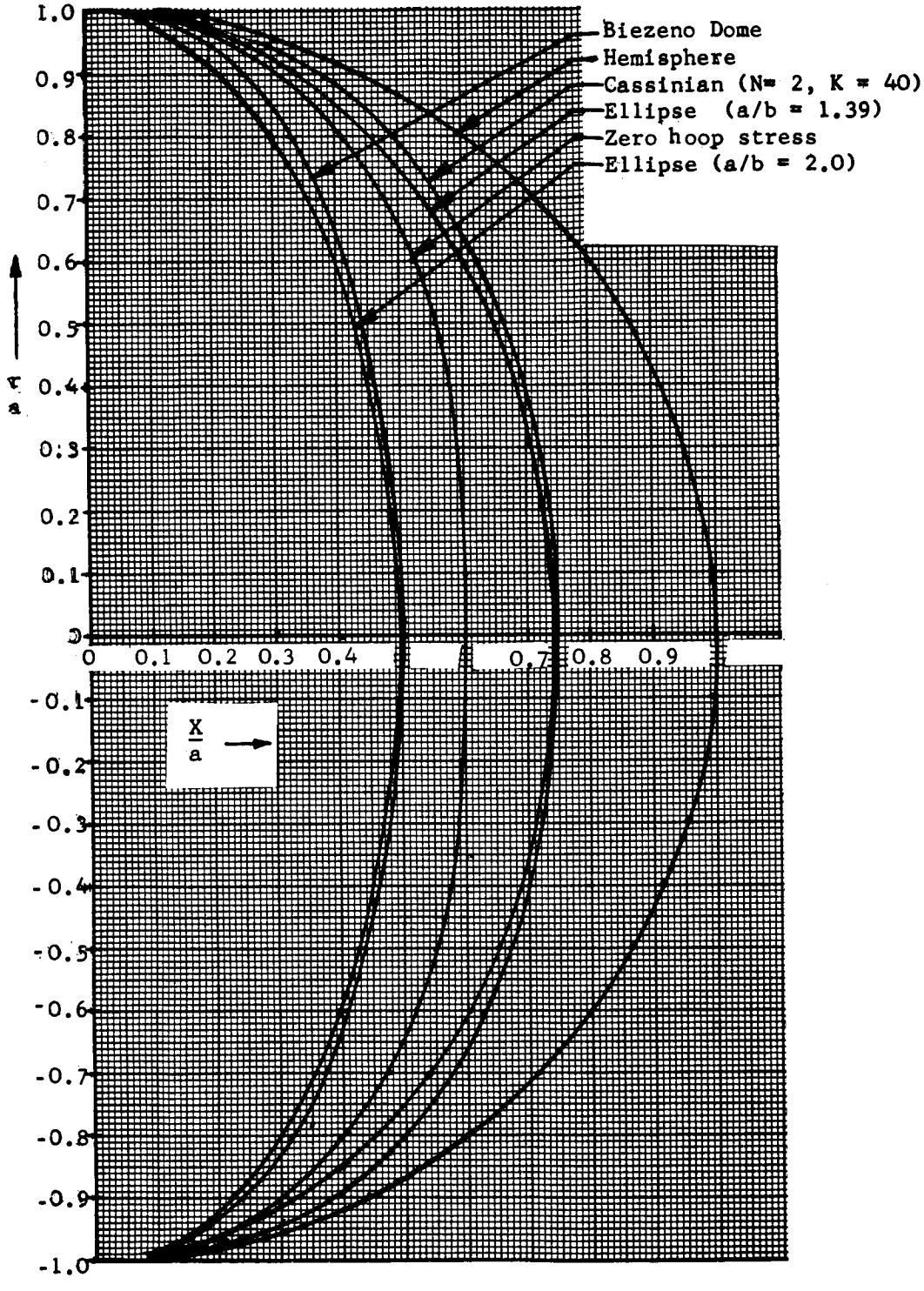

Fig. VII-4-22 Comparison of Head Shapes (Ref. 36)

$$R_1 = 2R_2 \tag{43}$$

The general shape of this head compared with a hemisphere is shown in Figure VII-4-21. As mentioned before the disadvantage with this shaped head is that the dome is extremely flat producing plate bending phenomena[36].

4. Biezeno Heads—Constant Shear Strength. This type of head is designed to produce the same shearing stress at each point. But this is not a good situation if the head material has low ductility and, as with the elliptical head, the edge will move inward under pressure[36]. Figure VII-4-22 summarizes the various head shapes discussed.

Openings in Shells

Consider first the case of a membrane with an unreinforced opening as shown in Figure VII-4-23.

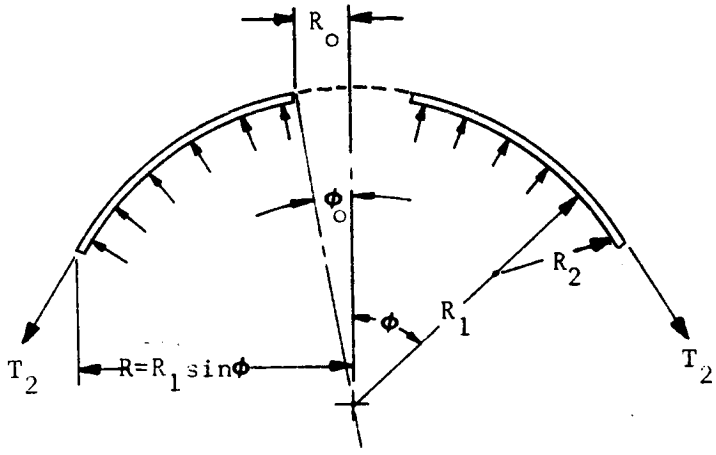

Fig. VII-4-23 Unreinforced Opening in a Membrane With Internal Pressure P

By equilibrium, T_2 is found to be:

$$2\pi R T_2 \sin\phi = \pi R^2 P - \pi R_o^2 P$$

or

$$T_2 = \frac{PR_1}{2}\left[1 - \left(\frac{R_o}{R_1 \sin\phi}\right)^2\right] \tag{44}$$

and then, with Equation (1), the relationship for T_1 becomes:

$$T_1 = \frac{PR_1}{2}\left\{2 - \frac{R_1}{R_2}\left[1 - \left(\frac{R_o}{R_1 \sin\phi}\right)^2\right]\right\} \tag{45}$$

When $R = R_o = R_1 \sin\phi$ (at the edge of the hole) Equations (44) and (45) reduce to the following:

$$\left.\begin{aligned} T_2 &= 0, \\ T_1 &= PR_1 \end{aligned}\right\} \tag{46}$$

This, when compared with Equation (9), shows that the hoop stress is twice that of the longitudinal stress if no hole is present.

By the previous analysis, the effect of a hole in a membrane is shown to be a stress concentration. Figure VII-4-24 shows how a hole effects the stress in a membrane.

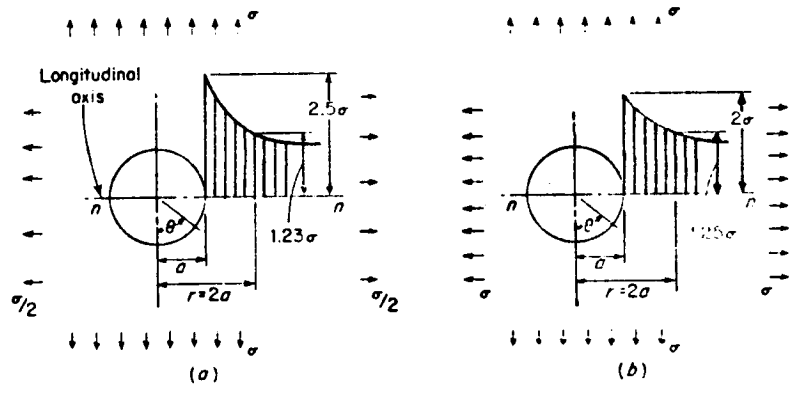

Fig. VII-4-24 Variation in Stress in the Region of a Circular Hole in (a) Cylinder, (b) Sphere Subjected to Internal Pressure (Ref. 14)

To compensate for this increase of stress near a hole, reinforcement must be added around the hole. As a general rule of thumb the reinforcement is placed within the limits of non-negligible stress concentration. This is shown graphically in Figure VII-4-25.

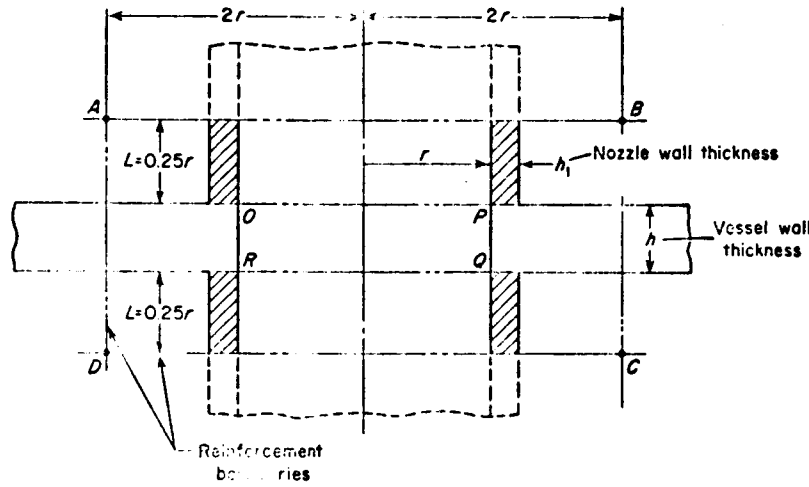

Fig. VII-4-25 Reinforcement Boundaries for Circular Openings in Cylindrical and Spherical Vessels (Ref. 14)

For an ideal amount of reinforcement the displacement of the reinforcing ring must be matched to that of the membrane. These displacement forces are shown in Figure VII-4-26.

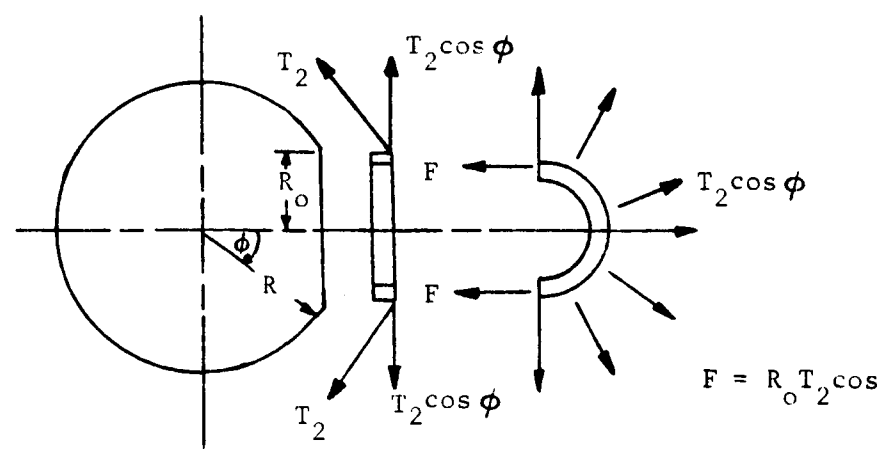

Fig. VII-4-26 Equilibrium Forces Around a Reinforced Hole (Ref. 36)

The displacements are as follows[36]:

$$\left.\begin{aligned} \delta_{ring} &= \frac{FR_o}{A_R E_R} \\ \delta_{sphere} &= \frac{T_2 R_o}{E_s t}(1 - \nu) \end{aligned}\right\} \qquad (47)$$

then since $S_R = S_s$ for continuity,

$$\frac{T_2 \cos\phi R_o^2}{A_R E_R} = \frac{T_2 R_o}{E_s t}(1 - \nu) \qquad (48)$$

or

$$A_R = \frac{E_s}{E_R}\left(\frac{R_o t \cos\phi}{1 - \nu}\right) \qquad (49)$$

if, as is usually the case, $E_R = E_s$, then:

$$A_R = \frac{R_o t \cos\phi}{1 - \nu} \qquad (50)$$

Many times, however, the area given by Equation (50) is too small to be practical, i.e., not enough area is provided for studs, etc.[36]. In cases such as this, "rigid" reinforcing rings are used. Figures VII-4-27 and VII-4-28 show the effect of reinforcement location on discontinuity stress in the membrane.

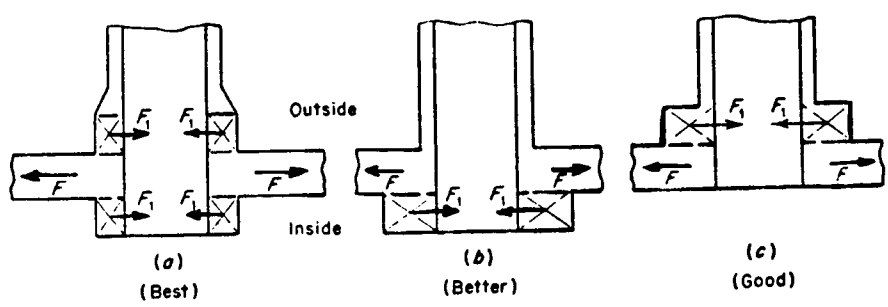

Fig. VII-4-27 Diagrammatic Location of Nozzle Opening Reinforcement, (a) Balanced, (b) Unbalanced Inside, (c) Unbalanced Outside (Ref. 14)

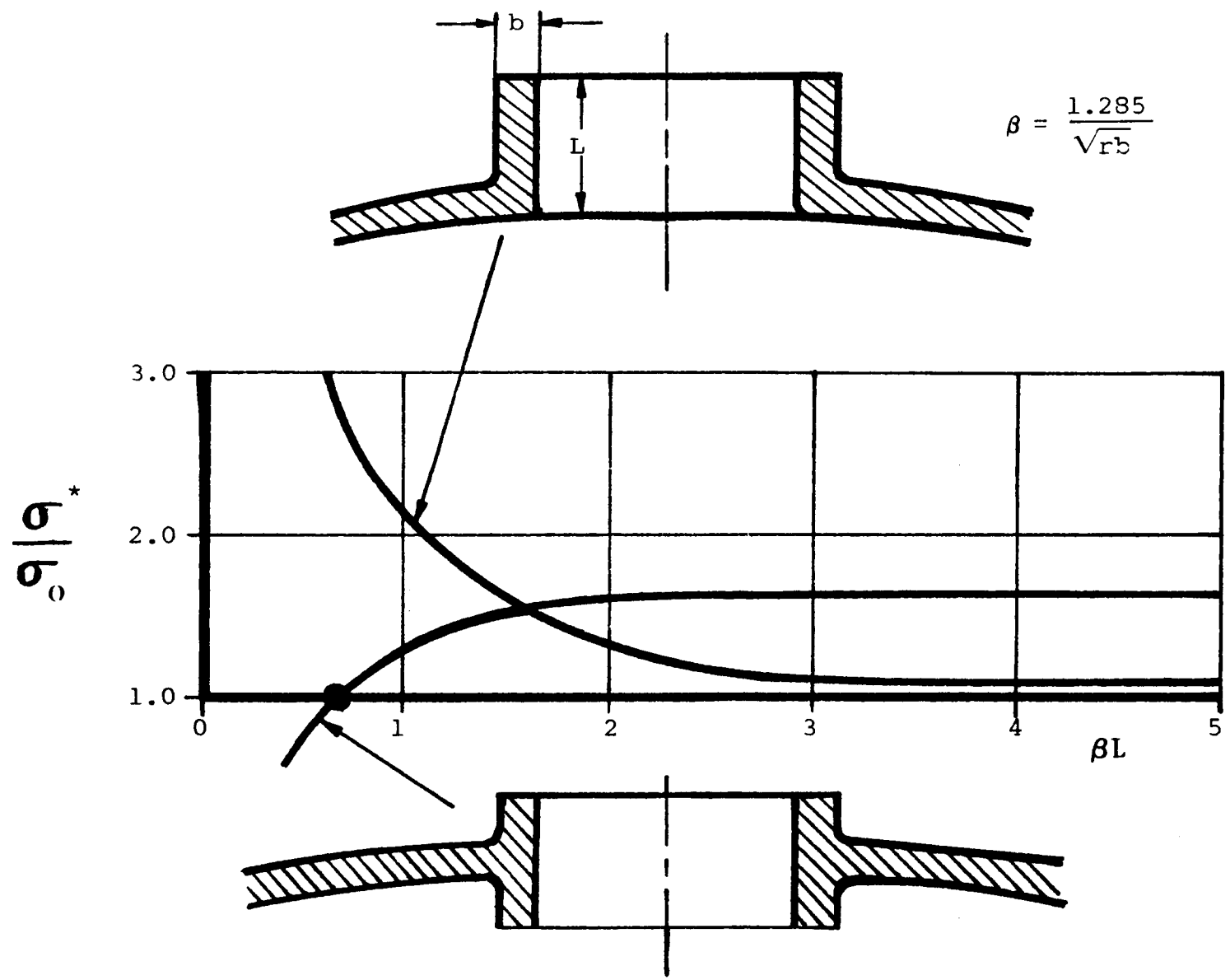

Fig. VII-4-28 Comparison of Symmetrical Versus Unsymmetrical Reinforcing Rings (Ref. 36)

When "rigid" rings are used as hole reinforcing the displacements must be equal to preserve continuity. Figure VII-4-29 graphically describes a typical case where, for continuity, the points O" and O' are brought together by applying moments and forces to the ring and shell.

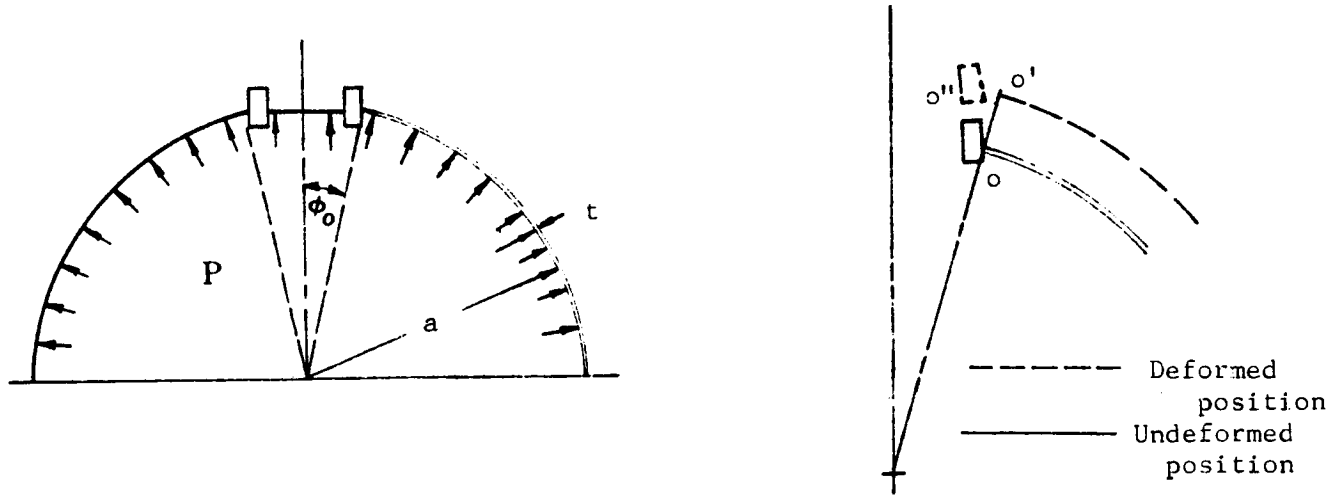

Fig. VII-4-29 Spherical Shell with a Reinforced Opening (Ref. 36)

The addition of the moments and forces to preserve continuity must, to preserve equilibrium, be such that their magnitudes are equal and their directions opposite. Figure VII-4-30 shows these forces in a ring to membrane junction.

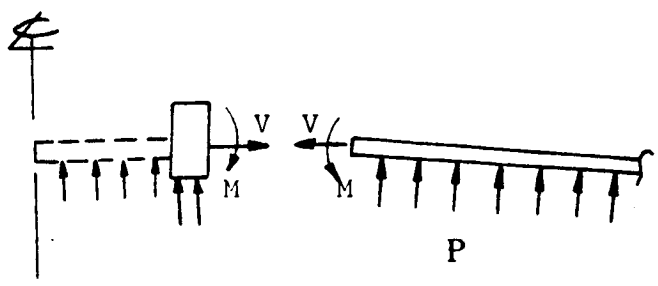

Fig. VII-4-30 Discontinuity Moments and Forces (Ref. 36)

To facilitate the analysis of a ring-membrane system of the type previously described, influence coefficients (displacements and rotations due to unit values of M and V) are defined as follows[36]:

Membrane:

θ_{MM}, u_{MM} $\equiv$ rotation and displacement due to a unit moment

θ_{MV}, u_{MV} $\equiv$ rotation and displacement due to a unit force

θ_{MP}, u_{MP} $\equiv$ rotation and displacement due to a unit pressure

Ring:

θ_{RM}, u_{RM} $\equiv$ rotation and displacement due to a unit moment

θ_{RV}, u_{RV} $\equiv$ rotation and displacement due to a unit force

θ_{RP}, u_{RP} $\equiv$ rotation and displacement due to a unit pressure

where the signs of θ, u, M and V are established as follows[36].

a) M and V are positive if they act in the direction shown in Figure VII-4-30

b) θ is positive counterclockwise

c) u is positive if the membrane displacement is increased

d) the membrane displacement is positive outward

Since these influence coefficients are unit values they must be multiplied by the loads to give the true rotation or displacement. The total values of rotation and displacement become:

Membrane:

total displacement:

$$u_M = u_{MP}P - u_{MH}H - u_{MV}V \tag{51}$$

total rotation:

$$\theta_M = \theta_{MM}M + \theta_{MV}V - \theta_{MP}P \tag{52}$$

Ring:

total displacement:

$$u_R = u_{RV}V + u_{RP}P - u_{RM}M \tag{53}$$

total rotation:

$$\theta_R = \theta_{RP}P + \theta_{RV}V - \theta_{RM}M \tag{54}$$

Compatibility then requires that:

$$\left.\begin{aligned} u_R &= u_M \\ \text{and} \qquad \theta_R &= \theta_M \end{aligned}\right\} \tag{55}$$

By substituting Equations (51) through (54) into (55) gives the following equations for M and V.

$$M = \frac{P\left[(u_{MP} - u_{RP})(\theta_{RV} - \theta_{MV}) + (\theta_{MP} + \theta_{RP})(u_{RV} + u_{MV})\right]}{(\theta_{MM} + \theta_{RM})(u_{RV} + u_{MV}) - (u_{MM} - u_{RM})(\theta_{MV} - \theta_{RV})} \tag{56}$$

$$V = \frac{P\left[(u_{MP} - u_{RP})(\theta_{MM} + \theta_{RM}) - (\theta_{MP} + \theta_{RP})(u_{MM} - u_{RM})\right]}{(\theta_{MM} + \theta_{RM})(u_{RV} + u_{MV}) - (u_{MM} - u_{RM})(\theta_{MV} - \theta_{RV})} \tag{57}$$

Hemispherical Heads

Reference 36 lists the following displacements and rotations for hemispherical heads. They will be reproduced here without comment.

Displacements:

$$\left.\begin{aligned} u_{MV} &= \frac{W_c}{E\phi_o} \\ u_{MM} &= \frac{X_c}{Et\phi_o} \\ u_{MP} &= \frac{a^2(1-\nu)\sin\phi_o}{2Et} \end{aligned}\right\} \tag{58}$$

Rotations:

$$\left.\begin{aligned} \theta_{MV} &= \frac{X_c}{Et\phi_o} \\ \theta_{MM} &= \frac{X_d}{Et^2\phi_o} \\ \theta_{MP} &= 0 \end{aligned}\right\} \qquad (59)$$

where W_c, X_c and X_d are functions of ξ_o. Figure VII-4-31 shows these relations.

For heads other than hemispherical, Equations (58) and (59) become[36]:

$$\left.\begin{aligned} U_{MP} &= \frac{PR_1 \sin\phi_o}{2Et}\left[R_1(2-\nu)1-\frac{R_1^2}{R_2}\right] \\ \theta_{MP} &\neq 0 \end{aligned}\right\} \qquad (60)$$

and the relationship for ξ_o becomes:

$$\xi_o = 1.82\frac{R_o}{\sqrt{R_1 t}} \qquad (61)$$

With these results, Equation (7) becomes, for the longitudinal stress, (if the reinforcing ring has an area greater than ideal, the longitudinal stresses at point o are larger than the hoop stresses[36]):

$$S_2 = \frac{T_2}{t} + \frac{V}{t\cos\phi_o} \pm \frac{6M}{t^2} \qquad (62)$$

where the plus sign before the last term is for the outer surface of the membrane and the negative sign for the inner surface[36]. Table VII-4-4 summarizes the influence coefficients for various reinforcement types.

In placing the reinforcement, one has the choice of placing the ring completely inside, completely outside or symmetrical with respect to the membrane. Figures VII-4-32 through VII-4-38 show the effect of this ring geometry on stresses which were summarized in Figure VII-4-28.

Table VII-4-4

FORMULAS FOR DEFLECTIONS & ROTATIONS

RING GEOMETRY, LOADING AND CASE NUMBER	DEFLECTIONS	ROTATIONS	LIMITATIONS FOR FORMULAS
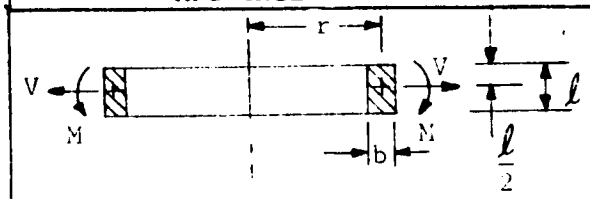 1. Symmetrical Ring	$U_{RV} = \frac{Vr^2}{EA}$, $(A = b\ell)$ $U_{RM} = 0$	$\theta_{RV} = 0$ $\theta_{RM} = \frac{Mr^2}{EI_x}$, $(I_x = \frac{b\ell^3}{12})$	$\frac{b}{r} << 1$ $\ell < 1.56\sqrt{rb}$
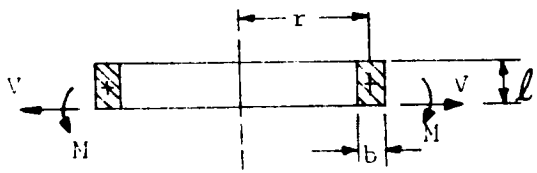 2. Unsymmetrical Ring	$U_{RV} = \frac{4Vr^2}{EA}$ $U_{RM} = \frac{6Mr^2}{EA\ell}$	$\theta_{RV} = \frac{Vr^2\ell}{2EI_x}$ $\theta_{RM} = \frac{Mr^2}{EI_x}$	$\frac{b}{r} << 1$ $\ell < 1.56\sqrt{rb}$
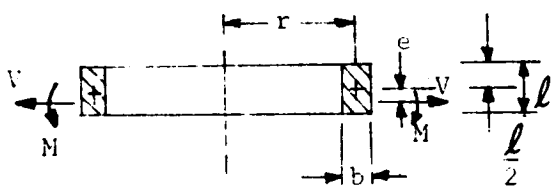 3. Partially Unsymmetrical Ring	$U_{RV} = \frac{Vr^2}{EA}\left[1 + 12\left(\frac{e}{\ell}\right)^2\right]$ $U_{RM} = \frac{12Mr^2}{EA\ell}\left(\frac{e}{\ell}\right)$	$\theta_{RV} = \frac{Vr^2e}{EI_x}$ $\theta_{RM} = \frac{Mr^2}{EI_x}$	$\frac{b}{r} << 1$ $\ell < 1.56\sqrt{rb}$
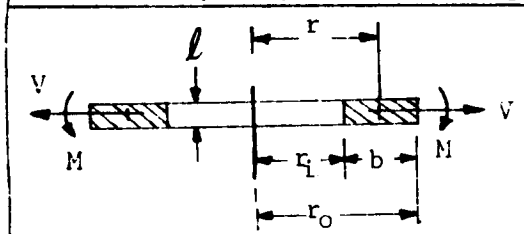 4. Annular Ring	$U_{RV} = \frac{Vr_o}{E\ell}\left[\frac{(1+\nu)\left(\frac{r_i}{r_o}\right) + (1-\nu)}{1-\left(\frac{r_i}{r_o}\right)^2}\right]$ $U_{RM} = 0$	$\theta_{RV} = 0$ $\theta_{RM} = \frac{12Mr}{E\ell^3 \ln\left(\frac{r_o}{r_i}\right)^2}$	
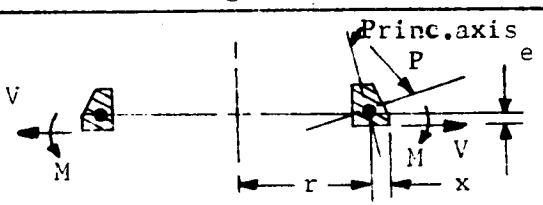 5. Compact Ring With Oblique Principal Axes	$U_{RV} = \frac{Vr^2}{EA} + \frac{Vr^2e^2}{E}\left[\frac{1}{I_x - I_{xy}^2/I_y}\right]$ $U_{RM} = \frac{Mr^2e}{E}\left[\frac{1}{I_x - I_{xy}^2/I_y}\right]$	$\theta_{RV} = \frac{Vr^2e}{E}\left[\frac{1}{I_x - I_{xy}^2/I_y}\right]$ $\theta_{RM} = \frac{Mr^2}{E}\left[\frac{1}{I_x - I_{xy}^2/I_y}\right]$	$x << r$

Table VII-4-4 (contd)

FORMULAS FOR DEFLECTIONS & ROTATIONS

RING GEOMETRY, LOADING AND CASE NUMBER	DEFLECTIONS	ROTATIONS	LIMITATIONS FOR FORMULAS
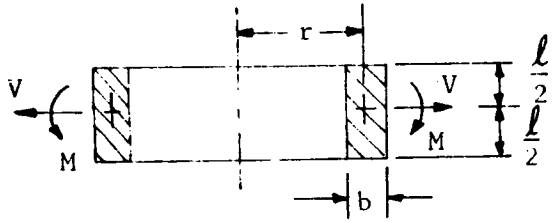 6. Symmetrical Reinforcement	$U_{RV} = \frac{Vr^2\beta}{2Eb} X_5$ * $U_{RM} = 0$ $\beta = \frac{1.285}{\sqrt{rb}}$ For $\nu = 0.3$	$\theta_{RV} = 0$ $\theta_{RM} = \frac{Mr^2\beta^3}{Eb} X_4$	$\frac{b}{r} \leq 0.2$
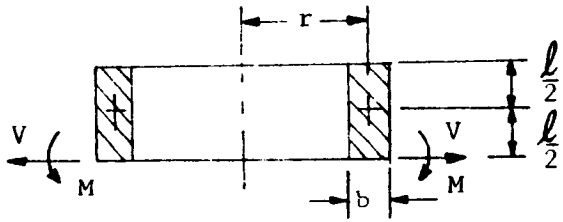 7. Unsymmetrical Reinforcement	$U_{RV} = \frac{Vr^2\beta}{2Eb} X_3$ $U_{RM} = \frac{Mr^2\beta^2}{Eb} X_2$	$\theta_{RV} = \frac{Vr^2\beta^2}{Eb} X_2$ $\theta_{RM} = \frac{Mr^2\beta^3}{Eb} X_1$	$\frac{b}{r} \leq 0.2$
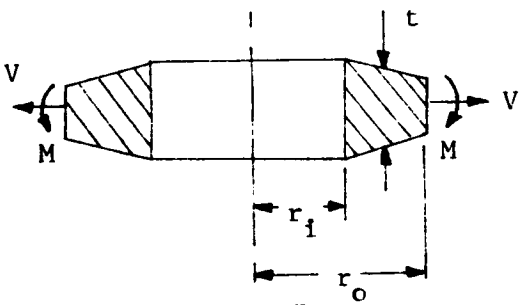 $t = \alpha r^n$ at $r = r_i$, $t = t_i$ at $r = r_o$, $t = t_o$ 8. Tapered Ring	$U_{RV} = \frac{(1-\nu^2) r_o^{1-n} V}{E\alpha \left(r_i^{m_2'} r_o^{m_1'} - r_i^{m_1'} r_o^{m_2'} \right)} \bullet \left\{ \frac{r_i^{m_2'} r_o^{m_1'}}{m_1' + \nu} - \frac{r_i^{m_1'} r_o^{m_2'}}{m_2' + \nu} \right\}$ $U_{RM} = 0$	$\theta_{RV} = 0$ $\theta_{RM} = \frac{12(1-\nu^2) r_o^{1-3n}}{E\alpha^3 \left(r_i^{m_2} r_o^{m_1} - r_i^{m_1} r_o^{m_2} \right)} \bullet \left\{ \frac{r_i^{m_2} r_o^{m_1}}{m_1 - \nu} - \frac{r_i^{m_1} r_o^{m_2}}{m_2 + \nu} \right\}$	

$$m_1 = \frac{-3n + \sqrt{9n^2 - 4(3n\nu - 1)}}{2}, \quad m_2 = \frac{-3n - \sqrt{9n^2 - 4(3n\nu - 1)}}{2}$$

$$m_1' = \frac{-n + \sqrt{n^2 - 4(n\nu - 1)}}{2}, \quad m_2' = \frac{-n - \sqrt{n^2 - 4(n\nu - 1)}}{2}$$

$$n = \text{Taper} \left(n = \frac{\ln t_o - \ln t_i}{\ln r_o - \ln r_i} \right)$$

Note: When $\ell < 1.56\sqrt{rb}$ (6) and (7) reduce to cases (1) and (2) respectively.

*Coefficients X_1 and X_5 are given in Fig. VII-4-16.

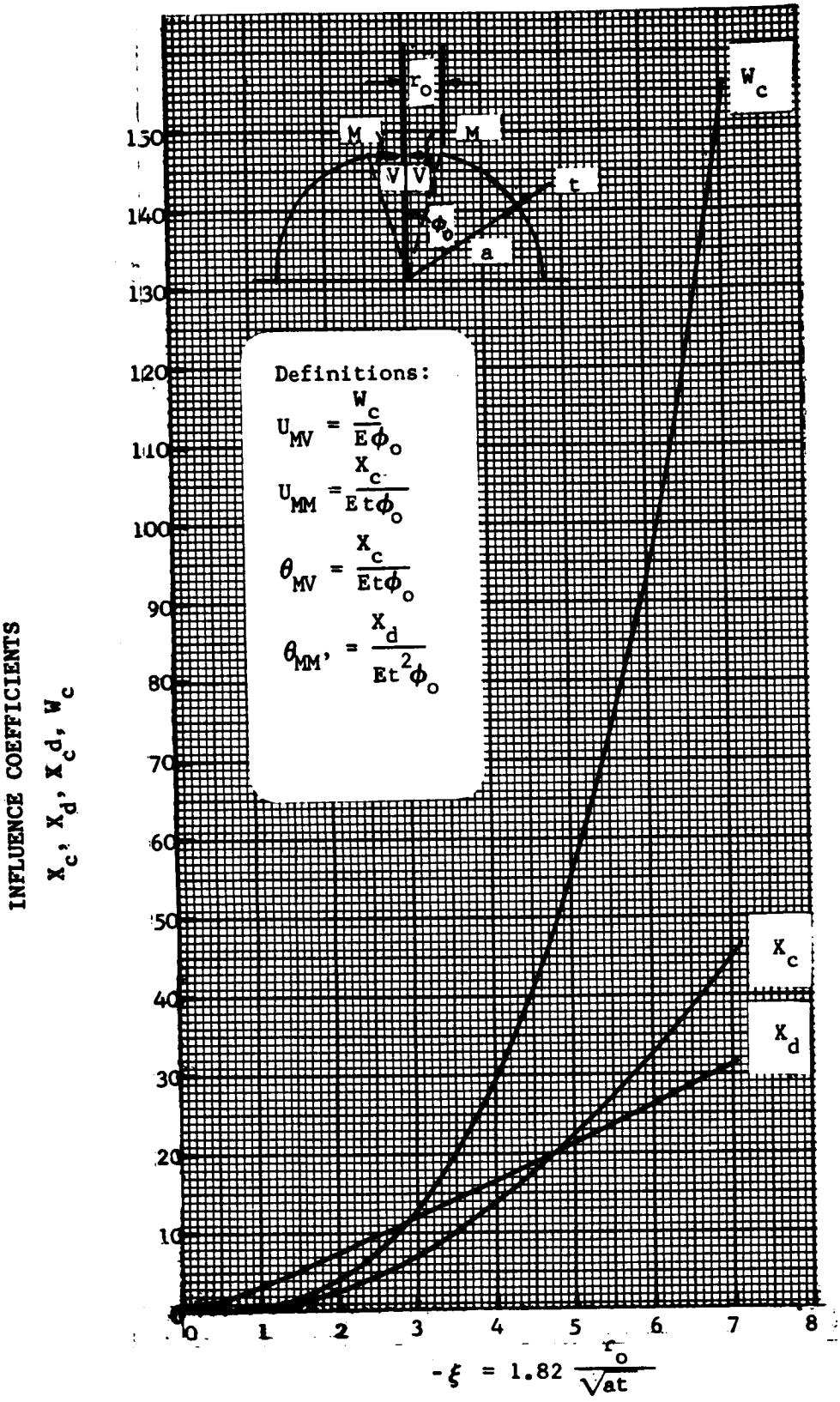

Notation:

U = Horizontal Deflection of a Point on the Shell

θ = Angle of Rotation of a Tangent to Meridian

$$\xi_o = P\sqrt{2}\,\phi_o = 1.82 \frac{r_o}{\sqrt{at}}$$

$$P = \left[3(1-\nu^2)\frac{a^2}{t^2} - \frac{\nu}{4}\right]^{\frac{1}{4}}$$

$$\approx 1.285\sqrt{\frac{a}{t}}$$

$\nu = 0.30$, Poisson's Ratio

Fig. VII-4.31 Influence Coefficients for a Small Opening ($0° < \phi_o < 10°$) (Ref. 36)

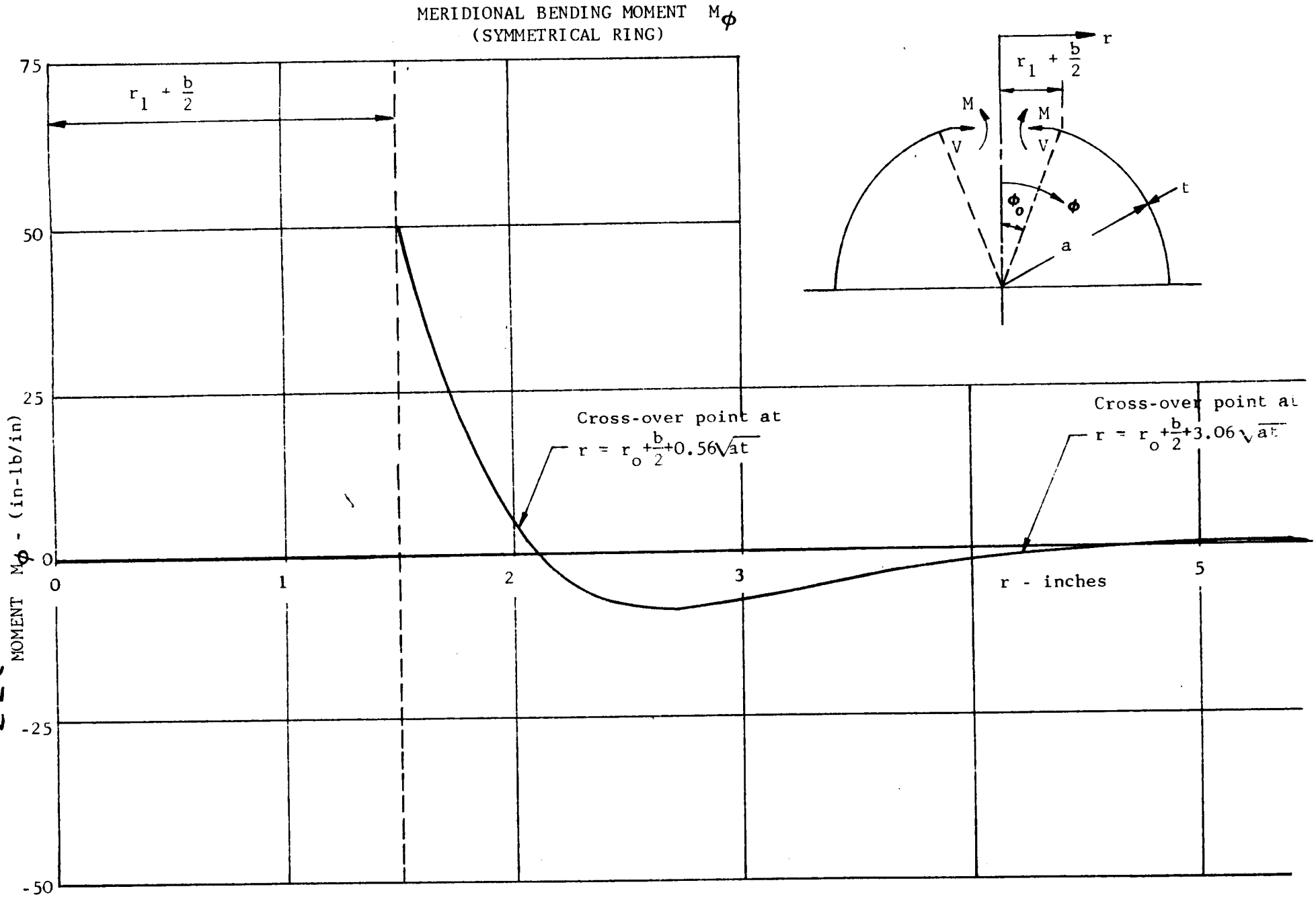

Fig. VII-4-32 Longitudinal Bending Moment M_2 for a Symmetric Ring (Ref. 36)

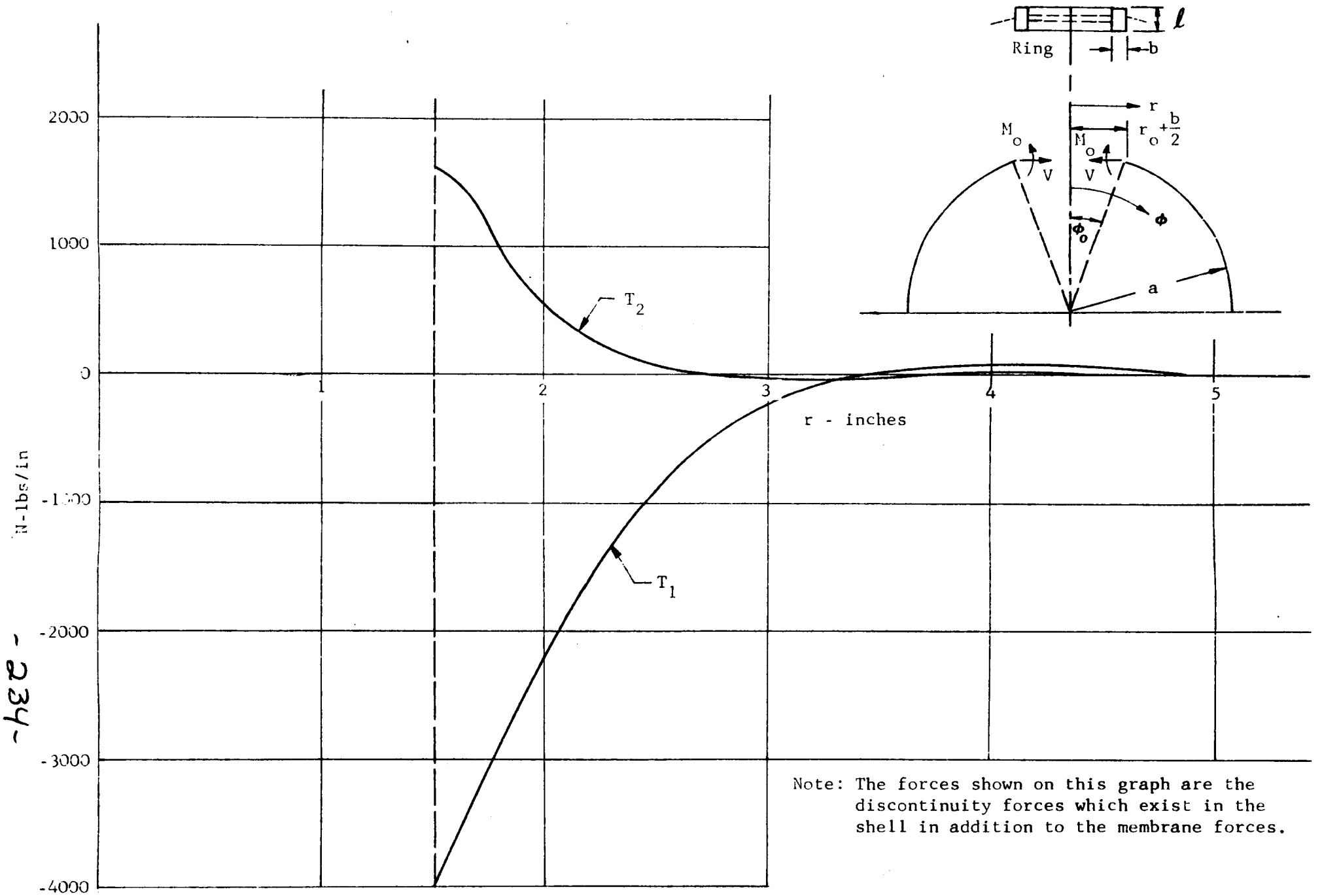

Note: The forces shown on this graph are the discontinuity forces which exist in the shell in addition to the membrane forces.

Fig. VII-4-33 Longitudinal and Hoop Forces for a Symmetrical Ring (Ref. 36)

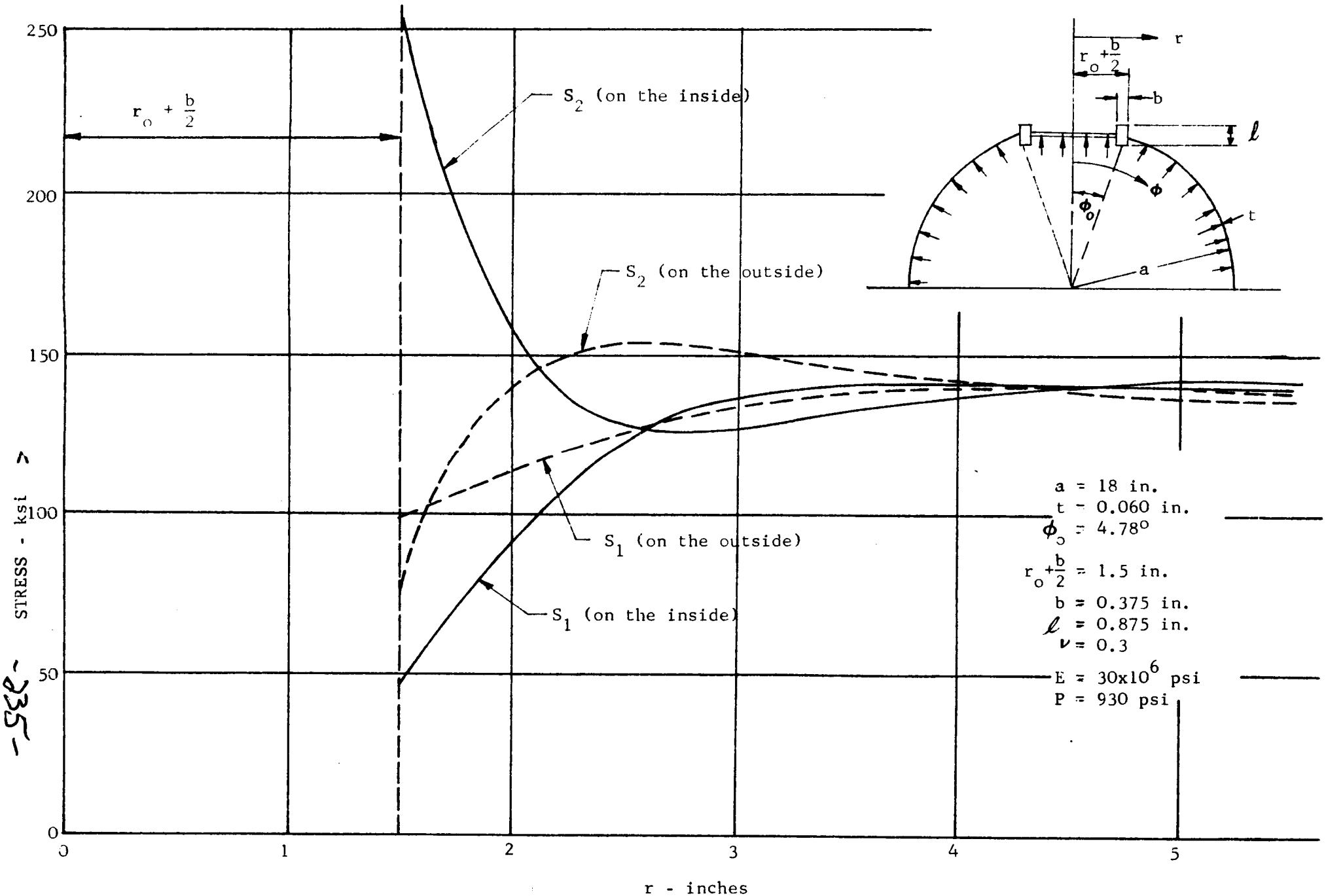

Fig. VII-4-34 Resultant Stresses Due to Moment, Horizontal Forces V, and Membrane Forces for a symmetrical Ring (Ref. 36)

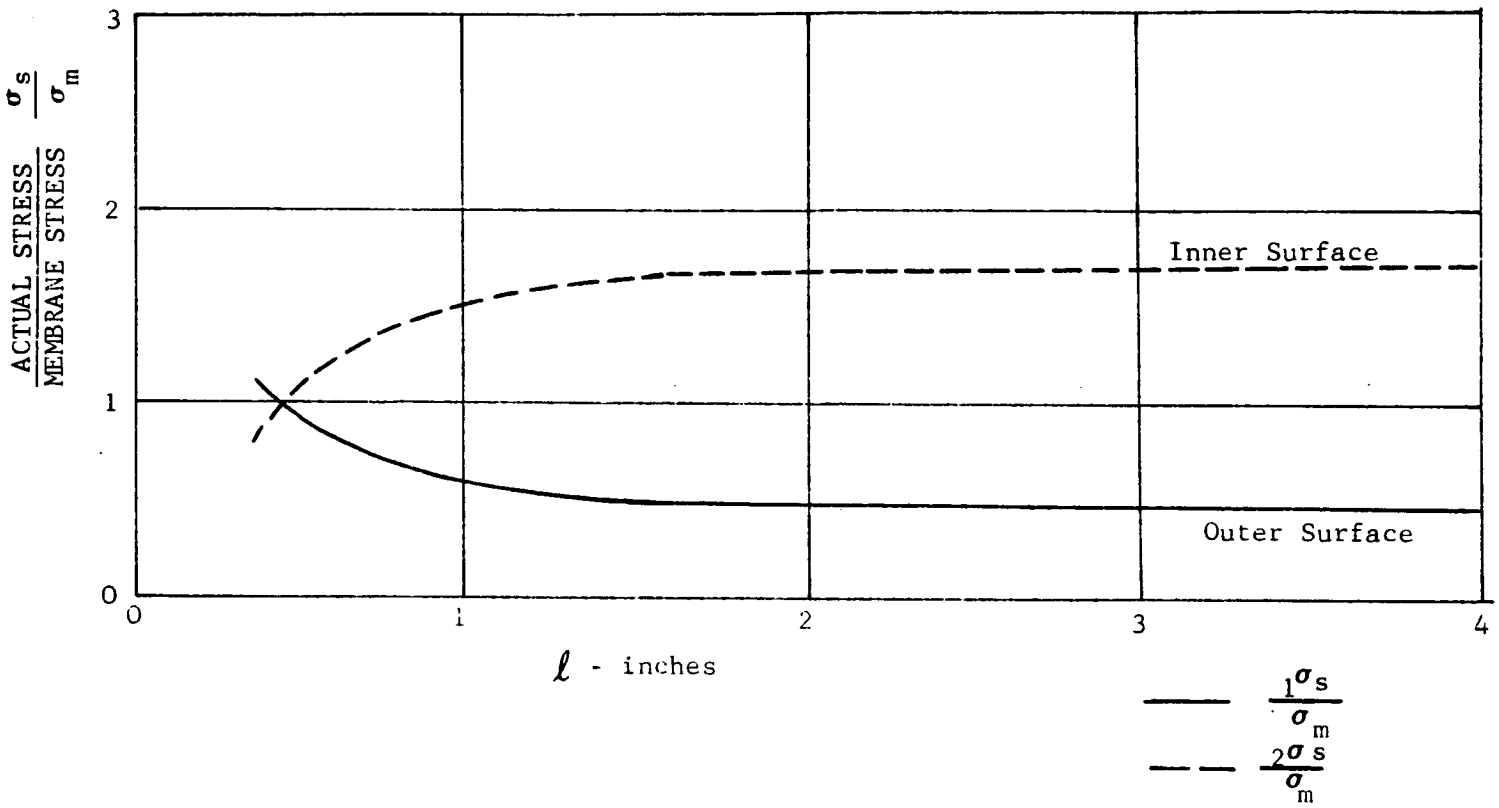

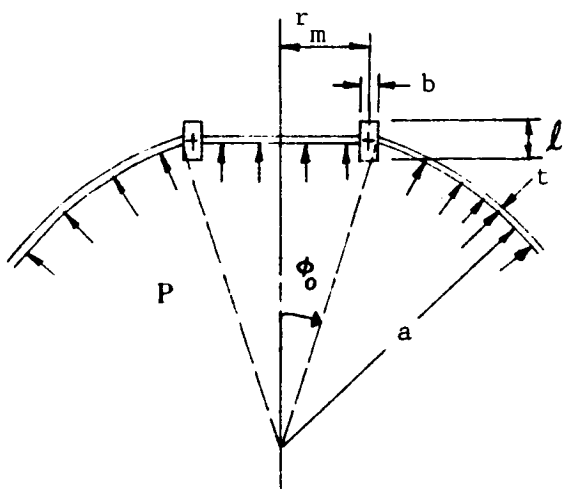

${}_1\sigma_s$ = Total Stress on the Outer Surface

${}_2\sigma_s$ = Total Stress on the Inner Surface

σ_m = Membrane Stress, $\frac{Pa}{2h}$

a = 18.0"

r_m = 2.338"

b = 0.375"

t = 0.048"

ℓ = Variable

P = Pressure

ν = 0.3

E = 30×10^6 psi

Fig. VII-4-35 Stresses at the Ring-Membrane Junction for a Symmetrical Ring (Ref. 36)

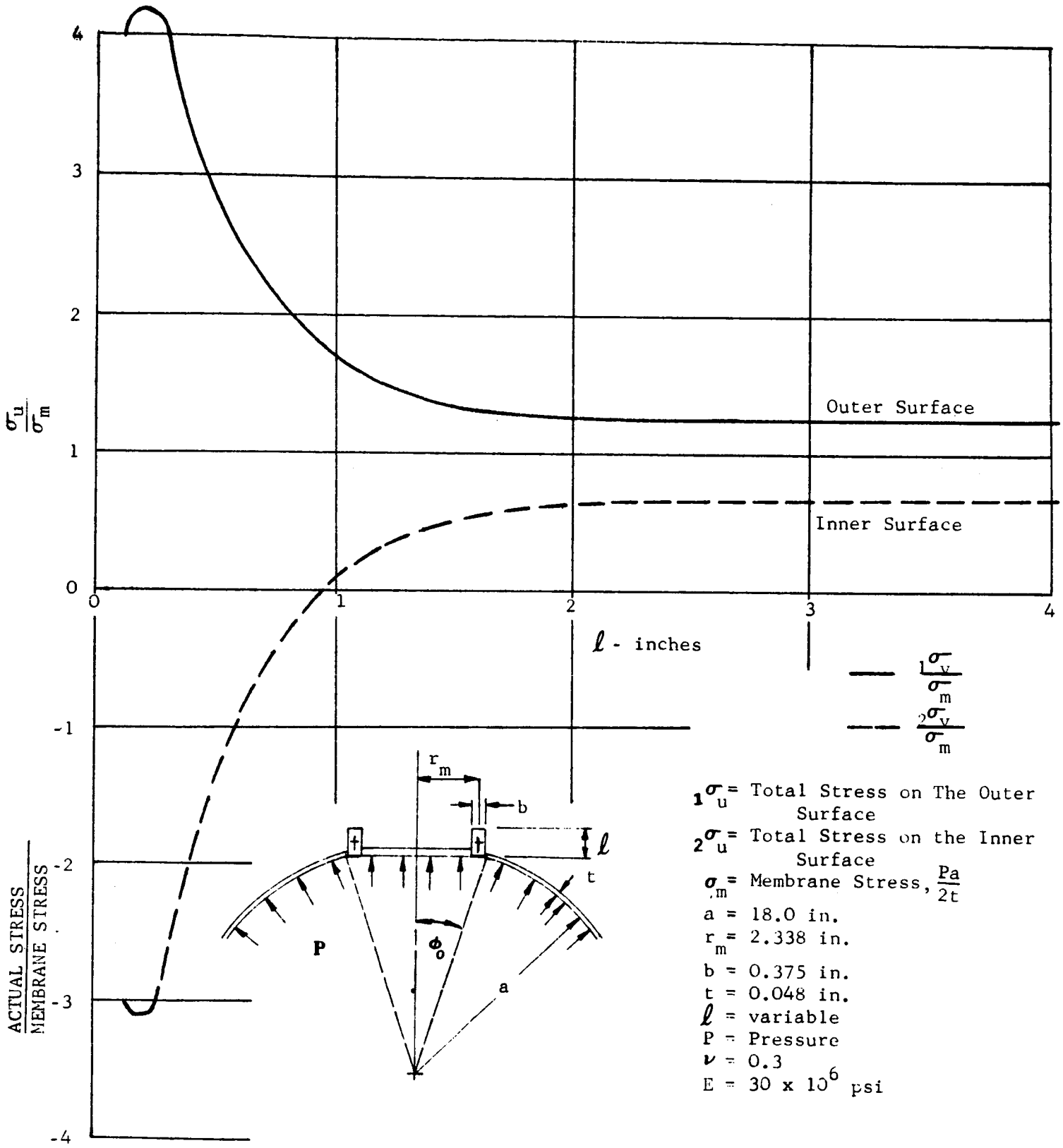

Fig. VII-4-36 Stresses at the Ring-Membrane Junction for an Unsymmetrical Ring (Ref. 36)

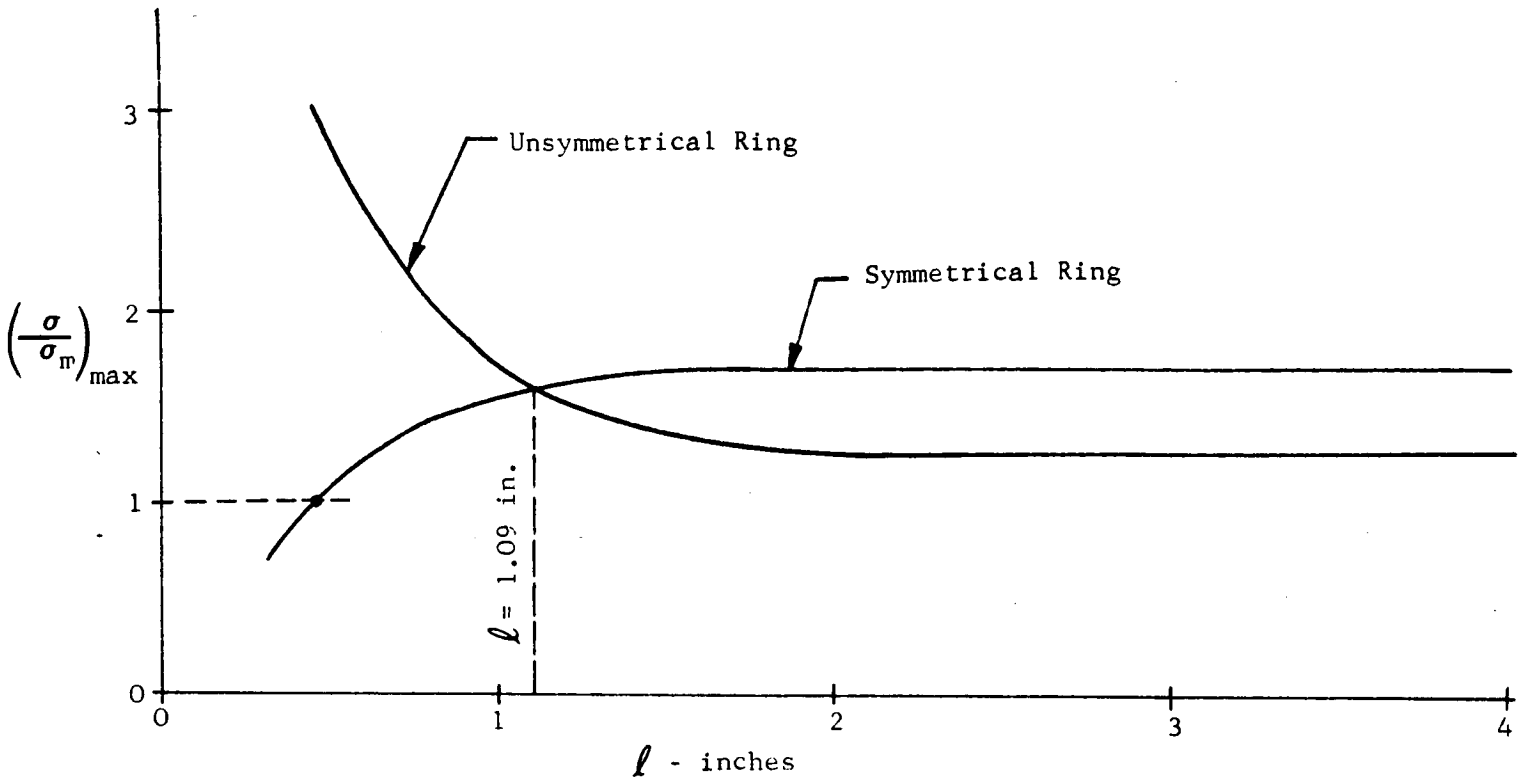

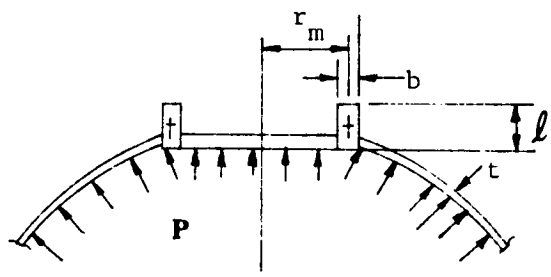

Unsymmetrical Ring

Ring and Shell Geometry:
a = 18.0 in Radius of the Shell
t = 0.048 in
r_m = 2.338 in

E = 30×10^6 psi
ν = 0.3, Poisson's Ratio
P = Pressure psi
$\sigma_m = \frac{pa}{2t}$ Membrane Stress
σ = Total Maximum Stress

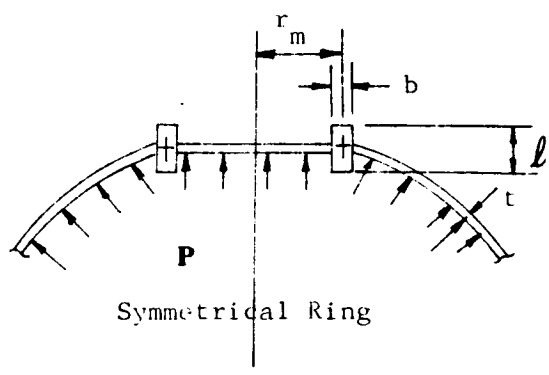

Symmetrical Ring

NOTE: For $\ell > 1.09$ the unsymmetrical ring is more efficient than a symmetrical one.

Fig. VII-4-37 Comparison of the Maximum Stresses at the Ring-Membrane Junction (Ref. 36)

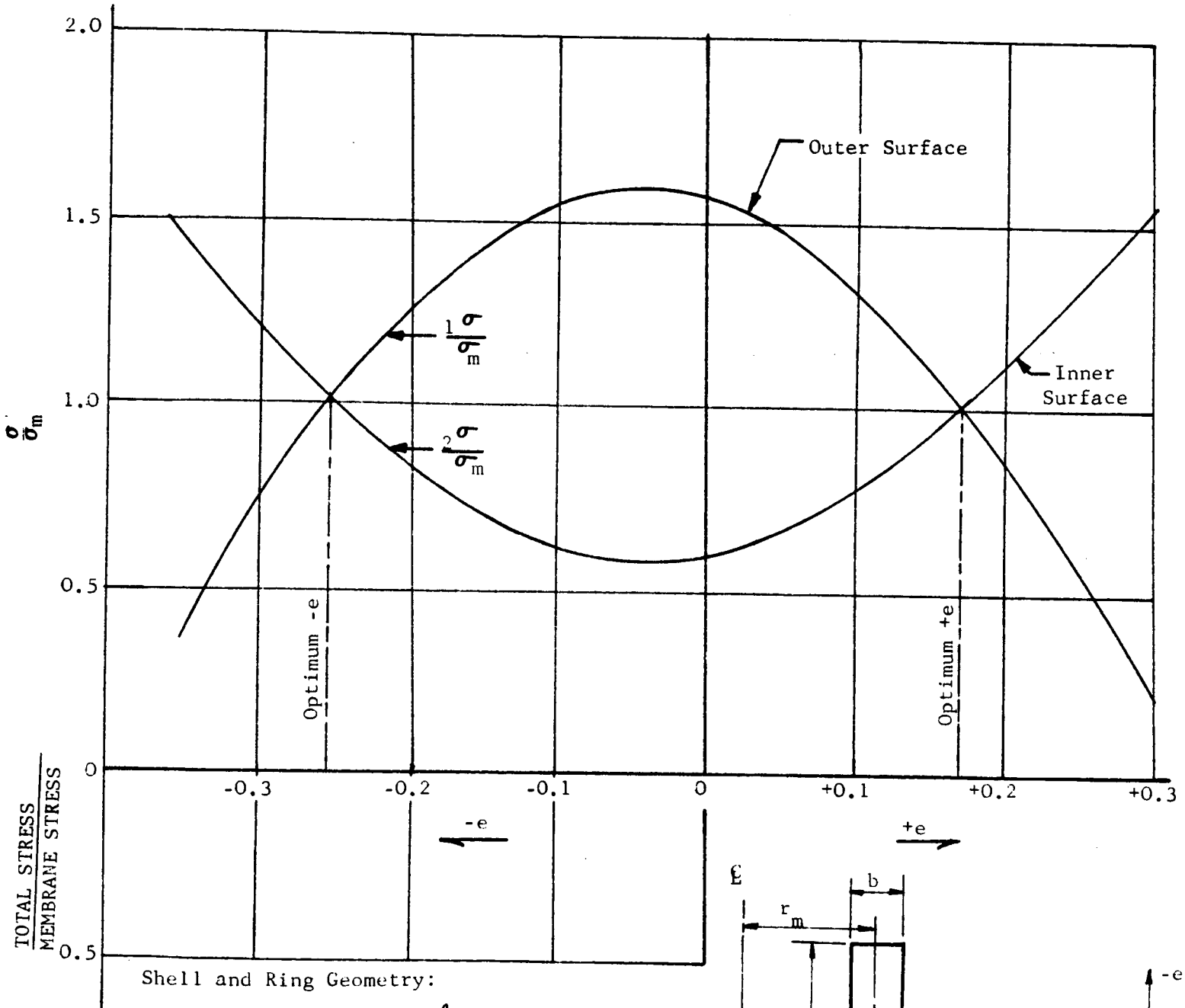

Shell and Ring Geometry:

$a = 18.0$ in
$\phi_o = 0.1403$ rad.
$r_m = 2.338$ in
$b = 0.375$
e = variable
${}_1\sigma$ = total stress on the outer surface of the shell.
${}_2\sigma$ = total stress on the outer surface of the shell.
$\sigma_m = \frac{Pd}{2t}$, membrane stress

$\ell = 0.724$ in
$t = 0.048$ in
$\nu = 0.3$
$E = 30 \times 10^6$ psi

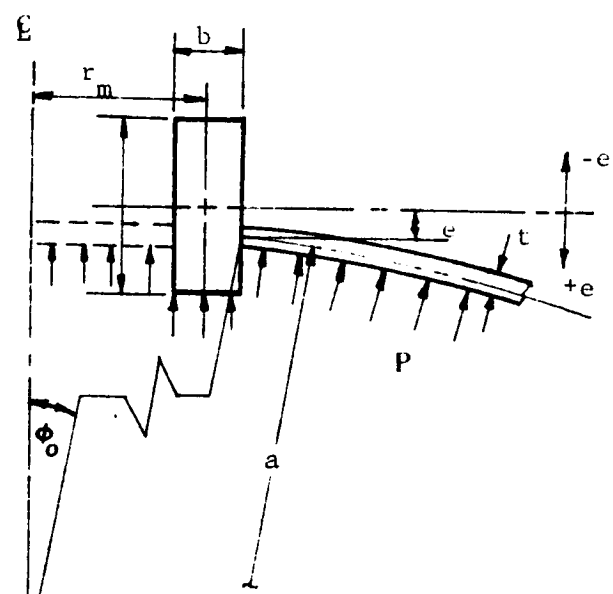

Fig. VII-4-38 Stresses at the Ring Membrane Junction Versus Eccentricity (Ref. 36)

The treatment of openings at points other than the apex of a head is extremely complicated and when a problem of this type arises it is wise to consult directly with the stress analysis people. Figure VII-4-39 shows the stress distribution around a typical off-apex reinforced opening.

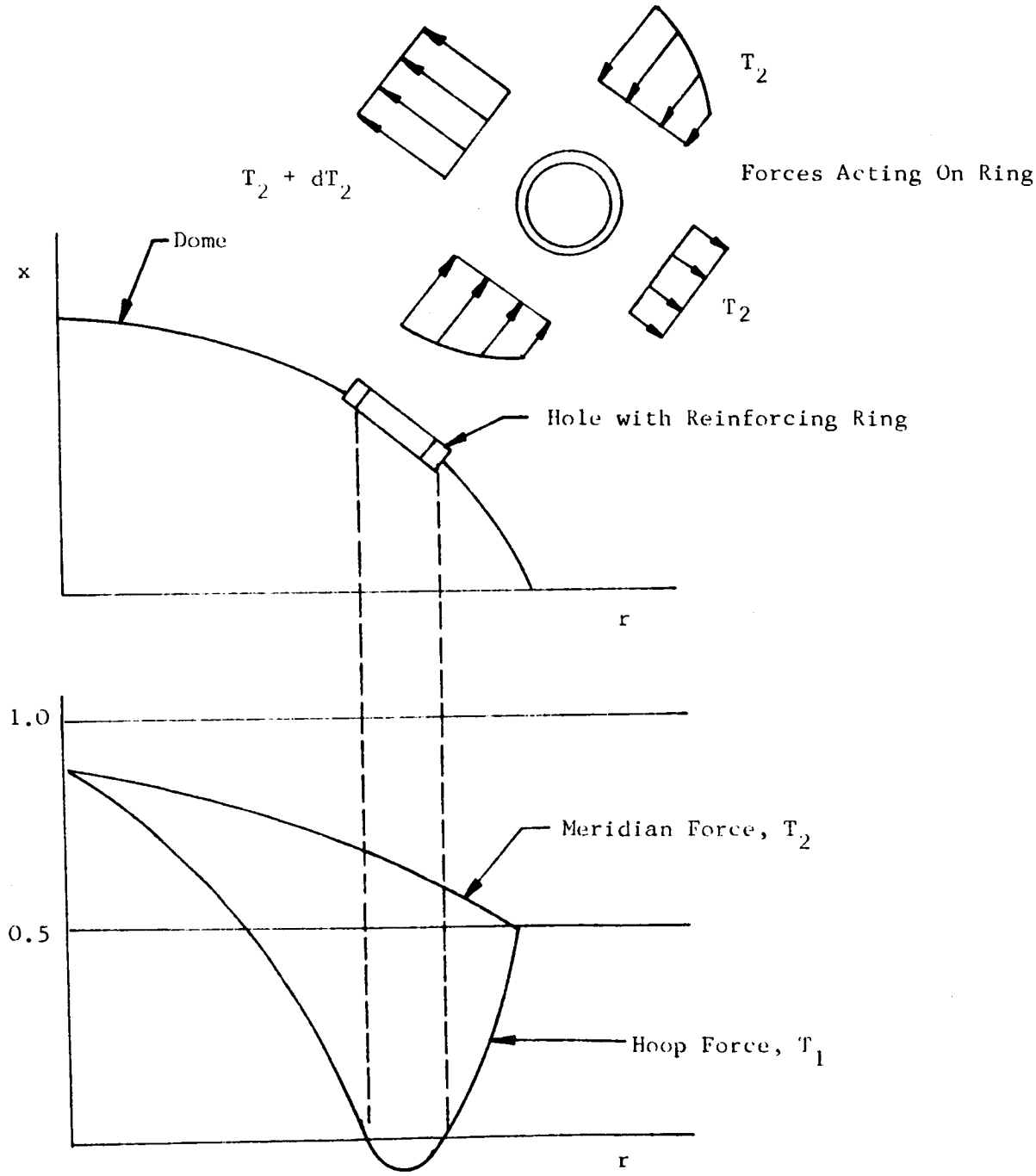

Fig. VII-4-39 Off-Apex Opening in a Head of Arbitrary Shape (Ref. 36)

Concentrated Loads

Many times a membrane will be subjected to loads which are concentrated in a small area. Here the membrane forces are extremely high and, if bending stresses were neglected, would approach infinity. Usually it is safe to assume that the effects of a concentrated load are negligible in a region defined by the radius r where $r > 1.9\sqrt{Rt}$ (Ref. 36). Figure VII-4-33 shows the stress concentration encountered when a membrane is reinforced with a rigid insert, while the following Figures (Ref. 41) show some common types of concentrated loads and their associated stresses and deflections. These stresses and deflections must be added to those due to other types of loading.

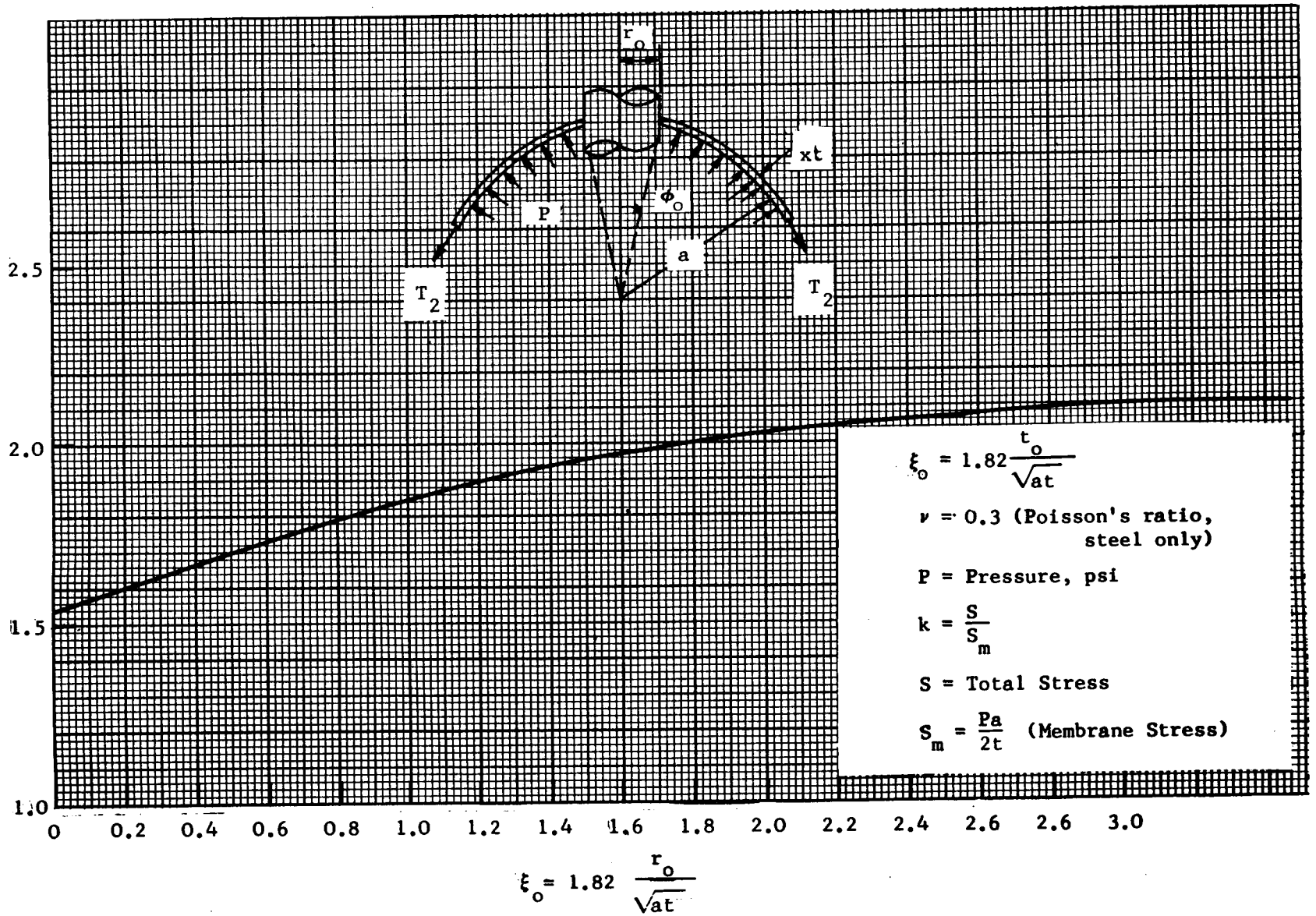

Fig. VII-4-40 Stress Concentration in a Membrane Reinforced with a Rigid Insert

Cylinders

Case 1.

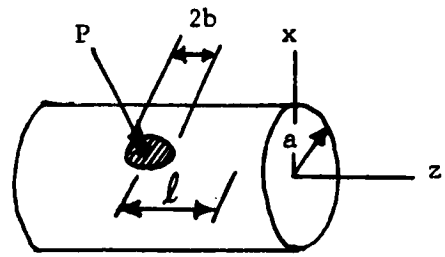

Fig. VII-4-41 Cylinder with Radial Load P (lb) Concentrated on Area of Radius b at a Distance ℓ from an End

The maximum bending stresses at the load are as follows:

ℓ remote from ends;

$$\left.\begin{aligned} S_1 &= -\frac{P}{t^2}\left[0.42 \ln \frac{0.215a}{b} + \frac{6\nu}{4\pi}\right] \\ S_2 &= -\frac{P}{t^2}\left[0.42 \ln \frac{0.215a}{b} + \frac{6}{4\pi}\right] \end{aligned}\right\} \quad (63)$$

for $b/a < 0.05$. If $b/a > 0.05$,

$$S_1 = S_2 = S_{max} = -\frac{P}{2t^2} \ln \frac{0.3a}{b} \quad (64)$$

ℓ close to an unsupported end,

$$S_1 = \left\{-\frac{P}{t^2}\left[0.42 \ln \frac{0.215a}{b} + \frac{6\nu}{4\pi}\right]\right\}\left(\frac{0.7a}{\ell + b}\right)^{\frac{1}{2}} \quad (65)$$

where, if $\ell + b > 0.7a$ the load is remote,

$$S_2 = -\frac{P}{t^2}\left[0.42 \ln \frac{0.215a}{b} + \frac{6}{4\pi}\right]\left(\frac{\ell}{0.2a}\right)^{\frac{1}{2}} \quad (66)$$

where, if $\ell > 0.2a$ the load is remote.

The maximum radial displacements at the load are:

ℓ remote from ends: $$\delta = -\frac{0.135Pa^2}{Et^3} \tag{67}$$

ℓ close to ends; $$\delta = -\frac{Pa^2}{Et^3}\left[0.48 - 0.22\left(\frac{\ell}{a}\right)^{0.35}\right] \tag{68}$$

where if $\ell > 2a$ the load is remote.

Case 2.

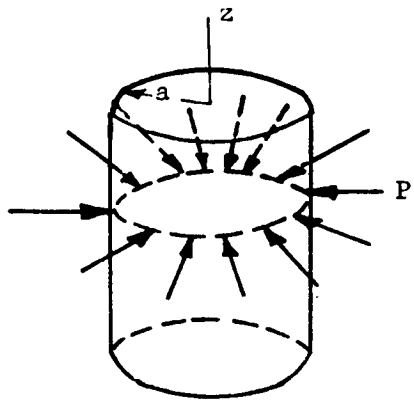

Fig. VII-4-42 Uniform Radial Pressure (P lb/in of Circumference)

The maximum moment and bending stress at the load are given by:

$$\left.\begin{aligned} M &= \frac{P}{A\lambda} \\ S_2 &= -\frac{3P}{2\lambda t^2} \\ \lambda &= \left[\frac{3(1-\nu^2)}{R_1^2 t^2}\right]^{\frac{1}{4}} \end{aligned}\right\} \tag{69}$$

where:

And the maximum hoop stress and radial displacement at the load is given by:

$$S_1 = -\frac{Pa\lambda}{2t} \tag{70}$$

$$\delta = -\frac{Pa^2\lambda}{2Et} \tag{71}$$

Case 3.

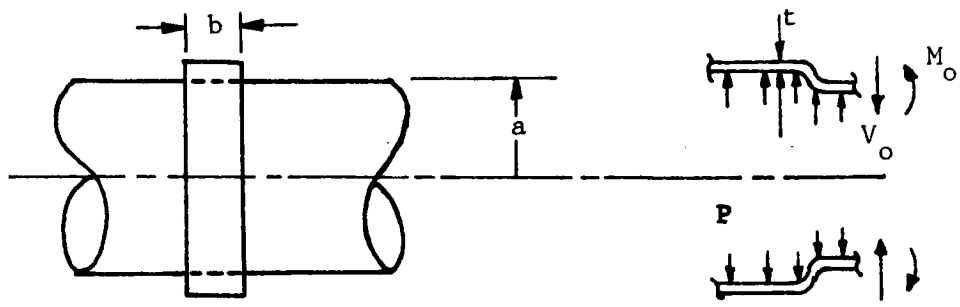

Fig. VII-4-43 Cylinder with Reinforcing Ring of Cross-Sectional Area A

M_o and V_o are given as follows:

$$\left.\begin{aligned} M_o &= 0.304\ Pat\left(\frac{A - bt}{A + 1.56t\sqrt{at}}\right) \\ V_o &= 0.78\ P\sqrt{at}\left(\frac{A - bt}{A + 1.56t\sqrt{at}}\right) \end{aligned}\right\} \tag{72}$$

And for a rigid ring or disk (Ref. 41):

$$\left.\begin{aligned} M_o &= 0.304\ Pat \\ V_o &= 0.78\ P\sqrt{at} \end{aligned}\right\} \tag{73}$$

Equation (72) leads to the following relation for the maximum bending stress at the edge of the ring:

$$S_2 = -\frac{6M_o}{t^2} \tag{74}$$

When a number of rings are used and are spaced at a distance equal to or greater than $4/\lambda$ the influence of one does not extend to the next.

Spherical Membrane

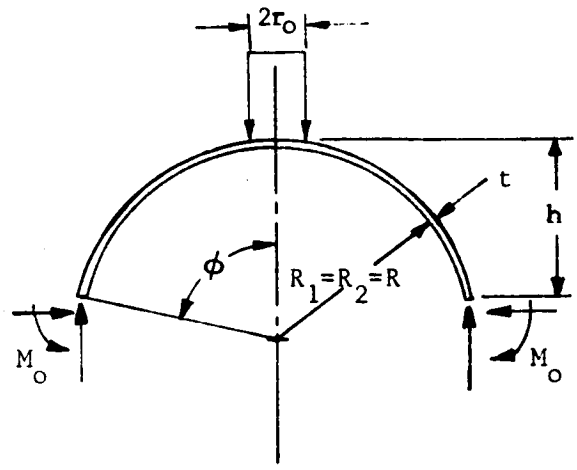

Fig. VII-4-44 Spherical Membrane with Load P (lb) Concentrated over a Circular Area with Radius r_o (Edges Fixed and Held)

The following equations give the deflection, y, and edge moment, M_o.

$$y = A\,\frac{PR^2 3(1-\nu^2)}{4\pi Et^3} \tag{75}$$

$$M_o = B\,\frac{P}{4\pi} \tag{76}$$

where A and B are coefficients that depend upon $\alpha = 2\left[3(1-\nu^2)\right]^{\frac{1}{4}}\sqrt{\frac{h}{t}}$ and are tabulated as follows:

α	0	1	2	3	4	5	6	7	8	9	10
A	1	0.985	0.817	0.515	0.320	0.220	0.161	0.122	0.095	0.075	0.061
B	1	0.975	0.690	0.191	-0.080	-0.140	-0.117	-0.080	-0.059	-0.034	-0.026

Thick-Walled Pressure Vessels

The membrane analysis previously developed assumed, among other things, that the stress distribution across the thickness, t, was constant. In an actual pressure vessel this is not true but the error introduced with this assumption is usually so small as to be insignificant and therefore, is ignored. Reference 23 describes the case of a cylinder where, if the outside radius, b, is 1.1 times the inside radius, a, the difference between the maximum (inside wall) and minimum (outside wall) stresses is only about 10%. Other authors[14] suggest that when the thickness is 20% of the inside radius, the maximum stress is only about 10% higher than the average (membrane) stress. This gives an a/t ratio less than 5 as the break-off point for membrane analysis. The best rule is, however, "if in doubt--check" since this ratio depends upon the material used and the designer's previous experience. References 14 and 23 provide the type of analysis presented here for thick-walled pressure vessels.

VII-5 MATERIAL BEHAVIOR

The analytical treatment of pressure vessels is accomplished through the two mutually complementary disciplines of stress analysis and failure criteria. Whereas stress analysis provides the distribution of stresses in the structure, it is the failure criterion which permits the prediction of limiting loads or the safe useful life of the structure. In recent years fracture has been the subject of a considerable research effort. This effort has borne three distinct fruits. The first benefit provides a degree of sophistication to the earlier, conventional theories. Secondly, analytical and experimental work has been performed which provides better insight into a relatively obscure phenomenon. Finally, much new theory has been developed in two relatively fertile fields which will be described herein as they pertain to pressure vessel design: fracture mechanics and statistical strength theory.

Phenomenological Theories

The stress at a point is completely defined by nine components of stress or by three principal stresses as follows:

$$\sigma = \begin{bmatrix} \sigma_x & \tau_{xy} & \tau_{xz} \\ \tau_{yx} & \sigma_y & \tau_{yz} \\ \tau_{zx} & \tau_{zy} & \sigma_z \end{bmatrix} = \begin{bmatrix} \sigma_1 & 0 & 0 \\ 0 & \sigma_2 & 0 \\ 0 & 0 & \sigma_3 \end{bmatrix}$$

A failure criterion can be simply a mathematical relation among these stress components which states that failure occurs when a certain combination of the stress components attains a critical value. Such a simple mathematical formula based on the stress state alone is called a phenomenological theory. The most common phenomenological theories which are found useful today are listed in Table VII-5-1.

As an example of how one employs the various fracture theories, consider the following. Using the maximum-tensile-stress theory of failure for elementary pressure vessel theory, $\sigma_{rr} = \tau_{r\theta} = \tau_{z\theta} = \tau_{zr} = 0$,

TABLE VII-3-1 PHENOMENOLOGICAL FAILURE THEORIES

FAILURE CRITERIA	TYPE OF MATERIAL TO WHICH CRITERION IS APPLICABLE	MATHEMATICAL FORM OF CRITERION (PRINCIPAL STRESSES)	MATHEMATICAL FORM OF CRITERION (COORDINATE STRESSES)
Maximum Tensile Stress	Used in Design With Brittle Materials	$\sigma_1 \geq \sigma_f$ *	$\sigma_f = \frac{\sigma_x + \sigma_y}{2} + \left[\left(\frac{\sigma_x + \sigma_y}{2}\right)^2 + \tau_{xy}^2\right]^{\frac{1}{2}}$
Maximum Tensile Strain	Brittle Materials Ceramics Glass Graphite	$\sigma_1 - \nu(\sigma_2 + \sigma_3) \geq \sigma_f$	$\sigma_f = (1-\nu)\left(\frac{\sigma_x + \sigma_y}{2}\right) + (1-\nu)\left[\left(\frac{\sigma_x - \sigma_y}{2}\right)^2 + \tau_{xy}^2\right]^{\frac{1}{2}}$
Maximum Shear Stress	Ductile Materials Metals Polymers	$\sigma_1 - \sigma_3 \geq \sigma_f$	$\sigma_f = 2\left[\left(\frac{\sigma_x - \sigma_y}{2}\right)^2 + \tau_{xy}^2\right]^{\frac{1}{2}}$
Maximum Strain Energy	Plastically flowing solids	$\left[\sigma_1^2 + \sigma_2^2 + \sigma_3^2 - 2\nu(\sigma_1\sigma_2 + \sigma_2\sigma_3 + \sigma_3\sigma_1)\right]^{\frac{1}{2}} \geq \sigma_f$	$\sigma_f = \left[\sigma_x^2 + \sigma_y^2 + \sigma_z^2 - 2\nu(\sigma_x\sigma_y + \sigma_y\sigma_z + \sigma_z\sigma_x) + 2(1+\nu)(\tau_{xy}^2 + \tau_{yz}^2 + \tau_{zx}^2)\right]^{\frac{1}{2}}$
Distortion Energy Theory	Ductile Materials	$\left[\sigma_1^2 + \sigma_2^2 + \sigma_3^2 - (\sigma_1\sigma_2 + \sigma_2\sigma_3 + \sigma_3\sigma_1)\right]^{\frac{1}{2}} \geq \sigma_f$	$\sigma_f = \frac{1}{\sqrt{2}}\left[(\sigma_x - \sigma_y)^2 + (\sigma_y - \sigma_z)^2 + (\sigma_z - \sigma_x)^2 + 6(\tau_{xy}^2 + \tau_{yz}^2 + \tau_{zx}^2)\right]^{\frac{1}{2}}$
Internal Friction Theory	Brittle Materials (Empirical)	$\sigma_1 - \sigma_3\left(\frac{1-\sin\alpha}{1+\sin\alpha}\right) \geq \sigma_f$ **	———
Mohr Theory	Brittle materials allow adjustable ratio of ultimate compressive strength to ultimate tensile strength	$\tau_{fs} = \frac{\sigma_{ft}\,\sigma_{fc}}{\sigma_{ft} - \sigma_{fc}}$ where σ_{ft} = tensile failing strength; σ_{fc} = compressive failure strength; τ_{fs} = shear failure stress	

* σ_f is the fracture stress in simple tension.

** $\alpha = \tan^{-1} f$ where f = coefficient of friction. This theory is postulated under the assumption of a frictional resistance to sliding on the plane of shear.

$\sigma_{\theta\theta} = pa/t$, and $\sigma_{zz} = pa/2t$. Clearly $\sigma_{\theta\theta} > \sigma_{zz}$ and therefore the limiting pressure for a given geometry is $p = \frac{t\sigma_f}{a}$. Also the design sizes for a vessel to sustain a given pressure are $\frac{a}{t} = \frac{\sigma_f}{p}$. Using a distortion energy failure criterion these same two relationships are

$$p = \frac{2t\sigma_f}{a\sqrt{3}} = 1.16t\,\frac{\sigma_f}{a}$$

and

$$\frac{a}{t} = \frac{2}{\sqrt{3}}\,\frac{\sigma_f}{p} = 1.16\,\frac{\sigma_f}{p}$$

Clearly, using a distortion energy criterion results in a 16% higher pressure capability for a given size tank and a fixed σ_f. Expressed another way, the thickness of the tank using the distortion energy failure criterion can be 16% lighter than that using the maximum-tensile-stress theory of failure.

In general the following comments should be applied to phenomenological failure theories. Currently, no theory yet developed will be seen to hold for all materials. Ductile materials appear to be best characterized by:

1) Maximum Shear Stress
2) Distortion Energy
3) Octahedral Stress Theory

For brittle materials which exhibit little or no flow prior to failure, those theories which appear to predict the behavior best are:

1) Maximum Normal Stress
2) Maximum Tensile Strain
3) Mohr Theory

For data on the limiting strength of metals used for pressurized gas containers see References 1 and 2.

Fracture Mechanics

Pressure vessel engineers employing high-strength steels are particularly interested in the following material properties: yield and tensile

strength, fatigue and corrosion resistances, and ductility and toughness.* While it would be desirable to increase the effectiveness of all of these properties simultaneously, it is an unfortunate but established fact that the ductility and toughness of high-strength metals tend to decrease as the ultimate tensile strength increases. Thus it becomes important for a designer to have some measure of the resistance of the material to crack propagation in addition to the usual tensile property data. In addition it is most meaningful if this knowledge consists of parameters which express toughness to a natural crack. Such a parameter, K, the stress intensity factor, or G, the crack extension force, has been well developed by Irwin and his co-workers.[4] The parameters, techniques for measuring K or G, the theoretical basis for these concepts and methods for applying these techniques are properly the scope of linear elastic-fracture mechanics. The concepts can be used to predict the loads to cause failure or the maximum tolerable crack size for a given material which will not lead to rapid crack propagation prior to failure by excessive plastic deformation.

Three modes of possible crack extension are shown in Figure VII-5-1. The three stress intensification factors associated with these three modes are K_I, K_{II}, and K_{III}. Since tensile-stress fields predominate in pressure vessels, and because the majority of practical applications result in failures typified by Mode I, this entire discussion will be limited to K_I.

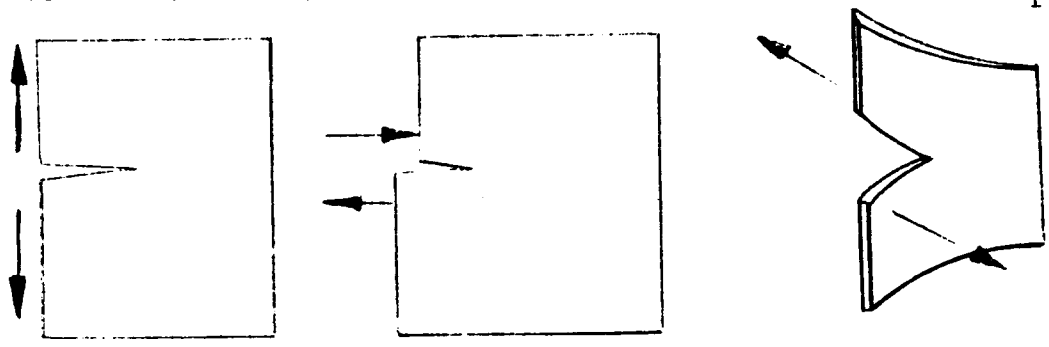

Mode I Opening Mode II Edge Sliding Mode III Tearing

Fig. VII-5-1 Three Possible Fracture Modes

* Defined as the ability of the material to resist failure in the presence of sharp notches, cracks, or flaws of internal and external location in the pressure vessel.

Essentially, the fracture mechanics approach states that a crack in the solid material will propagate when an incremental increase in crack area provides an increment of elastic strain energy equal to or greater than the work dissipated. The parameter, G, introduced earlier is the strain-energy release rate. The relationship between K and G is given by

$$K = \sqrt{GE} \qquad \text{For plane stress}$$

$$K = \sqrt{\frac{GE}{1-\nu^2}} \qquad \text{For plane strain}$$

For unstable crack growth (the point at which the energy available for crack growth exceeds the work done in extending the crack) critical values, G_c and K_c, occur. Through the use of toughness test, K_c and G_c for various materials can be determined.

Table VII-5-2 shows the relationship between K_I and various geometric and load parameters for several cases of practical interest. Table VII-5-3 gives the values of K_{Ic} for several high-strength materials currently used in practical pressure-vessel design.

As an example of the application of fracture mechanics to practical problems, consider the following problem. Suppose that in a specific application, such as is shown in Figure VII-5-2, under consideration a crack of length 2a is noted in the shape. The stress analysis of the component has shown that $\sigma = \frac{pr}{t}$. The material is Vascojet 1000. From Table VII-5-2 the stress intensity factor, K_I, is given by

$$K_I = 1.12\sigma\sqrt{\pi a}$$

Furthermore, from Table VII-5-3 we see that for Vascojet 1000, K_{Ic} = 34 ksi$\sqrt{\text{in.}}$ (for a 300-ksi ultimate tensile strength). In addition, the length of the longest crack in this structure has been determined to be 0.150 inches. Then the pressure at failure would be

$$p = \frac{t}{r}\,\frac{K_{Ic}}{1.12\sqrt{\pi a}} = 44\,\frac{t}{r}\ \text{ksi}$$

Also stated another way the geometric dimensions of the component to resist fracture at a given pressure would be

$$\frac{t}{r} = 0.0226p$$

If the problem of interest were to define nondestructive test techniques, the relationship

$$a = \frac{1}{\pi}\left(\frac{K_I t}{1.12pr}\right)^2$$

would enable the test engineers to establish the minimum required resolution of the equipment to locate critical size cracks.

Finally, although a comparison of the two methods for failure criteria cannot, in the strictest sense, be compared for the cylindrical pressure vessel, $\left(\sigma_\theta = pr/t,\ \sigma_z = \frac{pr}{2t}\right)$, some measure of the importance of the fracture mechanics concept can be gained from the following. Assume the same Vascojet 1000 material as before with a crack of length = 0.250 in. but oriented perpendicular to the $\sigma_z = pr/2t$ direction. From conventional failure criteria (distortional energy)

$$p = 1.16t\ \sigma_f/r = 348\frac{t}{r} \qquad [\text{ksi}]$$

From fracture mechanics (for a = 0.125)*, we use the stress intensity factor shown in Table VII-5-2, for the infinite cracked sheet with uniform normal stress at infinity, $K_I = \sigma\sqrt{\pi a}$. Thus

$$P = \left(\frac{2t}{r}\right)\sigma = \left(\frac{2t}{r}\right)\left(\frac{K_{Ic}}{\sqrt{\pi a}}\right) = 109\frac{t}{r} \qquad [\text{ksi}]$$

Thus the pressure capabilities of the same tank using fracture mechanics are shown to be only 31% of those using a conventional failure criterion even when the detected crack is oriented perpendicular to the smaller of the two principal stresses.

---

* A crack of length 1/8 in. seems to be the smallest detectable by current inspection techniques.

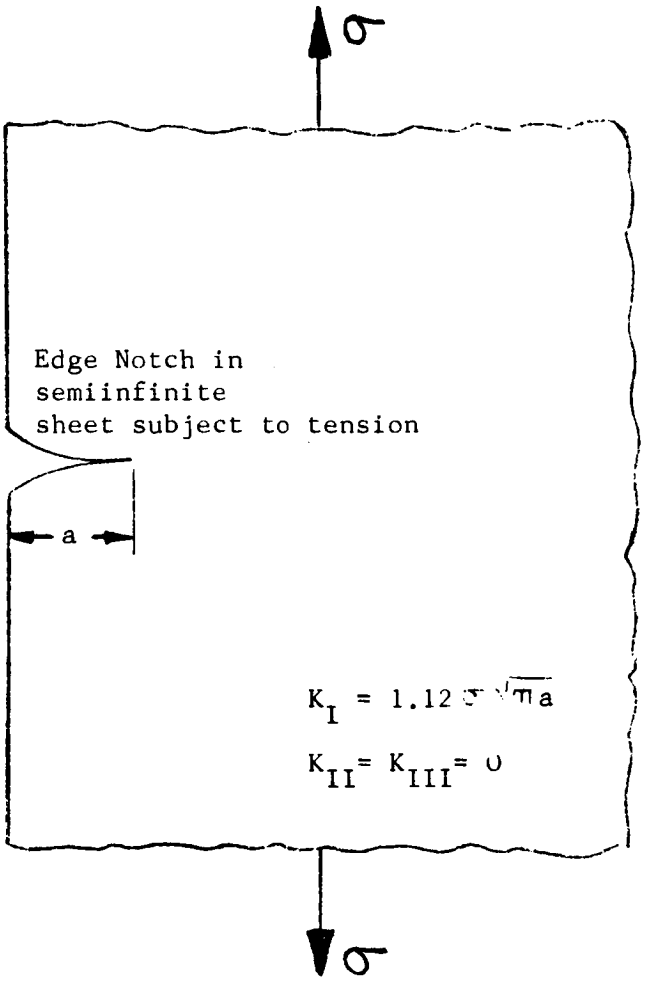

Fig. VII-5-2 Example of Practical Application of Fracture Mechanics

Table VII-5-2

STRESS INTENSITY FACTORS FOR VARIOUS SHAPES AND LOADS

STRESS FIELD AND GEOMETRY OF CRACK	STRESS INTENSITY FACTORS	REF.
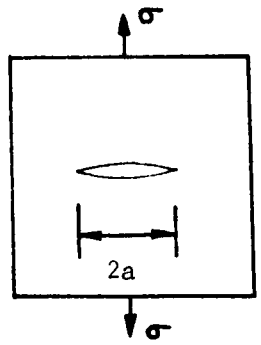 Infinite Cracked Sheet With Uniform No Normal Stress at Infinity	$K_I = \sigma\sqrt{\pi a}$ $K_{II} = K_{III} = 0$	47
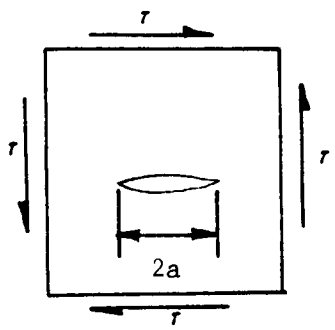 Infinite Cracked Sheet With Uniform In-Plane Shear at Infinity	$K_{II} = \tau\sqrt{\pi a}$ $K_I = K_{III} = 0$	47
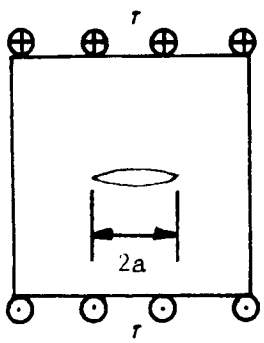 Infinite Sheet With Tunnel Crack Subject to Out of Plane Shear at Infinity	$K_{III} = \tau\sqrt{\pi a}$ $K_I = K_{II} = 0$	47

Table VII-5-2 (contd)

STRESS FIELD AND GEOMETRY OF CRACK	STRESS INTENSITY FACTORS	Ref.
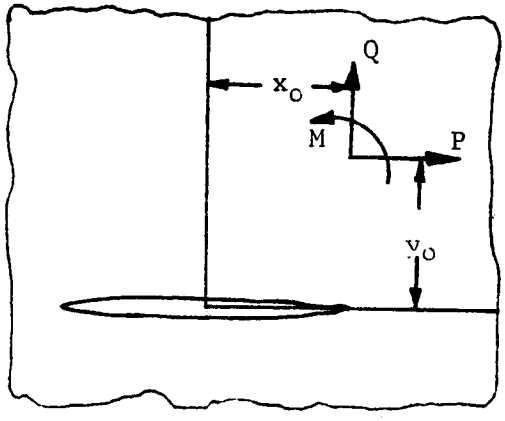 Crack in Infinite Sheet Subject to Arbitrary Force and Couple at a Remote Point	At right end: $K = \frac{1}{2\sqrt{\pi a}(1+K)}\left\{(P+iQ)\left[\frac{a+z_o}{\sqrt{z_o^2-a^2}} - \frac{K(a+z_o)}{(\bar{z}_o^2-a^2)^{\frac{1}{2}}} - 1 + K\right] + \frac{a(P-iQ)(\bar{z}_o - z_o) + ai(1+K)M}{(\bar{z}_o - a)(\bar{z}_o^2 - a^2)^{\frac{1}{2}}}\right\}$ $K = (3-\nu)/(1+\nu)$ for plane stress $K = 3 - 4\nu$ for plane strain $z_o = x_o + iy_o$ $\bar{z}_o = x_o - iy_o$	47
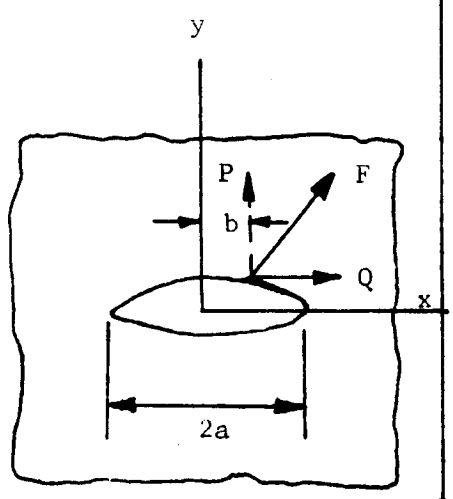 A Concentrated Force on the Surface of a Crack in an Infinite Sheet	$K_I = \frac{P}{2\sqrt{\pi a}}\left(\frac{a+b}{a-b}\right)^{\frac{1}{2}} + \frac{Q}{2\sqrt{\pi a}}\left(\frac{K-1}{K+1}\right)$ $K_{II} = \frac{-P}{2\sqrt{\pi a}}\left(\frac{K-1}{K+1}\right) + \frac{Q}{2\sqrt{\pi a}}\left(\frac{a+b}{a-b}\right)^{\frac{1}{2}}$ $K = 3.4\nu$ (for plane strain)	47

Table VII-5-2 (contd)

STRESS FIELD AND GEOMETRY OF CRACK	STRESS INTENSITY FACTORS	REF.
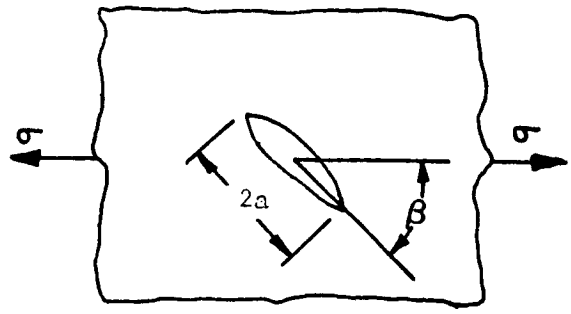 Inclined Crack in Uniform Tension in Infinite Sheet	$K_I = \sigma \sin^2\beta \sqrt{\pi a}$ $K_{II} = \sigma \sin\beta \cos\beta \sqrt{\pi a}$	47
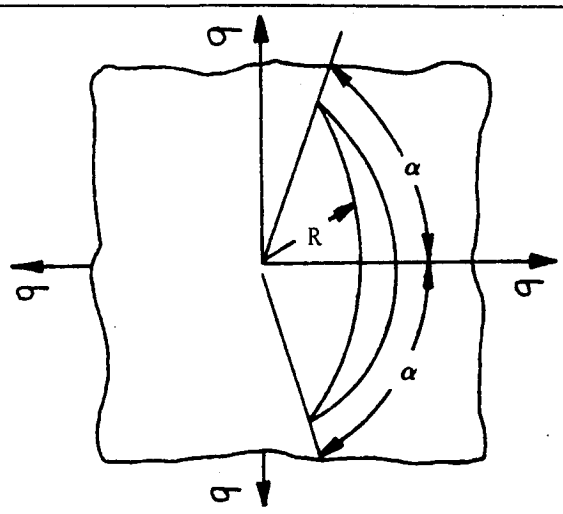 Curved Crack in Equal Biaxial Stress Field	$K_I = \dfrac{\sigma(\pi R)^{\frac{1}{2}}}{(1 + \sin^2\frac{\alpha}{2})} \cdot \left(\dfrac{\sin\alpha(1 + \cos\alpha)}{2}\right)^{\frac{1}{2}}$ $K_{II} = \dfrac{\sigma(\pi R)^{\frac{1}{2}}}{(1 + \sin^2\frac{\alpha}{2})} \cdot \left(\dfrac{\sin\alpha(1 - \cos\alpha)}{2}\right)^{\frac{1}{2}}$	47
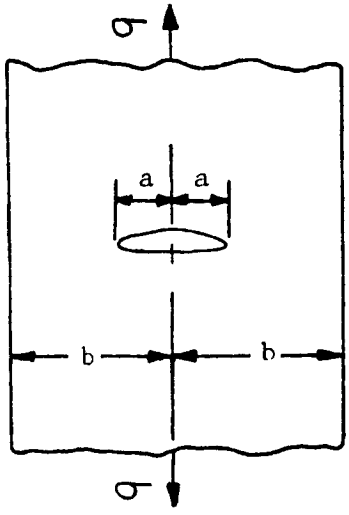 Central Crack in Strip Subject to Tension (Finite Width)	$K_I = \sigma \sqrt{\pi a}\, f(\lambda)$ $\lambda = a/b$ λ / $f(\lambda)$: 0.074 / 1.00 0.207 / 1.03 0.275 / 1.05 0.337 / 1.09 0.410 / 1.13 0.466 / 1.18 0.535 / 1.25 0.592 / 1.33	47 89 90 91 92 93

Table VII-5.2 (contd)

STRESS FIELD AND GEOMETRY OF CRACK	STRESS INTENSITY FACTORS	REF.
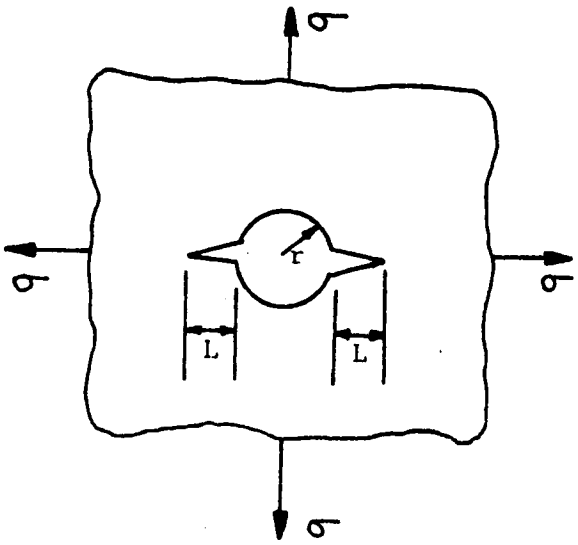 Cracks from Hole in Infinite Sheet	$K_I = \sigma\sqrt{L\pi}\, f\left(\frac{L}{r}\right)$ $K_{II} = 0$	47

$\frac{L}{r}$	ONE CRACK f(L/r) Uniaxial Stress	ONE CRACK f(L/r) Biaxial Stress	TWO CRACKS f(L/r) Uniaxial Stress	TWO CRACKS f(L/r) Biaxial Stress
0	3.39	2.26	3.39	2.26
0.1	2.73	1.98	2.73	1.98
0.2	2.30	1.82	2.41	1.83
0.3	2.04	1.67	2.15	1.70
0.4	1.86	1.58	1.96	1.61
0.5	1.73	1.49	1.83	1.57
0.6	1.64	1.42	1.71	1.52
0.8	1.47	1.32	1.58	1.43
1.0	1.37	1.22	1.45	1.38
1.5	1.18	1.06	1.29	1.26
2.0	1.06	1.01	1.21	1.20
3.0	0.94	0.93	1.14	1.13
5.0	0.81	0.81	1.07	1.06
10.0	0.75	0.75	1.03	1.03
∞	0.707	0.707	1.00	1.00

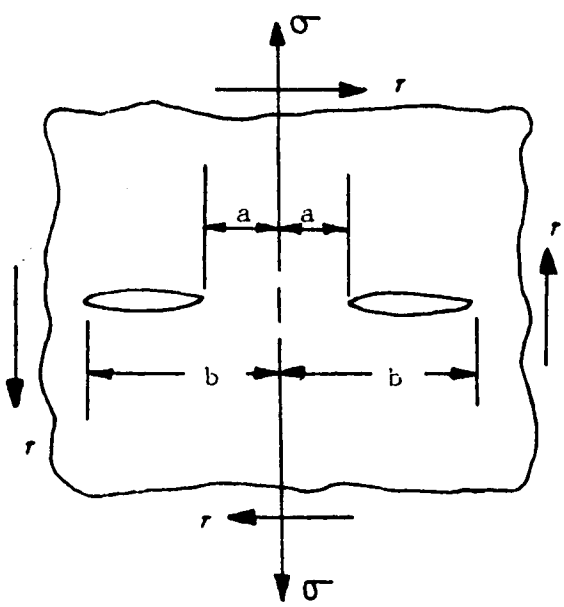 Two Equal Colinear Cracks in an Infinite Sheet Subject to Uniform Tension	At the near ends $K_I = \sigma\sqrt{\pi a}\,\frac{b^2\frac{E(\mu)}{K(\mu)} - a^2}{(b^2 - a^2)^{1/2}}$ $K_{II} = \tau\sqrt{\pi a}\,\frac{b^2\frac{E(\mu)}{K(\mu)} - a^2}{(b^2 - a^2)^{1/2}}$ At the far ends $K_I = \sigma\sqrt{\pi b}\left(\frac{1}{\mu} - \frac{E(\mu)}{\mu K(\mu)}\right)$ $K_{II} = \tau\sqrt{\pi b}\left(\frac{1}{\mu} - \frac{E(\mu)}{\mu K(\mu)}\right)$ where $\mu = \left[1 - \left(\frac{a^2}{b^2}\right)\right]^{1/2}$	47

Table VII-5-2 (contd)

STRESS FIELD AND GEOMETRY OF CRACK	STRESS INTENSITY FACTORS	REF.
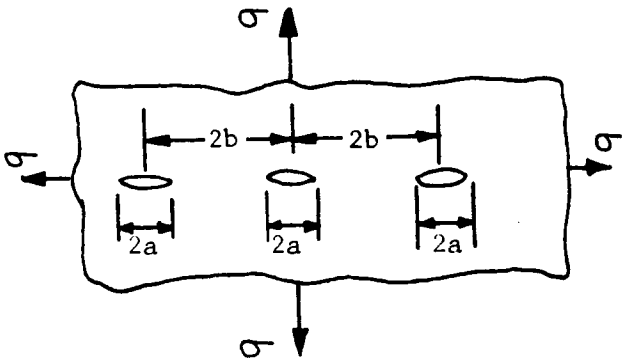 Periodic Array of Cracks Along a Line in a Sheet - Uniform Stress at Infinity	$K_I = \sigma\sqrt{\pi a}\left(\frac{2b}{\pi a}\tan\frac{\pi a}{2b}\right)^{\frac{1}{2}}$ $K_{II} = K_{III} = 0$	47 48
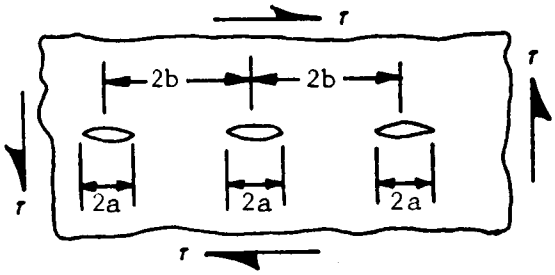 Periodic Array of Cracks Along a Line in a Sheet - Uniform In-Plane Shear Stress at Infinity	$K_{II} = \tau\sqrt{\pi a}\left(\frac{2b}{\pi a}\tan\frac{\pi a}{2b}\right)^{\frac{1}{2}}$ $K_I = K_{III} = 0$	47
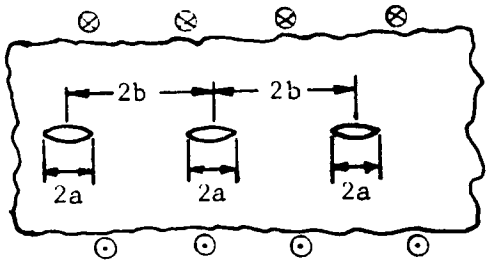 Periodic Array of Cracks Along a Line in a Sheet - Uniform Out-of-Plane Shear Stress at Infinity	$K_{III} = \tau\sqrt{\pi a}\left(\frac{2b}{\pi a}\tan\frac{\pi a}{2b}\right)^{\frac{1}{2}}$ $K_I = K_{II} = 0$	47

Table VII-5-2 (contd)

STRESS FIELD AND GEOMETRY OF CRACK	STRESS INTENSITY FACTORS	REF.
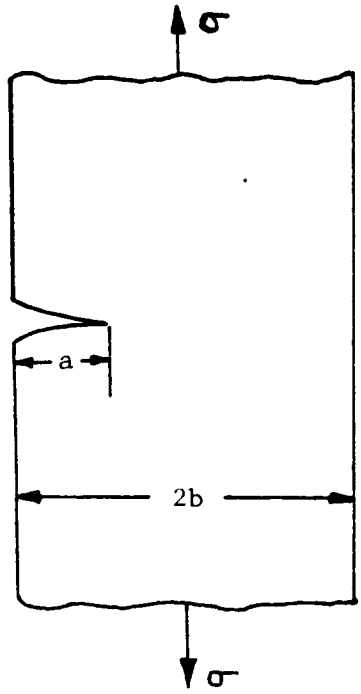 Single Edge Notch	$K_I = \sigma\sqrt{\pi a}\ f(a/b)$ $K_{II} = K_{III} = 0$	47 50 51

a/b	f(a/b) Ref. 50	f(a/b) Ref. 51
0.1	1.15	1.14
0.2	1.20	1.19
0.3	1.29	1.29
0.4	1.37	1.37
0.5	1.51	1.50
0.6	1.68	1.66
0.7	1.89	1.87
0.8	2.14	2.12
0.9	2.46	2.44
1.0	2.86	2.82

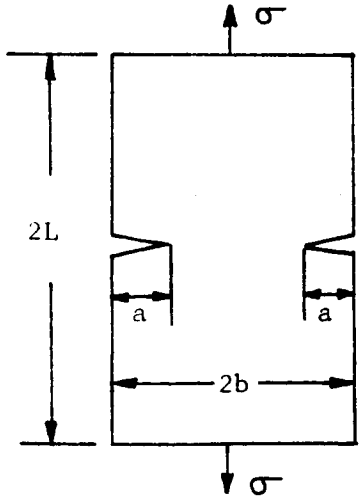 Double Edge Notch	$K_I = \sigma\sqrt{\pi a}\left(\frac{2b}{\pi a}\tan\frac{\pi a}{2b}\right)^{\frac{1}{2}} f(a/b)$ $K_{II} = K_{III} = 0$ for $L \to \infty$ use: $K_I = \sigma\sqrt{\pi a}\left[\frac{2b}{\pi a}\left(\tan\frac{\pi a}{2b} + 0.1\sin\frac{\pi a}{b}\right)\right]^{\frac{1}{2}}$ by Irwin (48)	47

a/b	f(a/b) L/b = 1	f(a/b) L/b = 3	f(a/b) L/b → ∞
0.1	1.13	1.12	1.12
0.2	1.13	1.11	1.12
0.3	1.14	1.09	1.13
0.4	1.16	1.06	1.14
0.5	1.14	1.02	1.15
0.6	1.10	1.01	1.22
0.7	1.02	1.00	1.34
0.8	1.01	1.00	1.57
0.9	1.00	1.00	2.09

Table VII-5-2 (contd)

STRESS FIELD AND GEOMETRY OF CRACK	STRESS INTENSITY FACTORS	REF.
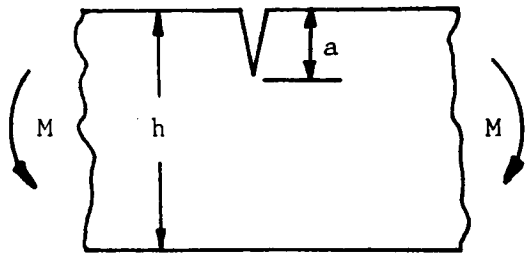 Notched Beam in Bending	$K_I = \frac{6M}{(h - a)^{3/2}} g(a/h)$ $K_{II} = K_{III} = 0$ a/h: 0.05, 0.1, 0.2, 0.3 g(a/h): 0.36, 0.49, 0.60, 0.66 a/h: 0.4, 0.5, 0.6, 70.6 g(a/h): 0.69, 0.72, 0.73, 0.73	47 49
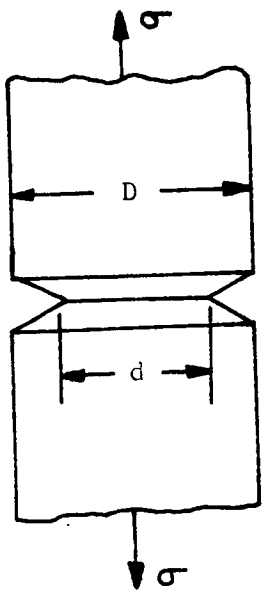 Round Bar in Tension With Circumferential Crack	$K_I = \sigma_{net}\sqrt{\pi D}\ f(d/D)$ $K_{II} = K_{III} = 0$ d/D: 0, 0.1, 0.2, 0.3, 0.4, 0.5, 0.6, 0.65 f(d/D): 0, 0.111, 0.155, 0.185, 0.209, 0.227, 0.238, 0.240 d/D: 0.70, 0.75, 0.80, 0.85, 0.90, 0.95, 0.97, 1.00 f(d/D): 0.240, 0.237, 0.233, 0.225, 0.205, 0.162, 0.130, 0	47

Table VII-5-2 (contd)

STRESS FIELD AND GEOMETRY OF CRACK	STRESS INTENSITY FACTORS	REF.
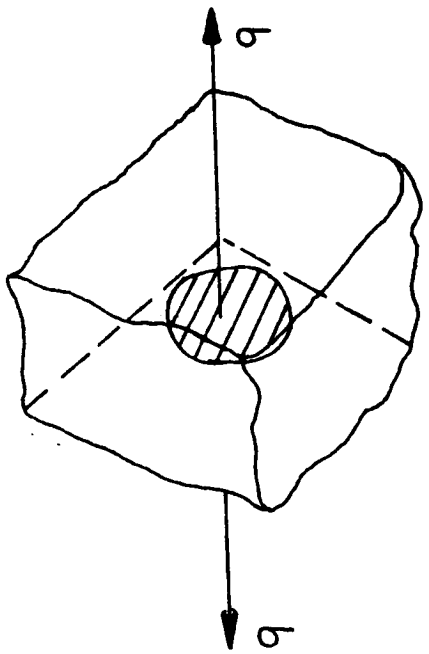 Penny-Shaped Crack in an Infinite Body Subject to Uniform Tension	$K_I = 2\sigma\sqrt{\frac{a}{\pi}}$ $K_{II} = K_{III} = 0$	47
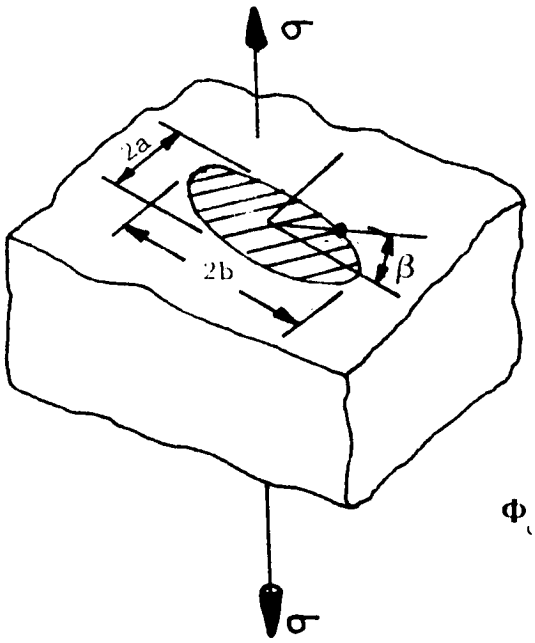 Elliptical Crack in Infinite Body Subject to Uniform Tension	For point on crack edge determined by angle β $K_I = \frac{\sigma\sqrt{\pi a}}{\Phi_o}\left(\sin^2\beta + \frac{a^2}{b^2}\cos^2\beta\right)^{\frac{1}{4}}$ $K_{II} = K_{III} = 0$ $\Phi_o = \int_0^{\pi/2}\left[1 - \left(\frac{b^2 - a^2}{b^2}\right)\sin^2\theta\right]^{\frac{1}{2}} d\theta$	87

Table VII-5-2 (contd)

STRESS FIELD AND GEOMETRY OF CRACK	STRESS INTENSITY FACTORS	REF.
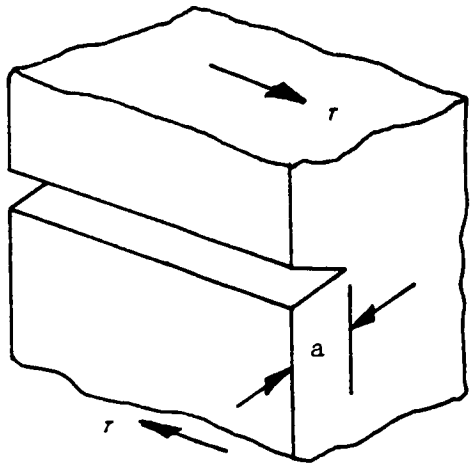 An Edge Crack in a Semi Infinite Body Subjected to Shear	$K_I = K_{II} = 0$ $K_{III} = \tau\sqrt{\pi a}$	88
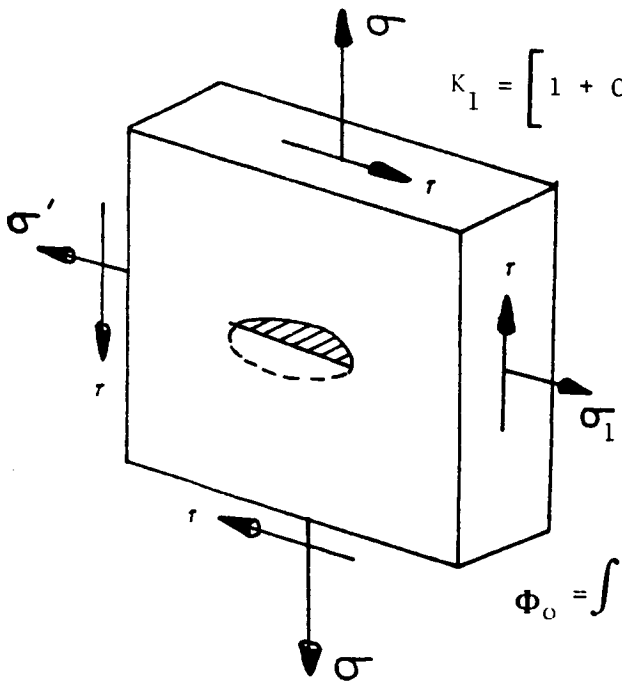 Semi-Elliptical Surface Crack in Plate Subject to General Extension	$K_I = \left[1 + 0.12(1 - \frac{a}{b})\right] \bullet \frac{\sigma\sqrt{\pi a}}{\Phi_o}\left(\frac{2t}{\pi a}\tan\frac{\pi a}{2t}\right)^{\frac{1}{2}}$ $K_{II} = 0$ $K_{III} = \frac{\tau\sqrt{\pi a}}{\Phi_o}\left(\frac{2t}{\pi a}\tan\frac{\pi a}{2t}\right)^{\frac{1}{2}}$ where Φ_o is given by $\Phi_o = \int_o^{\pi/2}\left[1 - \left(\frac{b^2 - a^2}{b^2}\right)\sin^2\theta\right]^{\frac{1}{2}} d\theta$	47 87

Statistical Fracture Techniques

If one measures the tensile strength of several samples of a ductile material, the results will usually fall within narrow bounds. On the other hand, normally "brittle" materials exhibit considerable scatter in the ultimate tensile strengths. As can be readily surmized from the preceding section, the orientation, size, and distribution of flaws within the material will give rise to various fracture-strength values. On this basis it is not possible to approach design against fracture by the conventional phenomenological theories. On the other hand, it may not be desirable or possible to inspect the final design for flaws. To overcome this deficiency in an approach to design with brittle materials, various statistical strength-design techniques are currently being explored.

The basis of these techniques is the distribution of strengths obtained from tests on simple specimens (tensile, bend, etc.). If the frequency with which a certain value occurs is plotted against the value itself, the frequency is generally shown to rise to some maximum value and then fall off again as we move across the range of values. It should be noted that the extreme (high and low) values do not occur as often as those which reside at the center. The cumulative distribution function is the integral of the normalized probability density function. Figure VII-5-3 shows a typical cumulative distribution for a brittle material (Hydrostone Plaster).

To predict the behavior of relatively complex components from the test behavior of relatively simple specimens, it must be implicitly recognized that the statistical input will yield statistical output. Thus, the behavior of the complex components will also have a statistical distribution of strengths. The design of a component for strength based upon statistical fracture methods cannot currently be performed for wide classes of problems. It is possible at present to predict the behavior of large components from a knowledge of the statistical behavior of a group of smaller-sized components. Although analytical techniques have been developed to go from one stress state to another, actual verification of these techniques for several materials or even any one class of materials is lacking. In recent years, this deficiency has been attacked but has not been resolved to date.

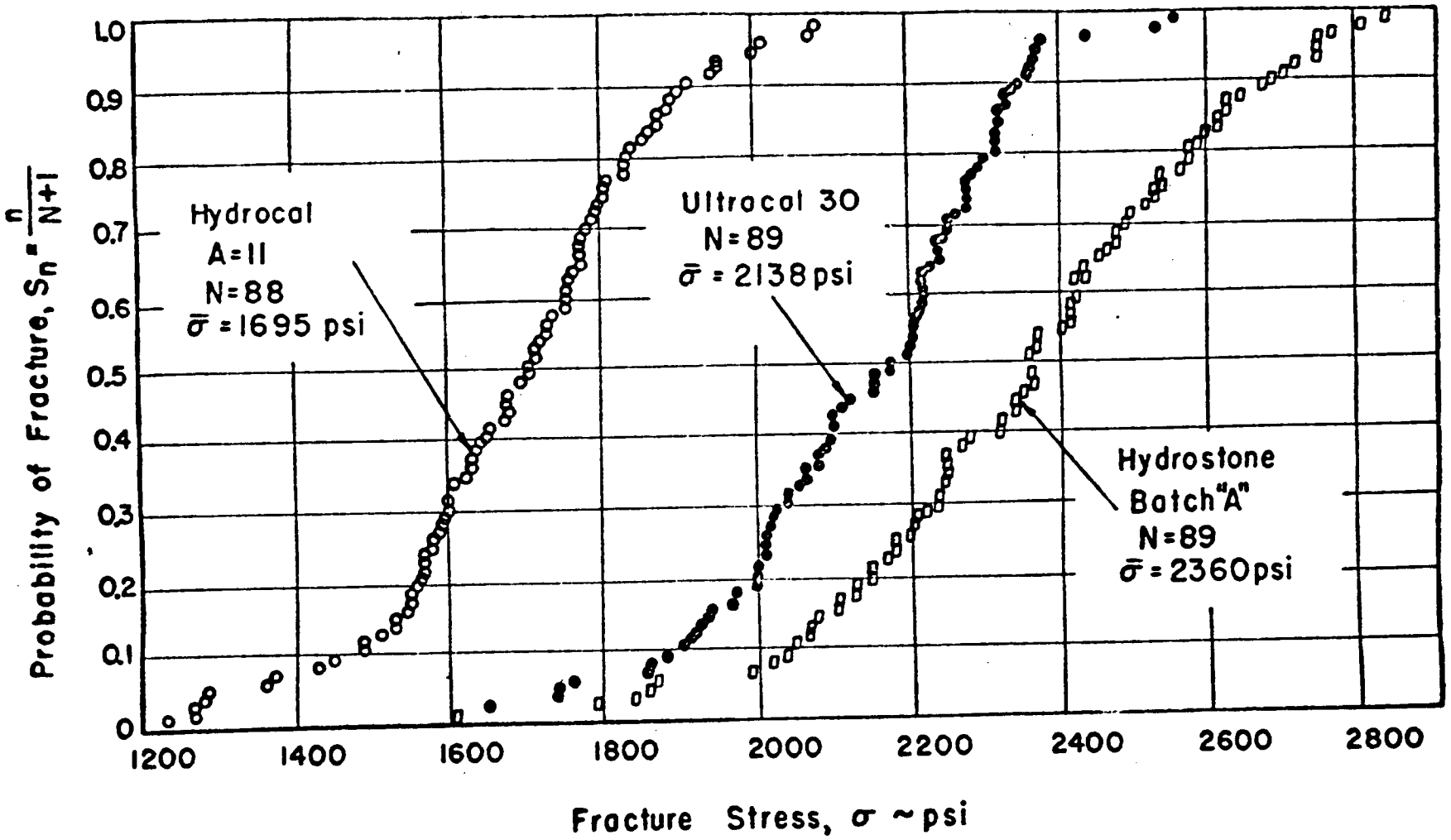

Fig. VII-5-3 Distribution Curve of Fracture Stresses For 1/4 in x 1/4 in x 4 in Bend Specimens of Three Gypsum Cements

Table VII-5-3

FRACTURE TOUGHNESS FOR SEVERAL MATERIALS
EMPLOYED IN PRESSURIZED TANKAGE

MATERIAL	ULTIMATE STRENGTH (ksi)	CRITICAL STRESS INTENSITY FACTOR K_c (ksi$\sqrt{in}$)	PLANE STRESS OR PLANE STRAIN
AISI-4340	280	86	Pl. Stress
"	260	200	" "
"	240	180	" "
300M	280	133	" "
"	260	194	" "
Airsteel X-200	300	85	" "
"	280	105	" "
"	260	90	" "
"	240	125	" "
AMS 6434	300	> 90	" "
"	280	>120	" "
"	260	>120	" "
"	240	200	" "
H-11 High Strength Steel	300	20-100	" "
"	280	47	" "
"	260	90	" "
"	240	108	" "
Vascojet 1000 Vanadium Steel	300	34	Pl. Strain
D6AC High Strength Steel	300	77	Pl. Stress
"	280	112	" "
"	260	98	" "
"	240	130	" "
18% Ni Maraging	300	175	" "
"	280	217	" "
"	260	160	" "
"	240	203	" "
PH 15-7 Mo Stainless Steel	240	77	" "
301 Stainless Steel	300	95	" "
301 Stainless Steel (60% cross-rolled)	224	204	" "
304 Stainless Steel	180	91-119	" "
310 Stainless Steel	180-200	86-132	" "
AM 355 Stainless Steel	223	60	Pl. Strain
410 Stainless Steel	188	163	Pl. Stress
4330 Low Alloy Steel	233	300	" "
2219-T87 Aluminum	69	110	" "
7075-T6 Aluminum	83	70	" "
7178-T6 Aluminum	88	26	" "
Ti6Al-4V	140	56-66	Pl. Strain

Crack toughness values should be determined by using standard specimens (recommended by the ASTM Special Committee for Fracture Toughness Testing) on the material of interest in the thickness range of interest. Handbooks containing values of interest do not seem to be available. Table VII-5-2 contains some of the more useful K_I stress factors used in specimen testing as well as factors used in pressure vessel analysis.

Temperature and Fracture Transition

Another approach to design against fracture depends upon the influence of temperature on the fracture behavior of the structural material.

The low-carbon steels have been noted to have a particular sensitivity to temperature. Above a certain temperature, the fractures are essentially ductile, but below this temperature the fractures are sudden with little or no shear or ductility evident and all of the traditional characteristics associated with brittle fracture. For this class of materials, design methods based on transition temperature are appropriate. The ultra-high-strength steels, aluminum alloys, and titanium do not exhibit this behavior but are brittle at almost all temperatures. This class of materials must incorporate complete stress analyses in the design, including fracture mechanics approaches. Finally, there is a class of metals, notably steels (tensile strength from 75 ksi to 200 ksi), which are essentially temperature sensitive since they exhibit mixed behavior at any temperature.

The primary utilization of the transition-temperature approach is in the selection of materials for a particular application. A material is generally selected which possesses a transition temperature below the lowest temperature experienced by the stressed component. Where the comparison is confined to a particular class of materials, this approach is usually reliable and useful and will most likely provide the most fracture-resistant material regardless of the transition-temperature criterion selected.

VII-6 MATERIALS TRACEABILITY AND CONTROL

Since the basic material for pressure vessels is purchased from outside vendors, usually in the form of rough forgings, it is important that some method be used to ensure uniform and reliable components throughout the length of the program. Traceability of materials is also important as a premature failure of a pressure vessel requires a thorough investigation and explanation.

Usually these controls begin with a specification of materials sent to the vendor. The content of these specifications varies depending upon the material, but in general the source of data for mechanical properties, etc. will be MIL-HDBK-5 or other published documents on material properties.[2]

A typical procedure for vendor control and material traceability of forgings will be outlined here. First, the vendor will record the ingot heat number and then cut the ingot into melts for forging. Usually the forging technique is established by the vendor.[2] This is obvious because a vendor usually has the necessary experience for the particular forging form, but this should be checked against the vendor's past performance. The vendor is usually allowed to select tensile specimen from any location on the forging for his own control, but the location of the tensile specimen for the post-heat-treat check are fixed. In most cases the forging is supplied with a skirt or ring which will provide a number of test specimens after heat treating.[3,8,12] This, however, does not always give the most representative results. A hemispherical head, for example, would have the skirt at the base (equator), while the properties of the forging near the top of the dome will be unknown. There are ways used to overcome this problem, one of which is to degrade the material in the test ring during the heat treating to match the expected lower properties near the top of the dome.[3] Another way is to control the heat-treating process so that higher properties are developed in areas where the forging operation would tend to lower them.[12] But perhaps the most positive technique (also the

most expensive) is to provide enough extra material on the forging to give a number of test specimens from each location on the forging.[2] Ultrasonic and/or radiographic inspection is usually done after the forging is rough machined. Since no repairs of forging defects are usually allowed,[3] it might be expeditious to have the forging vendor perform these inspections. After heat treating, the manufacturer will perform a number of tensile, notched-tensile, and fracture-toughness tests to establish compliance of the forged material to specifications.

VII-7 TESTING PROCEDURES

After the testing of the welds (Section VIII), a series of qualification tests are performed on a number of initial vessels.[6] This testing usually consists of some form of repeated loadings through a burst test.[3] However, some manufacturers perform much more extensive tests, i.e., ambient cycling, low-temperature cycling, vibration testing, long-term pressurization tests, acceleration tests, operating-cycle testing, and helium mass-spectrometer-leak testing.[3,5,9,10,12]

The routine inspection after qualification usually includes such tests as ultrasonic, radiographic, and dye-penetrant inspection; vibration tests; leak testing; strain-rate checks; repeated-load testing (if low-cycle fatigue is considered in the design, the number of cycles for this test must be considered); and proof testing.[2,3,4,5,6,10,11] In addition, some manufacturers may use a low-pressure leak test to ensure proper gasket seating.[5,8] One simple but often overlooked problem encountered while performing a hydrostatic proof test is that leaks cannot be detected if the vessel is sweating due to the cold test water inside. To overcome this the test water should be heated slightly so that when outside wetness is observed, one may be certain that a leak is its cause.

A great deal of design information may be gained from a well-conducted test program. If, for example, fatigue is expected to play a role in the design of a vessel, then components may be constructed and subjected to simulated loadings to determine their fatigue resistance. Strain gages may also be applied at questionable areas to determine a more accurate stress state.

Cleaning of the pressure vessels is usually performed in accordance with applicable government specifications and is established by contractural agreement. But it is important to provide adequate access openings in the vessel if internal weld inspection, cleaning inspection, or bladders are used.

VII-8 DESIGN EXAMPLE

Introduction

The following example is presented to illustrate the application of the equations developed in Part 4 (Stress Analysis) for the design of any pressure vessel under consideration. The particular vessel configuration (Figure VII-8-1) was selected to provide an example of the various problems that may be encountered during the course of a design evaluation. The design procedure requires, first, that a membrane analysis of the individual geometric elements be performed (Figure VII-8-2), and secondly, a discontinuity analysis to include junction or edge effects.

Membrane Analysis

The solution to the membrane equations will yield the minimum wall thickness of the individual elements. When these elements are joined together, discontinuity stresses develop because of differences in stiffness between elements. These stresses may be quite large and consequently must not be discounted in the computation of the final wall thickness.

It is assumed that a rigorous analysis will be performed after the competing designs have been evaluated and a selection made. Consequently, a number of time saving simplifications may be used. The use of these short-cuts, however, depend to a large extent on the experience of the designer to avoid the introduction of large errors.

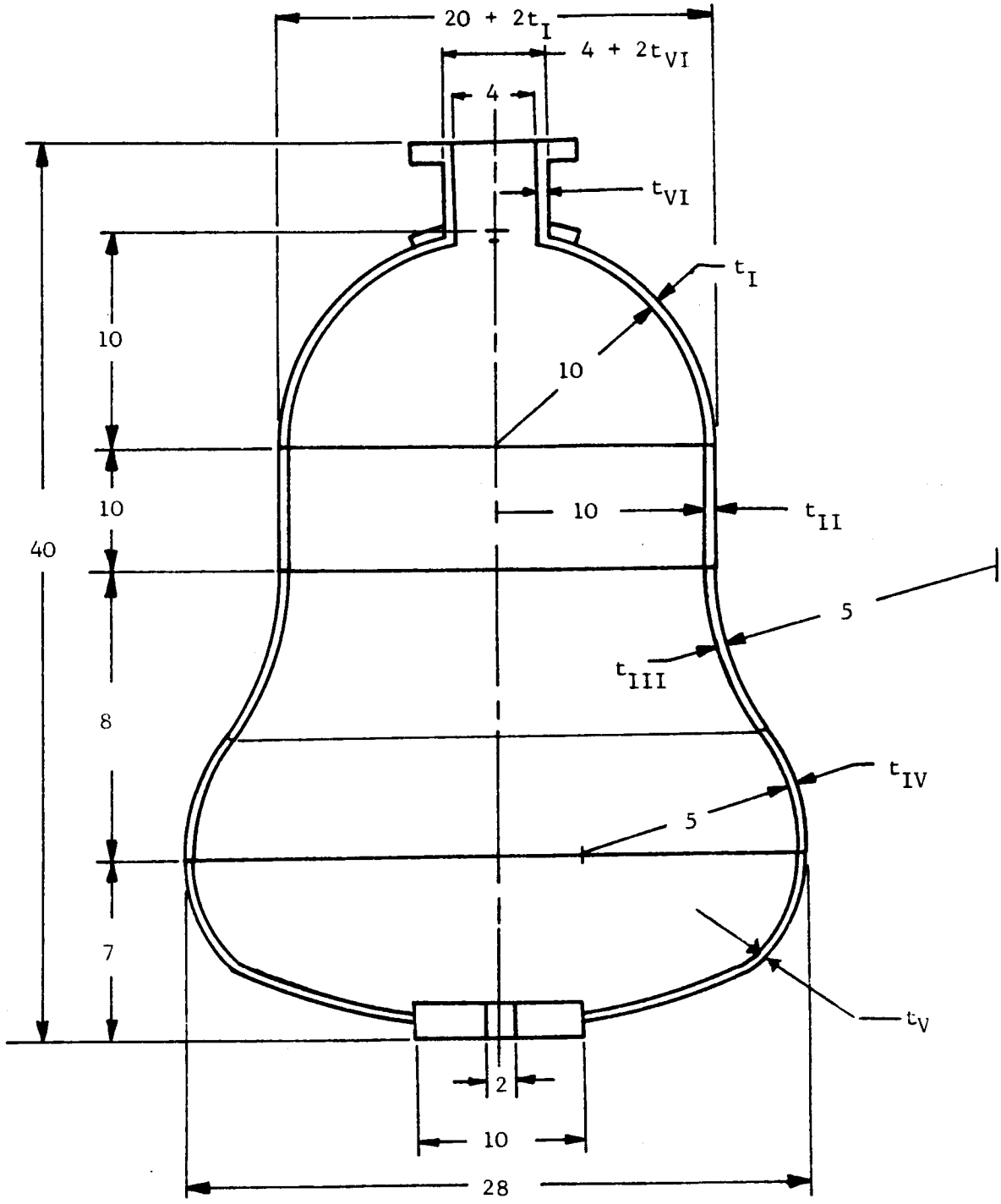

P = 800 psi, Internal gas pressure
T = Ambient temperature, °F
F_{tu} = 125 x 10^3 psi
F_{ty} = 75 x 10^3 psi
ν = 0.3, Poison's ratio

E = 28.0 x 10^6 psi
SF = 1.5 on F_{ty}
S = Maximum allowable stress, 50 x 10^4 psi

AISI Type 301 Stainless Steel

Fig. VII-8-1 Vessel Configuration and Specifications for the Design Example

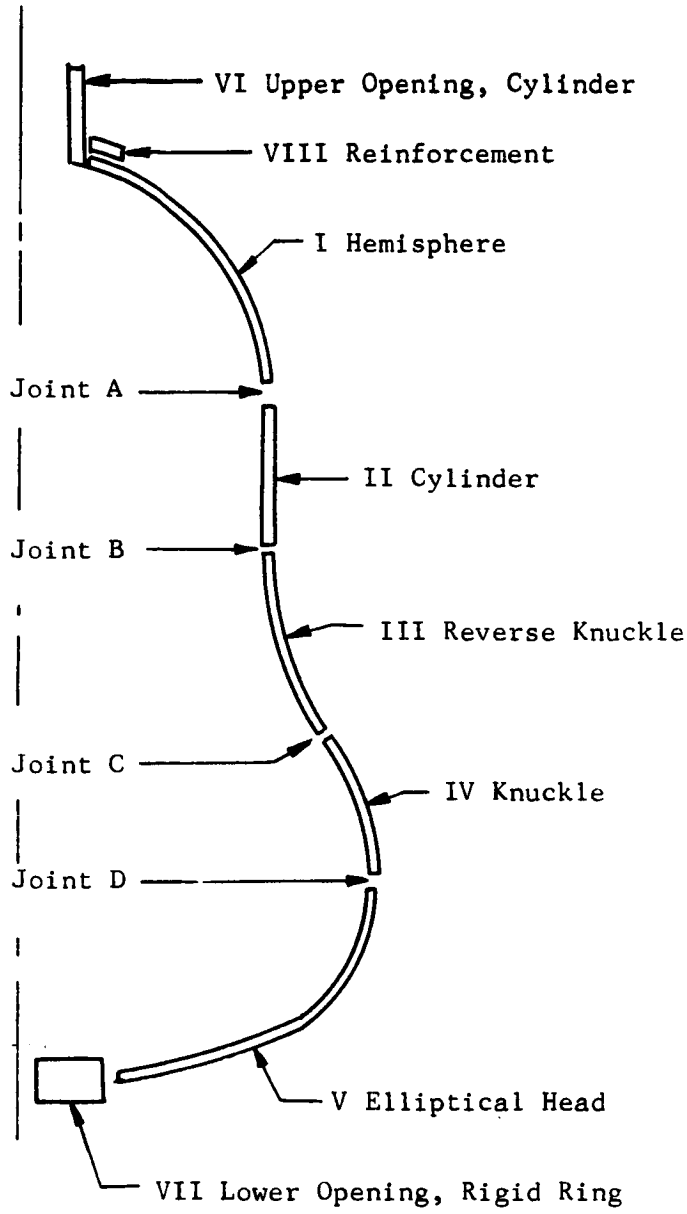

Fig. VII-8-2 Reduction of Vessel To Individual Geometric Elements

Section I (Hemisphere)

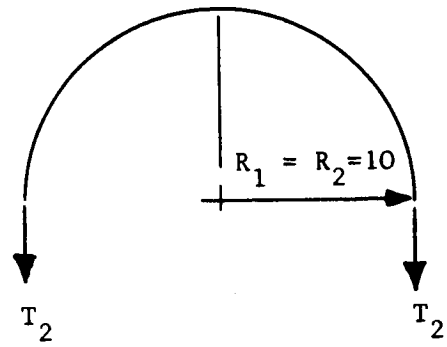

Fig. VII-8-3 Free Body Diagram of Section I, Hemisphere

$$T_2 = \frac{PR_1}{2} = \frac{800(10)}{2} = 4000 \text{ lb/in} \qquad (16)^*$$

$$S_2 = S = \frac{T_2}{t} \qquad (7)$$

$$t = \frac{T_2}{S} = \frac{4000}{50000} = 0.08 \text{ in}$$

$$T_1 = PR_1\left(1 - \frac{R_1}{2R_2}\right) = PR_1\left(1 - \frac{1}{2}\right) = T_2 \qquad (17)$$

If, for a thick wall, $\frac{R}{t} = \frac{10}{0.08} >> 10$, then the membrane analysis is adequate and:

$$\boxed{t_I = 0.08 \text{ in}}$$

Note that the same result would have been achieved using the formula given in Table VII-4-1.

---

*Equations numbered as previously cited in Section VII-4, Stress Analysis.

Section II (Cylinder)

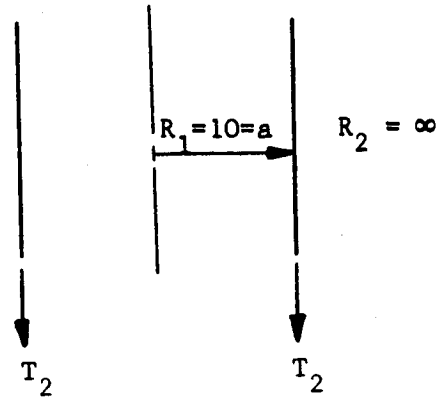

Fig. VII-8-4 Free Body Diagram of Section II, Cylinder

From Table VII-4-1, the hoop stress is twice that of the longitudinal stress; thus the hoop stress will be the governing factor.
Therefore,

$$S_1 = \frac{Pa}{t}; \quad t = \frac{Pa}{S} = \frac{800(10)}{50000} = 0.16 \text{ in}$$

and

$$\frac{a}{t} = \frac{10}{0.16} >> 10$$

This implies that the thickness need not be computed by the Lamé thick cylinder formula.[41] However this computation is included for information only.

$$t = R_1\left[\sqrt{\frac{S+P}{S-P}} - 1\right]$$

$$= 10\left[\sqrt{\frac{50800}{49200}} - 1\right]$$

$$= 10\left[\sqrt{1.03} - 1\right]$$

$$= 10(0.015) = 0.15 \text{ in}$$

The value of t = 0.15 inch obtained from the Lamé formula is approximately the same as the thickness computed using the membrane equations. If the

value of $\frac{r}{t}$ were less than 10, this thickness would become significantly larger than the membrane value.

Therefore the membrane thickness remains;

$$\boxed{t_{II} = 0.16 \text{ in}}$$

Section III (Reverse Knuckle)

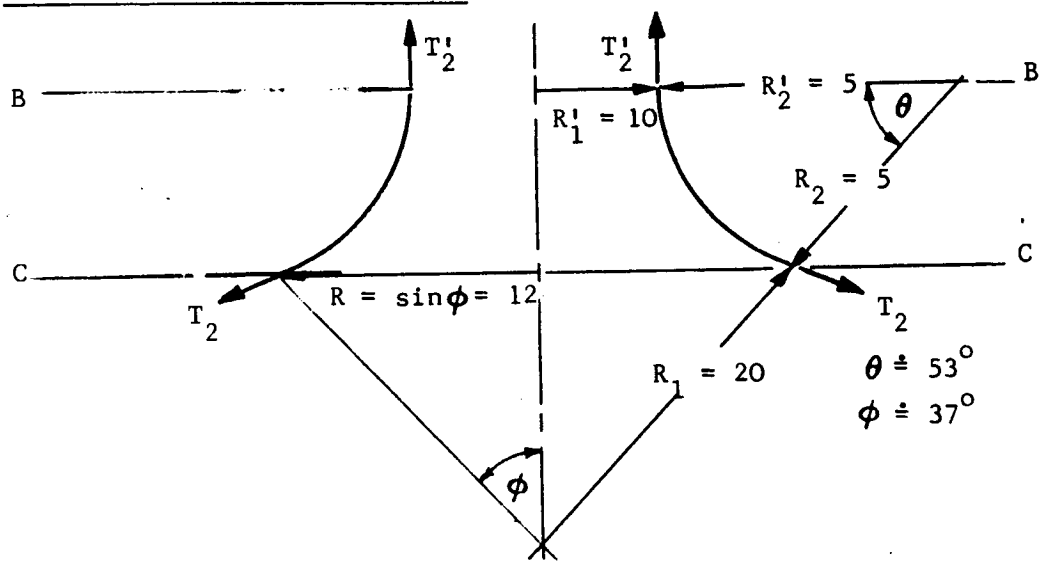

Fig. VII-8-5 Free Body Diagram of Section III, Reverse Knuckle

Since $R_1 \text{Sin } 37^\circ = 12$, $R_1 \cong 20$ inches. For the maximum stress S, T_1 and T_2 must be computed at both Section B and Section C.

Section B:

$$T_2' = \frac{PR_1'}{2} = \frac{800(10)}{2} = 4000 \text{ lb/in} \tag{16}$$

$$T_1' = PR_1'\left(1 - \frac{R_1'}{2R_2}\right) = 800(10)\left(1 + \frac{10}{2(5)}\right) = 16000 \text{ lb/in} \tag{17}$$

again, $T_1' > T_2'$, therefore $t_B = \frac{16000}{50000} = 0.32$ in

Section C:

$$T_2 = \frac{PR_1}{2} = \frac{800(20)}{2} = 8000 \text{ lb/in} \tag{16}$$

$$T_1 = PR_1\left(1 - \frac{R_1}{2R_2}\right) = 800(20)\left(1 + \frac{20}{2(5)}\right) \tag{17}$$

$$= 16000(3) = 48000 \text{ lb/in}$$

and since $T_1 > T_2$ from Equation (7) $t_C = \frac{48000}{50000} = 0.96$ in

For the sake of simplicity it is assumed that the thickness varies linearly from a minimum of 0.32 inch at B to a maximum of 0.96 inch at C. The error introduced by this simplification is negligible in this case. As such, it is not worth the extra effort required to compute the actual thickness at each station along the curve. The membrane thickness at these sections are:

$$t_B = 0.32 \text{ in}$$

$$t_C = 0.96 \text{ in}$$

Section IV (Knuckle)

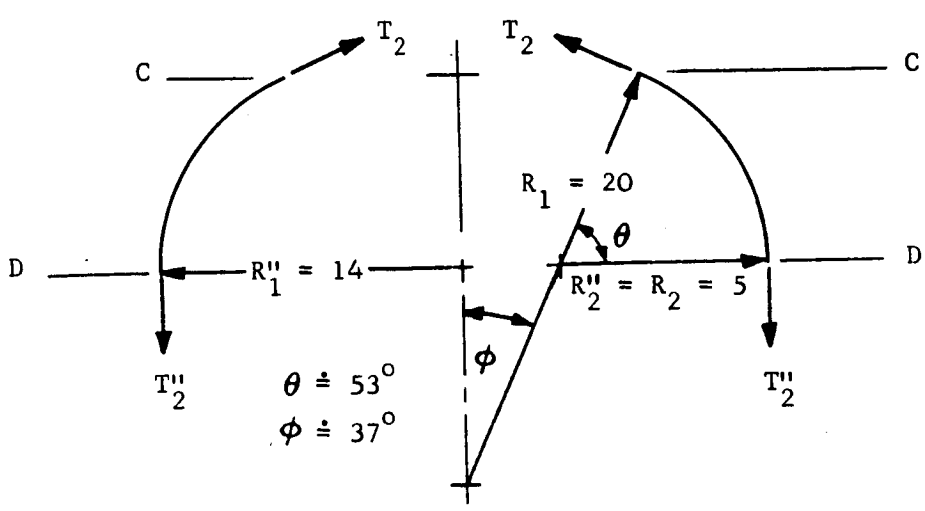

Fig. VII-8-6 Free Body Diagram of Section IV, Knuckle

Section C:

$$T_2 = \frac{PR_1}{2} = \frac{800(20)}{2} = 8000 \text{ lb/in} \tag{16}$$

$$T_1 = PR_1\left(1 - \frac{R_1}{2R_2}\right) = 800(20)\left(1 - \frac{20}{2(5)}\right) = -16000 \text{ lb/in} \tag{17}$$

At this section, T_1 is not only greater than T_2, but it is negative as well.

Section D:

$$T_2'' = \frac{PR_1''}{2} = \frac{800(14)}{2} = 5600 \text{ lb/in} \tag{16}$$

$$T_1'' = PR_1''\left(1 - \frac{R_1''}{2R_2}\right) = 800(14)\left(1 - \frac{14}{2(5)}\right) = -4480 \text{ lb/in} \tag{17}$$

The preceding solution server to point out a case discussed previously, namely, that when $2R_2 < R_1$, the hoop stress will be compressive. A compressive hoop stress in this knuckle implies that a buckling condition may exist, and so this loading must be approximated and analyzed. If a short cylinder $\left(\ell < 4.9R_1''\sqrt{\frac{R_1''}{t}}\right)$ (Ref. 41) is superimposed over the knuckle as shown in Figure VII-8-7, the technique in Reference 41, page 318, may be used to approximate the average thickness of the knuckle to resist buckling. This is done in the following manner.

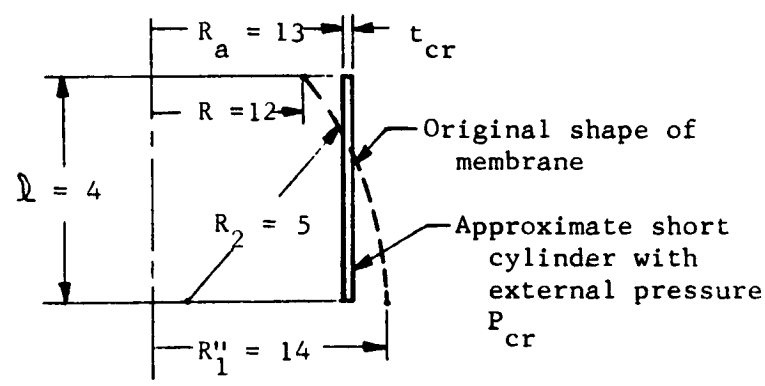

Fig. VII-8-7 Reduction of Membrane to Cylinder for Buckling Analysis

The cylinder shown above will buckle when the critical pressure is given by:

$$P_{cr} \cong 0.807 \frac{Et^2}{R_a}\left[\left(\frac{1}{\sqrt{1-\nu^2}}\right)^3 \left(\frac{t}{R_a}\right)^2\right]^{1/4} \qquad \text{(from Ref. 41)}$$

and the hoop stress in a cylinder is given by:

$$S_{cr} = \frac{P_{cr}R_a}{t_{cr}} \text{ and } S_{cr} = \frac{T_1}{t_{cr}} \qquad \text{(from Ref. 41)}$$

Rearrangement of terms in these equations yields the following formula for t_{cr}:

$$t_{cr} \cong \left(\frac{T_1}{0.807E}\left[(1-\nu^2)\ R_a^{\ 2}\right]^{1/4}\right)^{2/5}$$

Now, all that is required is a value for T_1. Since the radius of the cylinder is the average of the radii of the knuckle, choose T_1 as the average of the values of T_{1G} and T_{1D}. This gives T_1 = -10240 lb/in, and when substituted into the above equation the value for t_{cr} becomes:

$$t_{cr} = 0.129 \text{ in}$$

Another approach to this problem is to consider the local buckling of an axially loaded infinitely long cylinder with its axis perpendicular to the paper. This configuration is shown in Figure VII-8-8. The equation for the critical buckling stress, S', of a cylinder loaded as shown is as follows (Reference 41).

$$S' = \frac{1}{\sqrt{3}}\left(\frac{E}{\sqrt{1-\nu^2}}\right)\frac{t}{R}$$

where the approximation requires R to be equal to R_2 of the membrane. The membrane thickness required at Section C to resist the longitudinal load T_2 is:

$$t_C = \frac{8000}{50000} = 0.16 \text{ in}$$

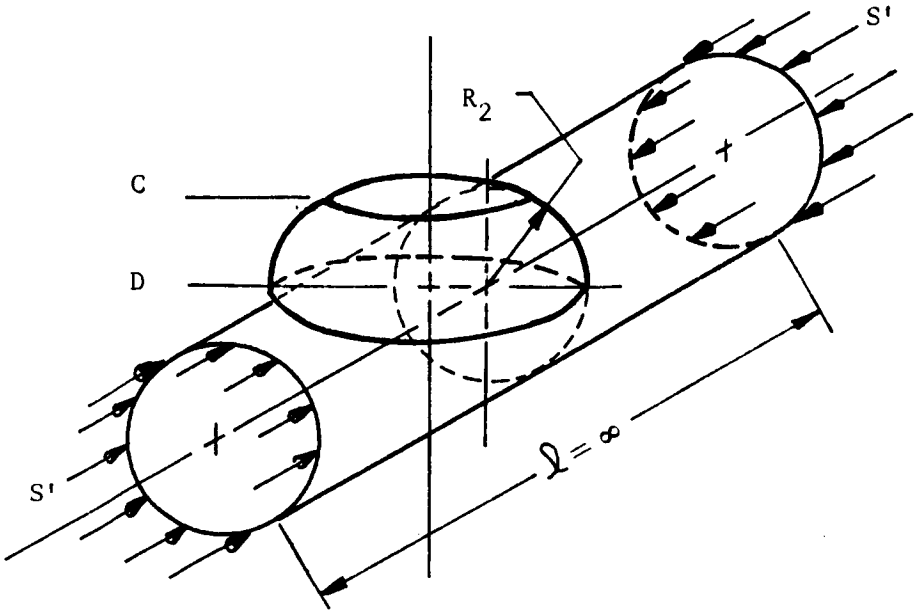

Fig. VII-8-8 Equivalent Axially Loaded Cylinder with End Stress S' Equal to the Maximum Value of the Negative Hoop Stress on the Membrane

and, at Section D becomes:

$$t_C = \frac{5600}{50000} = 0.112 \text{ in}$$

The average thickness thru this section then becomes:

$$t_{av} = \frac{t_C + t_D}{2} = 0.136 \text{ in}$$

Comparing this with the thickness of the equivalent cylinder having a critical buckling stress of S', t_{min} becomes:

$$t_{min} = \frac{S' R \sqrt{3(1-\nu^2)}}{E}$$

or since

$$S' = \frac{T_{1max}}{t_{min}}$$

then

$$t^2_{min} = \frac{T_{1max} \; R \sqrt{3(1-\nu^2)}}{E}$$

A solution for t_{min} follows:

$$t^2_{min} = \frac{16000(S)\sqrt{3(1-\ 3^2)}}{30x10^6} = 4\ 4x10^{-3}$$

or

$$t_{min} = 0\ 067\ in$$

t_{min} is clearly less than the thickness required to carry the longitudinal load and the thickness computed by considering the buckling of a short equivalent cylinder (Figure VII-8-7). However, since this is only an approximate solution to the actual buckling problem, a conservative approach to the final minimum membrane thickness is presented below. The final minimum membrane thickness should be the larger of the following: (1) average thickness required to resist the longitudinal loads, (2) the thickness required to resist buckling of a radially loaded short equivalent cylinder, or (3) the thickness required to resist buckling of axially loaded infinitely long cylinder.

These values are:

t_{Av} = 0 136 in (T_2 loads)

t_{cr} = 0 129 in (radially loaded cylinder)

t_{min} = 0.067 in (axially loaded cylinder)

Since t_{Av} is the governing factor, the membrane thickness becomes:

t_{C} = 0.16 in

t_{D} = 0.112 in

Section V (Elliptical Head)

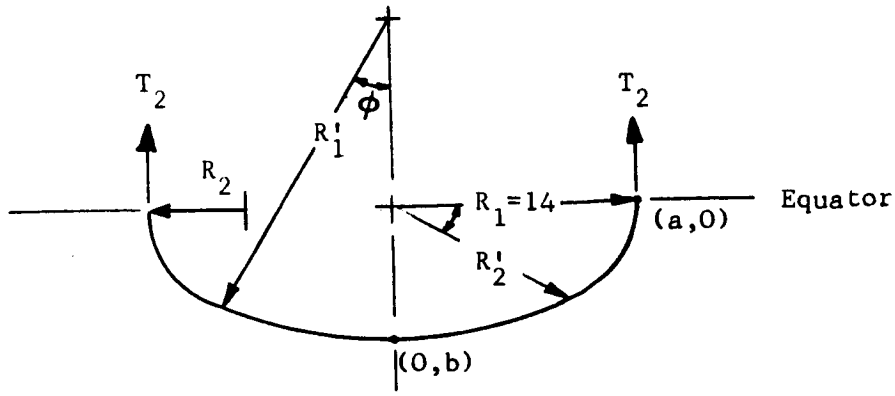

Fig. VII-8-9 Free Body Diagram of Section V, Elliptical Head

From Table VII-4-1, the maximum stresses occur at the equator (or junction) and are:

$$S_1 = \frac{P_a}{t}\left(1 - \frac{a^2}{2b^2}\right) \; ; \; S_2 = \frac{Pa}{2t}$$

where

$$a = 14 \text{ (semi-major axis)}$$
$$b = 7 \text{ (semi-minor axis)}$$

These stresses may also be derived using the radii of curvature given in Table VII-A-2 of the Appendix. From the above equation and a value of $a = 2b$, the hoop stress is again negative at the equator. Notice that the hoop stress for an elliptical head is negative when $\frac{a^2}{2b^2} > 1$, i.e.; when $a > b\sqrt{2}$, and is positive when $a < b\sqrt{2}$. Solving the equation for the longitudinal stress, the required membrane thickness becomes:

$$t = \frac{Pa}{2S_2} = \frac{800(14)}{2(50000)} = 0.112 \text{ in}$$

However, the resistance to buckling must be checked and, since thickness is derived from the longitudinal stress, the membrane thickness required at the junction of head and rigid ring must be checked. From Figure VII-8-1, the geometry in this area is as follows:

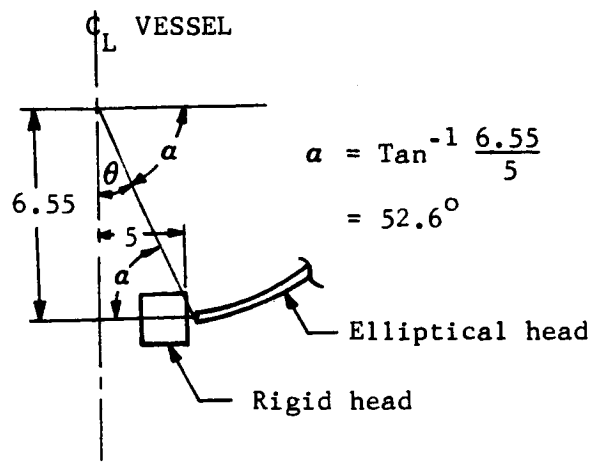

$$\alpha = \mathrm{Tan}^{-1}\frac{6.55}{5} = 52.6^{\circ}$$

Fig. VII-8-10 Membrane Junction with Rigid Ring

From Table VII-A-2 in the Appendix, the values for R_1 and R_2 are:

$$R_1 = \frac{a}{b}\sqrt{a^2\sin^2\alpha + b^2\cos^2\alpha}$$

and

$$R_2 = \frac{\left(a^2\sin^2\alpha + b^2\cos^2\alpha\right)^{3/2}}{ab}$$

where

$$\sin^2\alpha = (0.795)^2 = 0.632 \text{ and } \cos^2\alpha = (0.606)^2 = 0.368$$

Now

$$R_1 = \frac{14}{7}\sqrt{196(.632) + 49(.368)} = 23 \text{ in}$$

$$R_2 = \frac{\left[196(0.632) + 49(0.368)\right]^{3/2}}{14(7)} = 15.4 \text{ in}$$

The corresponding stresses are:

$$T_1 = PR_1\left(1 - \frac{R_1}{2R_2}\right) = 800(23)\left(1 - \frac{23.0}{30.8}\right) = 4675 \text{ lb/in}$$

$$T_2 = \frac{PR_1}{2} = \frac{800(23)}{2} = 9200 \text{ lb/in}$$

This gives a membrane thickness $t = \frac{T_2}{S} = \frac{9200}{50000} = 0.184$ inches in this area. For buckling of this head, first determine the point at which the hoop stress becomes zero; i.e., from Equation (17), $R_1 = 2R_2$. This point is at $a^2 = 2(a^2\sin^2\alpha + b^2\cos^2\alpha)$ and since $a = 2b$, then $\alpha = \cos^{-1}\sqrt{2/3} = 35.3^\circ$. The following diagram is now used to determine the extent of this negative hoop stress area.

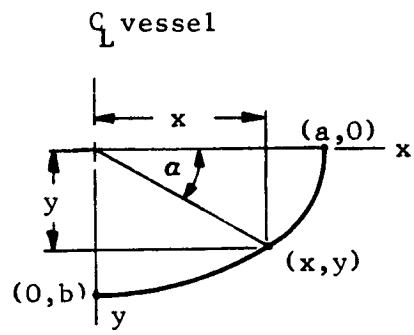

Fig. VII-8-11 Coordinate System for Elliptical Head

Since $\frac{x^2}{a^2} + \frac{y^2}{b^2} = 1$ defines the curve and $\tan\alpha = \frac{y}{x}$, $x \cong 8.1$ inches and $y \cong 5.7$ inches. Considering this area as a short cylinder as done for Section IV, the following geometry is used for a conservative approximation.

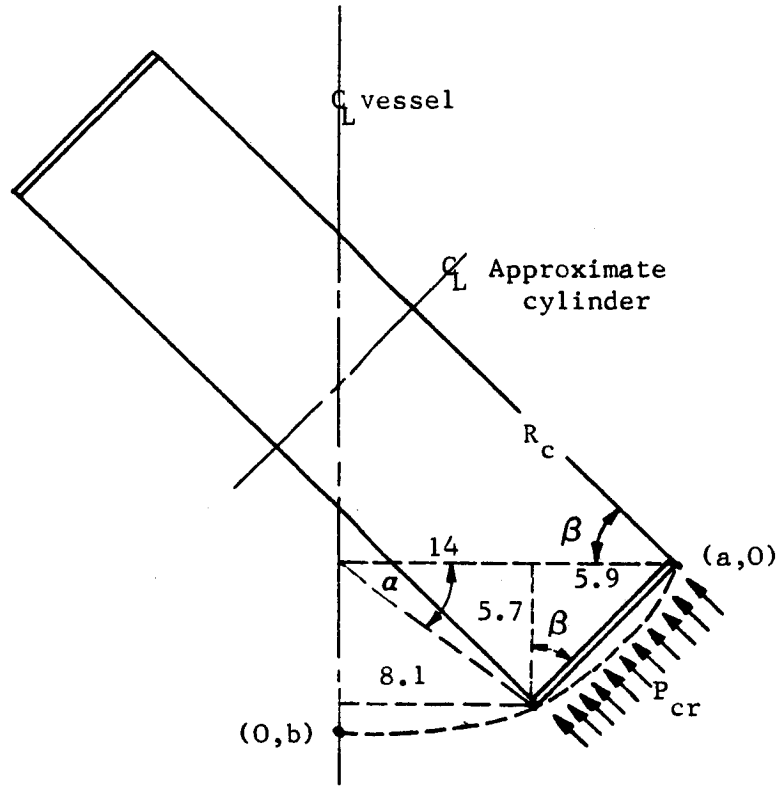

Fig. VII-8-12 Reduction of Membrane to Cylinder for Buckling Analysis

$\beta = \tan^{-1} \frac{5.9}{5.7} \cong 46^{o}$, therefore the length of the cylinder is

ℓ = 8.2 inches and the radius R_c = 15.9 inches. Again using the formula from Reference 41:

$$t_{cr} \left[\frac{T_1}{0.807E} \left((1-\nu^2)\ R_c^2 \right)^{\frac{1}{4}} \right]^{3/5}$$

where, as before, T_1 is the average value across the section and is:

$$\tfrac{1}{2}\ Pa \left(1 - \frac{a^2}{2b^2}\right) = \tfrac{1}{2}(800)(14)(1-2) = -5600\ \text{lb/in} \left(T_1 = \frac{T_{1(a,o)} - 0}{2}\right)$$

The value for t_{cr} then becomes:

$$t_{cr} \approx 0.140 \text{ in}$$

Now, as before, the average membrane thickness between (a,o) and (x,y) should be compared. At (x,y) R_1 = 20.1 inches and R_2 = 10.05 inches, therefore T_1 = 0 and T_2 = 8040 lb/in. Since $T_2 \neq 0$, the membrane thickness becomes $t_{(x,y)} = \frac{T_2}{S} = \frac{8040}{50000} = 0.161$ inches. This value, $t_{av} = \frac{1}{2}(0.161+0.112)$ = 0.136 inches, is less than the .140 inch required. Because the average and required thicknesses are almost equal, let the average be 0.140 and make the membrane thickness at (x,y) be such that $\frac{1}{2}(t_{(x,y)} + 0.112) = 0.140$ or, $t_{(x,y)} = 0.168$ in.

But, before the above value is selected as the membrane thickness at (x,y), the buckling of an equivalent axially loaded cylinder should be considered. In this case, R is taken to be equal to the average R_2 across the region of negative hoop stress. The value of R_2 at (a,o) is:

$$R_2 = \frac{b_2}{a} = \frac{45}{14} = 3.5 \text{ in}$$

and at (x,y) is:

$$R_2 = 10.05 \text{ in}$$

Therefore:

$$R_{2av} = 6.77 \text{ in}$$

The critical buckling stress, S', then becomes:

$$S' = \frac{1}{\sqrt{3}} \frac{E}{\sqrt{1-\nu^2}} \frac{t}{R_{2av}}$$

or since:

$$S' = \frac{T_{1av}}{t}$$

then, by rearranging terms:

$$t^2 = \frac{T_{1av} R_{2av} \sqrt{3(1-\nu^2)}}{E}$$

The minimum membrane thickness in this area then becomes:

$$t^2 = \frac{(5600)(6.77)}{30\text{x}10^6} \sqrt{3[1-(0.3)^2]}$$

$$= 2.08\text{x}10^{-3} \text{ in}^2$$

or

$$t_{min} = 0.046 \text{ in}$$

Now, comparing this value with the minimum values for t found previously it is clear that the following values of the membrane thickness are required.

$$\boxed{\begin{aligned} t_{(a,o)} &= 0.112 \text{ in} \\ t_{(x,y)} &= 0.168 \text{ in} \\ t_{(5,6.55)} &= 0.184 \text{ in} \end{aligned}}$$

Section VI (Upper Opening-Cylinder)

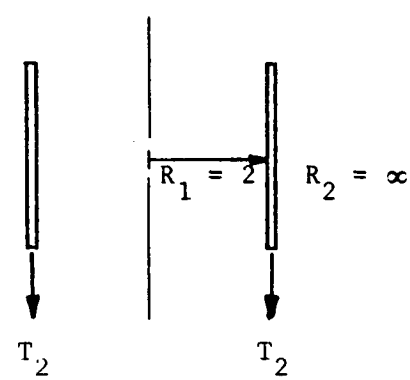

Fig. VII-8-13 Free Body Diagram of Section VI, Upper Opening, Rigid Ring

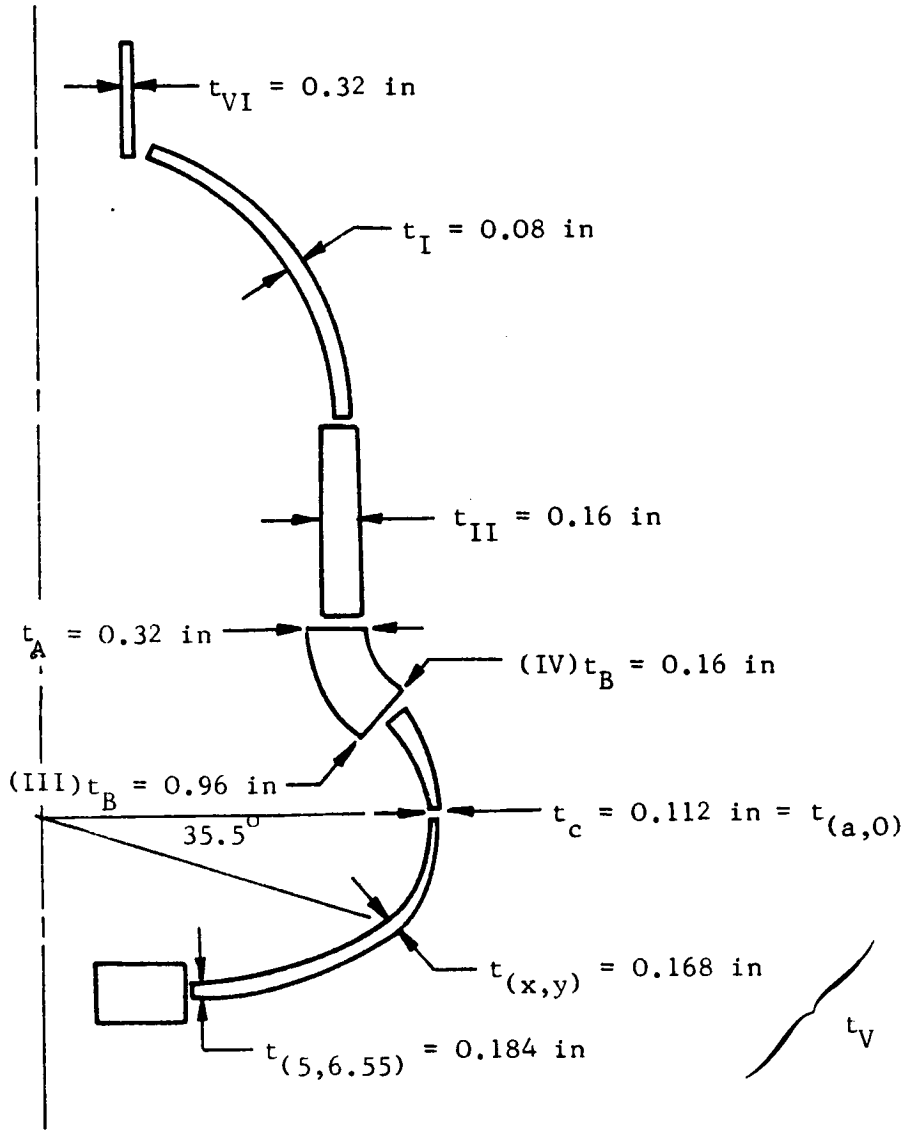

Fig. VII-8-14 Wall Thickness of Pressure Vessel From Membrane Analysis

For this section the analysis is straightforward and t_{VI} is:

$$t = \frac{T_1}{S} = \frac{PR_1}{S}\left(1 - \frac{R_1}{2R_2}\right) = \frac{PR_1}{S} = \frac{800(2)}{50000} = 0.32 \text{ inches}$$

$$\boxed{t_{VI} = 0.032 \text{ inches}}$$

A section thru the vessel would now have the membrane thicknesses as shown in Figure VII-8-14.

Discontinuity Stresses

Section I to Section II (Hemisphere to Cylinder)

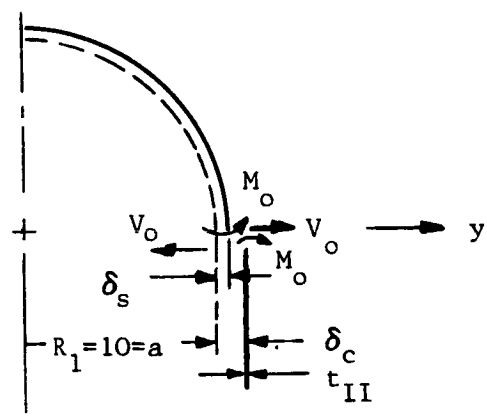

Fig. VII-8-15 Membrane Displacements when Pressurized

From Table VII-4-1 the displacements, δ_s and δ_c are as follows:

Hemisphere: $$\delta_s = \frac{Pa^2}{2Et_I}(1-\nu)$$

Cylinder: $$\delta_c = \frac{Pa^2}{2Et_{II}}(2-\nu)$$

The difference in displacement δ is equal to $\delta_c - \delta_s$, therefore:

$$\delta = \frac{Pa^2}{2E}\left[\frac{t_I(2-\nu) - t_{II}(1-\nu)}{t_I t_{II}}\right]$$

To find the magnitude of V_o and M_o the following continuity conditions at the junction must be met:

(1) The slope of the head must equal the slope of the cylinder ($\theta_s = \theta_c$)

(2) The equilibrium displacement of the head and cylinder must have the same ordinate.

This may be expressed as follows:

Slopes: $\theta_s = \theta_c$ implies the following:

$$\theta_{s,p} + \theta_{s,M_o} + \theta_{s,V_o} = \theta_{c,M_o} - \theta_{c,V_o}$$

Displacements: ($y_s = y_c$)

$$y_s = \delta_{s,p} + \delta_{s,V_o} + \delta_{s,M_o}$$

$$y_c = \delta_{c,p} - \delta_{c,V_o} + \delta_{c,M_o}$$

$$\delta = \delta_{c,p} - \delta_{s,p}$$

Therefore:

$$\delta_{s,p} + \delta_{s,V_o} + \delta_{s,M_o} = \delta_{c,p} - \delta_{c,V_o} + \delta_{c,M_o}$$

and

$$\delta = \delta_{s,V_o} + \delta_{s,M_o} + \delta_{c,V_o} - \delta_{c,M_o}$$

Welding also influences the junction geometry; this approximation will not be a great deal less accurate if the thickness of the adjoining membranes are made equal for a distance equal to the critical distance $x = 2.45\sqrt{Rt}$

For the hemispherical head this distance is:

$$2.45\sqrt{(10)0.16} \cong 3.1 \text{ in } = x_{cr}$$

The simplified junction now has $M_o = 0$ and $y = \delta/2$ (where δ now = $\frac{Pa^2}{2Et_{II}}$). Using Equation (34) (Part IV, Stress Analysis)

$$\frac{\delta}{2} = \frac{2V_o}{k} D_{\beta x}$$

which simplifies to

$$\frac{Pa^2}{4Et_{II}} = \frac{2V_o a^2 \beta}{Et_{II}}$$

or

$$V_o = \frac{P}{8\beta}$$

From Equation (28):

$$\beta = \frac{\sqrt[4]{3(1-\nu^2)}}{\sqrt{Rt}}$$

$$\beta = \frac{\sqrt[4]{3(1-0.09)}}{10(0.16)} = 1.016$$

And from Equation (35):

$$y_{max} = \frac{2V_o\beta}{k} = \frac{P}{4k} = \frac{Pa^2}{4Et_{II}}$$

This deflection gives rise to a negative hoop stress as the circumference tends to become smaller. The magnitude of this stress is $-\frac{Ey_{max}}{a}$, or at any point x, the stress becomes $-\frac{Pa}{t_{II}} D_{\beta x}$. There is also a contribution from the moment produced which tends to prevent cross-sectional strips from distorting. This stress has, from Equation (34), a magnitude at any point on the cylinder of $\pm \frac{3\nu P}{4t_{II}^2 \beta^2} \left(B_{\beta x}\right)$.

To include these stresses, the equation for the hoop stress (S_1) must be modified as follows:

$$S_1 = \frac{Pa}{t_{II}} - \frac{Pa}{t_{II}} D_{\beta x} \pm \frac{3\nu P}{4t_{II}^2} 2 B_{\beta x}$$

Since $D_{\beta x}$ varies from 1 to a small negative number (Table VII-4-1) and $B_{\beta x}$ varies from 0 to another small negative number thru a maximum at $\beta x = \pi/4$, the maximum stress should occur at $\beta x = \pi/4$. The value of this stress becomes:

$$S_1 = 50{,}000 - \frac{800(10)}{0.16}(0.322) + \frac{3(0.3)800}{4(0.16)^2(1.016)^2}(0.322)$$

$$= 50{,}000 - 16{,}100 + 2{,}250 = 36{,}050 \text{ psi at } x = \frac{\pi}{4\beta} \cong 0.77 \text{ in}$$

Since this stress is lower than the allowable working stress some reduction in thickness may be made. However, a recalculation of the discontinuity stresses would be necessary. This can easily lead to involved iterations and consequently will be ignored here.

Figure VII-8-16 shows the revised contour of the hemispherical head to accommodate the discontinuity stresses at the junction to the cylinder.

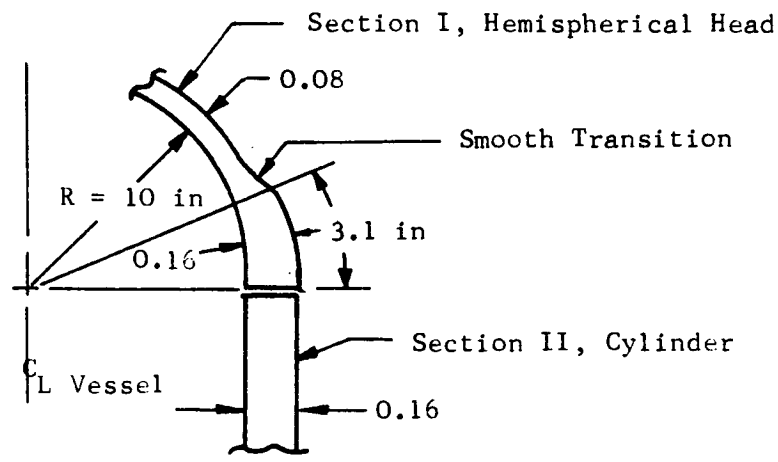

Fig. VII-8-16 Final Shape of Joint A

The discontinuity analysis of the remaining junctions will not be performed here but the procedure is straight forward and parallels the preceding discussion.

VII-9 REFERENCES

1. Gerard, G. (Allied Res. Assoc., Inc.) Aerospace pressure vessel design synthesis. NASA Contract NASw-928, NASA CR-287, Aug. 1965.

2. Hendry, G. (Grumman Aircraft, Bethpage, N.Y.) Private communication, Sept. 1965.

3. Hayes, J., et al. (General Motors, Allison Div., Indianapolis, Ind.) Private communication, Oct. 1965.

4. Smith, W., et al. (The Boeing Co., New Orleans, La.) Private communication, Nov. 1965.

5. Fuqua, C., et al. (McDonnell Aircraft Corp., St. Louis, Mo.) Private communication, Oct. 1965.

6. Meredith, R., et al. (North American Aviation, Inc., Downey, Calif. Private communication, Aug. 1965.

7. Fairbairn, G., et al. (North American Aviation, Inc., Rocketdyne Div., Canoga Park, Calif.) Private communication, Aug. 1965.

8. Felgar, R.P. Randall, P.N. and Goodman, J. (TRW Systems, Redondo Beach, Calif.) Private communication, Aug. 1965.

9. Edman, J. and Malthy, L.J. (Menosco Mfg. Co., Burbank, Calif.) Private communication, Sept. 1965

10. Miller, K., et al. (AiResearch Mfg. Co., Los Angeles, Calif.) Private communication, Sept. 1965.

11. Elias, L.G., et al. (Douglas Aircraft, Huntington Beach, Calif.) Private communication, Sept. 1965.

12. Engquist, R.D., et al. (Hughes Aircraft Co., Culver City, Calif.) Private communication, Sept. 1965.

13. Mischel, H.T. (Solar, San Diego, Calif.) Private communication, Sept. 1965.

14. Harvey, J.F. Pressure Vessel Design. Van Nostrand Co., Inc., Princeton, New Jersey, 1963.

15. Parker, E.R. (Ed.) Materials for Missiles and Spacecraft. McGraw-Hill Book Co., Inc., New York, 1963.

16. Thielseh, H. Defects and Failures in Pressure Vessels and Piping. Reinhold Publishing Corp., New York, 1965.

17. McClintock, R.M. and Gibbons, H.P. Mechanical Properties of Structural Materials at Low Temperatures. NBS Monograph 13, June 1, 1960.

18. Clauser, H.R., et al. How materials are selected. Materials in Design Engineering, pp. 109-28, July 1965.

19. Fager, J.A. Development of titanium alloy for lightweight LH_2 tankage. J. of Spacecraft 2, no. 3, 369-75, May-June 1965.

20. Engquist, R.D. Evaluating weldability of various materials. Welding Engineer, pp. 47-57, Oct. 1964.

21. Miller, K.J. Welding fabrication of high pressure oxygen vessels for life support in space. Welding J. pp. 187-93, March 1965.

22. Morita, W.H. Parametric booster tankage design studies. Fifth AIAA Annual Structures and Materials Conference, AIAA publication C-P-8, pp. 1-17, New York, April 1964.

23. Timoshenko, S. Strength of Materials, Part II. Van Nostrand Co., Inc., Princeton, New Jersey, 1930.

24. Rumbold, S.G. The application of cryogenic rocket propellants to space vehicles. Appl. Cryogenic Eng. pp. 380-90, 1962. Univ. of Calif. Eng. and Physical Sciences Extension Series, John Wiley and Sons, Inc.

25. Murphy, G.J. and Pearce, P.O. Contamination control in cryogenic fluids and systems. Appl. Cryogenic Eng. pp. 476-99, 1962. Univ. of Calif. Eng. and Physical Sciences Extension Series, John Wiley and Sons, Inc.

26. McKinley, C. Safety aspects of cryogenic systems. Appl. Cryogenic Eng. pp. 255-62, 1962. Univ. of Calif. Eng. and Physical Sciences Extension Series, John Wiley and Sons, Inc.

27. Flugee, W. Stresses in Shells. Verlag-Springen, Berlin, 1960.

28. Zick, L.P. and St. Germain, A.R. Circumferential stresses in pressure vessel shells of revolution. J. Eng. for Industry, May 1963.

29. Struik, D.J. Differential Geometry. Addison-Wesley Publ. Co., Inc. Reading, Mass., 1950.

30. Pascover, J.S., Matas, S.J. and Barclay, W.F. Tough high-strength steels for aerospace applications. Sixth National Symposium on Materials for Space Vehicle Use Vol. 2, Society of Aerospace Material and Process Engineers, Nov. 1963.

31. Richards, C.W. Engineering Materials Science. Wadsworth Publ. Co., Inc., Belmont, Calif. 1961.

32. Gohn, G.R., Herdrath, H.F. and Peterson, R.E. Fatigue of metals. Materials Research & Standards, pp. 105-39, Feb. 1963.

33. Manson, S.S. Fatigue: a complex subject - some simple approximations. Experimental Mechanics, pp. 193-226, July 1965.

34. Anon. (Gen. Motors Corp., Allison Div., Eng. Dept.) Pressure Vessel Presentation. Rept. no. 3410, June 1963.

35. Hurlich, S. Materials requirements for cryogenic temperature applications. Gen. Dynamics/Astronautics, San Diego, Calif.

36. Cunningham, J.H. Lecture notes on pressure vessel design. Douglas Aircraft, Santa Monica, Calif., Company Program, Acct. no. 81109-006, Aug. 2, 1961.

37. Love, G.G. Structural analysis of orthropic shells. AIAA J. 1, no. 8, 1843-7, Aug. 1963.

REFERENCES (contd)

38. Nelson, E.N. The non-linear pressure vessel theory. AIAA 1st. Ann. Mtg. Paper 64-438, Wash., D.C. June 29-July 2, 1964.

39. Timoshenko, S. Theory of Plates and Shells.

40. Muraca, R.F., et al. Design data for pressurized gas systems. NAS7-105, SRI Proj. PSU-4000, NASA CR-53393, Chapt. X, Nov. 1963.

41. Roark, R.J. Formulas for Stress and Strain. McGraw-Hill Book Co., Inc., New York, 1954.

42. Jaffe, L.D. and Rittenhouse, J.B. Behavior of materials in space environments. ARS J. pp. 320-46, Mar. 1962.

43. Pence, D.R. (Ed.) (Space Technology Lab., Inc.) Unmanned Spacecraft Weight Estimation Handbook. AF04 (695)-671, Dec. 1964.

44. Timoshenko, S. and Goodier, J.N. Theory of Elasticity (2nd edn.). McGraw-Hill Book Co., Inc., New York, 1951.

45. Whalley, E. Can. J. Technol. 34, pp. 268, 291, 1955.

46. Costes, W.M. Trans. ASME 52, no. 12, 1930.

47. Paris, P.C. and Sih, G.C.M. Stress analysis of cracks. ASTM Special Publ. no. 381, 1965.

48. Irwin, G.R. Analysis of stresses and strains near the end of a crack traversing a plate. Trans. ASME, 1957.

49. Bueckner, H. "Some stress singularities and their computation by means of integral equations", Boundary Value Problems in Differential Equations, Langer, R.E. (Ed.) Univ. of Wis. Press, Madison, Wis. 1960.

50. Bowie, O.L. Rectangular tensile sheet with symmetric edge cracks. Trans. ASME, J. Appl. Mech. 31, 208-12, June 1964.

51. Gross, B., Frawley, J.E. and Brown, W.F. Stress intensity factors for a single edge notch tension specimen by boundary collocations of a stress function. NASA TN D-2395.

52. Reissner, E. On the Theory of Thin Elastic Shells. Reissner Anniversary Volume pp. 231-47.

53. Timoshenko, S. Theory of Elastic Stability.

54. Potter, M.L. A matrix method for the solution of a second order difference equation in two variables. Math. Centrum Rept., MR 19, 1955.

55. Radkowski, P.P., Davis, R.M. and Bolduc, M.R. Numerical analysis of equations of thin shells of revolution. ARS J. Jan. 1962.

56. Spera, D.A. Analysis of elastic-plastic shells of revolution containing discontinuities. AIAA J. 1, no. 11, Nov. 1963.

57. Mendelson, A. and Manson, S.S. Practical solution of plastic deformation problems in elasti-plastic range. NASA TR R-28, 1959.

58. Ester, P.H. Multi-Layered thin shells of revolution with thermal and plastic strain. Proc. of Fifth Ann. Tech. Sym. Univ. of N. Mex. Oct. 1964.

59. Bogardus, K.O., et al. (Aluminum Co. of America) Results of tensile tests of various aluminum alloys at -18°, -112°, and -320°F made at the Aluminum Research Laboratories.

60. Howell, F.M. and Stickley, G.W. (Aluminum Co. of America) The mechanical properties of Alcoa wrought aluminum alloy products at various temperatures. Aluminum Res. Lab. Rept. no. 9-47-9, Dec. 12, 1947.

61. Strauss, J. Metals and alloys for industrial applications requiring extreme stability. Trans. Am. Soc. Steel Treating 16, p. 191, 1929.

62. NBS Cryogenic Eng. Lab. unpublished data.

63. McAdam, D.J., Jr., Mebs, R.W. and Geil, G.W. The technical cohesive strength of some steels and light alloys at low temperatures. Proc. ASTM 44, p. 593, 1944.

64. Zambrow, J.L. and Fontana, M.G. Mechanical properties, including fatigue, of aircraft alloys at very low temperatures. Trans. Am. Soc. Metals 41, p. 480, 1949.

65. Rosenberg, S.J. Effect of low temperatures on the properties of aircraft metals. J. Res. NBS 25, p. 673, RP1347, 1940.

66. Kostenetz, V.I. and Ivanchenko, A.M. Mechanical properties of metals and alloys in tension at low temperatures (-196°C and -253°C). Zhur. Tekh. Fiz. 16, p. 515, 1946, (in Russian). Abstracted in Metal Progr. 54, Dec. 1948 and 55, Jan. 1949.

67. Metals Handbook. Am. Soc. Metals, Cleveland, 1948.

68. Symposium on effect of temperature on the brittle behavior of metals with particular reference to low temperatures. ASTM, Special Tech. Publ. no. 158, 1954.

69. Templin, R.L. and Paul, D.A. The mechanical properties of aluminum and magnesium alloys at elevated temperatures. Symposium on Effect of Temperature on the Properties of Metals, 198, ASTM and ASME, 1931.

70. Spretnak, J.W., Fontana, M.G. and Brooks, H.E. Notched and unnotched tensile and fatigue properties of ten engineering alloys at 25°C and -196°C. Trans. Am. Soc. Metals 43, p. 547, 1951.

71. Anon. (Alleghany Ludlum Steel Corp.) Stainless Steel Handbook. 1951.

72. Hoke, J.H., Mabus, P.G. and Goller, G.N. Mechanical properties of stainless steels at subzero temperatures. Metal Progr. 55, p. 643, 1949.

73. Anon. (Linde Air. Eng. Lab.) AF04 (611)-373, Progr.Rept. no. 7, Jan. 12, 1959.

REFERENCES (contd)

74. McAdam, D.J., Geil, G.W. and Cromwell, F.J. Influence of low-temperatures on mechanical properties of 18-8 chromium-nickel steel. J. Res. NBS 40, p. 375, 1948.

75. Anon. (Union Carbide and Carbon Co. Res. Labs.) as quoted in Metals Handbook. Am. Soc. Metals, Cleveland, Ohio, 1948.

76. Krivobok, V.N. Properties of austenitic stainless steels at low temperatures. NBS circular 520, p. 112, 1952.

77. Krivobok, V.N. and Talbot, A.M. Effect of temperature on the mechanical properties, characteristics, and processing of austenitic stainless steels. Proc. ASTM 50, p. 895, 1950.

78. Schmidt, E.H. Low temperature impact of annealed and sensitized 18-8 Metal Progr. 54, p. 698, 1948.

79. Henke, R.H. Low temperature properties of austenitic stainless steels. Product Eng. 20, p. 104, 1949.

80. Anon. (Republic Steel Corp.) Republic Enduro Stainless Steel. 1951.

81. Klier, E.P. and Feola, N.J. Notch tensile properties of selected titanium alloys. J. Metals 9, p. 1271, Oct. 1957.

82. Anon. (Convair Astronautics Div., Gen. Dynamics Corp.) unpublished data.

83. McGee, R.L., et al. The mechanical properties of certain aircraft structural metals at very low temperatures. WADC Tech. Rept. 58-386, June 1958.

84. Bishop, S.M., Spretnak, J.W. and Fontana, M.G. Mechanical properties, including fatigue, of titanium base alloys RC-130B and Ti-150A at very low temperatures. Trans. Am. Soc. Metals 46, p. 993, 1954.

85. DeSisto, T.S. Automatic impact testing from room temperature to -236°C. Sym. on Impact Testing, ASTM, Special Tech. Publ. no. 176, 1956.

86. Tiffany, C.F. and Lorenz, P.M. (AF Matls. Lab. Res. and Technol. Div., Air Force Systems Command, Wright-Patterson AFB, Ohio) An investigation of low-cycle fatigue failures using applied fracture mechanics. AF 33 (657)-10251. Tech. Documentary Rept. ML-TDR-64-53, May 1964.

VII-A APPENDIX

Table VII-A-1

PROPERTIES OF VARIOUS HEAD SHAPES

	HEMISPHERICAL 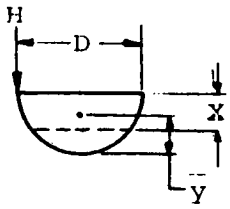	$\frac{D}{3}$ ELLIPTICAL 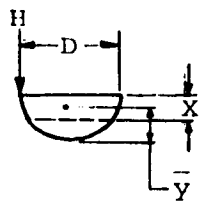	$\frac{D}{4}$ ELLIPTICAL 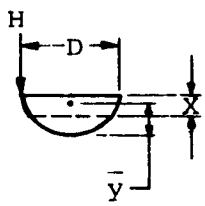	SEGMENTAL 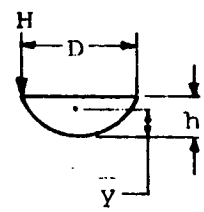	FLANGED AND DISHED HEAD 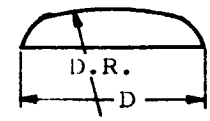 D.R. = D K.R. = 0.06D
Depth or Rise	$\frac{D}{2}$	$\frac{D}{3}$	$\frac{D}{4}$	h	0.169D
Volume, cu.ft.	$0.2618D^3$	$0.1745D^3$	$0.1309D^3$	$1.0472h^2(3r-h)$	$0.0810D^3$
Volume, gals.	$1.9584D^3$	$1.3056D^3$	$0.9792D^3$	$7.833h^2(3r-h)$	$0.6059D^3$
Surface, sq.ft.	$1.571D^2$	$1.24D^2$	$1.084D^2$	2 rh	$0.9286D^2$
Length of Arc	1.5708D	1.322D	1.211D	calculate angle	1.1043D
Projected Area	$0.3927D^2$	$0.2618D^2$	$0.1964D^2$	calculate sector-∇	$0.1255D^2$
to Centroid Proj. Ar.	0.2878D	0.1919D	0.1439D	$\pm \frac{5}{8}h$ (roughly)	0.1000D
to Centroid of Mass	0.3125D	0.2083D	0.1563D	$\frac{8rh - 3h^2}{12r - 4h}$	-
Stress (water) lbs. per inch	$1.3 \quad H+\frac{D}{2} \quad D$	$+1.95D \quad H + \frac{D}{3}$ or $-2.6D \quad \frac{H}{8} + \frac{D}{4}$	$+2.6D \quad H + \frac{D}{4}$ $-2.6D \quad H + \frac{D}{3}$	2.6r (H + h)	-
Stress due to Gas pressure "p" lbs per inch	epD	$+4.5pD$ or $-\frac{3pd}{4}$	$+6pD$ or $-6pD$	6pr	-
Partial Volume within depth X (cu.ft.)	$\pi x \quad \frac{D^2}{4} - \frac{x^2}{3}$	$\pi x \quad \frac{D^2}{4} - \frac{3x^2}{4}$	$\pi x \quad \frac{D^2}{4} - \frac{4x^2}{3}$	Calculate new vol. on basis (h-x) & subtract	-
Angle at edge	90°	90°	90°	calculate	90°

NOTE: All dimensions expressed in feet; H = water elev. above belt line (Shell Height).
W = total load carried, including dead load.

Table VII-A-2

R_1 AND R_2 FOR SHELLS OF REVOLUTION

Cylinder

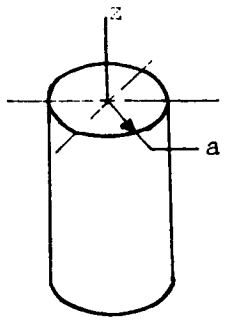

$R_1 = \infty$, $R_2 = a$

Torous

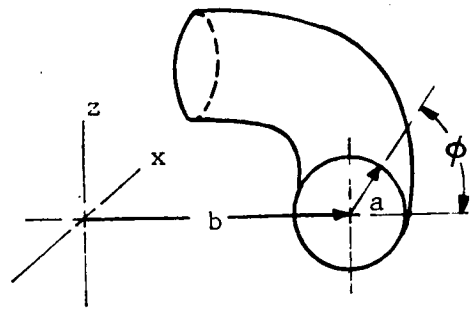

$$R_1 = \frac{2a(b+a\cos\phi)}{a(b+2a\cos\phi)+b}, \quad R_2 = \frac{2a(b+a\cos\phi)}{a(b-2a\cos\phi)-b}$$

Cone

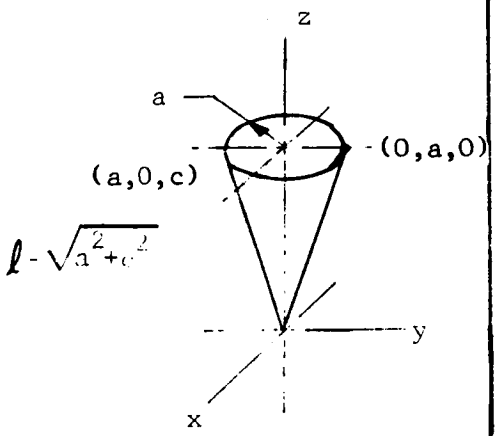

$$R_1 = \infty, \quad R_2 = \frac{\ell a z}{c^2}$$

Ellipse

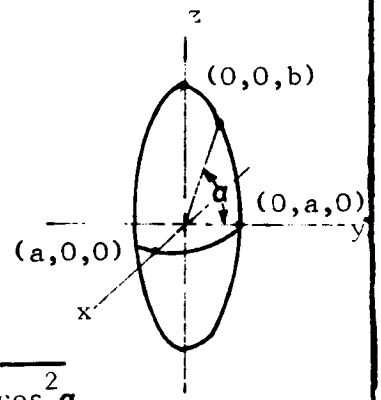

$$R_1 = \frac{a}{b}\sqrt{a^2\sin^2\alpha + b^2\cos^2\alpha}$$

$$R_2 = \frac{(a^2\sin^2\alpha + b^2\cos^2\alpha)^{\frac{3}{2}}}{ab}$$

Parabola

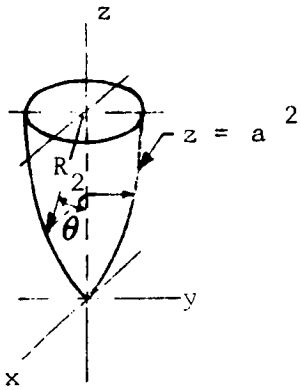

$$R_1 = \frac{\sin\theta}{r}\cos^2\theta, \quad R_2 = \frac{r}{\sin\theta}$$

Hyperbola

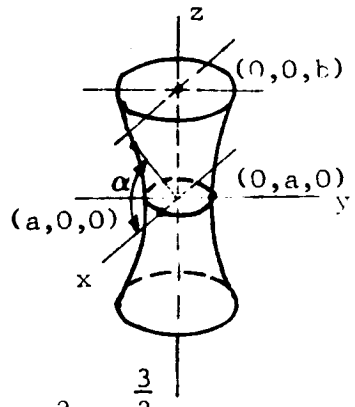

$$R_1 = \frac{(a^2\cosh^2\alpha + b^2\sinh^2\alpha)^{\frac{3}{2}}}{ab}$$

$$R_2 = \frac{a}{b}\sqrt{a^2\cosh^2\alpha + b^2\sinh^2\alpha}$$

Table VII-A-3

SHOCK AND VIBRATION LOADING FACTORS

Loading	Load Factor	Remarks
Vibration	$F = kW$	F is the force in lbs added to the system, k is the number of "g's" the system is subject to, W is the weight of the system.
Impact, vertical drop of a weight	$\frac{d_i}{d} = \frac{S_i}{S} = 1+\sqrt{1+2\frac{h}{d}}$ (Ref. 41)	d_i=impact vertical deformation, Si= impact stress, h=height of drop, d= vertical deformation due to the weight of the falling body applied as a static load, and s=static stress.
Impact, horizontal with velocity v	$\frac{d_i}{d} = \frac{S_i}{S} = \sqrt{\frac{v^2}{384.6d}}$ (Ref. 41)	V=velocity of horizontal impacting weight, d=deformation of same weight applied as a static load.

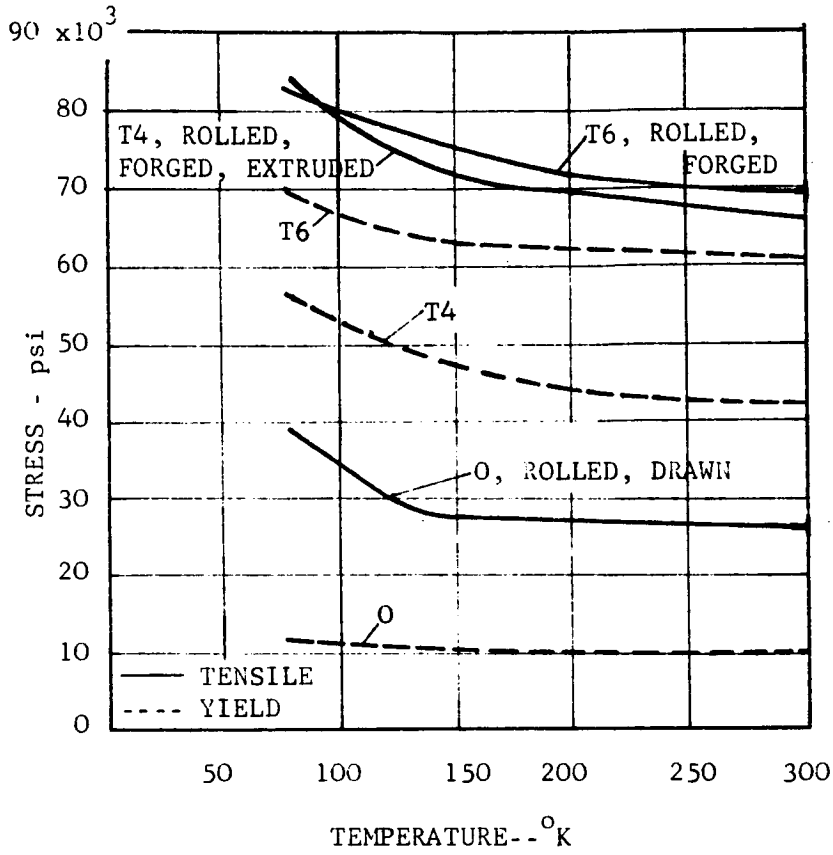

Strength of 2014 Aluminum

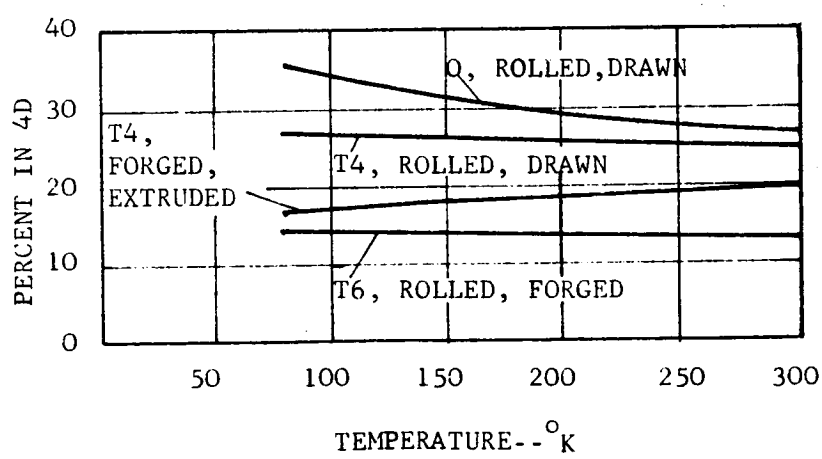

Elongation of 2014 Aluminum

Fig. VII-A-1 Properties of 2014 Aluminum (Ref. 17)

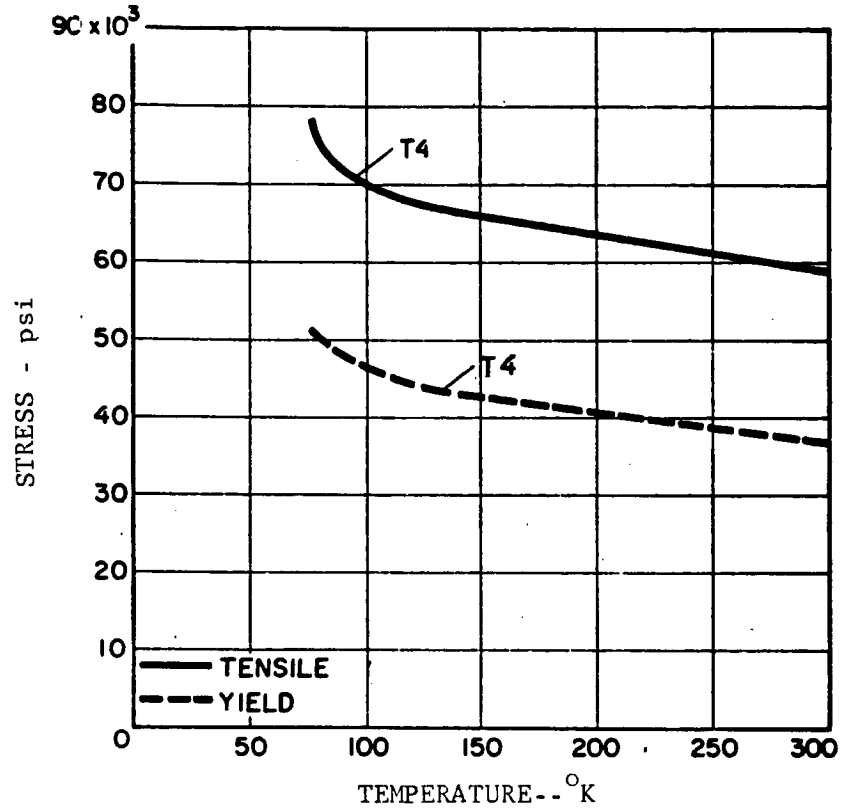

Strength of 2017 Aluminum

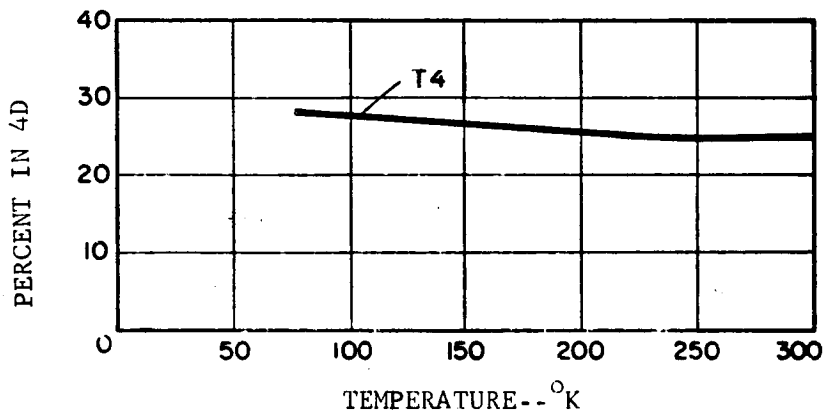

Elongation of 2017 Aluminum

Fig. VII-A-2 Properties of 2017 Aluminum (Ref. 17)

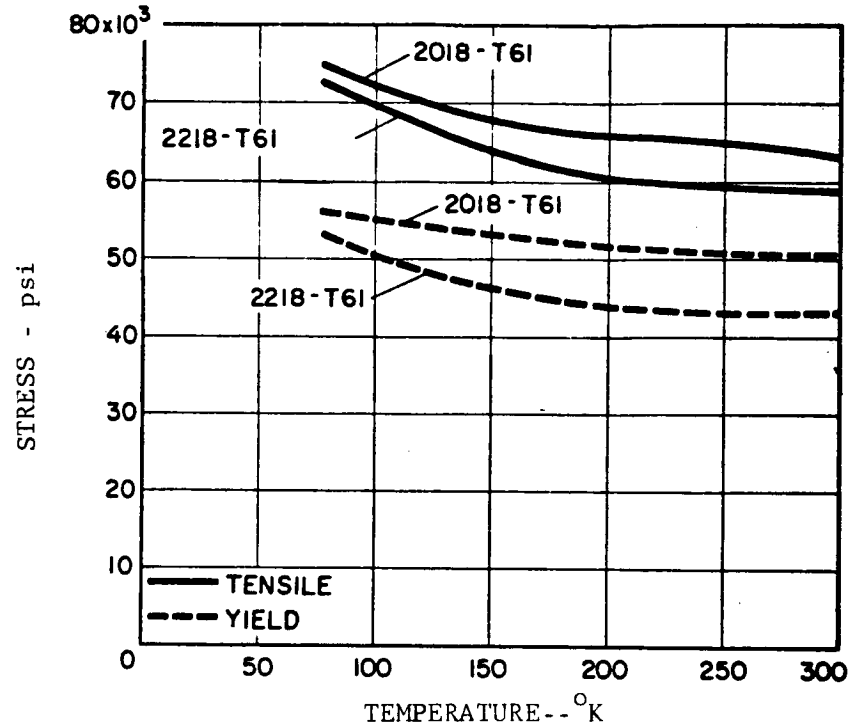

Strength of 2018 and 2218 Aluminum Alloys

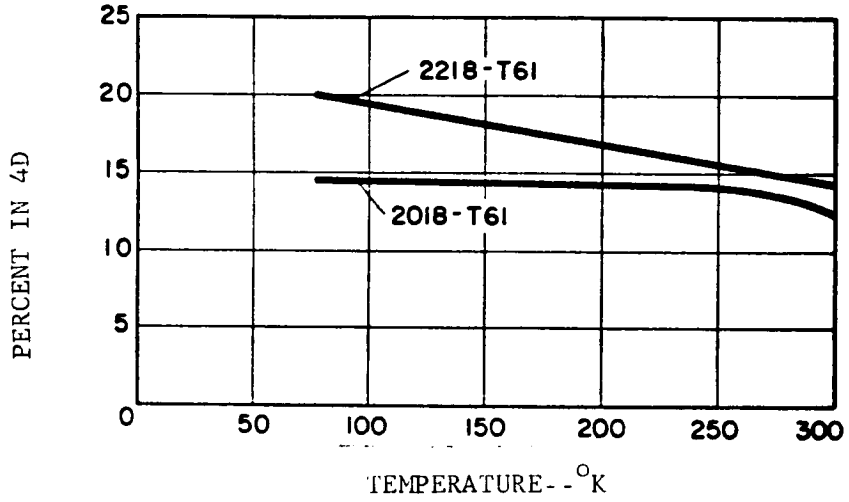

Elongation of 2018 and 2218 Aluminum Alloys

Fig. VII-A-3 Properties of 2018 and 2218 Aluminum (Ref. 17)

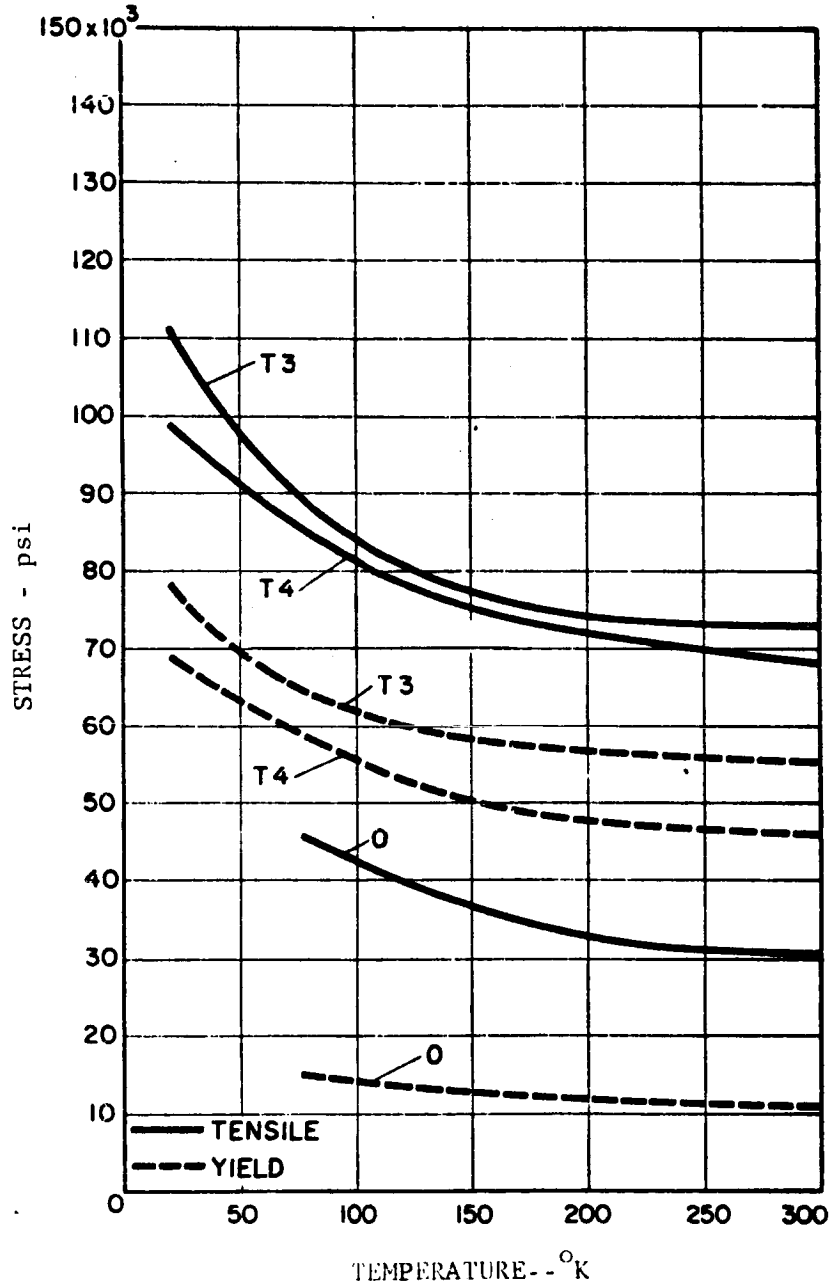

Fig. VII-A-4 Strength of 2024 Aluminum (Ref. 17)

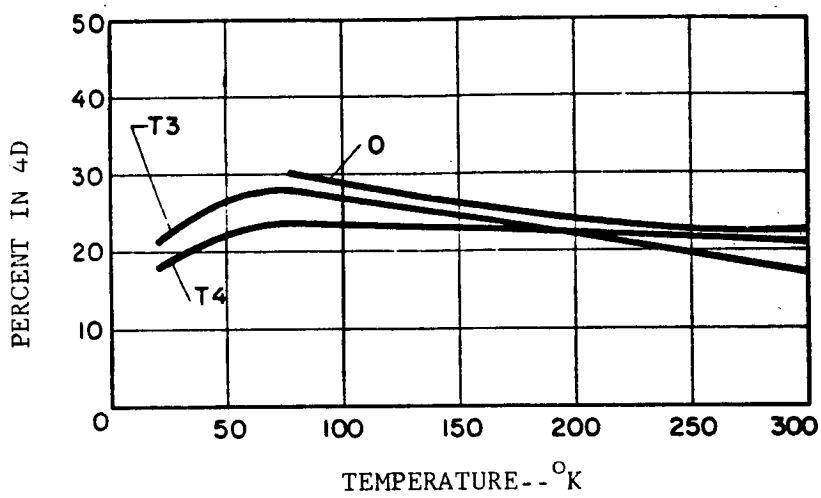

Elongation of 2024 Aluminum

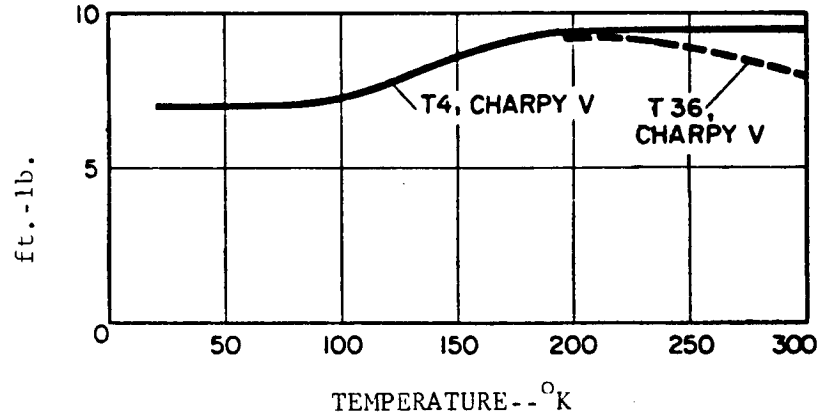

Impact Energy of 2024 Aluminum

Fig. VII-A-5 Properties of 2024 Aluminum (Ref. 17)

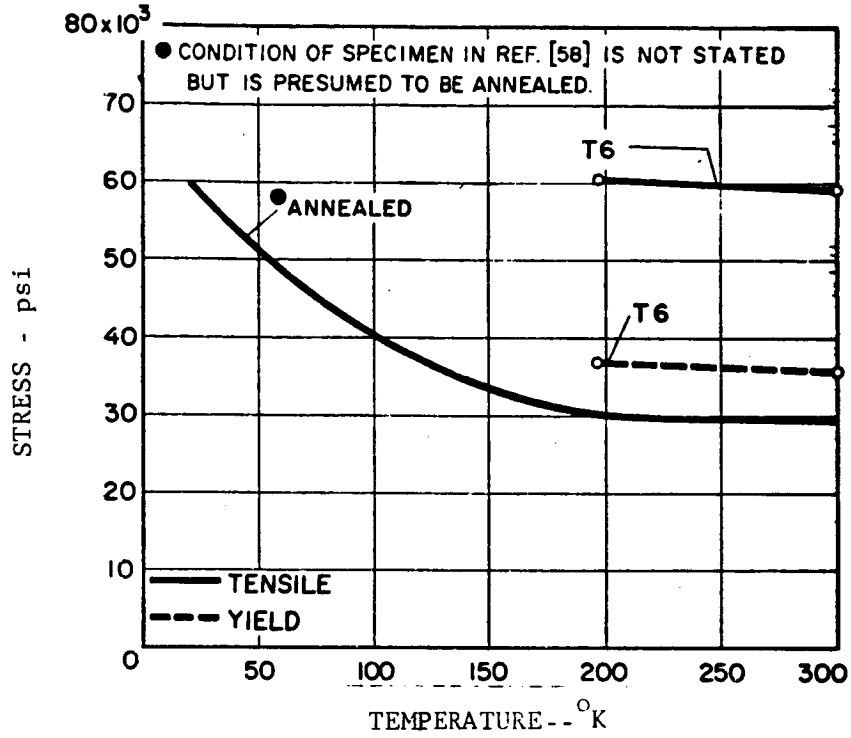

Strength of 2025 Aluminum

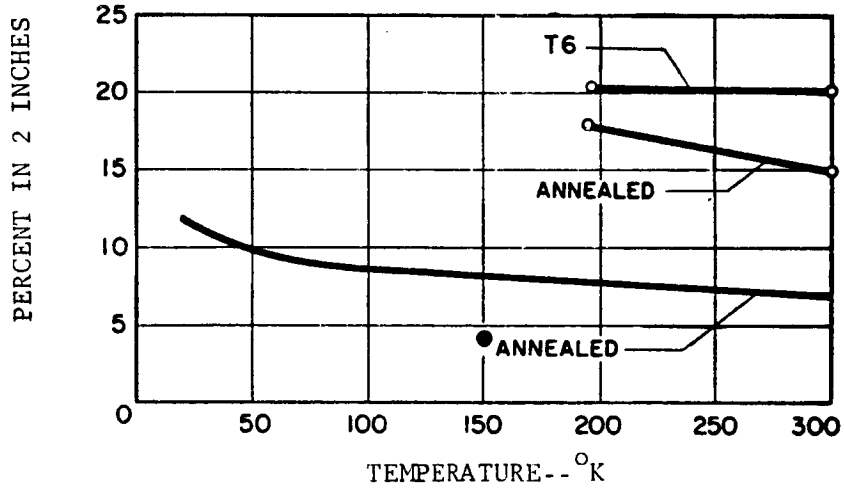

Elongation of 2025 Aluminum

Fig. VII-A-6 Properties of 2025 Aluminum (Ref. 17)

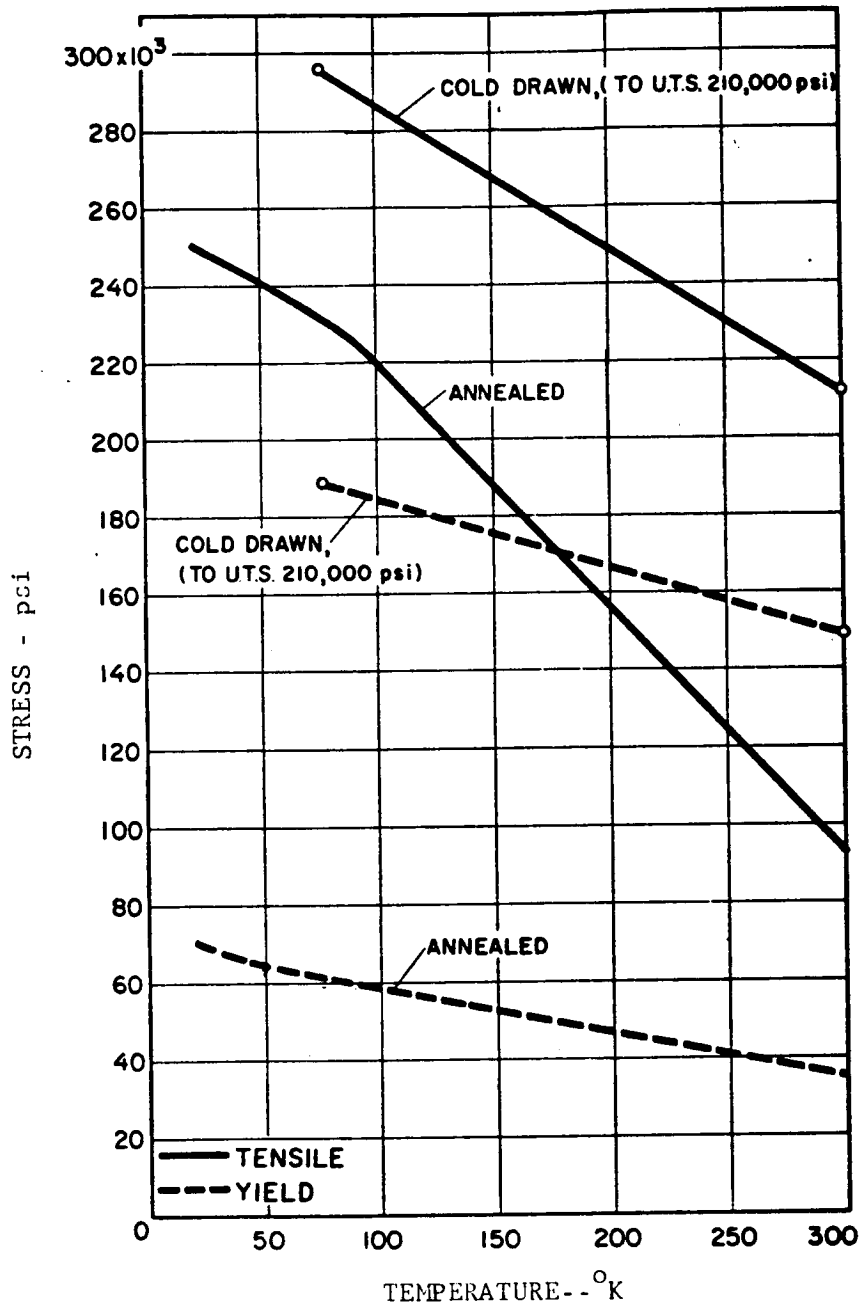

Fig. VII-A-7 Strength of AISI 304 Stainless Steel (Ref. 17)

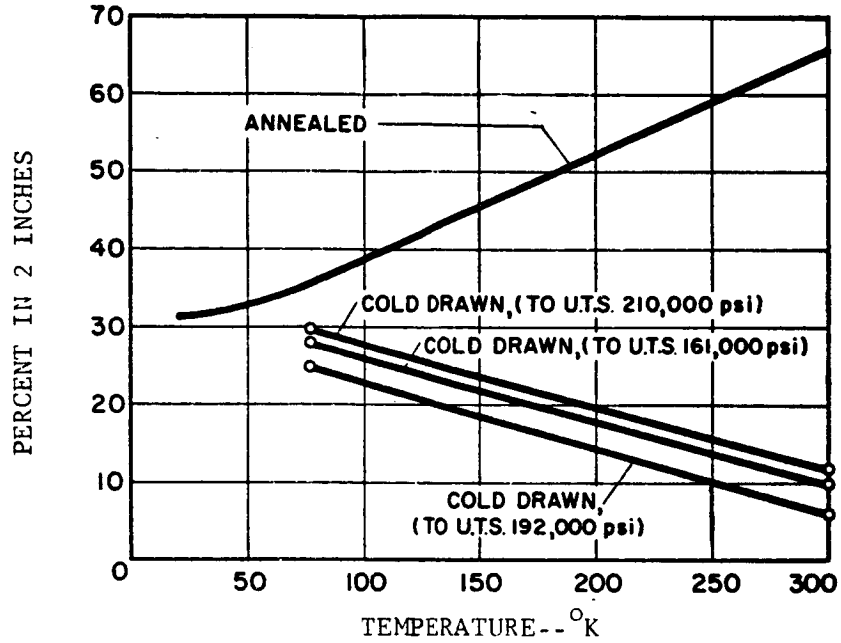

Elongation of AISI 304 Stainless Steel

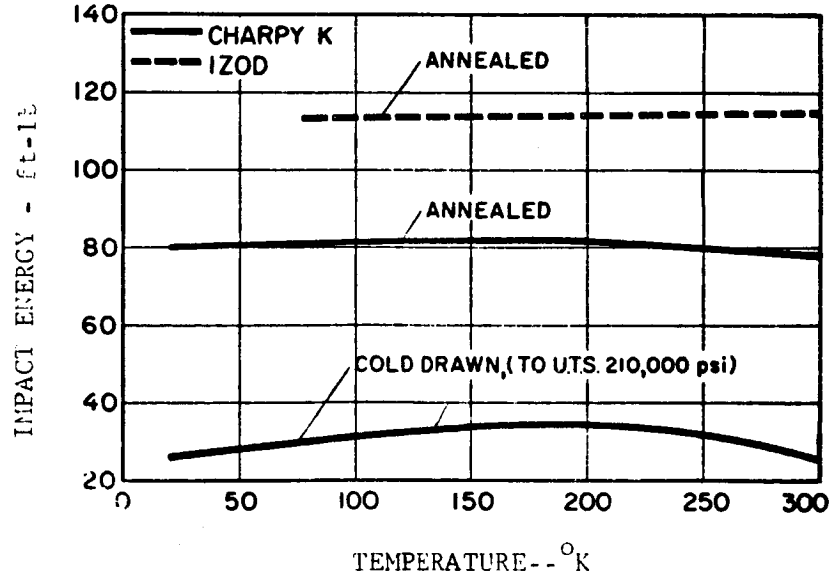

Impact Energy of AISI 304 Stainless Steel

VII-A-8 Properties of AISI 304 Stainless Steel (Ref. 17)

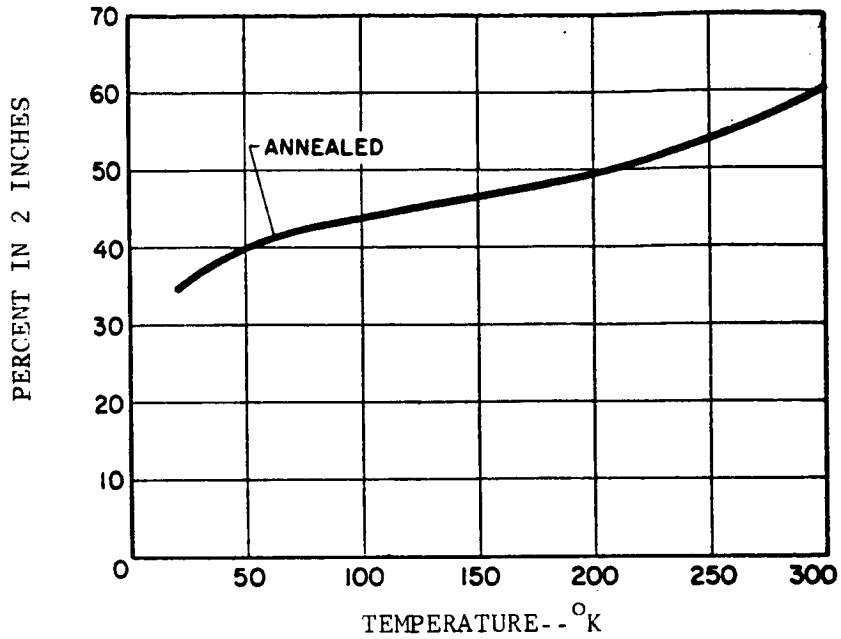

Elongation of AISI 321 Stainless Steel

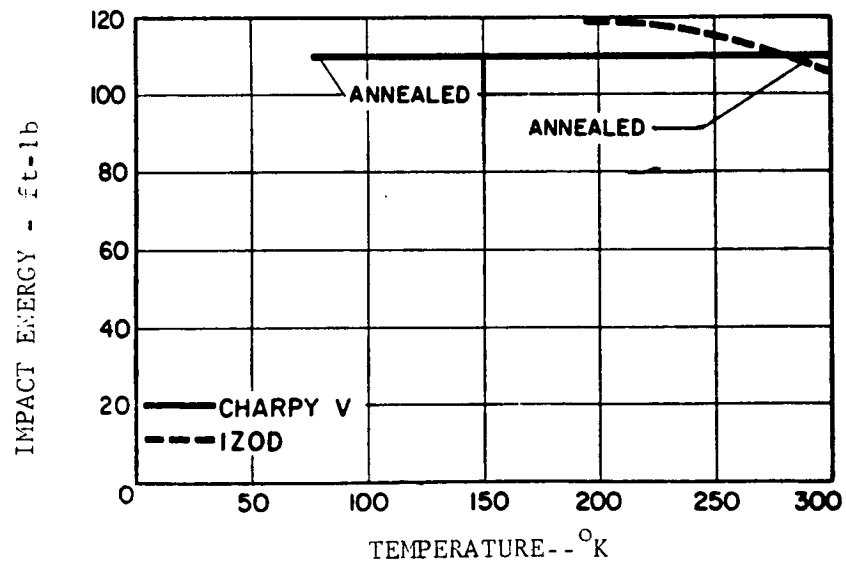

Impact Energy of AISI 321 Stainless Steel

Fig. VII-A-9 Properties of AISI 321 Stainless Steel (Ref. 17)

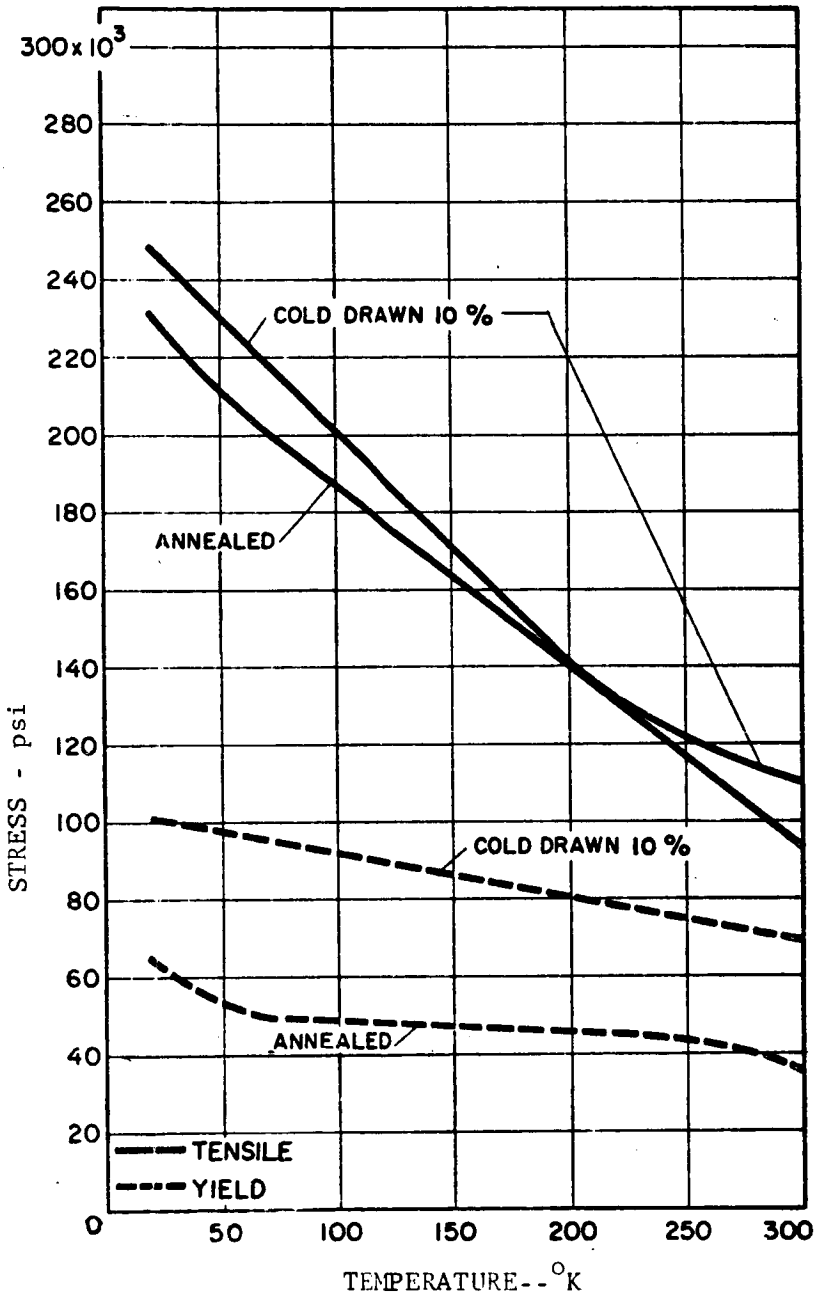

Fig. VII-A-10 Strength of AISI 347 Stainless Steel (Ref. 17)

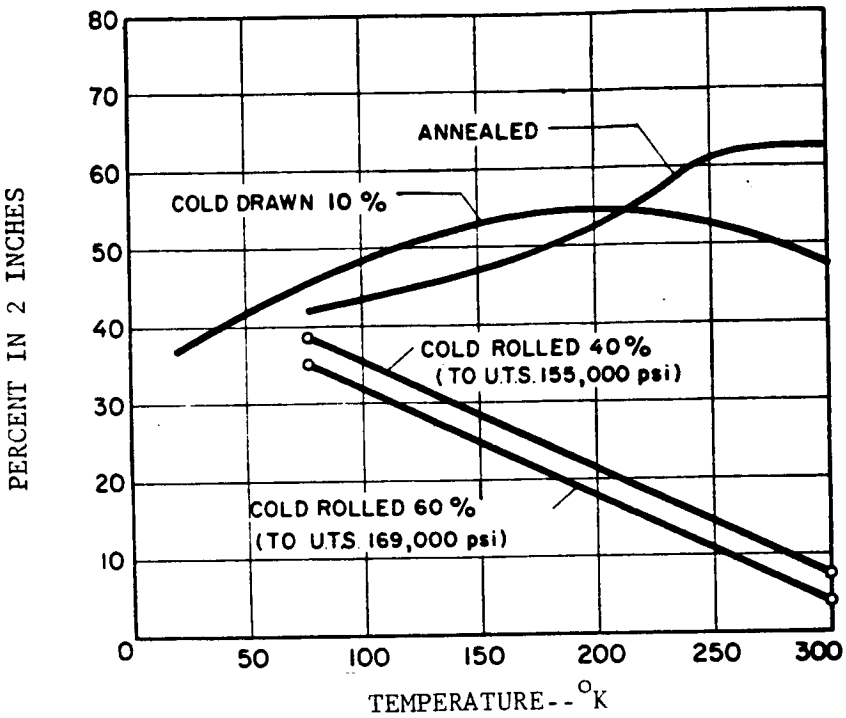

Elongation of AISI 347 Stainless Steel

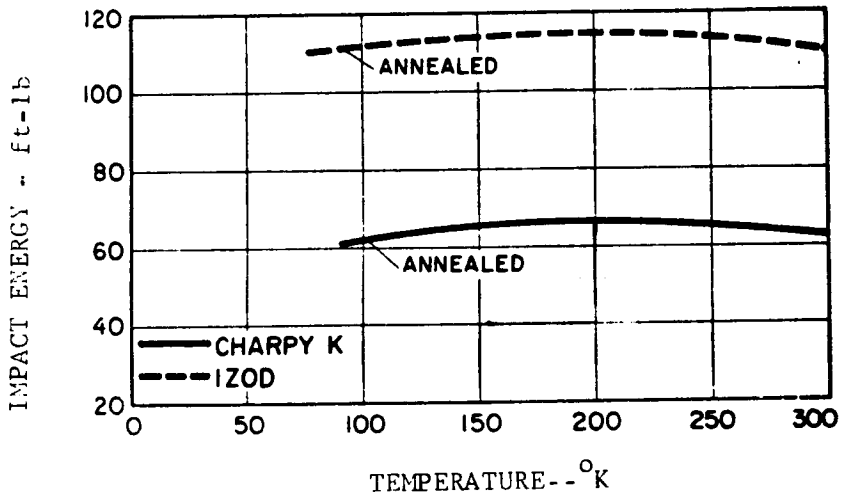

Impact Energy of AISI 347 Stainless Steel

Fig. VII-A-11 Properties of AISI 347 Stainless Steel (Ref. 17)

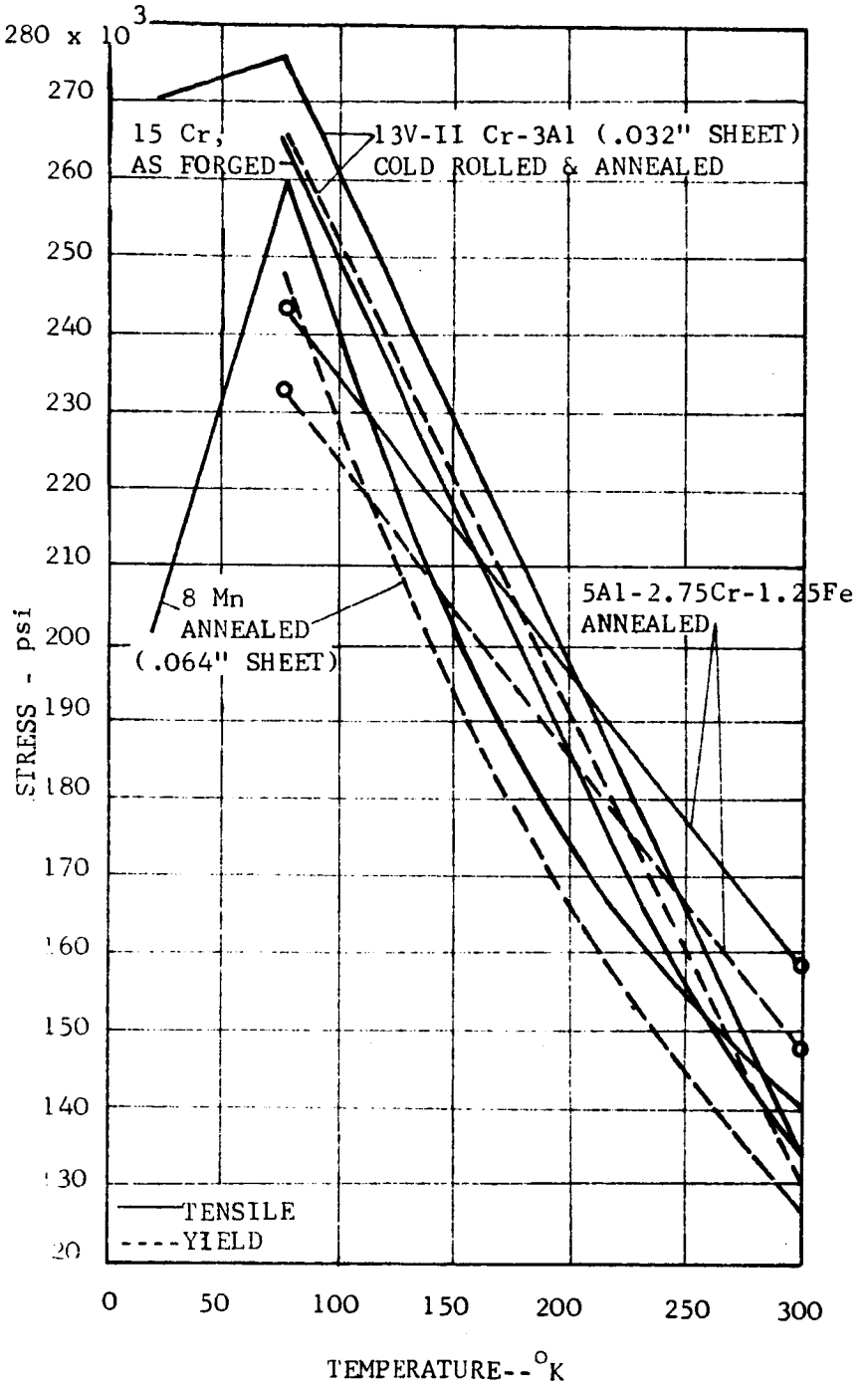

Fig. VII-A-12 Strength of Titanium Alloys (Ref. 17)

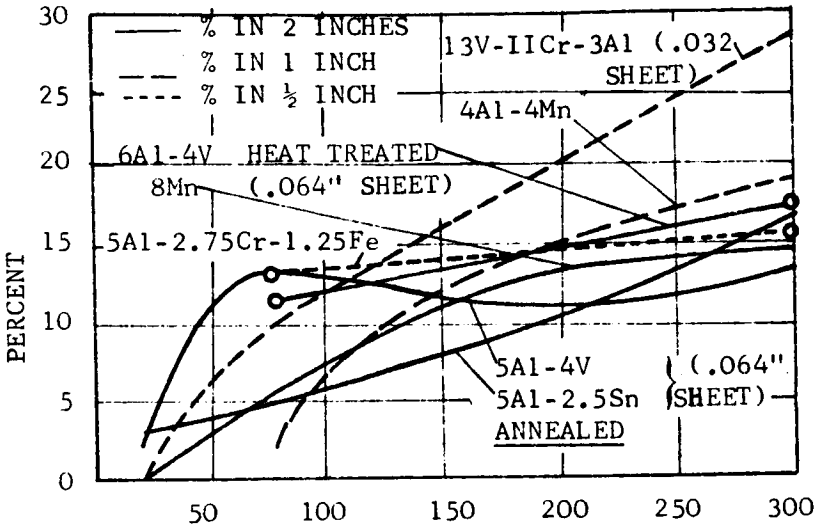

Elongation of Titanium Alloys

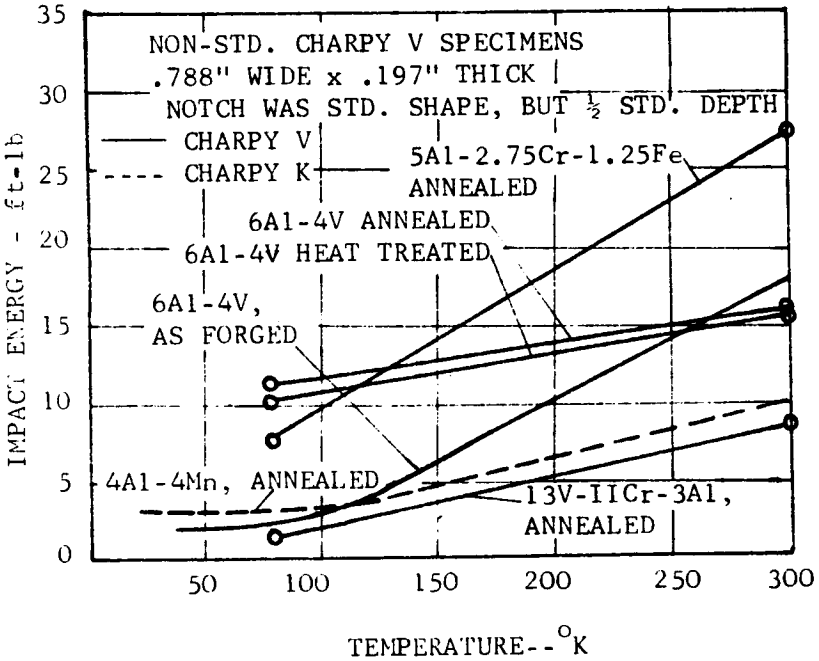

Impact Energy of Titanium Alloys

Fig. VII-A-13 Properties of Titanium Alloys (Ref. 17)

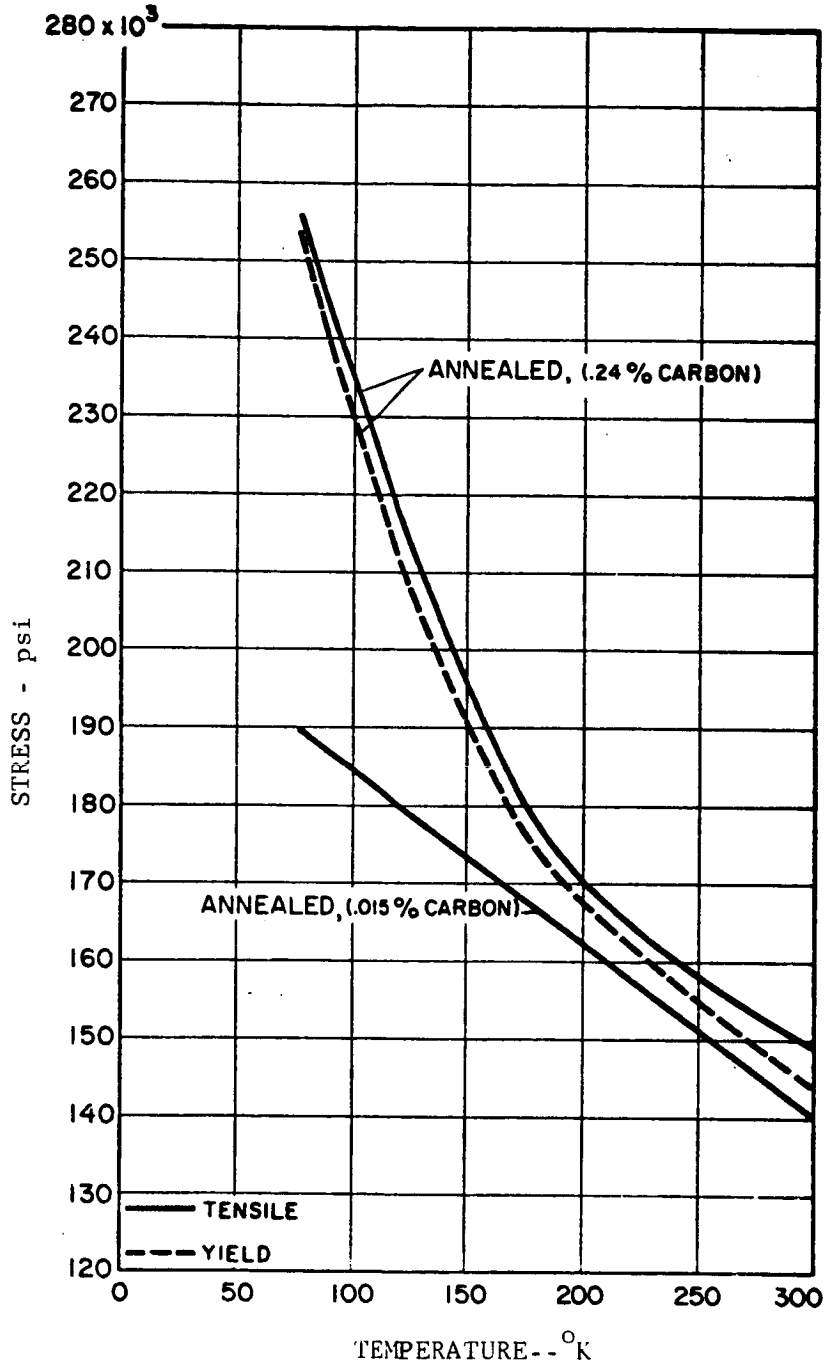

Fig. VII-A-14 Strength of 4A1-4Mn Titanium (Ref. 17)

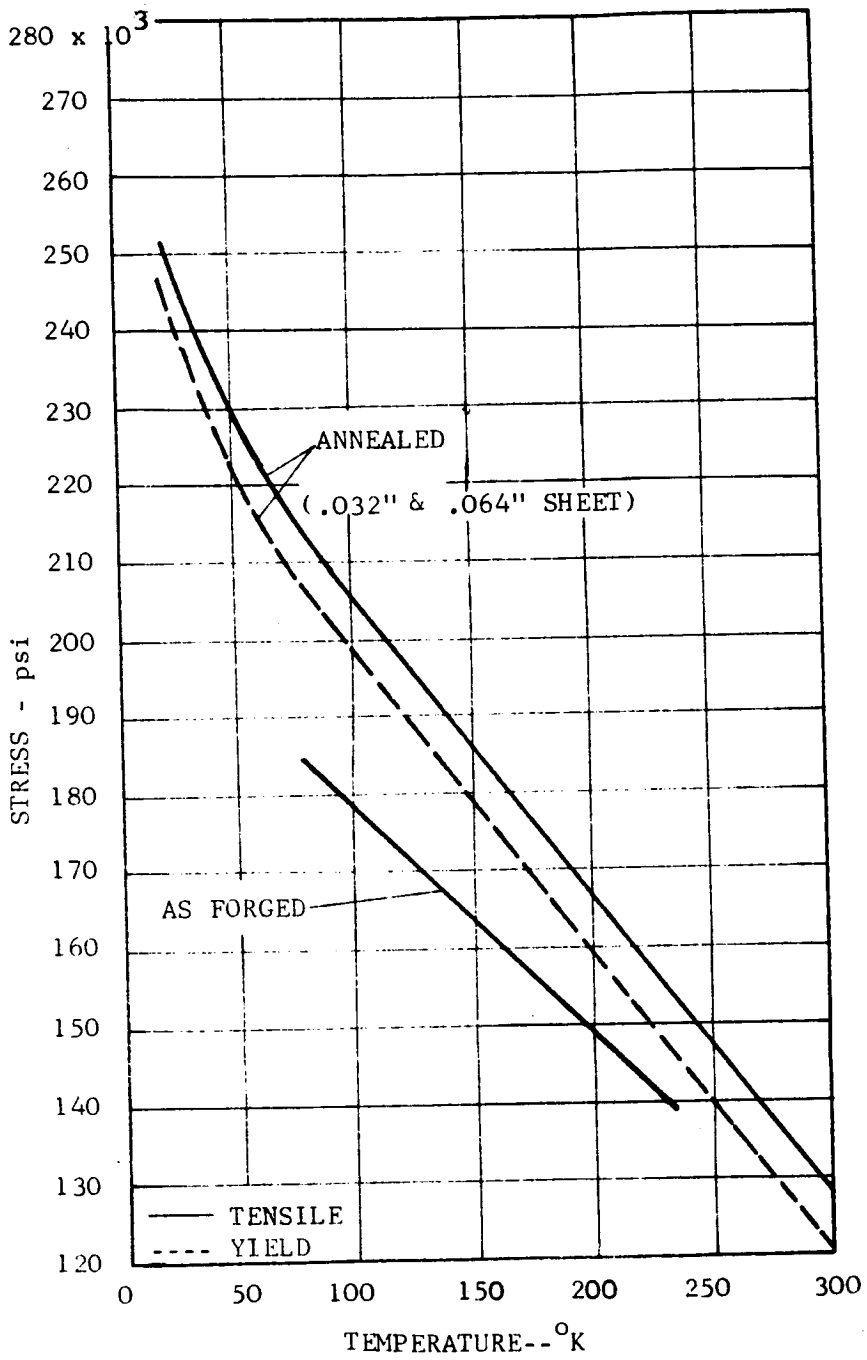

Fig. VII-A-15 Strength of 5Al-2.5 Sn Titanium (Ref. 17)

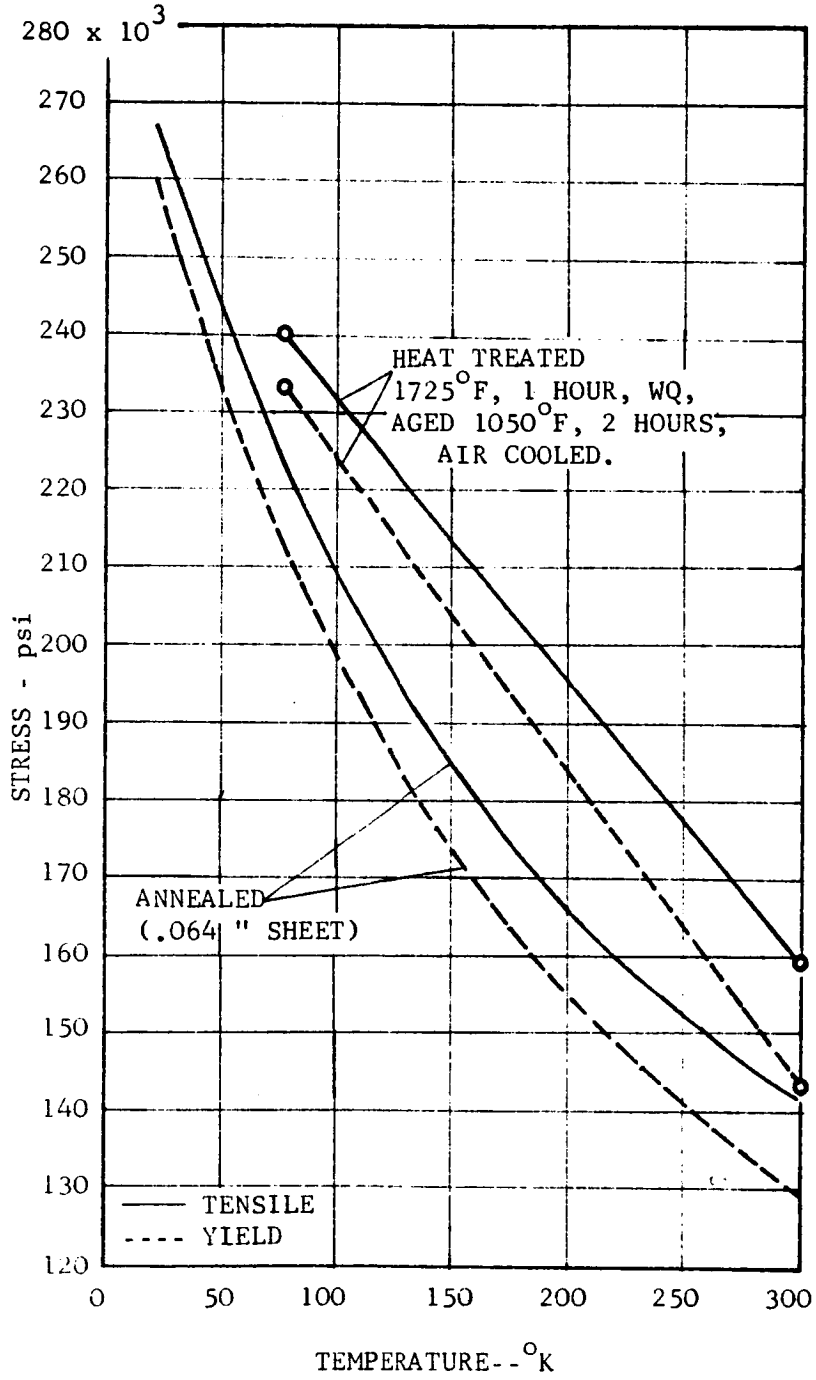

Fig. VII-A-16 Strength of 6 Al-4V Titanium (Ref. 17)

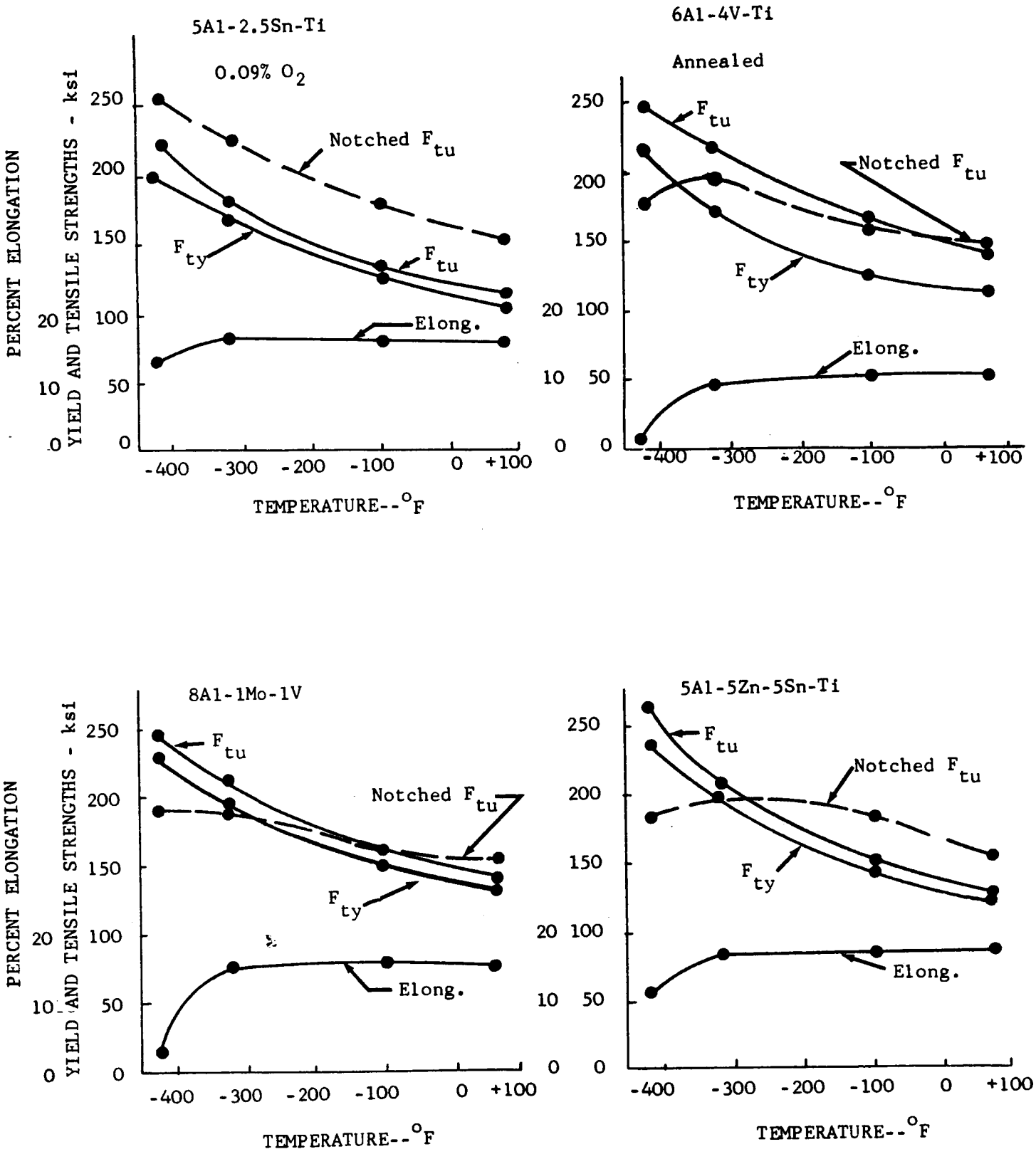

Fig. VII-A-17 Properties of Titanium Alloys (Ref. 35)

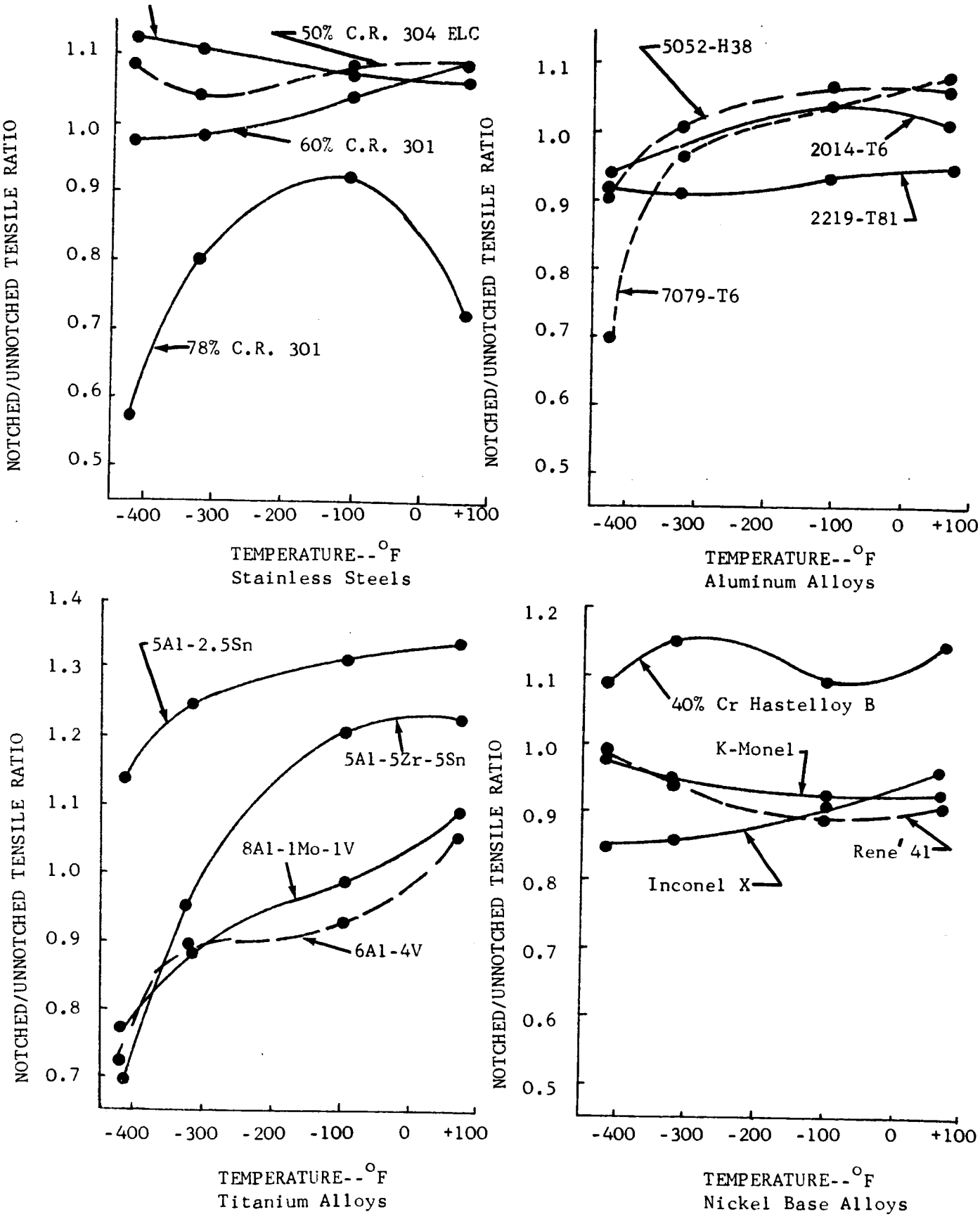

Fig. VII-A-18 Properties of Various Alloys (Ref. 35)

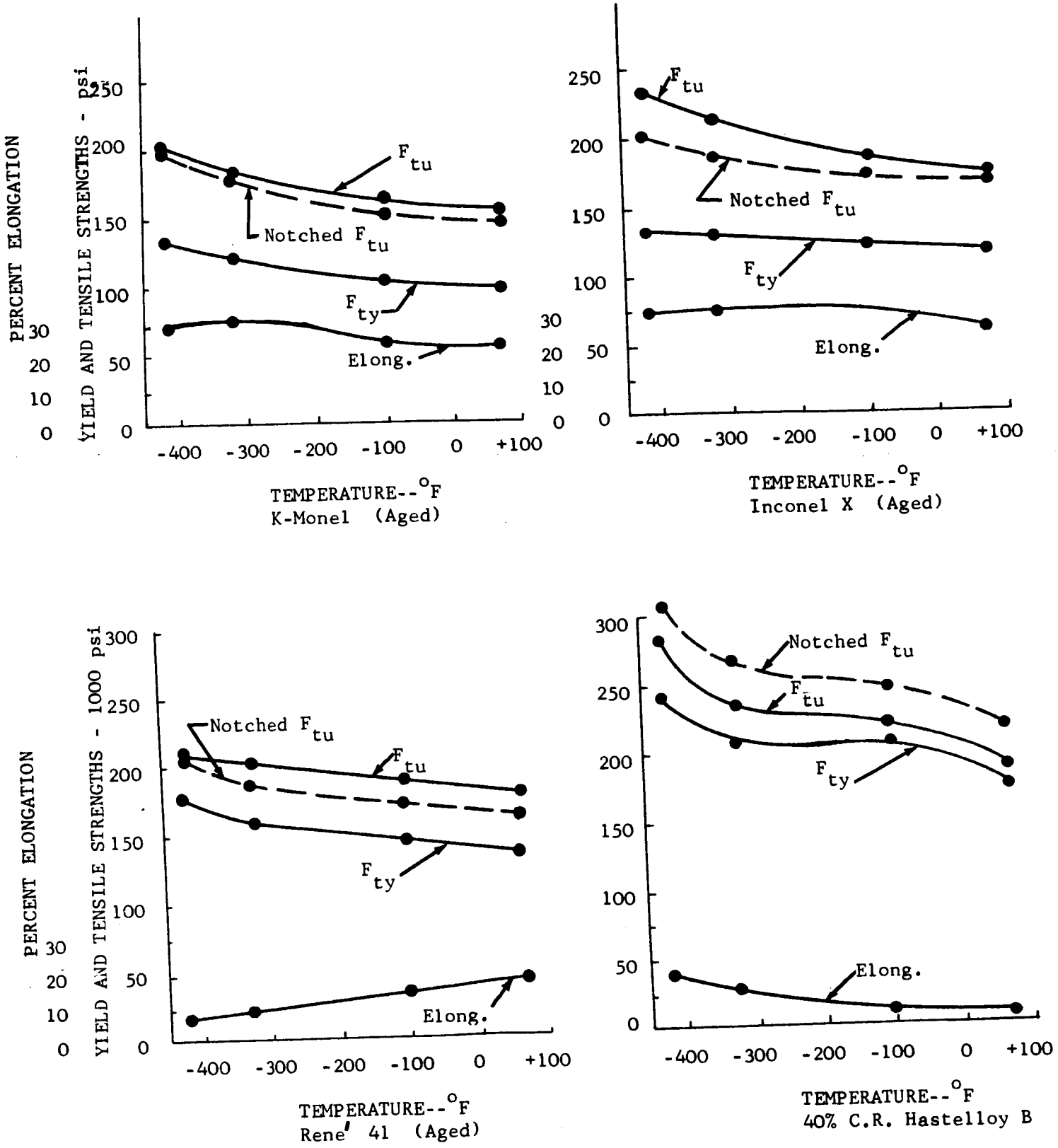

Fig. VII-A-19 Properties of Nickel Base Alloys (Ref. 35)

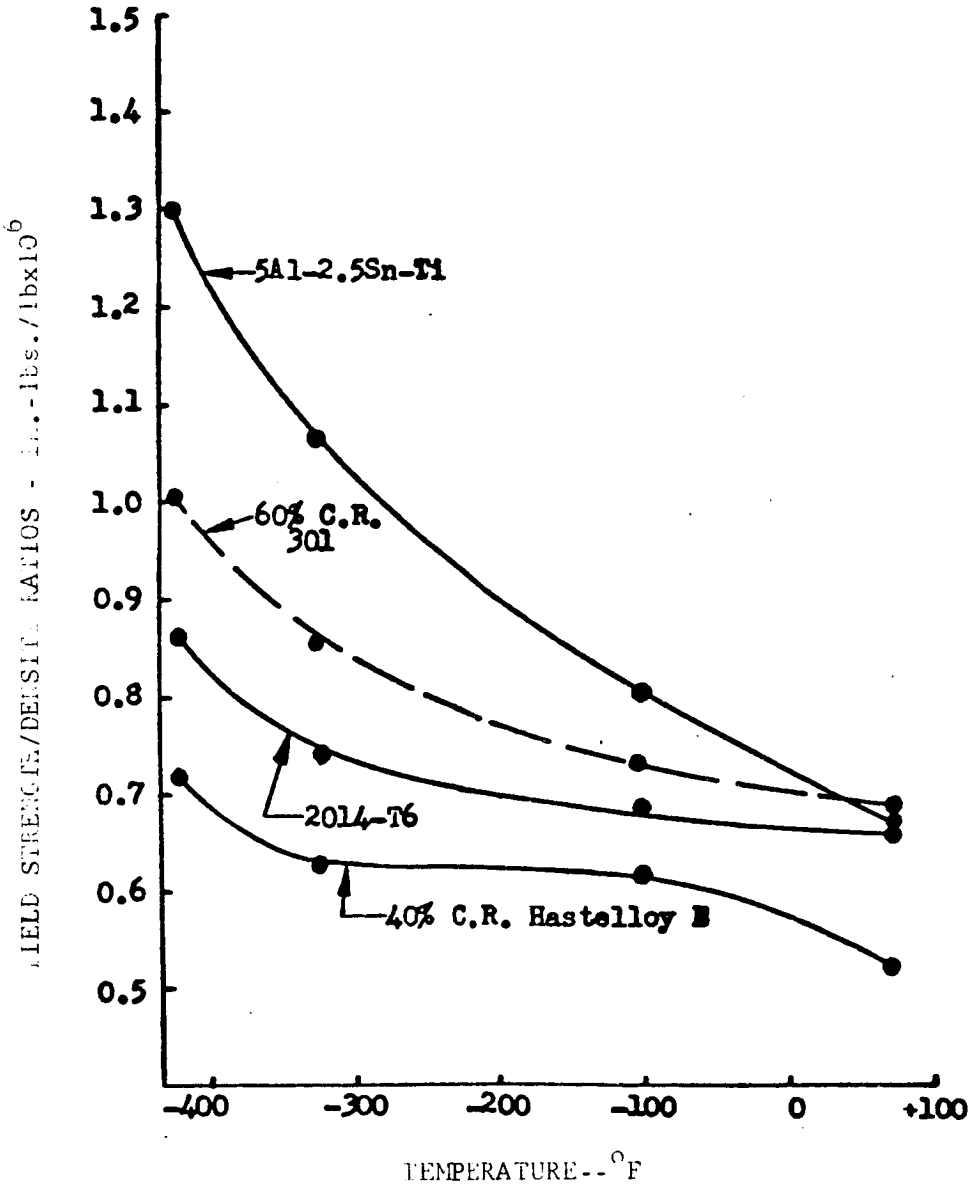

Fig. VII-A-20 Yield Strength Density Ratios vs. Temperature for Various Alloys (Ref. 35)

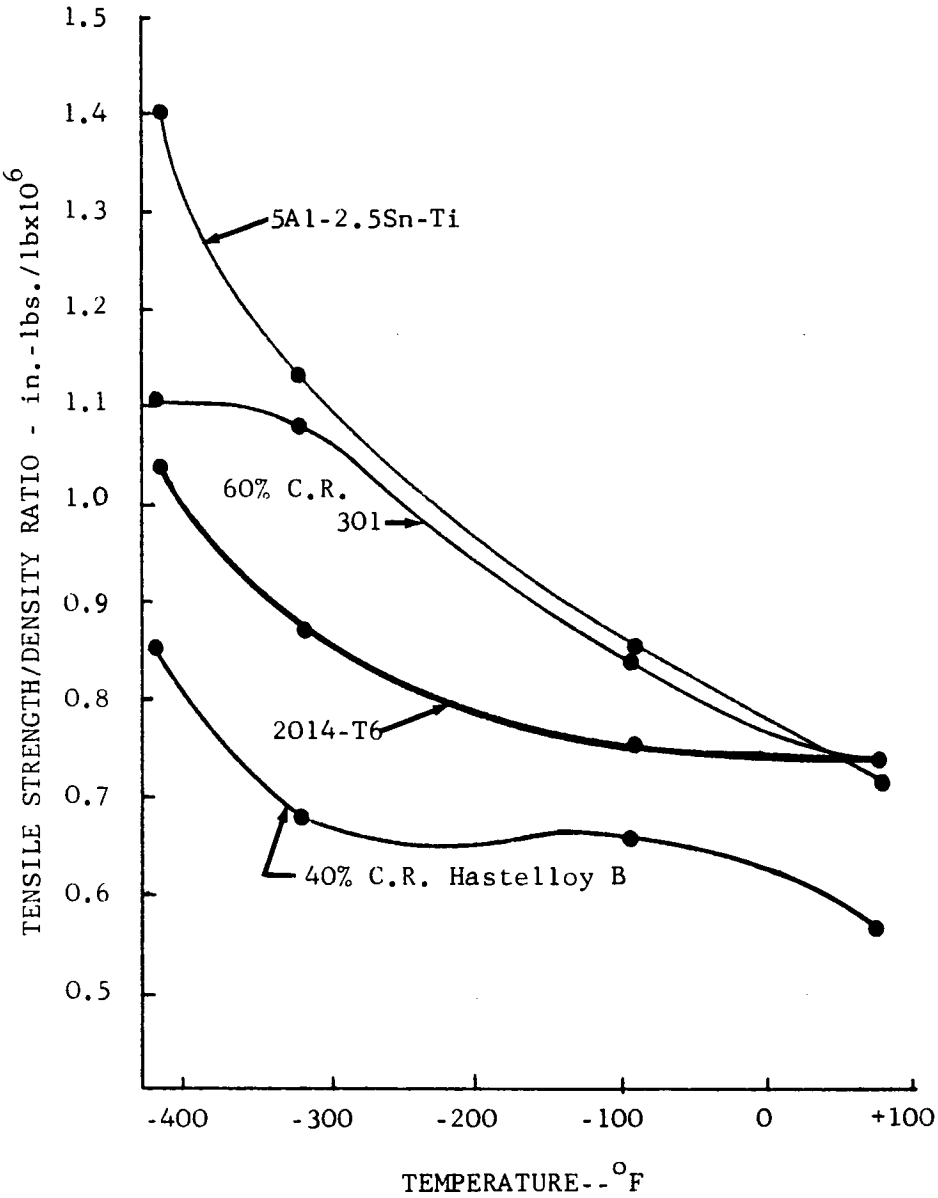

Fig. VII-A-21 Tensile Strength Density Ratios vs. Temperature for Various Alloys (Ref. 35)

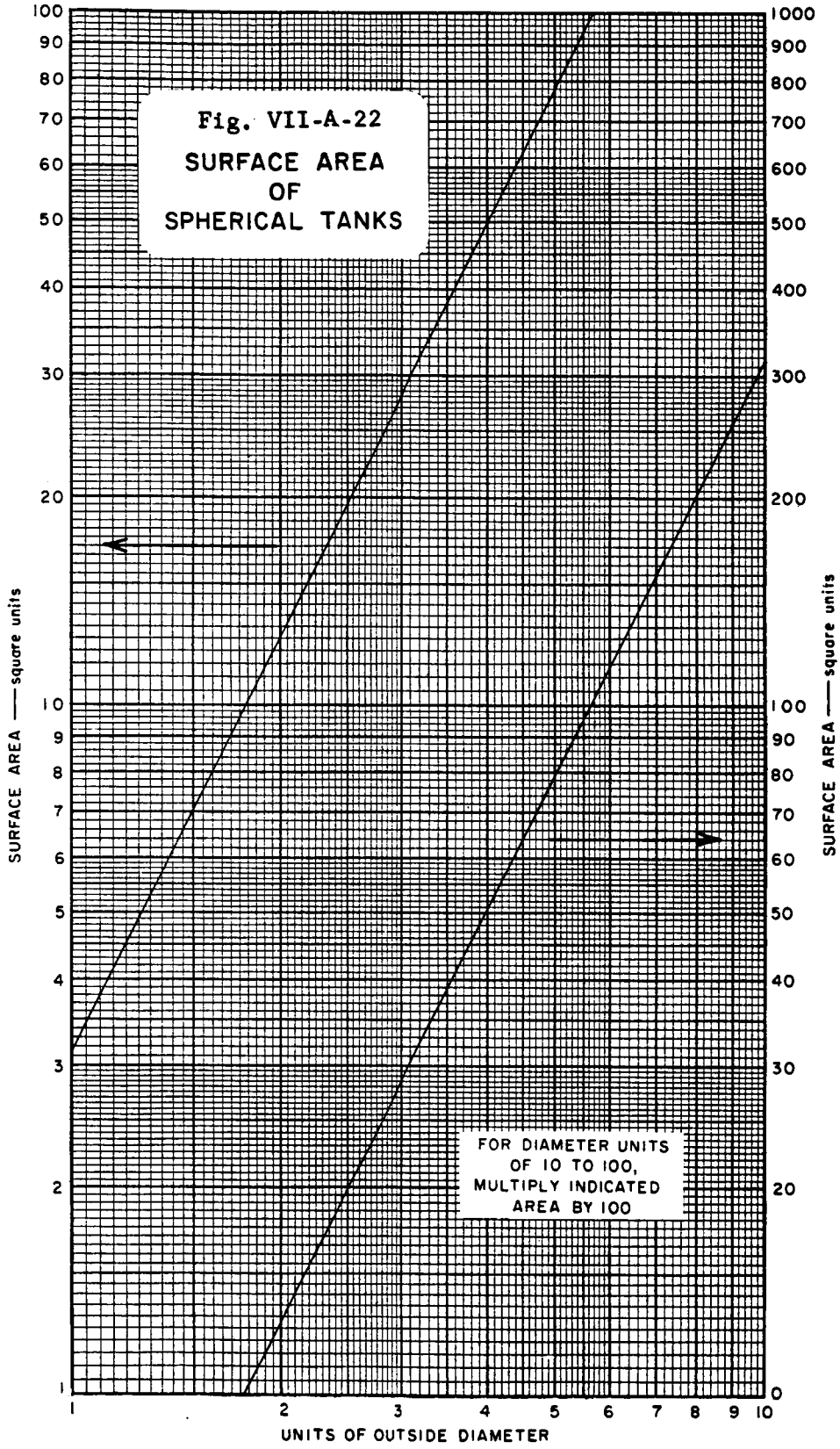
Fig. VII-A-22
SURFACE AREA
OF
SPHERICAL TANKS
FOR DIAMETER UNITS
OF 10 TO 100,
MULTIPLY INDICATED
AREA BY 100
SURFACE AREA —— square units
SURFACE AREA —— square units
UNITS OF OUTSIDE DIAMETER
100
90
80
70
60
50
40
30
20
10
9
8
7
6
5
4
3
2
1
1000
900
800
700
600
500
400
300
200
100
90
80
70
60
50
40
30
20
0
1
2
3
4
5
6
7
8
9
10

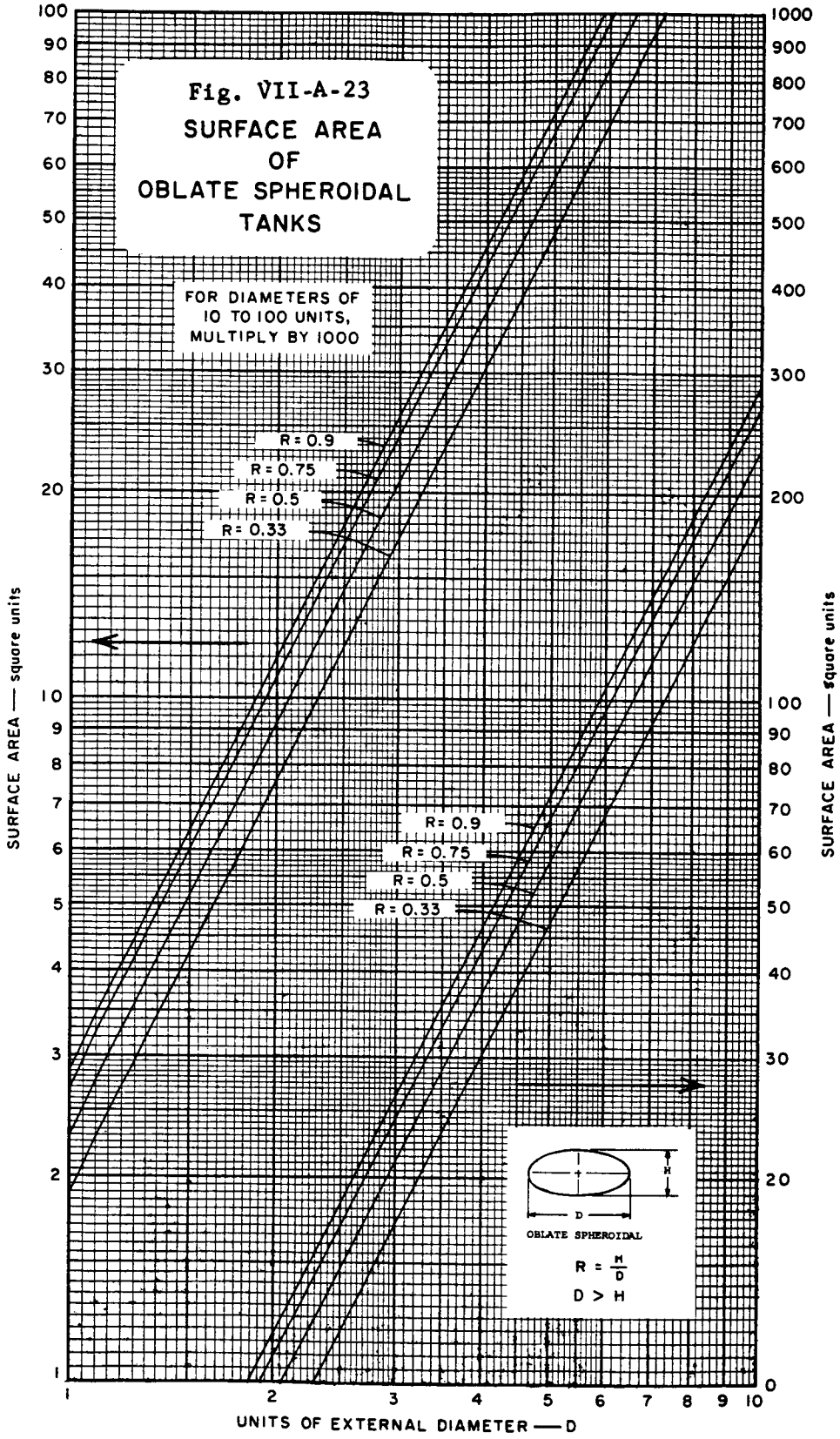
Fig. VII-A-23
SURFACE AREA
OF
OBLATE SPHEROIDAL
TANKS
FOR DIAMETERS OF
10 TO 100 UNITS,
MULTIPLY BY 1000
R = 0.9
R = 0.75
R = 0.5
R = 0.33
R = 0.9
R = 0.75
R = 0.5
R = 0.33
SURFACE AREA — square units
SURFACE AREA — square units
UNITS OF EXTERNAL DIAMETER — D
OBLATE SPHEROIDAL
R = H/D
D > H

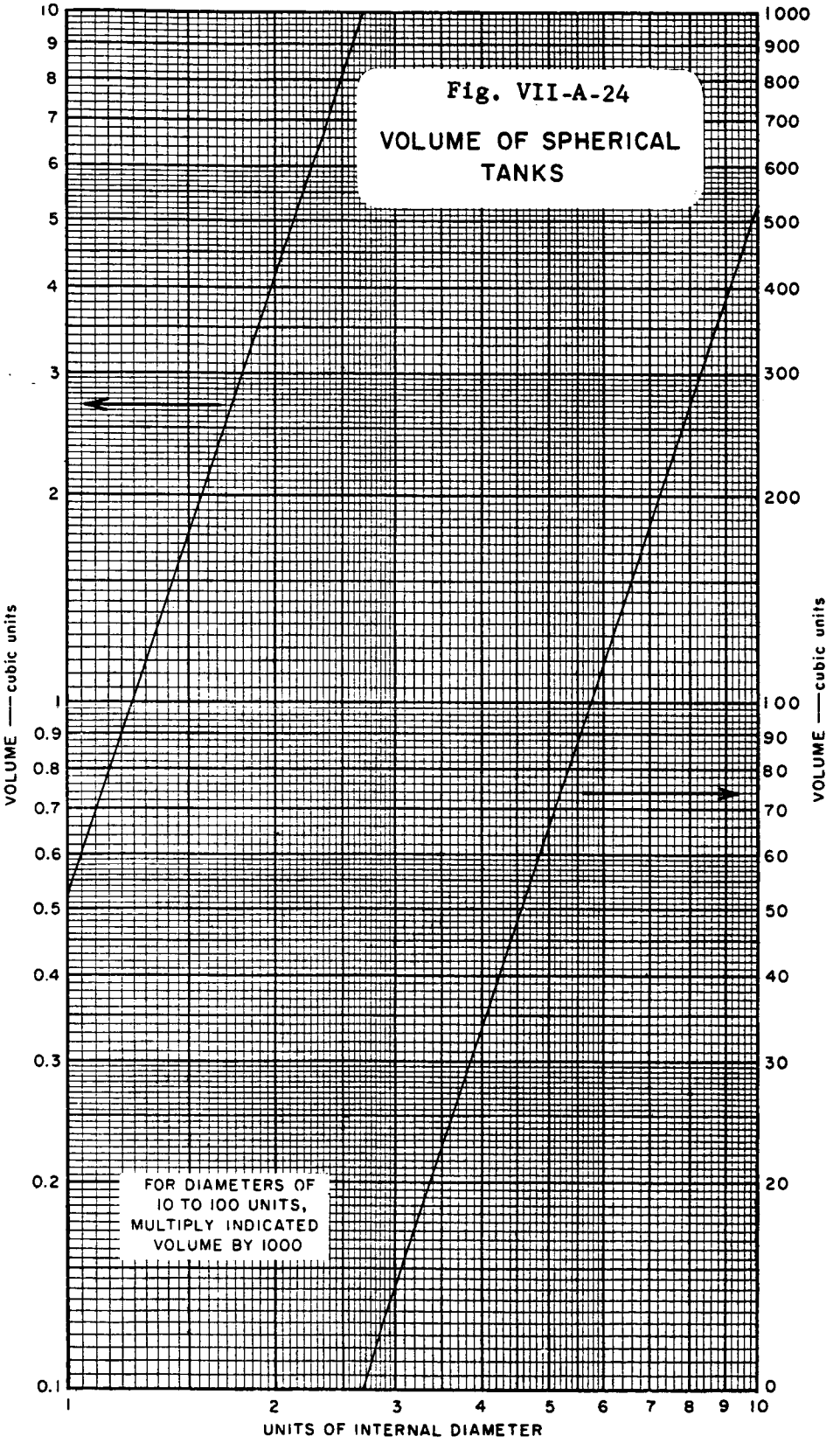
Fig. VII-A-24
VOLUME OF SPHERICAL TANKS
FOR DIAMETERS OF 10 TO 100 UNITS, MULTIPLY INDICATED VOLUME BY 1000
VOLUME — cubic units
UNITS OF INTERNAL DIAMETER
10
9
8
7
6
5
4
3
2
1
0.9
0.8
0.7
0.6
0.5
0.4
0.3
0.2
0.1
1000
900
800
700
600
500
400
300
200
100
90
80
70
60
50
40
30
20
0
1
2
3
4
5
6
7
8
9
10

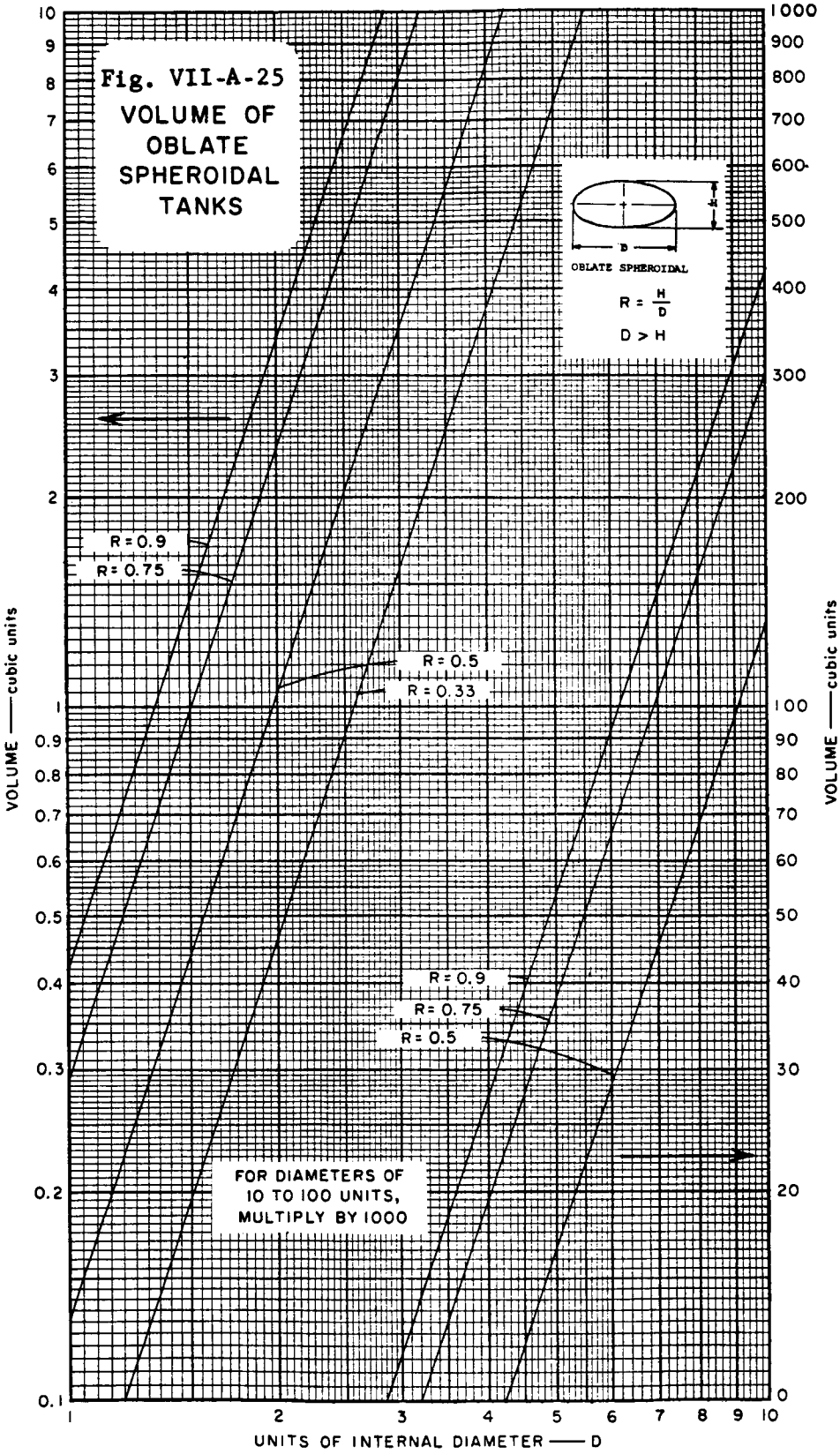
Fig. VII-A-25
VOLUME OF OBLATE SPHEROIDAL TANKS
OBLATE SPHEROIDAL
R = H/D
D > H
R = 0.9
R = 0.75
R = 0.5
R = 0.33
R = 0.9
R = 0.75
R = 0.5
FOR DIAMETERS OF 10 TO 100 UNITS, MULTIPLY BY 1000
VOLUME — cubic units
UNITS OF INTERNAL DIAMETER — D

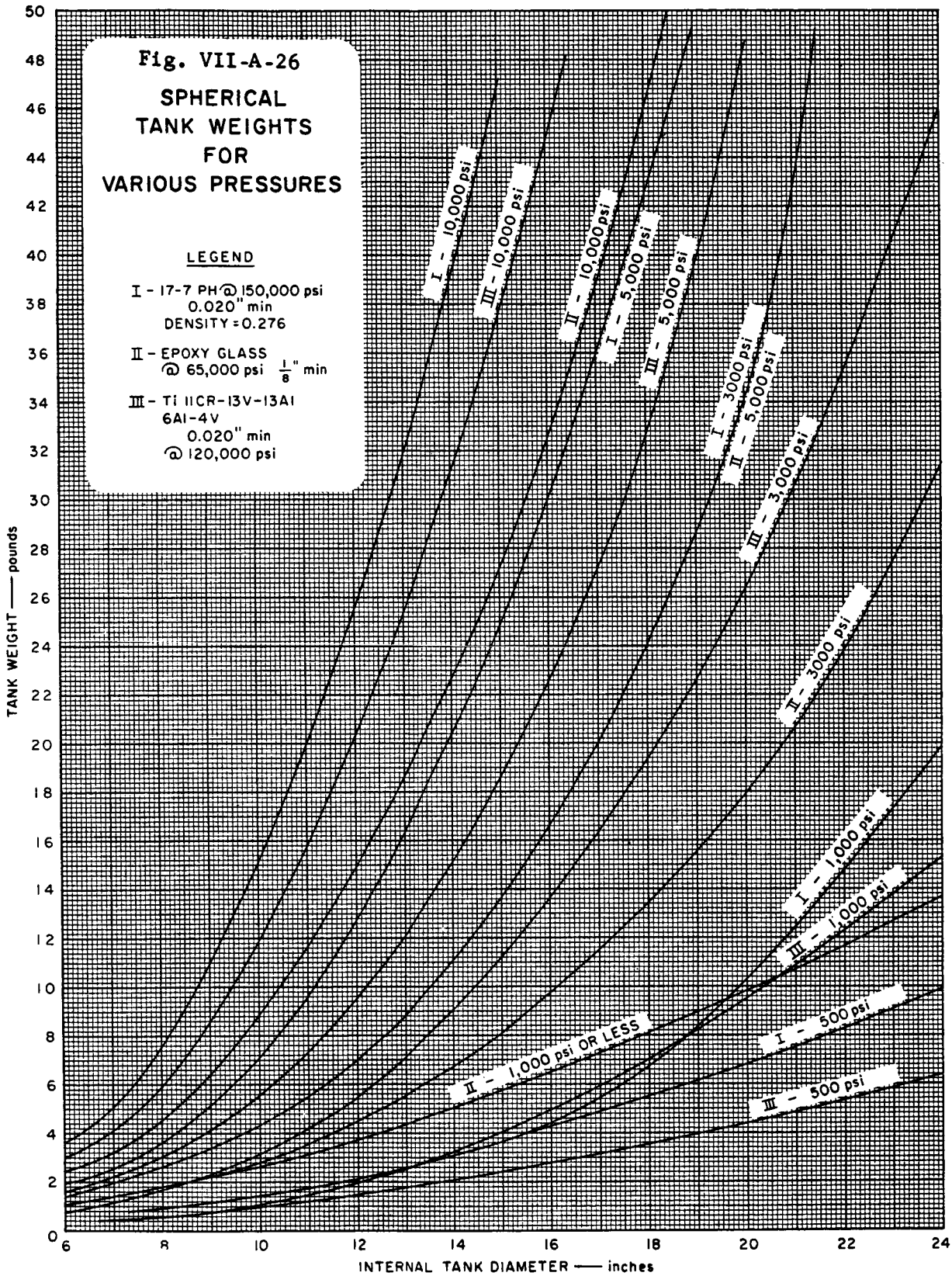
Fig. VII-A-26
SPHERICAL TANK WEIGHTS FOR VARIOUS PRESSURES
LEGEND
I - 17-7 PH @ 150,000 psi 0.020" min DENSITY = 0.276
II - EPOXY GLASS @ 65,000 psi 1/8" min
III - Ti 11CR-13V-13Al 6Al-4V 0.020" min @ 120,000 psi
I - 10,000 psi
III - 10,000 psi
II - 10,000 psi
I - 5,000 psi
III - 5,000 psi
I - 3000 psi
II - 5,000 psi
III - 3,000 psi
II - 3000 psi
I - 1,000 psi
III - 1,000 psi
I - 500 psi
II - 1,000 psi OR LESS
III - 500 psi
TANK WEIGHT —— pounds
INTERNAL TANK DIAMETER —— inches
0
2
4
6
8
10
12
14
16
18
20
22
24
26
28
30
32
34
36
38
40
42
44
46
48
50
6
8
10
12
14
16
18
20
22
24

VIII MATERIALS AND FABRICATION

Table of Contents

Section-Part	Title	Section-Part.Page
VIII-0	List of Tables	VIII-0.2
VIII-0	List of Figures	VIII-0.3
VIII-1	Introduction	VIII-1.1
VIII-2	Properties of Base Materials	VIII-2.1
	Means of Evaluating Mechanical Properties	VIII-2.1
	Properties of Material Between +300°F and Cryogenic Temperatures	VIII-2.4
	Compatability	VIII-2.27
	Delayed Failure	VIII-2.37
	Material Forms and Fabrication	VIII-2.39
VIII-3	Joining	VIII-3.1
	Introduction	VIII-3.1
	Welding Processes Applicable to Vessel Fabrication, Piping, Fittings and Repair	VIII-3.2
	Gas Shielded-Arc Welding	VIII-3.2
	Pressure Welding	VIII-3.7
	Electron Beam Welding	VIII-3.8
	Tubing Joints	VIII-3.11
	Welding Fabrication Variables and the Welding of Particular Alloys	VIII-3.16
	Some Preliminary Design Considerations for Welded Components	VIII-3.16
	Welded Fabrication Variables	VIII-3.17
	The Welding of Specific Alloys	VIII-3.19
	Titanium Alloys	VIII-3.19
	Aluminum Alloys	VIII-3.21
	Cold-Worked Stainless Steels	VIII-3.22
	Inconel 718	VIII-3.23
	Low-Alloy Hardenable Steels	VIII-3.23
VIII-4	References	VIII-4.1

VIII-0 LIST OF TABLES

Section-Part-Table	Table	Section-Part.Page
VIII-2-1	Strength-To-Density Ratios of Titanium Sheet Alloys at Cryogenic Temperatures.....	VIII-2.6
VIII-2-2	Fracture Toughness of 718 Sheet.....	VIII-2.10
VIII-2-3	Mechanical Properties of 2014-T6 Aluminum Alloy 0.063-in. Sheet....	VIII-2.11
VIII-2-4	Mechanical Properties of 2219-T81 Aluminum Alloy 0.063-in. Sheet....	VIII-2.12
VIII-2-5	Strength-To-Density Ratios and Notched-Unnotched Tensile Ratios of 2014-T6 Sheet 0.063-in. Thick.....	VIII-2.12
VIII-2-6	Evaluation of Coating Systems Used for Protection of Aluminum Alloys.....	VIII-2.33
VIII-2-7	Compatability of Selected Metals with Propellents and Oxidizers.....	VIII-2.35
VIII-2-8	Compatability of Selected Non-Metals With Cases and Liquid Propellants.	VIII-2.36
VIII-3-1	Electron Beam Welded Pressure-Vessel Specifications.....	VIII-3.11

VIII-O LIST OF FIGURES

Section-Part-Figure	Title	Section-Part.Page
VIII-2-1	Effect of Test Temperature on Un-Notched and Notched (K_t=21) Tensile Strength of Cryogenic Stretched 301S.S.....	VIII-2.8
VIII-2-2	Typical Tensile Properties of Alloy 718 Sheet.....	VIII-2.9
VIII-2-3	Modulus of Elasticity.....	VIII-2.13
VIII-2-4	Yield Strength of 6Al-4V Titanium...	VIII-2.14
VIII-2-5	Tensile Strength of 6Al-4V Titanium.	VIII-2.15
VIII-2-6	Notched Strength of 6Al-4V Titanium.	VIII-2.16
VIII-2.7	Yield Strength of Annealed 5Al-2.5Sn Titanium.....	VIII-2.17
VIII-2-8	Tensile Strength of Annealed 5Al-2.5 Sn Titanium.....	VIII-2.18
VIII-2-9	Notched Tensile Properties for Three Heats of 5Al-2.5Sn Titanium.....	VIII-2.19
VIII-2-10	Fracture Toughness (K_{Ic}) of 2219-T87 1 inch Thick Plate.....	VIII-2.20
VIII-2-11	Tensile Properties of 2219-T81 and 2219-T87 Aluminum Alloy Sheet....	VIII-2.21
VIII-2-12	Tensile Properties of 2014-T6 and 2014-T62 Aluminum Alloy Sheet in the Longitudinal Direction.....	VIII-2.22
VIII-2-13	Notched Tensile Strength of 2014 Aluminum.....	VIII-2.23
VIII-2-14	Notched Strength Ratio of 2014 Aluminum.....	VIII-2.24
VIII-2-15	Notched Tensile Strength of 2014 Aluminum.....	VIII-2.25
VIII-2-16	Notch Strength Ratio of 2014 Aluminum.....	VIII-2.26
VIII-2-17	Resistance to Stress-Corrosion Cracking of 7075-T6 Plate as Influenced by Direction of Stressing.....	VIII-2.31
VIII-3-1	Arc Column Shape for Gas Tungsten-Arc and Plasma-Arc.....	VIII-3.6

VIII-O LIST OF FIGURES (contd)

Section-Part-Figure	Title	Section-Part.Page
VIII-3-2	Schematic Representation of Pressure Welded Vessel.....	VIII-3.6
VIII-3-3	In-Place Tube Weld Joints.....	VIII-3.13
VIII-3-4	Edge Preparation For Welding In Tubing.....	VIII-3.15
VIII-3-5	Schematic Diagram of a Brazed Tubing Joint.....	VIII-3.15

VIII-1 INTRODUCTION

In this section will be discussed those elements related to materials selection and fabrication, especially welding of pressure vessels. The success of a particular design is obviously dependent upon the depth and quality of consideration given to materials selection and fabrication techniques. One must bear in mind the mechanical behavior of the candidate materials over the entire temperature range to be encountered in service, as well as problems of compatibility between container and material being contained. Welding is an essential fabrication tool, and several welding processes can be considered.

To assure the greatest likelihood of success, it is important that materials engineering (metallurgy) and welding engineering be incorporated as part of the team as early as possible, that is, in preliminary design. By anticipating problem areas and by providing knowledge of fabrication techniques, decisions can be made at this stage which may be inconvenient at later stages.

It is also important at an early point to establish material and fabrication control practices. For critical components, material must be highly pedigreed and adequate records must be maintained regarding all processing steps to assure the highest quality product. Furthermore, welding processes and operators must be qualified by adequate initial and periodic testing to provide that the welding process is under control.

VIII-2 PROPERTIES OF BASE MATERIALS

Means of Evaluating Mechanical Properties

The most important mechanical test imposed upon a pressurized gas system is the system proof test. Coupon testing, such as employed for material and process control purposes or laboratory evaluations, are of secondary importance. The proof test constitutes the final acceptance/rejection criterion prior to total system integration and checkout.

Proof testing conditions obviously depend upon the stresses and other environmental factors which must reflect the anticipated operating conditions.

The selection of proof testing conditions is perhaps one of the most difficult engineering decisions. The conditions obviously depend upon design specifications and operating conditions. However, nontechnical factors (e.g., cost and scheduling limitations) as well as technical compromises may impose significant deviations from the actual or anticipated operating conditions. Proof tests are often performed utilizing pressurizing media which are totally different from that to be employed in the actual system. Ambient temperature tests are sometimes used despite the fact that cryogenic or elevated temperature exposures are involved in actual service. Deviations such as the aforementioned may sometimes represent excessive departures from reality and should be accepted cautiously. For example, the fracture toughness of an alloy may exhibit a marked degradation below some specific temperature (generally termed the transition temperature). Both Ti-6Al-4V and Ti-5Al-2.5Sn alloys exhibit such a transition temperature somewhere between liquid nitrogen (-321°F) and liquid hydrogen (-423°F) temperatures. Susceptibility to catastrophic failure because of fabrication-induced defects (e.g., weld flaws, machining notches, etc.) is greatly magnified below the transition temperature. Tests performed above the transition temperature may result in the acceptance of a truly defective system. Substitution of the pressurizing medium may also result in the acceptance

of an unacceptable condition. For instance, until recently, inhibited water was often used to proof test titanium pressure vessels which were intended for N_2O_4 storage on the assumption that N_2O_4 was totally compatible with these titanium alloys. Testing costs are thereby significantly reduced. However, recent findings indicate that N_2O_4 may promote delayed failure in titanium alloys under certain conditions. Therefore, future tests may require N_2O_4 as a pressurizing medium unless the issue is otherwise resolved.

The lesson derived from the above examples is that proof testing conditions must not be arbitrary and should simulate the actual service conditions as closely as possible. Exact simulation is obviously impossible. Nonetheless, the engineering decisions should be based upon the known material behavior, and arbitrary decisions should be avoided, or if unavoidable, they should be clearly identified as such so that the risks may be estimated.

Generally common to all proof testing is a cyclic or sustained load test. Such a test tends to be conservative compared to a rapid load (single cycle) type of test. The rationale behind a cyclic or sustained load type of proof test is based, at least partially, on the observed cuase of failure of actual pressurized systems. Tiffiny and Masters (Ref. 1) illustrate several typical pressure vessel failures. Characteristically, the fracture origin is usually a small crack or crack-like flaw which existed in the structure prior to testing or service. Fabricated structures will invariably contain such flaws since fabrication processes are not perfect and generally produce defects. The types of potential defects are at least as numerous as the various fabrication processes. Machining may introduce small crack-like surface defects. Forming processes similarly may cause surface fissures. Heat treatments, if performed under poor atmospheric control, may result in surface stress corrosion cracking (e.g., chlorine induced stress-corrosion cracking of titanium alloys). Of all the fabrication processes, welding is probably the cause of the majority of pressure vessel defects. Porosity, lack of fusion, and both weld metal and heat-affected zone cracks may occur.

Furthermore, the case and chemically segregated nature of the weld deposit may often cause an added metallurgical infirmity which, if associated with a crack-like defect, may be especially damaging.

Operational pressures or loads in pressurized gas systems produce gross elastic, not plastic, stress fields during normal service proof testing conditions. Failed pressure bottles, therefore, ordinarily exhibit very little plastically deformed or yielded material. The importance of this cannot be overstated. The strength and operational life of pressurized gas systems must be based upon the fact that fabricated structures contain crack-like flaws. The lives of such real flawed structures are controlled by the flaw size required to cause fracture (termed the critical flaw size) at the particular operating stress level, the initial flaw size, and the sub-critical flaw-growth characteristics of the material (for the particular environmental conditions prevailing in service). Mechanical testing methods must be performed so as to assure the load-carrying ability of a structure containing fabrication-induced flaws. The initial flaw size may be sufficiently large to cause fracture upon initial loading. Alternatively, it may be small enough such that the structure can withstand a number of load cycles and/or a prolonged sustained load before the initial flaw grows to a size sufficient to cause failure. Hence, the use of cyclic or sustained load proof tests provides the opportunity for a "time delay" failure which could be unwittingly overlooked if only a short time static test is employed. The environmental conditions, as previously discussed, are exceedingly important. The rate of flaw growth from a sub-critical size to a size capable of producing failure may be greatly influenced by the environmental conditions (particularly temperature and the pressurizing medium).

Fracture mechanics is the discipline which analyzes and provides a predictive method for establishing the life duration of a flaw-containing structure such as a pressure vessel. Examples of application are described in Section VII-5 of this guidebook and a very comprehensive and complete review may be found in ASTM STP No. 381, "Fracture Toughness Testing and Its Applications."

Properties of Materials Between +300°F and Cryogenic Temperatures

Many factors determine the selection of materials for use in pressurized gas systems. Non-technical factors include cost and availability. The most important material properties are:

a. Strength-to-weight ratio
b. Toughness
c. Fabricability
d. Weldability
e. Modulus-to-weight ratio in cases where stiffness is important
f. Sensitivity to and compatibility with environment
g. Fatigue, especially low cycle

In this Part we will first give a general discussion of the most popular materials used in pressure vessel construction and the reasons for their use. Then a sampling of significant properties, mostly mechanical, between room and cryogenic temperatures will be presented in graphical form. These data presentations will not be comprehensive; many voluminous references can be consulted for implementation. Finally, a discussion of compatibility will be presented in later parts of this Section.

It is first important to discuss the significance of the various material properties. In order to achieve the strongest structure at the lowest weight, one wishes to use the material possessing the highest strength-to-weight ratio. An exception might occur under the circumstance of a material so strong and imposed loads so low that the section thickness would be so small as to have inadequate stiffness. Such a situation might be corrected by optimized design. (See Section VII-2 and 4 for discussions of vessel buckling under internal pressure and general vessel design.)

Materials used in pressurized gas systems must have sufficient toughness to prevent the growth of the largest defects existing in the system over the entire range of operating temperature. The loss in toughness exhibited by many materials at cryogenic temperatures is a strong determinant in selecting optimum alloys for cryogenic applications.

The components of the pressurized gas systems must be formed or shaped in some way and then welded. Fabricability and weldability are thus essential in dictating material selection.

Finally, fatigue or vibration characteristics of materials and structures are important. Low cycle fatigue is often germane even in one-shot systems because of the several proof tests that are imposed.

Although extensive past and current research has and is being performed on a variety of alloy developments and evaluations for cryogenic applications, the number of alloys actually and popularly used in pressurized gas systems is small as of this writing. These are the titanium alloys 6Al-4V and 5Al-2.5Sn with the highest strength-to-weight ratios, cryostretched 301 stainless steel, the nickel base alloy 718, and the aluminum alloys 2014 and 2219. Some vessels containing room temperature gases such as breathing oxygen may have been made of low alloy steels such as AISI4340 or Ladish D6AC. However, such materials are not used at cryogenic temperatures primarily because of their relatively poor toughness at these temperatures. There has been some interest in precipitation-hardenable stainless steels like A286, 17-4PH, and 17-7PH, but a recent survey has not revealed current inclination to apply them to pressurized gas systems. The nickel bearing, maraging steels are a relatively new class undergoing intensive development but here again they have not yet found wide favor in pressurized gas systems, one reason being that welding practices have not yet been routinized.

The two titanium alloys 6Al-4V (C120AV) and 5Al-2.5Sn (A110AT) possess a combination of virtues in their outstanding strength-to-weight ratio, good fabricability, and weldability. The main deterrents to their use in some cases is their impact sensitivity in the presence of liquid and gaseous oxygen, a much lesser impact sensitivity to N_2O_4, and a recently observed stress corrosion problem in the presence of N_2O_4. 6Al-4V is used in the annealed condition (room temperature yield strength from 120 to 155 ksi) or the heat treated condition, which includes solution treatment at 1700°F, water quenching, and aging at 1000°F (room temperature yield strength from 155 to 180 ksi). Although these alloys have been used to contain liquid hydrogen at temperatures down to -423°F, fracture toughness falls off at these temperatures, and there is some feeling in the industry that they should not be used at temperatures below -300°F.

Properties of these alloys are affected by the interstitial content (oxygen, nitrogen and hydrogen) and at least in some cases extra low interstitial grades (ELI) are specified for increased toughness. The higher the interstitial content the higher the strength and the lower the ductility.

Some typical properties of 6Al-4V and 5Al-2.5Sn are presented in Table VIII-2-1. According to these particular data, 5Al-2.5Sn is tougher to lower temperatures than 6Al-4V, but one must bear in mind the effects of such things as form and section size, particular heat treatment, and the presence of welds. Although it is commonly assumed that 5Al-2.5Sn is more weldable than 6Al-4V, the familiarity of a particular fabricator with a given alloy has a large bearing on success in welding. It is probably safe to say that with the current state of the art in the welding of 6Al-4V this material would be the present first choice of most fabricators for pressurized gas bottles because of its highest strength-to-weight ratio, neglecting problems of compatibility.

Table VIII-2-1

STRENGTH-TO-DENSITY RATIOS OF TITANIUM SHEET ALLOYS AT CRYOGENIC TEMPERATURES (Ref. 2)

ALLOY	TEST TEMP. °F	F_{ty}, psi/ DENSITY lbs/cu in x10^6	F_{tu}, psi/ DENSITY lbs/cu in x10^6	NOTCHED-UNNOTCHED TENSILE RATIO (K_t=6.3)	GAUGE	DENSITY
6Al-4V (Annealed)	+ 78	0.76	0.88	1.06	0.063	0.16
	-100	0.81	1.07	0.93		
	-320	1.13	1.36	0.89		
	-423	1.38	1.55	0.71		
5Al-2.5Sn	+ 78	0.70	0.74	1.34	0.040	0.161
	-100	0.84	0.88	1.22		
	-320	1.14	1.22	1.15		
	-423	1.43	1.52	0.97		

From the beginning of the space effort cold worked 300-series stainless steels have been attractive for cryogenic applications because of their combinations of strength-to-weight ratio, low temperature toughness, excellent formability, and good weldability and corrosion resistance. A relatively new modification which yields even higher strength-to-weight ratio is the cryogenic stretch forming of 301 stainless steel. Room temperature yield strength-to-density ratios exceeding 1,000,000 inches are reported by the commercial developers* of the process. Following are some of their data.[3,4]

Material	Yield Strength, psi	Density, lbs/cu-in	Strength-to-Density Ratio, inches
Ardeformed 301 SS			
Unaged	240,000	0.28	855,000
Aged	300,000	0.28	1,070,000
Ti-6Al-4V	147,000	0.16	920,000

In making cylindrical or spherical pressure vessels by cryogenic stretch forming, an undersize vessel is first made by conventional fabrication and welding methods. The preform is then cooled to -320°F and expanded to size (12 to 14% stretch for cylinders and 7-8% stretch for spheres) by internal pressurization with liquid nitrogen. The plastic deformation at -320°F transforms metastable austenite to martensite. Strength can then be further increased by a subsequent aging treatment at 800°F, typically for 20 hrs.

It is found that mechanical properties are sensitive to compositional variations that still lie within the 301 specifications, and current research is directed toward optimum compositions.

Among the advantages claimed for cryogenically stretched 301 SS, the following are perhaps the most significant:

1. High strength-to-weight ratio
2. Elimination of necessity for high temperature heat treatment of finished sized assembly
3. The stretching operation serves as a quality control measure for base material and welds

*Arde-Portland Inc., Paramus, N.J. who call their process Ardeforming.

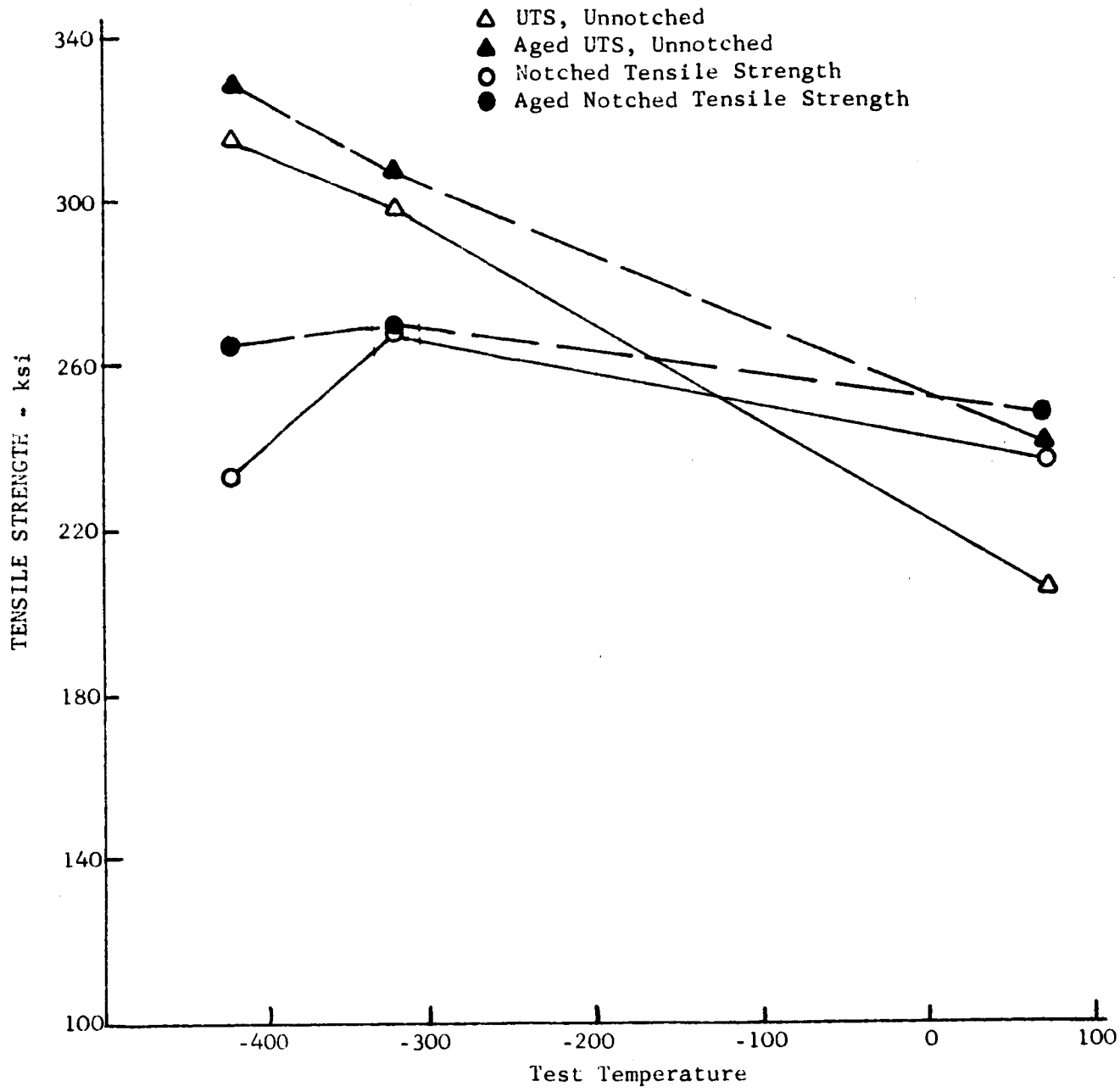

Fig. VIII-2-1. Effect of Test Temperature on Unnotched and Notched (K_t=21) Tensile Strength of Cryogenically Stretched 301 S.S. (Ref. 4)

Some unnotched and notched data (K_t = 21) for cryogenic temperature testing of cryogenically stretched 301 SS are shown in Figure VIII-2-1.

The highest strength nickel base alloy currently available is Inconel 718. It is an age hardening alloy containing nominally 19% each of Cr and Fe and lesser percentages of Mo, Cb, Ti, Al, C and B. Although it was primarily intended for use at elevated temperatures, it has assumed an important role for cryogenic applications because of the exceptionally good mechanical properties at room and cryogenic temperatures of the base metal and of weldments, because of its excellent formability and weldability, and because of its compatibility with cryogenic fluids. The solution treating temperature is in the range 1700-1800°F and the aging temperature around 1325°F. From the fabrication point of view, 718 possesses the virtue that weldments can be aged directly without resolution heat treatments.

Typical tensile properties of 718 sheet are given in Figure VIII-2-2 and fracture toughness data in Table VIII-2-2. From the Table it can be seen that tensile strength-to-density ratios range from 670,000 to 8,777,000 inches between +300° and -320°F.

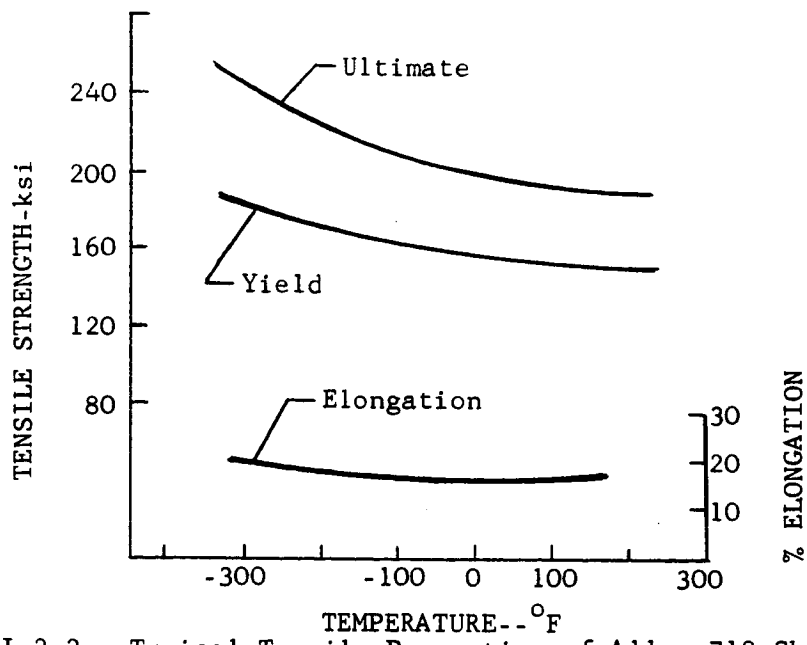

Fig. VIII-2-2. Typical Tensile Properties of Alloy 718 Sheet. (Ref. 10).

Table VIII-2-2

FRACTURE TOUGHNESS OF 718 SHEET (Ref. 5)

TEST TEMP., F	MELT NO.	THICKNESS, INCHES	THERMAL TREATMENT	YIELD STRENGTH 0.2% OFFSET, 1000 psi	TENSILE STRENGTH 1000 psi	ELONGATION %	NOTCHED TENSILE STRENGTH 1000 psi	Kc	TS/D	NTS/TS	NTS/YS	FRACTURE % SHEAR
-110	Y 8455	0.027	CRAH	168.5	212.0	25.0	195.5	-	713,000	0.92	1.16	100
85	Y 8455	0.027	CRAH	163.0	196.0	21.0	183.0	-	670,000	0.93	1.11	100
85*	Y 8455	0.027	CRAH	162.5	197.0	21.0	178.0	-	-	0.91	1.10	100
350	Y 8455	0.027	CRAH	153.0	191.0	20.0	-	-	-	-	-	-
650	Y 8455	0.027	CRAH	141.5	171.5	20.0	158.0	-	578,000	0.92	1.11	100
650*	Y 8455	0.027	CRAH	137.5	172.0	23.0	163.0	-	-	0.95	1.19	100
800	Y 8455	0.027	CRAH	141.0	188.0	23.0	156.0	-	-	0.83	1.22	100
1000	Y 8455	0.027	CRAH	135.0	169.0	24.0	143.0	-	570,000	0.85	1.25	100
-320	Y 8455	0.027	CRH	229.0	260.5	13.0	236.5	196.0	877,000	0.91	1.03	100
-110	Y 8455	0.027	CRH	206.5	232.0	17.0	209.0	185.5	781,000	0.88	1.01	100
85	Y 8455	0.027	CRH	198.5	221.0	12.0	196.5	174.5	745,000	0.89	0.99	100
85*	Y 8455	0.027	CRH	195.5	212.0	13.0	199.0	179.5	-	0.94	1.02	100
350	Y 8455	0.027	CRH	188.5	205.0	12.0	179.7	157.0	-	0.88	0.96	100
650	Y 8455	0.027	CRH	179.0	193.5	12.0	173.5	147.5	652,000	0.90	0.97	100
650*	Y 8455	0.027	CRH	182.0	198.5	13.0	172.0	150.0	-	0.87	0.95	100
800	Y 8455	0.027	CRH	-	-	-	169.0	-	-	-	-	100
1000	Y 8455	0.027	CRH	165.3	180.5	10.0	166.5	145.5	608,000	0.92	1.01	100
85	Y 8548	0.040	CRH	197.5	214.5	13.0	205.5	196.5	720,000	0.96	1.04	100
85	HT 4680 E	0.050	CRH	193.5	210.5	12.0	201.5	200.5	710,000	0.96	1.04	100

*--Stressed at 40,000 psi for 1000 hours at 650°F prior to testing.
CRAH--Cold rolled; annealed 1800°F/1 hour; aged 1325°F/8 hours, FC 20°/hour to 1150°F, AC.
CRH--Cold rolled; aged 1325°F/8 hours, FC20°/hour to 1150°F, AC.
Kc--Fracture toughness parameter, 1000 psi $\sqrt{\text{inch}}$.
TS/D--Tensile strength divided by room temperature density of alloy (0.297 lb/cu in).
NOTE--All tests transverse.

Of the aluminum alloys, the aluminum-copper 2014 and 2219 are favored for tankage over the 5000 magnesium bearing series or the 7000 zinc-copper-magnesium series. 2014 and 2219 have the best combination of strength, low temperature toughness, weldability, and formability. These alloys are heat treatable by an age hardening mechanism, an intermetallic compound of aluminum and copper (CuAl) being the hardening second phase. Solution treatment is performed in the temperature range from 900°F to 1000°F and aging at 200°F to 400°F. The T87 condition is sometimes used on 2219; this involves 7% straining prior to aging.

Some typical properties of 2014-T6 and 2219-T81 are given in Tables VIII-2-3 and VIII-2-4.

Table VIII-2-3

MECHANICAL PROPERTIES OF 2014-T6 ALUMINUM ALLOY 0.063-in. SHEET (Ref. 2)

TEST TEMP., °F	DIRECTION	F_{ty}, ksi	F_{tu}, ksi	ELONG. %	NOTCHED TENSILE STRENGTH, ksi (K_t = 6.3)	NOTCHED-UNNOTCHED TENSILE RATIO
+ 78	Long.	65.7	73.1	11	74.5	1.02
+ 78	Trans.	62.8	71.5	11	70.0	0.98
-100	Long.	69.3	76.4	12	79.2	1.04
-100	Trans.	63.3	74.1	11	71.0	0.96
-320	Long.	74.4	87.1	14	85.5	0.98
-320	Trans.	70.3	78.7	14	78.7	1.00
-423	Long.	86.2	104.0	17	97.8	0.94
-423	Trans.	82.3	102.0	15	84.5	0.83

Table VIII-2-4

MECHANICAL PROPERTIES OF 2219-T81 ALUMINUM ALLOY 0.063-in. SHEET (Ref. 2)

TEST TEMP., °F	DIREC-TION	F_{ty}, ksi	F_{tu}, ksi	ELONG. %	NOTCHED TENSILE STRENGTH ksi (K_t = 6.3)	NOTCHED-UNNOTCHED TENSILE RATIO
+ 78	Long.	52.0	67.5	10	64.4	0.95
+ 78	Trans.	51.0	67.2	10	66.0	0.98
-100	Long.	56.7	73.3	9	68.6	0.94
-100	Trans.	54.7	72.3	10	67.0	0.93
-320	Long.	62.2	85.2	11	77.4	0.91
-320	Trans.	61.4	84.6	12	76.1	0.90
-423	Long.	70.6	102.0	15	93.4	0.92
-423	Trans.	67.5	102.0	15	91.3	0.90

Some of the data from Table VIII-2-3 on 2014-T6 are converted to strength-to-density ratios in Table VIII-2-5.

Table VIII-2-5

STRENGTH-TO-DENSITY RATIOS AND NOTCHED-UNNOTCHED TENSILE RATIOS OF 2014-T6 SHEET 0.063 IN. THICK (DENSITY = 0.10 lb/in^3)(Ref. 2)

TEST TEMP °F	F_{ty}, psi/DENSITY lb/cu in x 10^6	F_{tu}, psi/DENSITY lb/cu in x 10^6	NOTCHED-UNNOTCHED TENSILE RATIO (K_t=6.3)
+ 78	0.66	0.73	1.02
-100	0.69	0.76	1.04
-320	0.74	0.85	0.98
-423	0.86	0.98	0.94

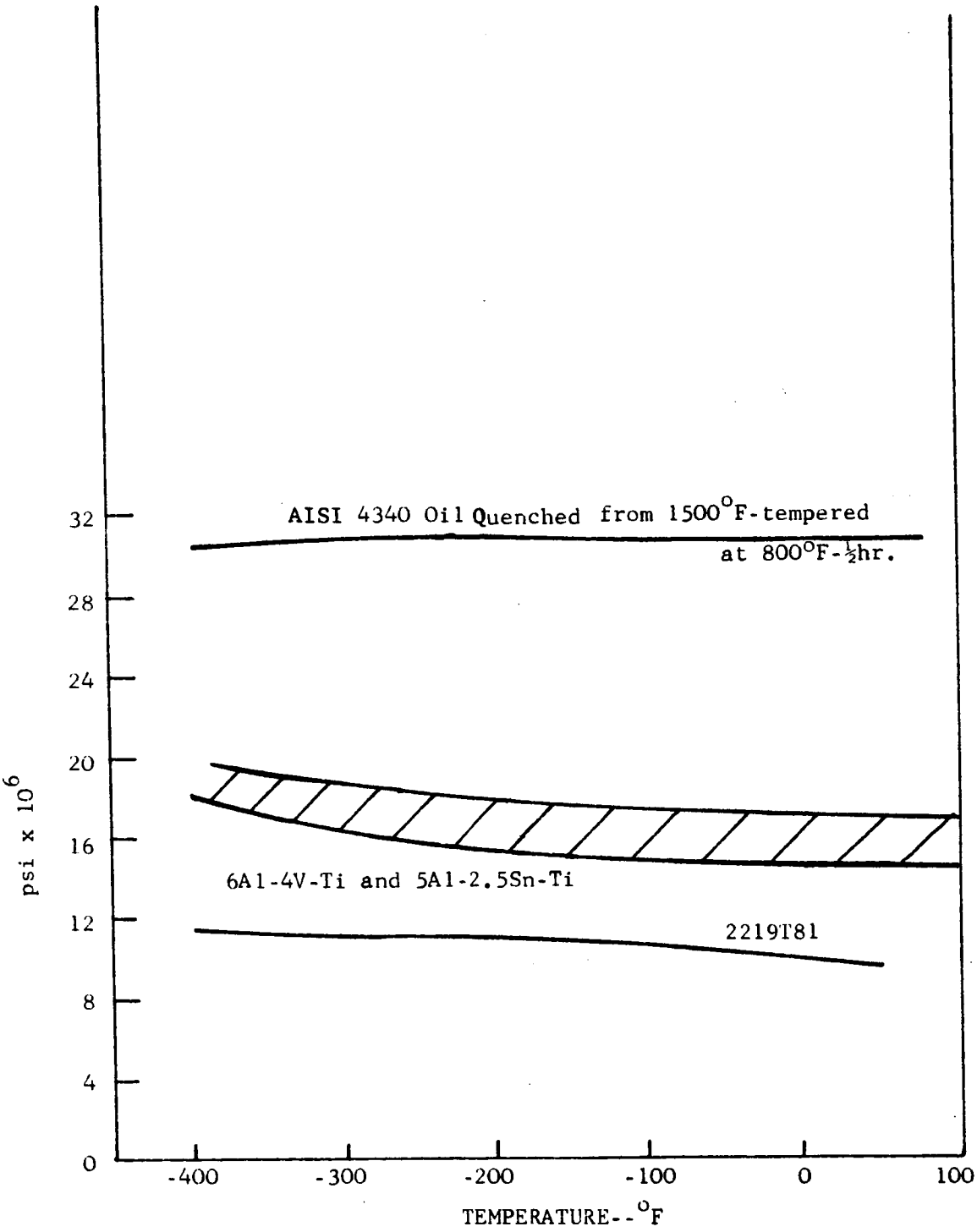

Fig. VIII-2-3. Modulus of Elasticity. (Ref. 9)

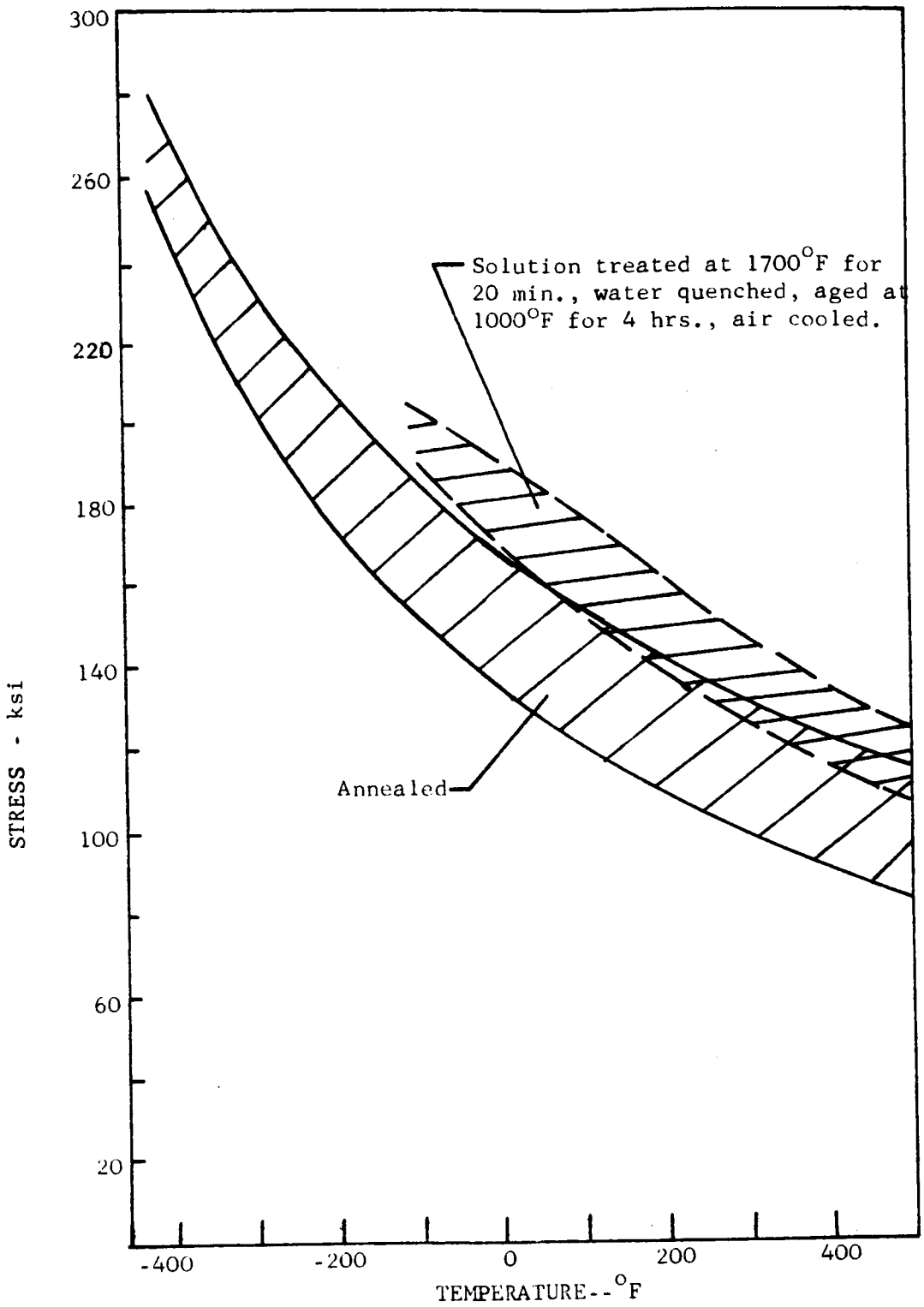

Fig. VIII-2-4. Yield Strength of 6Al-4V Titanium. (Ref. 9)

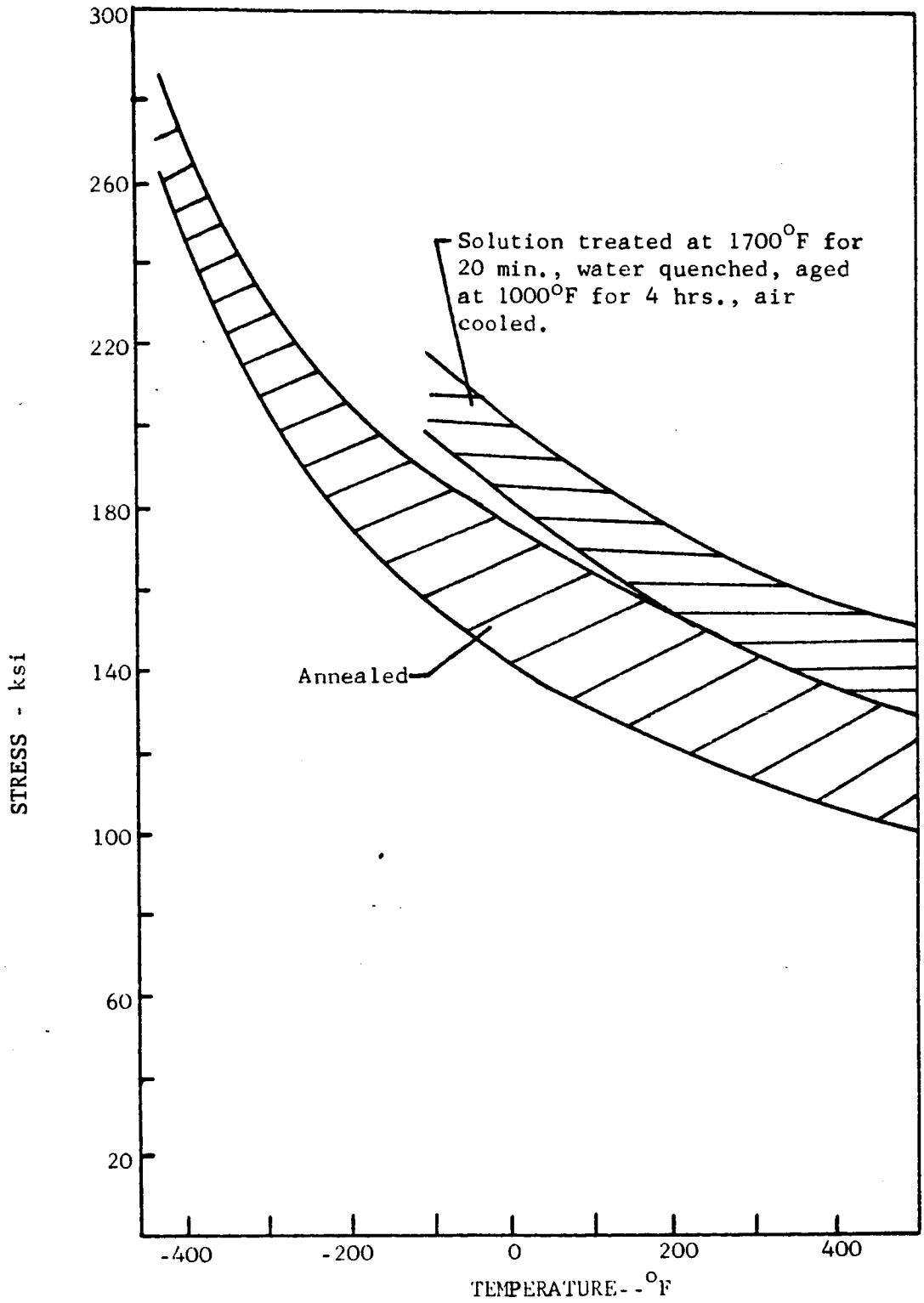

Fig. VIII-2-5. Tensile Strength of 6Al-4V Titanium. (Ref. 9)

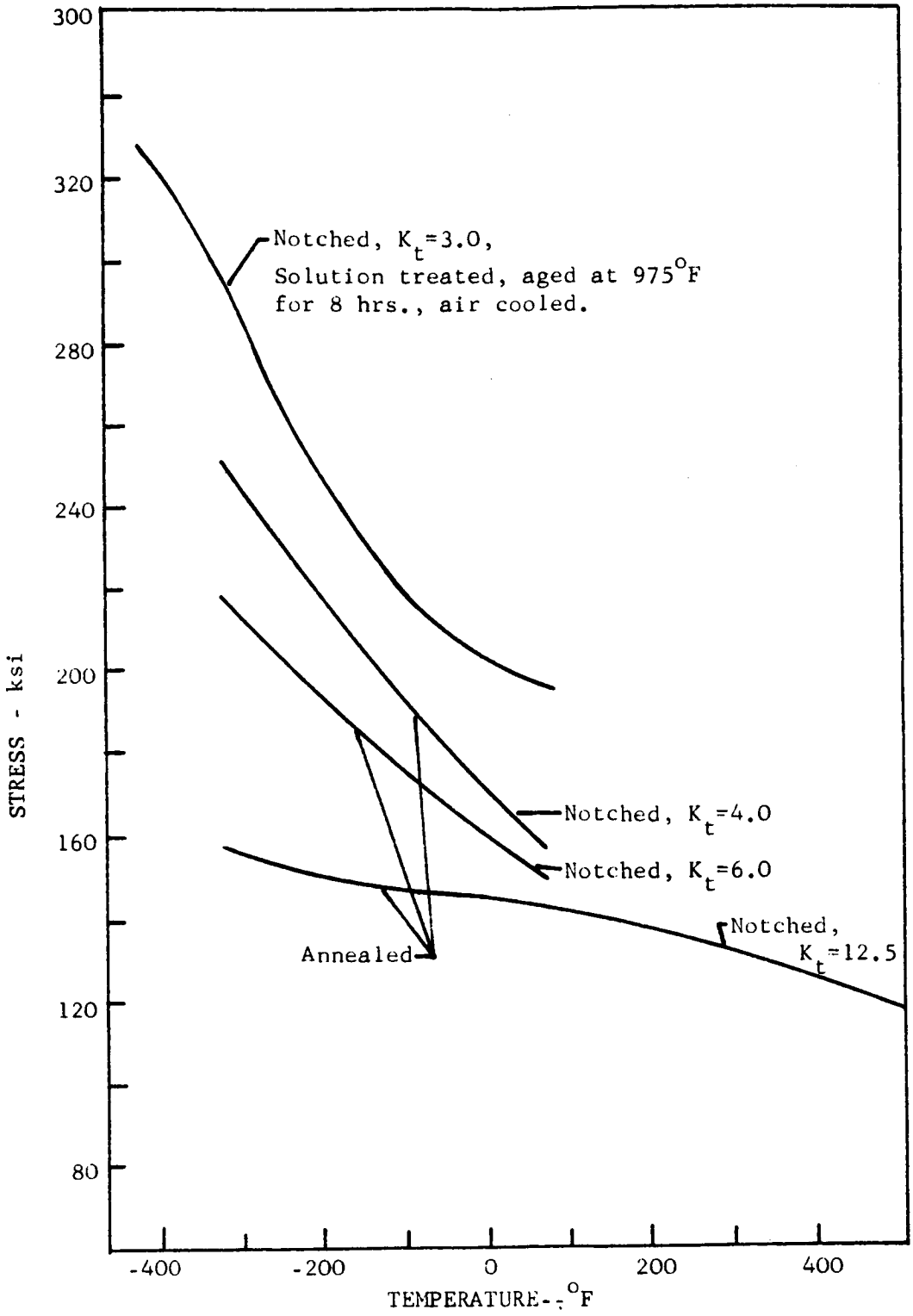

Fig. VIII-2-6. Notched Strength of 6Al-4V Titanium. (Ref. 9)

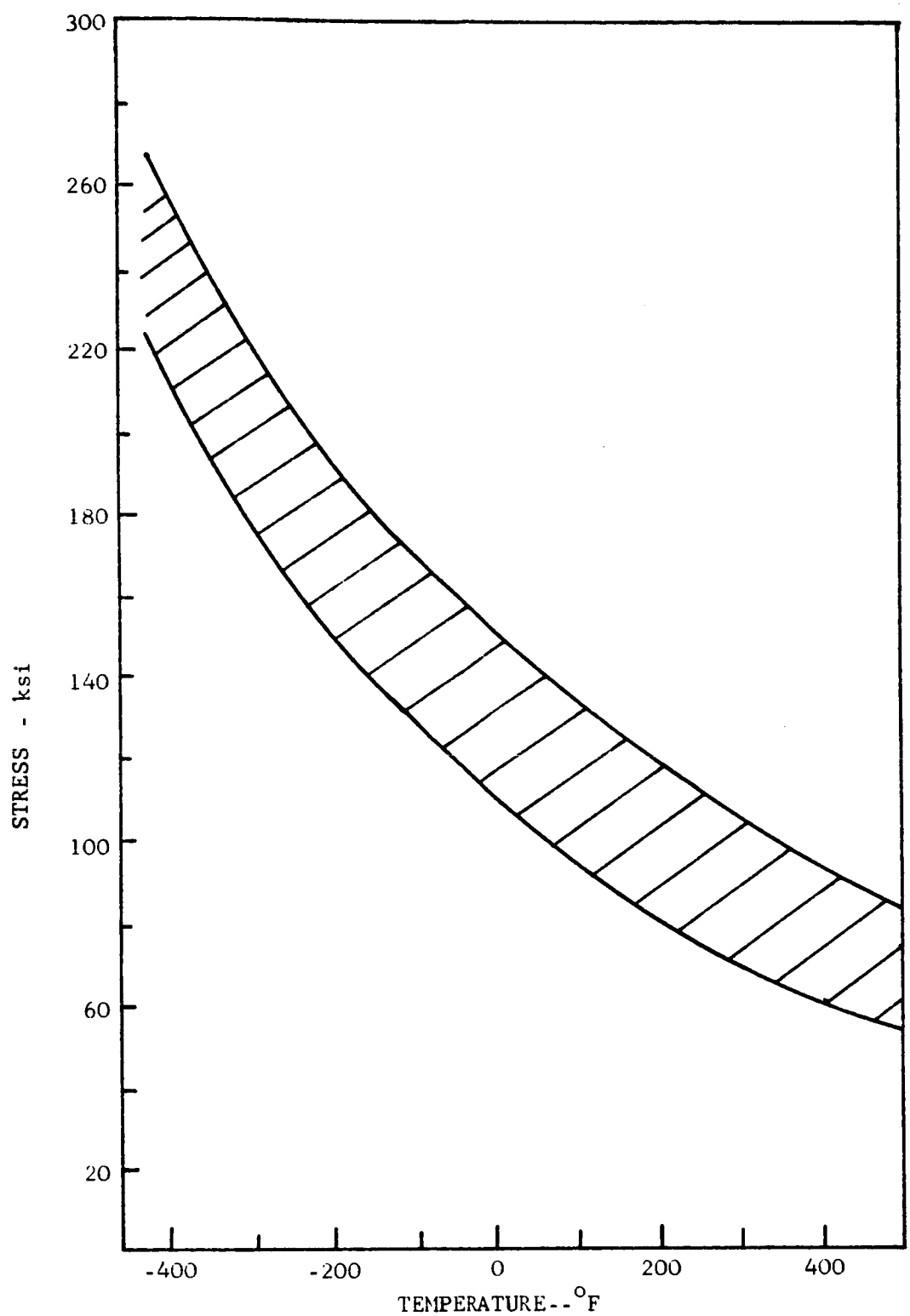

Fig. VIII-2-7. Yield Strength of Annealed 5Al-2.5Sn Titanium. (Ref. 9)

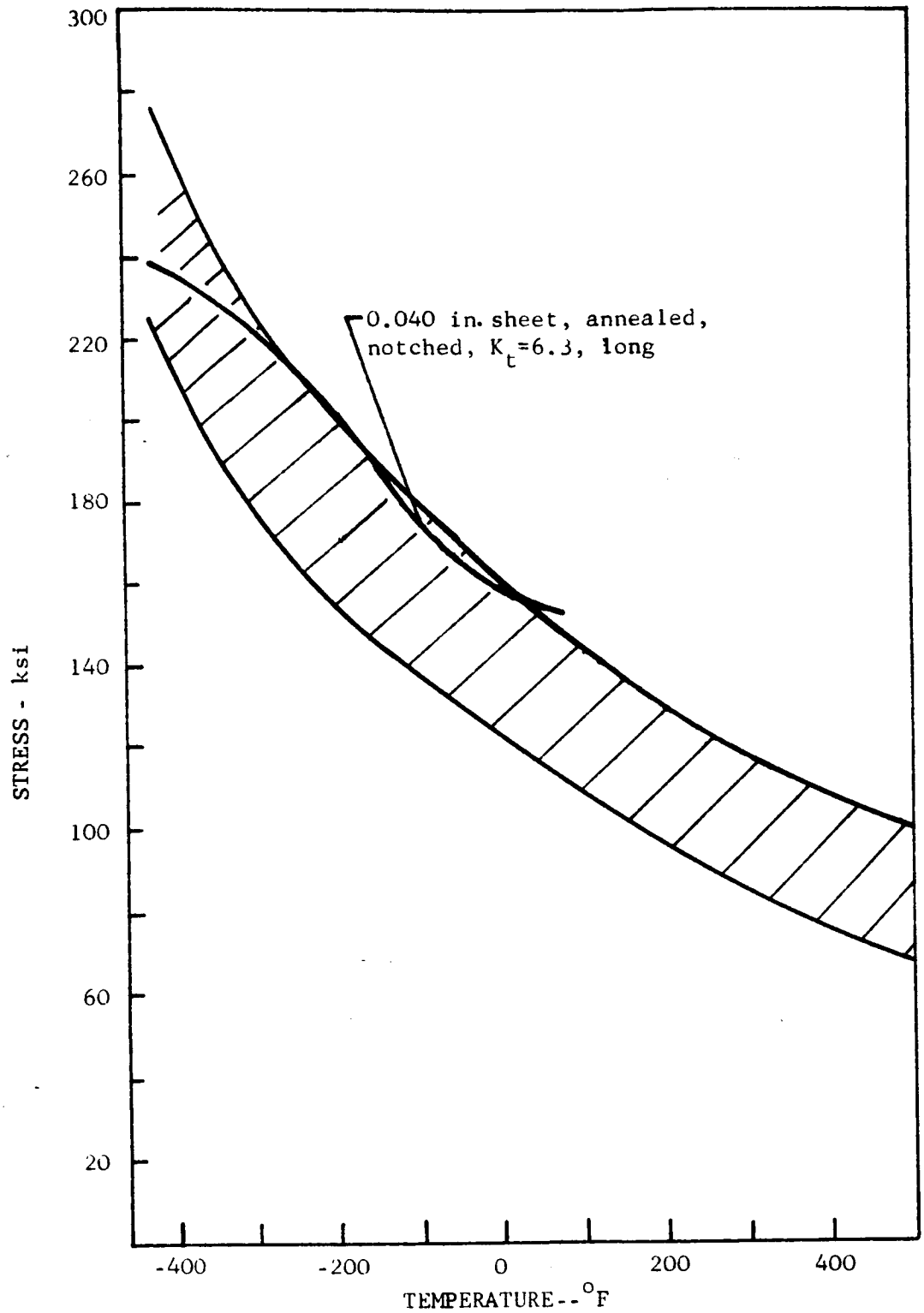

Fig. VIII-2-8. Tensile Strength of Annealed 5Al-2.5Sn Titanium. (Ref. 9)

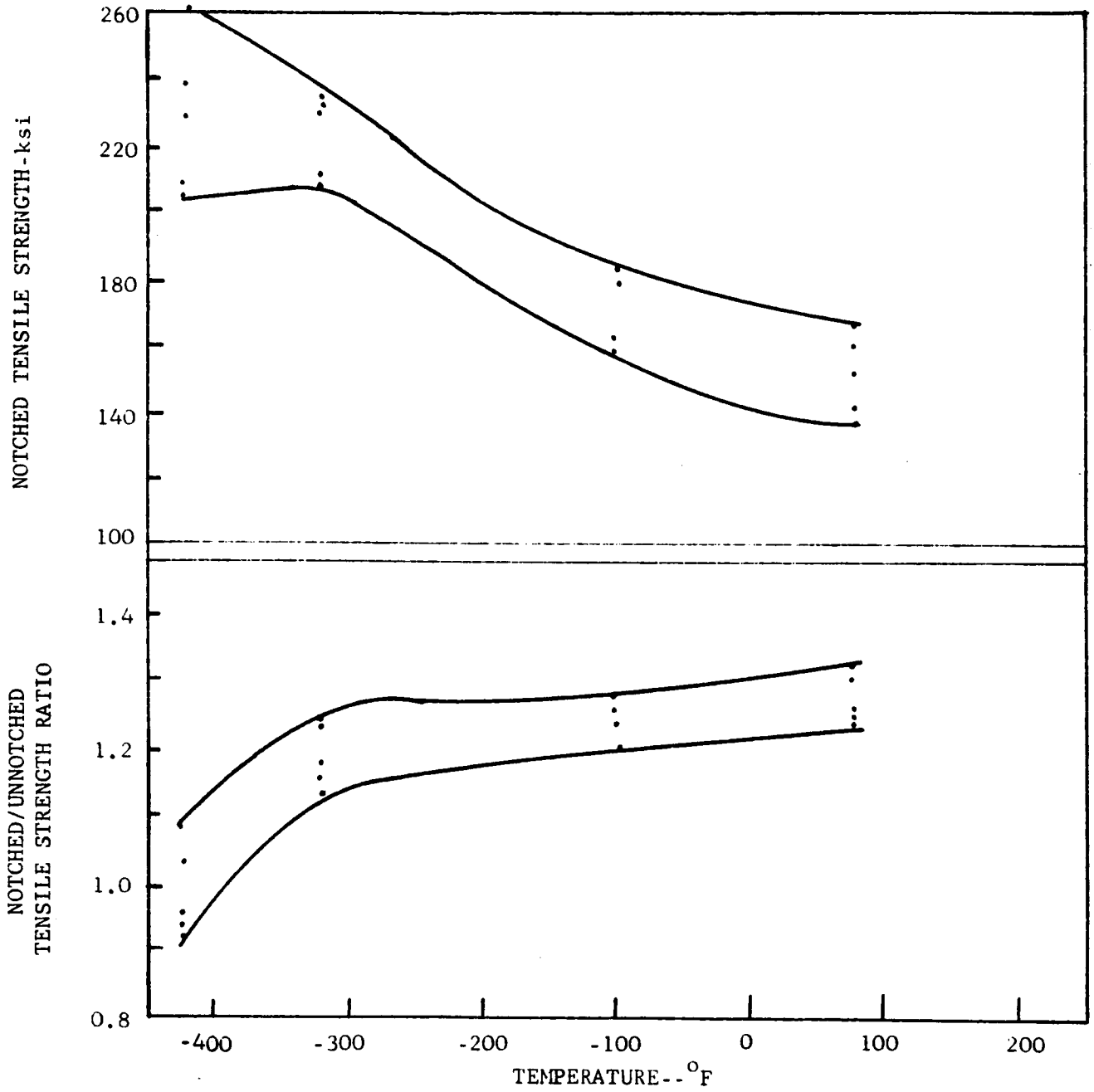

Fig. VIII-2-9. Notched Tensile Properties for Three Heats of 5Al-2.5Sn Titanium. (Ref. 6).

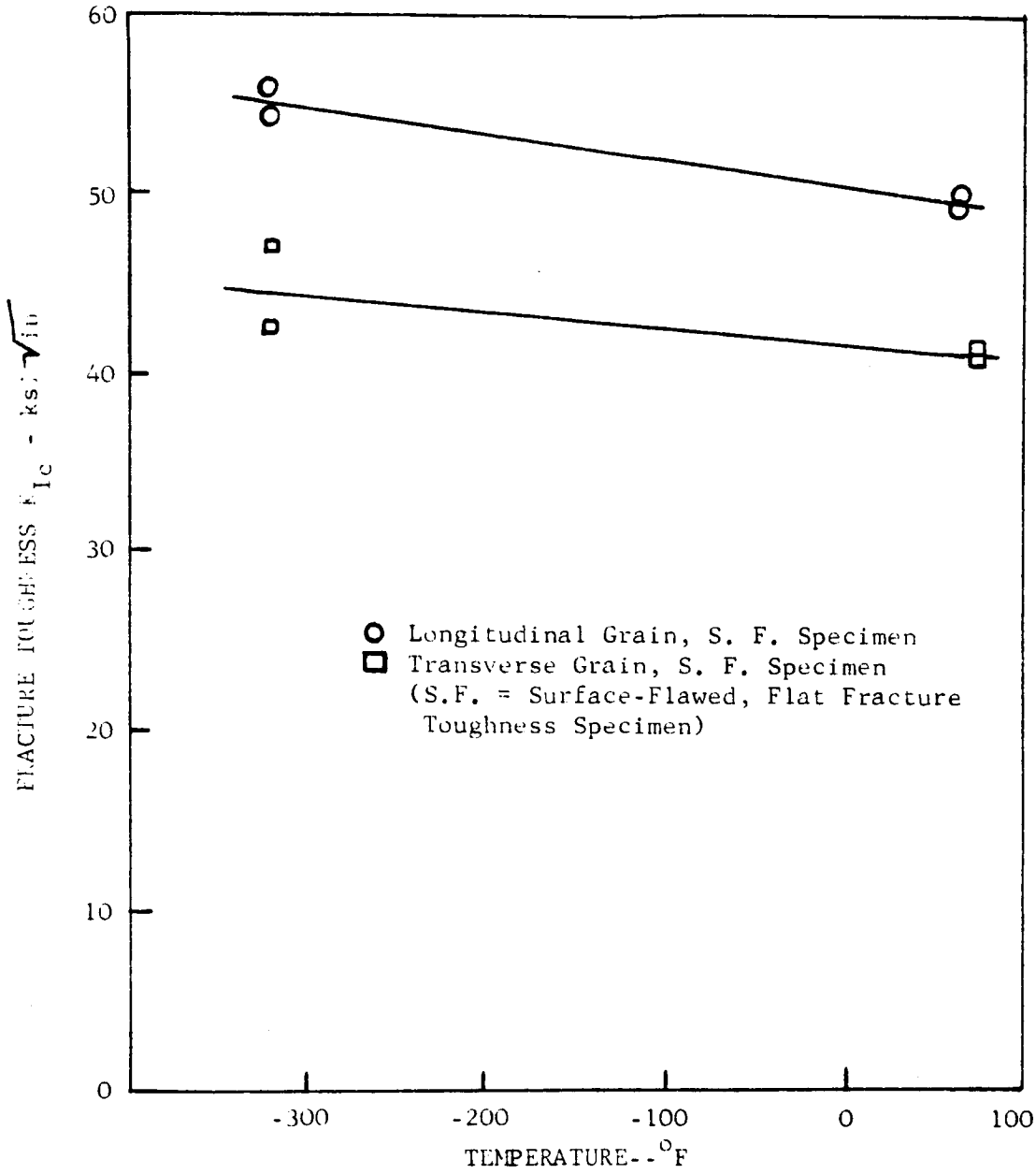

Fig. VIII-2-10. Fracture Toughness (K_{Ic}) of 2219-T87 1 inch Thick Plate. (Ref. 7).

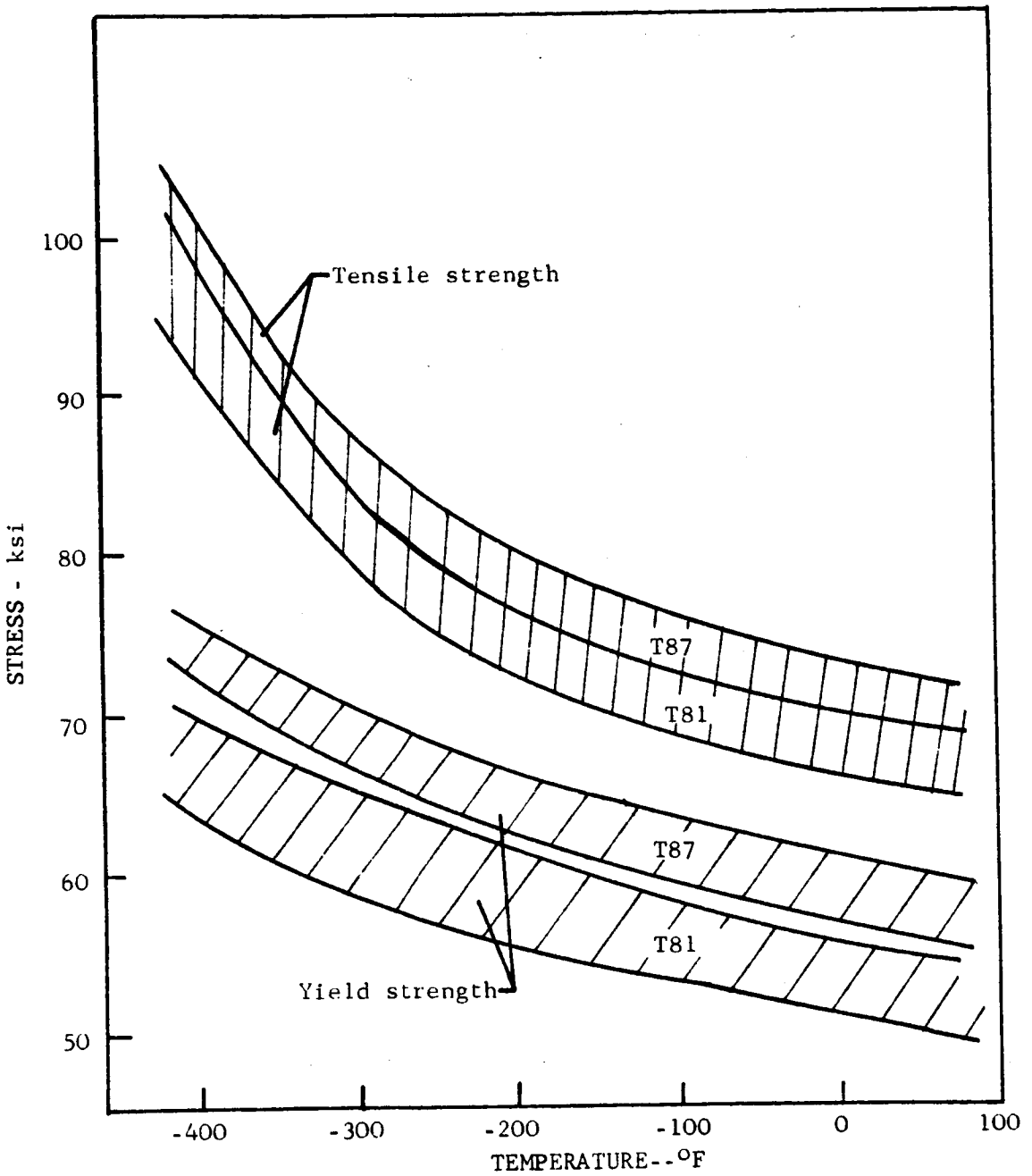

Fig. VIII-2-11. Tensile Properties of 2219-T81 and 2219-T87 Aluminum Alloy Sheet. (Ref. 8).

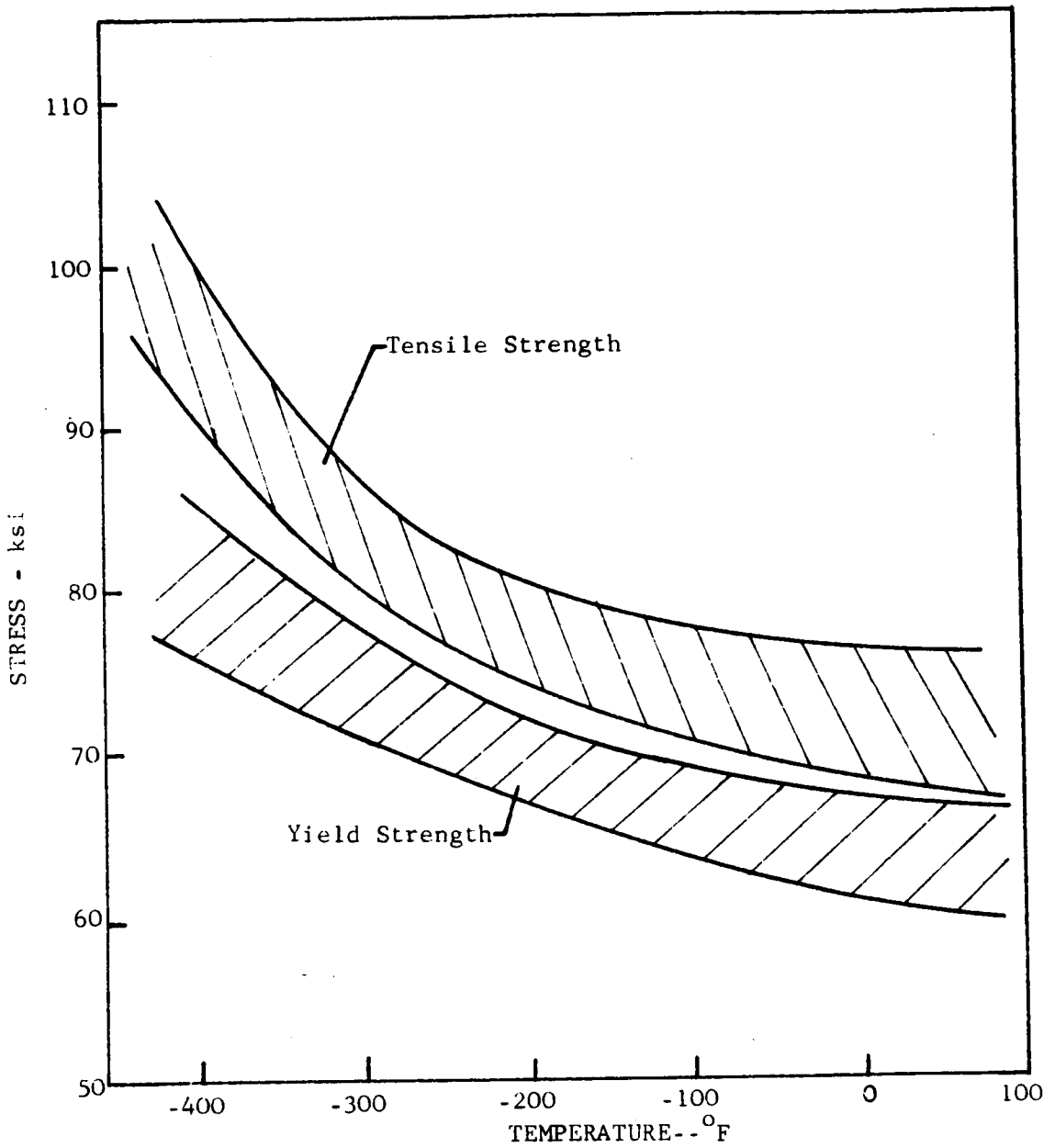

Fig. VIII-2-12. Tensile Properties of 2014-T6 and 2014-T62 Aluminum Alloy Sheet in the Longitudinal Direction. (Ref. 8).

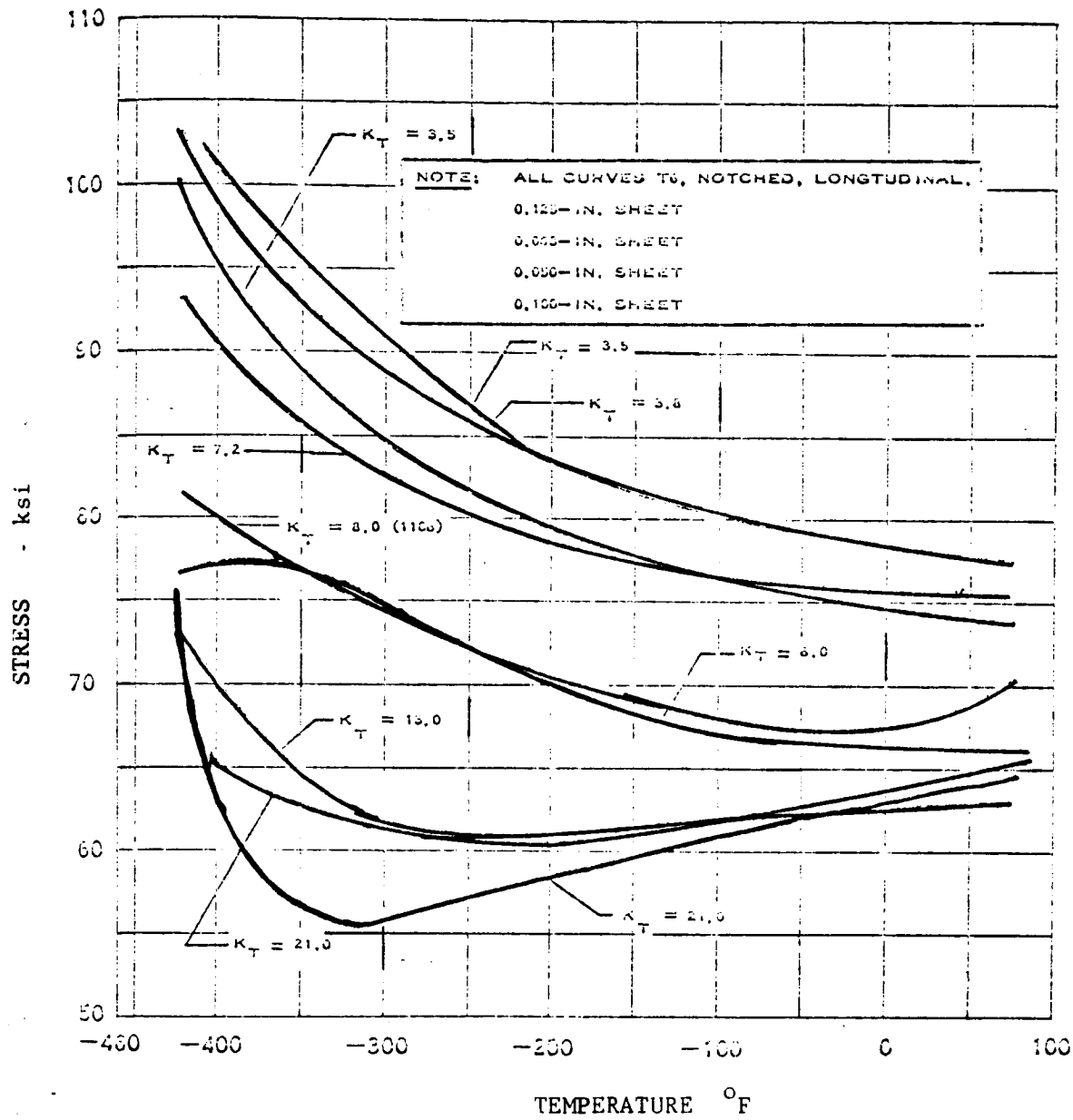

Fig. VIII-2-13. Notch Tensile Strength of 2014 Aluminum. (Ref. 9).

ORIGINAL PAGE IS
OF POOR QUALITY

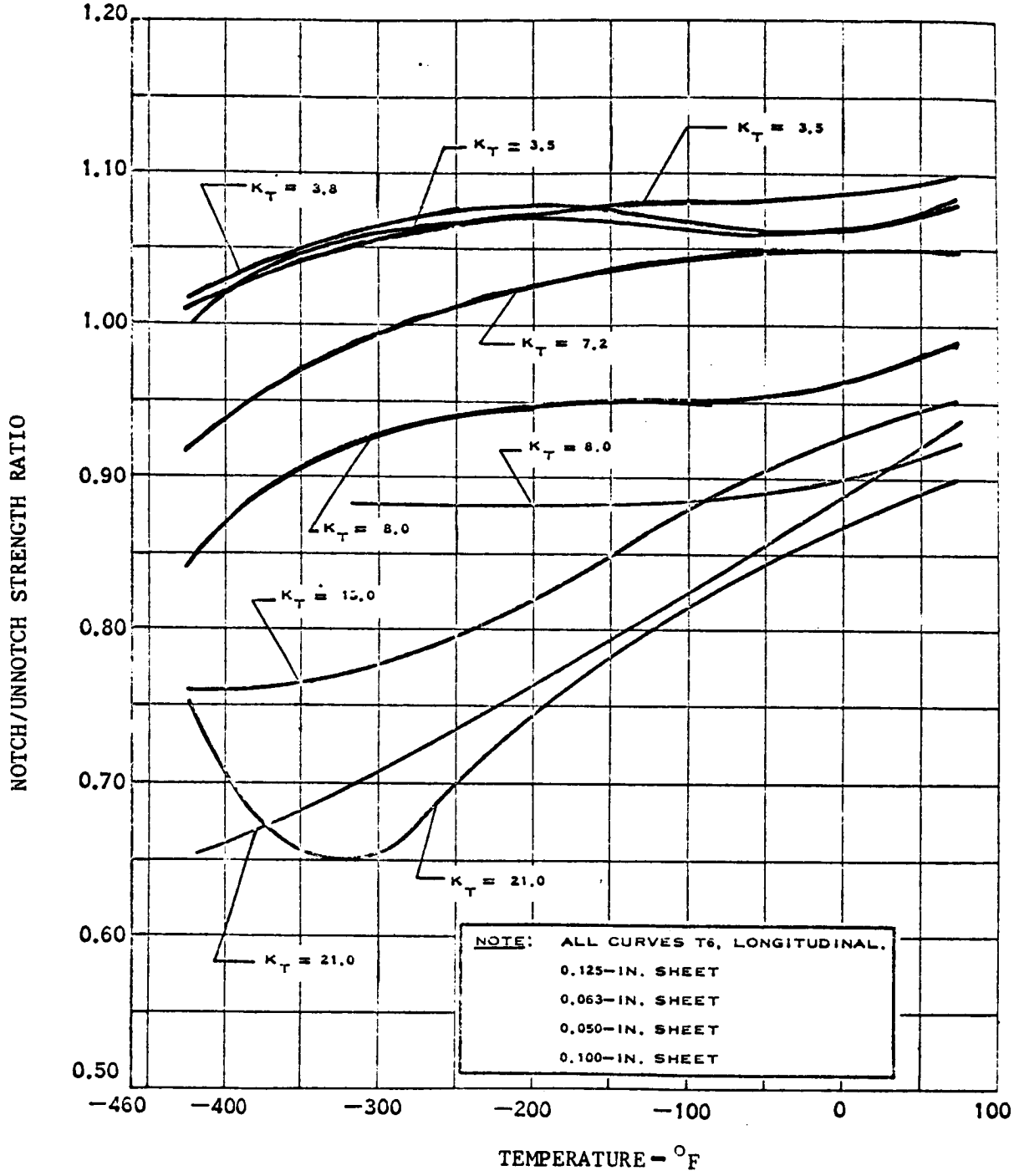

Fig. VIII-2-14. Notch Strength Ratio of 2014 Aluminum. (Ref. 9)

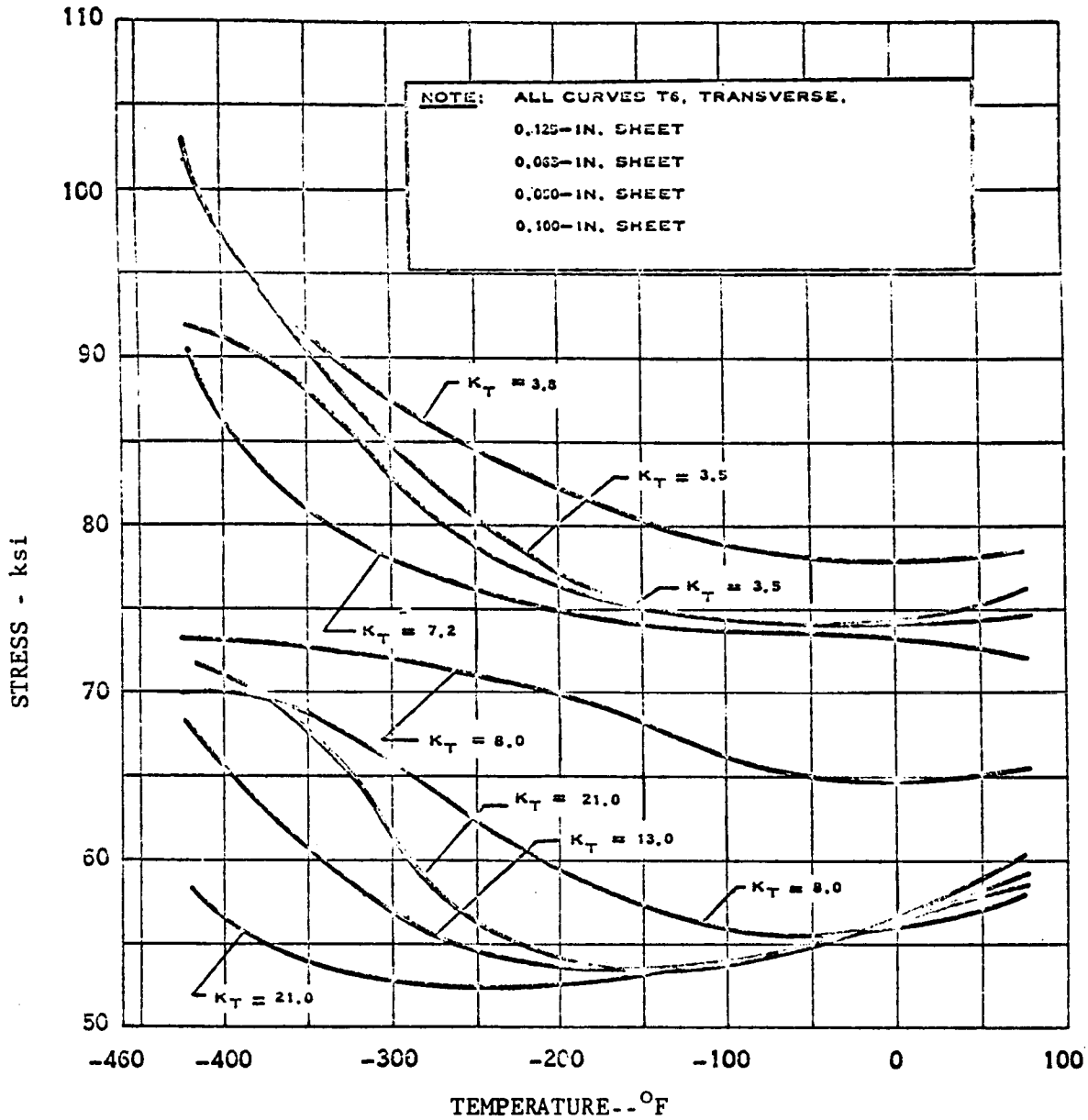

Fig. VIII-2-15. Notch Tensile Strength of 2014 Aluminum. (Ref. 9)

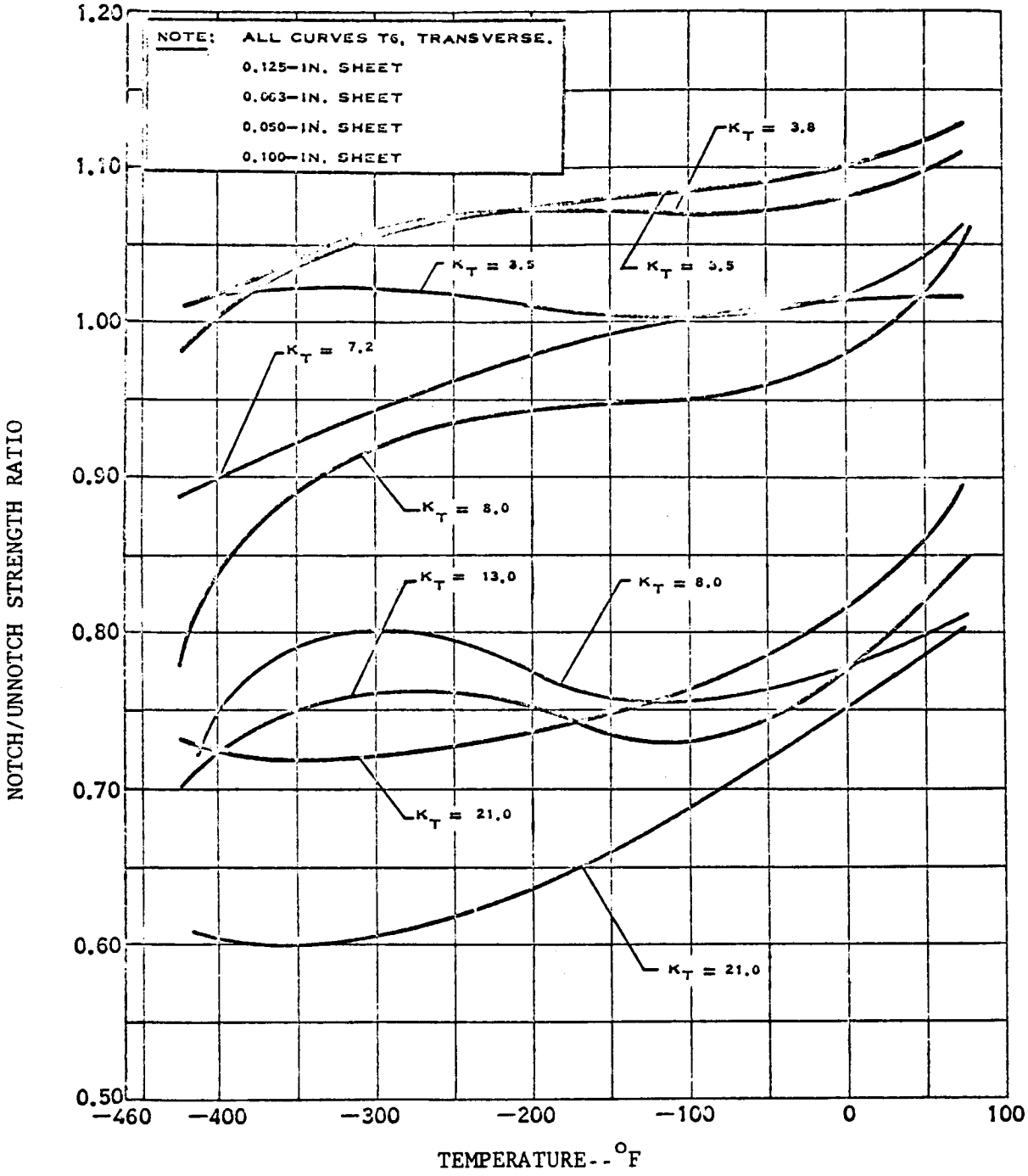

Fig. VIII-2-16. Notch Strength Ratio of 2014 Aluminum. (Ref. 9)

Compatibility of Materials

One of the most important criteria in selecting a material to contain a given working gas or liquid is the compatibility between the material of the container and the fluid being contained. In its broadest sense the term "compatibility" may be taken to mean an interaction between the container material and the contained fluid which affects the operation of the system. A host of mechanisms-- chemical, physical, or electrochemical-- may be involved, and, in some cases, the interaction between the two materials does not proceed automatically but requires some outside event to initiate or sustain the interaction. An example of the latter is the explosive interaction between titanium and liquid or gaseous oxygen when the metal is subjected to an impact while in contact with the oxidizer.

Although not all interactions are harmful to the functioning of the structure and some may be beneficial, we are mainly concerned here with interactions which decrease the load-carrying ability of the structure or promote catastrophic failure. In most cases, the mechanisms whereby the deleterious effects are produced are not understood in spite of intensive research, and the truth of the matter is that many mechanisms are involved and their isolation represents research tasks of major proportions. There is, first of all, the purely physical interaction in which the cryogenic nature of a working fluid may cool the container to a temperature at which an appreciable portion of its fracture toughness has been lost. In general, metals which have face-centered cubic lattice structures do not lose fracture toughness at cryogenic temperatures (aluminum alloys, nickel alloys, austenitic stainless steels), while metals which have body-centered cubic (alloy steels) and hexagonal close packed (titanium) lattice structures do lose fracture toughness at cryogenic temperatures. Thus, the currently popular alloy for pressure bottles, Ti—6Al-4V, is used with hesitation at temperatures below -300°F because of its decreasing fracture toughness at low temperatures.

The loss of fracture toughness associated with low temperatures is

not the primary type of interaction with which we are concerned in this Section. We are here mainly concerned with such things as corrosion of various types, LOX impact sensitivity, and possibly hydrogen embrittlement.

Corrosion may be considered as the destructive attack of a metal by its environment by a combination of chemical and electrochemical mechanisms. Electrochemical action may be established between two dissimilar metals in an electrolyte such as in galvanic corrosion or between different regions of a metal in an electrolyte.

One may distinguish at least five main types of corrosion which may occur singularly or in various combinations: (1) uniform corrosion, (2) pitting, (3) intergranular corrosion, (4) stress corrosion, and (5) galvanic corrosion.

Uniform corrosion occurs in completely homogeneous metals, so that no difference of potential exists between any two points. The material is removed evenly. Such attack is relatively rare since most metals are not so homogeneous.

Pitting corrosion occurs most commonly in metals that contain heterogeneities like inclusions or coring. Different points on the metal surface have different potentials, and local cells are established that result in pits.

Intergranular corrosion occurs when a difference of potential exists between the grain boundary and the grain body, leading to progressive attack at grain boundaries.

Stress corrosion is caused by the presence of a tensile stress, either applied or residual. Failure may be intergranular or transgranular, and its mechanism is the least understood.

Galvanic corrosion results from the contact of two dissimilar metals of different potential in an electrolyte.

The presence of stress or strain can accelerate corrosion. In Aluminum alloys one can distinguish between stress-accelerated corrosion and

stress corrosion. In the former, stress acts to rupture the corrosion-weakened grain boundaries, and the corrosive environment further penetrates the material. The load-carrying ability of the material is continually reduced to an extent proportional to the extent of corrosion damage.

Stress corrosion cracking is the most insidious form of corrosion. It is least understood and generates cracks which propagate, ultimately causing brittle fracture. It requires the presence of surface tensile stresses which may originate from service loads or be residual from prior thermal or mechanical history such as heat treatment, welding, plastic working, machining, or assembly.

Although the subject of stress corrosion cracking is much too complex and controversial to do it justice here, the subject is important enough to warrant the briefest kind of discussion.

Among the various alloys of interest in pressurized gas systems, stress corrosion cracking has been studied most extensively in aluminum alloys with NaCl solution as the electrolyte. Mild steels stress corrosion crack in hot concentrated aqueous solutions of nitrates and alkalis; commercial 18Cr-8Ni stainless steels, 304 and 347, crack in oxygenated NaCl solutions; and titanium alloys have been found to stress corrosion crack in elevated temperature chloride salt. Recently, problems suspected as resulting from stress corrosion cracking have been encountered in Ti-6Al-4V vessels containing N_2O_4. There are no universal environments that cause stress corrosion cracking in all materials. Occurrence of cracking is unique to a particular combination of material and environment.

Most of the ensuing discussion of stress corrosion cracking will be concerned with aluminum alloys since it has received great attention and it can be used to illustrate the significance of certain generalized effects such as that of residual stress.

In aluminum alloys cracking generally proceeds intergranularly by what is generally felt to be an electrochemical mechanism. Galvanic

action is established between anodic grain boundary areas and cathodic grain bodies. In susceptible alloys cracking can occur in the atmosphere with moisture on the specimen surface acting as the electrolyte. If the electrolyte contains certain chloride ions, as in a marine atmosphere, the rate of attack is increased.

A surface tensile stress is required to promote stress corrosion cracking. The propensity for stress corrosion cracking is usually determined by subjecting specimens to sustained stresses at various levels in a given environment and plotting a curve of time to failure as a function of applied stress. The aluminum wrought alloys that exhibit the greatest incidence of stress corrosion cracking in service are 2014, 2024, 2219, 7075, 7079, and 7178 in various heat treatments. Data for 7075-T6 plate in NaCl solution are presented in Fig. VIII-2-17. It can be seen that the propensity for failure is highly influenced by the mechanical working direction relative to the direction of stress applications. For the conditions represented in Fig. VIII-2-17 the maximum sustained stress that can be carried in the short transverse or thickness direction without the risk of failure is only 7000 psi.

The pronounced propensity for stress corrosion failure of high-strength aluminum alloys in the short-transverse direction has implications in the selection of fabrication methods for pressure vessels. An example will illustrate the point.

A particular pressure bottle is made of 2014-T6 and is fabricated by first extruding a tube 20 inches in diameter, 20 feet long and a 1 inch thick wall. The ends are nosed down by forging to a diameter of 4½ inches with an accompanying upsetting in wall thickness. The metal flow during this operation turns the flow lines normal to the surface of the vessel in the nosed-down region, and a stress corrosion problem is now anticipated because of the sharply reduced tolerance for sustained load if environmental conditions were to be encountered that would promote stress corrosion cracking.

To compound the problem in this particular bottle the end of the

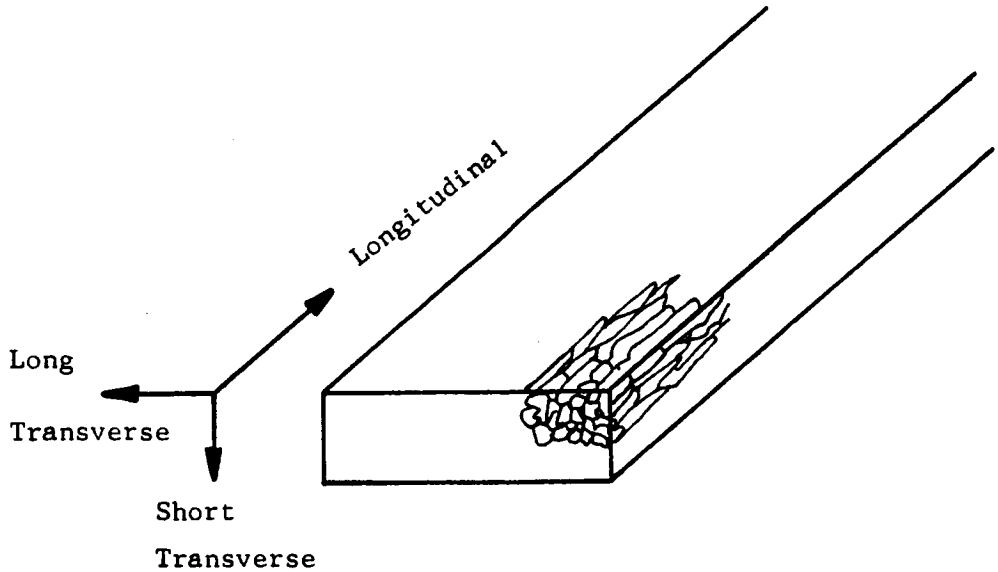

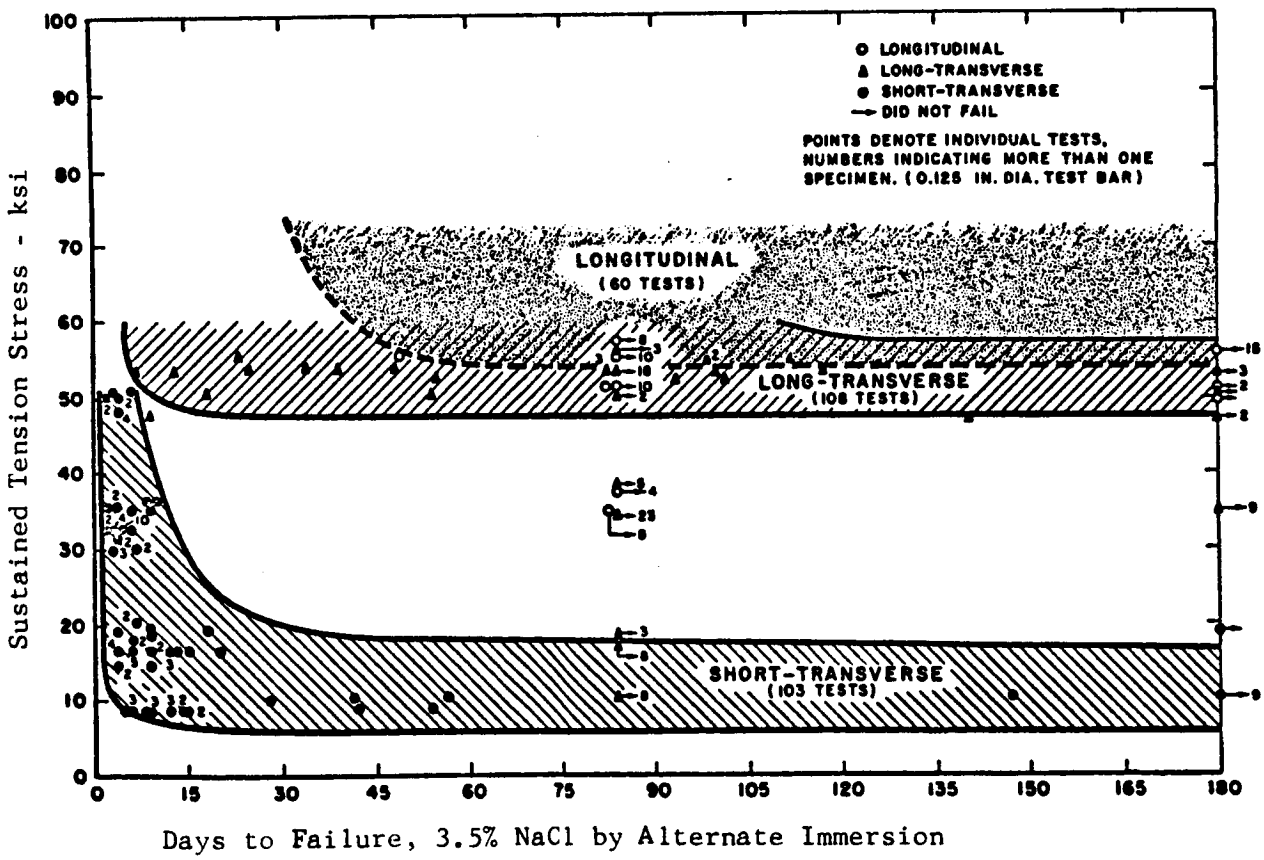

Fig. VIII-2-17. Resistance to Stress-Corrosion Cracking of 7075-T6 Plate as Influenced by Direction of Stressing. (Ref. 66).

nosed-down portion has threads cut into it for attaching a fitting. The notches cut into the end grain constitute a most undesirable condition for promoting stress corrosion cracking. One would expect rolled threads to be less insidious in such a circumstance than cut threads, and if the thread-rolling operation were performed so as to leave residual compression stresses at the thread roots, the expectation of a stress corrosion problem could be vastly if not completely eliminated.

We have now alluded to one effective means of minimizing the susceptibility to stress corrosion cracking. The benefit of induced residual compressive stresses on the surface of components, especially at holes or other geometrical discontinuities, is well-documented in the literature. This is especially important if the machining of the holes or forming of the geometrical discontinuities leave residual surface tensile stresses. Not only will the propensity for stress corrosion cracking be reduced, but an additional benefit is realized in an increase in fatigue life.

The most common method of inducing residual surface compression by surface plastic working is shot peening. Other methods include forcing tapered mandrels through holes, using expanding mandrels, surface rolling, and planishing or peening of welds.

Surface coatings or claddings can also be utilized to delay stress corrosion cracking. On aluminum, coatings may serve two functions: they may serve as an anodic sacrificial layer, or they may constitute a barrier to the corrosive environment. Some results of coating studies by various researchers are summarized in Table VIII-2-6.

Another form of catastrophic failure germane to pressurized gas systems is that due to the impact sensitivity of titanium alloys in liquid and gaseous oxygen and, to a much lesser extent, in liquid N_2O_4. The most commonly used device for testing the sensitivity of a given metal in a given atmosphere is the ABMA impact sensitivity tester, which drops a known weight a given distance onto a striker sitting on a sample which is immersed in the environment. The energy required to initiate an explosion or detonation is determined.

Table VIII-2-6

EVALUATION OF COATING SYSTEMS USED FOR PROTECTION OF ALUMINUM ALLOYS (Ref. 5)

NUMBER	COATING SYSTEM	ALLOY	STRESS LEVEL	FAILURE TIME, days	ENVIRONMENT	REMARKS BY RESEARCHER
1	Metal spray 7073 1-3 mils + zinc chromate primer + aluminum paint	7075-T6	75%	>800 ≥3500	Alternate[a] Industrial	-- --
2	Aluminum spray + zinc chromate primer + aircraft gray enamel	7079-T6	30 ksi	>190	Alternate	Excellent
3	Metal spray 7072, 1-3 mils	7075-T6	75%	200->1800 270->3500	Alternate Industrial	-- --
4	Aluminum spray + 2 coats zinc chromate primer + 2 coats enamel	--	--	--	--	Good protection
5	Alumite 204	--	--	--	--	(b)
6	Alumite 210	--	--	--	--	(b)
7	Zinc chromate primer + aluminum paint	7075-T6	75%	>200->1000 1500	Alternate Industrial	-- --
8	Anodizing + 2 coats zinc chromate primer	--	--	--	--	Effective
9	Anodizing + 2 coats epoxy primer	--	--	--	--	Effective
10	Zinc chromate primer + aircraft gray enamel	7079-T6	30 ksi	100-190	Alternate	Good
11	3M Primer + Pro-Seal 793 coating	7079-T6	30 ksi	90-190	Alternate	Fair
12	Pro-Seal 779 primer + Pro-Seal 793 coating	7079-T6	30 ksi	90-170	Alternate	Poor
13	Shot peened + iridited	7178-T6	45 ksi	63-100	Alternate	--
14	Iridite + BMS 10-39 (epoxy)	7178-T6	45 ksi	58-130	Alternate	--
15	Iridite + BMS 10-39 (epoxy)	Extrusions of 7079-T6 and 7178-T6	45 ksi	47-100	Alternate	--
16	Iridite + Buna top coat	7178-T6	--	30-130	Alternate	--
17	Glass peened + Iridite	7178-T6	--	35-100	Alternate	--
18	Sulfuric acid anodize	--	--	--	--	Good service[c]
19	Zinc chromate primer	Fasteners	--	--	--	Good service
20	Turko-Form No. 514 (rubber-base maskant)	--	--	--	--	(d)
21	Iridite + Buna top coat	Extrusions of 7079-T6 and 7178-T6	--	7-60	Alternate	--
22	Iridite	7178-T6	--	3-50	Alternate	--
23	Chromic acid anodize	7178-T6	--	3-50	Alternate	--
24	Iridite + zinc chromate primer	7178-T6	--	2-100	Alternate	--
25	Alodine 300 (conversion coating) + Alkatraz coal tar enamel	--	--	--	Kure Beach[e]	Poor
26	Alodine 300 (conversion coating) + Alkatraz Bitumastic	--	--	--	Kure Beach	Poor
27	Alodine 300 (conversion coating) + Del epoxy	--	--	--	Kure Beach	Poor
28	Alodine 300 (conversion coating) + Midland White Organosol	--	--		Kure Beach	Poor

(a) 3-1/2 percent NaCl alternate immersion 10 minutes in solution, 50 minutes in air.
(b) Improvement was about 10-fold at 75 percent stress and about 26-fold at 50 percent stress.
(c) Sulfuric acid anodize has proven superior to chromic acid anodize.
(d) Coating is used to protect stress-corrosion assemblies during tests.
(e) Eighty-foot lot at Kure Beach, North Carolina.

Sensitivity under other kinds of loading including penetration by a bullet, a simulated micrometeroid or other mechanical puncture tensile fracture, fatigue loading, explosive shock, electric discharge, cyclic pressure, vibration, and acoustic energy has been studied.

Experimentation has shown that rapid creation of fresh surfaces in titanium or its alloys in contact with liquid or gaseous oxygen produces detonation or violent burning. In fact, titanium is almost as reactive as many organic materials like greases and oils. The catastrophic reaction occurs over a fracture speed ranging from a few feet per second to several thousands of feet per second. Of all materials examined, only zirconium shows reactions similar to titanium. Stainless steels show almost no reactivity, and although aluminum is similarly unreactive under conditions of impact or rupture, it will ignite under conditions of high explosive shock.

Protection against impact sensitivity is afforded to varying degrees by anodizing, coating with Teflon or a fluoride-phosphate material, coating with copper, nickel, or aluminum, nitriding, or annealing to increase the thickness of the oxide film.

In view of the potential catastrophic failure in the presence of liquid or gaseous oxygen in the event of an impact or puncture, titanium alloys are not recommended. There does appear to be some current feeling in the aerospace industry that one can design systems that are virtually accident-proof. However, designers should be well acquainted with the risks involved.

Although there is great risk involved in attempting to present in a single table compatibility data for various metal-fluid combinations, an attempt has been made to do just this in Table VIII-2-7. It should be borne in mind that the recommendations made in this table may be controversial, but they represent an effort at systematizing, to some extent, the consolidated conclusions of many types of compatibility studies. Actually the particular performance of a given material in a given environment is so sensitive to system variables such as temperature, moisture content,

pressure, residual stresses, whether or not welds or brazes are present, and a host of other variables that compatibility tests should be performed under conditions simulating actual service as closely as possible before a final decision is made.

Compatibility of selected nonmetallic materials with propellants and oxidizers is presented in Table VIII-2-8.

Additional detailed compatibility data for both metallic and nonmetallic materials are available from the listed references.

Table VIII-2-7

COMPATIBILITY OF SELECTED METALS WITH PROPELLENTS AND OXIDIZERS*

	Al 1100	Al 2024	Ti 6Al-4V	Ti 5Al-2.5Sn	S.S. 302	S.S. 304	S.S. AM350	S.S. 17-4PH	S.S. 17-7PH
O_2	1	1	3	3	1	1	1	1	1
N_2	1	1	1	1	1	1	1	1	1
H_2	1	1	1	1	1	1	1	1	1
He	1	1	1	1	1	1	1	1	1
H_2O_2	1		3	3	2	2	2	2	3
N_2O_4	1	3	3	3	1	1	1	1	1
UDMH	1		1	4	1	1	1	3	1
Freon 11,12, 13,14 & 21	1		1	1	1	1	1	1	1
C_3H_8	1		1	1	1	1	1	1	1
C_4H_{10}	1		1	1	1	1	1	1	1
N_2H_4	1	3	4	4	1	1	2	1	1
CO_2	1		1	1	1	1	1	1	1
NH_3	2		1	1	1	1	2	1	1
ClF_3	2		3	3	2	2	2	2	2
ClO_3F	1		3	3	2	2	2	2	2

*The ratings in this table should be taken as only the roughest kind of guide since actual performance depends on many system details.

Ratings -
1. Acceptable
2. Acceptable (limited service)
3. Unacceptable
4. Check manufacturer's recommendations

Table VIII-2-8

COMPATIBILITY OF SELECTED NON-METALS WITH CASES AND LIQUID PROPELLANTS*

	TEFLON	KEL-F	MYLAR	VITON A	VITON B	POLY-ETHYLENE	EPOXY/ GLASS	NEO-PRENE	RUBBER
O_2	2	2	2	3	3	3	3	3	3
N_2	1	1	1	1	1	1	1	1	1
H_2	1	1	1	1	1	1	1	1	1
He	1	1	1	1	1	1	1	1	1
H_2O_2	1	1	1	3	3	1	4	3	3
N_2O_4	2	2	2	3	3	3	3	3	3
UDMH	2	2	2	3	3	3	3	3	3
Freon-11	4	4	4	4	4	4	4	4	4
Freon-12	4	4	4	4	4	4	4	4	4
Freon-13	4	4	4	4	4	4	4	4	4
Freon-14	4	4	4	4	4	4	4	4	4
Freon-21	4	4	4	4	4	4	4	4	4
C_3H_8	1	1	1	2	2	1	1	1	2
C_4H_{10}	1	1	1	2	2	1	1	1	2
N_2H_4	1	1	3	3	3	3	4	3	3
CO_2	1	1	1	2	2	1	4	2	2
NH_3	2	2	2	3	3	2	2	4	2
ClF_3	2	2	2	3	3	3	3	2	3
ClO_3F	1	1	1	4	4	1	1	2	3

Ratings

1 Acceptable
2 Acceptable (limited service)
3 Unacceptable
4 Check manufacturer's recommendations

*The ratings in this table should be taken as only the roughest kind of guide since actual performance depends on many system details.

Delayed Failure

In the preceding Part we discussed the degradation in the load-carrying ability of a metal due to interaction with its environment. The degradation may be continuous with slow crack growth until the remaining cross-sectional area is no longer adequate to sustain the applied load. At this point the member fractures completely, and in this sense one may refer to a stress corrosion failure as an instance of delayed failure.

Another possibly more common usage of the term delayed failure is that due to the presence of hydrogen in the material; the hydrogen does not necessarily originate from the service environment, but more usually originates in a previous processing operation. This type of delayed failure, sometimes called static fatigue, can most precisely be termed hydrogen-induced delayed brittle failure. It is "delayed" in the sense that in its most pernicious form failure occurs suddenly and in brittle fashion under the action of a sustained stress at levels as low as 15% of the uniaxial tensile strength. It is never observed in compression loading, i.e., tensile loads are necessary, and it is more pronounced in the presence of notches. In general, it is most prevalent in body-centered cubic transition elements and hexagonal close-packed metals, although it has been produced in face-centered cubic nickel and nickel-base alloys heavily charged with hydrogen. Ferritic steels (body-centered cubic) are especially susceptible to hydrogen embrittlement, while austenitic steels (face-centered cubic) are especially resistant. Titanium and its alloys (hexagonal-closed-packed) also have exhibited hydrogen embrittlement and hydrogen-induced delayed failure.

Most of the research in hydrogen-induced degradation has been performed on steels over a wide range of composition and strength level. Sources of hydrogen are plentiful, although it can enter the steel only in the atomic and not the molecular form. These sources are the steel-making operation itself, from water in the charged materials and refractories, hydrogen, and hydrocarbon gases in furnace atmospheres; pickling and many corrosion reactions can introduce hydrogen into steel; cathodic cleaning, electro-

plating, or electrolytic machining may also result in hydrogen pickup. Atomic hydrogen producing reactions among constituents being stored in a pressure vessel could also conceivably lead to embrittlement or delayed failure problems.

The presence of hydrogen can have three specific effects on mechanical behavior. It can reduce ductility as detected by percentage elongation or reduction of area in a tensile test, it can reduce the "true" fracture stress (terminal point on a true stress-strain curve), and it can cause sudden failure when subjected to a sustained load at very low applied stresses. The mechanisms are not understood but do depend upon diffusion of hydrogen in the steel to points of high stress. The driving force for the diffusion of hydrogen is either a hydrogen concentration gradient or a stress gradient. After an incubation period which allows sufficient hydrogen to diffuse to a point of high stress, a fracture is initiated at a point of maximum triaxiality. Fracture then progresses discontinuously; the time between fracture steps is determined by the time required for hydrogen to diffuse.

Since the diffusion of hydrogen is essential to the process, the effects of hydrogen are not seen in fast tests such as impact tests, but are more evident at the slowest strain rates, such as in a sustained load test. Also, the effects are reversible if no permanent damage has been suffered. Hydrogen will diffuse out of steel at room temperature and more rapidly at an elevated temperature. If cracking has not yet initiated underload, then properties will be restored to their nonhydrogenated values if all the hydrogen is diffused out of the steel.

In the delayed failure of steel under a sustained stress, a minimum value of applied stress is necessary to cause premature failure. This minimum value is strongly dependent on strength level, decreasing with increasing strength level so that, for example, SAE 4340 heat treated to high strength levels can fail prematurely in brittle fashion under sustained stresses even less than 10% of the nominal ultimate tensile strength. Such drastic degradation has been observed in unnotched specimens when a critical combination of stress, hydrogen content, and time was exceeded. The

minimum critical stress under which no premature failure occurred is also a function of hydrogen content; it decreases as hydrogen content increases.

Testing temperature has a strong effect on hydrogen embrittlement, the most severe effect being within an intermediate temperature range from -150°F to +210°F. Little effect of hydrogen is generally noted at -321°F or below, and it also drops off rapidly as temperature is increased above room temperature.

Another aspect of the hydrogen problem occurs when it is contained at high pressures and elevated temperatures. Under these conditions the molecular hydrogen can dissociate to atomic hydrogen, in which condition it can enter the steel and cause embrittlement and loss of load-carrying ability. Decarburization of the steel may also occur by what is thought to be a reaction between hydrogen and iron carbide to form methane.

Hydrogen-induced delayed failure or cracking in titanium and its alloys have not received nearly as much research attention as in the case of steel. In this case hydrogen has been observed to have deleterious effects in loading at high strain rates as, for example, in Charpy tests as well as at low strain rates or under static loading. Titanium alloys can absorb hydrogen at room temperature, and there is some suggestion that the extent or composition of the oxide film can affect the rate of hydrogen pickup. Some of the incidence of hydrogen embrittlement in titanium alloys, as well as in steel, is associated with weldments, where the residual stresses undoubtedly play an important role.

Material Forms and Fabrication

Two material forms are most commonly employed in fabricating pressure vessels for pressurized gas systems. Machined and welded forgings constitute the most common fabrication approach. The use of machined forgings with integral bosses and attachments requires only a circumferential girth weld for assembly. The probability of weld defects is thereby reduced to a relative minimum. However, material and machining costs may be significantly higher than those required for sheet-metal fabrication.

Formed and welded sheet metal constitutes the second most common method of fabricating the pressure vessels. Attachments and bosses are either machined bar stock or forged material which is welded to the vessel. Occasionally sheet metal is used for the cylindrical section of a cylindrical bottle. The end closures may be machined forgings or drawn heads. Longitudinal welds may be eliminated by using a flow-turned cylindrical section, and assembly is achieved by means of circumferential girth welds.

Pressure vessels fabricated by means if the Arde formed process represent a unique approach, which is described in Part VIII-3, Joining.

Introduction

Welding plays a key role in the fabrication of pressurized gas systems. Among its virtues are its efficiency and versatility in fabricating the lightest possible pressure vessels and for making attachments, fitting connections, and tubing joints. It is not, however, without its faults. Because of its possibility of producing defects and metallurgical impairments it must be closely controlled, and it must be used in its most advanced technological state if full advantage is to be taken of its potential.

Long experience of the aerospace industry with welding has bred certain basic tenets which are generally held in the industry, although exceptions are practiced. These are as follows:

1. There is some reluctance to permit any longitudinal welds in cylindrical pressure vessels since these are the most highly stressed, and in some cases they are absolutely forbidden. The vessel is made in these cases by girth-welding forged sections.
2. The locations of any welds are chosen so as to avoid the most highly stressed regions of the vessel, or points of stress discontinuity as, for example, the point of tangency between a dome and a straight cylindrical section.
3. There is usually reinforcement in the weld provided, first of all, by a thickened portion of the forged component prior to welding in the region of the weld, and, secondly, by using filler metal to provide a built-up bead. In some cases the as-welded bead is ground after welding to improve the bead contour and to provide a better surface for nondestructive testing. (Some refrain from grinding welds in titanium alloys to prevent the possibility of oxidation during grinding). The final thickness at the weld can be as high as 1.8 times the sheet thickness, the actual value varying among fabricators.
4. Usually no welding is done on the membrane portion of a vessel but only at thickened portions or at forged bosses or connections.

With this introduction, we can discuss the particular processes used in fabricating pressurized gas systems.

Welding Processes Applicable to Vessel Fabrication, Piping, Fittings, and Repair

The American Welding Society in its classification and definition of the welding processes recognizes between fifty and one hundred different processes which fall within the definition of welding. Of these, it is only necessary to discuss a few as being significant in the fabrication and repair of aerospace pressure vessels and in the making of piping or fitting joints. The most commonly used process is gas shielded-arc welding and, more specifically, gas tungsten-arc welding (commonly abbreviated TIG welding for tungsten inert-gas welding). TIG welding is used to make longitudinal and circumferential seams in cylindrical and spherical pressure vessels, for attaching heads of cylindrical vessels, and for attaching fittings. It is used for making joints in tubing, and special tooling has been developed for making such joints automatically. Weld repairs are also made by TIG welding.

Among the other welding processes, gas-pressure welding, brazing, electron-beam welding, and plasma welding require discussion. Gas-pressure welding is being used to make girth seams in cylindrical and spherical pressure vessels, and brazing is utilized in piping joints. Although electron-beam welding and plasma welding have not yet been widely adopted in fabricating pressurized gas systems, they offer some unique advantages.

Gas Shielded-Arc Welding

In the gas shielded-arc welding process the edges of two members being joined are melted by the heat of an arc maintained between the end of a nonconsumable or consumable electrode and the work. The electrode and the heated work are prevented from oxidizing by a protective gaseous atmosphere which may be inert and which issues, at least in part, from passages within the torch.

Two types of gas shielded-arc welding are practiced. These are differentiated by whether or not the electrode is consumed. The first type, and the more significant in aerospace fabrication, is gas tungsten-arc welding (TIG); in this case the electrode is a tungsten or tungsten alloy rod, which

is not consumed during welding. Filler metal may be added to the weld by means of a separate noncurrent-carrying wire fed into the puddle. The other type, gas metal-arc welding (MIG for metal inert gas), utilizes a spooled wire which is fed continuously to the arc which is maintained between the end of the wire and work. The wire in this case is consumed continuously.

It is sufficient for present purposes to elaborate only on the TIG welding process. The electrical circuit is comprised of the welding machine, which is a source of direct or alternating current, the work, and the electrode holder or torch. The torch also has passages and a nozzle for directing the shielding gas from the bottle supply to the region of the weld, the capability for holding the tungsten electrode, and water passages if the current rating of the torch is high enough to require water cooling. Appropriate gas regulating and metering equipment is also needed. If the welding operation is automated, then additional facilities for accomplishing the following functions may also be incorporated: electronic voltage controls for continuously checking and adjusting the torch position in order to maintain a uniform arc length and voltage; work and torch manipulating equipment; filler-wire feed mechanisms; arc initiation.

The power source provides either AC or DC current to the welding circuit. AC power is usually supplied by a transformer that converts commercial AC from power lines to values of current and voltage suitable for arc welding. DC power is supplied either by a motor-generator set or by rectifying the alternating current output from a transformer. When using DC power two alternatives exist in selecting the polarity of the electrode and the work. In direct-current-reverse polarity (DCRP) the electrode is positive and the work is negative, which means that electrons are emitted from the work and strike the electrode. This has several consequences: (1) Any oxide films on the surface of the metal are cleaned off to some extent, which is important in the welding of aluminum and magnesium. (2) The electrode gets hotter relative to the work than if the current flow were in the other direction. Therefore, relatively-large-diameter electrodes are required, and the weld puddle is shallow and wide. Therefore, DCRP is rarely

used. The more popular arrangement is direct-current straight polarity (DCSP) in which the electrons are directed to the positive plate at fairly high velocity causing the plate to heat more than the electrode. The weld puddle is deeper and narrower than when DCRP or AC is used. Heat-affected zones are narrower, distortion less, and higher welding speeds are possible. In using AC, the current flow changes direction 120 times a minute. Thus, one obtains the oxide cleaning action during the reverse part of the cycle.

Argon is generally used in TIG welding although helium or mixtures of argon and helium may also be used. When welding aluminum alloys, adequate shielding is provided by the inert gas issuing from the torch. However, when welding a reactive metal like titanium, additional shielding may be provided by inert gas introduced through leading or trailing shields or backup bars, or, as is frequently the case, the entire fabrication is placed within a welding chamber which has been filled with inert gas. Although flexible plastic bags have been used in the past as chambers, most current practice is to utilize rigid plastic chambers or steel chambers with windows to provide visibility. In some cases the chambers are purged by simply flushing with inert gas, but the highest-quality atmosphere is provided in tight chambers that are evacuated and backfilled with inert gas.

The purity of the gas is of prime importance in the welding of titanium and aluminum alloys. The purity of most commercial argon and helium averages over 99.95%, the impurities being mainly oxygen, nitrogen, oil, and water vapor. Impurities may also enter the arc atmosphere by aspiration through leaks in the hose lines or at connections, by diffusion through hose lines, or by leaks in the torch water-cooling system. Synthetic rubber or plastic tubing materials are generally more impervious than natural rubber.

Welding is generally done automatically to eliminate human error as much as possible although some vessels have been fabricated by manual welding. Filler metal is usually, although not always, added, and it may match the base metal in composition or be of different composition depending upon the composition of the base metal, thickness, and joint configuration.

Joint design is usually square butt or vee, and multipass welding is frequently practiced.

Frequently two or more passes are used for thicknesses which could be welded in a single pass for purposes of better control of bead geometry. Thus, a first pass may be optimized to yield the most satisfactory root contour, while a cover pass provides an optimum face contour.

Proper fixturing is important in assuring uniformity in terms of minimum mismatch, constant arc length, and travel speed.

Weld repairs are made by TIG welding either on a local basis or by completely routing out the full girth and rewelding, depending upon the fabricator's preference. The problem with local repair is the accompanying distortion. Those fabricators who do permit local repairs place a limit on the maximum number of repairs in one location, usually two or three. The most usual defect encountered is porosity, and a certain amount of porosity is accepted. The same is not true of crack-like defects, which are always cause for rejection or repair in any quantity.

Within the past few years a process somewhat related to TIG welding has been developed, and although it is not known to have been yet applied to the welding of pressurized gas systems, it does deserve some discussion because of current interest in its potential. The process, termed plasma-arc welding, may be considered a variation of TIG welding since the basic difference between the two lies in the fact that in plasma-arc welding the arc is constricted by a potential between the nozzle and the work. This is illustrated schematically in Figure VIII-3-1. In TIG welding the arc exists between the tungsten electrode and the work. The arc plasma is conically shaped, and the width-to-depth ratio of the weld bead is relatively high. In plasma-arc welding the arc exists usually between the tungsten electrode and the work (in another variation, the "nontransferred" arc, the arc exists between the tungsten electrode and the nozzle), but the imposition of a potential on the nozzle constricts the welding arc to a thin columnar geometry. The plasma argon is ionized as it passes at high velocity through the

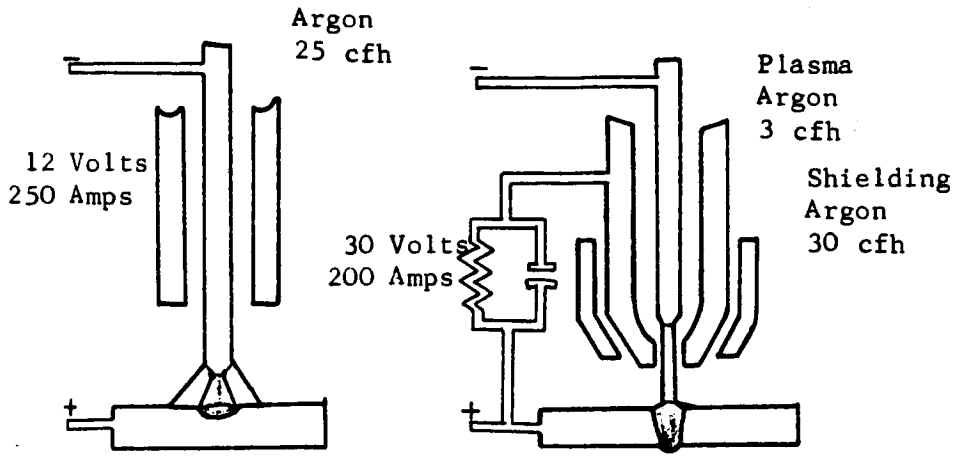

Fig. VIII-3-1. Arc Column Shape for Gas Tungsten-Arc (Left) and Plasma-Arc (Right). (Ref. 65).

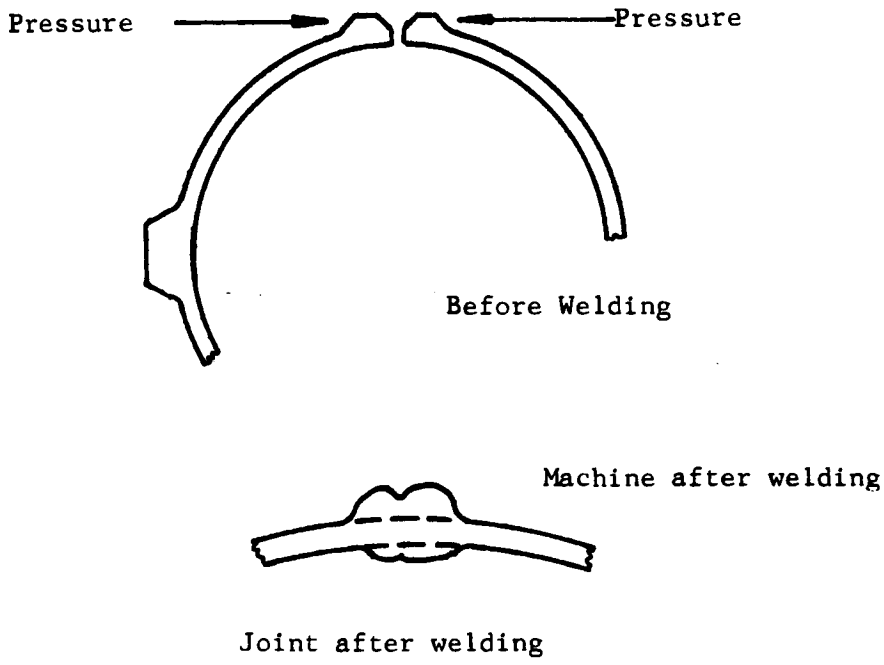

Fig. VIII-3-2. Schematic Representation of Pressure Welded Vessel.

arc, and arc temperatures are exceedingly high. Additional shielding gas is supplied through another annular nozzle or cup.

The advantages of plasma-arc welding over TIG welding are apparent from the comparison in Figure VIII-3-1. The greater energy concentration yields narrower beads and heat-affected zones, higher welding speeds (also a consequence of higher heat content), and less distortion. The high velocity and momentum of the plasma increases arc stability and makes it less sensitive to variations in joint alignment and arc length.

The principle disadvantages of plasma-arc welding are that (1) as in MIG welding, there are more process parameters than in TIG welding and this greater complexity increases the possibility of error, and (2) the bulkier torch and concomitant limits visibility. Plasma gas, shielding gas, and orifice cooling water must all be brought to the torch tip; this makes a somewhat bulkier torch than for TIG welding and limits the visibility. However, more sophisticated torch designs will undoubtedly evolve as plasma-arc welding finds greater acceptance.

Plasma-arc welding has already been utilized commercially, and its inherent advantages should make it worthy of consideration in the fabrication of pressurized gas systems.

Pressure Welding

Pressure welding is a joining process wherein coalescence is produced simultaneously over the entire area of abutting surfaces by heating either with induction or with gas flames obtained from the combustion of acetylene with oxygen and by the application of pressure without the use of filler metal. It is a nonfusion process (there is no melting) in contrast to arc welding, which is a fusion process. The process has been used to manufacture spherical and cylindrical pressure vessels by a company who applies the proprietary term "Uniwelding". Pressure-welded vessels have been made of titanium alloys, steels, and some nickel-base alloys in sizes up to 42 inches in diameter and in wall thicknesses down to 0.050 inch.

The practice of pressure welding can be best explained by referring to Figure VIII-3-2. The two forged halves of a pressure vessel are abutted in the welding machine. The forgings contain integral bosses for support and a thickened weld region through which pressure is applied during the heating cycle. Joint preparation is a vee configuration as shown. The joint area is surrounded by either a ring burner, which supplies gas heat, or by an inductor, which supplies induction heat for the largest size vessels. After the pressure is applied, heating is begun and is maintained until a given joint upset is achieved. The configuration of the joint after welding is shown in the bottom schematic. The configuration of the outside of the joint is a function of the original joint geometry and the thermal gradient which exists through the thickness of the weld. The excess metal in this region is always machined off. The fissure shown on the inside of the joint is obtained in steel vessels and is always machined off. Titanium alloy vessels do not exhibit this internal fissure, so no internal machining is performed.

The process is capable of making high quality joints and is ideally suited to mechanization. It is most important that the internal fissure sometimes obtained be completely removed; as it happens, the upsetting pressure causes this fissure to be tightly fitting, making it sometimes difficult to detect radiographically.

Among the advantages of pressure welding over the fusion-arc welding process is the fact that there is no spatter in the former since there is no melting. This simplifies the postweld cleaning operation.

Electron-Beam Welding

In the electron-beam welding process the work is bombarded by a concentrated high-velocity stream of electrons. The kinetic energy of the electrons is converted to heat upon impact. An electron-beam welding system includes an electron gun, which emits and accelerates electrons toward the workpiece, electromagnetic focusing coils which control the beam spot size at the work (it is sometimes desirable to defocus or oscillate the beam to accommodate less precise fit-up or to widen a bead as, for example,

on a cover or wash pass), a power supply which supplies voltages up to 150,000 volts to the equipment, a vacuum enclosure and vacuum pumping equipment capable of pump down to 1×10^{-4} torr or less, and appropriate auxiliary equipment for such functions as work manipulation and viewing.

The two main types of equipment that have evolved are (1) the so-called high-voltage welders, which operate at 60,000 volts and above and (2) low-voltage welders, which operate below 60,000 volts. Machines are built that deliver up to 30 kw of power and that have beam-welding currents ranging up to 1000 milliamps.

Although nuclear reactor fabrication provided the initial motivation for the development of electron-beam welding, it has been aerospace applications that have primarily fostered its principal acceptance in the decade or less since its development. The process is unique among all the welding processes in that it is performed in a vacuum. (Modifications of the process are possible in which the work to be welded need not be placed inside an evacuated chamber, but some of the inherent advantages of electron-beam welding are lost.) Since the process is performed in a vacuum one avoids the degradation associated with the pickup of gaseous contaminants like oxygen, hydrogen, and nitrogen which may arise from several sources in inert-gas welding. Thus, the interest in electron-beam welding for the joining of reactive metals like zirconium, titanium, molybdenum, tungsten, tantalum, and columbium is self-evident.

Another inherent advantage of electron-beam welding has come to be appreciated even more than the reduced opportunity for weld embrittlement by pickup of contamination. This is the extremely narrow, deep welds that can be achieved. In arc welding, the arc heats a relatively shallow depth of material by direct impingement, and thermal conductivity in the material accounts for additional penetration through the material and, concomitantly, laterally. In electron-beam welding, the energy concentration within the electron beam is so high that it instantly vaporizes a hole through the entire thickness being welded. As the beam is moved along the length of the weld, the molten metal along the sides of the hole flows to the rear of the direction of travel, solidifies, and affects the weld.

The high depth-to-width ratio of electron-beam welds has an important advantage in minimizing distortion since less material in the structure is being welded. The fact of lesser distortion can be important in itself and to the extent that undesirable distortions can sometimes decrease the load-carrying ability of a structure, electron-beam welded structures do not suffer from this type of structural degradation.

An indirect advantage follows from the greater dimensional precision and fit-up required in parts to be electron-beam welded. Since manufacturing tolerances need to be tightened for electron-beam welding, one might expect a more reproducible product. Or at least this is an argument advanced by the champions of electron-beam welding.

Two disadvantages of electron-beam welding are: (1) more weld spatter, which introduces more of a postweld cleaning problem and (2) greater difficulty of underside bead geometry control. A third disadvantage in some cases is the tendency to vaporize high-vapor-pressure constituents in welding some materials.

The economics of electron-beam welding relative to other processes is controversial; there is complete disagreement on this issue. In favor of electron-beam welding is the elimination of shielding gas costs and minimization of costs incurred because of the greater distortion in arc welds. On the other hand, initial equipment costs are higher for electron-beam welding equipment, and it is presumably more expensive to manufacture parts to the dimensional and fit-up requirements for electron-beam welding.

At least one fabricator, Beech Aircraft Corp., has developed successful electron-beam welding techniques for making girth welds in Inconel 718 and Ti-5Al-2.5Sn ELI spherical pressure vessels and plans to make such bottles for the Apollo program. A brief review of their welding practices is instructional.

The Inconel 718 will contain liquid oxygen, and the titanium alloy will contain liquid hydrogen. Some of the design requirements are shown in Table VIII-3-1. There is a long gradual taper from the membrane thickness to the weld land, which is melted down during the electron-beam

welding operation. The sequence of passes is as follows:

(1) Electron-beam tack welds are made through holes in the tooling after which the tooling is removed. The tack welds are 1/4 in. long and are placed at approximately 4-in. intervals.

(2) A shallow pass is made which smooths out small misalignments and results in what amounts to a continuous tack weld.

(3) A penetration pass is made which affects a weld through the entire thickness.

(4) A cover pass is made with a defocused beam, which improves the geometry on the top side.

Table VIII-3-1

ELECTRON-BEAM-WELDED PRESSURE-VESSEL SPECIFICATIONS

Parameter	Oxygen	Hydrogen
Material	Inconel 718	Ti-5Al-2.5Sn ELI
Configuration	Spherical	Spherical
Vessel Inside Diameter	25.060	28.245
Vessel Membrane Thickness	0.061	0.046
Peripheral Weld-land Thickness	0.139	0.088
*Design Stress (KSI)	110.0	50.0

*Stress limit at 1020 psig and 300 psig for oxygen and hydrogen vessels, respectively.

There is no postweld stress relieving or machining or grinding of the bead.

Nondestructive testing, leak testing, and pressure cycling at ambient temperature, plus burst testing at -300°F for the Inconel 718 and -423°F for the titanium alloy bottles have satisfied the fabricators of the suitability of electron-beam welding to make these bottles.

Tubing Joints

In the fabrication of pressurized gas systems in regions other than within the pressure vessel, it is necessary to make connections between tubes or between tubes and valves, fittings, regulators, or other such

components. Such connections are made by three general types of joining processes: (1) mechanical, (2) TIG-arc welding, and (3) brazing. Mechanical attachments utilize threads or other such schemes; these will be treated elsewhere in this guidebook. We will treat only TIG-arc welded and brazed, in other words, metallurgical-joining, processes in this part.

TIG welding has already been described in this section. In addition to using TIG welding to fabricate the pressure vessel it is also widely used to make connections between tubes and between tubes and fittings of all types. Some such joints in large diameters are made either manually or automatically using conventional TIG welding equipment. For small-diameter tubing, conventional equipment becomes difficult to use and is completely unsuitable for tubing under 1 in. in diameter. Several aerospace fabricators have developed specialized tube welding apparatuses of which one, termed in-place tube welding, is being used by North American Aviation. This process has been used to make joints in tubing as small as 1/4-in. diameter and 0.028-in. wall thickness.

In-place tube-welded joints are made by abutting two tubes to be welded and placing a sleeve over the joint. Several variations of this joint design are shown in Figure VIII-3-3. Using a special split welding torch, burn-thru lap welds are made as shown, either away from the abutting seam of the tubes being joined or over the abutting seam of the tubes being joined, as well as fillet welds at the end of the sleeve. The advantage of the joint type at the bottom of Figure VIII-3-3 is that there are no crevices in the joint to trap or retain corrosive media (the system is inherently cleaner), and the fatigue life of the joint is higher because of the absence of notches.

The welding torch consists of a split ring assembly, which fits around the tube sleeve. The small tungsten electrode is mounted in a cooper ring to which current is carried by a sliding contact and which revolves around the sleeve.

Some tubing connections are TIG welded utilizing novel joint preparations. One fabricator prefers a square butt joint in wall thicknesses that

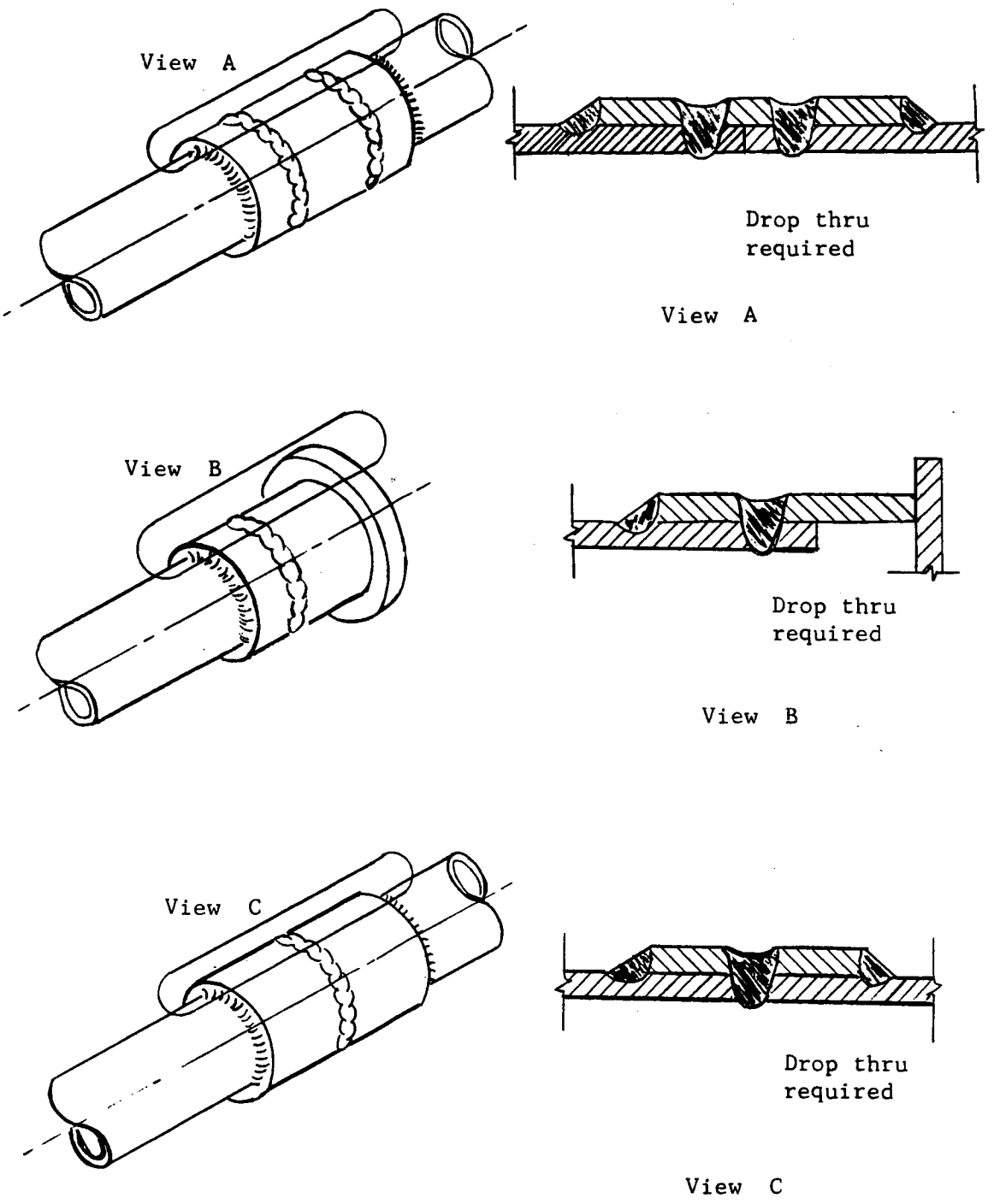

Fig. VIII-3-3. In-Place Tube-Weld Joints. (Ref.68).

are large enough to accommodate such a joint geometry, a lap-joint preparation for intermediate gages, and an edge-joint preparation for the lightest gages. These are illustrated in Figure VIII-3-4. The use of the lap- and the edge-joint preparations serves two functions: (1) The fit-up problem is made less critical and (2) The excess metal provides filler material when it is melted by the arc.

Brazing is also used to make tubing connections in pressurized gas systems. Brazing is a process in which the base metal is not melted. The connection is made by heating the joint to a temperature below the solidus temperature of the base metal but above the liquidus temperature of a dissimilar filler alloy. The filler alloy is distributed throughout and retained within the joint by the capillary force exercised within the spacing between the parts to be joined. In brazing, the filler metal melts above 800°F; in soldering the filler metal melts below 800°F. By definition, other than in respect to the melting point of the filler metal, brazing and soldering are identical processes.

Since only the highest quality brazing practices are permitted in aerospace fabrication, fluxes are not utilized; this avoids problems of flux entrapment.

Problems of compatibility may arise between the base metal and brazing filler metal in the presence of the working fluid and under the conditions of temperature and stress to be encountered in service. In this regard, brazing is not as attractive as welding since the compositions of base metal and filler metal are more dissimilar in brazing than in welding.

An induction, inert-gas brazing apparatus is marketed commercially* for making leak-tight high-integrity joints in the shop or in place in a spacecraft. A schematic of the joint is shown in Figure VIII-3-5. The portable brazing tool clamps around the joint and has facilities for supplying inert gas to the joint area. Inert gas is also supplied inside the tubes being joined. Heating is supplied from a high-frequency induction generator. Auxiliary tools are also supplied for cutting and cleaning.

*Aeroquip Corp., Jackson, Mich.

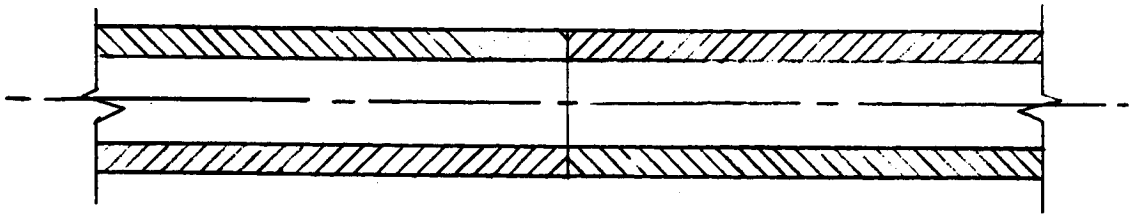

Large Wall Thickness

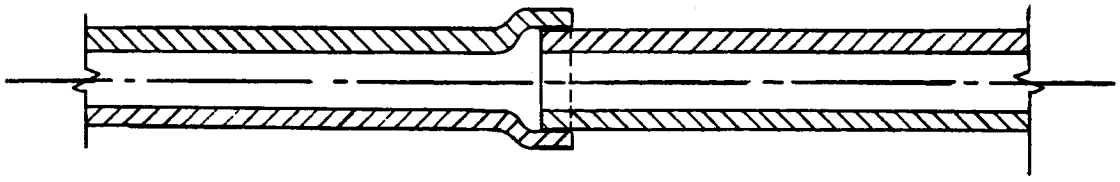

Intermediate Wall Thickness

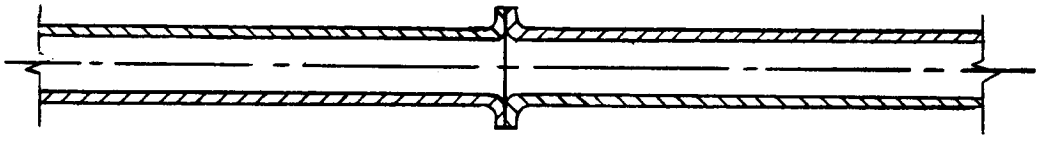

Small Wall Thickness

Fig. VIII-3-4. Edge Preparations For TIG Welding In Tubing.

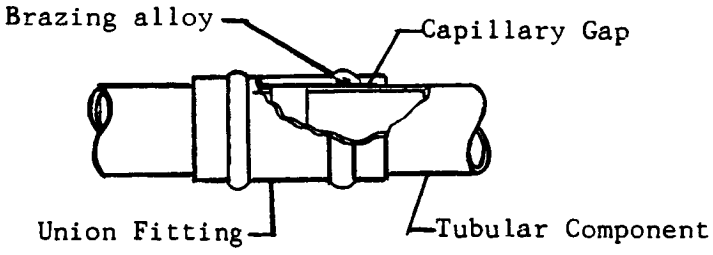

Fig. VIII-3-5. Schematic Diagram of a Brazed Tubing Joint. (Ref.67).

Welding Fabrication Variables and the Welding of Particular Alloys

The objective of this section is twofold: (1) to point out some frequently overlooked fabrication variables and (2) to discuss particular problems concerning the welding of specific alloys used for pressurized gas systems. The comments are neither comprehensive nor detailed but are instead presented to provide generalized background.

Some Preliminary Design Considerations for Welded Components

In designing a welded pressure vessel careful consideration must be given to all aspects of welding fabrication before the design is finalized and the materials have been selected. Design trade-offs may be necessary or material compromises may have to be accepted to assure fabrication within specific cost and schedule requirements. The complexity of welding fabrication is very dependent upon design requirements and alloy type. Tooling costs for the manufacture of welded structures often represent one of the most significant cost elements in the fabrication of a system, particularly where only a few of a kind are to be produced. Substantial savings may be realized by implementing rather minor design modifications which could permit the use of much simpler and less costly tooling. The fabricability of a particular design from the standpoint of accessibility and the sequence of manufacturing steps is sometimes overlooked in the early stages of design. Consequently, prolonged schedules and unexpected manufacturing delays may result.

The repairability of a structure represents another important consideration that is all too often neglected in the early design considerations. Disassembly of components for repair may entail prolonged schedule delays and added costs. Components not requiring repair may have to be disassembled to reach the defective component. Cutting of welded or brazed joints may be involved, and this could result in a very complicated and expensive reassembly job.

Clearly, it is essential that the design engineer, the manufacturing engineer, and the materials and process engineer should form a "team"

early in the design formulation phase. Such early coordination can help assure the successful fabrication of a system within the cost and schedule limitations.

Welding Fabrication Variables

It is informative to consider the fabrication variables in the manufacture of a welded system. The scope of this guidebook does not permit a detailed discussion of these variables. However, a mere listing of some of the more important variables serves to illustrate the complexity and scope of the welding fabrication problems.

I. General Design

A. Welded Types
1. Circumferential Joints
2. Longitudinal Joints
3. Closure Joints
4. Head Attachment
5. Port Attachment
6. Other Joints

B. Thickness and Contour Variations
1. Gradual
2. Abrupt

C. Dimensional Control
1. Longitudinal Shrinkage
2. Transverse Shrinkage
3. Buckling Deformation

II. Material Selection

A. Base Metal
1. Mill Form and Availability
a. Sheet
b. Forging
c. Extrusion
d. Casting
e. Other
2. Mill Heat Treatment
3. Surface Condition
a. Roughness
b. Coated
c. Spectral Reflectance
4. Chemical Composition
a. Alloy Range

b. Residual Element Range
c. Segregates
5. Mechanical Properties
a. Uniaxial Tensile Properties
b. Fracture Toughness
c. Others (dependent upon design requirements)
6. Metallurgical Properties
a. Heat-Treatment Response and Control
b. Metallurgical Stability
c. Soundness - Inclusions and Defects

B. Welding Filler Metal
1. Availability and Form
2. Chemical Composition (Alloy Range and Residuals)
3. Surface Cleanliness
4. Packaging and Storage

C. Shielding-Gas or Flux
1. Moisture Control
2. Gaseous Impurities
3. Contamination

III. Welding Factors

A. Preparation for Welding
1. Joint Preparation
a. Design
b. Machining
c. Cleaning
d. Clean Storage Prior to Welding
2. Fixturing and Tooling
a. Alignment
b. Distortion Control
c. Backup Tooling
d. Manipulators
3. Weld-Joint Fitup
a. Mismatch
b. Faying Interface Gap
4. Fabrication Sequence

B. Welding Process
1. Process and Equipment Selection
2. Welding Conditions
a. Number of Passes
b. Arc Current
c. Arc Voltage
d. Welding Speed
e. Gas Flow (Torch and Auxiliary)
f. Filler Wire
3. Preheat and Postheat and Heat Treatment

severely degraded by such reactions. Very small concentrations of carbon, hydrogen, oxygen, and nitrogen can produce severe embrittlement. Therefore, great care must be taken to assure against weld contamination. Special inert-gas shielding methods must be employed even when employing the inert-gas welding methods. Trailing shields and provisions for underside protection during welding are virtually mandatory. Very sophisticated vacuum-purgeable chambers are often used to achieve the high atmospheric purity that is required.

The preparation of titanium alloys for welding also requires special attention. Degreasing operations are usually employed to clean metal parts prior to welding. Chlorinated hydrocarbons such as trichlorethylene are frequently employed. However, chlorine-bearing residue can cause stress-corrosion cracking in titanium alloys during welding or during subsequent stress relieving or sizing operations. Therefore, the use of chlorinated hydrocarbon solvents for preweld cleaning should be avoided.

Porosity formation can represent a very severe problem in titanium alloys especially in the thinner gages (0.020 in. thick and less). Surface-adsorbed contaminants appear to cause porosity, although the specific contaminants have not been uniquely identified. Thin-gage material appears to be more susceptible to porosity formation than thicker gages presumably because of the higher surface area to volume ratio, hence, potentially higher concentrations of surface-adsorbed contaminants. Preweld cleaning procedures must be very carefully selected and controlled to avoid the porosity problem, especially in the thin-gage materials.

Generally the weld-joint efficiencies (from a uniaxial tensile strength standpoint) in Ti-6Al-4V or Ti-5Al-2.5Sn welds exceed 90% of the base material strength. However, ductility and fracture toughness may exhibit much more severe degradation due to welding, especially at cryogenic temperatures. Frequently, lower alloy or commercially pure filler metal is used for welding to achieve superior ductility and toughness at the expense of some small loss in strength. The loss in strength depends primarily upon the extent of filler metal and base metal mixing that results from the fusion that takes place during welding.

Titanium alloys cannot be readily welded to dissimilar metals. Severe embrittlement generally develops because of the formation of intermetallic compounds or excessive solid solution. Transition joints between titanium and other metals must be evaluated individually, and metallurgically bonded joints, if required, will very likely require special development.

Aluminum Alloys

Precipitation-hardenable aluminum alloys 2014 and 2219 are the most common alloys used for welded pressurized-gas systems. These alloys are generally welded by the inert-gas processes.

Undoubtedly the most troublesome problem encountered in the welding of aluminum alloys is porosity formation. Hydrogen is firmly established as the principal cause of porosity. Porosity forms when hydrogen, formerly dissolved in molten weld metal, coalesces out of solution upon solidification. Hydrogen originally may enter the molten weld pool as a result of the dissociation of hydrogen-containing contaminants in the welding arc. Water contamination, either surface adsorbed or in the atmosphere, is the most common source of hydrogen. Porosity control and minimization is achieved by implementing rigid process-control requirements to avoid contamination with hydrogen-bearing matter.

Unlike the titanium alloys, the aluminum alloys can suffer substantial strength loss when welded. For example, 2014-T6 or 2219-T87 will generally suffer a 40 to 60% loss in tensile strength after welding. A 10 to 20% increase in strength (compared to as-welded) may be realized if postweld heat-treatment is possible. Electron-beam welds generally exhibit superior strength compared to inert-gas-welded material, particularly for thicker sections. This is primarily due to the finer microstructure generally attainable in thick electron-beam welds.

Hot cracking is another problem area associated with the welding of 2014 and 2219 alloys. Hot cracking may occur in both weld metal and heat-affected regions of the parent metal. The problem is caused mainly by the

formation of low-melting-point constituents, which tend to form continuous networks. Cracking tends to follow these continuous networks. Cracking problems are minimized by the careful control of the welding process (heat-input control) and by the careful design of tooling.

Coarse-grained 2014 or 2219 extrusions are extremely susceptible to hot cracking and should, therefore, be avoided in critical welded structures. Occasionally, sheet material may exhibit an unusually coarse grain size because of prior forming and heat treatment exposures. Such material may also be very susceptible to hot cracking during welding, and precautions should be taken to avoid such a condition.

Structural fusion welds between aluminum alloys and dissimilar metals cannot be readily achieved because of the formation of brittle intermetallic compounds. The methods that have been developed incorporate the use of inter-mediate alloys, which are compatible one with the other. For example, the joining of aluminum to stainless steel has been accomplished by using Monel (a nickel/copper alloy) as a transition member to which both aluminum and steel may be welded. However, such joints have poor properties. Special diffusion bonding and brazing methods have also been employed, but they do not have wide-spread acceptance or application.

Cold-worked Stainless Steels

The use of cold-worked stainless steels, such as Am 355 and modified AISI 301, for pressurized gas systems has been very limited. These materials are normally welded in the annealed condition and are generally quite weldable. They are subsequently subjected to cryogenic exposures, cold-worked, and often subjected to a tempering treatment. The Arde-process, which employs a specially modified AISI 301 stainless, utilizes cryogenic stretch forming as a one-step operation. Joint efficiencies both from a tensile and toughness standpoint approach 100% when the weld-deposit chemical composition matches that of the base material.

These two alloys are probably the most weldable of all the alloys used in pressurized gas systems. Hot-cracking problems may occasionally develop, but they are usually solved by modifying the weld-deposit chemical

composition. The details of this problem and its solution represent a highly specialized metallurgical phenomenon, and it is beyond the scope of this guidebook.

Transition welds between stainless steel and other ferrous alloys are easily achieved by using austenitic filler metals (such as AISI 309 or 310).

Inconel 718

Inconel 718 is the only nickel-base alloy that is used as a pressure-vessel material for pressurized gas systems described in this guidebook. Most components are welded by the gas-tungsten arc process.

Porosity is often encountered if the preweld cleaning procedures are inadequate, although the specific cause (or causes) of porosity has not been identified.

Dissimilar filler metals are sometimes employed to weld Inconel 718, although a matching 718 filler is normally used.

The joint efficiencies of welds deposited in annealed material (in terms of base-metal tensile ultimate or yield strength) generally exceeds 90% in the as-deposited condition. Higher joint efficiencies may be attained if postweld aging treatments are employed, as they normally are. Weld toughness also appears to be quite comparable to the parent material after an equivalent postweld heat treatment.

Dissimilar metal joints to stainless steels and other ferrous alloys may be achieved using austenitic filler metals. Fusion joints to nonferrous alloys are not generally attainable.

Low-alloy Hardenable Steels

Low-alloy hardenable steels are not commonly used for pressure-vessel material in pressurized gas systems. Toughness and strength-to-weight ratios are considered inadequate.

Most of the steels are modifications of AISI 4340 that are employed at the 190,000-psi minimum-yield-strength level. Included in this category are AMS 6434, D6-AC, and AISI 4340.

These steels have good weldability if the proper preheat and post-heat treatments are used. Otherwise severe cracking problems can result.

Postweld heat treatment is mandatory to regain strength and ductility after welding. Weld toughness is generally quite inferior to the parent material under even the best conditions of welding and postweld heat treatment. Compared to the previously discussed alloys, this group has the worst welded toughness on a strength-to-weight basis.

New steel alloys, particularly the new maraging class (which does not belong in the low-alloy hardenable-steel group), have the potential of eventually being used for pressurized gas systems. These types of alloys appear to exhibit unusually high weld toughness even at very high strength levels.

VIII-4 REFERENCES

1. Tiffany, C. F. and Masters, J. N. "Applied fracture mechanics," Fracture Toughness Testing and Its Applications. ASTM STP No. 381, 1965.

2. Watson, J. F. "Materials at cryogenic temperatures," Materials for Missiles and Spacecraft. Parker (Ed.), McGraw-Hill Book Co., New York, 1963.

3. Alper, R. H. "Cryogenically stretch-formed type 301 stainless steel for cryogenic service," Materials Research and Standards. p. 525-32, Oct. 1964.

4. Anon. (Arde-Portland Inc.) High Performance Pressure Vessels Produced by Ardeform Process.

5. Anon. (International Nickel Co.) Supplementary Data Report, Inconel 718.

6. Christian, L., et.al. Mechanical Properties of Titanium-5Al-2.5Sn Alloy at Room and Cryogenic Temperatures.

7. Anon. (Boeing Co.) Fracture toughness and subcritical flaw growth characteristics of Saturn S-1C tankage materials. Final Report D2-22802.

8. Campbell, J. E. Properties and applications of Aluminum alloys at low temperatures. ASTM, Chicago, Ill., June 21-6, 1964.

9. Durham, T. F., McClintock, R. M. and Reed, R. P. (Cryogenic Engineering Lab., Boulder, Colo.) Cryogenic Materials Data Handbook. Supplement No. 6, OTS PB 171 809-6.

10. Campbell, C. M. Supercritical cryogenic storage tanks. Rept. No. W4-1-65, Presented at the Western Metal Congress, Los Angeles, Calif., Feb. 22-6, 1965.

11. Anon. Effects of low temperatures on structural metals. NASA SP-5012, NASA Technology Utilization Rept., Dec. 1964.

12. Jackson, J. O. and Boyd, W. K. Stress corrosion cracking of Aluminum alloys. DMIC Memo 202, Feb. 15, 1965.

13. Uhlig, H. H. Corrosion and Corrosion Control. John Wiley and Sons Inc., New York, 1963.

14. Jackson, J. D., Boyd, W. K. and Miller, P. D. Reactivity of metals with liquid and gaseous oxygen. DMIC Memo 163, Jan. 15, 1963.

15. Jackson, J. D., Miller, P. D. and Boyd, W. K. Reactivity of Titanium with gaseous N_2O_4 under conditions of tensile rupture. DMIC Memo 173, Aug. 1, 1963.

16. Levenson, E. O. Compatability testing of structural materials with rocket propellants. Presented at the 1965 Western Metal Congress, Feb. 22-6, 1965.

17. Chafey, J. E., Witzell, W. E. and Scheck, W. G. (General Dynamics/ Astronautics) Titanium - oxygen reactivity study. NASA-2664, AE62-0674, July 2, 1962.

18. Parker, E. R. Materials for Missiles and Spacecraft. McGraw-Hill Book Co., New York, 1963.

19. Anon. (Bell Aerosystems Co.) Storable propellant data for the Titan II Program. AFBMD TR-61-65, March 1962.

20. Coplan, H. I. (Aerojet-General Corp.) Screening tests on twenty elastomers for compatibility in nitrogen tetroxide. MN-146.

21. Eldridge, E. A. and Deem, H. W. Report on physical properties of metals and alloys from cryogenic to elevated temperatures. ASTM, Philadelphia, Penn.

22. Anon. (E. I. Du Pont de Nemours and Co., Inc.) Effect of 'Freon' Fluorocarbons on Elastomers. Booklet B-12A (preliminary).

23. Eiseman, B. J. Jr. Effect on elastomers of 'Freon' compounds and other halohydrocarbons. Refrig. Eng., Dec. 1949.

24. Liberto, R. R. (Bell Aerosystems Co.) Research and development on the basic design of storable high-energy propellants systems and components. AFFTC TR-60-61, May 19, 1961.

25. Liberto, R. R. (Bell Aerosystems Co.) Titan II Storable Propellant Handbook. AFBMD TR-62-2, 1962.

26. Anon. (Liquid Propellant Information Agency) Liquid Propellant Manual. LPIA/LPM-1, 1961.

27. Anon. (Lockheed-Georgia) Main Propellant Tank Pressurization System Study and Test Program, Design Handbook, Vol. III. AFFTC TR-61-21, 1961.

28. Lyons, R. H. (Aerojet-General Corp.) Materials for nitrogen tetroxide service. F-02668(101216-2).

29. Anon. (Pennsalt Chemicals Corp.) Perchloryl Fluoride. Booklet DC-1819.

30. York, H. J. (Aerojet-General Corp.) Compatibility of various materials of construction with nitrogen tetroxide. RM-13.

31. Elsea, A. R. and Fletcher, E. E. The problem of hydrogen in steel. DMIC Memo 180, Oct. 1, 1963.

32. Elsea, A. R. and Fletcher, E. E. Hydrogen-induced, delayed, brittle failures of high-strength steels. DMIC Rept. 196, Jan. 20, 1964.

33. Fletcher, E. E. and Elsea, A. R, The effects of high-pressure, high-temperature hydrogen on steel. DMIC Rept. 202, March 26, 1964.

REFERENCES (contd)

34. Altemose, V. O. J. Appl. Phys. 32, p. 1309, 1961.

35. Barrer, R. M. J. Chem. Soc. 1934, p. 378.

36. Barrer, R. M. Trans. Faraday Soc. 36, p. 1235, 1940.

37. Barrer, R. M. and Skirrow, G. J. Polymer Sci. 3, p. 549, 1948.

38. Barton, R. S. AERE-M599, 1960.

39. Borman, J. K. and Nardella, W. R. Vacuum 12, p. 19, June 1962.

40. Brubaker, D. W. and Kammermeyer, K. Ind. Eng. Chem. 44, p. 1465, 1952.

41. Brubaker, D. W. and Kammermeyer, K. ibid. 45, p. 1148, 1953.

42. Brubaker, D. W. and Kammermeyer, K. ibid. 46, p. 733, 1954.

43. Doty, P. M., Aiken, W. H. and Mark, H. ibid. 38, p. 788, 1946.

44. Flint, P. S. KAPL-659, 1951.

45. Hamm, W. R. J. Chem. Phys. 1, p. 476, 1933.

46. Hare, E. F. Interim Report No. 1, Contract No. NOnr 2848(00), July 1960.

47. Hsieh, P. Y. Interim Report No. 2, Contract No. NOnr 2848(00), Jan. 1961.

48. Johnson, F. M. G. and Larose, P. J. Am. Chem. Soc. 46, p. 1377, 1924; 49, p. 312, 1927.

49. Michaels, A. S. and Bixler, H. J. J. Polymer Sci. 50, p. 413, 1961.

50. Myers, A. W., et.al. TAPPI 44, p. 58, 1961.

51. Myers, A. W., Stannett, V. and Szwarc, M. J. Polymer Sci. 35, p. 285, 1959.

52. Myers, A. W., et.al. Modern Plastics 37, p. 139, June 1960.

53. Norton, F. J. J. Am. Ceramic Soc. 36, p. 90, March 1953.

54. Norton, F. J. J. Chem. Phys. 22, p. 1145, 1954.

55. Norton, F. J. quoted in Ref. 44.

56. Rudd, R. W. and Vetrano, J. B. NAA-SR-4898 Rev., 1961.

57. Rudd, R. W., Vose, D. W. and Johnson, S. J. Phys. Chem. 65, p. 1018, 1961.

58. Ryder, H. M. Elec. J. 17, p. 161, 1920.

59. Sarge, T. W. Anal. Chem. 19, p. 396, 1947.

60. Smithells, C. J. and Ransley, C. E. Proc. Royal Soc. (London) A150, p. 172, 1935.

61. Stout, L. E., Geisman, R. and Mozley, J. M. Jr. Chem. Eng. Progress 44, p. 219, 1948.

62. Van Amerongen, G. J. J. Appl. Phys. 17, p. 972, 1946.

63. Van Amerongen, G. J. J. Polymer Sci. 5, p. 307, 1950.

64. Waak, R., et.al. Ind. Eng. Chem. 47, p. 2524, 1955.

65. Anon. Welding Handbook (5th Edn.) American Welding Society, New York, N.Y.

66. Sprouls and Brown (Aluminum Co. of America) Resistance of high-strength Aluminum alloys to stress corrosion. Technical paper No. 17, 1962.

67. Anon. (Aeroquip Corporation/Aircraft Corp.) Space-craft tooling and fitting. Bulletins Nos. 278, 279 and 280.

68. Anon. (Rocketdyne) Rocketdyne reports on In-Place welding, MPTR 4-251-5, May 25, 1964.

N67-32148

DESIGN GUIDE FOR PRESSURIZED GAS SYSTEMS

Pages 400 through 792

399-A

IX PERMEABILITY THEORY

TABLE OF CONTENTS

Section-Part	Title	Section-Part. Page
IX-0	List of Tables	IX-0.2
IX-1	Introduction	IX-1.1
IX-2	Polymeric Materials	IX-2.1
IX-3	Glasses	IX-3.1
IX-4	Metals	IX-4.1
IX-5	Laminates	IX-5.1
IX-6	Distinction Between Permeation and Mass Flow	IX-6.1
IX-7	References	IX-7.1

IX-0 LIST OF TABLES

Section-Part-Table	Title	Section-Part. Page
IX-2-1	Permeability of Three Polyethylenes at 25°C	IX-2.7
IX-2-2	Permeability of Plasticized and Unplasticized Polychlorotrifluoroethylene	IX-2.7

IX-1 INTRODUCTION

The transmission of a gas or a vapor through a polymeric or metallic film is, in the absence of flaws such as cracks, pinholes and the like, a process of activated diffusion. The gas must first adsorb on the surface of the film, then dissolve in the material, diffuse through the bulk, and desorb on the low pressure side. These steps always occur when gases or vapors diffuse through any material, but the relative importance of the various steps and the rate-controlling processes are sufficiently different to make it convenient to discuss each type of material separately. Accordingly, permeation through organic polymers, through inorganic glasses, and through metals are discussed in this order. This is followed by a brief discussion of laminates (including a metal foil, which may have pinholes, deposited on a polymer) and finally, consideration of simultaneous permeation and mass flow.

Specific permeation data are given for a number of materials in the Fluid Systems Component Section (XI) of this guidebook.

IX-2 POLYMERIC MATERIALS

With permanent gases, such as He, H_2, O_2, N_2, CO_2, the solubility in the polymer is sufficiently low so that the gases are diffusing through essentially unchanged polymer. Under these circumstances, in the steady state the amount transmitted per unit time per unit area, J, is given by

$$J = -D \frac{dc}{dx} \tag{1}$$

where D is the diffusion constant and dc/dx is the concentration gradient within the polymer film. Because of the small solubility, Henry's law holds and thus $c = Sp$, where S is the solubility coefficient and p is the pressure of the gas. Substituting in Equation (1),

$$J = -DS \frac{dp}{dx} \tag{2}$$

The product DS is the permeability constant, P. Since in the steady state J is independent of x, Equation (2) can be integrated to give

$$P = \frac{-Jd}{\Delta p} \tag{3}$$

where d is the thickness of the film.

The usual method of measuring the permeability of a polymeric film is to establish a known pressure of the gas or vapor on one side of the film and to observe the transmission of the gas or vapor by the pressure increase on the other side. The low pressure side is generally at high vacuum, so that the pressure drop across the film is substantially constant during the course of the experiment. The method has the advantage of simple mathematical analysis but can be very slow under some circumstances. The method used by Stanford Research Institute measures the rate of permeation (as opposed to the total amount permeated) by means of a mass spectrometer, and allows the simultaneous determination of two or more species in a mixture.

ORIGINAL PAGE IS
OF POOR QUALITY

Both methods are amenable to the analysis of the transient state to separate the diffusion and solubility coefficient parts of the permeability coefficient. One means of analysis of the transient state can be termed the "late" approximation and the other the "early" approximation. The mass spectrometer method is particularly suitable for the latter, and in certain circumstances this can, in addition to separating diffusion and solubility, considerably shorten the time of the experiment.

Both means of analyzing the transient state start with Fick's second law and the assumption that the diffusion constant is independent of concentration which, in the one dimensional case, gives

$$\frac{dc}{dt} = D\frac{d^2c}{dx^2} \tag{4}$$

where t is the time. The late approximation was introduced by Daynes[7] and developed by Barrer.[3] Solution of Equation (4) by a Fourier series in the coordinates and an exponential in the time with the boundary conditions $c = c_0$ at $x = 0$ for all t, $c = 0$ for $0 < x < d$ for $t = 0$, and $c = 0$ at $x = 1$ for all t, leads to

$$Q = \frac{AD}{d}c_0\left[t - \frac{d^2}{6D} - \frac{2d^2}{\pi^2 D}\sum_{m=1}^{\infty}(-1)^m\frac{\exp(-m^2\pi^2 Dt/d^2)}{m^2}\right] \tag{5}$$

where A is the area of the film and Q is the quantity transported across the film in time t. At sufficiently long times Equation (5) reduces to

$$Q = \frac{ADc_0}{d}(t - \tau) \quad . \tag{6}$$

Thus Q becomes linear in t with a slope $(APp_0)/d$ (since $c_0 = Sp_0$, where p_0 is the upstream pressure) and an intercept on the time axis τ and

$$D = \frac{d^2}{6\tau} \quad . \tag{7}$$

Hence, by this method, one can obtain both P and D and, consequently, S. An independent check is to measure the solubility directly. Excellent

agreement has been reported for a number of elastomer-gas systems by van Amerongen.[33]

The "early" approximation was used by Rogers, Buritz and Alport.[24] By a transformation a solution of Equation (4) is

$$J = 2Sp_1(D/\pi t)^{1/2} \sum_{m=1}^{\infty} \exp\left[-(d^2/4Dt)(2m+1)^2\right] \quad . \tag{8}$$

At times sufficiently *short* only the leading term in the series is important. Multiplying both sides of Equation (8) by $t^{1/2}$ and taking natural logarithms leads to

$$ln\ (Jt^{1/2}) = ln\ [(2Sp_1)(D/\pi)^{1/2}] - d^2/4Dt \quad . \tag{9}$$

Thus plotting the left hand number against t^{-1} should give a straight line of slope $-d^2/4Dt$. Having determined D, the value of S is given by

$$S = \left(\frac{\pi}{D}\right)^{1/2}\left(\frac{Jt^{1/2}}{2p_1}\right)\exp\ (d^2/4Dt) \tag{10}$$

and, since $P = DS$, this quantity is also determined.

From the early approximation all the quantities of interest can be derived. It is especially useful in the mass spectrometer method because rates are required, which are determined directly. The late approximation requires an integration. Rogers *et al.* actually used the pressure rise method in their application of the early approximation which, of course, required a differentiation and its accompanying errors.

At $t = 2.7\tau$ both the early and the late approximation are in error by 1.2%, so this can be considered a rough dividing line for the region of validity of the two methods.

Both D and S obey the Arrhenius relations:

$$S = S_0 e^{-\Delta H/RT}$$

$$D = D_0 e^{-E_D/RT}$$

ORIGINAL PAGE IS
OF POOR QUALITY

where ΔH is the heat of solution of the gas in the polymer and F_d is the activation energy of diffusion within the polymer. Consequently,

$$P = P_0 e^{-E_p/RT}$$

where $E_p = \Delta H + E_d$. In all cases E_d is positive (rate of diffusion increases with increasing temperature). The quantity ΔH is small and positive for the permanent gases, but may be negative and large in the case of easily condensable gases owing to the contribution of the heat of condensation.[25] As a result, a plot of the logarithm of the permeability *vs.* the reciprocal of the absolute temperature gives very nearly a straight line in the case of the permanent gases (increase in permeability with increasing temperature), but with easily condensable gases (*e.g.*, water through Nylon 6-6 or polyvinyl alcohol,[19] methyl bromide through polyethylene[26]) when the temperature is decreased the permeability may first decrease, pass through a minimum, and actually increase at still lower temperatures.

A knowledge of the chemical nature of the polymeric film is not sufficient to define its permeability—one important factor is crystallinity. In Table IX-2-1 are given the permeability of some polyethylene films of different crystallinities (as determined by density) for selected gases. Fairly good correlation can be obtained by assuming that the gases are soluble only in the amorphous portion of the polyethylene; similar results have been reported for permeation of water vapor through polyethyleneterephthalate.[14] Table IX-2-2 illustrates another effect, that caused by plasticizer. Chemical analysis of the two polymers would be nearly identical, but it can be seen that the presence of low molecular weight material enormously increases the permeability. This effect, in contrast to the effect of crystallinity, is largely due to an increase in the diffusion constant. Polyethyleneterephthalate shows in addition crystallinity effects such as those illustrated for polyethylene.

It would be desirable to be able to predict the permeability of an arbitrary gas-polymer system through basic principles or an empirical correlation requiring very few measurements. Unfortunately, no method of general applicability has been found. The solubility portion can, in a given polymer, be correlated fairly well with the normal boiling point of the gas,[25] its critical temperature,[33] or its Lennard-Jones force constant.[16] Correlations of diffusion constants have not been nearly so successful.

Michaels and Brixter[17] have had some success in correlating diffusion in polyethylene with a geometric impedance factor, a chain immobilization factor, and a "reduced.diameter" (involving the mean unoccupied distance between two chain segments). However, use of this correlation requires a great deal of knowledge about the polymer and its extension to other polymers has not yet been made. Salame[29] has published a correlation of the permeability of various organic materials through polyethylene by use of a "permachore." Although useful for related polymers such as polypropylene, he specifically states that the method cannot be applied to polymers such as nylon, Delrin, and other nitrogen- or oxygen-containing polymers.

The simplest correlation suggested is that of Rogers *et al.*,[25] who noted that the ratio of the permeabilities of some of the fixed gases is roughly independent of the nature of the polymer. Hence they suggested a "*G* value" for the following gases (at 30°C): N_2 = 1.0 (arbitrary), O_2 = 3.8, H_2S = 21.9, CO_2 = 24.2. This may serve as a guide in many cases, but it fails badly in other cases. Thus from Table VIII-2-1 it can be seen that the ratio of the permeability of O_2 to that of N_2 is indeed approximately 3, but CO_2 is only about twice as permeable as N_2. In the case of polytrichloroethylene (Table IX-2-2), on the other hand, the CO_2/N_2 ratio is 13-19.

The above discussion has been confined to the permeability of permanent gases, except for brief mention of temperature effects with easily condensable vapors. If the vapor is appreciably soluble in the polymer, the situation can become quite complicated, since in general Henry's Law will not be obeyed; this plus the plasticizing effect of the permeant will cause a strong dependence of the permeability constant on the vapor pressure of the permeant and the more or less unpredictable temperature effects already mentioned. Under these circumstances, the polymeric material is generally not suitable for space applications. In some cases, however, the possibility of such behavior must be expected, as in the following example.

According to a Bell Aerosystems report[13] MON (and hence presumably N_2O_4) comes to equilibrium across a 7-mil Teflon sheet in a few days. For a long mission with a re-start, it might be desirable to know the permeability with a relatively low pressure differential and near saturation on both sides.

In the mass spectrometric method for measuring permeabilities, the pressure on one side is set at p_0 and on the other at essentially zero. By definition, the over-all permeability $\overline{P}$, the thickness t, the flux J, and p_0 are related by:

$$J = \overline{P}p_0/t \quad . \tag{11}$$

One can equally well define a differential permeability by ($0 < x < t$):

$$J = Pdp/dx \quad . \tag{12}$$

Equating (11) and (12) and integrating from $x = 0$, $p = 0$ to $x = t$, $p = p_0$ gives a relation analogous to a well-known case for integral and differential diffusion coefficients:

$$\overline{P} = \frac{1}{p_0}\int_0^{p_0} p\,dp \tag{13}$$

Differentiating (13) with respect to p_0 gives the relation sought:

$$P = \overline{P} + d\overline{P}/d\ln p_0 \quad . \tag{14}$$

For most "permanent" gases through most films, $\overline{P}$ is independent of p_0 and Equation (14) is trivial. Where swelling occurs, however, P and $\overline{P}$ may differ appreciably. For water through Nylon 6-6 at 25°C, P(sat.) = 7.5$\overline{P}$(sat.), calculated from data of Myers *et al.*,[18] and for methyl bromide through polyethylene at −15°C, P(sat.) ≈ 7.8$\overline{P}$(sat.), calculated from the data of Myer *et al.*[15]

Table IX-2-1

PERMEABILITY OF THREE POLYETHYLENES AT 25°C
(Ref. 17)
α = vol. fraction amorphous

GAS	PERMEABILITY [cc(STP)/cm-sec-atm] x 10^7		
	Grex (α = 0.23)	Alathon 14 (α = 0.57)	Hydropol (α = 0.71)
He	0.087	0.375	1.20
O_2	0.0308	0.220	0.86
A	0.129	0.208	0.84
CO_2	0.0275	0.113	0.47
N_2	0.0109	0.074	0.304

Table IX-2-2

PERMEABILITY OF PLASTICIZED AND UNPLASTICIZED
POLYCHLOROTRIFLUOROETHYLENE
(Ref. 20)

GAS	TEMP., °C	PERMEABILITY [cc(STP)/cm-sec-atm] x 10^8	
		Unplasticized	Plasticized[a]
N_2	50	0.014	0.42
	75	0.065	1.95
O_2	0	0.003	0.083
	30	0.040	0.42
	60	0.22	2.13
CO_2	50	0.27	5.70

[a] Plasticized with low molecular weight polychlorotrifluoroethylene.

IX-3 GLASSES

The permeability of fused silica and certain glasses to helium is well known and can be troublesome under certain circumstances. Vacuum Dewars of some types of glass, for example, can be used to store liquid helium only for a day or two since they will lose their vacuum through helium permeation. Hydrogen, deuterium, and neon will also permeate fused silica, but the permeabilities of molecules larger than these (a dividing line of about 2.5 Å diameter) are enormously less.[21]

The permeabilities of the small gas molecules through glass follow an Arrhenius law as in the case of polymeric films just discussed, $P = P_0 e^{-E_p/RT}$. The glass composition plays a dominant role. The rate of permeation decreases as the content of glass formers, $SiO_2 + B_2O_3 + P_2O_5$ decreases; when this sum drops to 20-30%, the helium permeation rate is cut down, compared to silica glass, by a factor of a million.[21] This effect is attributed to alkali and alkaline earth oxides blocking the passages in the relatively open network of the glass-forming oxides. A similar picture of channels closing explains the fact that the permeability of quartz to helium is less than that of vitreous silica by a factor of 10^7 or more.

In summary, glass could involve a permeability problem, particularly with helium, but one that can easily be circumvented by proper choice of composition.

IX-4 METALS

The permeation of metals by gases is considered separately from polymers and glasses because of three outstanding characteristics: impermeability to noble gases, dissociation of diatomic gases in the process, and influence of surface films on the permeability.

All attempts to measure the permeability of noble gases have been unsuccessful. As examples, Ryder[28] found negative results on the permeability of iron to argon, as did Bauklon and Kayser[5] on that of nickel to helium, neon, argon, and krypton. The rare gas *ions* can be forced into metals under a potential gradient, but penetration is relatively shallow and upon heating the metal the gas is released.[21]

The processes of adsorption, dissociation, solution, and diffusion of a diatomic gas can lead to quite complicated rate laws under certain circumstances. Various limiting equations are given by Ash and Barrer.[1] However, for most metals at pressures over one atmosphere a square root law is followed as is the exponential relation, already mentioned in the case of polymers and glasses, so the permeability may be expressed by

$$P = \frac{P_0(p_0^{1/2} - p_1^{1/2})e^{-E_p/RT}}{d}$$

where k is a constant and p_0 and p_1 are the upstream and downstream pressures. This law is not followed when there is an appreciable coherent film (usually oxide) on the metal, when there is radiative or chemical interaction, or when the solubility of the gas is very high. An example of the latter is H_2-Pd above about one atmosphere, where the permeation rate is proportional to the 0.8 power of the pressure.[8] Examples of chemical interaction are the diffusion of nitrogen and oxygen through titanium[34] and hydrogen through zirconium.[11] In these cases a new phase is formed above a limiting pressure (rather low unless the temperature is high) and the reaction becomes essentially a corrosion reaction, with the effective gas pressure in equilibrium with the upper limits of the new phase at the temperature in question. Under these circumstances the above equation becomes quite meaningless.

ORIGINAL PAGE IS
OF POOR QUALITY

In most studies on the permeation of gases through metals, precautions are taken to eliminate surface films as far as possible in order to simplify interpretation. From a practical standpoint, the effect of surface films must be taken into account. As Flint[9] points out, surface films may be expected to become important barriers to diffusion when the oxide coating has a specific volume equal to or greater than that of the base metal. Metals falling in this category are Al, Si, Cr, Mn, Fe, Co, Ni, Cu, Zn, Pd, Ce, and Pb. Very few systematic studies have been made in this field. Flint[9] prepared oxide films on Type 347 stainless steel by treatment in wet hydrogen and observed reduction in permeation rate of as much as 400 fold. However, these might be termed transient tests as the permeability increases with time, presumably as the oxide coating was reduced. Experiments with hydrogen and Inconel have given permeation rates independent of the thickness of the metal, thus indicating an over-riding effect of a surface film.[22] Several authors[32,12,30,27] have noted the effect of oxide films on aluminum or aluminum alloys; drops in permeability as much as 1000-fold have been found.

An effect that may become important for hydrogen (and possibly other gases) in space environment is production of atoms by radiation, although recent calculations[35] have tended to minimize this factor. Production of atomic hydrogen at iron surfaces by corrosion reactions with water and its subsequent diffusion into the metal is well known to corrosion engineers. The chemically produced atoms are equivalent to those at very high pressures and temperatures for normal hydrogen and, as previously mentioned, it is the atomic hydrogen that affords the mechanism for diffusion. One industrially important consequence of this effect was in the early days of metal vacuum tube manufacture, when it was found that water contained in sodium silicate paint was reacting with the iron, and hydrogen diffusing through the tubes made them gassy and inoperable.[21] Similarly, it has been found that a glow discharge increased the permeability of aluminum to hydrogen five-fold; conditions were not well enough defined in this case to attach quantitative significance to the result.[27]

IX-5 LAMINATES

The discussion up to this point has been concerned with homogeneous materials. There are, however, important practical cases where laminates are used. It is convenient for present purposes to distinguish two cases: one is where two or more plastics or elastomers are laminated and the permeabilities of the materials to the gas in question, while different, are not so far apart that any one of them can be neglected (an example is the use of styrene-butadiene rubber liners in continuous-filament glass fiber-reinforced epoxy pressure vessels); the second is where a metal foil is laminated onto a polymer film as a permeation barrier, in which case the foil may be considered (for noble gases at least) to have zero permeability but the possibility of pinholes and their influence must be considered.

In the plastic laminate case one can, as before, define an over-all permeability, P by

$$P = \frac{Jd}{\Delta p} \quad . \tag{15}$$

In the steady state J is the same for all elements i of the laminate, so in addition

$$P_i = \frac{Jd_i}{\Delta p_i}$$

and also

$$\Delta p = \sum_i \Delta p_i$$

$$= J \sum_i \frac{d_i}{P_i} \quad . \tag{16}$$

Substitution of (16) into (15) and rearranging gives,

$$\frac{d}{P} = \sum_i \frac{d_i}{P_i} \tag{17}$$

ORIGINAL PAGE IS
OF POOR QUALITY

Equation (17) has been experimentally verified by Phargava *et al.*,[6] for polyethylene-glassine laminates.

The case of a foil with pin-hole has been treated by Prins and Hermans.[23] For a foil, impermeable in bulk but with n circular holes/cm^2 of radius r, laminated onto a polymer of thickness d and permeability P, and for $d/r > 0.3$ (the only case of practical interest) they found (in the present notation)

$$J = \frac{P\Delta p}{d}\theta(1 + 1.18d/r) \quad ; \quad \theta << 1 \tag{18}$$

where $\theta = n\pi r^2$, the fraction of free surface. The first two terms on the right of Equation (18) simply express the reduction of permeation because of the reduction in free surface. The third term, however, can be a large multiplying factor, reflecting the spread of the diffusing gas in the polymer film. For very large value of d/r, Equation (18) reduces to

$$J = 3.7nrP\Delta p \tag{19}$$

and the flux becomes proportional to the perimeter of the holes rather than to their area.

IX-6 DISTINCTION BETWEEN PERMEATION AND MASS FLOW

The question often arises in permeability measurements whether the gas flux observed is all due to true permeation or whether part of it is due to flow through fine capillaries, whether they exist in the very nature of the film being studied (as is postulated by one group[31] for polystyrene below the glass transition temperature) or because of flaws such as cracks and pinholes. One pragmatic approach, and often a successful one, is to determine apparent permeabilities on a number of samples, with the presumption that they won't all have the same number of flaws, and with different sample thicknesses, with the presumption that a flaw is less likely to penetrate through in the case of the thicker samples. If substantially the same value for P is obtained in all cases it is fairly good evidence either that true permeability is being measured or that other means of passing gas are inherent and uniform in the film being studied.

Sometimes the above method is not practical, possibly because of a limited choice of samples or because individual experiments take too long. Further, if inherent capillaries are suspected, it may be desirable to confirm or disprove the hypothesis. In either case a great deal can be learned from the behavior of the apparent permeability with temperature. The development below will be confined to a slightly soluble gas. As already pointed out, this is the only case where the theoretical temperature behavior of the permeability is simple. For simplicity it will also be confined to the case where the film has uniform capillaries and the gas in the capillaries is in equilibrium with that dissolved in the film, although these simplifications do not appreciably affect the conclusions to be drawn.

In the steady state the over-all flux is simply the sum of that due to diffusion and that due to mass flow:

$$-J = D\frac{dc_f}{dx} + cv_g \qquad (20)$$

where c_f denotes the concentration of gas dissolved in the film, c_g that in the gas phase in the capillaries, θ the fraction of the cross section that consists of capillaries, and v the velocity of the gas in the capillaries. Substituting $c_f = Sp$ and $c_g = p/RT$, Equation (20) becomes

$$-J = DS\frac{dp}{dx} + \frac{\theta v}{RT}p \quad . \tag{21}$$

It is convenient to distinguish two cases: (1) the pressure is low enough, or the capillaries small enough, that Knudsen flow obtains, and (2) the capillaries are large enough that Poiseulle's law is followed.

In the Knudsen case, the velocity is given[10] by

$$v = -\frac{k_K}{\sqrt{\rho p}}\frac{dp}{dx} \quad ; \quad k_K = r/6 \tag{22}$$

where ρ is the density of the gas. If small gas imperfections are neglected, $\sqrt{\rho p} = p\sqrt{M/RT}$. With this relation and Equation (22), Equation (21) becomes

$$-J = DS\frac{dp}{dx} + k_K(RTM)^{-1/2}\frac{dp}{dx} \tag{23}$$

Equation (23) can be integrated directly, in x from 0 to d and in p from 0 to p_0 (for simplicity; a finite pressure on the low pressure side offers no difficulty) to give

$$-Jd = DSp_0 + \theta k_K(RTM)^{-1/2}p_0 \quad .$$

Recalling that the permeability is defined by $-Jd/p_0$, it is evidently given by

$$P = DS + \theta k_K(RTM)^{-1/2} \quad . \tag{24}$$

In the Poiseulle case the velocity is given by

$$v = \frac{k_p}{\eta}\frac{dp}{dx} \quad ; \quad k_p = r^2/8 \tag{25}$$

where η is the viscosity of the gas. Again neglecting gas imperfections, η can be expressed by $\eta = \eta_0(MT)^{1/2}$, where η_0 contains constants and the collision diameter. With this relation and Equation (25) substituted in (21), and proceeding exactly as before, the permeability is given by

$$P = DS + \frac{\theta k_p p_0}{2\eta_0 RM^{1/2}T^{3/2}} \qquad (26)$$

Frisch[10] using a somewhat different approach arrives at an equation formally identical with Equation (20) [his Equation (8)] and derives a relation identical with Equation (24) [his Equation (10)]. His Equation (12), however, is not the same as Equation (26) above, in that his implicitly contains $T^{-5/2}$ in the second term on the right. This appears to be an algebraic error [not typographical since it is carried on to his Equation (33)]. Intuitively one would expect that if the velocity is proportional to $T^{-1/2}$ the flux, which at a given velocity is proportional to $(RT)^{-1}$, would be proportional to $T^{-3/2}$.

The important point is that the product DS, which might be termed "true" permeability, depends exponentially on the temperature and almost invariably (in the case of permanent gases) strongly increases with increasing temperature. Any component of Knudsen flow, and even more strongly any component of Poiseulle flow, would *decrease* with increasing temperature. Thus the usual Arrhenius type plot of log P as ordinant *vs.* $1/T$ as abscissa should show strong curvature convex toward the origin as either of these types of mass transfer become important as the temperature is lowered. Indeed, as Frisch points out, a careful analysis of the temperature dependence of the apparent permeability should allow not only an estimate of how important mass flow is but what type of flow is important (molecular or viscous).

The above development has been based on mass transfer through a polymer film, where p is regarded as the driving force. There is no difficulty in extending it to metals, by simply substituting $c_f = Sp^{1/2}$ in Equation (20) and defining P as $Jd/p^{1/2}$. This would alter the pressure dependence of the second terms to the right in Equations (24) and (26), but the temperature behavior outlined in the previous paragraph would still obtain.

ORIGINAL PAGE IS
OF POOR QUALITY

IX-7 PERMEABILITY REFERENCES

1. Ash, R., and Barrer, R. M., *Phil. Mag.*, **48**, 1197 (1959).
2. Barrer, R. M., *Trans. Far. Soc.*, **35**, 628 (1939).
3. Barrer, R. M., "Diffusion in and Through Solids," Cambridge Press, London, 1951.
4. Barrer, R. M., and Skirrow, G., *J. Polymer Sci.*, **3**, 549 (1948).
5. Baukloh, W., and Kayser, *Z. Metallik.*, **26**, 156 (1934).
6. Bhargava, R., Rogers, C. E., Stannett, V., and Szwarc, M., *TAPPI*, **40**, 564 (1957).
7. Daynes, H., *Proc. Roy. Soc. (London)*, **A97**, 286 (1920).
8. DeRosset, A. J., *Ind. Eng. Chem.*, **52**, 525 (1960).
9. Flint, P. S., *KAPL-659*, 1951.
10. Frisch, H. L., *J. Phys. Chem.*, **60**, 1177 (1956).
11. Gulbransen, E. A., and Andrew, K. F., *J. Electrochem. Soc.*, **101**, 560 (1954).
12. Huffine, C. L., and Williams, J. M., *Corrosion*, **16**, 430t (1960).
13. Krivetsky, A., *et al.*, Bell Aerosystems Company, Report No. 7129-933003, March 1962.
14. Lasowski, S. W., and Cobbs, W. H., *J. Polymer Sci.*, **36**, 21 (1959).
15. Meyer, J. A., Stannett, V., and Szwarc, M., *Ind. Eng. Chem.*, **49**, 441 (1957).
16. Michaels, A. S., and Bixler, H. J., *J. Polymer Sci.*, **50** 393 (1961).
17. Michaels, A. S., and Bixler, H. J., *J. Polymer Sci.*, **50**, 413 (1961).
18. Myers, A. W., Meyer, J. A., Rogers, C. E., Stannett, V., and Szwarc, M., *TAPPI*, **44**, 53 (1961).
19. Myers, A. W., Meyer, J. A., Rogers, C. E., Stannett, V., and Szwarc, M., *TAPPI*, **44**, 58 (1961).
20. Myers, A. W., Tammela, V., Stannett, V., and Szwarc, M., *Modern Plastics*, **37**, 139 (1960).
21. Norton, F. J., *J. Appl. Phys.*, **38**, 34 (1956).
22. Norton, F. J., quoted by Flint, Ref. 9.
23. Prins, W., and Hermans, J. J., *J. Phys. Chem.*, **63**, 716 (1959).
24. Rogers, W. A., Buritz, R. S., and Alport, D., *J. Appl. Phys.*, **25**, 868 (1954).
25. Rogers, C., Meyer, J. A., Stannett, V., and Szwarc, M., *TAPPI*, **39**, 741 (1956).
26. Rogers, C. E., Stannett, V., and Szwarc, M., *TAPPI*, **44**, 715 (1961).
27. Russell, A. S., *Metal Progress*, **55**, 827 (1959).
28. Ryder, H. M., *Elect. J.*, **17**, 161 (1920).
29. Salame, M., *SPE Transactions*, October 1961, p. 153.
30. Sawatzky, A., and Rees, M. J., Atomic Energy of Canada, Ltd., *AECL-1252*, 1960.

ORIGINAL PAGE IS
OF POOR QUALITY

31. Schulz, G. V., and Gerrens, H., *Z. phys. Chem., N. Folge*, **7**, 182 (1956).

32. Smithells, C. J., and Ransley, C. E., Proc. Roy. Soc. (London), **A150**, 172 (1935).

33. VanAmerongen, G. J., *J. Appl. Phys.*, **17**, 972 (1946).

34. Wasilewski, R. J., and Kehl, G. L., *J. Inst. Metals*, **83**, 94 (1954-55).

35. Wiederhorn, N. M., 2nd Quart. Prog. Report, NASA Contract No. NAS5-664, 1961.

X SEALING AND LEAK DETECTION

Table of Contents

Section-Part	Title	Section-Part.Page
X-0	List of Tables	X-0.3
X-0	List of Figures	X-0.4
X-1	Introduction	X-1.1
	Leakage and Sealing	X-1.1
X-2	Static Seals	X-2.1
	Deformation of the Leak Path	X-2.3
	Material Properties	X-2.12
	Surface Topography and Fabrication Techniques	X-2.17
	Design Criteria-Metals and Plastics	X-2.23
	Design Criteria-Elastomers	X-2.37
X-3	Dynamic Seals	X-3.1
X-4	Recommendations for Minimum Leakage	X-4.1
	Static Sealing	X-4.1
	Dynamic Seals	X-4.4
	Comments	X-4.5
X-5	Leak Detection	X-5.1
	Source Locating Techniques	X-5.1
	Techniques for Method A	X-5.2
	Techniques for Method B	X-5.4
	Technique for Method C	X-5.6
X-6	Quantitative Leakage Measurements	X-6.1
	Techniques for Method D	X-6.2
	Technique for Method E	X-6.5
	Techniques for Method F	X-6.5
	Technique for Method G	X-6.6
	Technique for Method H	X-6.6
X-7	Accuracy of Leakage Measurements	X-7.1

Table of Contents (contd)

Section-Part	Title	Section-Part.Page
X-8	Sensitivity of Leakage Measuring Instrumentation	X-8.1
X-9	Conversion of Gas and Liquid Leakage Rates	X-9.1
X-10	Leak Detection Recommendations	X-10.1
X-11	References	X-11.1
X-A	Appendix	X-A.1
	Theoretical Leakage Considerations ...	X-A.1
	Modes of Leakage Flow	X-A-2
	Permeation Flow	X-A.7
	Molecular Flow through Long Channels .	X-A.12
	Theoretical Equations for Laminar, Incompressible Flow in a Uniform Channel (Liquid Flow)	X-A.16
	Theoretical Leakage Equations for Compressible Flow in a Uniform Channel	X-A.17
	Transition Flow	X-A.21
X-B	Appendix	X-B.1
	Calculation of Leakage Using Nomographs	X-B.1

X-O LIST OF TABLES

Section-Table	Title	Section-Part.Page
X-2-1	Meyer Hardness and Index for Various Materials	X-2.16
X-2-2	Calculated Leakage Rates	X-2.31
X-8-1	Instruments Suitable for Quantitative Leak Rate Measurements	X-8.1
X-A-1	Leakage Conversions	X-A.5
X-A-2	Time Conversion Table	X-A.6
X-A-3	Summary of the Nature of Gas Permeation	X-A.8
X-A-4	Mean Free Paths and Molecular Diameters for Various Molecules	X-A.15
X-A-5	Comparison of Leakage Rates	X-A.19
X-A-6	Comparison of Leakage Flow and Reynolds Number for Adiabatic Frictionless Flow (Case III) Exit Mach Number: 1	X-A.21

X-0 LIST OF FIGURES

Section-Figure		Section-Part.Page
X-2-1	Photomicrographs of Surfaces in Contact	X-2.2
X-2-2	Nondimensionalized Relationship Between Leakage Parameters	X-2.6
X-2-3	Leakage - Contact Stress Characteristics of a 2024-O Aluminum Gasket Pressed Between 1141 Steel Flanges. The Gasket Size was 2 1/8 x 2 1/2 x 1/8. The Pressure of the Sealed Fluid was Three Atmospheres	X-2.10
X-2-4	Leakage Characteristics of a 2 x 2 1/4 x 1/8 Square Buna N Ring Mated Against a 300-PVT Turned Steel Surface (Helium, 2 Atm Pressure, 85°F)	X-2.11
X-2-5	Typical Stress-Strain Diagram	X-2.15
X-2-6	Location of Topographical Measurements On a Circular Gasket Surface	X-2.19
X-2-7	Approximate Range of Waviness with Roughness for Various Fabrication Processes	X-2.20
X-2-8	Photomicrograph of a 321 Stainless Steel Surface Polished with Diamond Dust	X-2.24
X-2-9	Interferometer Photomicrograph of a 321 Stainless Steel Surface as Shown in Figure X-2-8.	X-2.24
X-2-10	Photomicrograph of a 321 Stainless Steel Surface with Fine Turned and Polished Grooves	X-2.24
X-2-11	Interference Photomicrograph of a 321 Stainless Steel Surface as Shown in Figure X-2-10. Roughness is approximately 15 μ in. PTV	X-2.24
X-2-12	Photomicrograph of a 321 Stainless Steel Lapped Surface	X-2.25

List of Figures (contd)

Section-Figure		Section-Part.Page
X-2-13	Interference Photomicrograph of the 321 Stainless Steel Surface Shown in Figure X-2-14. Roughness is approximately 2 μ in. PTV	X-2.25
X-2-14	Photomicrograph of a 6061T6 Aluminum Lapped Surface	X-2.25
X-2-15	Interference Photomicrograph of 6061T6 Aluminum Surface Shown in Figure X-2-14. Roughness is Approximately 5 μ in. PTV	X-2.25
X-2-16	Design Criteria for Turned Surfaces. Surface Roughness is Shown as a Parameter	X-2.26
X-2-17	Design Criteria for Ground Surfaces. Surface Roughness is Shown as a Parameter	X-2.27
X-2-18	Design Criteria for Lapped and Polished Surfaces. Surface Roughness is Shown as a Parameter	X-2.28
X-2-19	Geometry of a Sealing Cover	X-2.31
X-2-20	Hysteresis Effects for an Aluminum on Steel Interface (Aluminum Gasket 2A; Helium; 95 psi Pressure; 80°F)	X-2.34
X-2-21	Leakage - Normal Stress for Yatabe 347 Stainless Steel Specimens (First Set)	X-2.35
X-2-22	Circular Ring Pressed Between Two Flanges	X-2.39
X-2-23	Approximate Geometrical Representation of the Seal Interface	X-2.39
X-2-24	Theoretical and Experimental Leakage Characteristics of a Butyl Rubber Ring. The Net Interface Load is Normalized to the Maximum Pressure Load to Show the Relative Effects of Increasing Load. Pressure Difference Across the Ring is Shown as a Parameter	X-2.42

List of Figures (contd)

Section-Figure		Section-Part.Page
X-6-1	Experimental Mass Leak Measurement System	X-6.4
X-9-1	Flow Mode in Typical Hardware Leak; Needle Valve	X-9.3
X-B-1	Radial Channel	X-B.1
X-B-2	Nomograph for Incompressible Liquid Leakage	X-B.2
X-B-3	Schematic Representation of Nomograph	X-B.3
X-B-4	Nomograph for Gas Leakage	X-B.5
X-B-5	Schematic Representation of Figure X-B-4	X-B.6
X-B-6	Nomograph for Calculation of $1 + \frac{11.5\ P_o}{(P_1+P_2)}\ \frac{\lambda_o}{h_T}$	X-B.7
X-B-7	Schematic Representation of Figure X-B-6	X-B.8

X-1 INTRODUCTION

The topics of sealing and leak detection are closely interrelated in that the degree of sealing can only be established by suitable detection methods. Furthermore, the phenomena of sealing is somewhat independent of what is being sealed. To be more concise the mechanism of sealing can be viewed without consideration to applications such as valves, connectors, and other hardware items. Since most mechanisms of sealing may be found in all varieties of pressurization system components, certain generalizations can be considered with respect to sealing. This constitutes the objectives of this Section wherein fundamentals of sealing can be considered and subsequently applied to the hardware items as contained in Section XI.

Leakage and Sealing

The development of space vehicles imposes requirements of hitherto unknown severity on the leak-tightness of fluid systems. Losses of fluids contribute to detrimental decrease in space vehicle payload, influence mission accomplishment, and reliability, produce explosion hazards, and cause perturbations in vehicle trajectories due to leakage impulse.

The source of leakage can be described as gross or localized depending upon the mechanism of leakage. Gross effects are permeation or molecular diffusion through solid materials such as the walls of a pressure vessel. Localized leakage is generally attributable to seals where a seal is defined as a barrier to the transport of a fluid from one region to another formed by the mating of two materials together. Hence, the leakage is localized to the interface formed at the material juncture. The distinction between the mechanisms of leakage form a basis for an engineering definition of sealing, or specifically, seals. Since an objective of this Section is sealing, the sealing of primary interest is that of localized leakage which is consistant with the commonly accepted application of a seal. Gross leakage is considered in terms of effects rather than as a sealing problem and as such, is discussed separately in Appendix X-A of this Section.

Before Proceeding further, an additional distinction between seals must be made besides that of the simple joining of two materials together. If relative motion occurs between the materials, the seal is described as a dynamic seal while the absence of motion implies a static seal. Each of these topics is considered separately.

X-2 STATIC SEALS

When the surfaces of materials are placed together, void spaces and contact junctions are formed. It can be stated confidently that leak paths are formed by the interconnection of void spaces, whereas little can be said about the actual nature of leak paths except that they are generally small in size. The void spaces are produced by fabrication marks, damage, and foreign contaminants. An example of the nature of the interface between two materials is shown in Figure X-2-1. These photomicrographs are of a lathe-turned surface pressed against a flat glass plate. These figures, obtained from Reference 3, are helpful in providing a qualitative understanding of the leak path when viewed from the chance interconnection of void spaces (light areas) to produce a continuous leak path across the interface.

To achieve minimum or zero leakage, the most obvious requirement is to eliminate or diminish the number and size of the leak paths. Several methods are available for achieving this goal. These methods are associated with specific classes of seals identified as separable, semi-separable and non-separable seals.

Separable seals are formed by two surfaces forming an interface which after being joined together can be readily disengaged. The leak paths in the interface can be affected by:

(1) The pressing of the surfaces together producing microscopic deformation of asperities. The deformation is characterized as plastic, elastic, or both.

(2) The pressing together of surfaces where the mode of surface deformation is essentially elastic and is associated with the deformation of the substrate.

(3) The inclusion of a third material in the interface is used to fill the void spaces. These additional materials are usually liquids and are described as sealants. Other solid materials can be employed but the general effects are as described by the preceding two factors.

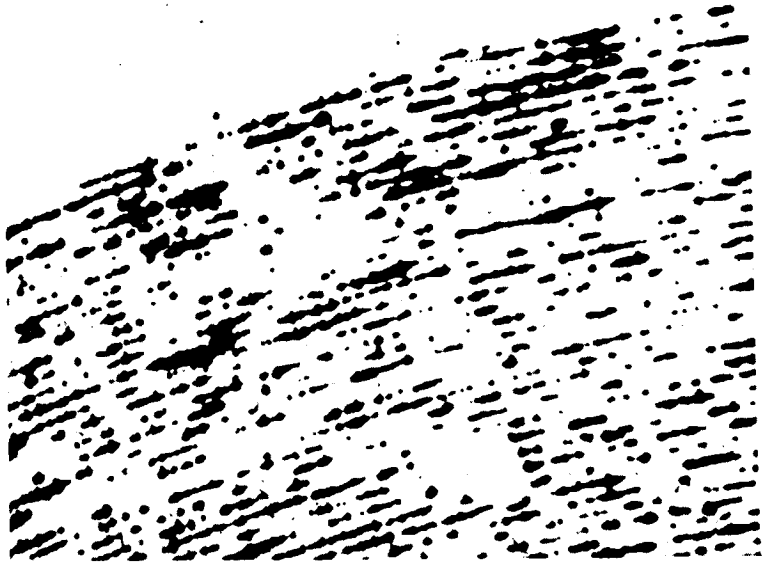

Contact Pattern for Aluminum Seal
at 6450 psi Sealing Stress

Contact Pattern for Aluminum Seal
at 17,500 psi Sealing Stress

Fig. X-2-1 Photomicrographs of Surfaces in Contact (Ref. 3)

Semi-separable seals are defined as seals which require the use of tools or some device to disengage the sealing surfaces. Typically, the seals fall into two categories:

(1) A seal composed of a separable and a non-separable seal. An example of this seal is a device where two separable surfaces are joined together and held together by a welded segment such as that employed in the Omega seal (see Section XI). the welded segment is constructed so that a tool can be employed to effect separation while still maintaining the primary seal.

(2) The inclusion of a third material in the interface such as adhesives. They provide a filling of the void spaces and additionally can produce a bond which often can be broken with minimum effort or suitable tools.

Non-separable seals are those formed by the filling of void spaces by welding, brazing, and diffusion bonding techniques.

Each of the preceding classes of seals are considered in this guidebook although in separate locations. Separable seals and the separable aspects of semi-separable seals are considered in this Section. Welding and brazing applications are considered in Section VIII. Additionally, separable seals possess the greatest challenge and problems and, consequently, require extensive discussion.

Deformation of the Leak Path

In the process of pressing materials together, microscopic deformation of the surface occurs, disrupting the chance interconnection of void spaces. Thus, the problems associated with leakage flow through an interface fall into two categories, which can be considered separately:

(1) Surface Interaction, the macroscopic deformation of the materials forming the interface.

(2) Formation of Leak Paths, the probabilistic interconnection of void spaces.

Gitzendanner[1] described a series of experiments using photomicrographic techniques involving the reflectivity of light from a surface pressed against a flat glass plate. Two of these surfaces were shown in Figure X-2-1. The objective of his investigation was to obtain a quantitative understanding of the leak path under load. Unfortunately, these visual techniques were not sufficient to provide this information. Following these early experiments, a statistical approach to the problem was undertaken by the General Electric Co.[2] In general, the technique consists of generating a three dimensional map of the topography of one surface forming a sealing interface using autocorrelation and probability distribution techniques with stylus type inspection instrumentation serving as input information. The purpose is to produce leak path statistics which, when coupled with Abbotts bearing assumption for the deformation process, yield a description of the leak path with changes in apparent contact stress. Their results, intended to yield a theoretical-statistical method for calculating leakage, are not available in final form at the present time.

IITRI[3] approached the problem somewhat differently by correlating experimental leakage data with the following factors:

(1) Applied load
(2) Material properties
(3) Initial surface topography
(4) Width of interface contact

The problem was to determine the parameters which have a hypothetical significance to the real leakage path. The interface leakage paths are probably very complicated judging from the studies of contact area. There may be a few large paths or many very small paths, depending on the initial surface topography and load. In any event, it is almost impossible to obtain dimensional descriptors of something which appears to be a random phenomenon. About the only conclusive fact that can be stated is that the interface of two materials provides resistance to the interchange of fluid. It was from this presumption that a conductance parameter was developed. The conductance parameter was derived from theoretical equations for fluid flow between two uniformly separated surfaces. The philosophy was simply an assumption of a hypothetical relationship between uniformly separated surfaces and the seal

sealing interface with its complicated leak path. For example, the transition flow equation for flow between two circular flat plates has the form:

$$Q_o = \left(\frac{\pi h^3 (r_o + r_i)(P_2^2 - P_1^2)}{12 \mu (r_o - r_i) P_o} \right) \left(1 + \frac{12.76 \epsilon P_o \lambda_o}{(P_2 + P_1) h} \right) \qquad (1)$$

where h^3 = conductance parameter normally identified as the uniform clearance between plates, in^3

Q_o = experimentally measured volume rate of leakage flow at standard conditions (STP) in^3/sec

r_o, r_i = outside and inside radii of the circular interface, in

μ = viscosity of the fluid, lb-sec/in

P_2 = sealed fluid pressure in the interior of the interface, psia

P_1 = external pressure on the interface, psia

P_o = standard atmospheric pressure, psia

λ_o = molecular mean free path at standard conditions, in

ϵ = correction factor $\sim$ 0.9 for a single gas and 0.66 for a mixture

Other theoretical expressions contained in the Appendix, Section X-A, were employed depending upon the flow regime. In all cases the cube of a hypothetical channel clearance was defined as the conductance parameter.

Leakage data from experiments on circular metal, plastic and elastomeric surfaces pressed together under varied loads were obtained from References 3, 4, 5, 6, 7, 8, 9, 10, 11, 12, and 13. The calculated conductance parameter was then correlated with interface loading, material properties and initial surface topography. These results are shown in Figure X-2-2 where:

F = normal load applied to the interface, lb

A_A = apparent contact area of the interface, in^2

n' = Meyer strain hardening index

σ_m = Meyer hardness, psi

$(PTV)^3$ = peak-to-valley interface surface roughness measured in the direction of leakage flow

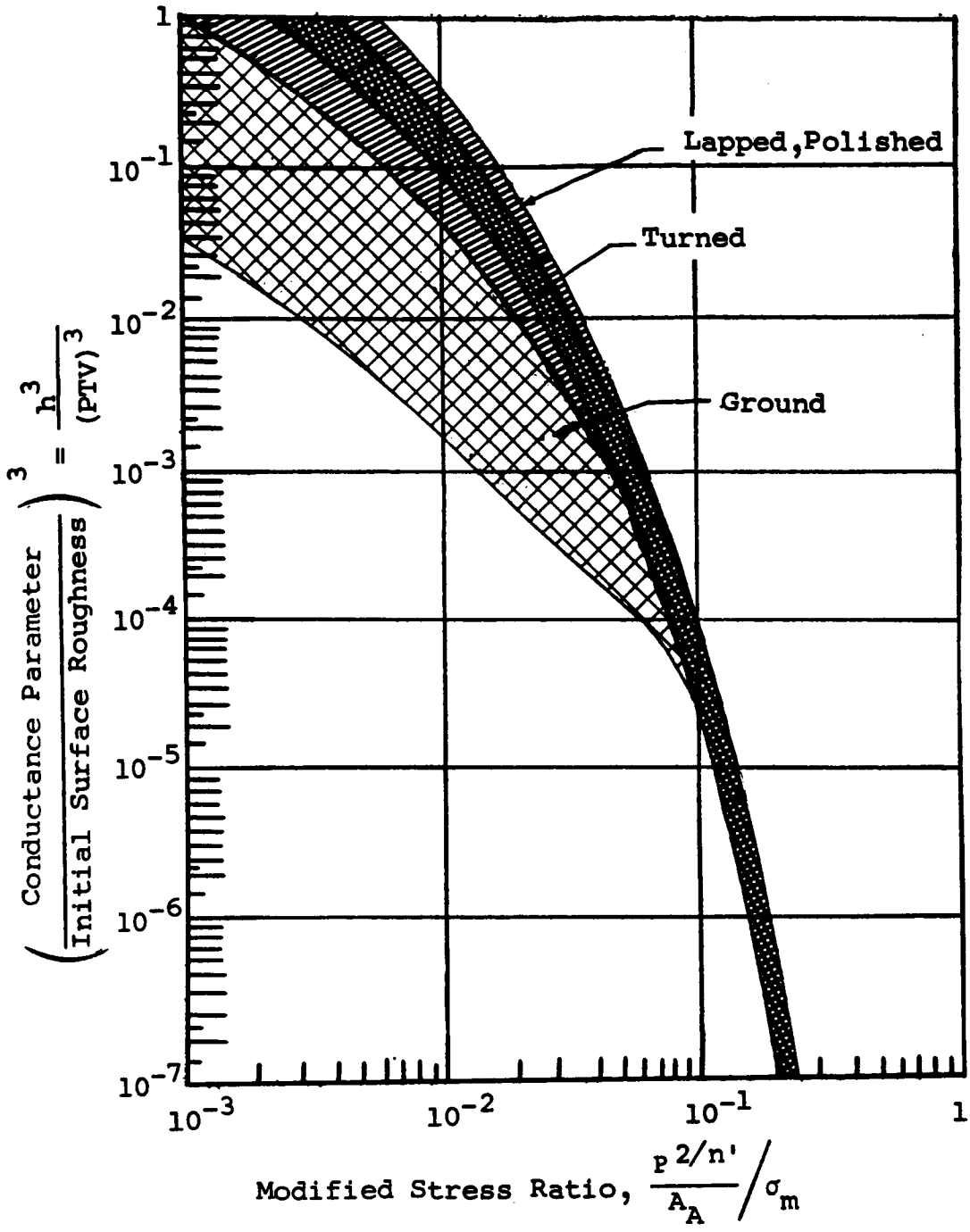

Fig. X-2-2 Nondimensionalized Relationship Between Leakage Parameters (Ref. 3)

The criteria developed by IITRI[3] must be viewed as yielding only approximate results; perhaps within an order of magnitude of the leakage which may actually be encountered. This data, however, does yield quantitative data which can be utilized to predict seal performance and, additionally, serves to show general influences between parameters.

Of the several modes of deformation previously described, many may occur simultaneously in any interface. Additionally, metals, plastics, and elastomers behave differently from one another, and must be considered separately.

The forces acting at an interface are composed of contributions due to transmitted loads at the points of contact and the effects of fluid pressure within the interface. The contact loads transmitted between the mating surfaces are located at the microscopic surface irregularities. Hence, the actual contact area is that formed by all of the individual contact junctions. Since the actual contact area is unknown, and, additionally, has little significance to the leak path, the applied load is assumed to be uniformly distributed over the apparent interface area. The resulting stress is defined as the net, normal, apparent contact stress. It should be noted that any separation effects due to fluid pressure are not included.

Deformation of metal to metal surfaces can be described and classified into five regimes.

Regime I

Any metal surface, whether it be machined, ground, lapped, or diamond burnished, will have surface asperities existing on it. Most machining or grinding techniques tend to make most of the asperities of generally uniform height. There will always exist, however, a certain number of the asperities that are higher than the mean values. When two surfaces having such distributions are brought together, they will initially touch each other on the higher than average asperities. These asperities will be local in nature and will not cause appreciable barriers to fluid flow. As a normal force presses the surfaces together, the stress on the few asperities which are touching will be extremely high and they will deform readily. As the

asperities are deformed, initial contact between other asperities occurs until the tops of the asperities of average height have come into contact. The first phase of material deformation, therefore, is the mating and deformation of the extremely high asperities. During this regime of material flow, the two surfaces will move together under extremely low normal sealing stresses. During this regime, however, little decrease in fluid flow between the surface can be expected unless significant elastic deformation of the surface substrate occurs. This regime is characterized by modified stress ratios of 10^{-2} to 10^{-3} as shown in Figure X-2-2. It should be kept in mind that h^3 is somewhat proportional to leakage under given conditions.

Regime II

After the peaks of the most dominant size of asperity on each surface have come into contact, the next increment of material deformation is the plastic deformation of individual asperities as they mate with those asperities immediately opposite. The equilibrium stress level on each asperity during this regime of deformation will be between two and three times the yield stress of the weaker material, depending on the asperity shape. As long as the pile-up of material from one asperity does not significantly interfere with the material pile-up from adjacent asperity deformation, the increase in area of contact between the two surfaces will be linear with the increase in normal load. During this regime of material deformation, it can be expected that the leakage rate will be reduced drastically with the ever increasing area of contact. This regime can be approximately identified as the range of modified stress ratio from 10^{-1} to 10^{-2} in Figure X-2-2.

Regime III

As the load is further increased, the material that is piled-up between asperities radically effects the deformation. As the material pushed to the side from the reduction in height of one asperity interferes with the similar material from the adjoining asperity, a further resistance to material flow occurs. The response of the total deformation process is more the product of a complex stress field in the bulk material, than of asperity deformation. This complexity is further complicated by whatever strain hardening characteristics the material in question may have. This regime, which is called

the transition regime, may occur when stress levels in the bulk material are not high enough to cause bulk flow of the material. This regime may be associated with modified stress ratios in the range of 1×10^{-1} to 1.5×10^{-1}.

Regime IV

During the previous three regimes of material deformation, stresses in the bulk of the material were not high enough to cause bulk flow of that material. When the stress field in the solid is sufficient to produce yielding in a large portion of the material, drastic geometrical deformations will occur. In the case of flat gaskets, this deformation resembles very closely that of the Prandtl plastic flow problem. Surface shear stresses tend to reduce the bulk flow during this regime. Where tie deformable material is in a flat gasket form, or in any shape that will allow the material to slide along the surface with which it is mating, a further decrease in leakage can be expected due to the shear deformation. Where no increase in apparent area is effected by bulk flow of the material, this phenomenon is not useful. The range of modified stress ratio shown in Figure X-2-2 corresponding to this regime is in the vicinity of 2 to 2.5×10^{-1}.

Regime V represents the effects of load or stress reduction. The characteristics of the leakage curve in this region is indicative of the degree of plastic or permanent deformation. The general characteristics of this region are defined as hysteresis effects. Since the deformation is permanent and depends upon the maximum stress achieved, it is expected that the leakage would remain constant for large decreases in stress. If the stress is sufficiently reduced, elastic deformation effects predominate and leakage changes significantly. Figure X-2-20 illustrates the relationship between the leakage and contact stress in terms of the flow conductance factor.

Each of the preceding regimes of deformation are shown in Figure X-2-3 for a typical gasket pressed between two surfaces. The deformation is characterized by changes in helium leakage rate.

Deformation of metal-to-plastic surfaces can be described similarily to metal-to-metal surfaces. Because of the lower loads required for

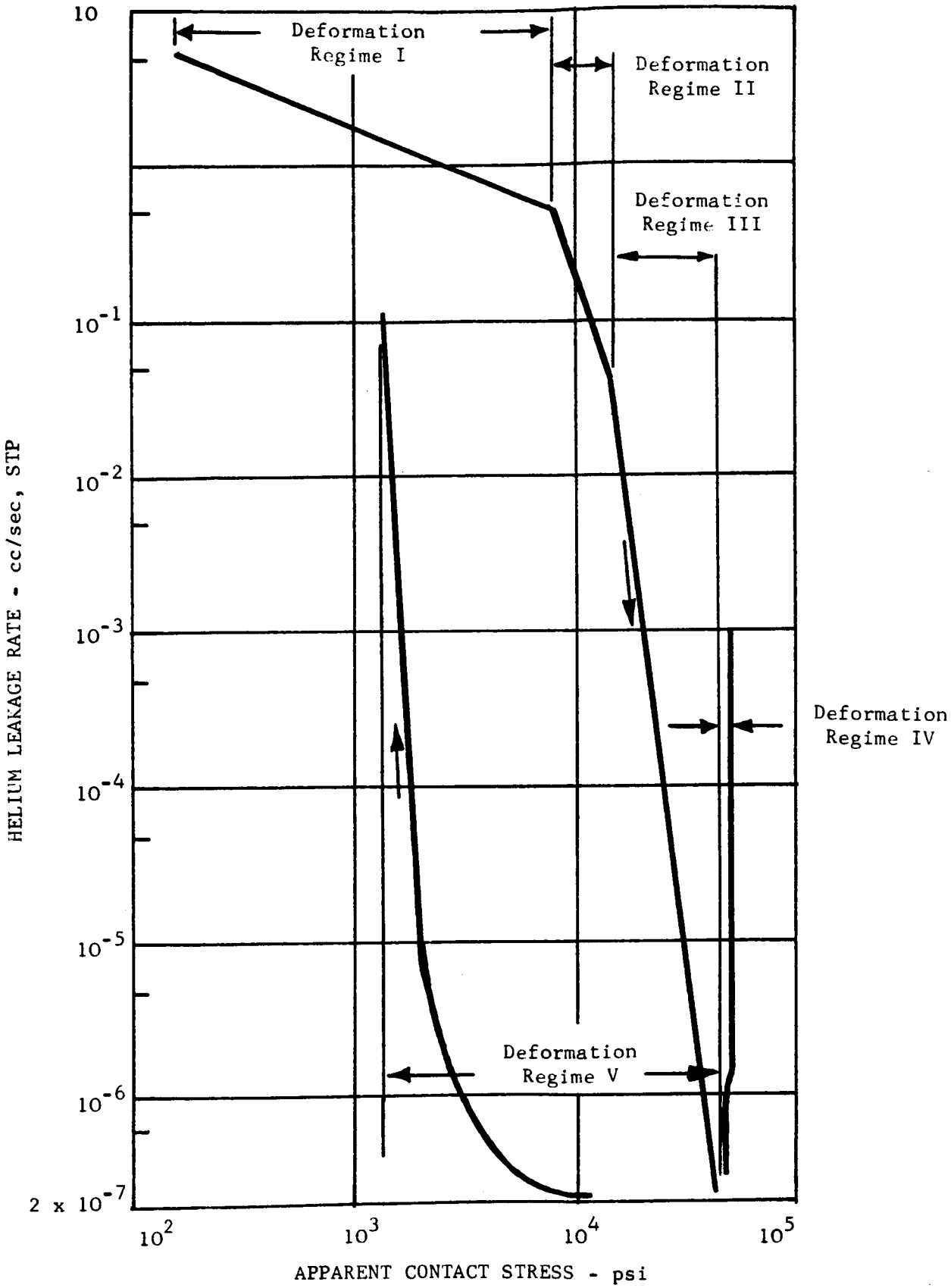

Fig. X-2-3 Leakage-Contact Stress Characteristics of Aluminum 2024-0 Gasket Pressed Between 1141 Steel Flanges. The Gasket Size was 2-1/8 x 2-1/2 x 1/8. The Pressure of the Sealed Fluid was Three Atmospheres.

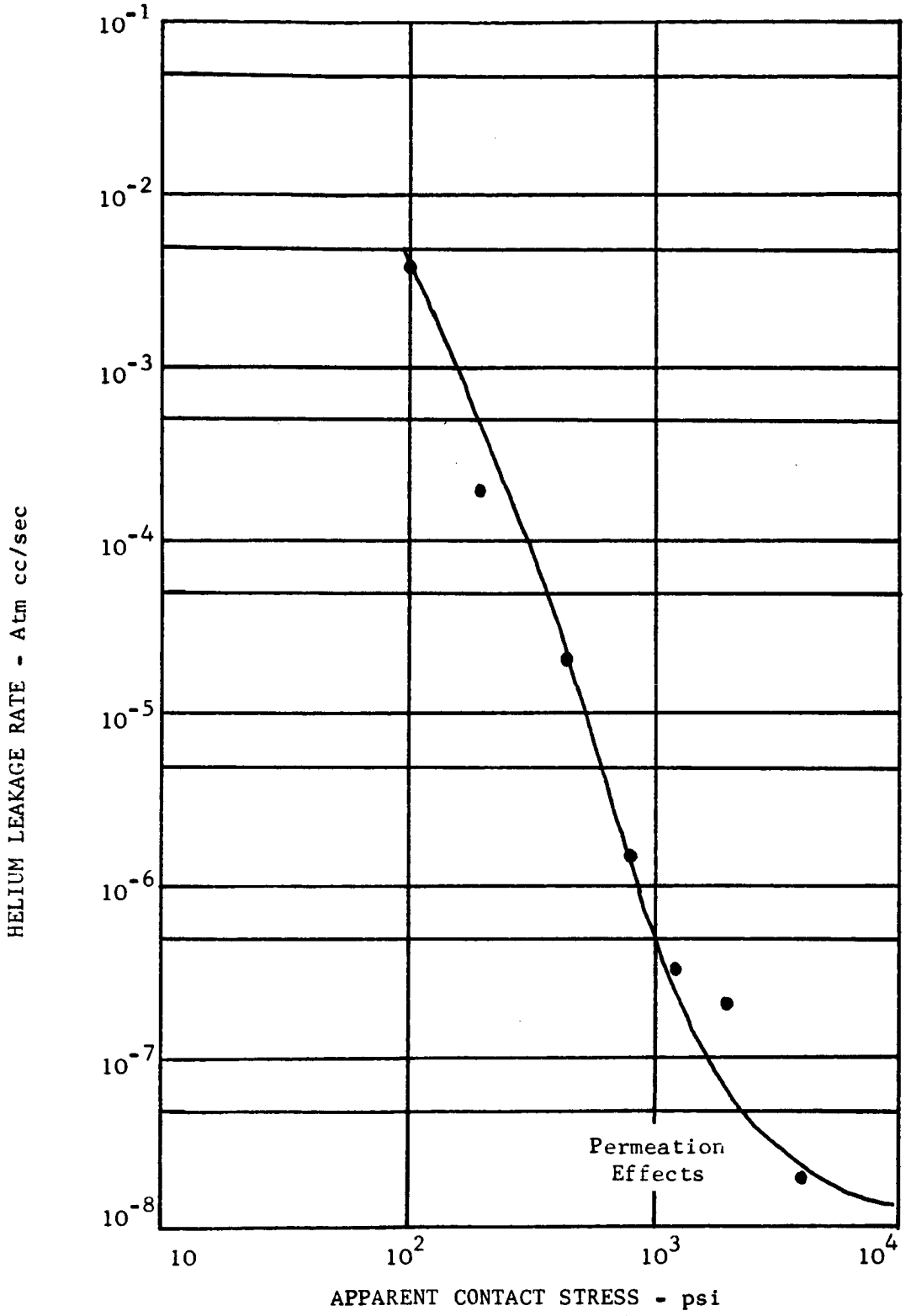

Fig. X-2-4 Leakage Characteristics of a 2 x 2-1/4 x 1/8 Square Buna N Ring Mated Against a 300-PTV Turned Steel Surface (Helium, 2 Atmospheres Pressure, 85°F)

deformation, the regimes of I and II are relatively insignificant compared to regime III and IV which predominate.

Deformation of elastomers can be identified as completely elastic and, hence, does not fit into the regimes already identified. The interface deformation of elastomers is almost proportional to the applied load. This was experimentally demonstrated by the inverse relationship between the conductance parameter and contact stress[3]. At low normal loading, equivalent to stresses less than 1000 psi, the predominant leakage occurs at the interface formed by the rubber and solid materials. Higher loads produce close conformability at the interface and the leakage rate reaches an almost constant value, suggesting the predominance of permeation flow. Typical leakage rate characteristics for a confined rubber ring are shown in Figure X-2-4.

Material Properties

Hardness of the interface materials was found by IITRI[3] to be the most important measure of the ability of a material to deform under load. The hardness of interest, defined as the Meyer hardness of the softer material forming the interface, can be obtained using a Brinell test apparatus. This differs somewhat from the concepts of General Electric Co.[5] in that the 0.2% yield stress was chosen as an important factor in the deformation process.

Yield stress and hardness are closely related. Tabor[14] demonstrated, theoretically and experimentally, that the hardness H of many metals and nonmetals is $\sim 3\sigma y$. At first glance it would appear that either property could be used to describe the plastic flow of materials, particularly in respect to the filling of leak path void spaces in a seal interface. However, the relationship between hardness and yield stress is not sufficiently unique and is dependent upon other factors. These factors plus other seal-related advantages qualify hardness as a more important parameter. The argument may be stated as follows:

(1) Hardness can be measured more easily than yield stress.

(2) The hardness measuring process is geometrically close to the pressing of an asperity into a surface.

(3) Hardness measurement instrumentation is more consistent

with respect to the reproducibility of results. Yield strength instrumentation is also consistent, but the shape of the material specimens varies as do the results.

The Brinell hardness number (BHN) is expressed as the load P divided by the surface area of the indentation:

$$BHN = \frac{F}{(\pi D/2)\ (D - \sqrt{D^2 - d^2})} \qquad (2)$$

where

F = applied load, kg

D = diameter of ball, mm

d = diameter of indentation, mm

Several deficiencies exist that limit the interpretation of hardness measurements:

(1) The human error in measuring the impression diameter that is caused by ill-defined edges of the indentation.

(2) The elastic recovery of the indentation induces an error that is a function of the indenting load.

(3) The interpretation of the contact area and its relationship to the deformation phenomena.

(4) The variation in results that is due to the magnitude of applied load and the geometry of the indenter. Unless geometrical similarity is maintained, strain-hardening effects can predominate and prevent the correlation of test results.

The definition of Brinell hardness is an example of improperly defined surface area. The applied load is assumed to be distributed over the apparent surface area of the dent. It can be shown that the Brinell hardness number of a material is constant only for one applied load and diameter of ball. To obtain consistency of results at nonstandard loads, geometrical similarity must be maintained. This problem was investigated by Meyer (discussed by Dieter[15]), who suggested that the projected area of contact is an improved parameter. The mean contact stress between the surface of the indenter and indentation is defined as projected area of the indentation.

$$\text{Meyer Hardness} = \sigma_m = \frac{4F}{d^2} \tag{3}$$

Meyer hardness is reportedly less sensitive to applied load than Brinell hardness. For a cold-worked material, the Meyer hardness is essentially constant and independent of load while the Brinell hardness decreases as the load increases. For an annealed material, the Meyer hardness increases continuously with increasing load, whereas the Brinell hardness first increases and then decreases. Additionally, the Meyer hardness based on the projected area of contact, is independent of the indenter shape.

Meyer[15] also proposed an empirical relation between load and the diameter of the indentation considering the effects of strain hardening. This relation, usually called Meyer's Law, is

$$P = kd^{n'} \tag{4}$$

where

n' = material constant related to strain hardening (Meyer index)

k = a material constant representing the resistance of a metal to deformation

The material constant in the exponential equation for the true law is approximately equal to the strain-hardening coefficient n plus 2; i.e.,

$$n' = n + 2 \tag{5}$$

The strain-hardening coefficient can be readily determined from the slope of a log-log plot of a plastic portion of the stress-strain curve, as shown typically in Figure X-2-5.

When indentations are made with different diameter indenters, different values of k and n' are obtained.

$$P = k_1 D_1^{n_1'} = k_2 D_2^{n_2'} = k_j D_j^{n_j'} \tag{6}$$

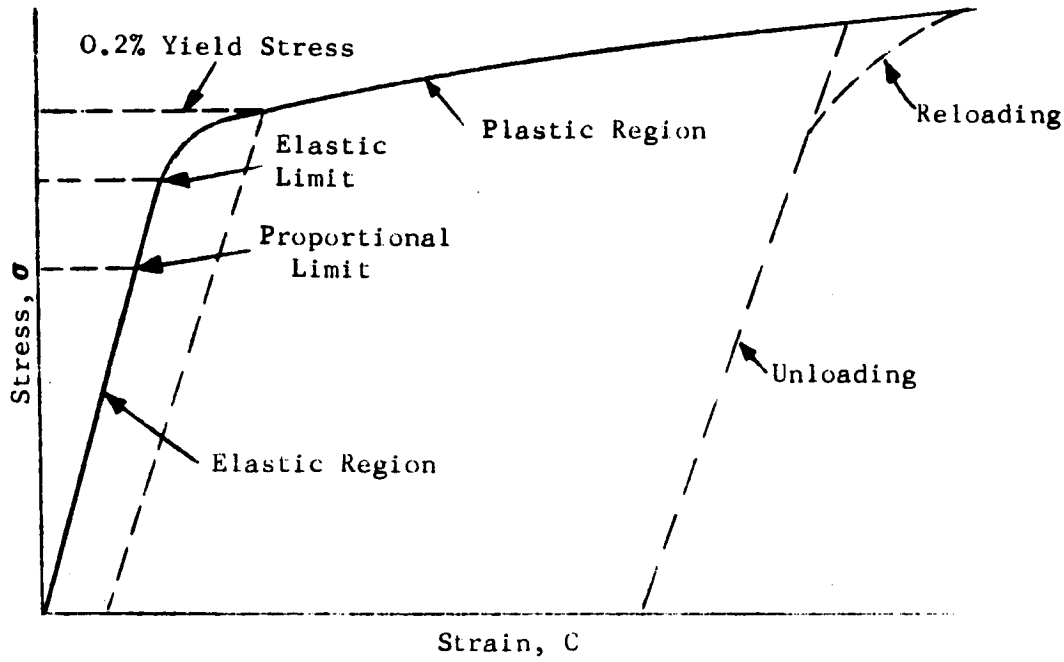

Fig. X-2-5 Typical Stress - Strain Diagram

Meyer also found that n' was almost independent of the indenter D but that k decreased with increasing D. The general expression of Meyers' law becomes:

$$P = \frac{Cd_1^{\,n'}}{D_1^{\,n'-2}} = \frac{Cd_2^{\,n'}}{D_2^{\,n'-2}} = \ldots\ldots \frac{Cd_j^{\,n'}}{D_j^{\,n'-2}} \qquad (7)$$

where

$$C = k_1 D_1^{\,n'-2} = k_2 D_2^{\,n'-2} = \ldots\ldots k_j D_j^{\,n'-2} \qquad (8)$$

An easy method for determining the Meyer index n' is through a hardness test. By pressing an indenter against a surface under varied load conditions, the dent diameter can be measured. The Meyer index can be determined from a log plot of the data if we consider Meyer's law in the form

$$\log P = \log k + n' \log d. \tag{9}$$

The slope of the curve is n'. For hard materials, the various loadings available in a Brinell testing machine may be used and for softer metals a standard testing machine may be used to provide the load, and a precision steel ball used for an indenter. In making these measurements care should be exercised to maintain geometrical similarity in the ratio of the impression diameter to the ball diameter (d/D) for all of the metals tested. The range of validity for Meyer's law is $0.1 < d/D < 1.0$[15]. A series of experiments was conducted on a number of metals and nonmetals. These results, shown in Table X-2-1 were obtained for a d/D of approximately 0.5.

Table X-2-1

MEYER HARDNESS AND INDEX FOR VARIOUS MATERIALS

MATERIAL	MEYER HARDNESS (psi)	MEYER INDEX
102 Copper	109,000	2.09
1100 - O Al	48,700	2.19
2024 - O Al	89,600	2.44
5086 - H32 Al	139,000	2.14
6061 = T6 Al	159,000	2.00
2024 - T351 Al	202,000	2.00
7075 - T6 Al	262,000	2.00
Teflon	3,870	2.80
Lead	4,390	2.33
321 CRS	202,000	2.35
C1141 Steel	308,500	2.22

Creep may have an important effect on the magnitude of Meyer hardness and index, particularly for Teflon and lead. The results shown in Table X-2-1 were obtained for a load application of one minute. While it is recognized that the results may not be completely accurate, they are sufficient for use in the development of interface deformation correlations.

Surface Topography and Fabrication Techniques

Of all the parameters influencing sealing, surface topography is the most important and also the most nebulous. It is a complex parameter that is difficult to measure and impossible to describe simply. It is a parameter that varies with material properties, substrate geometry, and fabrication processes. To present a comprehensive survey of each of these aspects would require the repetitious presentation of very adequate discussions available in the literature. To maintain continuity, however, each will be briefly considered with the suggestion that the reader refer to References 4, 5, and 6 for additional details.

An appreciation of the problem can be best developed by considering the cause and effect of surface topography with emphasis on the formation of the leakage path when two surfaces are mated together. Although a majority of surfaces appear to have random topographies and consist of many irregular, jagged protrusions, there are definite patterns that characterize a surface. These patterns can generally be classified according to the number of occurrences or, if viewed as a periodic disturbance, by wavelength. The irregularities of longest wavelength are caused by flexure of the part being formed, by deflections of shafts and slideways in the machine tool. Superimposed upon this waveform are other vibrational effects. The next shorter wavelength is that contributed by the method of fabrication, such as the formation of spiral crests formed in a lathe-turning process. This predominant orientation of a surface pattern is defined as lay of a surface. The controlling factor of lay is in the fabrication process producing variations described as spiral, parallel, circular, and multidirectional, relative to some reference.

The smallest distrubance is produced by localized tearing and shearing between the cutting element and the surface. In addition to these surface characteristics, there is a class of random irregularities called flaws. These occur at one place or at infrequent intervals on a surface. Scratches, ridges, holes, cracks or checks are examples of flaws.

The preceding characteristics are often broadly classified by the terms <u>surface roughness</u> or <u>waviness</u>. Roughness takes into account the finer irregularities caused by the cutting tool and the machine tool feed, while waviness

is the wider spaced irregularity, resulting from machine or work deflections, vibrations, heat treatments, etc. To distinguish between these two forms, a roughness-width cutoff is often defined to specify the maximum width of surface over which roughness is measured. Wide disagreement exists concerning instrumentation and techniques for the evaluation of surfaces. It is not the intent here to suggest that the following methods described are the ultimate. They are, however, commonly used and the results obtained have been reasonably satisfactory. Three instruments for surface evaluation are:

(1) Stylus instrument for roughness and waviness measurement. This instrument records the surface topography in a single plane normal to the surface.

(2) Optical flat for over-all waviness. The optical flat provides a three-dimensional view of large surface irregularities and is limited to flat and fairly reflective surfaces.

(3) Interferometer for microscopic measurements of surface topography. The interferometer provides a three-dimensional view of small surface irregularities.

The measurement and identification of surfaces discussed in this Section are based on a human interpretation of information obtained from the stylus, optical flat and interferometer instruments. The real surface, being complex, introduces substantial variations in interpretation of data. To completely describe a surface, the following information must be known as a minimum:

(1) The waviness of the over-all surface (assuming a definition of waviness based upon the 2nd, 3rd, or n^{th} order wave-length characteristics of the topographical distrubances).

(2) The average roughness

(3) The maximum average roughness (peak-to-valley variations)

(4) The statistical distribution of asperities by height, wavelength, and location over the entire surface

(5) The directional pattern of the surface lay

Each of these factors can be described, but not in simple terms. Unless the language is simple, the factors cannot be interrelated. In view of the limitations on surface interpretation, waviness and average peak-to-valley

roughness were chosen as the factors for use in the development of empirical correlations. The selection was based solely on the ability to define the factors easily with existing instrumentation.

Waviness is interpreted as a maximum surface variation having a wavelength greater than 0.030 in. and conforms with MIL-STD-10A. The surface waviness of importance to sealing is that normal to the direction of leakage flow, as shown typically in Figure X-2-6. Roughness, on the other hand, is measured either in the direction of, or normal to, the leakage flow. When surface lay predominates, the roughness in the direction of flow is used while surfaces possessing no lay effect are measured normal to leakage flow. Roughness is interpreted as an average peak-to-valley variation since it has some similarity to the seal leak path and is more reliable than Root-Mean-Square or Arithmetic Average descriptors.[4] Following this procedure, two numerical descriptions are developed, one to describe waviness and the other roughness. Other directions of waviness could be described but this would induce another descriptor and it is not known how this additional number could be gainfully employed.

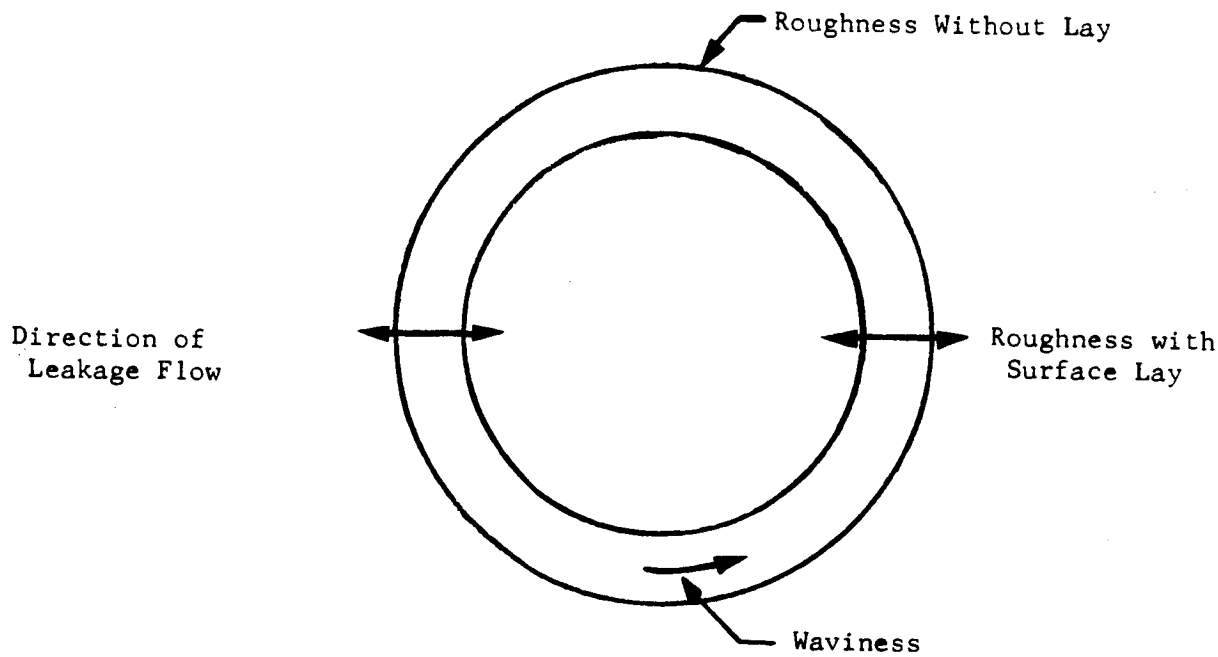

Figure X-2-6 Location of Topographical Measurements on a Circular Gasket Surface

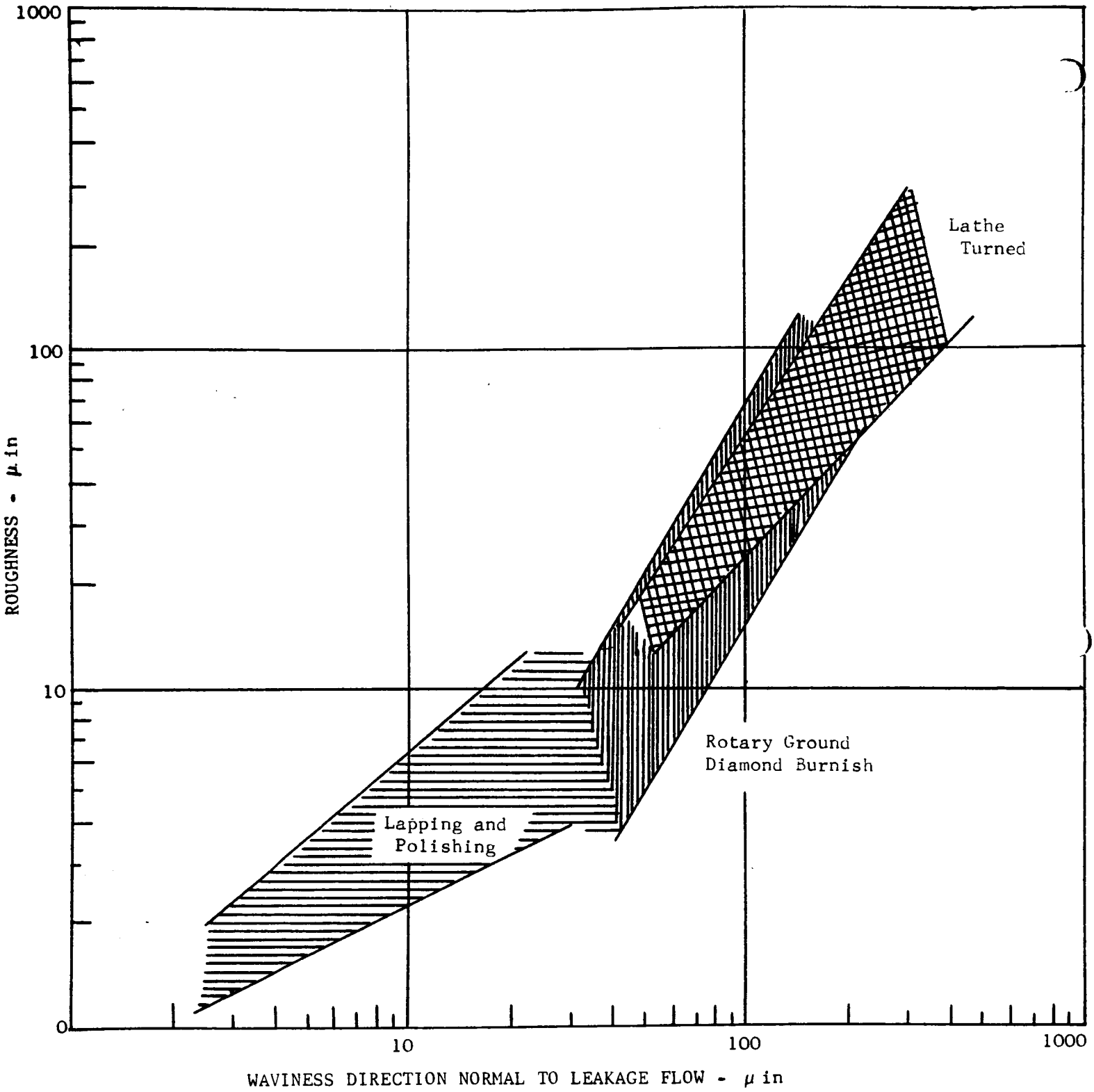

Fig. X-2-7 Approximate Range of Waviness with Roughness for Various Fabrication Processes

Waviness is primarily determined by the surface fabrication process. Even with the same process, substantial variations occur. Thus, it is not possible to associate a specific waviness with any fabrication process or other factor. It is possible, however, to assign ranges of waviness variations which can be associated with the fabrication process. Since an eventual correlation is based on considerable data, it is felt that the waviness influence becomes an averaged effect. Figure X-2-7 shows approximate range of waviness obtained from many experimental surfaces. It should be noted that this information is restricted to interface size geometries less than 3 in. in diameter.

The influence of surface lay can be hypothesized almost intuitively. When surfaces are rough, > 15 μin. PTV, the orientation of lay should be normal to the average direction of leakage flow for minimum leakage.[4] This observation is reasonable if we consider that a surface possessing lay has uniform crests and valleys. Thus, a leak is easily formed by the valleys when their orientation is in the same direction of leakage flow. Surface variations < 15 μin. PTV do not require preferential orientation because the valleys usually have the same depth as the irregularity in the crests. It should be noted that multidirectionally-formed surfaces do not have preferentially formed crests and valleys. These surfaces often have variations <15 μin. PTV and, consequently, can be expected to produce leaks similar to fine-finish, preferentially oriented surfaces.

Surface fabrication techniques can be grouped into four classes based on the degree of surface finish and the mode of surface deformation. The classes are:

> Class I - No surface disturbances on either mating surface observable with common microscopes (1000 X). These surfaces when pressed together produce a minimum leakage path by almost perfect mating. Any waviness effects are diminished by elastic deformation of the material substrate.
>
> Class II - Few random disturbances not exceeding 2 μin. PTV.
>
> Class III - Preferential orientation of the surface lay so that a uniform barrier to leakage may be created.

Class IV - Many random surface disturbances greater than 2μin. PTV.

The first two classes of surfaces are very similar in that an attempt is made to achieve surfaces having minimum surface variations. Actually, it is difficult to achieve Class-I surfaces because of contaminants, imperfections in the fabrication process, and damage due to handling. General Electric[2,12] obtained surfaces which came close to having no surface variations. These surfaces were generated by Jones Optical Company, Cambridge, Massachusetts and the Up-Hi Company, Ltd., Tokyo, Japan. These references give photomicrographic evidence of the degree of surface perfection that can be achieved. The distinction between Classes I and II is not well defined except that the Class-II surface has slightly more topographical protusions. Figure X-2-8 shows a photomicrograph of a Class-II surface prepared on 321 stainless steel. A corresponding interferometer photo is shown in Figure X-2-9. The minor surface disturbances are indeed small and beyond the range of interferometer measurement. A small scratch having a depth of $\sim$ 2μin. is shown in the center of the photo.

The generation of Class-II surfaces is accomplished by polishing lapped surfaces using fine diamond or oxide dust. Class-I surfaces are probably obtained in a similar manner, but using special techniques. The process used in producing Class-I surfaces by the two firms cited, is considered proprietary information.

Class-III surfaces are typically those that have a preferentially oriented and undisrupted lay obtained by lathe-turning very small spiral grooves on a surface. This is followed by a diamond-polishing operation to remove the last vestages of gross waviness variations. Figure X-2-10 shows the resulting surface on 321 stainless steel while Figure X-2-11 shows a corresponding interferometer photomicrograph. The depth of the valleys was approximately 15μin.

Class-IV surfaces encompass the vast majority of surfaces encountered in most engineering practice. Two typical 321 stainless steel and 6061T6 aluminum surfaces are shown in Figure X-2-12 and X-2-13. These surfaces may be considered good lapped surfaces and yet, when compared with Figure X-2-8, are extremely rough. The topographical variations shown on the

interferometric photographs (Figures X-2-14 and X-2-15) are in the range of 2 to 5μin. The aluminum surface is slightly rougher than the steel. This rougher surface on soft materials is common in lapping and polishing processes.

Design Criteria - Metal and Plastics

The correlation of parameters influencing leakage through an interface were derived by IITRI[3] encompassing the four classes of surface fabrication processes. These correlations are shown in Figures X-2-16, X-2-17, and X-2-18, for turned, ground, and lapped and polished surfaces, respectively. The charts contain all of the important parameters describing the leakage path. These include the hardness of the softer interface material, the apparent interface geometry and the initial surface topography of the harder material. Thus, for any interface where the preceding conditions are known, the designer can predict the leakage rate. Leakage is given as

ω = f (conductance parameter, sealed fluid pressure, fluid properties, and gross geometry of the interface).

The functional relationship in this expression is given by an assumed state of fluid flow through hypothetically separated surfaces. The functional relationships are presented in Appendix X-A.

The criteria for predicting leakage has several limitations. The first limitation concerns the minimum width of interface contact in the direction of leakage flow. Generally, insufficient information is available to place a positive value on the width of contact because of the influence of scratches, surfaces defects, and fabrication marks. Some experiments by IITRI[3] did show that the criteria for predicting leakage will apply to interface surfaces greater than 0.012 in. in width. This, however, must be accepted on an individual basis. Further work is needed to determine absolute minimum widths of contact. It should be noted that leakage can be expected to be substantially large, and unpredictable when contact areas are too narrow. The second limitation of the criteria pertains to the prediction of leakage under full plasticity conditions. This region is designated at modified stress ratios greater than 0.2 and represents the very steep portion of the curves shown in Figures X-2-16, X-2-17, and X-2-18.

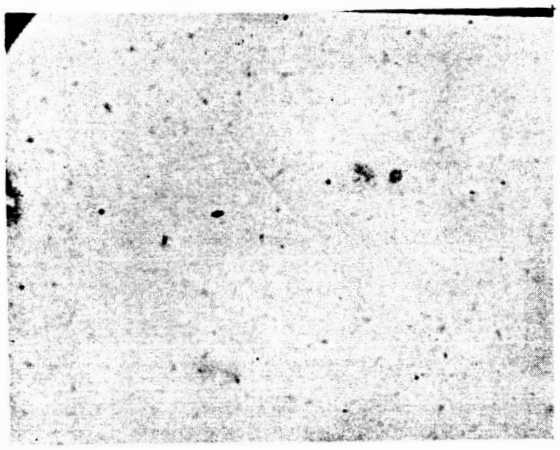

X960

0.0005 in.

Fig. X-2-8 Photomicrograph of a 321 Stainless Steel Surface Polished with Diamond Dust

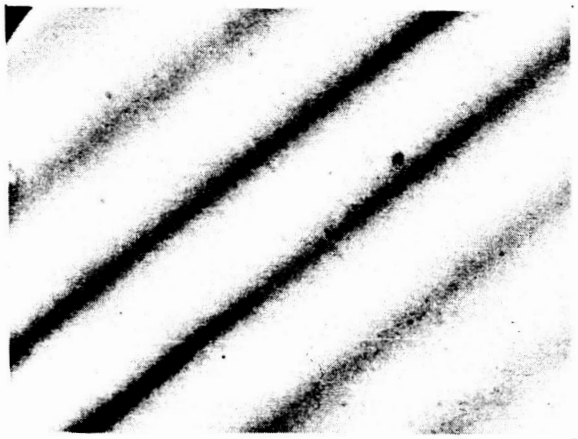

0.0005 in.

Fig. X-2-9 Interferometer Photomicrograph of a 321 Stainless Steel Surface as Shown in Fig. X-2-8.

X960

0.0005 in.

Fig. X-2-10 Photomicrograph of a 321 Stainless Steel Surfaces with Fine Turned and Polished Grooves

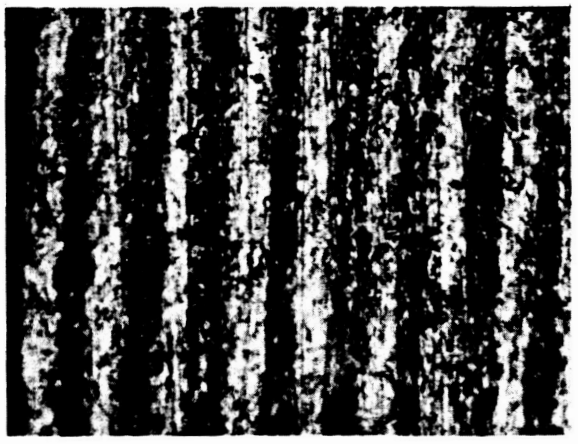

0.0005 in.

Fig. X-2-11 Interference Photomicrograph of a 321 Stainless Steel Surface as Shown in Fig. X-2-10. Roughness is approximately 15 μin. PTV

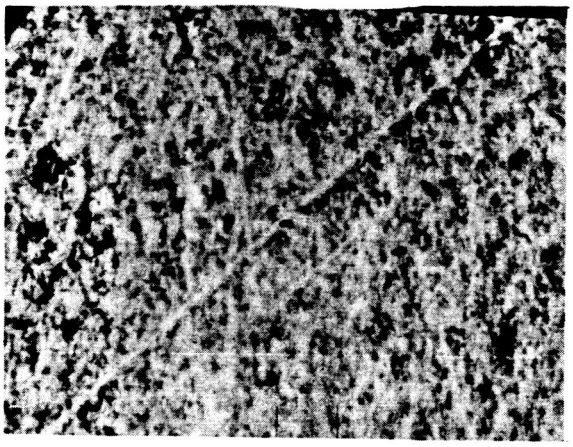

X960

0.0005 in.

Fig. X-2-12 Photomicrograph of a 321 Stainless Steel Lapped Surface

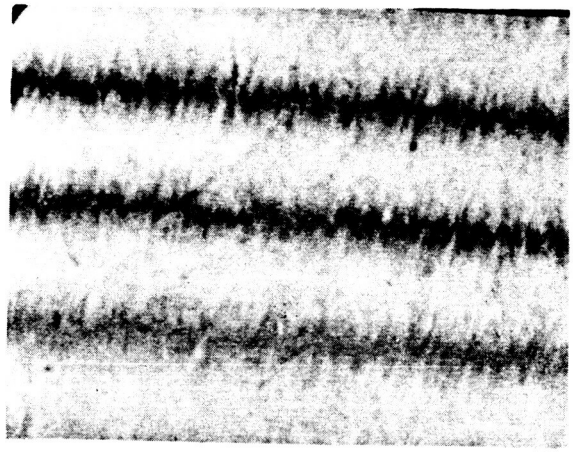

0.0005 in.

Fig. X-2-13 Interference Photomicrograph of the 321 Stainless Steel Surface Shown in Fig. X-2-12. Roughness is Approximately 2 μin. PTV

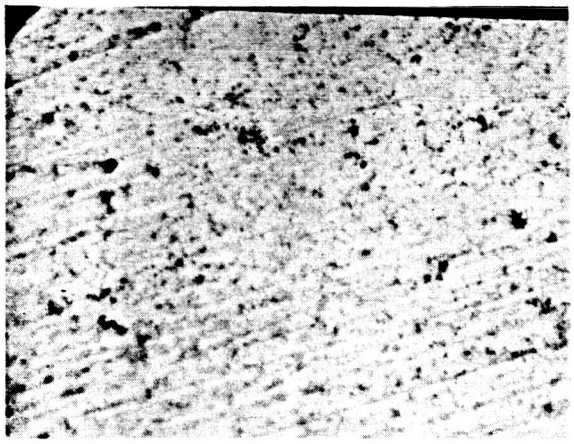

X960

0.0005 in.

Fig. X-2-14 Photomicrograph of a 6061T6 Aluminum Lapped Surface

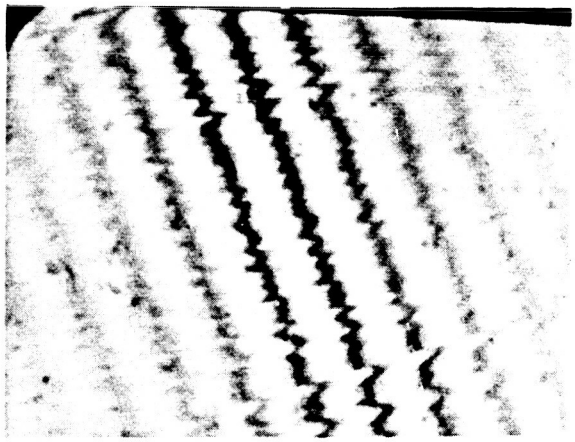

0.0005 in.

Fig. X-2-15 Interference Photomicrograph of a 6061T6 Aluminum Surface Shown in Fig. X-2-14. Roughness is Approximately 5 μin. PTV

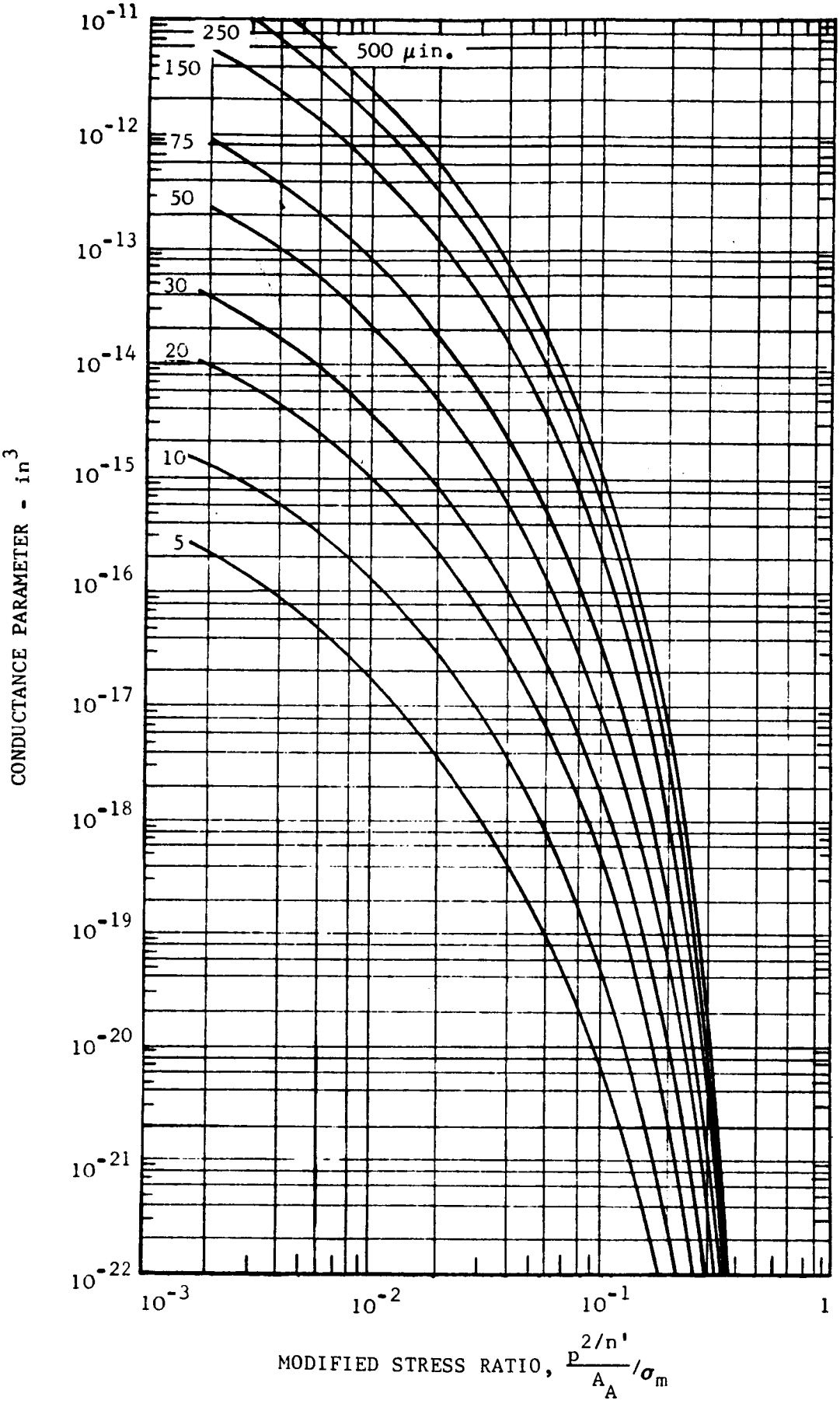

Fig. X-2-16 Design Criteria for Turned Surfaces. (Surface Roughness is Shown as a Parameter)

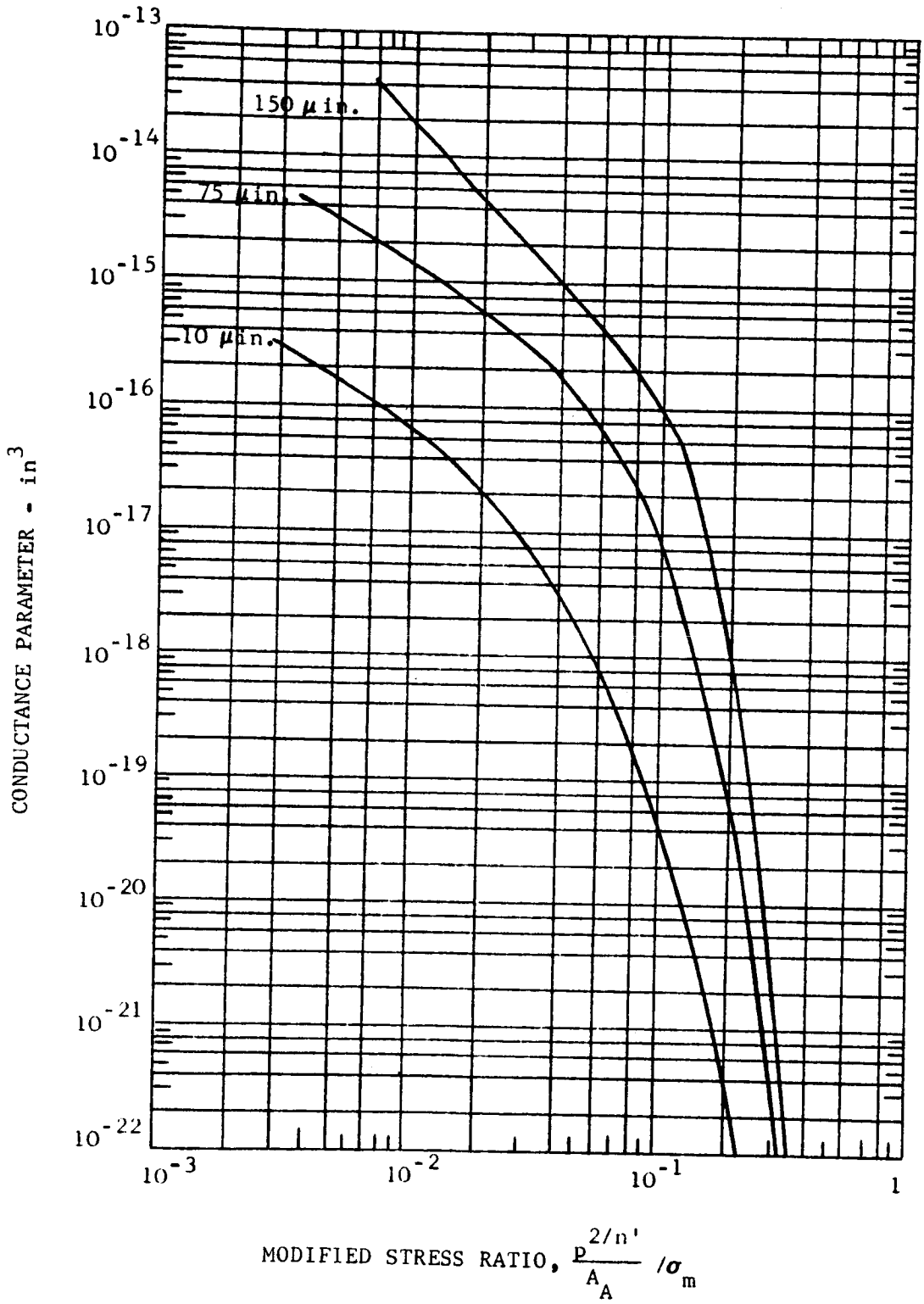

Fig. X-2-17 Design Criteria for Ground Surface. (Surface Roughness is Shown as a Parameter)

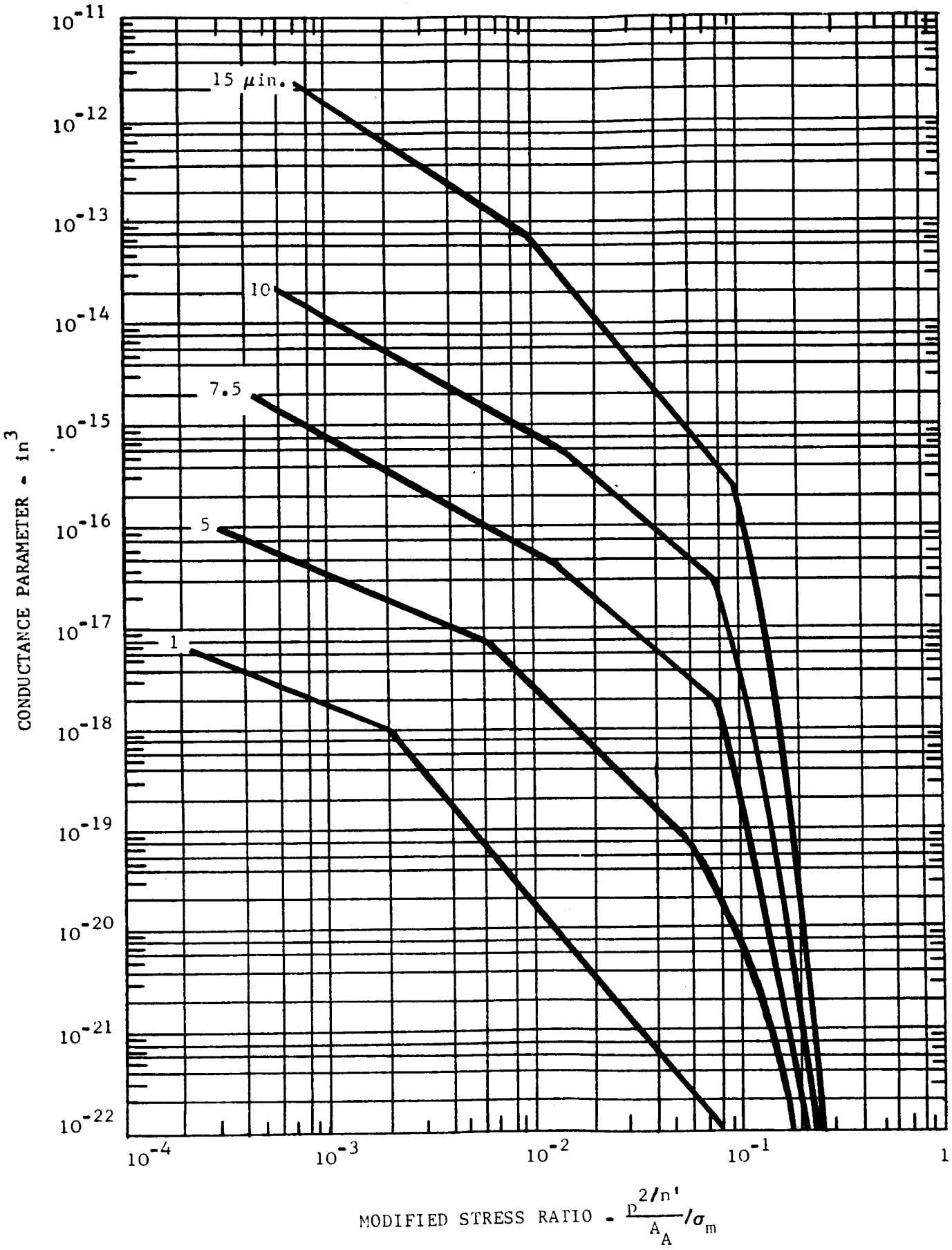

Fig. X-2-13 Design Criteria for Lapped and Polished Surfaces. (Surface Roughness is Shown as a Parameter)

Since leakage is close to being a proportional function of the conductance parameter, the exact value of the conductance parameter (hence leakage) will not be readily predictable. For example, the curves shown in the Figures terminate at values of approximately $h^3 = 1 \times 10^{-22} in.^3$ Values lower than this are possible but not predictable due to the rapid closing of the leak pattern as shown by the steepness of the curves.

An example showing the application of criteria can be demonstrated by considering a cover, as shown in Figure X-2-19, to seal a cavity containing helium gas at varying pressure. The objective is to produce a relationship between the load restraining the cover and the requirements for minimum leakage. The input information is:

Cover material - 17-7 PH, age hardenable stainless steel
Meyer hardness 238,000 psi (Brinell 168)

Mating surface - AM 355, age hardenable stainless steel
Meyer hardness 540,000 psi (Rockwell-C-53)

Surface finish - Both surfaces rotary to 10μ in. PTV

A net load relationship can be obtained from Figure X-2-17 for a low value of conductance, say $h^3 = 10^{-22} in.^3$ which yields:

$$\frac{F^{2/n'}}{A_A} \Big/ \sigma_m \cong 0.25 \qquad (10)$$

where $n' = 2.3$ (strain hardening index of the softer 17-7 PH material)

$A_A = 0.012$ in $\frac{2}{\text{in}}$ of contact

σ_m = Meyer hardness of 17-7 PH material

F = net interface load per inch of interface circumference

Hence,

$$F \cong \left[0.25(238{,}000)(0.012)\right]^{1.15}$$
$$F \cong 1890 \text{ lb/in} \qquad (11)$$

The total load $\bar{F}$ which must be applied to the parts shown in Figure X-2-19 is given:

$$\bar{F} = F + \pi(P_2 r_i^2 - P_1 r_o^2) + \left(\frac{P_2 - P_1}{2}\right)\left[\pi(r_o + r_i)(r_o - r_i)\right] \qquad (12)$$

The preceding equation contains all of the forces, including fluid pressure gradient effects, in the interface. A linear gradient $\frac{P_2 - P_1}{2}$ is assumed for a close approximation.

Leakage through the interface can be calculated by assuming the pressure of the sealed helium ranges between 100 and 2000 psi. Applying the equation for transition flow between two circular flat plates, the volume rate of leakage flow can be calculated as shown in Table X-2-2 for the following conditions:

$$Q_o = \frac{W}{\gamma_o} = \frac{W}{P_o} R_o T_o$$

Q_o = leakage rate, in^3/sec (STP)

$P_1 = P_o = 14.7$ psia

$T_o = 68^oF$

$R_o = 4630$ in/^oR

$\mu = 2.8 \times 10^{-9}$ lb-sec/in^2 (viscosity of helium)

$\epsilon = 0.9$

$\lambda_o = 13.0 \times 10^{-6}$ in (STP)

$r_o = 1.006$ in

$r_i = 0.994$ in

Table X-2-2

CALCULATED LEAKAGE RATES

P_2 (psia)	LEAKAGE RATE (cc/sec)(STP)
114.7	3.01×10^{-6}
514.7	1.54×10^{-5}
1014.7	3.26×10^{-5}
2014.7	7.05×10^{-5}

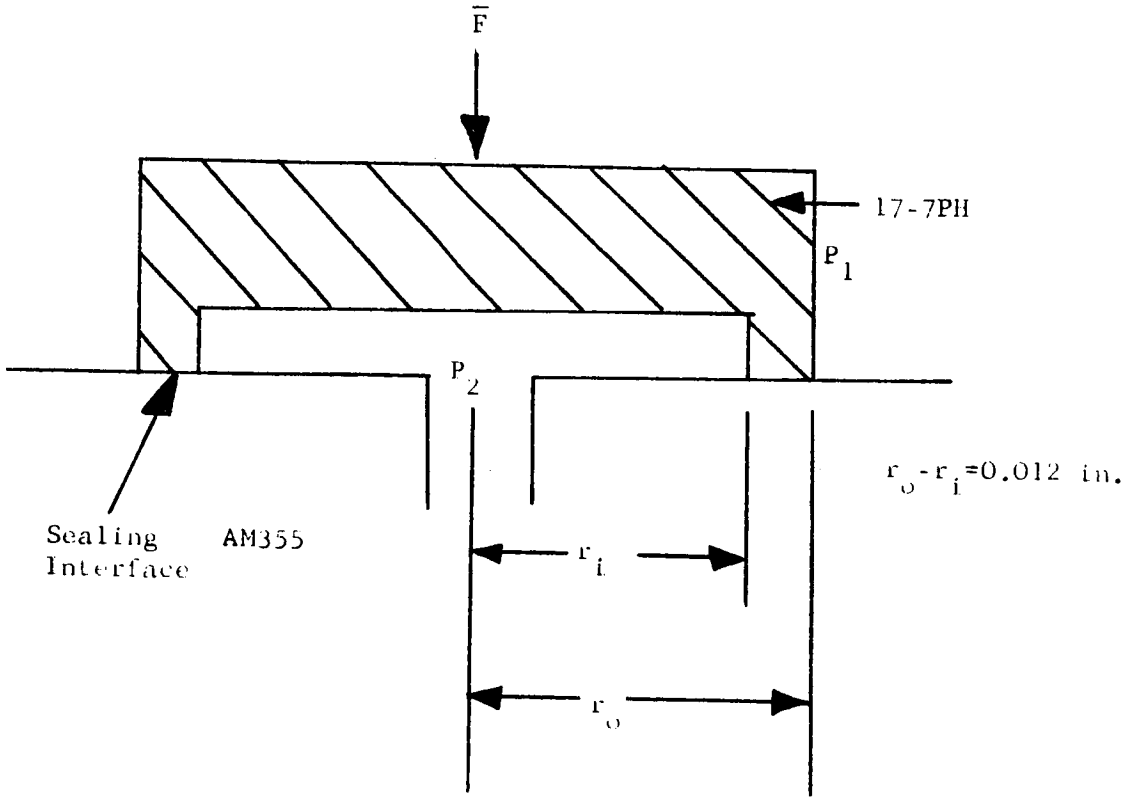

Fig. X-2-19 Geometry of a Sealing Cover

Caution must be exercised when calculating liquid leakage. Surface tension effects may be the dominant factors in the flow process when the conductance is small. An estimate of the effects of surface tension can be obtained by assuming surface tension in a hypothetical channel of a dimension equal to the cube root of the conductance. Unfortunately, the influence of surface tension is unknown because the variables of wetting angle, surface contamination, and leak path geometry cannot be precisely defined. Related to this topic is the deliberate clogging of the interface by liquids in gas sealing applications. This method of sealing has been referred to as "wet seals".[16]

The leak paths formed by the contacting of two materials forming a sealing interface can be clogged by liquids that have an ability to wet the mating surfaces. Wetting of the surfaces by the liquid produces capillary or surface tension forces which oppose the transgression of another liquid or gas through the leak paths.

The capillary force between a liquid-solid interface depends upon the manner in which they meet. The contact angle between a liquid and a solid is the angle between the solid and the tangent to the liquid (at the point of contact normally observed at the boundries of the liquid). The surface tension of the solid and liquid phases and interfacial tension between these phases determines the magnitude of the contact angle and thus the capillary force.

TRW Systems[16] reviewed the literature concerning applications of liquid metals to surfaces. Particular attention was given to physical properties, wettability characteristics and wetting techniques, corrosiveness, known compatibilities, and related usage. Subsequently, two liquid metal systems were selected consisting of: (1) mercury-indium-thallium and (2) gallium-indium-tin.

Under certain conditions, circular, flat interface surfaces were found to provide minimum leakage sealing (less than 10^{-6} cc/sec) with these materials. Several problems encountered concerned surface reaction including chemical effects, reusability, undefined bonding due to long term contact, and poor lubrication properties in dynamic seals. Another conclusion

reached by TRW Systems[16] was that surface finish for the sealing surface is a very important condition relating to the ability of liquid metals to produce essentially zero leakage under high and low pressure conditions. Surface finish requirements are in the vicinity of one micro inch or less.

Another aspect in the application of the criteria concerns the use of coatings, plating, and thin films. Generally, the plastic deformation of the interface will be governed by the properties of the softest material present. Hence, the effects of soft material coatings, etc. may be expected to be the same as though the entire substrate were of the soft material.

The hysteresis phenomenon is described as the relative effects of permanent interface deformation compared with the elastic deformation. This phenomenon (Deformation Regime V) can be described as follows: Two surfaces pressed together under load produce a given leakage rate. When the load is relaxed, little change in leakage occurs until the load is sufficiently relaxed, whereupon a significant increase in leakage occurs. A further increase in load produces a lower leakage rate and if the load is again relaxed, the same phenomenon occurs. The magnitude of load relaxation permissible depends upon the maximum applied stress. Typical results from Reference 4 are shown in Figure X-2-20.

The exact nature of the hysteresis phenomenon is tied in very closely with the elastic deformation of the interface substructure. This would include the seal structure and other seal-related parts. Hence, it is impossible to define rigid guidelines for its effect. Another problem is to define the limits of acceptance in terms of increase in leakage. For example, in Reference 4 it was found that the stress on flat mating surfaces could be relaxed as much as 50 per cent without a 100 per cent increase in leakage. A corresponding one-order-of-magnitude change in leakage for stresses between the yield and σ_m. When the stresses are below yield, the effects of hysteresis are variable and should not be depended upon for sealing. When the maximum stress is equivalent to σ_m, the load on the surface can be relaxed until the load is approximately equal to 1/10 the load necessary for minimum interface contact width. An increase in leakage less than one order of magnitude can be expected.

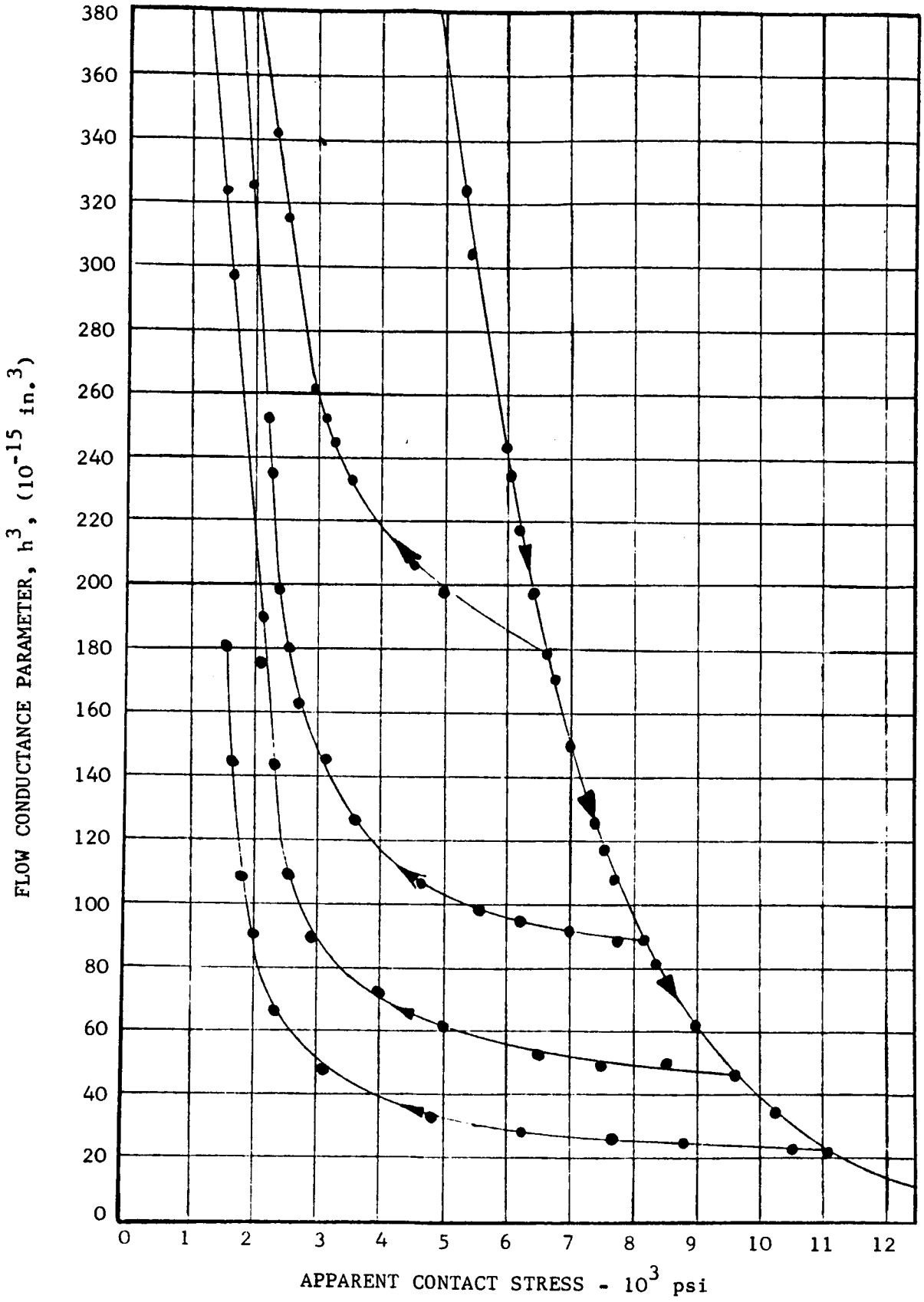

Fig. X-2-20 Hysteresis Effects for an Aluminum on Steel Interface (Aluminum Gasket 2A; Helium; 95 psi Pressure; 80°F)

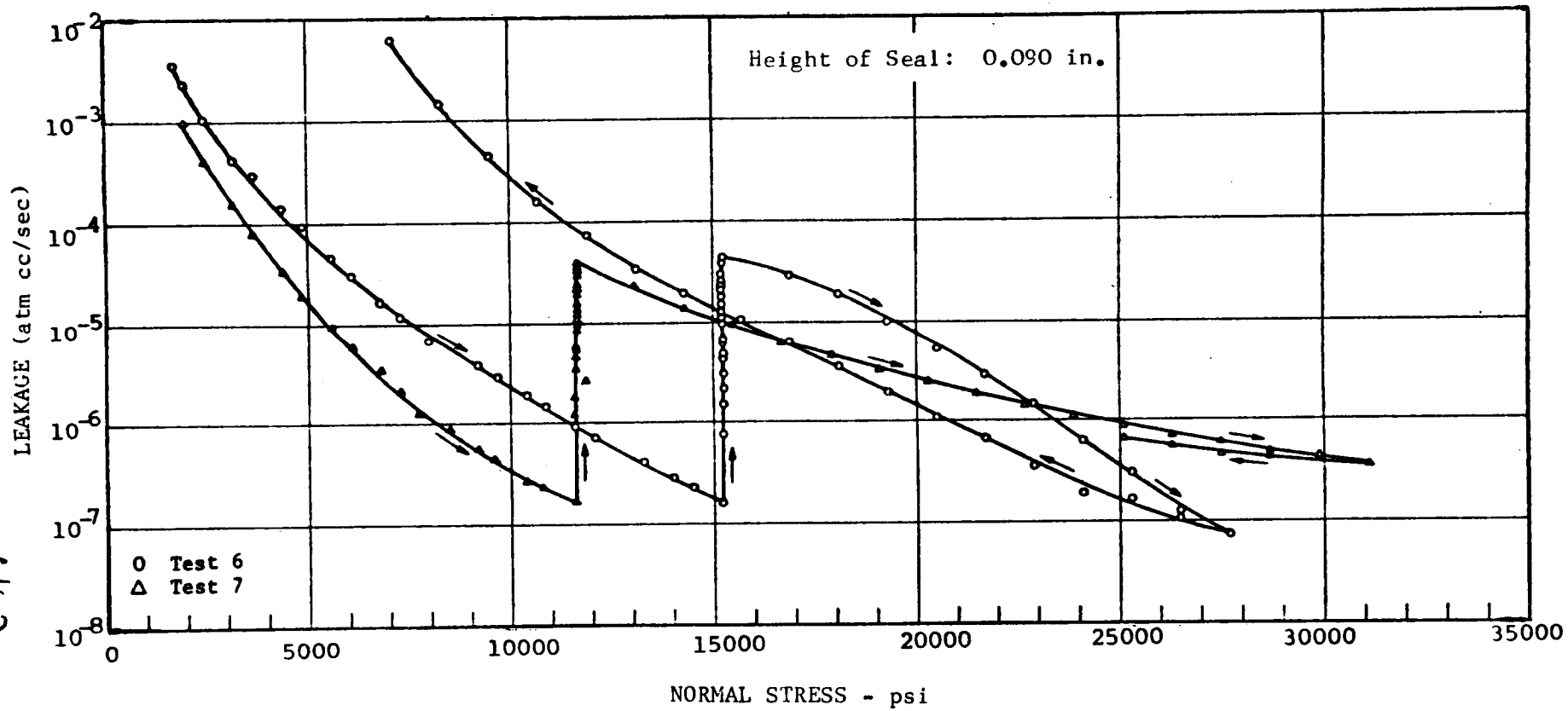

Fig. X-2-21 Leakage - Normal Stress Response for Yatabe 347 Stainless Steel Specimens (First Set)

The reusability of static sealing interfaces after separation is not permissible unless an increase in interface load accompanies each reuse. The increased load is required to produce additional deformation of the bulk surface or localized disturbances. The most promising surface classes for reuse are as follows:

> Class I or II. The deformation of these surfaces, being mostly elastic, should require no increase in load prior to each reuse. However, solid and liquid contaminants are often present when the surfaces are disjoined. To achieve elastic contact when rejoined, all contaminants must be removed. This implies that particles less than 1/40 micron must be cleaned from the surface. This is indeed a difficult task employing the best cleaning techniques. Another source of contamination is the sealed fluid. When the surface substrate relaxes due to a decrease in load, leakage increases corresponding with a small separation of the surfaces. The separation permits small particles of fluid-borne contaminants to enter the sealing interface and, when the load is reapplied, the surfaces no longer contact each other. To improve the contact, a higher load must be applied causing localized elastic and plastic deformation around the contaminants. This effect was shown by General Electric.[12] Typical leakage results of a Yatabe polished surface are shown in Figure X-2-21. Two polished surfaces were pressed together and a one atmosphere differential was impressed across the system. Leakage was measured with increases in normal stress until a leakage rate of 10^{-6} cc per sec (helium) was reached. At this time the internal pressure was increased and the load adjusted so that the normal stress remained constant although leakage increased as a result of the higher pressure. Again, the normal stress was increased and leakage was observed. It can be observed that after each successive increase in leakage, a higher stress was required for minimum leakage. This is attributed to the gas contaminants entering the interface. After the fourth repetition of this process, it required 31,000 psi contact stress to achieve a minimum leak rate of 5×10^{-7} cc per sec. This stress is approximately equal to $0.13\sigma_m$. At this stress, a leakage of the same range could have been obtained by plastically deforming rougher surfaces.

Class III. These surfaces depend entirely on plastic deformation for sealing. When the surfaces are disjoined and rejoined, a load increase of 5 per cent is sufficient to again produce full plasticity.

In summary, neither surface or deformation mode is entirely satisfactory from a reusability standpoint. The Class III surface offers greatest reliability since the magnitude of load increase is not dependent on very small contaminants. However, the load required for initial deformation is substantially higher than the Class I or II surface. The Class I or II surfaces are susceptible to handling as well as to contaminants and the load increase is not readily predictable. Hence, a compromise must be made on the choice of surface when reusability is a requirement.

The deformation of plastics requires additional considerations to the extent that without proper constraints, the phenomenon of cold flow can exist. The reliability of plastic materials cannot be assured unless the bulk flow of the material is precluded by proper geometric constraints. This problem exists to a lesser extent with metallic materials and is associated with creep and the region of full plasticity (modified stress ratio >0.1).

Design Criteria - Elastomers

Elastomers deform to mate with rigid surfaces by large elastic deformation. The normal stress required for minimum leakage is a function of the material hardness as measured by various Shore Instruments.[17] The softer the material, the lower stress required for sealing. IITRI[3] developed a relationship for the conductance of elastomeric interfaces of the form:

$$h(x) = \frac{5.7\times10^{-10}\ H^{3.25}}{\sigma_x} \tag{13}$$

where

$h(x)$ = cube root of the conductance parameter and is a function of a point (x) in the interface

H = Shore A hardness of the material

$h\ max$ = PTV surface finish of the mating material normal to leakage flow

σ_x = contact stress at a point (x) in the interface

In the case of the deformation of metals and plastics, the conductance was assumed to be an average value for the entire interface. In other words, the deformation across the interface was assumed to be constant. This was a reasonable assumption since the contact forces were of primary interest and the effects of fluid pressure were insignificant in magnitude. Elastomers, however, are readily deformed and consequently, the effects of fluid pressure must be considered. This is the primary reason for designating h and σ as functions of (x). The following example shows the application of the criteria and further explains the preceding effects.

The general case of a rectangular cross-section ring is chosen for analysis. The ring is assumed to be confined between two flanges, as shown in Figure X-2-22. The radial displacement of the rubber is constrained by two substantial rings.

If the curvature of the seal ring is neglected, the geometry of flange A can be represented as a rectangular flange with no leakage past the edges. This approximation is valid when the ring width is small compared with the diameter. The approximate geometry is shown in Figure X-2-23.

Forces Acting at the Interface are:

$$\frac{P_N}{bX} = \frac{P - \frac{p \pi D_i^2}{4}}{bX} = P_{(x)} - \sigma_{(x)} \qquad (14)$$

where

P_N/bX = average net interface stress

X = width of interface in the direction of leakage flow

b = depth of interface normal to flow

P_N = net load

P = flange load

p = sealed fluid pressure

$P_{(x)}$ = fluid pressure at any point x

$\sigma_{(x)}$ = normal stress at any point x

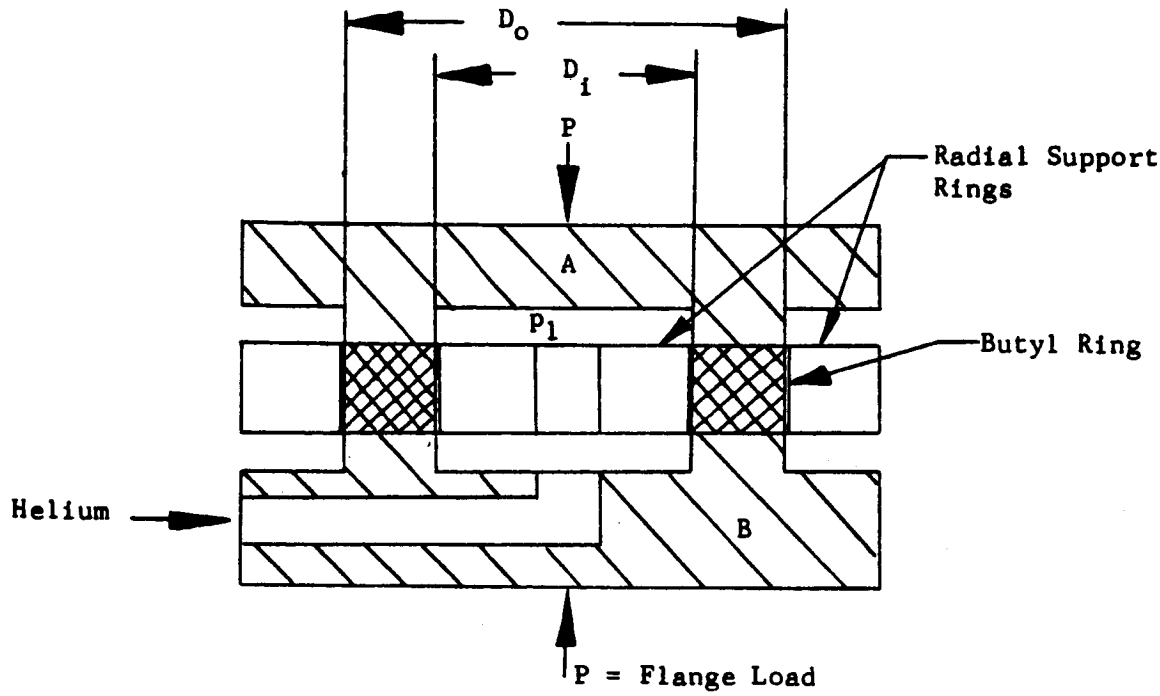

Figure X-2-22 Circular Ring Pressed Between Two Flanges

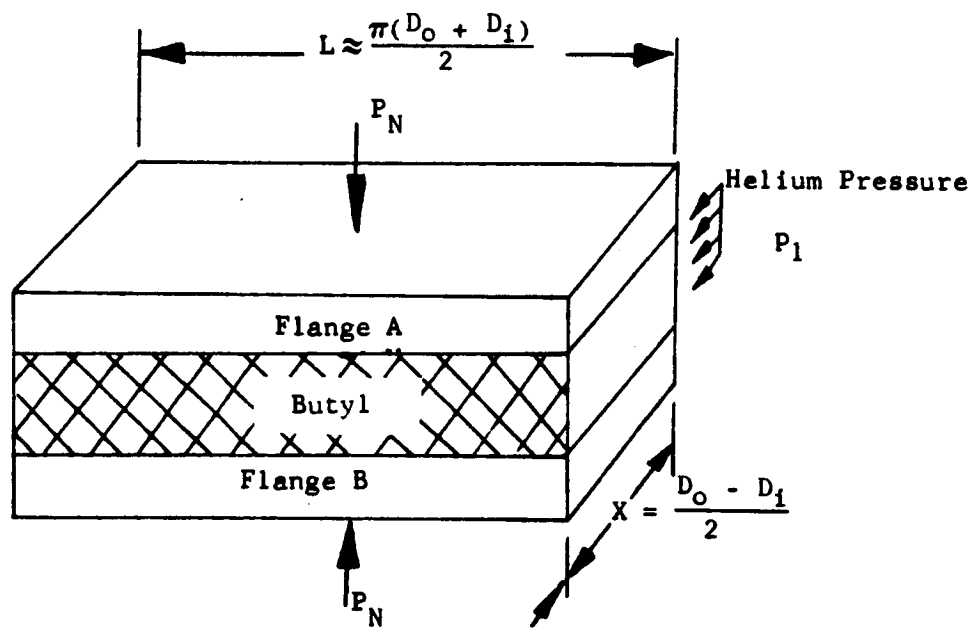

Figure X-2-23 Approximate Geometrical Representation of the Seal Interface

The weight rate of flow simultaneously through two interfaces, shown in Figure X-2-23 under the assumptions of laminar, compressible flow is:

$$W = \gamma Q = \frac{\gamma b h^3}{6\mu} \frac{dp}{dx} \tag{15}$$

Rearranging terms;

$$W \int_{o}^{X} dx = \int_{p=p}^{p=p_o} \frac{bh^3 p}{6\mu RT} dp \tag{16}$$

Combinding Equations (13), (14) and (16) gives:

$$W = - \frac{b(1.85x10^{-28})H^{9.75}}{6X\mu RT} \int_{p=p_1}^{p=p_o} \frac{p}{\left[a + \frac{P_N}{bX} - p\right]^3} dp \tag{17}$$

Integration yields:

$$W = \frac{b(1.85x10^{-28})H^{9.75}}{6X\mu RT} \left\{ \frac{a + \frac{P_N}{bX} - 2p_o}{2\left(a + \frac{P_N}{bX} - p_o\right)^2} - \frac{a + \frac{P_N}{bX} - 2p_1}{2\left(a + \frac{P_N}{bX} - p_1\right)^2} \right\} \tag{18}$$

where

$$a = \frac{\left(5.7 \times 10^{-10}\right)H^{3.25}}{h_{max}} \tag{19}$$

If the following actual identities are substituted into Equation(23) the volume leakage rate at ambient conditions can be calculated. The results are shown graphically in Figure X-2-24 along with comparative experimental data.

Butyl Rubber Seal

H = 70 Shore A

h_{max} = 46 μin PTV

P_1 = 360 psia

P_o = 14.7 psia

μ = 2.83×10^{-9} lb-sec/in^2 (viscosity of helium)

X = $(D_o - D_i)/2$ = 0.134 in

D_o = 2.500 in

D_i = 2.232 in

$$b = \frac{\pi(D_o - D_i)}{2} = 7.42 \text{ in}$$

$$Q_o = \frac{W}{\gamma_o} \text{ and } RT = \frac{P_o}{\gamma_o}$$

γ_o = specific weight of helium (STP)

The conductance clearance Equation 13 applies to any rubber material. In most cases, high contact loading produces permeation flow. Thus, limitations must be placed upon Equation 13 from the standpoint of minimum leakage prediction. The permeation rate can be estimated from the data in Appendix X-A and the procedures and data contained in Volume II, of Reference 4.

The rubber material must be devoid of all contaminant's including large surface scratches. If a grease lubricant is applied to the surfaces, the properties of the lubricant should be used initially to predict its flowrate through the interface.

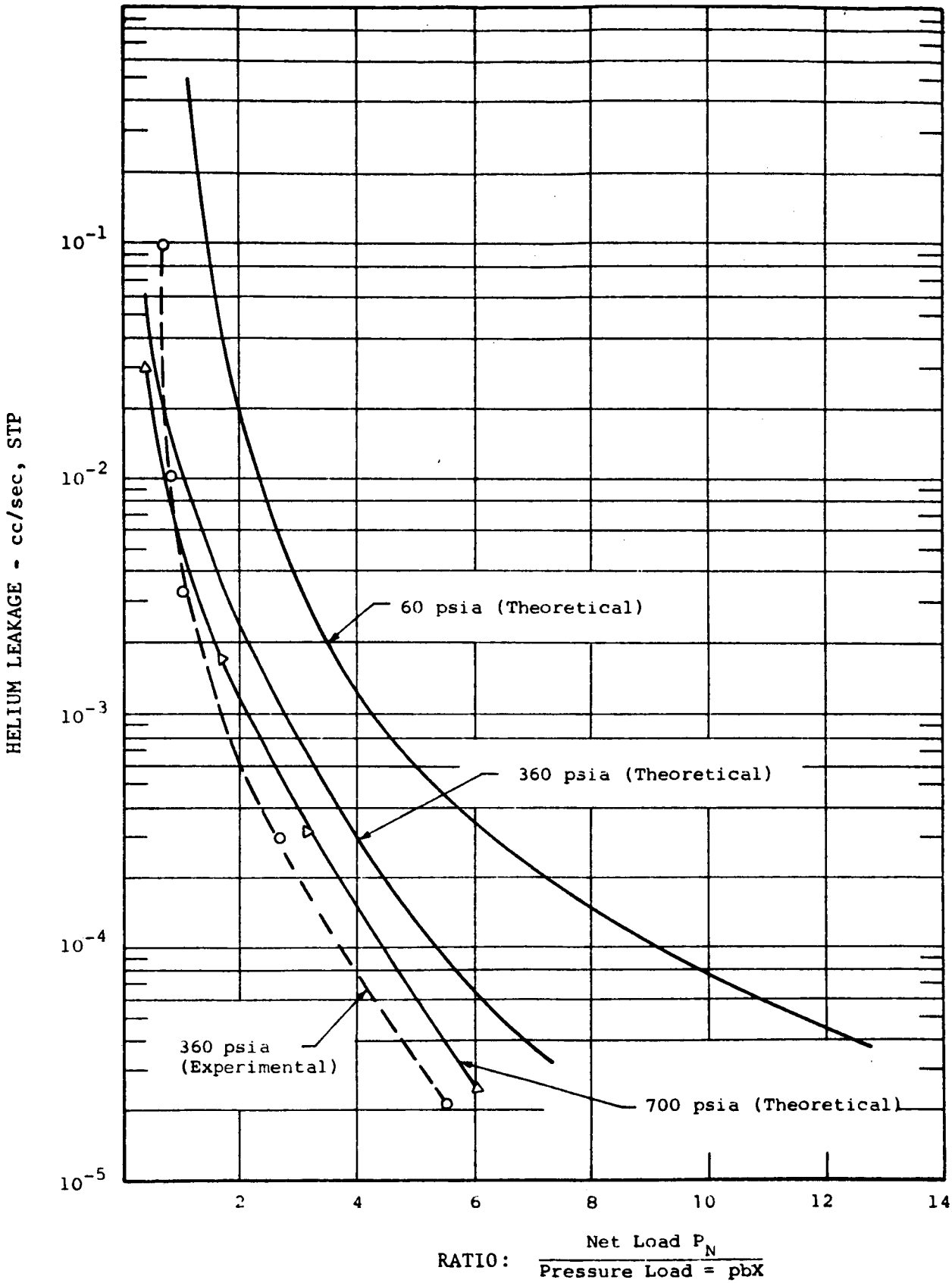

Fig. X-2-24 Theoretical and Experimental Leakage Characteristics of a Butyl Rubber Ring. The Net Interface Load is Normalized to the Maximum Pressure Load to Show the Relative Effects of Increasing Load. (Pressure Difference Across the Ring is Shown as a Parameter)

X-3 DYNAMIC SEALS

Leakage flow occurs through the interconnection of void spaces formed by the topographical variations of static mating surfaces. Deformation of the surfaces by applied loads produced a change in the interconnection of void spaces. Leakage, therefore, was shown to be dependent upon the degree of deformation. When gross relative motion occurs between surfaces, the magnitude of applied loading must intentionally be small to minimize energy dissipation. Hence, the deformation exhibited by rubbing surfaces is not expected to be the same as that by static surfaces. Another form of deformation caused by wear predominates in rubbing contact. A disruption in the chance orientation of void spaces is accompanied by changes in surface topography through the various mechanisms of wear.

The factors influencing the magnitude of fluid interchange or leakage through a static interface have been identified as material properties, applied load, and the initial topography of the surfaces. Similarly, these factors may be expected to be of significance for interface surfaces having relative motion. The imposed motion, however, introduces two additional factors, wear and friction. Each of these factors, while somewhat related, has different effects from the viewpoint of sealing. Friction is of interest because of detrimental energy dissipation, in the form of low system efficiency, heat generation, thermal deformation of seal parts, and heat generation producing physical or chemical changes in the fluid between the interface surfaces. Wear, on the other hand, is of interest because of the loss of material from the rubbing surfaces and, more importantly, the topographical changes of the surfaces associated with the wear process. The latter aspect is considered significant solely from experimental observations of leakage through static interfaces[3,4,5] and the resulting roughness observed when surfaces rub together. For example, two mild steel surfaces of 10 μin. finish, when statically pressed together, produce an equivalent leakage

channel gap* of approximately 10 μ in. Observations by Finken,[18] however, showed that the rubbing of similar surfaces in air produced a surface roughness of 200 μ in. Hence, rubbing may be expected to produce a larger equivalent leakage channel with a corresponding three-order-of-magnitude increase in leakage through the interface. Unfortunately, little information that ties wear, surface topographical changes, and leakage together is available.

To fully describe the effects of wear, consider the following example. Two surfaces possessing an initial roughness are rubbed together. The various mechanisms of wear produce an increase or decrease in roughness depending upon load, material properties, and initial finish. Simultaneously wear debris and transfer are generated. If the debris and transfer particles are larger than the roughness, the surfaces will be separated by a distance determined by the debris size. If the debris and transfer particle size are smaller than the roughness, the surfaces will be in contact. Thus, the following statement logically follows:

> The physical condition (leakage path) of an interface is determined by the magnitude of surface roughness or the size of wear debris and transfer particles depending upon which is larger.

Experimental investigations of wear fragment generation show that the fragments are large in number and in size. An estimate of the wear particle diameters for sliding systems can be obtained from material surface energy considerations.[19]

---

* The concept of an equivalent leakage channel gap is based on the results of experimental leakage measurements and theoretical flow equations. The equivalent channel represents a model of the interconnected void spaces in the interface.

$$d = 2.3 \times 10^{-4} \frac{W_{ab}}{H} \text{ in.} \tag{20}$$

where

W_{ab} = surface energy in ergs/cm^2

H = hardness in kg/mm^2

A review of the literature and experimental evidence has shown that the average particle diameter for the best combination of sliding materials is $\sim$ 50 to 100 μ inches.

An estimate of the number of particles generated, N, can be obtained by experimentally determining wear coefficients, k, using the formula

$$N = \frac{kP}{3Hd^3} \tag{21}$$

where P is normal surface loading and the wear rate is equal to Nd^3. From the preceding formulas, the magnitude of wear and particle size can be estimated. The leakage rate through a seal can, therefore, be determined by applying the appropriate flow equation derived from principles of fluid mechanics.

Another type of dynamic seal is the intersticial seal. These seals employ surfaces which are separated by a finite distance through the mechanism of fixed clearances such as a throttle bushing, hydrodynamic lift hydrostatic separation, and viscous seals. Generally, these seals are not used in pressurization systems because:

(1) The throttle bushing requires a finite clearance resulting in high leak rates.

(2) The hydrodynamic, hydrostatic and viscous seals are applied principally in rotary shaft applications which are not found in pressurization systems.

Further detailed discussion on the topic of wear and other types of dynamic seals can be found in Reference 3.

X-4 RECOMMENDATIONS FOR MINIMUM LEAKAGE

Static Sealing

The easiest and most reliable sealing can only be achieved through the use of semi-and non-separable seals. This implies such techniques as welding and brazing. Unfortunately, this form of sealing is suitable only when the functioning parts are not required to separate as in the case of tube connections. Pressurization systems, however, do require other forms of separable seals such as valve seats and component enclosures which cannot be permanently joined. For these cases, wet seals and freeze seals appear to offer the greatest advantages from a minimum contact load and surface deformation standpoint. These seals, however, are still in the development stage. Consequently, the only recourse at the present time is to employ one or more of the various modes of deformation for separable seals.

Minimum leakage is usually desirable with minimum interface loading. This can be achieved by elastically deforming rubber or metallic materials. At higher loads, metals and plastics can be employed through plastic deformation of the materials.

Elastic deformation of metallic surfaces requires the surfaces to be very highly polished with few surface disturbances smaller than 1 μinch. The waviness must be approximately the same value, depending upon the geometry of the substrate material. These surfaces are difficult and expensive to produce and susceptible to handling damage and foreign contaminants. The performance of the elastically deformed interface can be superior to the plastically deformed interface. The performance, however, is unreliable because of factors over which one has little control. In addition, the elastic seal surface is difficult to evaluate in large diameter seals (greater than 4 inches) due to limitations of inspection techniques.

Plastic deformation of the sealing interface offers reliable performance, but at the expense of very high contact loads. Minimum leakage can be achieved when the interface loads approach the Meyer hardness of the materials. Hence, materials with low hardness are preferable to harder materials. To illustrate this point, the Meyer hardness, σ_m, of plastics is $\sim$4000 psi compared with

ORIGINAL PAGE IS
OF POOR QUALITY

over 1,000,000 psi for hard metals. An average elastic stress for rubber materials is ~ 1000 psi.

It has been found that sealing generally occurs within a reasonably predictable range of stress. Even though the leak rate depends on numerous parameters such as width of contact, initial roughness of the surfaces, etc. it has been found that the leak rate decreases precipitously as the average stress over the seal area reaches a critical value. This effect may be observed in Figures X-2-16, X-2-17, and X-2-18. For systems of surfaces pressed together, the approximate range of applied stress has been found by IITRI[3] to be between 0.2 and 0.33 times the Meyer hardness of the softer material forming the interface. This compares with the conclusion reached by General Electric[20] that the applied stress should be between 1.5 and 2.5 times the yield strength. If a comparison is made between Meyer hardness and yield strength, the hardness is found to be 4 to 8 times greater than the yield strength.

Using the maximum difference factor of eight and IITRI's results based on 0.2 and 0.33 times the Meyer hardness, the stress required for sealing is 1.6 and 2.7 times the yield strength. These results corroborate General Electrics' conclusion. However, if the choice of a softer material is such that the Meyer hardness to yield strength ratio is four, the stress required for sealing from IITRI results in 0.8 times the yield strength. A review of the work conducted by General Electric and their conclusions suggests that minimum leakage is a function substantially of the initial surface finishing process and the yield strength. IITRI results, however, showed that minimum leakage is substantially affected by the Meyer hardness and strain hardening effects. The influence of initial surface finish was only 60% compared to a value of 200% as determined by General Electric.[20] At leakage rates higher than the minimum (lower corresponding stress), however, a greater influence of initial surface finish was demonstrated by IITRI as shown in Figure X-2-16, X-2-17, and X-2-18.

In any event the preceding arguments can be settled by accepting General Electric's statement[20] "It can be stated that, for most designs, a stress of 2.75 times the yield stress of the softer material would be conservative". From this standpoint, IITRI's conclusions concur.

The shape or geometry of the interface should lend itself to gross plastic deformation. Most commercial seals have relatively flat interface surfaces, which, when pressed together, produce microscopic deformation of the asperities. Consequently, large loads must be imposed before sufficient plastic deformation of the leakage path can be realized for minimum leakage. Wedge-shape interfaces, on the other hand, produce substrate and surface deformation upon the first application of load. Consequently, full plasticity occurs. The most beneficial shape of the interface appears to be a 60-deg wedge, however, other shapes offer similar advantages.

Minimum leakage through wedge-deformed interfaces depends upon the load applied, material properties and the resulting width of contact normal to the average direction of leakage flow. On the basis of limited experiments, the width of contact must not be less than 0.012 in. This suggests that the ability to produce minimum leakage is a function of the load per unit length of circumference and the material properties. For minimum leakages, an approximation for the load per inch of circumference is $P = 0.012\,\sigma_m$. Thus, a metal with a hardness of 100,000 psi would require an interface load of 1200 pounds per in. This loading is normal and may be excessive in some applications. Design innovations whereby mechanical advantage can be utilized can overcome this problem.

Minimum leakage is associated with the deformation of the softest material forming the interface. Hence, surface platings and coatings will govern the deformation process while the substrate has little or no effect.

Whether the interface deformation be elastic or plastic, the topography of the surface must be a minimum. Rough surfaces greater than 10 μ in. PTV should possess a lay pattern normal to the direction of leakage flow. Surface waviness, usually a controlling factor in rough interfaces, must be a minimum. Unfortunately, waviness is machine-produced, and minimizing it depends on the fabrication process and quality of the machine tool. Surface finishes less than 10 μ in. can be multidirectionally oriented. These surfaces are produced by precision machine tools where waviness is approximately

the same as the roughness.

The effects of contaminants are most pronounced on elastically deformed metal interfaces. The detrimental contaminant size is estimated as 1/20 micron. On the other hand, plastically deformed interfaces can tolerate contaminants equivalent in size to the maximum rough variations. For a 10 μ inch PTV surface, the contamination level would be 1/4 micron. While the contaminant size is still small, the chances of removal are improved by exceptional cleanliness procedures. The removal of 1/20-micron particles is, indeed, difficult if not impossible. It can be stated, therefore, that plastically deformed interfaces are less susceptible to small contaminants and, therefore, are more reliable.

Dynamic Seals

Interfacial seals were described as contacting-type seals where one face rubs against the other. It was concluded that fragments resulting from wear are of such a size and number that substantial separation of the seal surfaces occurs. These fragments, even under well-lubricated conditions, have an average size generally not less than 50 μ inch and can range to 10,000 μ inch. Consequently, interfacial seals could be more appropriately classed as fixed clearance seals where the wear fragment size determines the size of the leakage path. To achieve minimum leakage, the fragment size must be as small as possible. This can be accomplished through low contact loads and a choice of rubbing materials having low surface interaction. Low surface interaction can be achieved with hard materials having low energy of adhesion, preferably a metal rubbing against a nonmetal, e.g., hardened steel against aluminum oxide.

Hydrostatic or hydrodynamic seals offer improved leakage performance by producing a smaller leakage path than that produced in interfacial seals. The criteria for these seals have not been fully developed and, additionally, pertain primarily to rotating shaft seals.

Sliding seals appear relegated to the interfacial variety because of the nature of the motion and the problems associated in the fabrication of seals and seal-related parts. Since most sliding seals are cylindrical, the problem is one of fabricating and inspecting cylindrical surfaces. To achieve minimum leakage, the maximum mismating (out-of-roundness of both interface surfaces) must be at least less than the average size of the wear fragments. This suggests out-of-roundnesses less than 0.0001 inch. In some cases this can be achieved, depending on the geometry of the cylindrical parts. In any event, inspection instrumentation and procedures must be improved before reliable advances in fabrication can be achieved.

Even with optimum criteria, it seems unlikely at the present time that leakage rates of 10^{-5} cc per sec of gas leakage can be achieved without resorting to such devices as liquid barriers, or bellows seals. A review of the criteria for static seals shows that substantial surface loading and deformation are required to achieve this leakage rate. These requirements placed on dynamic seals would undoubtedly produce severe wear and large debris fragment size.

Comments

It may be concluded that it is impossible to achieve zero leakage; at best, minimum leakage can be achieved where minimum leakage is defined as the leakage produced by all seals in the system. Often a tolerable leakage rate will have to be acceptable which is an optimum compromise between mission requirements and seal construction features. This topic is considered in Section XI.

It is suggested that References 3,4,5,6 and 20 be reviewed if further information concerning seals is required.

X-5 LEAK DETECTION

The detection of leakage may be defined as the "pin point" identification of the leak source and the quantitative measurement of leakage. Each of these objectives in leak detection requires a different technique. As a result, only one objective is usually sought because of the procedures involved and complexity of the necessary instrumentation.

Leak detection is employed in virtually all stages in the development and utilization of pressurized gas systems. The important applications are:

(1) Laboratory investigations involving research on seals, valve seats, and other fluid containing components. A high degree of measurement and location accuracy is required.

(2) Quality control of manufactured system components. This presupposes that adequate standards have been established for this purpose. A high degree of measurement accuracy is also required while location detection may be of secondary importance. Since the success of a mission depends upon the overall performance, the degree of measurement accuracy is the same as that sought in the laboratory.

(3) Field evaluation and check-out procedures. In this case the location of the leak is of prime importance. Quantitative measurements may also be used where known, tolerable leakage rates have been established. The success in detecting leakage on a fully assembled gas storage system is limited by the instrumentation available and the accessibility of components.

(4) In-flight inspection and repair. During manned missions it may be necessary to locate and repair leaks which occur in the pressurization system, and other critical areas. Satisfactory, light weight, and easily used instrumentation must still be developed for in-flight applications.

Source Locating Techniques

The detection and pin point location of leaks is most important when a failure or malfunction of a component has occurred. Considering that leaks could develop at many points, such as seals or cracks, it is necessary to pin point the source so that corrective action can be taken.

Several methods and instrumentations can be employed depending upon the hardware to be inspected. A limitation of virtually all the methods is accessibility to the area being investigated for leakage. For example, internal valve leakage is often impossible to pin point without partially dismantling the component. Consequently, source locating leak detection methods are usually applied to external leaks. Three common methods employed can be described as follows:

Method A - The pressurization system or individual component is evacuated to pressures of 10 Torr or lower. This requires that the component can be readily evacuated and the leakage rates are very small. This method is not recommended when the total leak rate is unknown because, substantial contaminants may enter the system in attempting evacuation.

Method B - The system under investigation is pressurized with a gas. The gas may be that normally used or another gas. The choice of gas depends upon the instrumentation or techniques utilized.

Method C - The system under investigation is pressurized as described in Method B. However, the hardware item is then placed in a vacuum chamber.

Each of the preceding methods require different techniques to pin point leakage although the instrumentation required may be the same. The specific techniques for each method can be described as follows.

Techniques for Method A

A-1 Detection of Tracer Gas with Thermal Conductivity or Ionization Gage. Change in pressure within the system may be monitored using the thermocouple, Pirani or ionization gage. A tracer gas applied to the exterior enters the localized leak and changes the thermal conductance or ionization current originally produced by the gas initially in the system. A small gas dispensing probe is usually employed to scan the part being inspected. A rise in indicated pressure shows the presence of a leak. Similar techniques employing substances on the outside of the system may be used also. In this case sealers such as water, lacquer, Glyptal, acetone, or ether clog the leak and produce a decrease in indicated pressure. Some of the sealers such as ether, provide a temporary seal where lacquer is permanent.

A-2 Radioactivity Measurement. A material, such as krypton 85, is allowed to enter a leak from a suitable probe dispenser. The amount of radioactive material which enters the system continuously being evacuated is measured by a scintillation counter.

A-3 Argon Leak Detector - One commercially sold detector uses the pressure rise in a vacuum system to detect leaks. The leak detector consists of a vacuum system which uses a getter pump. This type of pumping is efficient for all but the inert gases. Argon or helium is therefore used as a tracer gas. When Argon enters the vacuum system through the leak, the pump is not capable of gettering it efficiently and the pressure in the system rises. The sensitivity of this type of pressure rise method is reported to be extremely high, 10^{-9} STP cc/sec. The major disadvantage of this method of leak testing is that it is not readily applicable to large volume systems, because of the large amount of argon needed to be pumped from the air in the system.

A-4 Hydrogen Sensitive Leak Detector - A hydrogen sensitive leak detector consists of an ionization gauge connected to the vacuum system by a heated paladium diaphragm. Hydrogen, which is used as the tracer gas, permeates through the hot paladium to the ion gauge. The advantage of this system is that it is relatively insensitive to pressure changes. This detector has a reported sensitivity of about 10^{-8} STP cc/sec.

A-5 Electron Emission Leak Detector - The electron emission from a tungsten or oxide coated filament decreases greatly upon contact with oxygen. This phenomenon,[21] has been applied to leak detection. The sensitivity of this method, using oxygen as a tracer gas, is reported to be approximately 10^{-8} STP cc/sec.

A-6 The Halogen Leak Detector - Early investigations of thermionic emission showed that platinum, even in air, at red heat emits positive ions. This emission at any given anode temperature of positive ions in air is increased very markedly when vapors of compounds containing a halogen strike the electrode surface. This observation forms the basis of the halogen leak detector. Leak detectors using this principle are marketed by several companies. Two types of models exist. One type consists of a detector head mounted in the vacuum system and the halogen gas, usually Freon, used as a tracer outside the vacuum system. A second type consists of a small gas pump probe; the system to be leak tested is pressurized with halogen-containing gas. The gas pump probe contains the detection apparatus. The sensitivity of this method of leak detection is approximately 10^{-6} STP cc/sec. Special units are claimed to be as sensitive as 10^{-9} STP cc/sec.

A-7 Helium Leak Detector - A very sensitive method for detection of leaks is the use of a mass spectrometer and helium as the tracer gas. The mass spectrometer is attached to the vacuum system and a probe of helium gas is passed around the suspected leak area. The mass spectrometer is set directly on the helium mass peak. Detection and measurement consists of observation of the intensity of the ion current. Helium is chosen as the tracer gas for the following reasons:

(1) Low value of molecular weight - the rate of effusion through the leak is greater than for any other gas except hydrogen.

(2) Helium occurs in the atmosphere only to the extent of one part per 200,000 parts of air.

(3) There is no possibility that an ion, due to any other gas will give an indication that can be mistaken for helium.

Several companies manufacture commercial leak detection equipment using this principle. The sensitivity of most of these units is 10^{-10} STP cc/sec. One company manufactures a helium leak detector which operates on a pressure build-up by getter-ion pumping prior to detection of the peak. The sensitivity of this instrument is claimed to be 10^{-14} STP cc/sec. Because the vacuum equipment in this apparatus is similar to the equipment in the argon leak detector previously described, this instrument could be used as a binary leak detector. For gross leaks the pressure build-up using an argon probe would be used. After all the large leaks were detected, helium gas could be used to hunt for the small leaks.

Techniques for Method B

B-1 Sonic Detectors - Leak detectors are available to physically detect the sound made by the outflow of a gas, presumably choked flow. Manufacturers stated sensitivity of these instruments is approximately 10^{-1} STP cc/sec.

B-2 Bubble Testing by Soap Solution - A container to be tested is pressurized and painted with a soap solution. Any leak can be seen by the growth of bubbles. The efficiency of this method depends upon: the observation abilities of the operator, the ability to completely wet the tested area, the surface tension of the soap solution, and the complexity of the part. It has been estimated that under proper conditions the sensitivity of this method is 10^{-4} STP cc/sec.

B-3 Bubble Testing by Immersion - A pressurized vessel may be immersed in a liquid; the bubbles rising to the surface will indicate a leak. This method is dependent on the pressure capability of the vessel, surface tension of the liquid and the size of the testing area. This method is obviously not suitable to large vessels. However, modifications can be made to cover one area by a liquid. This technique is simpler than soap solution testing because the observation abilities of the operator are not as important. The sensitivity of this method is about 10^{-5} STP. cc/sec.

B-4 Probe Method - Another method, perhaps the most common, utilizes the oxygen, helium, hydrogen, argon, or halogen leak detectors described under A-3, A-4, A-5, A-6 and A-7. A small vacuum probe collects air from outside the suspected leak area and passes it into the vacuum system containing the gas sensitive instrument. This method has a sensitivity of about 10^{-6} STP. cc/sec. which is limited, not by the instrument, but by the probe and its ability to collect small leakage flow before it diffuses into the atmosphere.

B-5 Halide Torch Leak Detector - The halide leak detector consists of a propane gas torch with a copper plate in the flame and a rubber tube supplying the flame with air. The system to be tested is pressurized with Freon gas and the end of the rubber tube which supplies air to the flame is passed over the suspected area. A leak is detected when the flame turns bright green, since a piece of copper in a flame containing halogen atoms gives off a characteristic green flame. This equipment is often used by household refrigerator repairmen because the refrigerant (Freon) acts as the tracer gas and the equipment is inexpensive. The sensitivity of this method is reported to be approximately 10^{-5} STP. cc/sec.

B-6 Radioactivity Measurement - One nondestructive method of leak testing hermetically sealed components is by using a radioactive gas. This type of leak detecting equipment is commercially available. The basic principle involves the detection of radioactive Krypton 85, which has been allowed to diffuse into the leaking components. The components to be tested are placed in an activating tank and sealed. Air in the tank is evacuated and diluted. Krypton 85 is pumped into the tank to a pressure up to 7 atmospheres. The radioactive gas diffuses into the existing leaks in the component. After a prescribed soaking period, the Krypton is pumped out and returned to storage for reuse. Air is circulated over the components to remove any residual Krypton 85 from the external surface. The components are then removed from the activating tank and tested with a scintillation counter. Under favorable conditions, leakage rates in the order of 10^{-12} STP. cc/sec. can be measured.

B-7 Chemical Reaction Methods - Coating of components with thin films subject to chemical change with the leaking fluid may be employed if the chemical change produces a discoloration of the film and is not detrimental to the component. Another method, not requiring a pressurized system, is the use of fluorescent dyes. A penetrating fluorescent dye solution is made which may be painted onto a weld and then wiped away. This dye will penetrate into any cracks and fissures. The material that is not wiped away is observed due to fluorescence, under ultra-violet light. This method of leak detection will display flaws in machining and joining. No quantitative estimates can be made as to the leak size which can be detected by this method.

Technique for Method C

Spark Coil Over Outside of Component - A high potential electrode is traversed over the outside of a system or component located within a vacuum environment. The leak is found by spark passing through the leakage flow or by a change in discharge color with materials such as ether, alcohol, or carbon dioxide. View ports in the vacuum chamber are necessary to observe the source of leakage.

X-6 QUANTITATIVE LEAKAGE MEASUREMENTS

The requirements for long term space missions has imposed an extremely low leakage criterion for the pressurization system designer to satisfy. Zero leakage, always an ideal objective, must be realistically viewed as an impossible objective. Consequently, a tolerable or optimum leakage rate specification must be generated which is compatible with the limitations of the state-of-the-art of hardware design. Having established a realistic leakage rate goal, the problem then becomes one of determining whether a system meets this criterion.

The problems associated with quantitative leakage measurements are substantially greater than those for source leak detecting. The major problem is the determination of the accuracy of the leakage measurement. This, in turn, is directly related to the reliability of the system and the ability to meet mission requirements. The general techniques and, particularly, instrumentation used in source leak detecting are the same for quantitative measurements. The differences are attributable to the methods employed.

Five methods of leakage measurement can be applied to individual pressurization system components or the entire, assembled system. The latter may often be difficult because of the system size or spacecraft design limitations. The methods can be briefly described as follows:

<u>Method D</u> - The component or system to be evaluated is pressurized and placed within a chamber.

<u>Method E</u> - The hardware is evaluated by placement within a chamber. The chamber is slightly pressurized with a gas while the component is evacuated by an external vacuum system. The leak detection instrumentation is incorporated into the external vacuum system.

<u>Method F</u> - The hardware is pressurized by an external gas supply. Leakage flow of gas into or out of the hardware is measured by suitable instrumentation. No external chamber is required.

<u>Method G</u> - The hardware element is pressurized by a gas and a connection is made between the element and a leak measuring instrument. This method may be employed, for example, to measure internal leakage such as that produced within a valve.

Method H - The hardware element is pressurized and isolated. A physical observation of the change in pressure with time within the element is related to leakage.

Before proceeding in a discussion of techniques and instruments associated with each method, several points must be clarified. First, some instruments and techniques measure mass or volume rates of leakage flow while others measure total leakage over a period of time. No specific distinction is attempted to differentiate these devices on this basis. Secondly, the fluid contained in the system may be a liquid rather than a gas. Where liquid measurement techniques are similar to that for gases, this point is identified. In general, however, when liquids are encountered it is preferrable to evaluate the system with a gas and convert the leakage to that of a liquid. This topic is considered independently. Finally, the description of instruments previously described in Part X-5 are referred to but not repeated.

Techniques for Method D

D-1 Pressure Rise in the Chamber - A hardware element can be placed in an isolated vacuum system; the leakage rate can be determined by the pressure increase measured by gauges such as the Pirani, thermocouple or ionization gauge. Care must be exercised in the selection of the gas for use as a pressurant since the pressure measurement instrumentation is effected by the thermal properties of the gas such as heat conductivity. Substantial error in actual pressure measurement can result when gas mixtures are involved. The leak rate can be calculated when the properties of the gas, chamber volume, and time increment between readings are known. The ultimate sensitivity of this method is controlled by the length of the time increment and the sensitivity of the gauge, and is also effected by temperature changes in the environment that produce independent pressure changes.

D-2 Helium Leak Detectors - Technique A-7 may be employed by connecting the leak detector to the isolated vacuum chamber. The procedure followed is usually to rough pump-down the system and then connect the leak detector. The detector must have its own pumping system and must, additionally, be capable of maintaining a high vacuum in the chamber. These devices provide a rate of leakage flow and must be carefully calibrated.

D-3 Buoyancy Technique - The concept evolved by TRW Systems[16] utilizes a vacuum container with a sensitive measuring device which measures the change in weight of an evacuated sphere due to the buoyancy of the gas within the container which surrounds the evacuated sphere. The outer container is first evacuated to an adequately low pressure and the leak whose mass flow rate is to be determined is admitted to the container, the mass admission rate is the mass flow rate to be determined. Figure X-6-1 shows a typical schematic use of the system. The mass flow rate is given by:

$$\frac{\Delta M}{\Delta t} = \frac{\Delta W}{\Delta t} \frac{Vc}{Vs} \tag{22}$$

where

ΔM = total mass of fluid introduced into the detector chamber during time interval, Δt

ΔW = indicated weight increment (buoyancy force) on the sensitive weight electrobalance

Vc = net active gas volume of chamber

Vs = volume of evacuated sphere

Test results have shown a leak sensitivity of measurement of 10^{-5} gm is possible and it is anticipated that with improvements, leak sensitivity of 10^{-8} gm will be realistic. In terms of free air, the present sensitivity is approximately 7×10^{-3} cc which, over a 5 min. time interval, is equivalent to 2.3×10^{-5} cc/sec. Hence, the anticipate improvement of three orders of magnitude enhance this concept considerably. The ultimate sensitivity, however, will probably be limited by the degree of sealing which can be incorporated into the chamber and vacuum valves. Air leaking into the system and outgassing of components may significantly induce measurement errors. (See Page X-10.1 for Leak Detection and Recommendations).

D-4 Vented Chamber - The chamber enclosing the component being evaluated can be vented through flow measuring instruments. The most common devices are:

(1) Vane displacement meters. Instruments of this type are used to measure relatively large leakage rates. The rotational displacement of the device may be used to indicate total volume flow or flow rate.

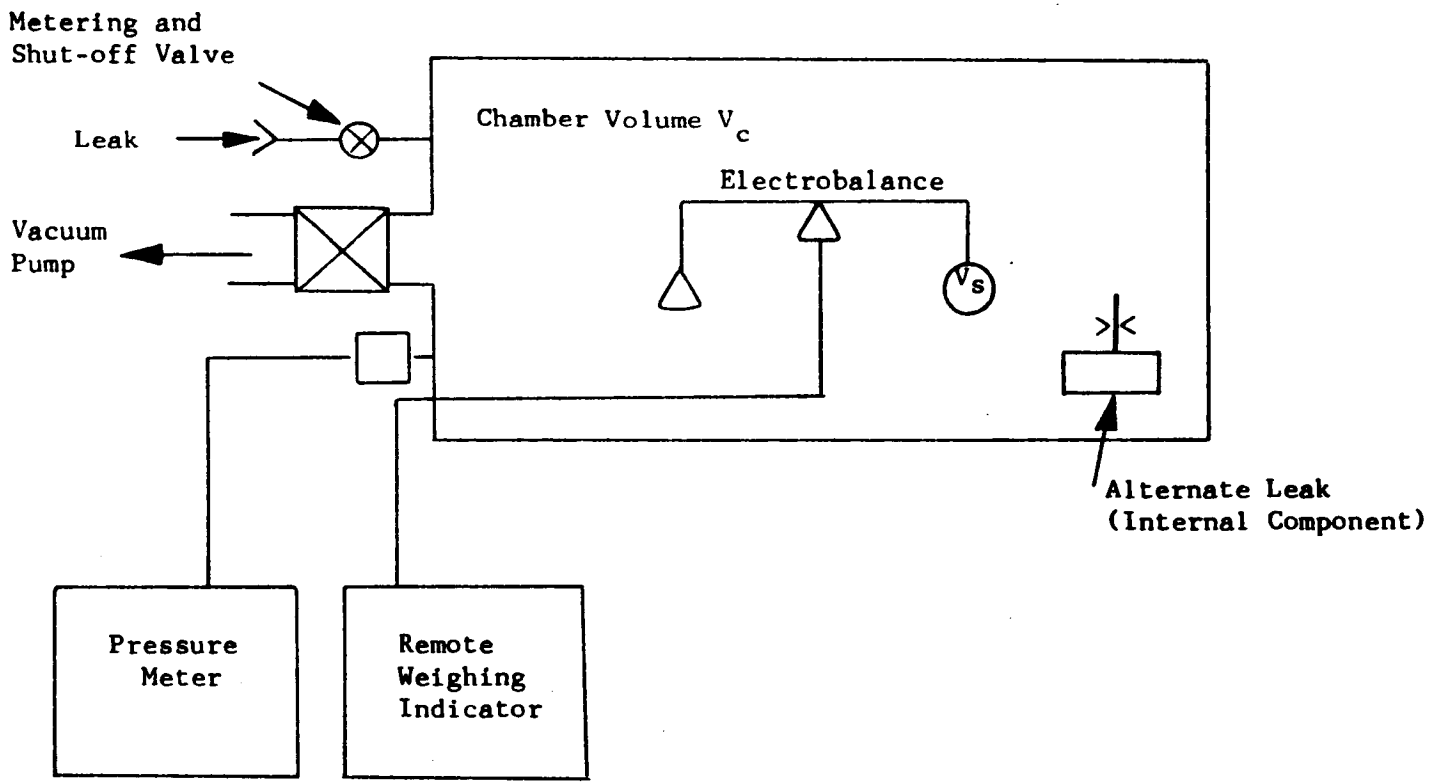

Fig. X-6-1 Experimental Mass Leak Measurement System* (Ref. 16)

---

* The buoyancy technique is described here with the permission of TRW Systems

(1) Vane displacement meters. Instruments of this type are used to measure relatively large leakage rates. The rotational displacement of the device may be used to indicate total volume flow or flow rate.

(2) Bellows displacement meters. The displacement of a pleated bellows or diaphragm may be used to measure volume change or, with suitable instrumentation, flow rate.

(3) Glass capillary tubes. Very small diameter glass tubes containing a nonwetting fluid bubble may be employed to measure small leakage. The movement of the bubble must be visually observed.

(4) Rotameters. A tapered tube containing a flow is commonly used to measure large flow rates. The position of the float in the tube indicates a flow rate. Since the tube is tapered, the flow area about the flat varies with position.

The preceding instruments can be used for liquids or gases.

Technique for Method E

Helium Leak Detector - The technique is essentially the same as D-2 but the detector is connected to the interior of the hardware item. In this case the leakage into the component is measured. An advantage of this technique over D-2 is that a vacuum chamber is not required. The external chamber required for this method could be a plastic bag enclosure slightly pressurized with a tracer gas. However, the sensitivity of measurement will be low due to the slightly pressure difference across the leak. This method is most suitable for large leak measurements.

Techniques for Method F

F-1 Flowmeters - Flow measuring instruments, such as the vane, bellow displacement, and glass capillary tube described in D-4 can be used to measure leakage rates into or from a component or system. These devices can be used for high and low gas pressure measurements depending upon their design.

F-2 Bubble Testing - The techniques described under B-2 and B-3 can be used to quantitatively measure leakage out of a component. The procedures used are:

(1) Immersion - Bubble counting with average size measurement over a time period.

(2) Soap bubble - Application of soap solution and approximating the bubble size at the end of a time period.

Technique for Method G

The technique employed is the same as E (leak detectors) and is usually applied to the evaluation of internal seals which can be readily evaluated by external connections.

Technique for Method H

The technique is the same as D-1 except that a pressure decrease is measured using conventional pressure measuring devices. The internal volume of the system or component must be precisely known. Accuracy of small leakage measurement is greatly influenced by thermal environment changes.

X-7 ACCURACY OF LEAKAGE MEASUREMENTS

The accuracy of leakage rate measurements is related to the instrument design and methods of calibration. Three methods of calibration can be employed which can be described:

(1) Weight or volumetric methods for large leakage rate instruments. These calibration techniques can be readily found in the literature.

(2) Comparison with another instrument whose range overlaps and is more sensitive than the instrument of interest. This presumes that another reference was used to determine the accuracy of the reference instrument.

(3) Calibration of leak detectors with standard leaks for use in measuring small leakage rates (10^{-4} STP cc/sec). Calibrated leaks are commercially available with eight decades of leakage values. Unfortunately, no standards for the calibration of the leaks are available resulting in wide comparative variations even though the vendor states a specific value. Methods of calibrating leaks are isobaric volume change, pressure rise method, pressure drop across a known conductance, pressure measurement at a constant pumping speed, and the measurement of alpha radiation. Each of these methods are described in Reference 22.

Estimated accuracy of various flow measuring devices is shown in Table X-8.1. Leak measuring instruments, like most instruments, should only be used within their design range. Instruments used to detect leakage rates smaller than they have been designed for, will cause leakages to be masked by the noise of the instrument. Additionally, non-linear effects attributed to electronic circuitry can induce errors. Some instrument manufacturers are overly optimistic about the sensitivity of their instruments. Conversely, the use of an instrument on leaks larger than its designed range will cause the purchase of an instrument much more expensive than necessary.

X-8 SENSITIVITY OF LEAKAGE MEASURING INSTRUMENTATION

The sensitivity of leakage measuring devices in influenced by essentially the same factors which influence accuracy. To assign specific ranges to all techniques would be difficult because of the wide variety of instrumentation available. However, certain generalizations can be made and are shown in Table X-8.1. It should be noted that all source detecting devices are not suitable for quantitative leakage measurements.

Table X-8-1

INSTRUMENTS SUITABLE FOR QUANTITATIVE LEAK RATE MEASUREMENTS

Instrument or Techniques	Range of Measurable Leakage Rates Std cc/sec										Accuracy
	10^{2}	1	10^{-2}	10^{-4}	10^{-6}	10^{-8}	10^{-10}	10^{-12}	10^{-14}		
Helium Leak Detector					▬	▬	▬	▬	▬		± 100%
Halogen Leak Detector					▬						± 100%
Bubble Methods				▬							± 500%
Pressure Rise	▬	▬	▬	▬							± 50%
Positive Displacement	▬	▬	▬	▬							± 1/2%
Rotameters	▬	▬	▬								± 2%
Buoyancy		▬	▬	▬	▬	▬					Unknown

X-9 CONVERSION OF GAS AND LIQUID LEAKAGE RATES

In Section X-A, the appendix, the theoretical equations describing the various types of fluid flow are presented under modes of leakage flow beginning on page X-A.1. The equations were developed for known leak paths or channel sizes. While it is impossible to describe completely the dimensions of a real leak, such as that in a seal, some relationships between variables can be deduced. The leak rate can be expected to be dependent upon pressure, viscosity, molecular weight. Fortunately, the theoretical expressions for flow through a fixed arbitrary leak closely agree with experiment[22]. The relationship between variables are principally:

Gas Flow

Molecular: $$Q \sim \frac{\left(P_1 - P_2\right)\lambda}{\sqrt{M}}$$

Laminar: $$Q \sim \frac{P_1^{\,2} - P_2^{\,2}}{\eta}$$

Turbulent: $$Q \sim \frac{\left(P_1 - P_2\right)}{\sqrt{M}}$$

Choked: $$Q \sim \frac{\left(P_1 - P_2\right)\sqrt{\frac{\gamma}{\gamma + 1}}}{\sqrt{M}}$$

Liquid Flow

Laminar: $$Q \sim \frac{P_1 - P_2}{\eta}$$

Turbulent: $$Q \sim \sqrt{P_1 - P_2}$$

where

Q = Volume rate of leakage flow

$P_1 - P_2$ = Pressure difference across the leak

M = Molecular weight of the gas

γ = Heat capacity of the gas

η = Absolute viscosity

λ = Molecular mean free path

In order to convert a known leakage rate under known fluid and pressure conditions to other conditions, the mode of flow must be first determined. This is not accomplished theoretically, but can be arrived at by successive leakage measurements at different pressures. Fig. X-9-1 shows typical leakage rate measurements of a needle valve.[22] After determining the flow mode, a conversion can be obtained by calculating a conductance parameter from the theoretical flow rate equations. Additionally, gas and liquid leakage equivalents can be similarily determined. The conversion results may be approximate due to changes in flow modes across the leak. It is suggested that Reference 22 be referred to for a discussion on the limitations of leak rate conversions.

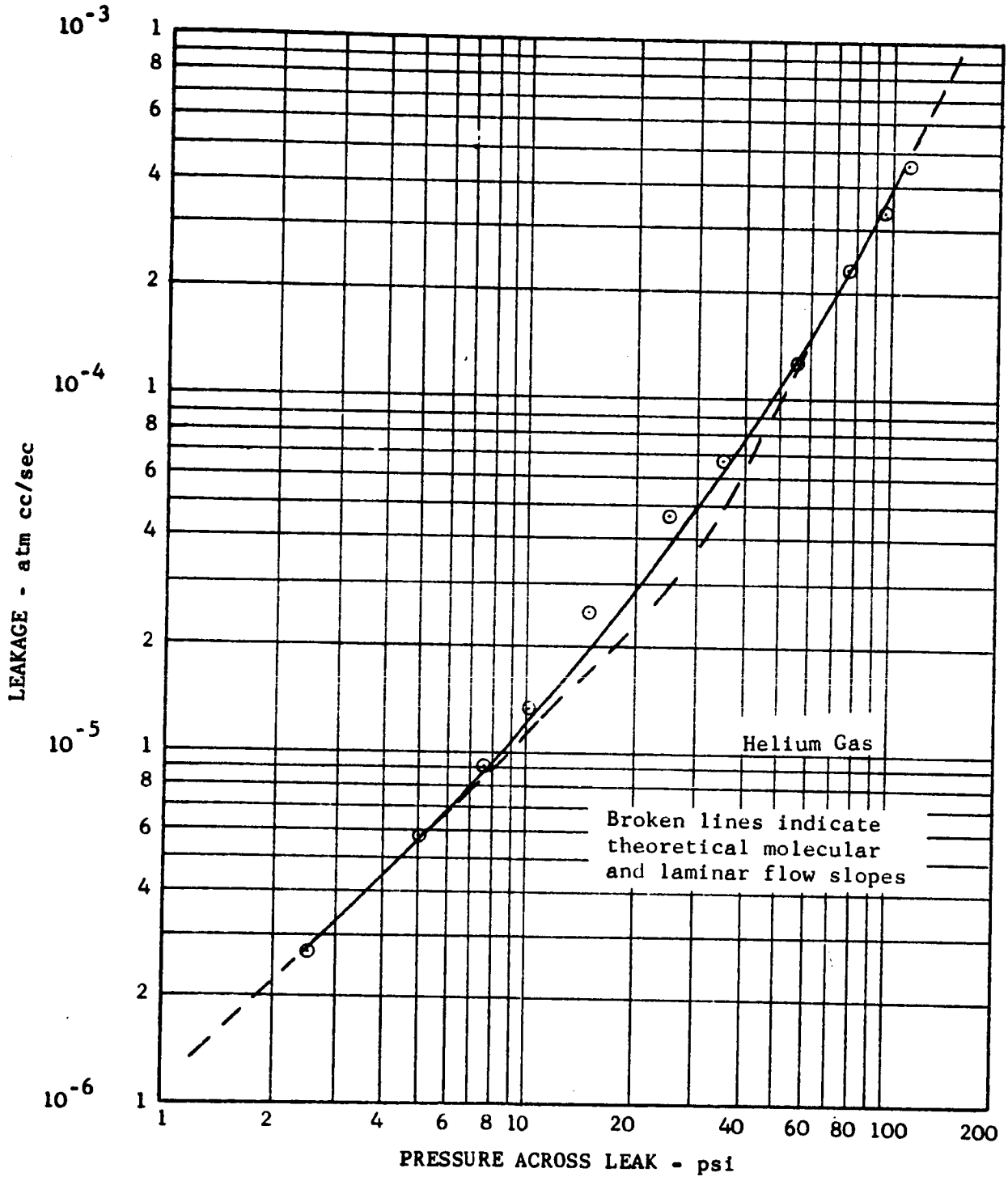

Fig. X-9-1 Flow Mode in Typical Hardware Leak; Needle Valve (Ref. 22)

X-10 LEAK DETECTION RECOMMENDATIONS

The source location of leaks is a time consuming task when utilizing the most sensitive instruments. An adequate instrument is the helium leak detector using a probe or tracer gas techniques. Unfortunately, when large components or systems are involved, the entire surface area must be scanned very carefully. Other methods such as the bubble and chemical reaction tests provide a much faster scanning of the surface but with reduced sensitivity. Hence, a suggested approach to the problem is that of employing several instruments.

A recommended procedure for locating leaks is to:

(1) Measure quantitatively the total leakage rate from the system or component. If possible, the entire system should be pressurized with helium and place in a vacuum chamber. Pressure rise techniques should be initially employed to establish a range of leakage. If the leakage rate is in the range of a helium leak detector, it should then be employed.

(2) After the gross leak rate has been established, a selection of leak source instruments must be made. When large leakage rates are encountered, the immersion bubble test can be considered. If many small leaks contribute to the total leakage, partial or no reaction may be observed. At this point, there is no choice other than the use of the helium leak detector probe. When very large leaks occur, the sonic detector can be utilized.

It must be noted that the buoyancy instrument being developed by TRW Systems[16] appears to have substantial promise for use in quantitative measurements. This statement is based on its wide range of leakage rate capability. The successful development of this technique would permit the use of a singular instrument to cover very large (10^2 cc/sec) to very small (10^{-7} cc/sec) leak rates.

Whenever possible, leak detection should be made at operating pressure or higher. This not only increases sensitivity but locates "check valve" and self cleaning leaks. Check valve leaks can be described as leaks which occur under certain conditions of flow but disappear at higher

flow velocities, probably due to clogging by contaminants. An additional prime reason for using the operating pressure as the testing pressure for leak detection measurements is that the structural distortion which occurs at that pressure may reveal more or larger leak path than would be indicated at very low pressures.

Leakage extrapolations to other gases or liquids may be made with the realization that errors can be encountered. The surveys and analysis of leakage measurement and evaluation by Dr. J. W. Marr[22,23] are suggested for additional source information.

X-11 REFERENCES

1. Gitzendanner, L.G. Optical observations of sealing phenomenon. Proc. Conf. and Design of Leak-tight Separable Fluid Connectors. NASA March 24, 1964.

2. Anon. (General Electric) Statistical interface-leakage analysis and feasibility of superfinished interfaces for sealing. NAS 8-4012 Geo. C. Marshall Space Flight Center, Final rept., 3rd contract period, May 1, 1965.

3. Bauer, P.A. (IITRI) Investigation of leakage and sealing parameters. AFRPL-TR-65-153, Aug. 1965.

4. Bauer, P.A., Glickman, M. and Iwatsuki, F. (IITRI) Analytical techniques for the design of seals for use in rocket propulsion systems. Vol. I and II, AFRPL-TR-65-61, May 1965.

5. Anon. (General Electric) Design criteria for zero-leakage connectors for launch vehicles. NAS 8-4012, Geo. C. Marshall Space Flight Center, Final rept. March 15, 1963.

6. Anon. (North American Aviation, Rocketdyne Div.) Rocket engine valve poppet and seat design data. Rept. RPL-TDR-64-68, May 1964.

7. Anon. (North American Aviation, Rocketdyne Div.) Analytical design data on rocket propulsion system seats and poppets. AF04(611)-9712, Contract status rept. 64RC17154, Sept. 18, 1964.

8. Anon. (North American Aviation Rocketdyne Div.) Analytical design data on rocket propulsion system seats and poppets. AF04(611)-9712, Contract status rept. 64RC13616, Aug. 17, 1964.

9. Anon. (General Electric) Design criteria for zero-leakage connectors for launch vehicles. NAS 8-4012, Geo. C. Marshall Space Flight Center, Quarterly rept. 3, Jan. 1963.

10. Anon. (General Electric) Design criteria for zero-leakage connectors for launch vehicles. NAS 8-4012, Geo. C. Marshall Space Flight Center, Quarterly rept. 4, June 15, 1963.

11. Anon. (North American Aviation, Rocketdyne Div.) Analytical design data on rocket propulsion system seats and poppets. AF04(611)-9712, Contract status rept. 64RC15455, Sept. 18, 1964.

12. Anon. (General Electric) Design criteria for zero-leakage connectors for launch vehicles. NAS 8-4012, Geo. C. Marshall Space Flight Center, Quarterly rept. 7, July 1964.

13. Anon. (General Electric) Design criteria for zero-leakage connectors for launch vehicles. NAS 8-4012, Geo. C. Marshall Space Flight Center, Quarterly rept. 8, Oct. 1964.

14. Tabor, D. The Hardness of Metals. Oxford Univ. Press, Oxford, Eng., 1951.

15. Dieter, G.E., Jr. Mechanical Metallurgy. McGraw-Hill Book Co., Inc., New York, 1961.

REFERENCES (contd)

16. Anon. (TRW Systems) Advanced valve technology for spacecraft engines. NAS 7-107, Final rept. 8651-6042-SU000, Aug. 1965.

17. Anon. (Shore Instrument and Mfg. Co., Inc.) Bulletin Catalog R-12, Jamaica, N.Y.

18. Finken, E. Surface roughness in wear. Wear 6, 293-302, 1963.

19. Rabinowicz, E. Friction and Wear of Materials. John Wiley and Sons, Inc., 1965.

20. Rathbun, F.O. (Advanced Technology Lab., Schenectady, N.Y.) Design criteria for leakage connections for launch vehicles. General Electric rept. 64GL202, Dec. 1, 1964.

21. Nelson, R.B. Rev. Sci. Instr. 16, p. 55, 1945.

22. Marr, J.W. (Advanced Technology Lab., Schenectady, N.Y.) Leakage measurement and evaluation. General Electric rept. 64GL163, Oct. 12, 1964.

23. Marr, J.W. (Advanced Technology Lab., Schenectady, N.Y.) Leak detection and measurement. General Electric rept. 65GL28, Feb. 1, 1965.

24. Norton, F.J. Permeation of gases through solids. J. Appl. Phys. 28, 1957.

25. Dushman, S. and Lafferty, J.M. Scientific Foundation of Vacuum Technique. (2nd edn.) John Wiley and Sons, Inc., 1962.

26. Reid and Sherwood Properties of Gases and Liquids. McGraw-Hill Book Co., Inc., 1958.

27. Loeb, L.B. Kinetic Theory of Gases. McGraw-Hill Book Co., Inc., 1934.

28. Kennard, E.H. Kinetic Theory of Gases with an Introduction to Statistical Mechanics. McGraw-Hill Book Co., Inc., 1938.

29. Espe, W. Werkstoffkunde der Hockvakuumtechnik. Deutcher Verlag der Wissenschaften, 1959.

30. Pao, R.H. Fluid Mechanics. John Wiley and Sons, Inc., 1961.

31. Hunsaker, J. and Rightmise, B. Engineering Applications of Fluid Mechanics. McGraw-Hill Book Co., Inc., 1947.

X-A APPENDIX

AND

X-B APPENDIX

X-A APPENDIX

Theoretical Leakage Considerations

In vacuum technology, a hole or porosity in the wall of an enclosure capable of passing gas from one side of the wall to the other under a pressure or concentration differential is defined as a leak path. A leak path is not usually indicated by certain dimensions but is hypothetically characterized as a physical hole of a certain length and width. However, since a leak path is not intentionally formed into an item, its dimensions are generally unknown. In leak detection, the dimension used to describe the leak is the leak rate. While this de facto information is beneficial, it is not suitable for use by the systems designer. To predict leakage, the designer must have criteria to establish the characteristic geometry of the leak paths and a knowledge of the influencing factors governing the transport of fluid. To proceed in the presentation of design criteria, the transport of fluid is considered first with respect to the flow of fluid in very small passages or channels. Some of the theoretical concepts presented have serious limitations and are used solely for comparison. The limitations are due to the assumptions made in obtaining solutions. Unfortunately, more encompassing assumptions quite often make the problem unsolvable. The assumptions made in arriving at solutions for leakage flow are presented for hypothetical flow models consisting of geometrically defined small channels. The assumptions are sufficiently valid for certain conditions of flow; however, the regime of flow is not easily defined mathematically on the basis of experimental results. An example of this inadequacy is the case of laminar-to-molecular flow transition. Experiments show that the flow may be laminar while theoretical analysis indicates molecular flow. Guide lines for estimating the flow regime are presented in this Part. The major difficulty in defining flow regions is attributed to the irregular and undefinable leakage path inherent in most seals whereas the theoretical solutions are based on well defined channels.

Modes of Leakage Flow

The leakage of fluid occurs by a variety of flow mechanisms: permeation, molecular flow, laminar flow, transition flow, turbulent flow and choked flow. These, as well as the circumstances leading to this flow, will be described in this Part. Before proceeding, however, it is necessary to define the term leakage rate since it is often expressed in a multiplicity of units. Consequently, conversion constants often must be used to convert volume rates of leakage flow to other units of measurement because of the widespread use of virtually all dimensional units. In vacuum technology and other scientific areas, gas leakage is commonly expressed in pressure, volume, and time. The most commonly used unit, the micron-liter per second, represents the basic factors. The micron-liter is the mass of fluid that would occupy one liter at a pressure of one micron (10^{-3} mm Hg). The relationship between weight and volume flow is:

$$W \propto \frac{m}{R} \frac{PV}{\Delta t} \Bigg|_{T = \text{constant}} \tag{23}$$

$$Q \propto \frac{1}{\Delta t} \frac{R}{m} V \Bigg|_{T = \text{constant}} \tag{24}$$

where

W = Weight rate of flow
Q = Volume rate of flow
V = Volume
P = Pressure
Δt = Time increment
R = Universal gas constant
m = Molecular weight
T = Temperature

Thus, the micron-liter flow rate may be readily converted to mass flow rate if the gas properties and temperature are known. Unless otherwise stated, volume rates of leakage are usually specified at $0^{\circ}C$.

Another commonly used unit is cubic centimeters per second. This unit is usually specified at standard conditions and is denoted as STP cc/sec. In the sciences, standard atmosphere is 760 mm Hg at $0^{\circ}C$. In engineering practice, it is 760 mm Hg at $20^{\circ}C$ ($68^{\circ}F$). In engineering, units of cubic inches per second and cubic inches per minute are commonly used for small flow rate measurements. For large flow rates, cubic feet per minute is the unit employed. Long-term leakage, such as that occurring from a fuel tank on a space vehicle, is commonly expressed in terms of cubic centimeters per month or cubic centimeters per year. Tables X-A-1 and X-A-2 contain conversion factors relating the various units.

Continuing with the development of a description for flow in small channels, some generalizations must be considered. When a fluid flows steadily past a stationary wall, the particles next to the wall adhere to it, and there is in the fluid a velocity gradient normal to the direction of flow. The force exerted by the boundary on the fluid depends upon the velocity gradient at the boundary and the viscosity of the fluid. For Reynolds Numbers less than 2000,

$$N_{Re} = \frac{\bar{u}h\rho}{\eta} \tag{25}$$

the flow is defined as laminar or viscous flow. The shear stress is defined as

$$\tau = \eta \frac{du}{dy} \tag{26}$$

For $N_{Re} > 2000$, the flow may consist of random motions superimposed on the average velocity of the stream. The streamlines no longer exist and, under these conditions, the relationship between shear stress and velocity gradient is very complex. No exact theories are available to describe this flow region. However, considerable empirical information is available which permits close approximation of the flow.

The shear stress is given as:

$$\tau = f\left(\frac{\bar{u}^2}{2}\right) \tag{27}$$

where f is a friction coefficient. The friction coefficient is a function of the Reynolds Number, wall roughness, and distance from the pipe inlet. In both laminar and turbulent flow, collisions between molecules occur more frequently than collisions of molecules with the channel wall. The coefficient of viscosity reflects the influence of intermolecular interactions. When the pressure of a fluid is sufficiently reduced, the mean free path of the molecule, λ, becomes large compared to a characteristic dimension h of the channel. When the fluid molecules collide more often with the wall than with each other, the flow is called free-molecular flow.

Free molecular flow occurs when λ/h is approximately 1.00. The dimensionless ratio λ/h is called the Knudsen number. The transition of flow between laminar and molecular flow is called transition flow. Other flow concepts are also presented in the ensuing discussion based on frictionless conditions. In many cases the flow can be adequately described using frictionless and other assumptions. However, applicability depends upon complex factors and is discussed in other sections of the report. A summary of the flow regimes and their identification is shown below:

$\frac{\lambda}{\alpha} < 0.01$	Laminar flow
$\frac{\lambda}{d} > 1.00$	Molecular flow
$0.01 < \frac{\lambda}{d} < 1.00$	Transition flow
$N_{Re} < 2000$	Turbulent flow
$N_{Re} < 1200$	Laminar flow
$1200 < N_{Re} < 2000$	Mixed flow

Table X-A-1

LEAKAGE CONVERSIONS

Unit / Equiv.	1 STD cc/sec	1 STD cu ft/yr	1 STD cu in/min	1 STD cu ft/min	1 STD cu ft/hr	1 STD cc/min	1 STD cc/hr	1 $\frac{\mu \text{ liter}}{\text{hr}}$	1 $\frac{\mu \text{ ft}}{\text{hr}}$
Std cc/sec	1	1.112×10^{3}	3.61	2.117×10^{-3}	1.27×10^{-1}	60	3.60×10^{3}	2.736×10^{6}	9.66×10^{4}
Std cu ft/yr	8.99×10^{-4}	1	3.29×10^{-3}	1.90×10^{-6}	1.14×10^{-4}	5.39×10^{-2}	3.24	2.56×10^{3}	86.8
Std cu in/min	2.77×10^{-1}	3.04×10^{2}	1	5.79×10^{-4}	3.474×10^{-2}	16.4	9.84×10^{2}	7.58×10^{5}	2.68×10^{4}
Std cu ft/min	4.72×10^{2}	5.26×10^{5}	1.73×10^{5}	1	60	2.83×10^{4}	1.7×10^{6}	1.29×10^{9}	4.56×10^{7}
Std cu ft/hr	7.87	8.77×10^{5}	2.88×10^{3}	1.67×10^{2}	1	4.72×10^{2}	2.83×10^{4}	2.15×10^{7}	7.6×10^{5}
Std cc/min	1.67×10^{-2}	1.86×10^{3}	6.1×10^{-2}	3.53×10^{-5}	2.12×10^{-3}	1	60	4.57×10^{4}	1.61×10^{3}
Std cc/hr	2.78×10^{-4}	3.09×10^{-1}	1.02×10^{-3}	5.88×10^{-7}	3.53×10^{-5}	1.67×10^{2}	1	7.61×10^{2}	26.85
$\frac{\mu\text{-liter}}{\text{hr}}$	3.65×10^{-6}	3.91×10^{-4}	1.32×10^{-6}	7.75×10^{-10}	4.65×10^{-8}	2.19×10^{5}	1.31×10^{-3}	1	3.53×10^{-2}
$\frac{\mu\text{-cu ft}}{\text{hr}}$	1.63×10^{-5}	1.15×10^{-2}	3.73×10^{-5}	2.19×10^{-8}	1.32×10^{-6}	6.21×10^{-4}	3.72×10^{-2}	28.33	1

Table X-A-2

TIME CONVERSION TABLE

Unit / Equiv.	1 Second	1 Minute	1 Hour	1 Day	1 Week	1 Month	1 Year
Seconds	1	60	3.6×10^{3}	8.6×10^{4}	6.1×10^{5}	2.6×10^{6}	3.1×10^{7}
Minutes	1.7×10^{-2}	1	60	1.4×10^{3}	1.0×10^{4}	4.3×10^{4}	5.2×10^{5}
Hours	2.8×10^{-4}	1.7×10^{-2}	1	24	1.7×10^{2}	7.2×10^{2}	8.8×10^{3}
Days	1.2×10^{-5}	6.9×10^{-4}	4.2×10^{-2}	1	7	30	3.7×10^{2}
Weeks	1.6×10^{-6}	9.8×10^{-5}	5.9×10^{-3}	0.14	1	4.3	52
Months	3.8×10^{-7}	2.3×10^{-5}	1.4×10^{-3}	3.3×10^{-2}	0.23	1	12
Years	3.2×10^{-8}	1.9×10^{-6}	1.1×10^{-4}	2.8×10^{-3}	1.9×10^{-2}	0.83	1

Permeation Flow

Transport of gases through a solid wall separating regions of higher and lower gas pressure can occur by means of two mechanisms:

(1) A series of voids in the solid may form capillary passages through which the gas may flow. This condition is commonly called porosity and may extend from the macroscopic to the microscopic field of view. Further discussion on this mechanism of flow is presented under the topics of molecular, transition and laminar flow.

(2) Transport may occur by molecular adsorption and solution on the outer wall surface layer, molecular or atomic diffusion through the interior, and dissolution and desorbtion on the inner wall.

The general formulas for diffusion flow given in References 24 and 25 are:

Molecular Diffusion:

$$Q = KDA \frac{(P_2 - P_1)}{L} \tag{28}$$

Atomic Diffusion:

$$Q \propto \sqrt{P_2} - \sqrt{P_1} \text{ or for } P_1 - 0_{abs} \tag{29}$$

$$Q = Q_e \frac{P_2}{P_e}$$

where

A = area of leakage
D = diffusion coefficient
K = solubility
L = thickness of the wall
P_1 = exit pressure
P_2 = inlet pressure
P_e = experimental pressure difference usually P_o (atmospheric)
Q = volume rate of flow at any pressure difference $(P_2 - P_1)$
Q_e = flow rate at pressure P_e, determined by experiment

The general rules in applying the formulas for various materials are outlined in Table X-A-3.

Table X-A-3

SUMMARY OF THE NATURE OF GAS PERMEATION

METALS
(1) None of the rare gases will permeate any metal.
(2) Hydrogen permeates most metals, especially iron.
(3) Oxygen permeates silver.
(4) Hydrogen through iron by corrosion electrolysis.
(5) Flow rates vary as $\sqrt{P}$ (Atomic Diffusion).
(6) Very small halogen gas leakage through metal.
POLYMERS
(1) All gases permeate all polymers.
(2) Water leak rate apt to be high.
(3) All rates vary as pressure (Molecular Diffusion).
(4) Permeation rate varies exponentially with temperature.

A permeation rate Z may be defined as a conductance factor for molecular and atomic diffusion. The permeation rate is an experimentally determined value and often expressed in the units.

$$Z = \frac{cm^3\text{-}mm}{sec\text{-}cm^2\text{-}torr} \tag{30}$$

For molecular diffusion:

$$Q = \frac{Z\,A\,(P_2 - P_1)}{L} \tag{31}$$

For atomic diffusion:

$$Q = Q_e \sqrt{\frac{P_2}{P_e}} \tag{32}$$

where

$$Q_e = \frac{ZA(P_e)}{L} \tag{33}$$

Thus,

$$Q = \frac{ZA(P_e)}{L}\sqrt{\frac{P_2}{P_e}} \tag{34}$$

In these formulas, the units of measurement must be:

P in torr = 10^{-6} mm Hg
A in cm^2
L in mm
Q in cm^3/sec

Permeation rate is converted into common engineering units using the factor,

$$\left(Z\right)\left(131.2\right) = \text{cc/sec x in/psi-in}^2$$

where the units of measurement may be given:

P in psia
A in in^2
L in in
Q in cm^3/sec

In general, very little permeation rate data are available for a variety of materials. Section XI contains permeation rates for selected materials.

To show the method of estimating molecular and atomic diffusion flow, the following examples are presented:

Molecular Diffusion

Given: A circular rubber ring seal with a rectangular cross section with the dimensions:

Outside diameter, D_o = 2.00 in

Inside diameter, D_i = 1.75 in

Thickness, t = 0.10 in

Helium is sealed at P_2 = 14.7 psi inside seal and P_1 = 0 psi external. Temperature is 68°F.

P_2 = 14.7 psi Helium sealed inside seal

P_1 = 0 psi external pressure

Calculate: Leakage rate in cubic centimeters per second. Since the material selected is an elastomer, the leakage mechanism is molecular. The diffusion rate is 8.6×10^{-10} cc-mm (STP)/sec-cm^2-torr. When the units are converted to engineering units

$$Z = 1.13 \times 10^{-7} \frac{cc}{sec} \quad \frac{in}{(psi)\ in^2}(STP) \tag{35}$$

The volume rate of flow may be calculated from the formula for molecular diffusion

$$Q = \frac{Z\ A\ (P_2 - P_1)}{L} \tag{36}$$

$$Q = \frac{1.13(10^{-7})(\pi D_o T)(P_2 - P_1)}{\frac{D_o - D_i}{2}}$$

$$Q = \frac{1.13(10^{-7})(\pi \times 2 \times 0.10)(14.7)}{0.125}$$

$$Q = 8.4 \times 10^{-6}\ cc/sec\ (STP)$$

Correction of permeation rate for other temperature conditions may be accomplished using the procedures described in Reference 25.

Atomic Diffusion

Given: Ring seal having the same dimensions as the rubber ring. Atomic diffusion describes the leakage process. Hydrogen is sealed at P_2 = 30 psia and P_1 = 14.7 psia.

The permeation rate for metals is usually given for a pressure difference across the material of close to 760 mm. The internal pressure is usually close to zero absolute. The leakage rate for this condition may be defined as an experimental rate Q_e.

$$Q_e = K\ A\ (P_e)/h \tag{37}$$

where P_e = 760 mm Hg.

The permeation rate for steel and hydrogen is given as

$$8 \times 10^{-13}\ \frac{cm^2\text{-}mm(STP)}{sec\text{-}cm^2\text{-}torr}$$

which when converted to engineering units becomes

$$1 \times 10^{-10}\ \frac{cm^3}{sec}\ \frac{in}{in^2}\ \frac{1}{psi}\ (STP)$$

Calculate: Leakage rate Q_e when P_e = 14.7 psia.

$$Q_e = \frac{1 \times 10^{-10}\ (\pi D_o t)(P_e)}{\frac{D_o - D_i}{2}}$$

$$Q_e = \frac{1 \times (10^{-10})\ \pi \times 2 \times 0.10 \times 14.7}{0.125}$$

$$Q_e = 7.4 \times 10^{-8}\ cc/sec\ (STP)(at\ 1\ atm)$$

The atomic diffusion flow rate when P_2 = 30 psia is

$$Q = Q_e \sqrt{\frac{P_2}{P_e}} \tag{38}$$

$$= 7.4 \times 10^{-8} \sqrt{\frac{30}{14.7}}$$

$$Q = 1 \times 10^{-7} \text{ cc/sec}$$

Molecular Flow Through Long Channels

When the clearance space becomes extremely small, assumptions based on: (1) no slip at the wall, and (2) intermolecular collisions solely within the fluid can no longer be applied in a flow analysis. When the clearance space is in the same order of magnitude as the molecular free path, considerations must be given to the collision of molecules with the wall. The method of attacking the problem was first introduced by Knudsen and employs analysis based on the kinetic theory of gases. For a long tube, the fundamental deduced by Knudsen[25] is

$$W = \frac{4}{3}\frac{\gamma}{P} \frac{\nu a}{\int_0^L \frac{H}{A_p^2}\, dl} (P_2 - P_1) \tag{39}$$

where

A_p = cross section of channel

H = perimeter of channel

L = channel length

m = molecular weight of gas

W = weight rate of flow

ν_a = mean molecular speed $= \sqrt{\frac{8\,R\,T}{\pi\, m}}$

γ = specific weight $= \frac{Pm}{RT}$

From the kinetic theory of gases, the mean molecular free path is:

$$\lambda \approx \frac{1}{0.31}\sqrt{\frac{\pi}{8}}\ \frac{\eta}{P}\sqrt{\frac{RT}{m}} \tag{40}$$

Substituting this equation into the leakage equation we obtain:

$$W = \frac{1.064\ \bar{\lambda}\ \bar{P}\ (P_2 - P_1)}{\eta} \tag{41}$$

where $\bar{\lambda}$ is defined as the mean free path at a mean pressure $\bar{P} = \frac{P_2 + P_1}{2}$

For a rectangular channel having width w and height h:

$$H = 2(w + h) \quad \text{and} \quad A_p = hw \tag{42 \& 43}$$

The weight rate of flow is:

$$W = \frac{0.532\ \bar{\lambda}\ (P_2^{\ 2} - P_1^{\ 2})\ w\ h^2}{R/m\ T\eta L} \tag{44}$$

To utilize the preceding formula, the properties of fluids and equations of state must be known. On the basis of the kinetic theory of gases, a relationship is established between viscosity of molecular properties. The general form of this relationship[26,27,28] may be written:

$$\eta = B\ \nu_a\ \lambda \tag{45}$$

where

B = constant

ν_a = average molecular velocity

λ = molecular free path

η = viscosity

Equation (45) and the ensuing discussion stipulates that the product $\gamma\lambda$ is constant and independent of pressure for a constant temperature.

The molecular mean free path is given:

$$\lambda = \frac{\text{constant}}{\gamma} \tag{46}$$

Applying the ideal gas equation of state it follows that:

$$P/P_1 = \gamma/\gamma_1 = \lambda_1/\lambda \quad \text{for } T = \text{constant} \tag{47}$$

and

$$\lambda = \frac{\lambda_1 \gamma_1}{\gamma} \tag{48}$$

where

λ = mean free path at pressure P

λ_1 = mean free path at pressure P_1

Equation (48) may be used to calculate the mean free path for any pressure condition if the mean free path is known at some pressure condition. Table X-A-4 shows mean free path values for typical gas. Additional information may be obtained from Reference 29.

Table X-A-4

MEAN FREE PATHS AND MOLECULAR DIAMETERS FOR VARIOUS MOLECULES

MOLECULE	MEAN FREE PATH cm x 10^{-3} at 1 Torr and 25°C	MOLECULAR DIAMETER
H_2	9.31	2.75
He	14.72	2.18
Ne	10.45	2.60
A	5.31	3.67
O_2	5.40	3.64
CO_2	3.34	4.65
H_2O	3.37	4.68
benzene	1.34	7.65
methane	4.15	4.19
ethane	2.53	5.37
propane	1.82	6.32
n-butane	1.46	7.06
n-pentane	1.19	7.82
n-hexane	1.03	8.42

Theoretical Equations for Laminar, Incompressible Flow in a Uniform Channel (Liquid Flow)

The solution to the case of laminar incompressible flow in a uniform channel can be reviewed in detail in References 30 and 31. The solution is given:

$$W = \frac{\gamma w h^3 (P_2 - P_1)}{12 \eta L} \tag{49}$$

where

h = channel height
L = length
P_1 = exit pressure
P_2 = inlet pressure
w = channel width

In many seal applications, the leakage channel is not uniform with respect to width and length. This channel is described by two circular plates with radial flow predominating between the plates. The weight rate of flow between circular plates is given:

$$W = \frac{\gamma h^3 (P_2 - P_1)}{6 \eta \ell n \, r_i / r_2} \tag{50}$$

where r_1 = inside radius of the plate
r_2 = outside radius of the plate

In these equations, the viscosity and density are indicated as being an invariable property of the fluid. Actually density and viscosity are influenced by temperature and pressure.

Simplifying the Geometrical Aspects of Laminar Flow Between Circular Plates

The volume rate of flow between two circular plates can be accomplished by assuming that the geometry of the plate is represented by a uniform channel of width w and length L.

The rate of flow may be written:

$$W = \frac{\gamma h^3}{12} (P_2 - P_1) \pi \frac{(r_2 + r_1)}{(r_2 - r_1)} \tag{51}$$

for ratios of $\frac{r_2}{r_1}$ up to 1.7 without incurring an error greater than 2%.

Theoretical Leakage Equations for Compressible Flow in a Uniform Channel

To determine the appropriate equation describing leakage flow in a seal analysis, it is necessary to compare the assumptions made in the analysis and typical calculated results. In the following three cases of one-dimensional flow, a small uniform channel is assumed having the geometry:

h = channel height

L = length

w = width

Case I - Isothermal Laminar Flow

Infinite heat transfer is assumed.

$$W = \frac{wh^3}{24R_o T \eta L} (P_2^2 - P_1^2) \tag{52}$$

Case II - Isothermal Laminar Flow with Inertia

Infinite heat transfer is assumed. An approximation for laminar flow is included in the analysis to obtain a solution when inertia in c is considered.

$$\frac{2W^2 h}{gw} \ln \frac{P_1}{P_2} = - \frac{wh^3}{R_o T} (P_2^2 - P_1^2) + 24W \eta L \tag{53}$$

Case III - Adiabatic Frictionless Flow

No heat transfer is assumed.

$$W = wh \frac{\sqrt{2kg}}{R_o (k-1)} \frac{P_2}{T_2} \left(\frac{P_1}{P_2}\right)^{1/k} \sqrt{1 - \left(\frac{P_1}{P_2}\right)^{k-1/k}} \tag{54}$$

where k = ratio of specific heat c_p/c_v.

If the ratio of P_1/P_2 is less than the critical pressure ratio of 0.532 then the weight rate of flow is choked and given:

$$W = wh \left[\frac{2}{k+1}\right]^{k/k-1} \sqrt{\frac{2gk}{R_o(k+1)}} \quad \frac{P_2}{\sqrt{T_2}} \tag{55}$$

We shall <u>illustrate</u> the results obtained in each of the three cases using the following information.

Air at 68°F is leaking through a seal interface from a reservoir at two assumed pressures P_2 = 100 psig and 5000 psig

g = 386 in/sec^2

h = 10^{-2}, 10^{-4}, and 10^{-6} in. (Equivalent Channel Clearance)

k = 1.4

L = 1 in.

η = 2.6×10^{-9} lbF - sec/in.^{2}

P_1 = 14.7 psia

R_o = 640 in./°R

w = 1 in.

λ_o = 2.64×10^{-6} in.

The results obtained in each case are shown in Table X-A-5.

Table X-A-5

COMPARISON OF LEAKAGE RATES

	CLEARANCE, h, (in.)		
	1×10^{-2}	1×10^{-4}	1×10^{-6}
LEAKAGE RATE AT P_2 = 100 psi (lb/sec)			
Case I	4.7×10^{-1}	4.7×10^{-7}	4.7×10^{-13}
Case II	1.6×10^{-2}	4.7×10^{-7}	4.7×10^{-13}
Case III	2.7×10^{-2}	2.7×10^{-4}	2.7×10^{-6}
LEAKAGE RATE AT P_2 = 5000 psi (lb/sec)			
Case I	1.2×10^{3}	1.2×10^{-3}	1.2×10^{-9}
Case II	1.6×10^{-1}	1.4×10^{-4}	1.4×10^{-10}
Case III	1.2	1.2×10^{-2}	1.2×10^{-4}

These examples show that:

(1) The flow equations of Cases I and III are not applicable at P_2 = 100 psi and 5000 psi for h = 1 x 10^{-2} in. Case I cannot be applied because the equations predict a Mach number greater than one in the channel. Case III considers only frictionless, adiabatic flow. Case II considers fluid friction and inertial effects and appears to be the most applicable expression for flow under these conditions.

(2) For h = 1 x 10^{-4} and 1 x 10^{-6} inch at P_2 = 100 psi, Case I and II yield identical results and appear to describe the flow in this region. The flow equation of Case I is suggested for calculations in this region.

(3) When the inlet pressure is substantial, P_2 = 5000 psi, the inertia effects are significant. The flow equation for Case II considers viscous and inertia effects and, thus, produces the lowest flow rate calculation.

Before any definite conclusions may be made on the selection of the appropriate flow equation, other factors must be considered. The most important additional factor is the effects of turbulance and wall roughness. Since the Reynolds number N_{Re} is an indication of the flow regime, it is necessary to make further calculations. The Reynolds number is defined:

$$N_{Re} = \frac{u\,D\,\rho}{\eta} \tag{56}$$

where D = Hydraulic radius = $\frac{4\,w\,h}{2(w + h)}$

or

$$N_{Re} = \frac{2\,u\,h\,\rho}{\eta} \tag{57}$$

Since the adiabatic flow equation, Case III, is a conservative and limiting approximation describing the flow, it is used in the calculation of the Reynolds number. The preceding numerical information is used to obtain the results shown in Table X-A-6.

Table X-A-6

COMPARISON OF LEAKAGE FLOW AND REYNOLDS NUMBER FOR
ADIABATIC, FRICTIONLESS FLOW (CASE III)
Exit Mach Number: 1

CLEARANCE, h, (in.)						
	1×10^{-2}		1×10^{-4}		1×10^{-6}	
P_2 (psi)	W (lb/sec)	N_{Re}	W (lb/sec)	N_{Re}	W (lb/sec)	N_{Re}
100	2.7×10^{-2}	4.6×10^{-4}	2.7×10^{-4}	4.6×10^{2}	2.7×10^{-6}	4.6
500	1.1×10^{-1}	2.3×10^{5}	1.1×10^{-3}	2.3×10^{3}	1.1×10^{-5}	23.0
1000	2.4×10^{-1}	4.6×10^{5}	2.4×10^{-3}	4.6×10^{3}	2.4×10^{-5}	46.0
3000	7.0×10^{-1}	1.4×10^{6}	7.0×10^{-3}	1.4×10^{4}	7.0×10^{5}	1.4×10^{2}
5000	1.2	2.3×10^{6}	1.2×10^{-2}	2.3×10^{4}	1.2×10^{-4}	2.3×10^{2}

These examples show that the Reynolds number is large for clearances greater than 1×10^{-5} inch and pressures up to 5000 psi. If the flow rate values for Cases I and II in Table X-A-5 are compared with those shown in Table X-A-6, it may be concluded that the Reynolds number is less than 2000 for clearances less than 1×10^{-4} inch and pressures up to 5000 psi. The preceding discussion is based upon air as a fluid medium. Since the properties of most gases do not vary to a great extent, the preceding conclusions may be acceptable for other gases. In summary, the final choice of a flow equation requires sample calculations, past experience and experimental correlation if available for equation applicability.

Transition Flow

For a description of the flow in the transition range between laminar and molecular flow, an empirical relationship has been established:

$$W = W_{laminar} + \epsilon W_{molecular}$$

where $\epsilon = 0.9$ for a single gas and $\epsilon = 0.66$ for a mixture. It is dependent upon the gas properties and clearance dimension. When the free molecular and viscous flow equations for flow in a uniform channel are combined, the transition flow rate may be defined,

$$W = \frac{w\, h^3\, (P_2^{\,2} - P_1^{\,2})}{24\, R_o T\, L} \left(1 + 6.38\, \epsilon\, \frac{\lambda}{h} \right) \tag{58}$$

A comparison of molecular and laminar flow shows that:

$$\frac{W_{free\ molecular}}{W_{laminar}} = 6.38\, \frac{\bar{\lambda}}{h} \tag{59}$$

where $\bar{\lambda}/h$ is defined as a dimensionless parameter called the Knudsen number. More generally defined, the Knudsen number is the ratio of the mean free path of a molecule to a characteristic dimension of a channel. When $\bar{\lambda}/h > 1$, the flow is assumed to be molecular. For a given flow passage size, pressure difference, fluid and temperature, it can be seen that for $\bar{\lambda}/h > 1$, the calculated free molecular flow rate is greater than the calculated laminar flow rate. Thus:

$$W_{molecular} > W_{laminar}$$

and, correspondingly, the resistance to flow under molecular flow conditions is less than the laminar flow.

Calculation of Leakage Using Nomographs

To Calculate Incompressible Laminar Leakage Flow in a circular interface having a uniform clearance Figure X-B-1, the nomograph shown in Figure X-B-2 may be used.

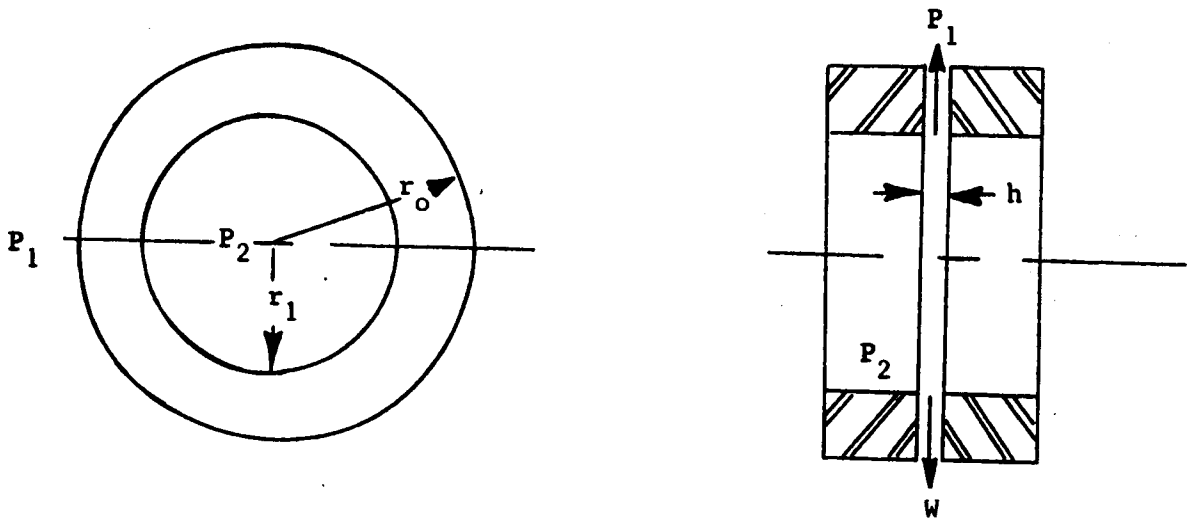

Figure X-B-I Radial Channel

The nomograph represents the flow equation

$$W = \frac{\pi \gamma h^3 \Delta P}{6 \mu \ln r_o/r_i} \tag{60}$$

Where W is the weight rate of flow in lb per sec, and

h = channel height (in.)

$\Delta P = (P_2 - P_1)$

P_1 = exit pressure (psi)

P_2 = inlet pressure (psi)

μ = viscosity(lb-sec/in.^{2})

γ = specific weight

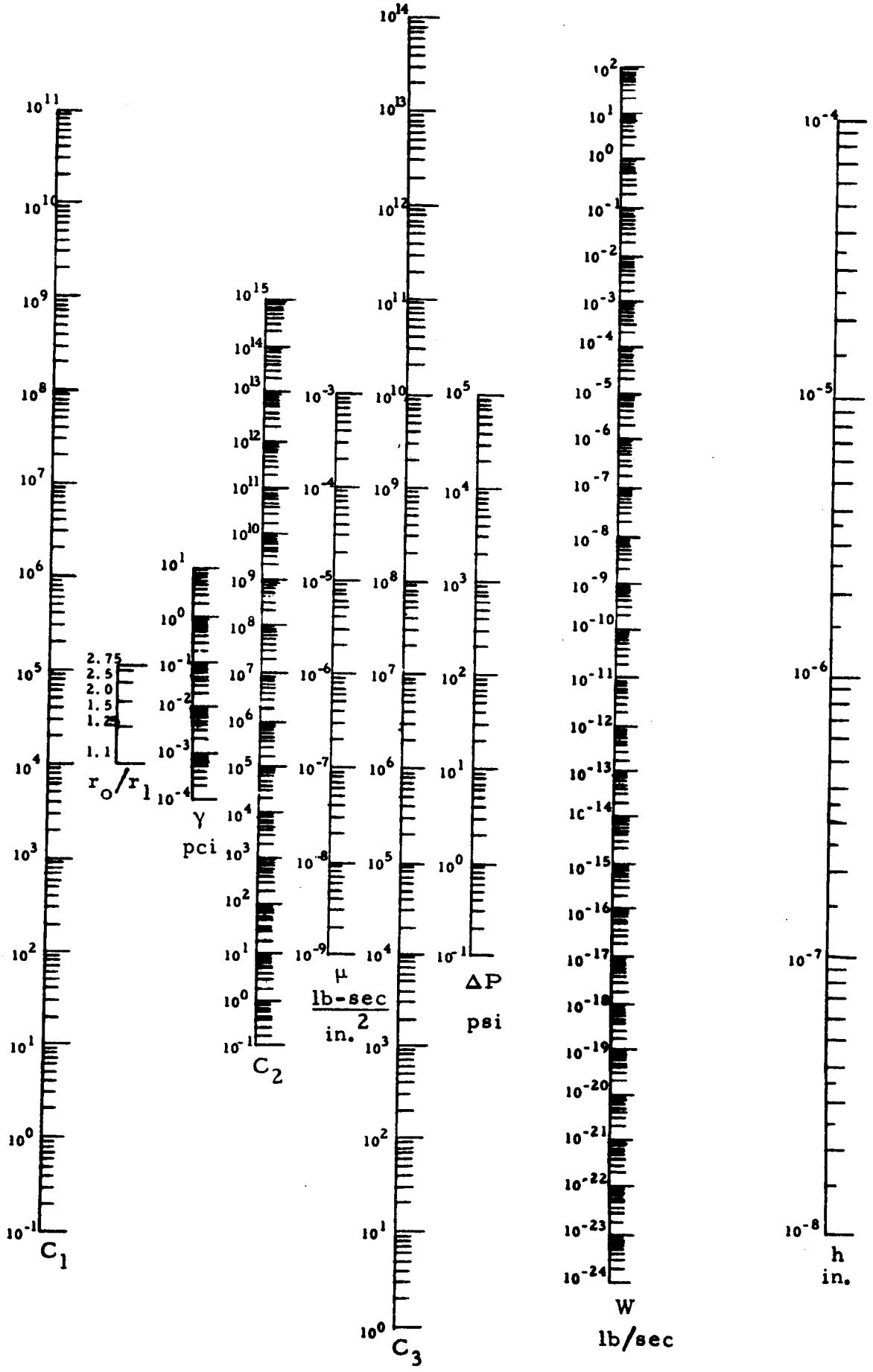

Fig. X-B-2 Nomograph for Incompressible Liquid Leakage

The chart is composed of nine scales. Six of the scales represent geometrical and environmental variables, three the ratios between the variables. The ratios are identified as the C_1, C_2, and C_3 scales and represent

$$C_1 \sim \gamma/\mu$$

$$C_2 \sim \Delta\rho C_1$$

$$C_3 \sim C_2/\ln r_o/r_i$$

$$C_3 \sim h^3/W$$

A step-by-step procedure is outlined below using Figure X-B-3 as an example.

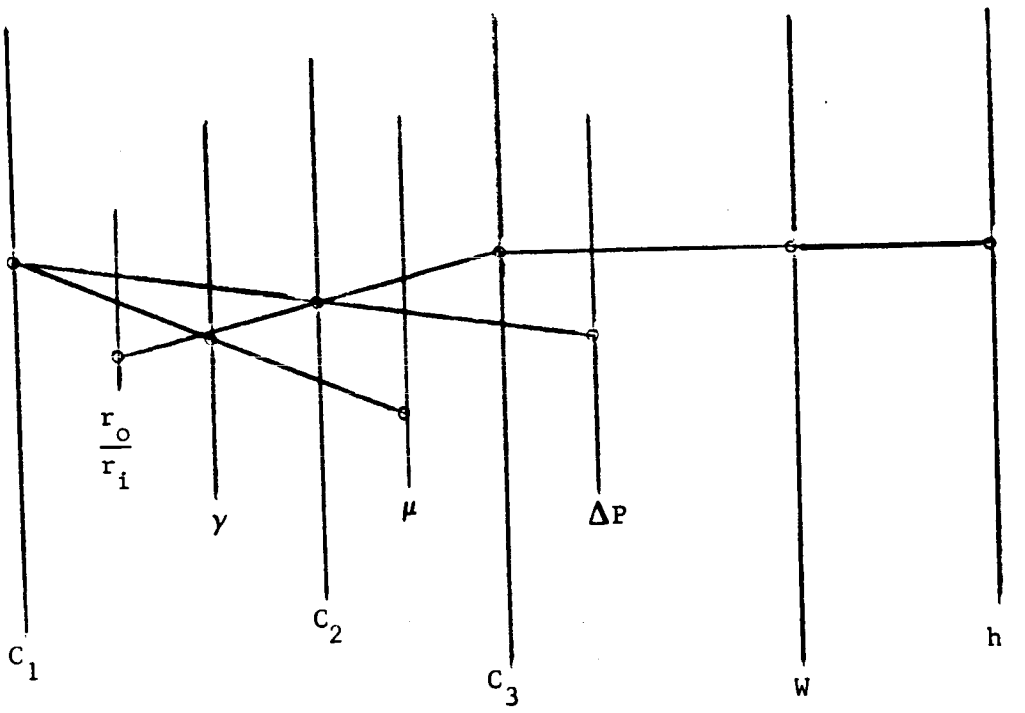

Figure X-B-3 Schematic Representation of Nomograph

Given: γ, μ, r_o/r_i, ΔP, and h

To find: W, weight rate of flow:

(1) Draw a line connecting γ and Δ and intersecting the C_1 scale.

(2) Connect the C_1 intersection point with the value of ΔP and observe the line intersection on the C_2 scale.

(3) Draw a line between the C_2 intersection and r_o/r_i. This line should be extended to intersect the C_3 scale.

(4) Connect the C_3 intersection point with the value of h clearance.

(5) Read the weight rate of flow on the W scale.

To Calculate Compressible Laminar Leakage Flow through the flow channel shown in Figure X-B-1.

$$W = \frac{\pi \gamma_o h^3 (P_2^2 - P_1^2)}{12\mu(\ln r_o/r_i)(P_o)} \tag{61}$$

where

γ_o = specific weight at pressure P_o. The nomograph (Figure X-B-4) represents this equation. The following procedure (shown in Figure X-B-5) is used to calculate the weight rate of flow:

(1) Draw a line connecting γ_o and μ and intersecting the C_1 scale.

(2) Connect the C_1 intersection point with the value of $(P_2^2 - P_1^2)/P_o$ and observe the line intersection on the C_2 scale.

(3) Draw a line between the C_2 intersection and r_o/r_i. This line should be extended to intersect the C_3 scale.

(4) Connect the C_3 intersection point with the value of h clearance.

(5) Read the weight rate of flow on the W_L scale.

To Calculate Compressible Laminar Transition Leakage Flow, the nomograph Figure X-B-6 and Figure X-B-7 must be employed. The transition flow equation may be represented:

$$W = \frac{\pi \gamma_o h^3 (P_2^2 - P_1^2)}{12\mu(\ln r_o/r_i)(P_o)} \left[1 + \frac{11.5\, P_o}{P_2 + P_1} \frac{\lambda_o}{h}\right] \tag{62}$$

where γ_o = specific weight at pressure P_o

λ_o = molecular mean free path at P_o

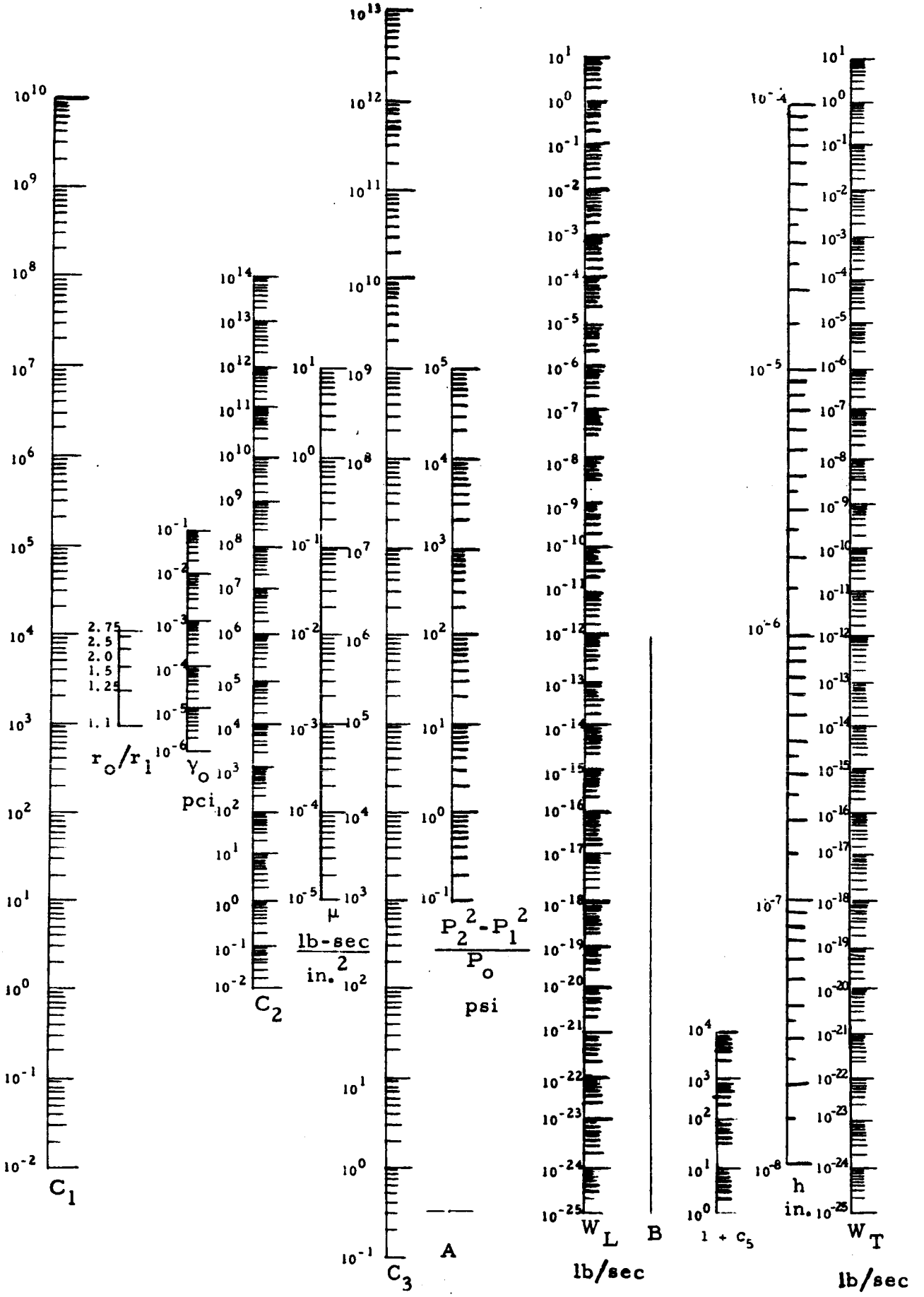

Fig. X-B-4 Nomograph for Gas Leakage

-526-

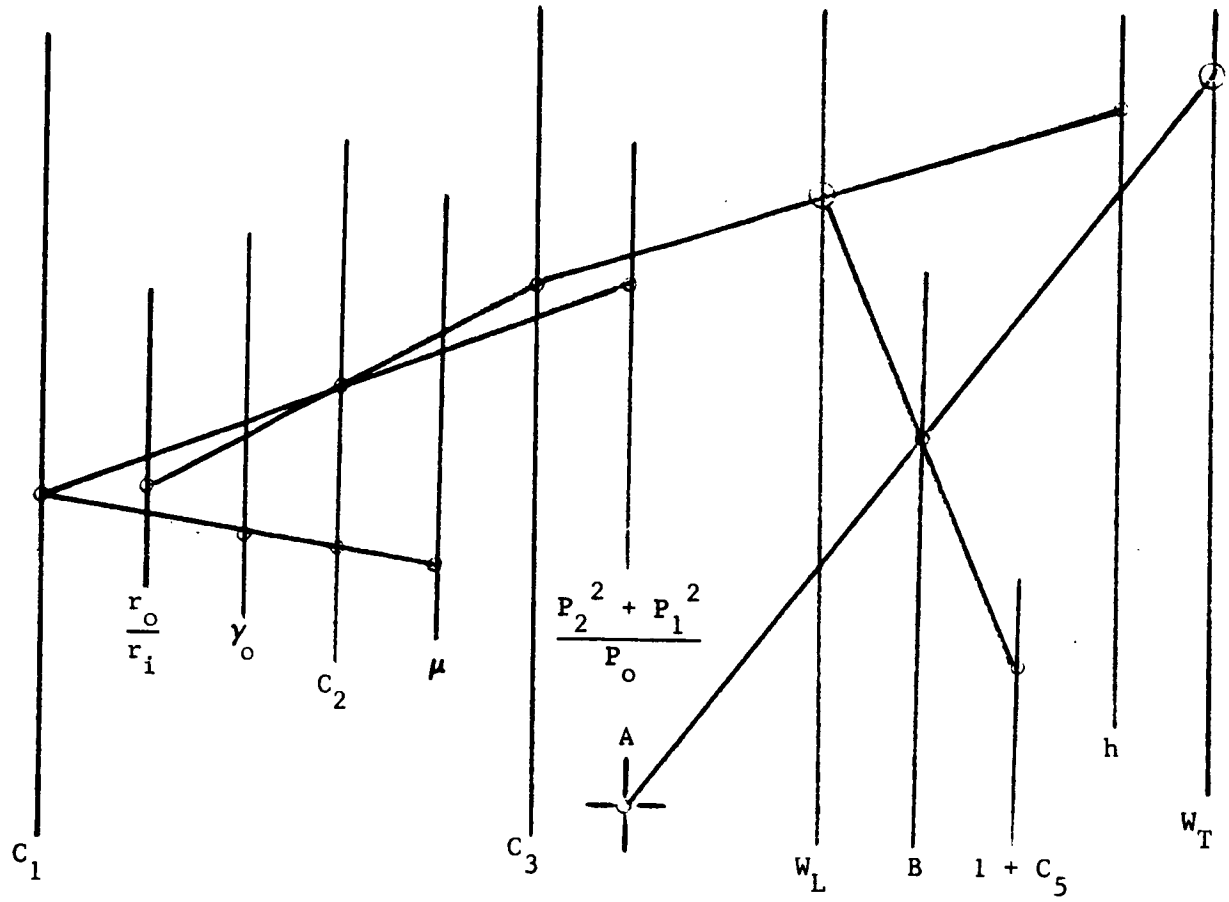

Figure X-B-5 Schematic Representation of Figure X-B-4

A step-by-step procedure is outlined using Figures X-B-5 and X-B-7:

(1) Draw a line connecting γ_o and intersecting the C_1 scale with μ.

(2) Connect the C_1 intersection point with the value of $P_2^2 - P_1^2/P_o$ and observe the line intersection on the C_2 scale.

(3) Draw a line between the C_2 intersection and r_o/r_i. This line should be extended to intersect the C_3 scale.

(4) Connect the C_3 intersection point with the value of h clearance.

(5) Read the weight rate of flow on the W_L scale.

(6) On Figure X-B-6 connect a line between points on the $P_2 + P_1$ and λ_o scale and observe the point of intersection on the C_4 scale as shown. This is illustrated in Figure X-B-7.

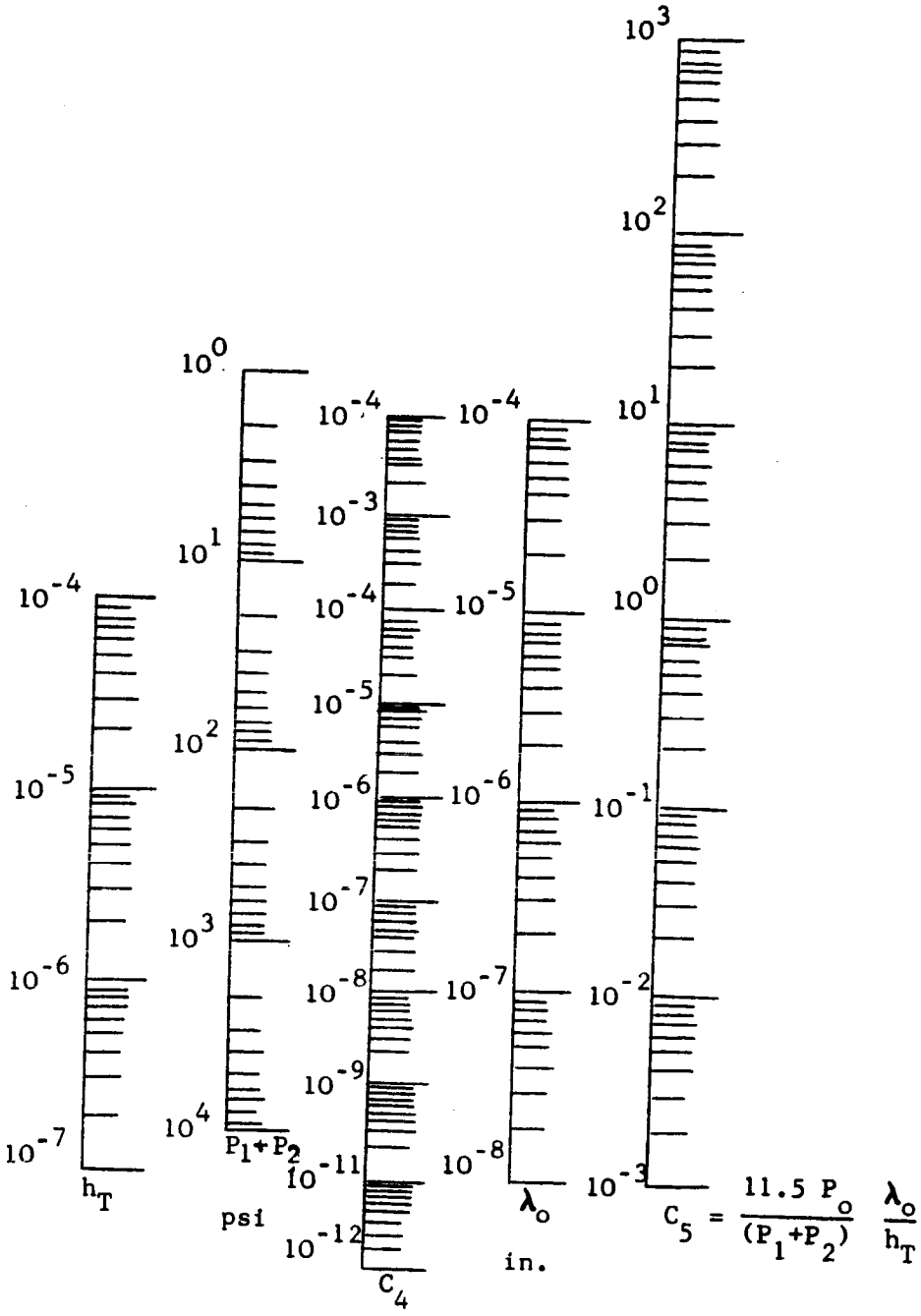

where P_o = 14.7 psia

Figure X-B-6 Nomograph for Calculation of $\left(1 + \frac{11.5\ P_o}{(P_1+P_2)} \frac{\lambda_o}{h_T}\right)$

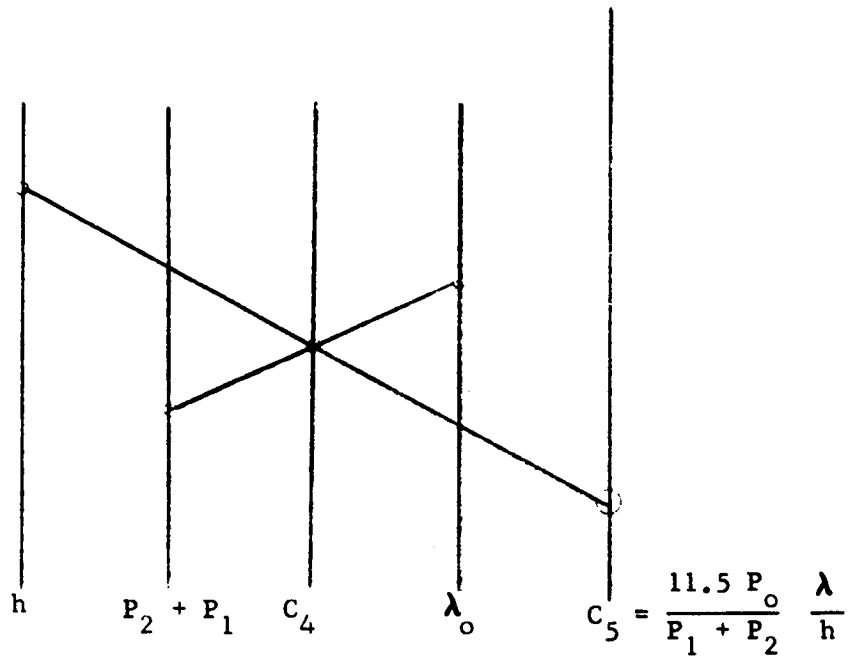

Figure X-B-7 Schematic Representation of Figure X-B-6

(7) Draw a line between the C_4 intersection and h, and intersecting C_5. Observe the value of C_5.

(8) Referring again to Figure X-B-6, place the observed value of C_5 on the corresponding scale, $1 + C_5$.

(9) Connect a line between the points on the W_L scale and $1 + C_5$ scale. Observe the point of intersection on the B scale.

(10) Connect the B scale intersection with a line drawn through point A intersecting the W_T scale.

(11) Read the value of transition leakage flow on the W_T scale.

XI FLUID SYSTEM COMPONENTS

Table of Contents

Section-Part	Title	Section-Part.Page
XI-0	List of Tables	XI-0.4
XI-0	List of Figures	XI-0.5
XI-1	Introduction	XI-1.1
XI-2	Valves - General	XI-2.1
	Introduction	XI-2.1
	Control Elements	XI-2.1
	Sealing Elements	XI-2.3
	Elastomeric Sealing Elements	XI-2.6
	Plastic Sealing Elements	XI-2.7
	Metallic Sealing Elements	XI-2.9
	Summary of Sealing Element Requirements	XI-2.10
	Fluid Forces Acting on the Control and Sealing Elements	XI-2.11
	Static Pressure Forces	XI-2.11
	Forces Due to Leakage at the Sealing Interface	XI-2.15
	Flow Induced Forces	XI-2.17
	Summary of Forces Acting on the Control Element	XI-2.21
	Sealing Element Leakage	XI-2.21
	Isentropic Flow	XI-2.23
	Turbulent Channel Flow	XI-2.24
	Laminar Flow	XI-2.25
	Transition and Molecular Flow	XI-2.26
	Interface Loads and Leakage	XI-2.27
XI-3	Factors Influencing Valve Design and Selection	XI-3.1
	Introduction	XI-3.1
	Fluid Effects	XI-3.1
	Pressure Drop and Flow Capacity	XI-3.2
	Poppet Stroke	XI-3.6
	Sealing and Control Element Configuration	XI-3.9
	Contamination	XI-3.12
	Actuation Methods	XI-3.17
	Solenoids	XI-3.17
	Response Time	XI-3.19
	Pressure Effects	XI-3.19
	Housing Construction	XI-3.20

Table of Contents (contd)

Section-Part	Title	Section-Part.Page
XI-4	Types of Valves	XI-4.1
	Start Valves	XI-4.1
	Fill and Vent Valves	XI-4.2
	Relief Valves	XI-4.6
	Direct Operated Relief Valves	XI-4.8
	Seat Load Sensitive Valves	XI-4.8
	Seat Load Non-sensitive Valves	XI-4.8
	Pilot Operated Relief Valves	XI-4.10
	Check Valve	XI-4.12
	Explosive Valves	XI-4.15
	Explosive Initiation	XI-4.16
	Typical Explosive Cartridge	XI-4.17
XI-5	Filters	XI-5.1
	Introduction	XI-5.1
	Woven Wire Mesh	XI-5.2
	Wound Wire Mesh	XI-5.2
	Sintered Wire Mesh	XI-5.2
	Dutch Weave Wire Mesh	XI-5.2
	Disc or Ribbon Edge Filter	XI-5.3
	Sintered Metal	XI-5.3
	Composite Sintered Metal and Wire Cloth	XI-5.3
	Etched Disc	XI-5.4
	Pressed Paper	XI-5.4
	Matted Fibers	XI-5.4
	Comparison Factors for Filters	XI-5.5
XI-6	General Purpose Seals	XI-6.1
	Introduction	XI-6.1
	Static Seals	XI-6.1
	Metallic Pressure-Energized Seals	XI-6.1
	Metallic Non-Pressure-Energized Seals	XI-6.3
	Combination Pressure-Energized Seals	XI-6.4
	Combination Non-Pressure-Energized Seals	XI-6.4
	Nonmetallic Pressure-Energized Seals	XI-6.6
	Nonmetallic Non-Pressure-Energized Seals	XI-6.7
	Sliding Seals	XI-6.8
	Rotating Shaft Seals	XI-6.9
XI-7	Seal Design and Selection Methods	XI-7.1
	Introduction	XI-7.1
	Seal Housing	XI-7.1
	Thermal Expansion	XI-7.9

Table of Contents (contd)

Section-Part	Title	Section-Part.Page
	Other Thermal Effects.....	XI-7.13
	Seal Structure.....	XI-7.14
	Application of Analytical Methods.....	XI-7.16
	Leakage Prediction.....	XI-7.21
	Summary of Seal Structural Requirements	XI-7.22
XI-8	Expulsion Devices.....	XI-8.1
	Introduction.....	XI-8.1
	Positive Expulsion Devices.....	XI-8.1
	Non-Positive Expulsion Devices.....	XI-8.4
XI-9	Fluid Connectors.....	XI-9.1
	Introduction.....	XI-9.1
	Separable Connectors.....	XI-9.1
	General Design and Selection Factors..	XI-9.3
	Threaded Connectors.....	XI-9.8
	Bolted Flange Connectors.....	XI-9.12
	Semi-Separable Connectors.....	XI-9.15
XI-10	References.....	XI-10.1

XI LIST OF TABLES

Section-Part-Table	Table	Section-Part.Page
XI-2-1	Comparative Ratings of Control Elements with Elastomeric Seals....	XI-2.7
XI-2-2	Comparative Ratings of Control Elements with Plastic Seals.....	XI-2.8
XI-3-1	Common Poppet Configurations.....	XI-3.10
XI-5-1	Mechanical Filter Comparison Chart.	XI-5.8
XI-7-1	Leakage Prediction of a Naflex Seal	XI-7.22

XI LIST OF FIGURES

Section-Part-Figure	Title	Section-Part.Page
XI-2-1	Typical Poppet Configurations.....	XI-2.2
XI-2-2	Schematic Sideview of an Eccentric Butterfly Valve.....	XI-2.2
XI-2-3	Blade Valve.....	XI-2.2
XI-2-4	Tappered Gate Valve.....	XI-2.2
XI-2-5	Poppet Valve with Elastomeric Seal Element Retained by a Special Seal Cavity.....	XI-2.7
XI-2-6	Anti-Extrusion Method for a Plastic Seal Poppet Valve.....	XI-2.9
XI-2-7	Four Configurations of a Solenoid Operated Poppet Valve.....	XI-2.13
XI-2-8	Effect of Pressure on Start Valve Bellows Unbalance.....	XI-2.14
XI-2-9	Pressure Profiles.....	XI-2.16
XI-2-10	Pressure Distribution Across the Face of a Poppet Valve.....	XI-2.18
XI-2-11	Pressure Distribution on the Disc of a Butterfly Valve.....	XI-2.19
XI-2-12	Butterfly Valve Torque Characteristics.....	XI-2.19
XI-2-13	Compensation for Flow Induced Forces.....	XI-2.20
XI-2-14	Typical 1.0 Inch Poppet and Seat Model.....	XI-2.22
XI-2-15	Theoretical Nitrogen Flow Through the Valve Model Shown in Fig. XI-2-14.....	XI-2.22
XI-3-1	Approximate Values of C_v Versus Valve Diameter.....	XI-3.5
XI-3-2	A Comparison of Control Valve Flow Characteristics.....	XI-3.7
XI-3-3	Conical Poppet Stroke Relation for Various Half Angles.....	XI-3.8
XI-3-4	Typical Pilot Operated Valves.....	XI-3.11
XI-3-5	Conical Poppet Seat Design, Tank Vent Valve (Rocketdyne).....	XI-3.13

FIGURES (contd)

Section-Part-Figure	Title	Section-Part.Page
XI-3-6	Flat Poppet Seat Design, Vent Port Check Valve (Rocketdyne).....	XI-3.13
XI-3-7	Spherical Poppet Seat Design, High Pressure Relief Valve (Aqualite Corp.).....	XI-3.13
XI-3-8	Conical Poppet Seat Design, Pro-Pellant Control Solenoid Valve I (Rocketdyne).....	XI-3.13
XI-3-9	Conical Poppet Design, Propellant Control Solenoid Valve II (Honey-well).....	XI-3.14
XI-3-10	Conical Poppet Seat Design, All Metal Check Valve (Randall Engi-neering Corp.).....	XI-3.14
XI-3-11	Spherical Poppet Seat Design, Snap Action Relief Valve (Frebank Co.).	XI-3.14
XI-3-12	Flat Poppet Seat Design, Metal-to-Metal (Randall Engineering Corp.).	XI-3.14
XI-3-13	Self Aligning Bi-Polar Solenoid Valve (Parker Aircraft).....	XI-3.15
XI-4-1	Simple Fill and Vent Valves.....	XI-4.4
XI-4-2	Typical Quick-Disconnect Couplings	XI-4.5
XI-4-3	Pressure Flow Characteristics of a Relief Valve.....	XI-4.7
XI-4-4	Ball Poppet Valve.....	XI-4.9
XI-4-5	Conical Poppet Valve.....	XI-4.9
XI-4-6	Sleeve Type Poppet Valve.....	XI-4.9
XI-4-7	"V" Seal Valve to Provide Snap Open Characteristics.....	XI-4.9
XI-4-8	Inverted Seat Valve.....	XI-4.11
XI-4-9	Inverted Seat Valve with Diaphragm Retainer.....	XI-4.11
XI-4-10	Pilot Operated Valve.....	XI-4.11
XI-4-11	Inverted Seat Pilot Operated Valve	XI-4.11

FIGURES (contd)

Section-Part-Figure	Title	Section-Part.Page
XI-4-12	Typical Check Valve Pressure Drop Curves.....	XI-4.13
XI-4-13	Typical Ball Check Valve.....	XI-4.14
XI-4-14	Typical Pressure Versus Time Record for an Explosive Actuator....	XI-4.16
XI-4-15	Typical Explosive Cartridge.....	XI-4.17
XI-4-16	A Normally Open and a Normally Closed Explosive Valve.....	XI-4.19
XI-4-17	Normally-Open Explosive Valve.....	XI-4.20
XI-4-18	Normally-Closed Explosive Valve...	XI-4.20
XI-5-1	Woven Wire Mesh.....	XI-5.5
XI-5-2	Wound Wire Mesh.....	XI-5.6
XI-5-3	Dutch Twill Weave Wire Mesh.....	XI-5.6
XI-5-4	Ribbon Edge Filter.....	XI-5.6
XI-5-5	Sintered Porous Metal Filter.....	XI-5.6
XI-5-6	Composite Sintered Porous Metal with Wire Mesh.....	XI-5.7
XI-5-7	Etched Disc Filter.....	XI-5.7
XI-5-8	Pressed Paper Filter.....	XI-5.7
XI-5-9	Membrane Filter.....	XI-5.7
XI-6-1	Metallic Seal Structure with Plated Sealing Surfaces.....	XI-6.3
XI-6-2	Metallic Structure with Plastic Sealing Surface in a Separable Flange.....	XI-6.3
XI-6-3	Wedge Shaped Flange Soft Flat Gasket.....	XI-6.4
XI-6-4	Solid Metal Profiled.....	XI-6.4
XI-6-5	Molded Elastomer Seal Metal Loading Spring.....	XI-6.5
XI-6-6	General-Purpose Flange (Soft Metal) Gasket (Elastomer) and Metal Jacket Filler (Asbestos)....	XI-6.6
XI-6-7	Ring Type Solid Elastomer.....	XI-6.7
XI-6-8	Metallic Pressure Energized Seal..	XI-6.10

FIGURES (contd)

Section-Part-Figure	Title	Section-Part.Page
XI-6-9	Nonmetallic - Nonpressure Energized Seal.....	XI-6.10
XI-6-10	Metallic Nonpressure Energized Seal.....	XI-6.11
XI-6-11	Nonmetallic - Pressure Energized Seal.....	XI-6.11
XI-6-12	Metallic Split Piston Ring Seal...	XI-6.12
XI-6-13	Rolling Diaphragm Seal.....	XI-6.12
XI-6-14	Face-Type Seal.....	XI-6.12
XI-6-15	Lip-Type Seal.....	XI-6.12
XI-6-16	Circumferential Split-Ring Seal...	XI-6.13
XI-6-17	Packing or Stuffing Box Seal.....	XI-6.13
XI-7-1	General Cover Geometry.....	XI-7.3
XI-7-2	Flat Cover Geometry.....	XI-7.5
XI-7-3	Flat Cover Plate Geometry.....	XI-7.5
XI-7-4	Bolted Cover.....	XI-7.6
XI-7-5	Bolt Cover with Seal.....	XI-7.8
XI-7-6	Simplified Cover and Seal Geometry	XI-7.12
XI-7-7	Seal with Cantilever Leg of Constant Thickness.....	XI-7.15
XI-7-8	Two-Inch Diameter Navan Seal.....	XI-7.17
XI-7-9	Load Deflection Characteristics of a Naflex Seal.....	XI-7.19
XI-7-10	Leakage of a Two-Inch Naflex Seal at 80°F.....	XI-7.23
XI-7-11	Leakage of a Naflex Seal at Low Temperatures.....	XI-7.24
XI-8-1	Piston-Like Positive Expulsion Devices.....	XI-8.2
XI-8-2	Typical Bladder Type Expulsion Devices.....	XI-8.3
XI-8-3	Life Cycle of a Convoluted Metal Diaphragm.....	XI-8.4
XI-9-1	Typical Threaded Connector Configuration.....	XI-9.2

FIGURES (contd)

Section-Part-Figure	Title	Section-Part.Page
XI-9-2	Simple Bolted Flange.....	XI-9.2
XI-9-3	Flange with Pressure Energized Seal.....	XI-9.6
XI-9-4	Schematic of an AN Flared Fitting.	XI-9.7
XI-9-5	Temperature Compensated Flange Design.....	XI-9.7
XI-9-6	"MC" Tube Connector.....	XI-9.9
XI-9-7	"MC" Fitting with Voi-Shan Washer.	XI-9.11
XI-9-8	AN Fitting with "O"-Ring.....	XI-9.11
XI-9-9	AFRPL Flanged Tube Connector.....	XI-9.12
XI-9-10	Tube Connector Utilizing Super-finished Surface Sealing Principle	XI-9.13
XI-9-11	Flange Contact Inside the Bolt Circle.....	XI-9.14
XI-9-12	Flange Contact Outside the Bolt Circle.....	XI-9.15
XI-9-13	Typical Omega Seal Configuration..	XI-9.16
XI-9-14	Omega Seal Connector Schematic....	XI-9.16
XI-9-15	Diffusion Bonded Connector Schematic.....	XI-9.17
XI-9-16	Swaged Connector Union, Unassembled.....	XI-9.18
XI-9-17	Swaged X-Fitting.....	XI-9.18
XI-9-18	General Electric Cold Welded Connector Seal.....	XI-9.19
XI-9-19	Formation of Cold Welded Seal.....	XI-9.19

XI-1 INTRODUCTION

The purpose of this Section is to discuss basic fluid components which can be employed in the construction of a pressurized gas storage system. The discussion is limited to individual components without regard to their interrelationship with one another or the design philosophy governing the entire pressurization system with respect to the spacecraft. This topic is considered in Section X.

The major items of interest in this Section are valves, filters, general purpose seals, connectors and fittings and expulsion devices. Several of these topics comprise more than one item, for example, valves are further cataloged as shut-off or start, fill, vent, check, and relief valves. Each of these components are considered individually. However, each potentially possess common features. To proceed rationally in their discussion, therefore, the common features are considered first, followed by a discussion of the individual item.

The format of this Section is to briefly survey and assess the design merits and limitations of the individual component features. Based upon certain conclusions, design and selection criteria are outlined for the most promising components. Since the conclusions are subject to present state-of-the-art knowledge and individual interpretations, information sources for design and the less promising components are appropriately referenced. The inclusion of criteria for a broad spectrum of candidate components is a substantial task and beyond the scope of this guidebook.

XI-2 VALVES - GENERAL

Introduction

A valve is a device used to control the direction, flowrate, or pressure of a fluid. To provide these functions the device normally contains a movable control element within a fluid-containing housing. The valve element is composed of one or more sealing elements formed between the control element and the fluid-containing housing. The contacting surface of the valve element on the housing is defined as a sealing element seat. In addition, a means of actuating the control element is required. This latter aspect, however, is associated with the specific component. The common features of all valves can, therefore, be specifically identified as the control element and the seal element. In the following discussion the various types of control elements are briefly described with a subsequent assessment of their applicability to long term gas storage systems in terms of the sealing elements.

Control Elements

The pertinent control elements are one direction flow control devices. This distinction is made to eliminate such devices as four-way servo valves from the survey. The general classes of one direction control devices applicable to pressurized gas systems include poppet, butterfly, gate and blade valves. For lower pressure applications, ball, rotary slide, spool and rotary plug valves are used in addition to those listed above. These latter valves will not be covered in this guidebook, but are mentioned to make the reader aware of their relative usage.

Poppet valves contain a control element which moves parallel to the flow passage. The shape of the control element commonly has the form of a sphere, cone, plug or flat plate as shown in Figure XI-2-1. The sealing element is formed at the contacting surfaces of the poppet and seat.

A butterfly valve, Figure XI-2-2, consists of a disc supported on a shaft which is rotated within a housing forming the flow passage. To provide a seal element at closure, the disc is either canted or eccentric with

respect to the actuating shaft. The seal element is formed at the perimeter of the disc.

Gate and blade valves contain control elements which slide normal to the flow passage as shown in Figures XI-2-3 and XI-2-4. The seal element is formed by urging the control element against the seat. A variation of this arrangement is shown in Figure XI-2-4 where the gate is depicted as a wedge. In this case, two sealing elements are present.

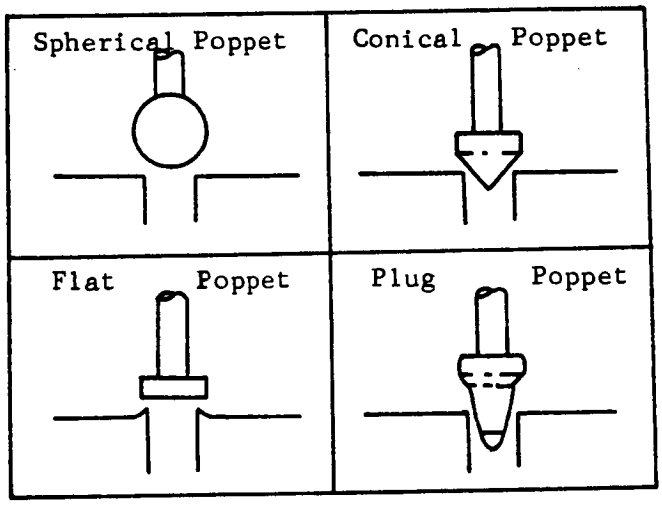

Fig. XI-2-1 Typical Poppet Configurations

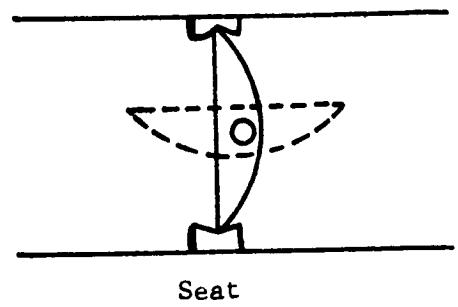

Fig. XI-2-2 Schematic Side View of an Eccentric Butterfly Valve

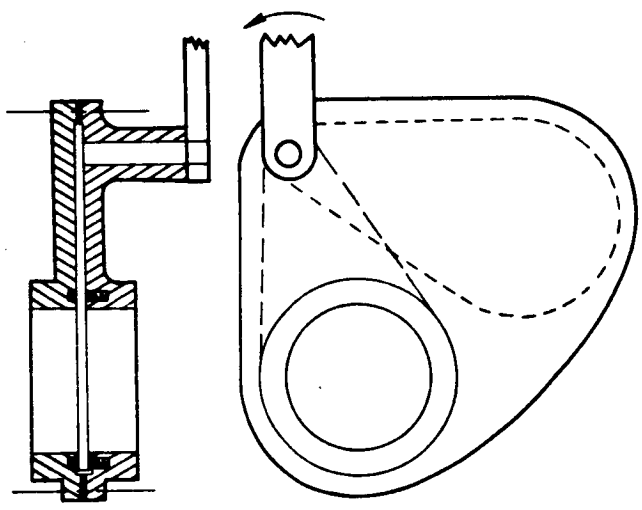

Fig. XI-2-3 Blade Valve (Ref. 6)

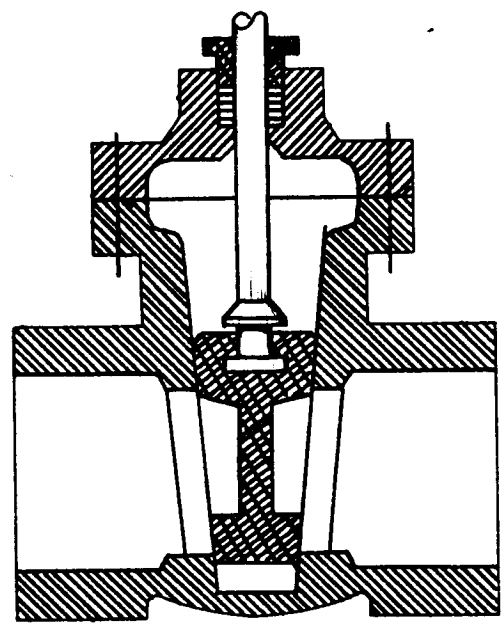

Fig. XI-2-4 Tapered Gate Valve (Ref. 6)

Sealing Elements

To assess the merits of the preceding control elements, the qualitative requirements for minimum leakage sealing as discussed in Section X-4 must be used as guidelines. These guidelines are in the form of requirements for interface seal loads, material properties, surface finish and other surface variations. The sealing element can be specifically defined as the interface formed by the control element and the housing.

The factors influencing valve sealing can be categorized into four basic groups depending upon their origin and identified as (1) design, (2) fabrication, (3) environment and (4) fluid effects. The groups can be further subdivided as follows:

A. Design Factors

(1) Configuration of the Control Element

a. Geometry of the interface
b. Designated tolerances, surface finish, and other dimensional influences producing such factors as deformation resulting from fluid pressure acting on housing and control elements

(2) Forces Acting at the Sealing Interface

a. Static pressure forces in the control element
b. Pressure forces due to leakage flow
c. Mechanical forces
d. Actuation or other external forces acting on the control element
e. Friction forces
f. Impact forces

(3) Material Properties (Macroscopic and Microscopic)

a. Modulus of elasticity
b. Yield strength
c. Hardness
d. Wear
e. Thermal conductivity
f. Thermal expansion
g. Impact
h. Friction
i. Fretting corrosion and surface fatigue
j. Chemical corrosion
k. Permeability
l. Chemical compatibility
m. Creep and other long term effects on material properties

B. Fabrication Factors

1. Fabrication Processes

   a. Dimensional variations attributed to the machine tool capability.

      1. Concentricity
      2. Flatness
      3. Sphericity
      4. Roundness
      5. Straightness
      6. Angularity
      7. Surface finish
      8. Size
      9. Geometry and location of critical surfaces

   b. Dimensional variations attributed to the material properties such as machinability

2. Inspection Processes

   a. Limitations of inspection instrumentation to reach all critical areas. This is attributed to the valve configuration.
   b. Limitations of the inspection instrumentation with respect to absolute values of measurement. This refers to the reliability of the measurement based on a standard calibration using an instrument of greater sensitivity and reliability

C. Environmental Factors

1. Storage procedures to prevent scratches, atmospheric corrosion and other "shelf" induced effects including packaging
2. Operational temperature and dimensional stability of parts
3. Sterilization temperature
4. Fluid contaminants including water and ice
5. External contaminants such as space debris, lunar dust, etc.
6. Vacuum degradation
7. Radiation
8. Vibration, acceleration and impact
9. Cold welding

D. Fluid Factors

1. Viscosity
2. Thermal conductivity
3. Specific heat
4. Vapor pressure
5. Lubricity and corrosivity
6. Density
7. Surface tension
8. Pressure

To assess each of the control element configurations on the basis of the preceding factors is indeed a difficult task because many of the factors are interrelated. Some generalizations can be made, however, which reduce the number of factors to a working level. In achieving this simplification, common factors are omitted from consideration and additional factors are introduced. The new factors are minimum leakage, cost and the resistance to fluid flow produced by the control element. The latter factor is introduced in general but applies specifically to start valves. The influencing factors can be restated:

(1) The sealing interface must be composed of completely contacting surfaces. From the viewpoint of geometry and fabrication problems, simplicity is a good description of an optimum sealing element.

(2) The net loads acting at the sealing interface must be uniformly distributed. This can only be achieved by uniform contacting surfaces.

(3) The net load acting at the interface must be commensurate with the surface finish and material properties.

(4) No gross plastic deformation of the sealing interface is permitted unless unusual circumstances prevail. These circumstances entail compensating devices or "one time" operational valves.

(5) The control element should provide minimum resistance to flow.

(6) There should be no relative motion between contacting surfaces which produces wear. Relative changes in the sealing surface position is permissible provided that uniform contact is maintained.

Following the preceding arguments, each of the control elements can be assessed with respect to the materials forming the interface.

Elastomeric Sealing Elements

With nominally precise fabrication processes employed in their manufacture, all of the valve elements considered in this Section can provide minimum leakage, 10^{-5} cc/sec or less, when elastomers are used as part of the sealing element. This assumes that good design practice is employed in each case with respect to the seal element, control element, housing, and actuating mechanism.

From an optimization viewpoint, however, certain factors must be considered. These factors are identified and related to the specific configurations in Table XI-2-1. From an obvious consideration, simplicity and cost are somewhat related and are of primary consideration when equal leakage performance is chosen as a basis for comparison. The next factor of importance is whether the design is suitable for elastomeric sealing. For example, the sliding motion of a sharp metallic edge across a seal element can destroy the element. The fourth consideration is the proximity of the sealing element to the flow stream. Seal elements in the direct flow stream are subject to erosion. Additionally, elastomeric seal elements located in regions of high velocity flow, particularly when the element is close to closure, have a tendency to erode and wash away unless special restraining techniques are utilized. The latter effect is due to a pressure difference across the sealing element. The fifth factor is related to the geometry of the element and its influence on reducing the flow path or causing changes in momentum of the flow. This effect is described as resistance to flow and is related to system efficiency. The sixth factor is related to friction induced by the sealing element and the consequent increase in actuating force required to operate the element.

If each comparison factor is weighed on a 1-Good, 2-Fair, and 3-Poor basis, it can be seen from Table XI-2-1 that the lower total weighed values can be assigned to the poppet valve. From Table XI-2-1, the optimum valve is the poppet device. The influences of flow on the elastomeric sealing element of a poppet valve can be minimized through design features such as that shown in Figure XI-2-5.

Table XI-2-1

COMPARATIVE RATINGS OF CONTROL ELEMENTS WITH ELASTOMERIC SEALS

FACTORS	POPPET	BUTTER-FLY	BLADE & GATE	BALL	ROTARY SLIDE	SPOOL	PLUG
Simplicity	1	3	2	3	2	1	3
Cost	1	3	3	3	3	2	3
Design pertinent to elastomeric sealing	1	1	1	1	3	1	1
Influence of flow on on sealing element	3	2	1	1	2	3	1
Resistance to flow	2	2	1	1	2	2	1
Seal element induced friction	1	1	2	3	3	3	3
Total	9	12	10	12	15	12	12

Rating Method: 1-Good, 2-Fair, 3-Poor.

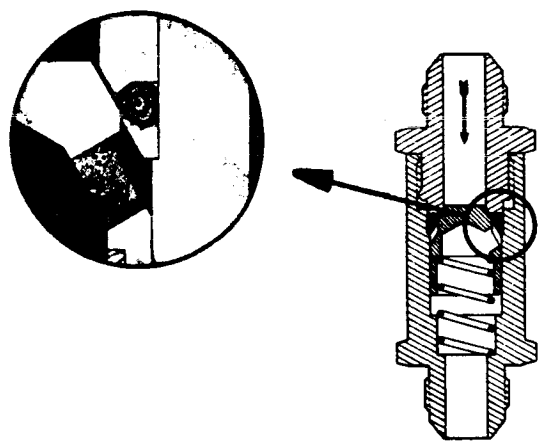

Fig. XI-2-5 Poppet Valve with Elastomeric Seal Element Retained by a Special Seal Cavity (Courtesy of Kepner Products Co.)

Plastic Sealing Elements

A conclusion reached in Section X is that minimum leakage (less than 10^{-5} cc/sec) in metal to plastic interfaces can be achieved by either plastically deforming the plastic or having precision finishes on the metallic parts such that the deformation is elastic. Compared to elastomer sealing elements, the dimensional tolerances in either case must

significantly improve. These tolerances include out-of-roundness, surface finish, straightness, waviness, etc. The tolerances of interest are dependent upon the geometry of the sealing element.

Interface stresses less than that required for full plasticity require fabrication finishes less than 1 microinch PTV. The out-of-roundness variation of a cylindrical or spherical part must be in the range of 50 microinches or less. It must be recognized that the preceding dimensions and leakage limitation are generalized. The size of the component and leakage are somewhat related. Small sealing elements leak less than larger elements. Additional detrimental effects are occasioned by a diminishing ability to fabricate and measure precision tolerances as size increases.

Contact stresses equal to the full plasticity stress produce a high friction contribution to the control element actuation function and additionally, introduces severe creep and extrusions problems. Another factor of significance is the influence of wear at any semi-dynamic seals.

A review of the construction features of the control elements yields a weighed comparison as shown in Table XI-2-2. The factors upon which the table is based are low friction, wear and debris formation, and creep and extrusion control.

Table XI-2-2

COMPARATIVE RATINGS OF CONTROL ELEMENTS WITH PLASTIC SEALS

FACTORS	POPPET	BUTTER-FLY	BLADE OR GATE	BALL	ROTARY SLIDE	SPOOL	PLUG
Low Friction	1	2	3	3	3	3	3
Wear and Debris Formation	1	1	3	3	3	3	3
Creep and Extrusion Control	3	3	3	3	3	3	3

Rating Method: 1-Good, 2-Fair, 3-Poor

Since the poppet moves normal to a sealing surface, the seal element can be described as frictionless. The remaining control elements possess dynamic seals which contribute to friction and the generation of wear and the formation of contaminants. In all cases, the problem of creep and extrusion apply. Special backup devices and composite construction of the plastic are often used to reduce this effect. A technique to provide minimum extrusion and simultaneously compensate for any losses of material in a poppet valve is shown in Figure XI-2-6. This design requires a reaction spring and sealed fluid pressure to provide the high normal stress at the sealing interface.

In summary, a comparative performance of each control element yields the conclusion that the poppet configuration possesses the greatest advantages for use with plastic sealing elements. The second choice is the butterfly valve followed by a modified version of the conventional blade or gate valve. In both cases, additional linkage mechanisms are employed so that the final sealing is accomplished in poppet valve fashion. When these valves open, no contact with the sealing surface occurs.

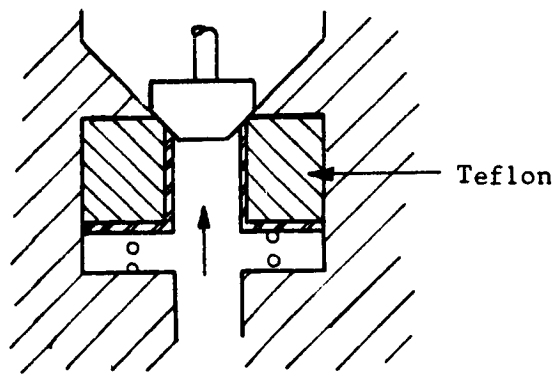

Fig. XI-2-6 Anti-Extrusion Method for a Plastic Seat Poppet Valve

Metallic Sealing Elements

The problems of sterilization temperature and radiation damage can limit the choice of sealing materials to metals. When employed, the possibility of cold welding in high vacuum exists. Contamination from all

sources impose a much greater influence on metal to metal sealing than plastic or elastomeric sealing.

To achieve minimum leakage (10^{-5} cc/sec or lower) in metal to metal interfaces, the following criteria must be applied to the sealing element:

(1) When surfaces are rough ($>1\mu$ inch PTV); high interface loads sufficient to produce full plasticity are required. This results in high friction and wear.

(2) When surfaces are highly polished ($<1\mu$ inch PTV) low interface loads are permissable but not reliable from an operational viewpoint.

A functional comparison of all valve elements shows that the optimum choice of sealing element is the poppet configuration. This conclusion is based solely on the influence of wear debris particles which prevent the sealing surfaces from mating closely. Consequently, all control elements containing a dynamic seal are eliminated from consideration. A weighed rating comparison for metallic elements would yield the same comparison as shown in Table XI-2-2 for plastic elements. Another factor eliminating all valve elements except the poppet is the precise tolerances required even when higher leakage rates can be tolerated. Complex control element components such as the ball and plug valve must be made to dimensions varying not more than 20 microinches PTV. The cost of fabrications is quite high and precautions in preserving the sealing surfaces from damage must be exercised.

Summary of Sealing Element Requirements

The preceding discussion leads to the conclusion that the poppet type control element possesses optimum characteristics for minimum leakage. This conclusion must be qualified as follows:

1) When high leakage rates (greater than 10^{-3} cc/sec) are encountered, the blade, gate, or butterfly valve may be more suitable particularly when high flow rates are involved.

2) The degree of minimum leakage depends on many factors as described in Section X-9. It is suggested that leakage calculations be made before assuming absolute merits of any poppet valve. The

procedures for leakage calculations are outlined in Section X B

3) Since at least four basic poppet configurations are available (see Figure XI-2-1), one type may have advantages over another. This depends upon the valve application and is discussed separately. In general, the factors governing the selection of sealing materials is the hardness of the softer interface material Hence, elastomers, plastics, and metallics are the order of preference. The susceptability to contaminant influences also follow in the same order. The interface surfaces must be finished as smooth as possible commensurate with a tolerable leakage requirement. The integrity of the surface must not be influenced by variations of element and seat orientation or from any of the environmental effect.

Fluid Forces Acting on the Control and Sealing Elements

Several fluid pressure forces act on the control and sealing element and are somewhat interdependent. When the valve element produces closure, two forces are prevalent One force is due to static pressure acting on the configuration of the element and the second force is a contribution due to leakage flow through the sealing interface. The resultant of these forces produces a net interface contact loading However, when the control element is unseated and permits flow, additional forces are contributed by the dynamics of the flow. Hence, three distinct fluid forces must be considered in any valve design

Static Pressure Forces

Static pressure forces result from differences in fluid pressure acting on areas of the control element or the same pressure acting on unequal areas of the element The resultant of these forces is described as unbalanced or balanced depending on the valve element design The term balanced does not imply that all forces on the element are balanced. Only the static pressure forces are balanced

The techniques for controlling the degree of balance vary and in the case of several valve designs, balance cannot be controlled. In these cases the valve element is usually completely unbalanced. Before considering the

merits of either effect, a solenoid operated, poppet type valve is chosen to illustrate the terms.

A completely unbalanced valve is shown in Figure XI-2-7(a) where inlet pressure acts over the full seating area To compensate for the force due to the inlet pressure, an opposing poppet can be included in the valve element as shown in Figure XI-2-7(b) In this case the valve contains two sealing surfaces which can be classed as semi-static seals. To completely balance the valve element, the seat and poppet geometry must be identical. Another method of balancing requires the use of a sliding seal in lieu of one poppet, as shown in Figure XI-2-7(c). In this case, complete balance requires that the poppet seat and element geometry be equal to that of the portion of the valve element containing the sliding seal. The sliding seal element can be replaced by a bellows seal as shown in Figure XI-2-7(d). The degree of balancing on the valve elements shown in Figures XI-2-7(b), (c), and (d) can be controlled by varying the geometric area relationships between the two sealing elements. For example, the diameter of the sliding seal in Figure XI-2-7(c) can be reduced thus increasing the unbalanced force

The degree to which pressure forces can be controlled is difficult to assess In the cases of all four valves shown, manufacturing tolerances are most important The second requirement is that no detrimental frictional effects are present This is particularly pertinent to the valve shown in Figure XI-2-7(c) Unfortunately, minimum leakage sliding seals do possess significant frictional increases with increasing pressure or vice-versa. Attempts to minimize sliding friction effects by using wet seals is being investigated by TRW Systems (Ref. 1, 2) Gallium and DC705 liquids have been deposited on sliding surfaces where the wetting action produces surface tension within the liquid thus blocking the leakage path.

The bellows seal, shown in Figure XI-2-7(d) induces pressure dependent forces due to a change in geometry of the bellows. These changes are difficult to predict except from past experience. Typical variations of bellows unbalance are shown in Figure XI-2-8 for a 0.151 square inch seat [illegible] 3) In addition to the design and fabrication induced force variations, operational deformation of the valve element seats produce balancing variations due to creep or fretting corrosion.

Valves which are usually completely unbalanced by virtue of their design are gate, blade, single poppet, rotary plug and ball valves. The remaining valve types can be balanced to the extent that the configuration, fabrication and functional operation will permit.

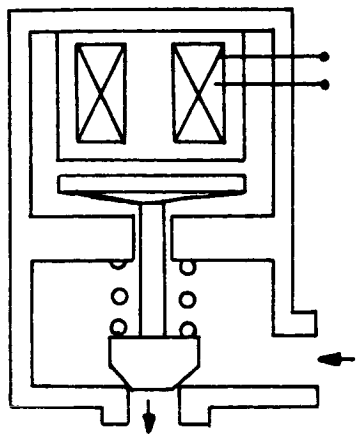

(a) Unbalanced Poppet

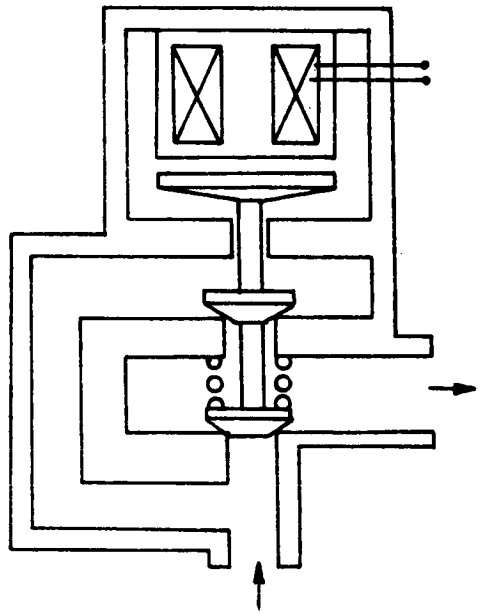

(b) Balanced Valve with Double Poppet

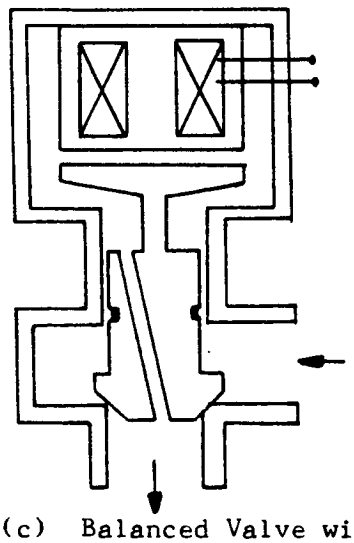

(c) Balanced Valve with Sliding Seal

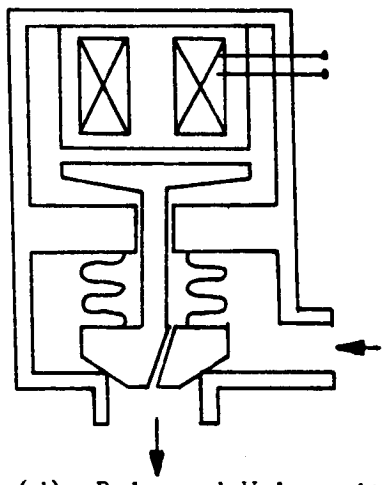

(d) Balanced Valve with Bellows Seal

Fig. XI-2-7 Four Configurations of a Solenoid Operated Poppet Valve (Ref. 9)

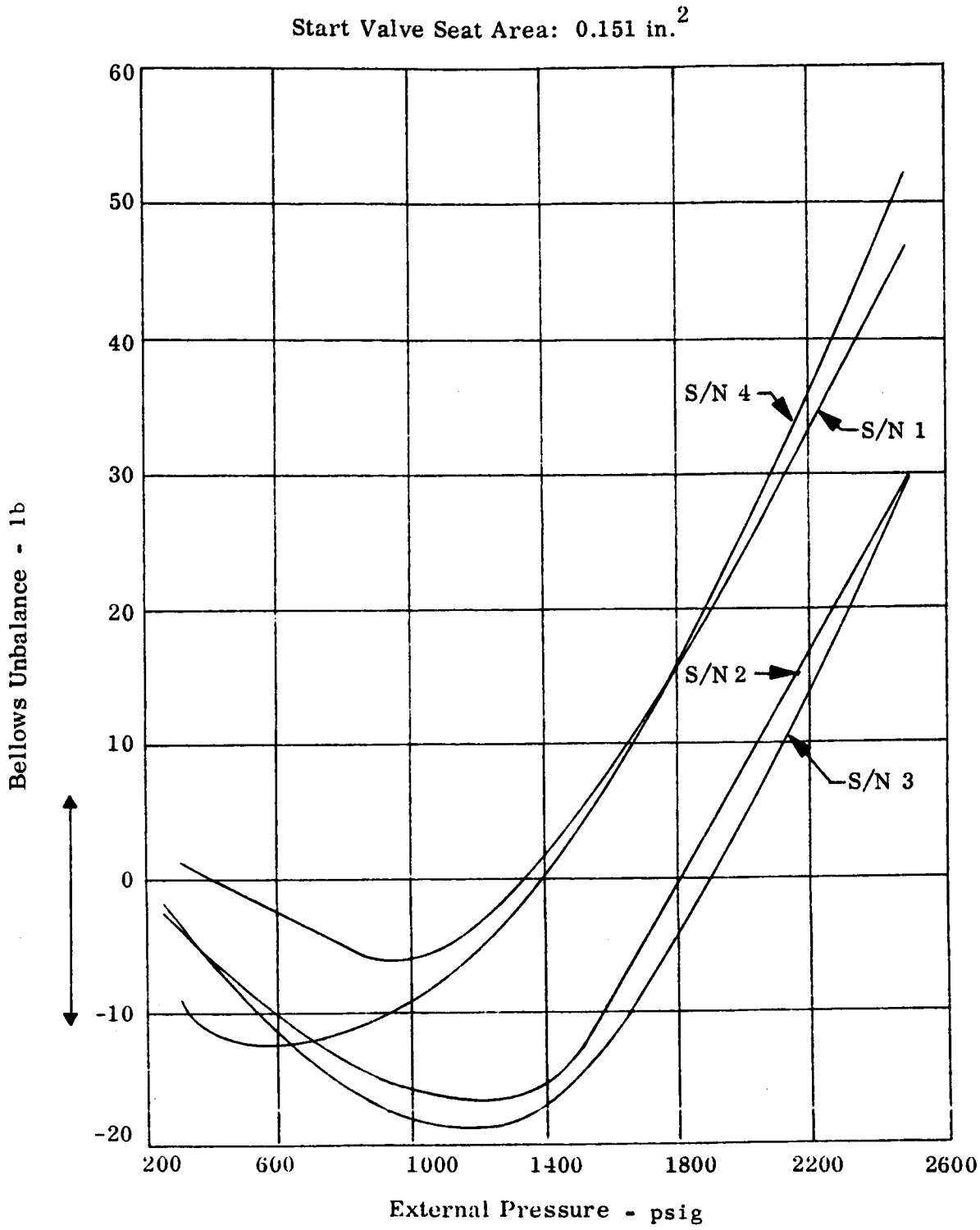

Fig. XI-2-8 Effect of Pressure on Start Valve Bellows Unbalance (Ref. 3)

Forces Due to Leakage at the Sealing Interface

Fluid flowing in small channels formed by the sealing surfaces in contact produce a pressure distribution or gradient due to energy losses accompanying the flow. An integration of this gradient over the entire interface produces a force tending to separate the surfaces. These forces determine such external performance parameters as start valve actuating force, cracking and reseat requirements for relief valves or influence stability in the case of regulators and flow modulating valves.

The theoretical aspects of fluid flow in small channels simulating a sealing interface are discussed in Section X-A. When the leakpath is large and the flow is compressible, choking can occur at the exit. The problem is difficult to treat theoretically and with some simplifying assumptions it can be considered analogous to isentropic flow through a short tube orifice. Reference 8 contains a discussion of flow through short tubes. Because the analysis is basically qualitative, the pressure gradient is most often determined experimentally. For turbulent incompressible fluid flow, the pressure drop is a direct function of the length of the path; therefore, the pressure profile is linear across the seat land. This results in an effective seat load resultant at the mid point of the interface. The pressure distribution for the compressible, turbulent gas flow is somewhat more complex and depends upon the equivalent interface clearance. In general, the pressure profile along a channel is linear for high Reynolds numbers but, as the clearance decreases, the profile progressively approaches the parabolic shape found in the laminar flow regime. Fortunately, leakage flow through the interfaces of most valves is in the laminar or molecular flow region. Unlike the analysis of pressure distribution in the choked and turbulent channel regimes, the laminar consideration is straightforward. Because the density is essentially constant for the incompressible fluid, the pressure profile will be a straight line with the effective area located at the midpoint, Figure XI-2-9.

Based on the laminar flow equation for compressible media, the following formula can be derived which expresses the variable pressure P as a

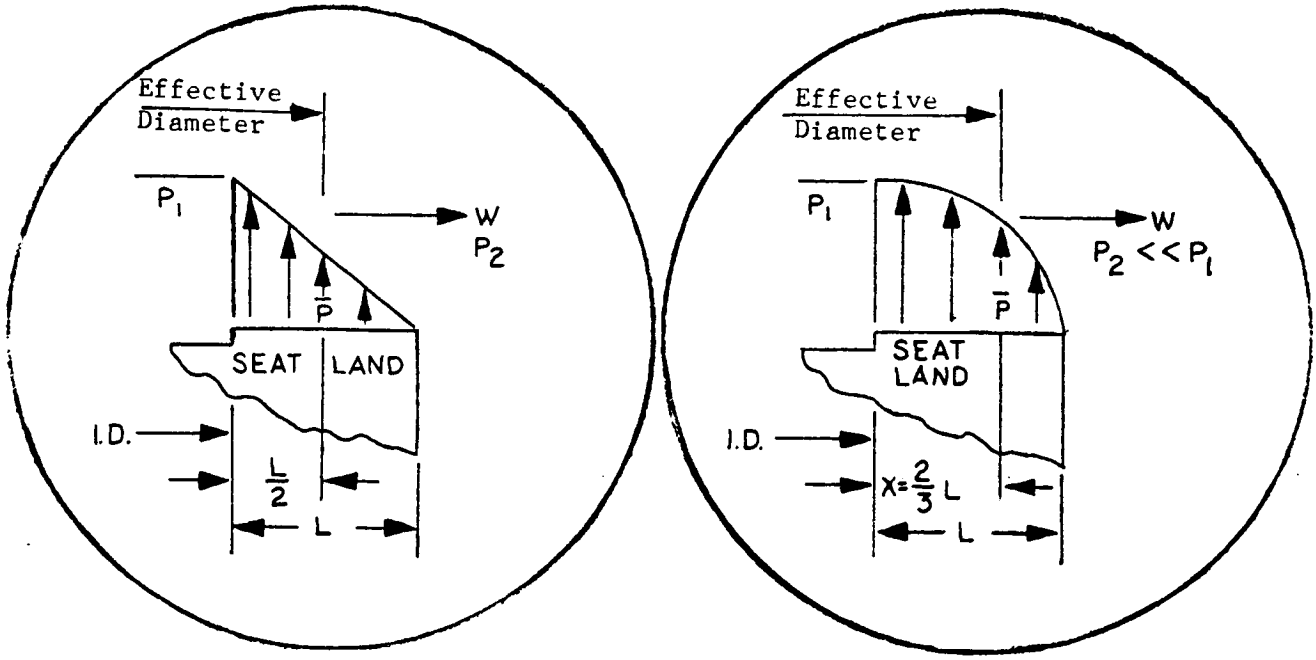

(a) INCOMPRESSIBLE FLUID (b) COMPRESSIBLE FLUID

Fig. XI-2-9 Pressure Profiles (Ref. 5)

function of the distance along the seat land X:

$$P = P_1 \left\{ 1 - \frac{X}{L} \left[1 - \left(\frac{P_2}{P_1} \right)^2 \right] \right\}^{1/2} \qquad (1)$$

The resulting curve is parabolic in shape (Figure XI-2-9(b)). To find the average pressure $\overline{P}$ over the entire land, the previous equation is integrated to give the following relationship:

$$\overline{P} = \frac{2}{3} \frac{P_1^{\,3} - P_2^{\,3}}{P_1^{\,2} - P_2^{\,2}} \qquad (2)$$

If P_2 can be neglected, the average pressure for the seat land reduces to:

$$\overline{P} \cong \frac{2}{3} P_1 \qquad (3)$$

It follows that for L small relative to the ID and $P_2 << P_1$, the effective seat diameter for compressible media is located at 2/3 of the distance across the seat land.

For the special case where the radial divergence must be taken into account, i.e., when L is large relative to the ID, Equation (1) must be modified. It can be seen in the following equation that X/L in the original equation, has been replaced by a radius function and the variable pressure P is now a function of the radial distance r along the seat land.

$$P = P_1 \left\{ 1 - \frac{\ln \frac{r}{r_1}}{\ln \frac{r_2}{r_1}} \left[1 - \frac{P_2^{\,2}}{P_1} \right] \right\}^{1/2} \qquad (4)$$

Since both r_1 and r_2 are variables in the general solution of the equation, a single pressure profile curve cannot be determined. However, the general effect of radial divergence is to straighten out the parabolic curve, and for the extreme case, actually reverse the curve so that the effective diameter is less than the land midpoint.

Detail consideration was not given to the transition and molecular pressure distributions because these flow regimes almost always occur under highly stressed seating conditions, and therefore, the force resulting from small differences in the effective seat area is often negligible relative to the total seat force.

Flow Induced Forces

Flow induced forces are attributable to the flow of fluid in the region of the sealing surfaces and all other additional surfaces prevailing in the flow stream. The cause of these forces differ from the previously considered forces in that the control element is not seated and geometric relationship between the seat and control element vary.

The effect of the flow induced forces can be described in a qualitative manner. Consider two positions of a conical poppet valve, as shown in Figure XI-2-10. Because of the proximity of the poppet to the seat, the net upward force due to pressure is greater in Figure XI-2-10 (a) than (b).

This effect is induced by an increase in flow velocity across the poppet surface as the minimum flow area comes closer to the center of the poppet. The net force can be obtained by integrating the pressure distribution curve if the distribution is known. Often a large scale model can be employed and actual pressure measurements made through a series of small holes in the poppet surface. For the case of the poppet valve the resultant force acts through the center of the poppet, if the poppet is symmetrical with the flow stream. Often, the poppet is not adequately guided and a slight eccentricity occurs causing the center of reaction to shift. This can result in lateral motion instability of the poppet. In some valves, the pressure distribution is more complicated and the direction of the reaction force is not readily determined. The butterfly valve shown in Figure XI-2-11 contains these features. The operating torque required to position the disc of a butterfly valve results from friction and non-symmetrical pressure loading around the disc. Depending on the angular position of the disc, the flow induced force will change. This change is reflected in actuating torque and variations in support shaft bearing friction. Often the change in actuation force will differ in opening the valve compared to valve closure as shown in Figure XI-2-12. Methods are available to compensate for these forces and hinge largely upon design ingenuity.

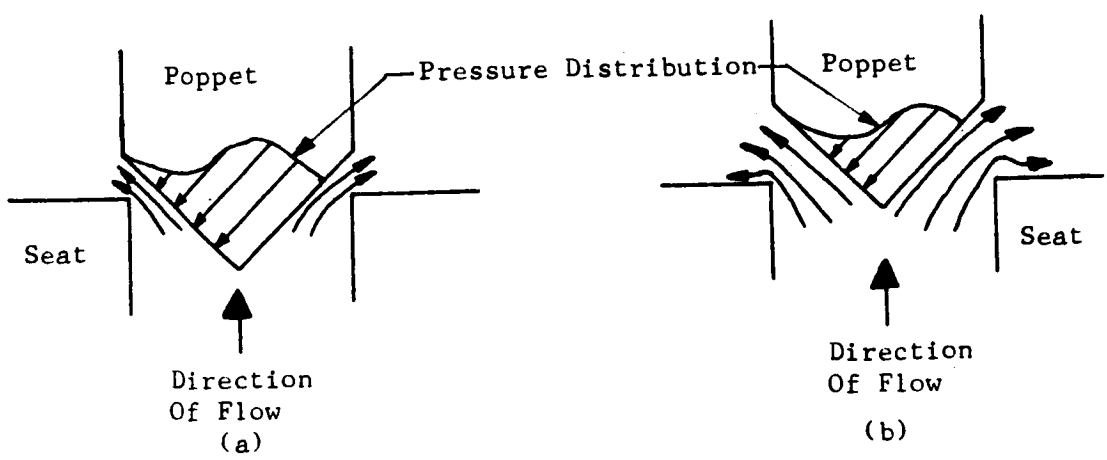

Fig. XI-2-10 Pressure Distribution Across the Face of a Poppet Valve

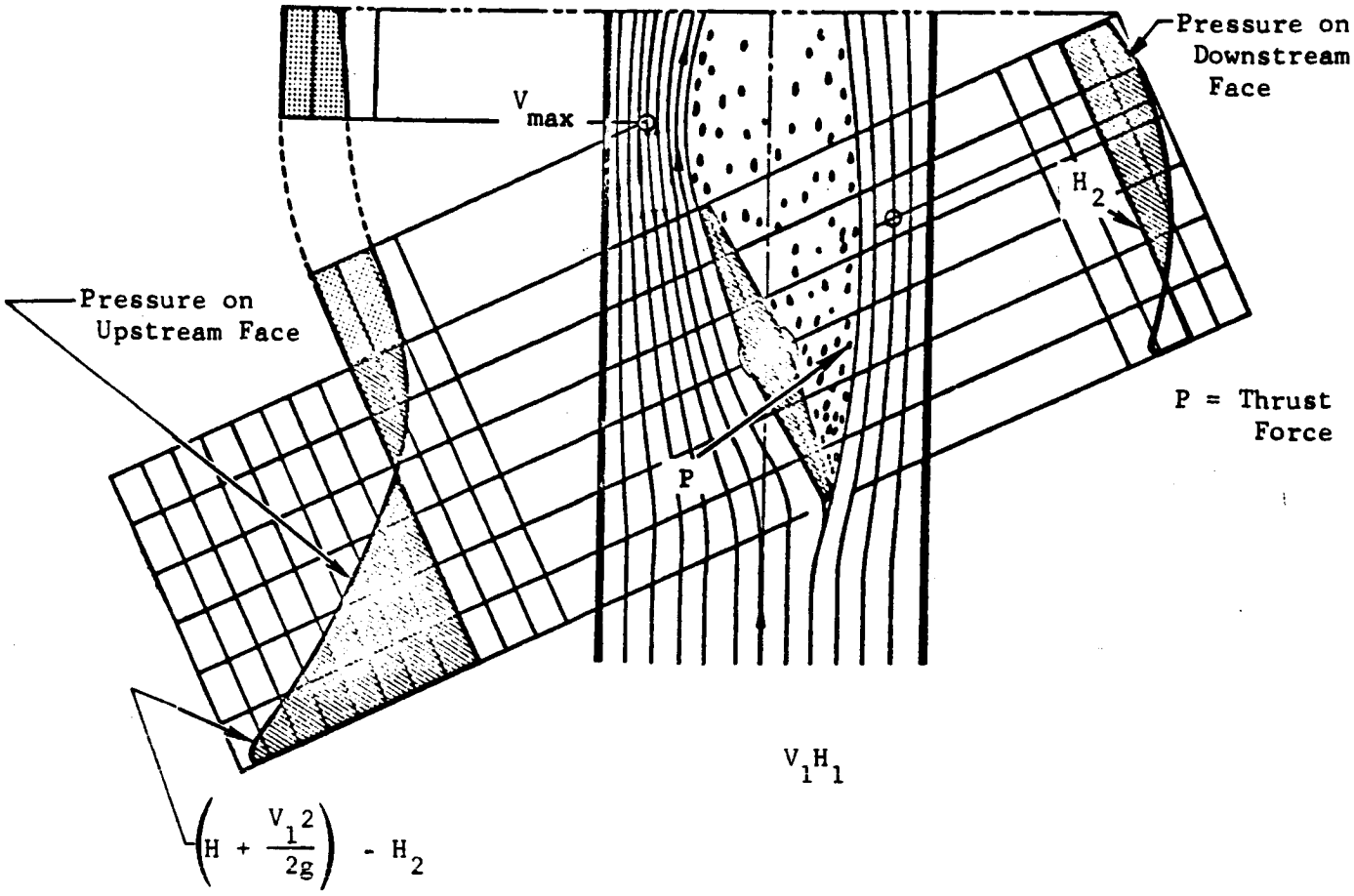

Fig. XI-2-11 Pressure Distribution on the Disc of a Butterfly Valve (Ref. 6)

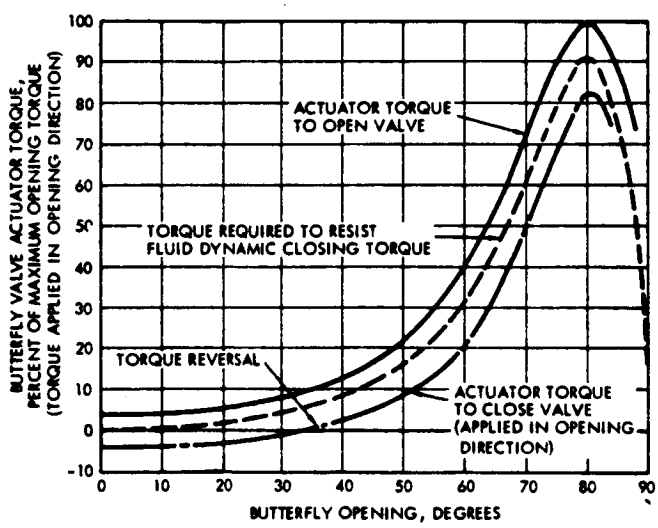

90° = Full Closed

Fig. XI-2-12 Butterfly Valve Tourque Characteristics

Figure XI-2-13 shows a cross section of a differential poppet relief valve where the fluid pressure in the spring chamber can be made to vary with the relative position of the poppet to the seat. These techniques vary with the control element configuration and the degree of force compensation required. In general, all control elements are influenced to an extent by these forces.

Two analytical methods for estimating the steady state flow forces on a control element have been developed (References 4 and 6). The first method employs momentum considerations and requires empirical coefficients based on the element geometry. Reference 4 outlines an investigation of poppet valve performance using this technique. The second method is based on an integrated surface pressure or free streamline potential flow consideration. The development of stream functions is complex and requires large computer facilities to solve the Navier-Stokes equations with a few restrictions on boundary conditions.

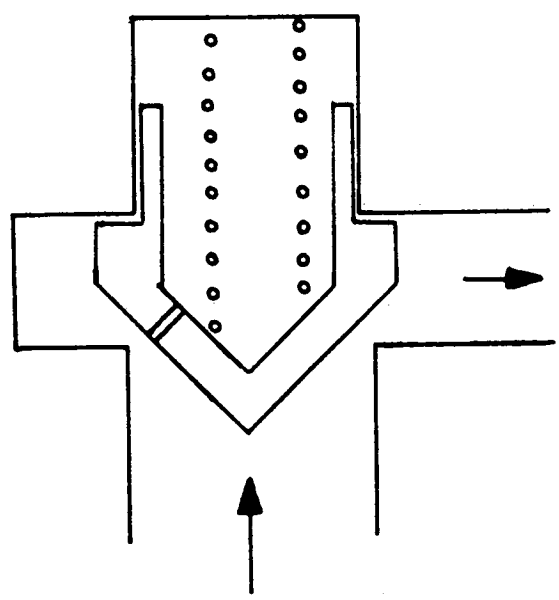

Fig. XI-2-13 Compensation for Flow Induced Forces

Summary of Forces Acting on the Control Element

The influence of all pressure forces acting on the control element depend upon the function of the valve. In an ideal relief valve, the summation of forces should be zero at any position of the control element. This would produce a coincident cracking, reseat pressure, and maximum pressure at rated flow. Attempts are usually made to achieve this objective. Since other mechanical forces are usually involved, these also must be taken into consideration.

A start valve could be force biased to open but would require an additional force for closure. Generally, the effects of flow induced forces are minimized without any attempt to utilize their effects.

Flow modulating valves, like the relief valve, are very sensitive to any changes in pressure forces. The changes can result in instability and valve malfunction. This is particularly pertinent to valves which are static pressure balanced.

Sealing Element Leakage

To illustrate how the leakage equations presented in Section X-A can be used, the following sample calculation is presented. A flat plate poppet valve model, shown in Figure XI-2-14, is selected with the interface dimensions as shown and leakage flow is from the inside to the outside through a 0.060 inch flat seat. The sample calculations were obtained from Reference 5 for nitrogen gas sealed at a 100 psig, 70°F, and a 14.7 psia outlet pressure.

Figure XI-2-15 presents the leakage spectrum for the sample computation. The various flow regimes, i.e., isentropic, turbulent channel, laminar, transitional, and molecular are identified on the curve. Also, the limits of each regime are shown. A range of theoretical parametric data has been computed for various pressures and gases and is presented with test data in Reference 5.

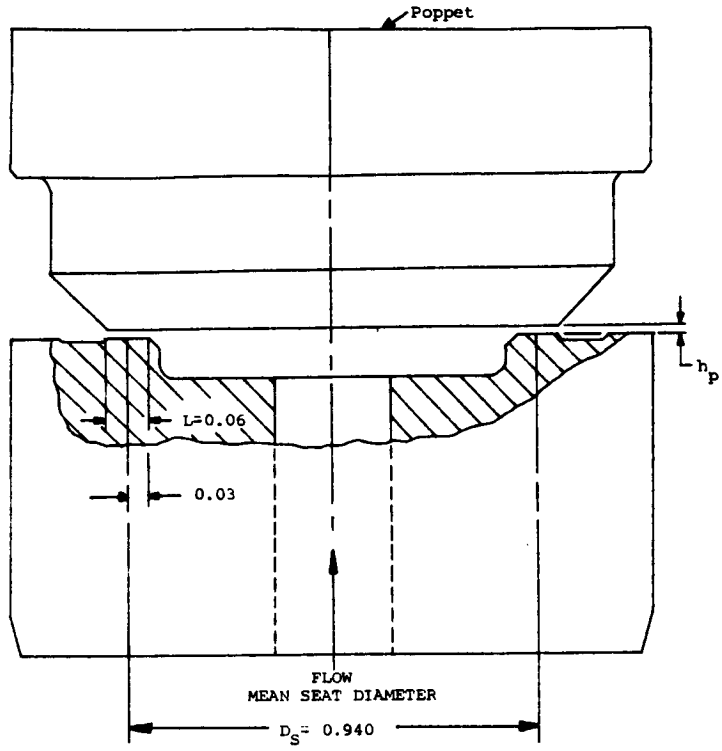

Fig. XI-2-14 Typical 1.0 inch Poppet and Seat Model (Ref. 5)

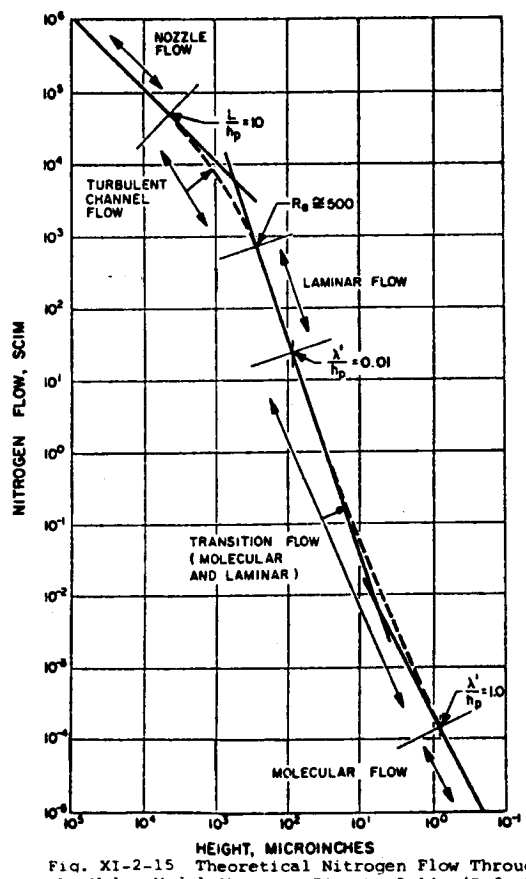

Fig. XI-2-15 Theoretical Nitrogen Flow Through the Valve Model Shown in Fig. XI-2-14. (Ref. 5)

The following parameters are known values for this seat configuration and are used in the flow equations to compute the noted leakage characteristics:

$C = 0.95$, Discharge coefficient

$g = 1.39 \times 10^6$ in/min^2, Gravitational acceleration

$k = 1.4$, Specific heat ratio

$L = 0.060$ inch, Channel length

$P_1 = 114.7$ psia, Inlet pressure

$P_2 = P_s = 14.7$ psia, Discharge pressure

$R = 663$ in/R, Gas constant

$T_1 = T_s = 530^\circ R$, Absolute temperature

$W = 2.95$ inches, Channel perimeter (πD_s)

$\mu = 4.40 \times 10^{-11}$ lb-min/in^2, Absolute viscosity

Isentropic Flow

For a compressible fluid flowing sonically the following equation is used:

$$Q = \frac{RT_s}{P_s}\left[\frac{C\,Wh_p\,P_1}{\sqrt{RT_1}}\sqrt{gK\left(\frac{2}{k+1}\right)^{\frac{k+1}{k-1}}}\right] \tag{5}$$

Using the assumptions and data outlined previously

$$Q = 1.045 \times 10^7\ h_p \tag{6}$$

The orifice flow ceases, and turbulent channel flow commences at a height h_p of approximately 6×10^3 microinches (Figure XI-2-15). The land width is 0.060 inch giving an L/h_p ratio of 10 as the breaking point.

Turbulent Channel Flow

Flow in this regime is defined by a curve on log-log paper. A sample calculation of one point will illustrate the method used. Leakage is computed for a stroke height h_p of 0.001 inch using the following steps:

(1) Hydraulic diameter, $D = 2h_p = 0.002$ inch

(2) A friction coefficient (f) is estimated at 0.040. This is the starting point for the trial and error solution; (f) will be verified at the conclusion of this computation.

(3) Compute $fL/D = 1.20$

(4) Compute the entrance Mach number, M, from the following equation:

$$\frac{fL}{D} = \frac{1 - M^2}{kM} + \frac{k+1}{2k} \ln \frac{(k+1)\, M^2}{2\left(1 + \frac{k-1}{2} M^2\right)} \tag{7}$$

where

$fL/D = 1.20$, entrance Mach number

$M = 0.49$

(5) Assuming an isentropic entrance condition, the entrance static pressure, P_1, can be computed from Equation (8) where P_o is the stagnation (total) pressure of 114.7 psia, and M is the entrance Mach number:

$$\frac{P_o}{P_1} = \left(1 + \frac{k-1}{2} M^2\right)^{\frac{k}{k-1}} \tag{8}$$

Therefore, static pressure, P = 97.3 psia.

(6) Again, assuming isentropic conditions, the entrance static temperature, T_1 is computed from Equation (9) for a total temperature T_o of 530°R.

$$\frac{T_o}{T_1} = 1 + \frac{k-1}{2} M^2 \tag{9}$$

Therefore, static temperature $T_1 = 506^{\circ}R$.

(7) The following series of equations are used to compute the flow, Q, in the channel:

$$\left.\begin{aligned} V_1 &= M\sqrt{kg\ RT_1} \\ \rho_1 &= \frac{P_1}{RT_1} \\ A &= Wh_p \\ \omega &= \rho_1 AV_1 \\ Q &= \omega \frac{RT_s}{P_s} \end{aligned}\right\} \qquad (10)$$

from which the flow, Q = 7960 scim

(8) To prove the flow computation, the originally estimated friction coefficient, f, is checked. The Reynolds number is first computed:

$$R_e = \frac{DV_1\rho_1}{\mu} = 3.95 \times 10^3 \qquad (11)$$

Using the computed value for Reynolds number, a friction coefficient is determined from the Moody diagram. The friction coefficient determined from this curve is 0.0395, and is close enough to the original estimate of 0.040 so that a recomputation is not necessary.

The curve plotted from this and other data points is shown as a dashed line in Figure XI-2-15. This flow regime extends into the initial portion of laminar flow, i.e., R_e below 2000 where fluid momentum is still an important consideration.

Laminar Flow

Laminar flow for nitrogen gas is computed from the Poiseuille equation

in the following form:

$$Q = \frac{RT_s}{P_s} \left[\frac{Wh_p^{\,3} (P_1^{\,2} - P_2^{\,2})}{24 \mu L RT} \right] \qquad (12)$$

Using the assumptions and data outlined:

$$Q = 4.08 \times 10^{13} h_p^{\,3}$$

This flow regime continues until molecular flow can be detected and the transition flow (laminar + molecular) begins.

Transition and Molecular Flow

The equation used to compute leakage in the molecular regime is as follows:

$$Q = \frac{RT_s}{P_s} \left[\frac{4}{3} \sqrt{\frac{2}{\pi}} \; \frac{Wh_p^{\,2} (P_1 - P_2)}{L \sqrt{RT/g}} \right] \qquad (13)$$

Using the assumptions and data outlined:

$$Q = 2.49 \times 10^{8} h_p^{\,2}$$

This flow regime is plotted on the lower right of Figure XI-2-15. The dashed line connecting the laminar and molecular flow regimes is simply the sum of the two leakage values. Therefore, the transition equation is:

$$Q_{Transition} = Q_{Laminar} + Q_{Molecular} \qquad (14)$$

The boundaries of this transition regime are defined by the following limits.

$$\bar{\lambda}/h = 0.01 \text{ to } 1.0\ h_p$$

The molecular mean free path, λ', is 3.61 microinches for nitrogen at standard conditions (70°F and 14.7 psia). For a mean pressure of 50 psig, $\bar{\lambda}' = 0.82$ microinch.

The corresponding height limitation of the transition regime is between 0.82 and 82 microinches (Figure XI-2-15).

Interface Loads and Leakage

The resultant of all forces acting on the seated control element produce contact stresses acting at the interface. To show how leakage can be calculated for given contact loads, the poppet valve and conditions of sealing given on pages XI-2.1 to XI-2.11 are employed. The poppet material is assumed to be 6061-T6Al aluminum and the seat material is steel and substantially harder. Additionally, it is assumed that the surfaces are lapped to a surface finish of 5 microinch (PTV). When these surfaces are mated together with zero net contact load, the leakage rate is approximately given as 6×10^{-3} in^3/min (STP) in Figure XI-2-15.

Next assume that loads equivalent to contact stresses of 1,000, 10,000, and 50,000 psia are applied to the interface. The actual loads per inch of interface circumference are given:

$$F = \sigma (0.060) \tag{15}$$

where

$L = 0.060$

σ = apparent contact stress

F = net load per inch of interface circumference. This is the sum of all forces acting on the control element.

σ (psi)	F(lb/in)
1,000	60
10,000	600
50,000	3,000

The properties of 6061-T6Al are given in Section VIII.

Meyer hardness = 159,000 psi = σ_m

Meyer Index = 2.00 = n'

Following the procedures outlined in Section X-2, the modified stress ratio and values for three different loads are tabulated below.

F(lb/in)	Modified Stress Ratio = $\frac{P^{2/n'}}{A_A/\sigma_m}$
60	0.0063
600	0.063
3,000	0.314

From Figure X-2-18, Section X-2, the conductance parameter, and equivalent clearance for lapped and polished surfaces is given and tabulated below.

F(lb/in)	h^3 (inch^3)	$h \approx h_{in}$
60	6×10^{-18}	1.8×10^{-6}
600	4×10^{-20}	7.4×10^{-7}
3000	10^{-22}	2.2×10^{-7}

Again referring to Figure XI-2-15, the approximate leakage rates are given and tabulated below.

F(lb/in)	Nitrogen Leakage (in^3/min (STP))	Nitrogen Leakage (cc/sec (STP))
0	6×10^{-3}	1.6×10^{-3}
60	7×10^{-4}	1.9×10^{-3}
600	1×10^{-4}	2.7×10^{-5}
3000	1×10^{-5}	2.7×10^{-6}

The preceding results show the sensitivity of seating loads on leakage. If leakage rates at higher pressures are encountered, a close approximation can be obtained by applying the pressure squared relationship. For example, the nitrogen leakage rate at 1,000 psi is approximately 100 times greater than at 100 psi. It can be seen that even large loads such as 3000 lb/in of interface circumference are necessary to provide leakage rates of $\sim 3 \times 10^{-3}$ cc/sec (STP) at 1,000 psi.

XI-3 FACTORS INFLUENCING VALVE DESIGN AND SELECTION

Introduction

The following discussion enumerates various factors influencing the design and selection of valves for use in pressurized gas systems. The characteristics presented are common to the valves considered in this guidebook but are specifically directed towards poppet type valves and in particular, start valves.

Six methods of relating the various resistance parameters and the flow capacity of any given valve configuration are presented. The resulting flow coefficients serve the important function of providing comparison factors for the evaluation of different valve geometries under similar flow conditions. Other factors affecting the selection and the design of valves, i.e., fluid effects, poppet stroke, sealing and control element, configuration, contamination, actuation methods, response time, pressure effects and valve housing, are discussed briefly.

Fluid Effects

Compatibility of the fluid with materials of valve construction is one of the foremost considerations in valve selection. In some cases a certain amount of material degradation can be tolerated provided that it does not contribute to contamination of the fluid, or malfunction of the valve. This applies only to non-critical areas and not the important critical area in the sealing element. The sealing element should be completely impervious to the fluid media.

The state of the fluid, liquid or gas, influences the size of the flow passageways and imposes different requirements on the seal element design. High velocity gas flow can cause seal damage by erosion.

Often fluids other than the principal fluid are employed during cleaning or evaluation tests. Careful selection of these fluids is required to prevent degrading effects and should be purged immediately after use.

Pressure Drop and Flow Capacity

The flow capacity of a valve is a predetermined rate of fluid flow which must pass through the valve with a given loss in energy. Pressure drop is a measure of the energy loss due to the resistance to flow within the valve. The resistance to flow is produced by the size, shape, roughness and length of the flow passageway within the valve. Additionally, resistance to flow is produced within the fluid itself, attributed to shear stresses, and related to the viscosity of the fluid. Hence, the flow capacity, pressure drop and resistance to flow are all interrelated.

Six methods of relating these parameters together have been developed yielding a coefficient or an equivalent orifice area and are presented below. The purpose of each method is to arrive at a single descriptor for the flow resistance of a valve.

(1) Discharge coefficient, C_D, which is an adaptation of the sharp edged orifice equation for imcompressible flow.

$$Q = C_D A_o \sqrt{\frac{2g\Delta p}{\gamma}}$$

where

Q = volumetric flowrate

C_D = discharge coefficient

A_o = throat or minimum flow area

g = gravitational constant

Δp = pressure drop across the valve

γ = specific weight of the fluid

The application of this expression requires the insertion of experimental flow data and the discharge coefficient is calculated. This coefficient reduces the total losses in a valve to that of an equivalent orifice area.

(2) A flow coefficient, C_v, which is an experimentally determined measure of the volumetric flowrate in gallons per minute of water that will flow through a valve with a pressure drop, Δp, of 1 psi across the valve.

$$Q = C_v \sqrt{\frac{\Delta p}{s}}$$

where

s = specific gravity of the liquid

(3) Equivalent orifice area, A_o. In this case a discharge coefficient C_D is assumed and the relationship between variables is the same as Method (1).

$$Q = C_D A_o \sqrt{\frac{2g\Delta p}{\gamma}}$$

A discharge coefficient value of 0.60 is often assumed and is based upon a typical value for a sharp edged orifice.

(4) A resistance coefficient, K, which relates the pressure drop to the velocity head.

$$\Delta p = K \gamma \frac{V^2}{2g}$$

where

V = fluid velocity based on some nominal flow path area within the valve. The inlet or exhaust port areas are usual choices.

When the port areas are selected, the coefficient K can be related to an equivalent length of pipe or tubing by the relationship:

$$\Delta p = f \frac{L}{D} \gamma \frac{V^2}{2g}$$

where

f = Darcy friction factor for pipe flow
L = equivalent pipe length

(5) National Bureau of Standards flow factor, F, a measure of gas flow through valves and orifices defined as the ratio of air flow in standard cubic feet per minute to the upstream pressure in psia when

$$P_2/P_1 = 0.5 \quad \text{or}$$

$$F = \frac{Q(max)}{P_1}$$

F = flow factor SCFM/psia

Q(max) = air flow in SCFM e $P_2/P_1 = 0.5$

P_1 = upstream pressure

P_2 = downstream pressure

(6) A discharge coefficient C_w based on the assumption of unchoked isentropic flow where the mass rate of flow is given:

$$W_t = A_o \sqrt{\frac{2gk}{k-1} p_1 \gamma_1 \left(\frac{P_2}{P_1}\right)^{2/k} \left[1 - \left(\frac{P_2}{P_1}\right)^{\frac{k-1}{k}}\right]}.$$

and the overall discharge coefficient is defined as:

$$C_w = \frac{W_a}{W_t}$$

where

W_t = theoretical isentropic weight of flow

W_a = actual weight rate of flow

k = ratio of specific heats

When the flow becomes choked, the theoretical flow-rate is given:

$$W_t = A_o \sqrt{kg \left(\frac{2}{k+1}\right)^{\frac{k+1}{p-1}} p_1 \gamma_1}$$

Additional details on each of the preceding methods are described in Reference 6. Each of the preceding methods of relating variables possess limitations from the standpoint of useful criteria for valve selection. Even the relationships for incompressible flow yield coefficients which are dependent upon Reynolds number. The compressible relationships are further influenced by Mach number and not easily defined contraction and expansion losses.

Although much has been done to standardize flow tests and incorporate correction coefficients, a problem of test procedures still exists. These problems are associated with the location and type of pressure measuring taps and size of connections leading to and from the valve. The recommended criteria for valve selection should be based on actual experimental data in the graphical form of Δp versus Q for incompressible flow or

$$\frac{W_a}{P_1}\sqrt{\frac{2gkRT_1}{k-1}} \quad \text{versus} \quad \frac{P_2}{P_1} \text{ for compressible flow}$$

where

R = gas constant

P_1 = upstream stagnation pressure

T_1 = upstream stagnation temperature

The preceding experimental data permits the designer to evaluate a valve design under other possible flow conditions particularly when a gas other than the operational gas is used in the performance evaluation test.

The various flow coefficients, however, do have an important function in that they can serve as comparison factors between specific valve geometries when evaluated under similar circumstances. Preferably, these circumstances should be limited to incompressible flow. A typical comparative relationship is shown in Figure XI-3-1 where C_v is related to valve size and valve configuration.

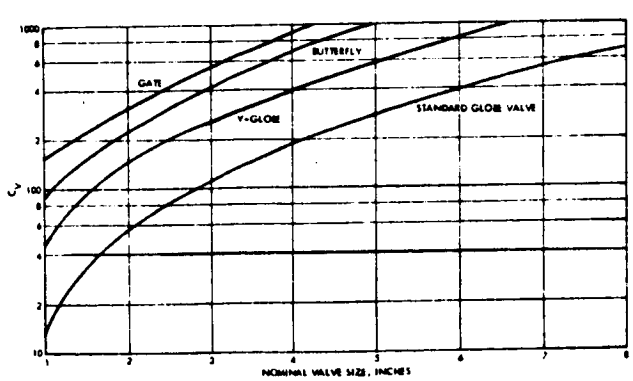

Fig. XI-3-1 Approximate Values of C_v Versus Valve Diameter (Ref. 6)

From a valve design standpoint, the prediction of pressure drop or energy loss characteristics in a valve is difficult. Some theoretical attempts can be made by assuming orifice shapes, changes in section, etc.; however, the results usually yield a poor approximation. Thus, the designer must often be guided by past experimental performance and by the application of scaling relationships can often improve the performance prediction.

In general, when minimum energy losses or maximum flow capacity are required in a particular valve, the valve should possess a full-open flow path from inlet to outlet without any change in direction of flow with minimum wall roughness and change in shape. Some valves such as the ball, rotary plug, gate and blade valves inherently possesses these characteristics. Other valves whose configuration make the preceding requirements impossible should have a minimum of changes in direction of the flow and gradual changes in flow passage areas.

The two principal factors influencing the resistance to flow can be specifically identified as the shape of the control element, the size of the sealing element, and the relative displacement of the control to sealing element.

Poppet Stroke

The maximum flow capacity of a valve may be determined by the seal diameter or the distance the poppet moves from the seat. In the latter case, the configuration of the control element and seat determine the general flow characteristics of the valve. As the poppet moves off its seat, flow characteristics of various types can be obtained by varying the minimum flow area-stroke relationships. Common flow characteristics are linear, modified linear, equal percentage, and square root. Figure XI-3-2 shows typical characteristics which can be obtained. In general, almost any characteristic shape can be obtained above the square root or quick-opening configuration. It should be noted that the preceding stroke area modifications can be introduced into other control element configurations.

Quick opening characteristics can be obtained with flat poppets while other characteristics can be achieved with various types of conical poppets.

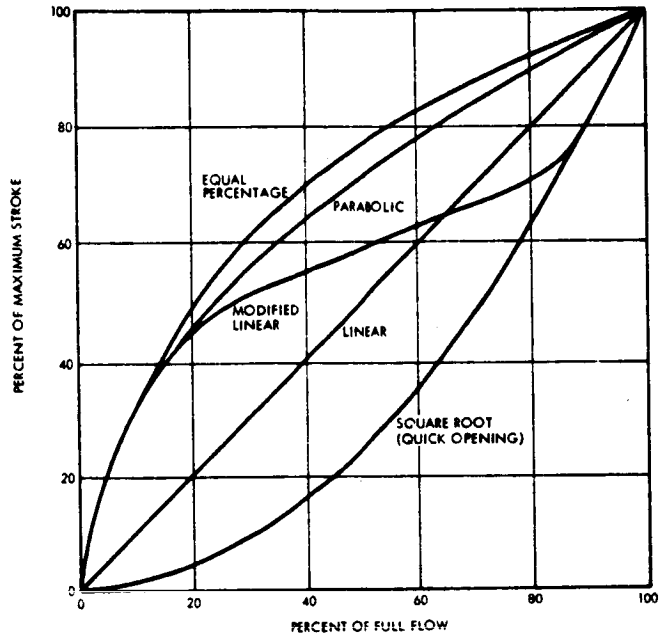

Fig. XI-3-2 A Comparison of Control Valve Flow Characteristics (Ref. 6)

Figure XI-3-3 represents the stroke to orifice diameter ratio for a conical poppet at various cone angles. The curve is valid if a perpendicular line can be drawn from the poppet cone to and intersecting the outer edge of the seat contact face. As the cone half angle θ is increased, the stroke required to form the effective orifice area is reduced. However, for half angles above 45°, small reductions in stroke per degree increase of poppet angle is evident. The limiting maximum is 90° (flat poppet) where the stroke is equal to 25% of the seat hole diameter. For this condition, the seat usually consists of a thin raised shoulder which increases the turning losses during flow. For metal-to-metal contact seats and poppets, surfaces must be lapped for a low leakage fit. In general, it is more difficult to lap surfaces with the very low cone angles. Solenoids exhibit a characteristic decreasing of actuating force with increasing stroke. As cone half angle is decreased, solenoid design may become critical, particularly for direct action solenoid valves.

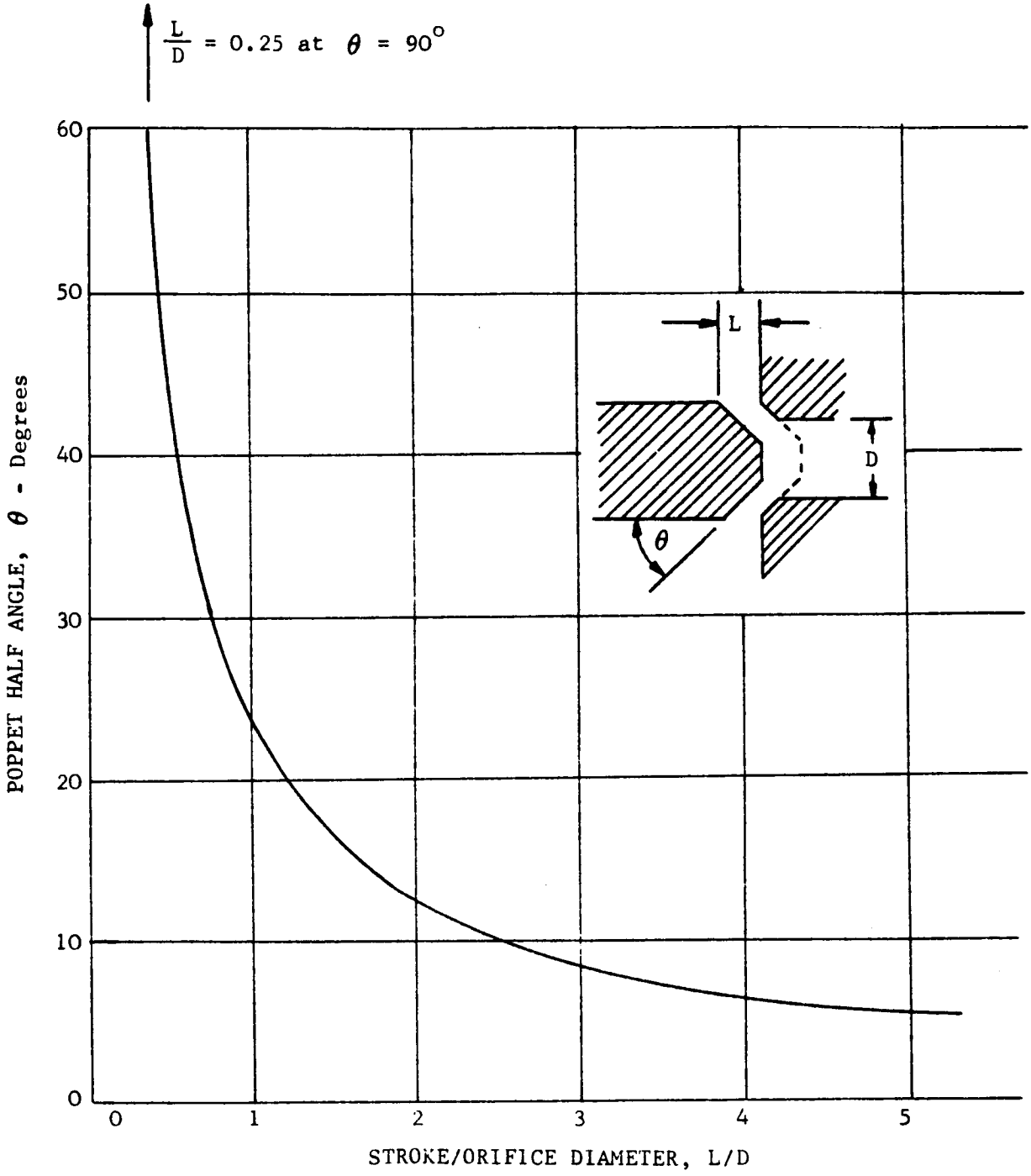

Figure XI-3-3 Conical Poppet Stroke Relation for Various Half Angles (Ref. 3)

Furthermore, there is a tendency to "wedge" on closing when a shallow half angle is used. For these reasons, conical poppets of half angles from 30 to 45° are often preferred.

The flat ($\theta = 90^{\circ}$) poppet requires minimum stroke. When a spherical poppet surface is used, the stroke is dependent on the spherical radius and the seat bore diameter. Normally, the stroke requirement is less than that of the 45° half angle conical poppet and the stroke is decreased as the spherical radius is increased.

Sealing and Control Element Configuration

Recognizing that pressurization systems for most spacecraft applications require small valves, the present discussion is limited to the poppet design. The actual poppet configurations can be a multitude of shapes for any particular application. Each design has its advantages and disadvantages in leakage control, manufacturing, and flow performance. Table XI-3-1 lists the primary elements shown in Figure XI-3-4 and relates the configuration defining variables to common combinations of seats and poppets.

The sealing reliability of poppets and seats has resulted in the use of this control element in some of the most demanding applications where no other valve has proven satisfactory. The effectiveness, however, is dependent upon the seat and poppet configuration and the materials forming the sealing element. To proceed objectively in discussing the merits of each configuration, the materials of seat construction must form the basic consideration. The general guidelines for minimum leakage material selection were stated in order of preference in Section XI-2, as elastomers, plastics and metals. In each poppet configuration the combination of possible materials is as follows.

(1) Hard poppet on soft seat
(2) Soft poppet on hard seat
(3) Hard poppet on hard seat
(4) Soft poppet on soft seat

Table XI-3-1

COMMON POPPET CONFIGURATIONS (Ref. 6)

POPPET / SEAT	FLAT 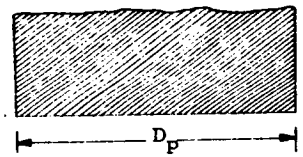	FLAT WITH RAISED SEAL LAND 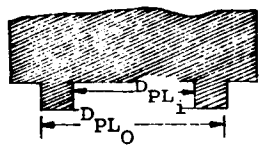	CONICAL 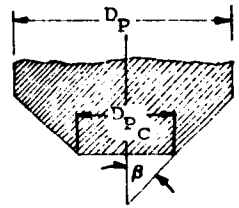	SPHERICAL 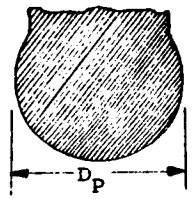
FLAT 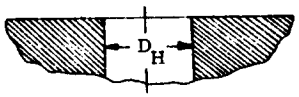	$D_P > D_H$	$D_{P_{L_i}} > D_H$	$D_{P_C} < D_H < D_P$	$D_P > D_H$
FLAT WITH RAISED SEAL LAND 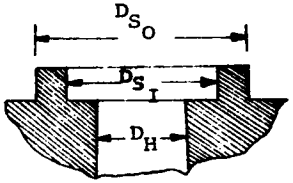	$D_P \geq D_{S_O}$	SELDOM USED $D_{PL_O} \approx D_{S_O}$ $D_{PL_i} \approx D_{S_i}$	NOT USED	NOT USED
CONICAL 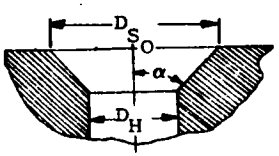	SELDOM USED $D_P > D_{S_O}$	SELDOM USED $D_{P_{L_i}} > D_{S_O}$	$D_P > D_H$ USUALLY $\alpha \geq \beta$ SELDOM $\alpha < \beta$	USUALLY $D_H \cos^{-1} < \alpha D_P < D_{S_O}$ SELDOM $D_P > D_{S_O}$ SELDOM $D_H < D_P < D_H \cos_\alpha^{-1}$
SPHERICAL - INTERNAL 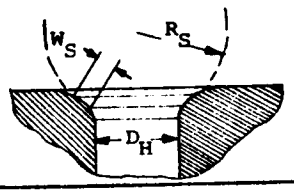	NOT USED	NOT USED	NOT USED	$D_P = 2R_S$
SPHERICAL - EXTERNAL 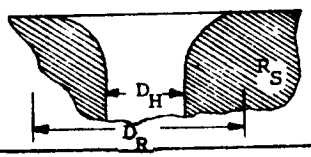	SELDOM USED $D_P > D_R$	SELDOM USED $D_{P_{L_i}} > D_R$	$D_P > D_H$	$D_H < D_P < D_R$

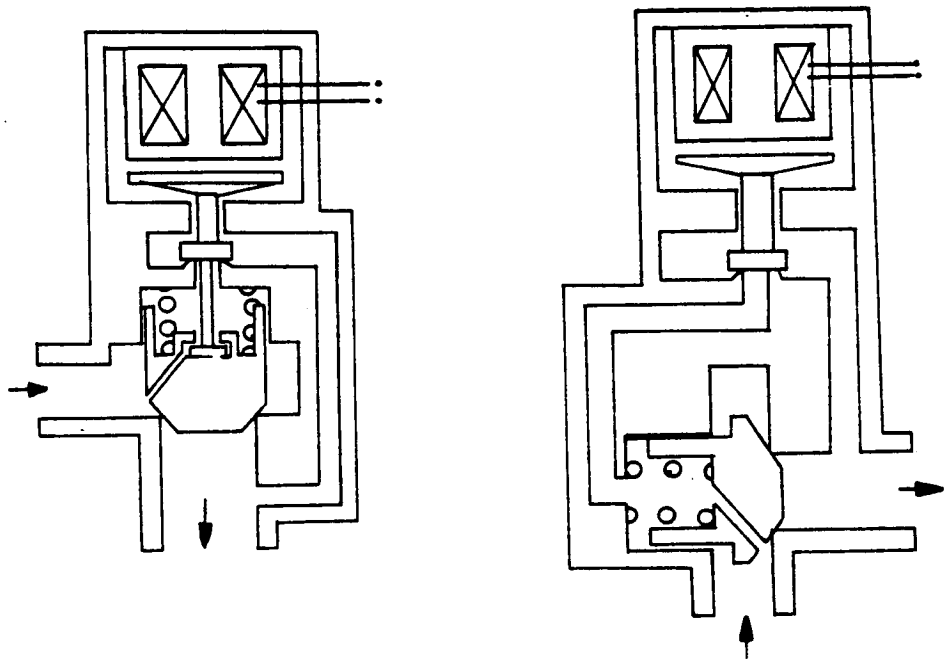

Fig. XI-3-4 Typical Pilot Operated Valves (Ref. 9)

The choice of material selection can be narrowed by relegating soft-on-soft and soft-on-hard seats to low pressure and flow applications. At higher pressures composite seals are usually employed consisting of metal-to-metal seat contact combined with the soft material serving as the actual sealing element. The most common method of sealing is a hard poppet mated against a soft seat. Among the materials used for soft seats or poppets are Teflon, Kel-F, Nylon, Mylar and elastomers such as Buna N, Viton, and Silicone. Figures XI-3-5, XI-3-6, XI-3-7 and XI-3-8 show typical applications of soft seats in flat, conical and spherical hard poppet designs. These were obtained from Rocketdyne, Reference 5.

It is interesting to note that the soft sealing element can be placed in either the seat or the poppet. However, it is much easier to produce fine finish metallic sealing surfaces on a removable part such as the poppet rather than deep within the valve housing.

Pitfalls which must be guarded against when designing for soft seals include seal blow out and cold flow. Elastomeric seals exposed to high velocity gas flow are particularly susceptible to blow out. Minimizing

exposure of the seal to the fluid stream aids in avoiding this problem. Cold flow is minimized by confining the seal particularly in the loaded condition.

The recent use of highly reactive rocket propellants such as fluorine, and requirements for controlling the flow of hot gases have resulted in increased interest in the metal-to-metal seat poppet valves for aerospace applications. Typical of the hard materials used for seats and poppets are 440C stainless steel, stellites, and carbides. Hard metal seats and poppets have been used in aircraft hydraulic systems for many years, but usually with relatively high permissible leak rates of comparatively viscous hydraulic fluid. Four applications of metal to metal seats and poppets are shown in Figures XI-3-9, XI-3-10, XI-3-11, and XI-3-12 (Reference 5). To date hard-to-hard seat-poppet combinations have been limited to relatively small sizes largely because of difficulty in meeting stringent leakage requirements. The most promising seat-poppet configuration is the flat plate or disc mated against a flat seat surface. (This configuration is suggested because the interface surfaces can be finished to produce a roughness and waviness of less than 1 microinch and easily inspected). The degree of finish is well below that achievable on cylindrical, spherical, or conical surfaces. These surfaces however, are susceptible to contaminants and ice formation.

It is preferable to have minimum shift in the elemental contact of any valve sealing element. This rotational restraint is necessary to provide the proper alignment of the mating surfaces and a continuous contact of the same sealing areas. A metal bellows can be used to provide this function. On the other hand, the sealing element can also be completely self aligning as demonstrated in the flexure support, solenoid valve shown in Figure XI-3-13.

Contamination

Since no system is completely free of particulate contamination, valves themselves being contamination generators, sensitivity of a valving element to contamination is an important consideration in valve design. Contamination can lodge between the seal faces, thus (1) creating a leak

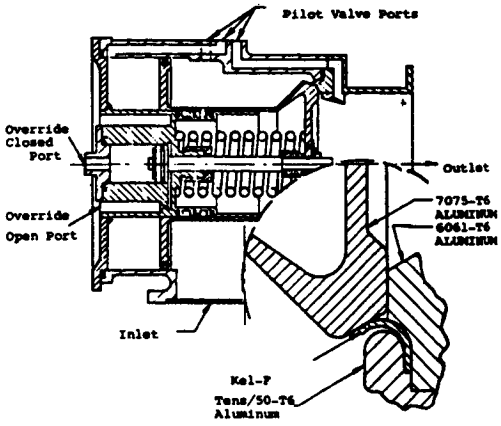

Key Parameters

Valve Type: Main Valve, Pilot Operated Vent and Pressure Relief Valve
Flow Media: Air, Nitrogen, Helium, Liquid Oxygen
Operating Pressure: Adjustable 30 To 60 psig
Operating Temperature: -300°To +160 °F
Leakage: 200 SCIM Max Helium At -290°F
Size: 4-Inch Line
Life: 5000 Cycles at 68 psig and -250°F
Vibration: 10 G To 500 cps

Fig. XI-3-5 Conical Poppet Seat Design, Tank Vent Valve, Rocketdyne

This design illustrates the pressure-loaded plastic lip seal used in the main valve of a pilot actuated vent and relief valve.

Development of this poppet seal took place during a state-of-the-art improvement program* for extreme environment components. No major problems were encountered.

The success of this seal is directly attributable to its flexibility and deformation control fabrication provided by the positive stop design. However, seal fabrication does require the use of hot forming techniques and special dies. Close control of the poppet and seal surface finish is required.

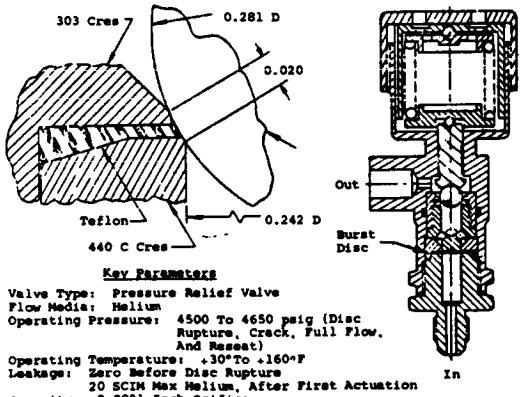

Key Parameters

Valve Type: Pressure Relief Valve
Flow Media: Helium
Operating Pressure: 4500 To 4650 psig (Disc Rupture, Crack, Full Flow, And Reseat)
Operating Temperature: +30°To +160°F
Leakage: Zero Before Disc Rupture
20 SCIM Max Helium, After First Actuation
Capacity: 0.0021 Inch Orifice
Life: 1000 Cycles
Tube Size: 1/4 Inch

Fig. XI-3-7 Spherical Poppet Seat Design, High-Pressure Relief Valve, Aqualite Corp.

This Valve was designed and developed to operate as a thermal relief valve for the main helium supply tank of a space vehicle. The use of Teflon burst disc guarantees extremely low leakage prior to the initial activation. (Burst and flow are both accomplished in the piston annulus.) Disc rupture, cracking, full flow and reseat to 20 scim helium leakage is maintained within 3.3%. Unique in the design is the combination Teflon-metal seat which affords low leakage. Accuracy is maintained by almost complete freedom form friction and bind through the use of ball joints.

While this component has proved its capability as a relief valve, the burst disc function has not been thoroughly demonstrated. Annular width, Teflon thickness, edge radius, installation and temperature change all cause variation in burst pressure. A statistical test program is required to ensure design feasibility.

*AFBMD-TR-60-55, "Design, Development, and Testing of Advanced Liquid Oxygen Tank Vent and Relief Valve, Part No. 551430", North American Aviation Inc., March 1960.

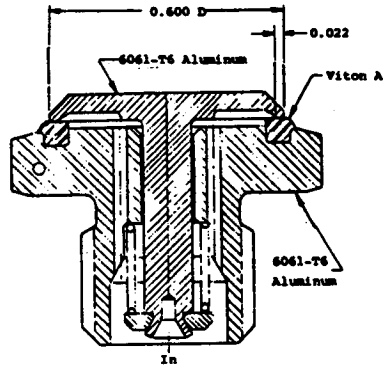

Key Parameters

Valve Type: Check Valve
Flow Media: Air, Nitrogen, Helium, Oxygen or RP-1 Fuel Vapors
Operating Pressure: 0 To 1000 psig
Cracking Pressure: 3 To 5 psig
Full Open Pressure: 10 psig
Operating Temperature: -320°To +160°F
Leakage: Measured in Free Flow Direction At 0.5 psig
-320°F: 10 SCIM Max Helium
-65°To +160°F: Zero Bubble Leakage For 3 Minutes
Capacity: 0.60 Inch Orifice
Life: 10,000 Cycles
Vibration: 25 G To 2000 cps
Tube Size: 1/4 Inch

Fig. XI-3-6 Flat Poppet Seat Design, Vent Port Check Valve, Rocketdyne

This component represents a series of valves designed to protect the internal portion of components (which require a vent to atmosphere) against the entrance of moisture or contaminants. The large external seat configuration ensures the maintenance of a low cracking pressure in the event of ice formation over the valve. The flat-lapped molded Viton A rubber seat construction results in an excellent seal throughout a wide range of temperatures and conditions.

After considerable service experience it was found that following several days storage the Viton rubber would cling to the poppet causing a substantial increase in cracking pressure. This problem was solved by the application of a nonremovable dry film lubricant to the rubber.

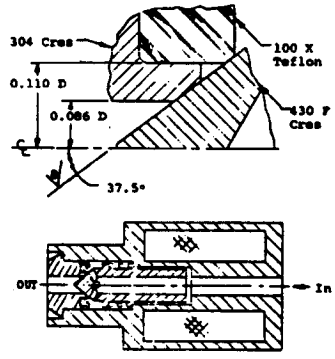

Key Parameters

Valve Type: 2-Way Direct Operated Solenoid Valve, 28vdc
Flow Media: Nitrogen,Tetroxide, UDMH, Hydrazine
Operating Pressure: 325 psig
Operating Temperature: -65°To +160°F
Leakage: 0.02 SCCM Max GN$_2$
Capacity: 0.06 Inch Orifice
Response: 90 cps At 24 vdc
Life: 10,000 Cycles
Tube Size: 1/4 Inch

Fig. XI-3-8 Conical Poppet Seat Design, Propellant Control Solenoid Valve I, Rocketdyne

This valve must maintain an effective seal of chemically active rocket engine propellants. A controled stress "soft" seat is obtained by utilizing a plastic seal in combination with a centering metal stop. While enhancing the probability of a tight seal, the seat design necessitates a larger solenoid due to additional unbalance pressure area between the sealing surface and the metal-to-metal stop. The major problem encountered with the design is the tendency of the plastic seal to take a permanent set (cold flow) while operating near maximum material operating temperatures.

ORIGINAL PAGE IS
OF POOR QUALITY

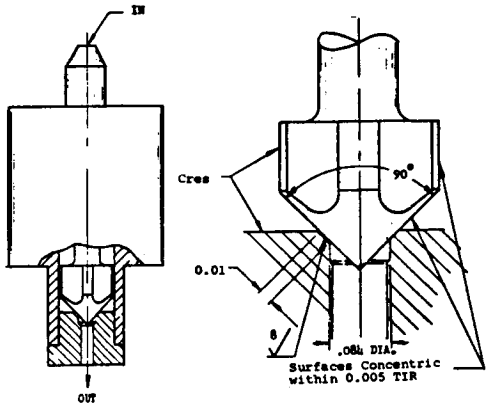

Key Parameters

Valve Type: 2-Way Direct Operated Solenoid Valve, 28 vdc
Flow Media: Nitrogen Tetroxide, UDMH, Hydrazine
Operating Pressure: 300 psia
Operating Temperature: -65° to +165 °F
Leakage: 1.0 SCC/hr Max Nitrogen at 200 psig
Capacity: 0.07 Inch Orifice
Life: 80,000 Cycles Water at 70°F and 200 psi

Fig. XI-3-9 Conical Poppet Design-Propellant Control Solenoid Valve II, Honeywell

The conical closure shown illustrates a simple approach to design an economical, fast-response, hypergolic propellant valve. While this design does not match the performance capabilities of the spherically seated valve, careful attention to finish concentricity and normality result in an endurance life and leakage level suitable to many applications.

The primary disadvantages of this design are the close match lapping and poppet to seat alignment necessary to obtain suitable leakage-life characteristics. Additionally, fine (10 micron) filtration of fluid contaminants is necessary.

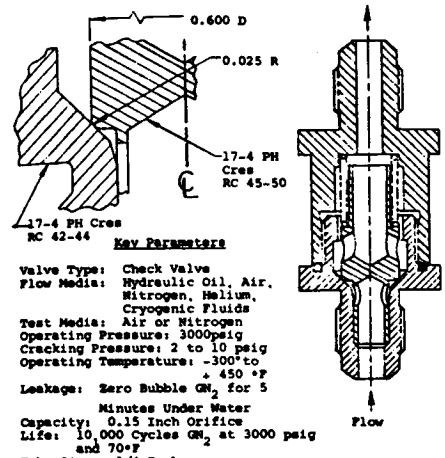

Key Parameters

Valve Type: Check Valve
Flow Media: Hydraulic Oil, Air, Nitrogen, Helium, Cryogenic Fluids
Test Media: Air or Nitrogen
Operating Pressure: 3000psig
Cracking Pressure: 2 to 10 psig
Operating Temperature: -300° to + 450 °F
Leakage: Zero Bubble GN_2 for 5 Minutes Under Water
Capacity: 0.15 Inch Orifice
Life: 10,000 Cycles GN_2 at 3000 psig and 70°F
Tube Size: 1/4 Inch

Fig. XI-3-10 Conical Poppet Seat Design, Randall Engineering Corp.

This all metal check valve is designed for high endurance and low leakage rates with multiple fluids, over a wide temperature range. The metal-to-metal closure seal is provided by seating a radiused corner of the poppet on a conical seat. A 16 microinch finish is ground on the poppet and seat preliminary to match lapping.

Utilization of the inlet port to guide the poppet reduces the size and weight of the unit, but provides a broken flow pattern with the associated additional pressure drop.

Modifications of the design shown have utilized stellite on the seating surfaces for ultra-high endurance (100,000 cycles) and a Teflon-coated (0.002 inch) poppet for cryogenic service.

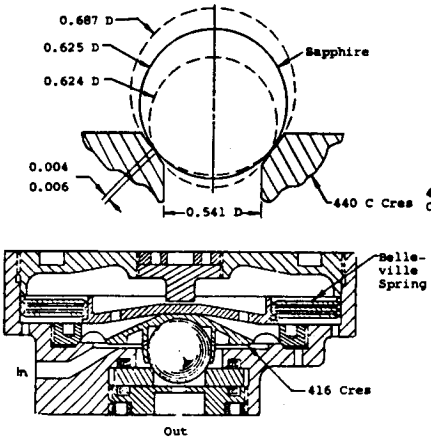

Key Parameters

Valve Type: Pressure Relief Valve
Flow Media: Air, Nitrogen, Helium
Cracking Pressure: 50 to 100 psig
Full Flow Pressure: Within + 2.5% Cracking Pressure
Reseat Pressure: Not Less Than 94% of Cracking Pressure
Operating Temperature: -450°To +300°F
Leakage: 5SCCM Max Helium
Capacity: 0.12 Orifice
Response: 5 Milliseconds
Life: 50,000 Cycles
Vibration: 65 To 2000 cps

Fig. XI-3-11 Spherical Poppet Seat Design, Snap Action Relief Valve, Frebank Co.

This snap action pressure relief valve employs a pressure sensing diaphragm and the inherent instability of a Belleville spring to actuate the poppet at a set cracking pressure. The design was the subject of considerable development effort under a state-of-the-art improvement program[*] A sapphire-to-metal poppet and seat was selected to provide positive stroke control for operation of the Belleville springs in the negative rate region, maintain material compatibility with storable propellants, and improve the vibration characteristics by decreasing the weight of the poppet. The spherical ball seats on a narrow land width seat to provide a low leakage rate with relatively low seat loads and to closely control the effective diameter of the seating surface.

The horizontal deflection of the metal diaphragm is unpredictable when the poppet and diaphragm are assembled in the body, with the resultant inconsistent concentricity of the poppet to the seat for each assembly.

Notable in the development of the valve was the attempt to eliminate the problem by guiding the poppet onto the seat. The perpendicular spring force of the installed diaphragm was sufficient to cause galling of the guide. The addition of dry film lubricants did not eliminate the problem.

Due to the above problem the valve must be repetitously assembled and tested to obtain an assembly that meets the delineated requirements.

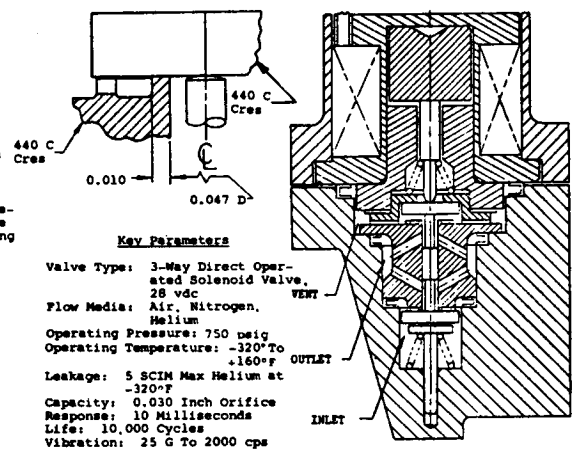

Key Parameters

Valve Type: 3-Way Direct Operated Solenoid Valve, 28 vdc
Flow Media: Air, Nitrogen, Helium
Operating Pressure: 750 psig
Operating Temperature: -320°To +160°F
Leakage: 5 SCIM Max Helium at -320°F
Capacity: 0.030 Inch Orifice
Response: 10 Milliseconds
Life: 10,000 Cycles
Vibration: 25 G To 2000 cps

Fig. XI-3-12 Flat Poppet Seat Design, Randall Engineering Corp.

Metal-to-metal flat poppets and seats are used in this design to obtain low leakage over a wide range of temperatures. The combination of size and operating pressure economically allows an unbalance design which eliminates the need for dynamic seals and external bleed.

The poppet discs and seats are lapped extremely flat (less than 1 light band) to obtain bubble-tight leakage of helium at room temperature. The proved cycle life is due to the extreme hardness of the seat materials in addition to the outer seat land used to facilitate lapping and uniform application of seating load (or stress).

[*] AFBSD-TR-61-71, "Design Development and Testing of Non-Modulation Pressure Control Valves", Frebank Company, December, 1961.

ORIGINAL PAGE IS OF POOR QUALITY

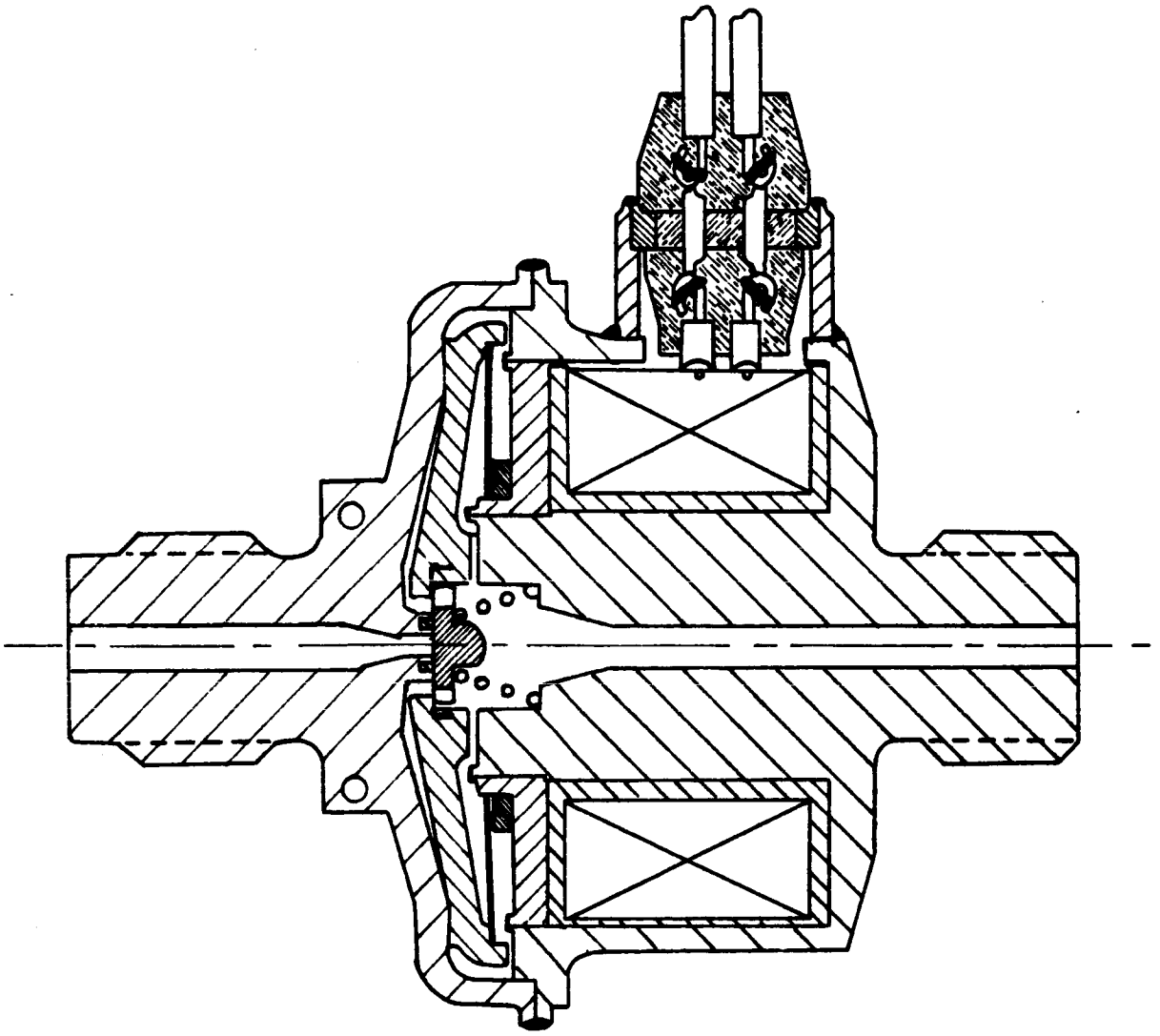

Fig. XI-3-13 Self Aligning Bi Polar Solenoid Valve, (Courtesy Parker Aircraft Company, Drawing 92003)

path (although the particles may be crushed in the interfaces, they may deform the valve seat as it is mated with the valving element) and (2) depending upon the size and hardness of the contaminant, may permanently scratch or deform the valving element or seat, reducing the valve's further usefulness as a sealing device. The damage susceptibility of hard seats to particulate contamination is acknowledged by most valve manufacturers and is cause for concern. Where pressure drop limitations permit, many manufacturers of small valves incorporate filters at the inlet port to screen out particulate matter. Others tend to de-emphasize the contamination problem by claiming the probability of a particle of sufficient size to cause failure by lodging itself on a seat land at the time of closure is low. Narrow seats may minimize contamination probability and increase crushing stresses on those particles which are trapped. On the other hand, wide seats minimize the effect of pits in the seat or poppet faces resulting from contamination or corrosion. The damage susceptibility of soft seats or seals depends greatly on the resiliency of the nonmetal used. With elastomeric seal materials, the contaminant can be pressed locally into the valve seat during closure without plastically deforming the seal. However, a continual subjection to such treatment may cause seat fretting and feathering. If the nonmetallic seat is relatively hard the size of the contaminant which can be impressed is diminished, and at the same time the material may become scratched or nicked, creating a leak path.

The formation of ice on the valving unit surfaces of cryogenic valves may be treated as a form of contamination. Such ice formations have been the source of numerous problems with practically all types of cryogenic propellant valves, including:

(1) Interference and adhesive action at the valve seat which prevents valve opening, especially with butterfly valving units

(2) Ice formation on the seat or valving element while the valve is open, preventing seating when valve is closed

(3) Damage to lip or other soft seals when the seal slides over ice formed on the valve body or valving element, especially in sleeve valve designs.

Actuation Methods

The most common method of pressurization system valve actuation is the use of the solenoid although manual override features may be employed. The forces which must be overcome by the solenoid have been described in Section XI-2. These forces were attributed to pressure, flow, and frictional forces. The factors defining the static forces acting on the poppet in the closed position include:

(1) Seat land diameter and width
(2) Pressure differential across valve
(3) External force either seating the poppet or tending to open it

The forces acting on a poppet after lifting off the seat are somewhat more complex and depend upon:

(1) Poppet configuration
(2) Seat configuration
(3) Housing configuration in immediate vicinity
(4) Seat land width
(5) Pressure differential across valve (magnitude and direction)
(6) Fluid properties (density, viscosity)
(7) Port diameter
(8) Stroke

The curves presented in Figure XI-3-14 (Ref. 6) show fluid flow forces as a function of stroke for conical, spherical, and flat poppet valving units with flow in either direction. Unlike rotary-element or gate-type valving units, poppet valving units have no clearly defined limit of stroke, for it is possible that the poppet may be translated so far away from the seat that any further motion will have absolutely no effect upon flow through the port.

Solenoids

A solenoid must be designed so that it will provide the required operating force when the coil is at its maximum operating temperature. Assuming that the solenoid is normally deenergized when the valve is in the closed condition, the forces which the solenoid must overcome in opening the valve must be equal to the forces required to close the valve. In the

general case these forces can be tabulated:

Forces required to open valve:

(1) acceleration (response time)
(2) friction (fluid and rubbing)
(3) energy storage device (i.e. a spring)
(4) fluid pressure and displacement effects

Forces required to close valve:

(1) acceleration (response time)
(2) friction (fluid and rubbing)
(3) flow induced forces
(4) fluid pressure and displacement effects
(5) seating loads

The force-stroke (flux gap) characteristics of a solenoid armature are interrelated with the current, rate of change of current, coil windings, flux losses, and materials. The interrelationship between all of these variables are non-linear and quite complex. Most often past experience serves as the most important design criteria. An insight into solenoid construction, design criteria, and theory can be obtained from Reference 7.

Temperature effects impose the greatest limitations on solenoid performance. The coil temperature is somewhat higher than the maximum external environment temperature because of the heat generated by the coil itself. Consequently, the ambient environment and cycle of operation are necessary input information in solenoid design. High temperature coils over 800°F have been designed with special insulating material. These materials, however, have adverse effects resulting in increased weight due to decreased flux density.

When the solenoid is subjected to low environmental temperatures, or is deenergized for an extended period, the coil temperature will be considerably below the maximum. The resistance of copper wire decreases as the wire temperature is decreased and is almost zero at -423°F. To prevent a direct current coil from drawing excessive current at reduced coil temperatures a short winding of constantan wire is often used in series with the copper. There is a trade-off between the degree of temperature compensation and coil weight.

The alternating current coil has an inherent temperature compensating feature. The impedence of the alternating current coil is the resultant of the ohmic resistance of the wire and the inductive reactance of the coil. The inductive reactance is usually dominant and is the result of the physical arrangement of the coil and is little influenced by temperature changes. The net result is that the alternating coil impedance does not change significantly within the usual range of operating temperature and no temperature compensation is required. This makes the alternating current coil preferable for operation in environmental temperature extremes where alternating current is available.

Response Time

The total valve response time is the sum of the response time of the actuator and control element. The factors influential in valve response are:

(1) Mass of moving parts
(2) Friction
(3) Unbalanced pressure forces
(4) Dynamic fluid forces
(5) Friction forces
(6) Displacement of fluid

Response times less than 5 milliseconds are possible if large actuating forces are available. A trade-off, however, may be necessary to preserve the sealing element from impact degradation in the form of extrusion (elastomers and plastics) and fretting corrosion (metals).

When fast response is required, significant electrical power drain can occur while the valve is being held open. A latching mechanism can be employed such as an over center bellville spring in a modified version of the valve shown in Figure XI-3-13.

Pressure Effects

A valve housing must be capable of withstanding the maximum operating pressure to which it will be subjected. Flow transients can cause line pressure to rise several times in excess of normal operating pressure. In cases where critical tolerances exist, care must be taken to assure that

the resulting pressure deformation does not alter the tolerances to a degree that would affect operation. If the valve is subjected to many cycles of pressure application, consideration must be given to possible fatigue failure.

Since valve housing and control elements are usually complex, a theoretical stress analysis is usually accomplished by gross simplifications. Consequently, the prediction of maximum operating pressure is often a poor estimate. The final qualification must be generated by burst tests. Once a burst pressure rating has been established, a lower value non-destructive proof pressure test can be devised. The range between maximum operating, proof and burst pressures depends upon whether the system is man-rated and the degree to which a weight saving can be evolved without sacrificing performance such as that attributed to deformation of critical areas.

Housing Construction

The valve housing may be composed of a lightweight material with special inserts for the sealing elements. The actual sealing surface should be relatively independent of the body from the standpoint of pressure and thermal distortion. Connections to the valve may be threaded, brazed, or welded. These connections should not influence the critical tolerance areas of the valve or impede the flow of fluid. The connections can be inline or at 90° depending on the control element design.

XI-4 TYPES OF VALVES

Start Valves

The term "start" is used in pressurization systems although the class of valves under consideration can be more adequately described as "shut off" valves. The term shut-off applies to a class of valves which contain a control element that is normally open or closed. The element does not assume an quasi-steady intermediate position and, therefore, does not provide a flow or pressure modulating function. The basic elements of a start valve include (1) a housing with provisions for inlet, exit and auxilliary flow connections, (2) a control element, (3) a seal element(s) and (4) a means of actuation for the control element.

The design optimization of a start valve requires trade-offs between leakage, and sealing loads, flow capacity, actuation force, response, size, and weight. If leakage is the principal criterion, the optimum seal element configuration is the unbalanced poppet type valve (see Section XI-2). Generally for small valve seat areas, less than 1 inch diameter, the unbalanced poppet type valve is compatible with the actuation forces of the magnitude produced by solenoids. When larger valves are required, pilot operated designs can be considered such as those shown in Figure XI-3-4. In each case a smaller pilot is used to operate an unbalanced main valve. When even larger valves are required, other control element designs can be considered.

The actuators for start valves may be solenoids, handwheels, levers, motors, and pneumatic or hydraulic diaphragms or pistons. The final choice is dependent upon:

(1) the valve size
(2) power available
(3) response
(4) remote operation requirements
(5) available space
(6) weight
(7) forces required to move and seat the control element

While each of these factors are considered in this Part, a distinction is made between the general class of valve actuators and the explosive or propellant actuated valves which are discussed separately.

Other design and selection parameters include:

(1) the fluid media
(2) pressure drop and flow capacity
(3) operating temperature and pressure
(4) sealing element
(5) control element
(6) leakage

These parameters are considered in Section XI-3 although a detailed discussion on control elements, seal elements, and leakage is presented in Section X-2. Hence, the latter parameters are reconsidered solely from an optimization viewpoint.

Fill and Vent Valves

Fill and vent valves may assume numerous configurations with respect to type of valve used and method of connecting and disconnecting. In the simplest case wherein a man-rated tank is to be filled to a low pressure, the valve can be of almost any type of manual shutoff. For added insurance against leakage, a secondary closure, such as a cap, can be attached and locked in place. As the requirements become more rigorous, fill valves become more complex. High pressures and toxic, corrosive, or cryogenic fluids must be transferred by more elaborate couplings which may include requirements for remote operation, balanced valve element design, and very low spillage upon engagement or disengagement.

Disconnects are required to meet extremely stringent leakage requirements because of the necessity of preventing pressurant or propellant loss and the need to avoid hazards to personnel that might result from spillage or leakage. Soft seats are used in these valves almost exclusively in order to meet these requirements. Polymers can be used with many fluids but not with fluorine and fluorine vapors. All metal construction is required for the fluorines.

Other problems that exist for disconnects include that of the effects of sterilization temperature on soft seats in contact with propellants. It is considered very possible that the combination of high temperatures for long periods of time (36 hours) and propellant contact would degrade elastomeric materials used as seals or seats. As the disconnect port in a spacecraft subsystem is exposed to the vacuum of space, sublimation of the material occurs to some degree, and radiation effects could degrade the polymers if the dosage became sufficiently high. A secondary seal upstream of the disconnect such as a cap or a soldered closure can be used to help prevent fluid contamination. It should be noted that some pressurizations systems have been sealed by crimping and welding the fill tubing.

The selection of pressurant fill and drain components is dependent on the contractors past experience and system sealing requirements for such areas as the auxiliary ground equipment-spacecraft interface and for such considerations as ground abort and personnel safety. Once the vessel is filled and the disconnect is released, the airborne connection on a spacecraft should be securely capped to minimize high pressure fluid leakage during the mission life of the vehicle. To insure a leak tight seal, brazing or welding of the cap and tube may be required. The use of nonmetallic sealers is limited because the combination of a vacuum environment and high material vapor pressure results in sealant evaporation. Closure of the disconnect may require that personnel work around high pressure lines. The overall hazard can be minimized by keeping manual operations short. This can be accomplished by remote actuation of the disconnect and valves. The latter applies particularly to conditions where a corrosive gas such as OF_2 is used as a pressurant. In such a case, safety considerations necessitate special fill and drain operations even when protective clothing and self-contained breathing systems are used.

Deactivation of a pressurized system after mission abort may be accomplished through the fill disconnect, provided gravity expulsion of the main propellants or pressurization of the propellants from a ground source is permitted. The former technique is preferred for spacecraft where the

pressurization system controls and any positive expulsion devices will be intact after fluid drainage. Another approach to fluid drainage is the use of an explosively actuated jettison valve.

A simple fill and vent valve can be composed of a hard spherical ball pressed into a relatively hard seat. Relative displacement of the sealing elements should be avoided to prevent the generation of contamination. Two typical valves are shown in Figure XI-4-1.

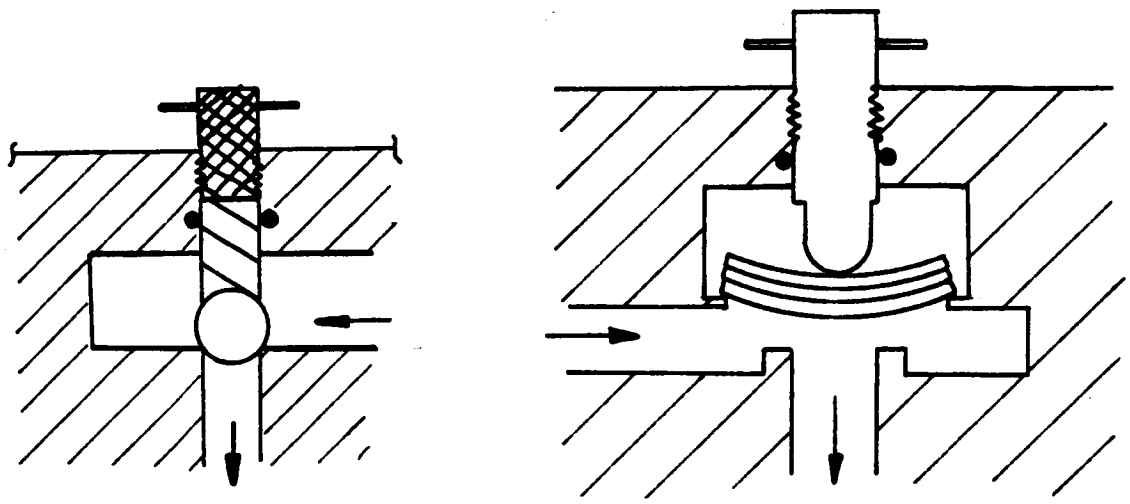

Fig. XI-4-1 Simple Fill and Vent Valves

Since closure is produced manually on the ground, the seating load applied can be varied according to the number of times the valve is operated. In addition, leak checks can be readily accomplished.

Quick disconnect couplings are used when frequent repairs, rapid connecting and disconnecting to ground vents are necessary, and when remote breakaway features are desirable. The parameters of importance are self-sealing features, air inclusion and fluid loss and pressure drop.

Based on system requirements, self-sealing of both ends of the disconnected line may be mandatory, required for one end only, or may be unnecessary for either disconnected end. When the requirement is established, the field of coupling configurations is narrowed to a few types, differing principally in the valve arrangement. The air inclusion and fluid loss

characteristics apply only to self-sealing, double valved couplings where a discrete volume of air is trapped within the coupling during connecting, and an equivalent volume of fluid is lost during disconnecting. This results in air being forced into the system and fluid being lost during coupling. Additional fluid is lost in disconnecting due to leakage past the valves during closing. The quantity of fluid lost will depend upon such factors as the fluid properties, fluid temperature, fluid pressure, valve closure rate, wear, and valve seal design. This additional leakage can be determined accurately by test, and must be added to the trapped volume to determine the total fluid loss.

The pressure drop across a quick-disconnect coupling is determined by the shape of the flow path through the coupling, the fluid flow rate, and the fluid properties. The flow-path differs markedly between the various types of valve designs. Typical designs are shown in Figure XI-4-2.

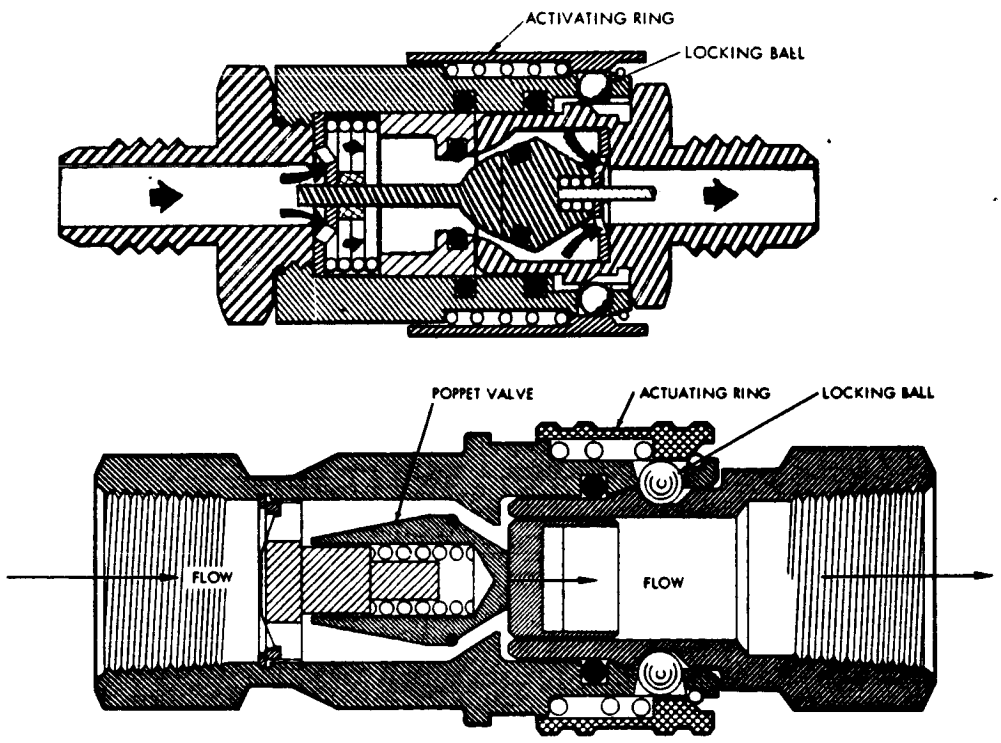

Fig. XI-4-2 Typical Quick-Disconnect Couplings

The system pressure dictates the coupling's strength requirement, which is a function of the yield strength and thickness of the stressed materials. The material thicknesses in turn affects the coupling weight, pressure drop and size. The material chosen is of such strength that the thicknesses of the stressed parts do not result in excessive weight, restricted flow causing excessive pressure drop, or excessive space. This is significant in that an unrealistic restriction on weight, size, or pressure drop will result in unwarranted compromising of the other factors and/or the body material.

Locking devices have two functions to perform: to lock the plug and socket together, and to hold the coupling valves open. The strength of the locking device is determined by the type of locking materials and the size and number of locking balls, threads, fingers, pins or other devices incorporated within the socket which mate with a locking groove or slot in the plug. In selecting a locking device, other factors which are to be considered are number of required operating cycles while pressurized and depressurized, mode of locking and unlocking, forces required to connect and disconnect, and space allowed for actuation of the locking device. Consideration should also be given to remote disconnection using pneumatics, squibs, or lanyards.

Relief Valves

A relief valve is a device which opens at a predetermined pressure and vents fluid from a chamber until the pressure is below the opening pressure. Essentially, a relief valve functions as a safety device limiting the maximum pressure in a pressurization system to a level below that required to cause system component failure. In the course of its operation, it does expel fluid from the pressurization system and consequently reduces the system performance and efficiency.

If a system is designed for optimum mission performance, pressures above safe limits theoretically cannot occur. Hence, in some instances relief valves are unnecessary. The guidelines which determine when a relief valve is necessary in a system can be summarized.

When required

(1) On man rated systems where all conditions of the mission are not known. For example, radiation or other heat generation effects can increase the pressure within the pressure vessels. The fluid lost may be excess fluid deliberately stored or it may result in an aborted mission.

(2) On non-man rated systems where excess fluid can be stored without compromising mission requirements.

When not required

On non-man rated one way voyages where weight efficiency must be a maximum.

To achieve minimum losses of fluid, a relief valve must open and close almost at the same pressure and simultaneously not leak at pressures below the maximum pressure. Typical characteristics of a satisfactory valve would exhibit little hysteresis effects. Figure XI-4-3 shows a so-called regulation curve where the operating pressure at rated flow are close to the cracking and reseat pressures.

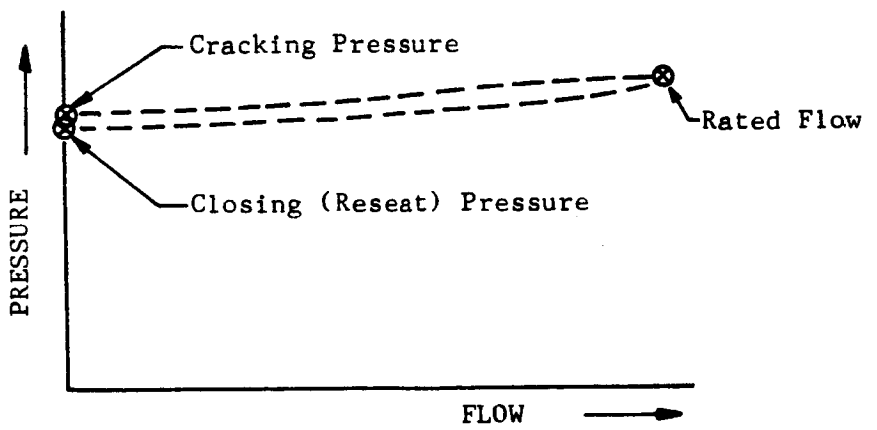

Fig. XI-4-3 Pressure Flow Characteristics of a Relief Valve

A typical value of cracking pressure is 110% of maximum operating pressure. The reseat pressure can approach 97% of the cracking pressure depending upon the design.

A relief valve consists of a valve body, a valve element, and a reference load. The reference load is coupled to the valve element and opposes the effects of fluid pressure. The reference load is usually a spring or spring-like device.

Direct Operated Relief Valves

Direct operated relief valves can be subclassed as seat load sensitive and non-sensitive. Each of these types is considered separately.

Seat Load Sensitive Valves

The most common type of relief valve is the simple ball poppet valve as shown in Figure XI-4-4. Increasing fluid pressure acting on the projected area of the poppet decreases the seating load. This reduction in load produces an increase in leakage which is particularly detrimental when one considers that virtually no seating load exists at maximum operating pressure. Additionally, vibratory forces can easily unseat the poppet. Other poppet types are shown in Figures XI-4-5, XI-4-6, and XI-4-7. The leakage past the valve element shown in Figure XI-2-14 is controlled by close clearances, which for minimum leakage pressurization systems must be held unrealistically small. The valve shown in Figure XI-4-7 contains a "V" seat closure which produces pop-open effects when fluid flows through the seat. This is produced by a change in momentum of the fluid which opposes the spring and causes the valve seat opening flow area to increase rapidly. This performance is also achieved by using bellville springs. This valve usually possesses poor opening-reseat to pressure characteristics.

Seat Load Non-Sensitive Valves

The inverted relief valve valve depicted in Figure XI-4-8 is designed to minimize undesirable vibratory response through the application of relatively high seat loads at normal operating tank pressures. A force is exerted by the poppet against the seat due to the applied pressure and spring loads. As the pressure increases, both the seat and poppet are

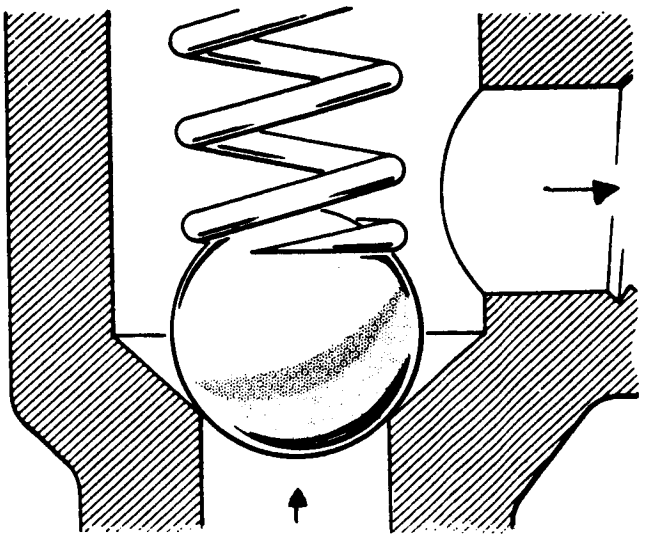

Fig. XI-4-4 Ball Poppet Valve (Ref. 6)

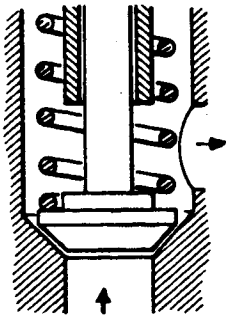

Fig. XI-4-5 Conical Poppet Valve (Ref. 6)

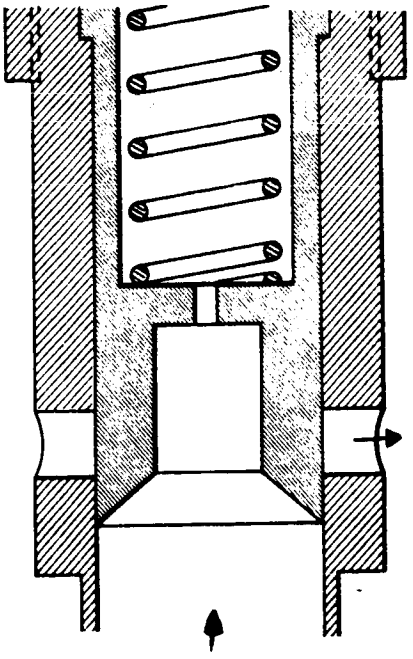

Fig. XI-4-6 Sleeve Type Poppet Valve (Ref. 6)

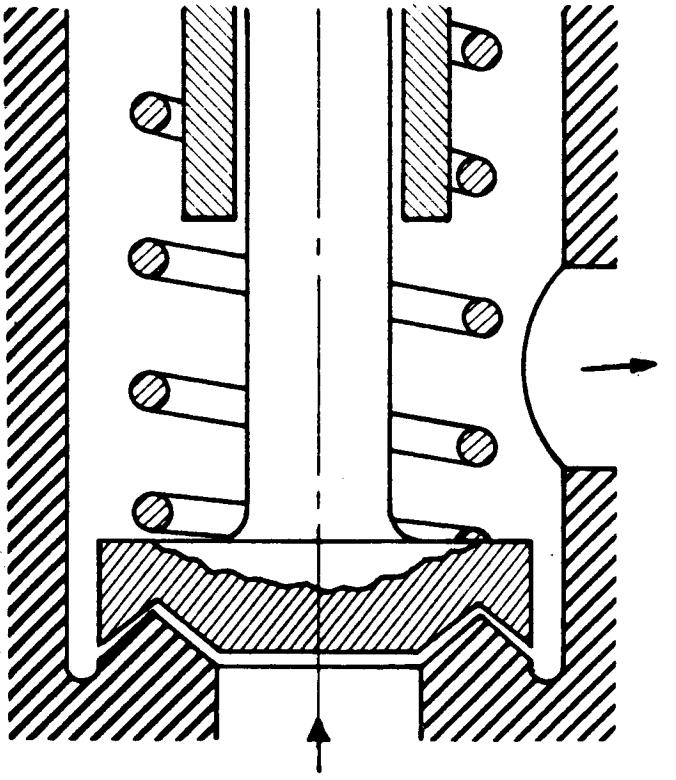

Fig. XI-4-7 "V" Seal Valve to Provide Snap Open Characteristics (Ref. 6)

displaced equal amounts until a lip or shoulder on the poppet is intercepted by a stop. At this point, the pressure force on the poppet is transferred to the stop and a finite increase in pressure, equivalent to this transferred load, must be exerted on the piston to lift the seat off the poppet. High seating forces are maintained during normal operating tank pressures if interception of the poppet occurs at a slightly greater pressure. However, to keep the required increase in pressure relatively small, the annular piston area must be relatively large compared to the port area. In addition, the piston requires a dynamic seal which may introduce undesirable friction forces and gas leakage.

Another concept shown in Figure XI-4-9 employs an integral spring and diaphragm which is well suited for relief applications in which small differences between cracking and reseat pressures are desired. Because of the non-linear characteristics of the inverted cone end, changes in relief pressure with flow capacity are substantially smaller than those incurred with comparable helical springs. The absence of dynamic seals and associated hysteresis results in very small differences between cracking and reseat pressures. Bell (Ref. 3) reported a reseat pressure 1 psi below a cracking pressure of 250 psi.

Pilot Operated Relief Valves

As the capacity requirements for direct-acting relief valves become large the leakage through seat load sensitive valves becomes intolerable. To overcome this deficiency, an unbalanced main valve is operated by a pilot valve.

A pilot valve of the type shown in Figure XI-4-10 vents a cavity above the main valve at a maximum pressure. This negatively unbalances the main valve and permits fluid pressure to open the valve. The greater the initial positive unbalance force, however, the greater variation between opening and reseat pressures. When the main valve element is balanced, it is subject to vibratory forces. To overcome this deficiency a pilot operated, non-seat load sensitive main valve can be used, as shown in Figure XI-4-11, in conjunction with a non-seat load sensitive pilot

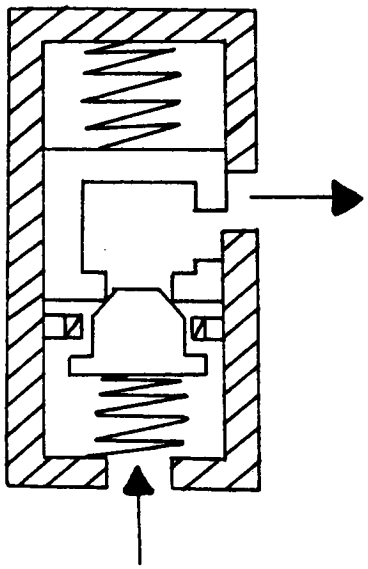

Fig. XI-4-8 Inverted Seat Valve

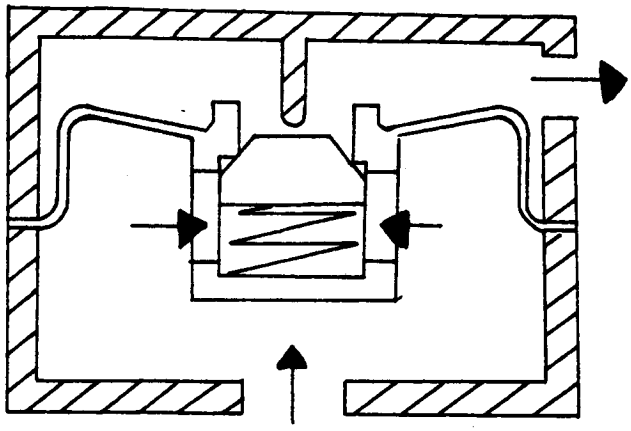

Fig. XI-4-9 Inverted Seat Valve with Diaphragm Retainer

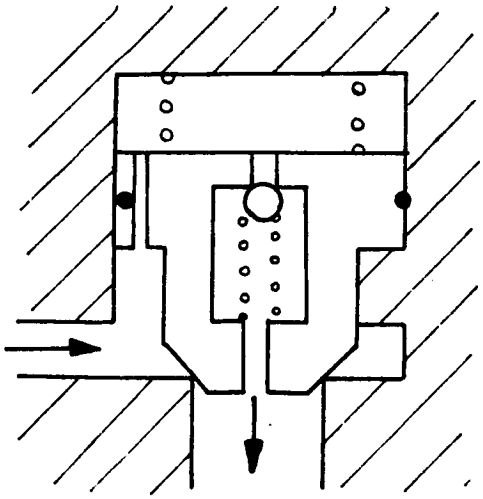

Fig. XI-4-10 Pilot Operated Valve

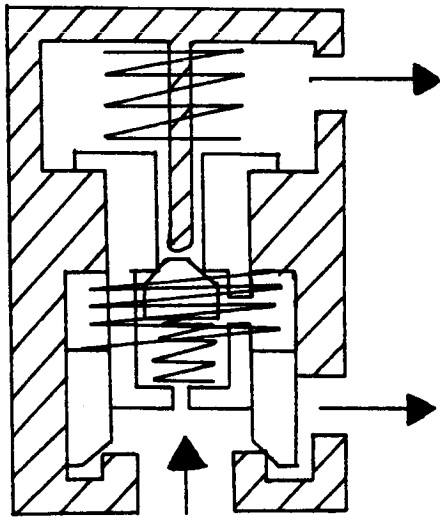

Fig. XI -4-11 Inverted Seat Pilot Operated Valve

valve. The opening and closing response rates are slower than a comparable direct-operated valve.

A desirable characteristic in any relief valve for pressurization systems is to open and close as rapidly as possible such as might be achieved by snap open valves. To date, snap action valves have demonstrated poor opening and reseat characteristics.

Chattering is a common characteristic of many relief valves and can be controlled by:

(1) Having a small sealing seat compared to the control area. This reduces the net effects of flow induced forces on the valve elements.

(2) Inclusion of a dashpot or other damping devices on the valve element.

(3) Use of a pilot operated valve which inherently increases the time constant of the main valve element.

Check Valve

The primary function of a check valve is to prevent flow reversal. Check valves pass fluid freely in one direction and, if pressure reverses, close quickly to stop flow in the other direction. Flow reversal in fluid systems may be programmed as a normal occurrence or may be caused by accidental occurrences or failures. Accidental flow reversal must be promptly and effectively halted or reservoirs may overflow, tanks may be overpressurized, reactive fluids may combine, rotating equipment may overspeed, or other types of equipment damage may occur.

Check valves are entirely automatic in their operation and require no external actuation signals or sources of power. Their valving elements are activated by the forces of the flowing media. Valving elements of check valves are either spring-loaded closed or gravity closed. The spring-loaded type is the only one of significant interest in aerospace applications, due to the uncertainty of vehicle attitude or of the existence of gravitational forces.

Check valves are the simplest of valve types. However, in spite of their simplicity, they are often one of the most troublesome components in

a fluid system. Having no actuators, check valves often lack sufficient seating force to accomplish a good seal. Most check valve designs are a compromise between good sealing and low pressure drop. In aerospace fluid systems, it is usually desirable to minimize pressure drop across the valve as a function of flow rate. The comparative pressure drop characteristics for several types of check valves are shown in Figure XI-4-12. When specifying the pressure drop of the check valve, it is important that the actual operating conditions of flow rate, pressure, temperature, and flow medium are accurately stated.

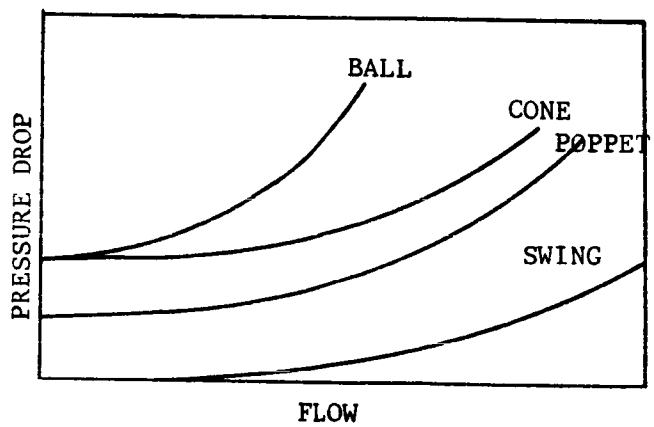

Fig. XI-4-12 Typical Check Valve Pressure Drop Curves

The sealing characteristics of the check valve are dependent upon the seal material, initial spring-loading, and differential pressure across the closure element. When pressure reversal occurs, the check valve will leak until the back pressure becomes high enough to provide an adequate seating force. The requirement for zero leakage at zero or very low reversal pressure necessitates the use of higher initial spring load, which will result in higher pressure drops through the valve in the forward flow direction. The use of resilient seat materials wherever possible will aid in achieving minimum leakage at low seat loadings.

Cracking pressure is defined as the forward differential pressure which is required to pass some specified minimum flow rate. Reseat pressure is that reverse differential pressure required to reduce leakage to some minimum specified value. With sufficient spring-loading and proper seat characteristics, the reseating pressure can be zero. Both the cracking and reseating pressure characteristics of the valve are related to the pressure drop and leakage characteristics.

The most significant consideration for operating pressure is that the valve housing must be designed for the maximum pressure to which it may be subjected. The possibility of rapid valve closure causing water hammer must be taken into consideration, in that it may cause a pressure rise several times the normal operating pressure. A maximum differential pressure in the reverse direction must be considered in the design of the valve closure and seals to prevent fracture of closure and extrusion of seals. If the valve may be subjected to a large number of pressure cycles, consideration must be given to the possibility of fatigue failure.

Other pertinent selection factors are sealing element, operating temperature, flow media, and contamination sensitivity. These aspects are considered in Sections XI-2 and XI-3 and are applicable to check valves. A typical check valve is shown in Figure XI-4-13.

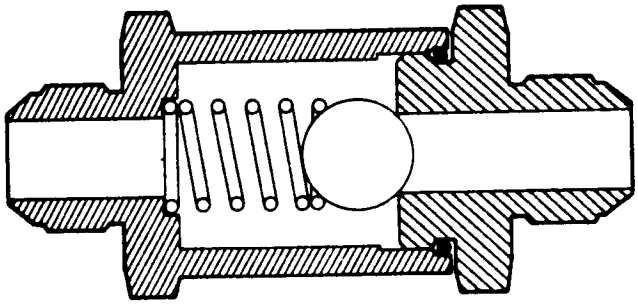

Fig. XI-4-13 Typical Ball Check Valve (Ref. 6)

Explosive Valves

Explosive or squib valves are one time, quick open or close elements which are activated by extremely compact energy sources. These valves are actuated by the sudden conversion of potential chemical energy into mechanical energy. The chemical energy can be released either by deflagration (fast burning), or detonation (the propagation of a shock wave through a high explosive).

In the case of deflagration, work is done by the high pressure of the hot explosive gases acting on a piston. A typical chamber pressure versus time record is shown in Figure XI-4-14. Pressure is contained in the cylinder by one or two piston O-rings and backup rings. Some combustion gas generally leaks past the rings, since the seal reaction time is not sufficient to resist the initial pressure buildup. (The gas leakage is usually insignificant to the performance of the valve). However, when leakage does occur into the system, combustion product contaminant may (and have been known to) adversely affect system operation. It is also possible to use a deflagrating charge to drive an interference fit, but extremely high pressures must be obtained. In the case of detonation, the momentum of the shock wave in the explosive is transferred to a piston, equivalent to hitting the end of the piston a sharp blow. The use of a detonating charge permits the piston to be an interference fit in the cylinder. If extremely tight contamination control is required, shock waves from a detonating charge can pass through a permanent metal barrier to actuate the piston.

In either case, a small amount of explosive is used. For example, a typical 0.75 inch diameter, 4000 psi working pressure, normally-closed valve uses 140 milligrams of propellant or about 1/20th ounce. The explosive pressure in this valve is approximately 25,000 psi.

A deflagrating charge used in an explosive valve generally consists of small flake-like particles of powder similar to shotgun powder. A typical design would consist of discs approximately 0.010 inch thick and 0.050 inch in diameter. This shape is used to present a large surface area

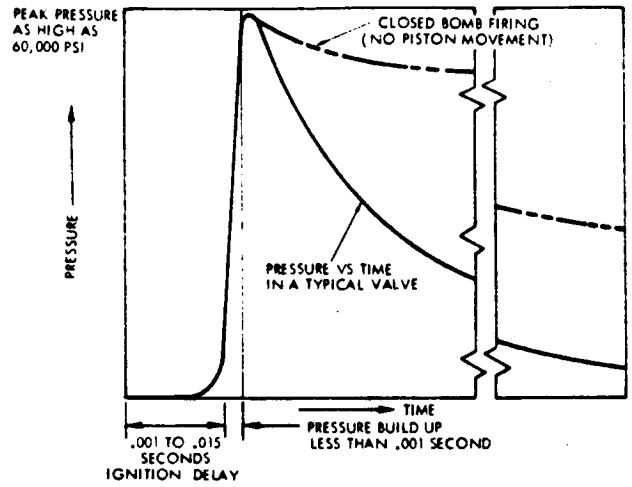

Fig. XI-4-14 Typical Pressure Versus Time Record for an Explosive Actuator (Ref. 6)

to the advancing flame front, permitting rapid pressure buildup. A detonating charge consists of a high explosive such as PETN or RDX, generally compressed at high pressure to a solid cylindrical pellet.

Explosive Initiation

Explosion charges are generally initiated by the transfer of either electrical or mechanical energy to a sensitive primer such as lead styphnate. Ignition may be started by striking the primer a sharp blow through a metal barrier, like the firing pin of a gun, by abruptly piercing the primer container with a sharp probe, or by electrically heating the primer through a bridgewire.

A deflagrating charge can be initiated directly by a primer, while a detonating charge requires a booster to transform the primer output into a detonation wave. A typical booster would be a lead azide pellet pressed against the output charge.

Both detonating and deflagrating charges can be directly initiated without the primer by using an exploding bridgewire. This method requires a firing pulse of approximately 25,000 volts, as compared to a conventional firing pulse of 5 volts. The extremely high potential first

vaporizes the bridgewire, then discharges through the ionized particles remaining in the path, creating an explosion which, in turn, ignites the main charge. Ignition by the exploding bridgewire is extremely insensitive to accidental firing, but requires a more complex firing circuit, resulting in a heavier unit, than conventional electrical ignition systems.

Typical Explosive Cartridge

A typical explosive cartridge is shown in Figure XI-4-15. The charge is electrically initiated, an electrical connector being integral with the cartridge. The unit is hermetically sealed to protect the explosive charge from moisture and damage. This cartridge is a specific example of a type of cartridge common to explosive valves. Many variations are possible. Some cartridges have wires leading from the bridgewire to the outside power source instead of using an integral electrical connector; others use a single ceramic or glass seal for the connector pins instead of individual seals for each pin. Some use four pins, two for each bridgewire, while others have but a single bridgewire. Some have a ground pin in addition to the power pins, while some explosive valves use no cartridge at all, instead incorporating the charge directly into the body of the valve.

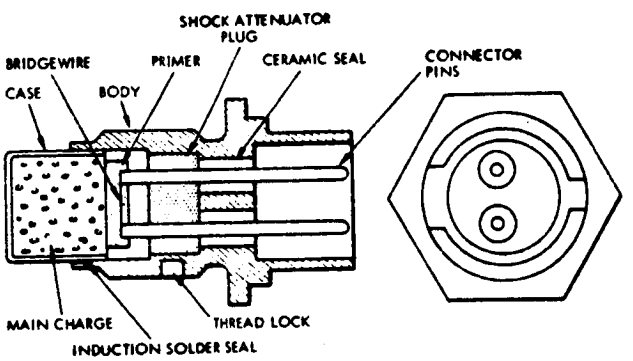

Fig. XI-4-15 Typical Explosive Cartridge (Courtesy of Holex, Inc., Hollister, California)

The cartridge shown contains a nominal 188 milligrams of deflagrating charge, sufficient to produce pressures up to 60,000 psi, depending inversely on the dead volume in the firing chamber.

Cartridges such as the one shown in Figure XI-4-15 can have a firing current from 1.0 to 5.0 amps, and a firing time from 0.001 to 0.020 second. Cartridges with 5.0 amps firing current can be made to survive 1.0 watts bridgewire power dissipation without igniting. Many cartridges of this type have 2 bridgewires for reliability. Typical units are capable of withstanding 300°F soak for 24 hours without deterioration.

The cartridge shown in Figure XI-4-15 weighs 0.03 pound, most of the weight being in the stainless steel case. The electrical conductors, two stainless steel connector pins, are locked into the case by fused ceramic seals. Fused glass seals can be used for low pressure cartridges. Fused ceramic seals are capable of withstanding pressures of 60,000 psi. The cartridge incorporates a plastic shock plug to attenuate the shock waves generated by the explosive before they reach the ceramic seals. The explosive charge is contained in a thin metal shell which is induction solder sealed to the cartridge body. The thin shell bursts when the explosive fires. The cartridge incorporates two nylon pellets to lock the threads against vibration, and is designed to accept a standard O-ring for sealing.

A normally open and a normally closed valve are shown in series in Figure XI-4-16. Both valves use a wedge to shear the walls of the flow passage. In each case, the valve provides an unobstructed flow path. Other variations are available utilizing the various forms of sealing such as the normally open tapered poppet shown in Figure XI-4-17.

A similar normally closed explosive valve is shown in Figure XI-4-18.

In small port sizes, usually less than one inch, squib valves are directly actuated. As the size increases, piloting techniques become more practical because of size of cartridge and heat generation. The pilot section is a squib actuated device which in turn directs a high pressure gas supply to operate the main valve or unlatch a spring device which, in turn, opens or closes the main valve.

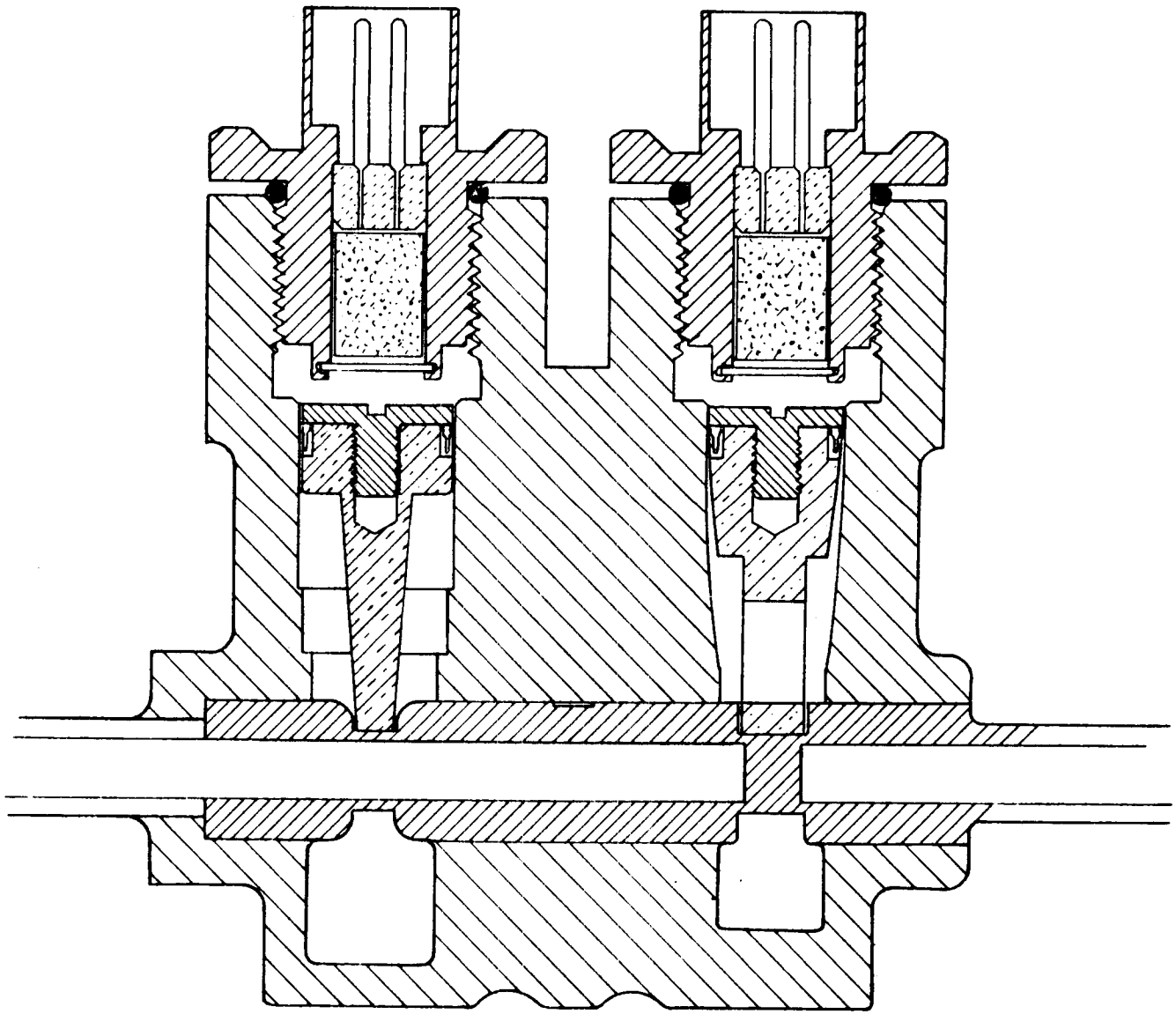

Fig. XI-4-16 A Normally Open and Normally Closed Explosive Valve

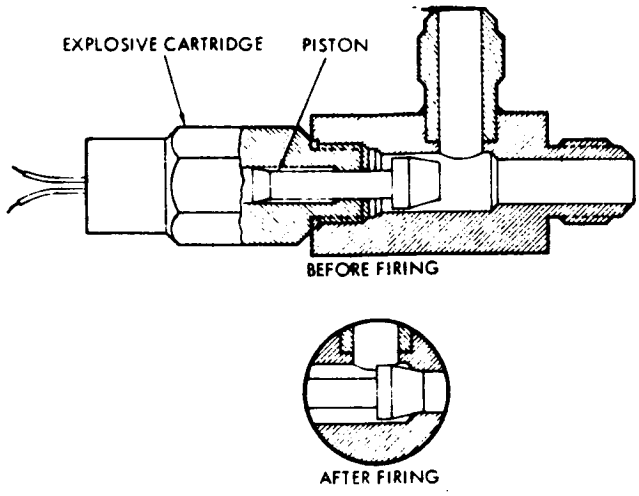

Fig. XI-4-17 Normally-Open Explosive Valve (Ref. 6)

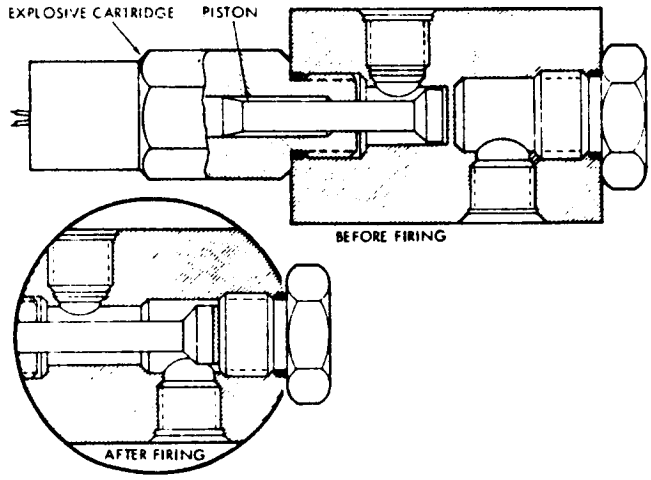

Fig. XI-4-18 Normally-Closed Explosive Valve (Ref. 6)

A parallel combination of valves such as shown in Figure XI-4-16 can be used when multiple cycling is required. The response of the valve varies from 2 to 25 ms depending upon the ignition system. The severity of the opening and closing shock in the fluid system can cause problems.

Lower electrical power requirements are another feature of the explosive valve. A typical valve can be operated with a 25 watt supply through a 1 ohm bridgewire. Consideration must be given to possible electrical short circuits which could prevent other valves from functioning. Additionally, the squib ignition system should be designed to prevent accidental firing due to static electricity.

The size and weight of the valves are smaller and lower than conventional valves. However, multiple cycle operation can quickly offset this advantage. Reliability of even single cartridge explosive valves is extremely high, due partly to their mechanical simplicity and partly to the high reliability of all explosive cartridges. Redundant cartridges can be used to actuate a valve where either extremely high reliability is required or the expense of demonstrating required reliability with a single cartridge would be excessive. These devices can function successfully at temperatures ranging from -320°F to +250°F.

Other reliability factors which must be considered are contamination due to products of combustion and metal particles fragmenting during firing. Usually the combustion contaminants are contained within the explosive chamber and are prevented from entering the fluid system by the seals at the points of closure. A necking down of the flow passageway, such as shown in the design of the valve in Figure XI-4-16 assists in producing precise fractures with no contaminant generation. Finally, the nature of the valve design requires substantial qualification testing since non-destructive methods cannot be employed.

XI-5 FILTERS

Introduction

As a protection against component malfunction, particularly of valve seats, filtration of the fluid media is required. The process of filtration is one of separating particles from the fluid by mechanical, chemical, magnetic, gravitational or electrostatic methods.

Particles are defined and measured by the largest dimension, which is usually given in terms of microns. One micron is approximately equivalent to 40 microinches. Filters are rated by two methods:

(1) an absolute basis where particles no larger than a given size can pass through

(2) a nominal rating corresponding to the ability of the filter to remove 98 percent of incident particles of a given size.

Both of these ratings are based on experiments using standard contaminates. The nominal rating is determined by first adding a standard contaminant such as glass beads or aluminum dust of a known quantity and size distribution to the fluid. The ratio of particles larger than a given size in the fluid to the quantity in the fluid is used to determine the nominal rating. The two percent passing through may be of any size up to the maximum of the test contaminant.

The capacity of a filter refers to the maximum weight of contaminant which can be retained without exceeding a specified pressure drop. Other factors of importance are the pressure drop at rated flow through a clean element and the collapse pressure of the element due to clogging of the filter.

The method of filtration pertinent to pressurization systems is the mechanical method which employs such devices as woven, wound and sintered wire mesh filters; disc or ribbon edge filters; sintered matel filters and pressed paper and matted fibers filters.

Woven Wire Mesh (Figure XI-5-1

The wire mesh cloth filter (Figure XI-5-1) develops a square opening pattern and presnets a straight-through opening. Twilled weaves are also available, which present a straight-through opening to fluid flow. Since there is no mechanical bond between points of intersection of the wire, the cloth will distort under high mechanical stress and vibration, and pore size will vary allowing particles to pass. This type of filter is suitable for non-critical hydraulic, pneumatic, and propellant feed applications. The filter will pass fibers and random large particles.

Wound Wire Mesh (Figure XI-5-2)

Cleanliness is difficult to attain in this type of filter due to contaminants wound into the cloth and the placement of the filter in the system by means of welding. Migration of media is comparable to other sintered cloth elements and will continue under dynamic flow, mechanical vibration, and stresses. The elements have depth and are more effective in stopping fibers than single layer cloth filters. Dirt holding capacity is good. This type of filter is suitable for critical hydraulic, pneumatic and pressurization systems applications if thoroughly cleaned initially.

Sintered Wire Mesh

Both the woven wire and wound wire mesh can be sintered. The sintering process fixes the pore size and reduces the possibility of changes in pore size under mechanical stress and vibration. The sintered wire mesh has the same general filtration capability as unsintered mesh and presents a straight-through path for contaminants. The sintered process introduces another source of contaminant. Initial cleanliness is more difficult to achieve than with unsintered cloth, and migration tends to be more severe. This type of filter is suitable for non-critical hydraulic, pneumatic, and propellant feed applications. The filter will pass fibers.

Dutch Weave Wire Mesh (Figure XI-5-3)

Cloth of the dutch weave or dutch twill type presents a somewhat more intricate flow path than square mesh patterns and for this reason the

material has somewhat better ability to stop fibers. This medium cannot be classed as a cloth filter, however, even though its performance will be somewhat better than square weave cloth. This type of filter is suitable for non-critical, hydraulic, and propellant feed applications.

Disc or Ribbon Edge Filter (Figure XI-5-4)

Edge filters consist of stacked washers or ribbon wound to form a hollow cylinder. The filtration surface is the outside diameter of the cylinder. The pore size of such elements is fixed and will not vary with flow mechanical stress, vibration or temperature if properly supported. Initial cleanliness of the element can be attained to the level of the environment in the assembly room. Migration of media will depend upon the method used to stamp, cut, or fabricate the discs or ribbon. These filters are surface filters and will pass fibers of larger dimensions than the nominal pore size. Dirt holding capacity is poor since the element has no depth. Depending upon the construction, this type of filter may be recleaned by back flushing, if the stack can be loosened. It is suitable for non-critical hydraulic, pneumatic, and propellant feed applications. The element will pass fibers. The size and weight may be excessive for airborne propellant feed applications.

Sintered Metal (Figure XI-5-5)

Initial cleanliness of this type of element is difficult to achieve and migration of element material including flakes, beads, or large granules is possible. The ability to withstand thermal shock is very critical with this material, and mechanical shock and vibration resistance of these materials is poor. This type of element may be suitable for removal of gross contamination of fluids in non-critical airborne hydraulic, pneumatic, or propellant feed applications.

Composite Sintered Metal and Wire Cloth (Figure XI-5-6)

Laboratory tests have demonstrated that this construction is very poor from the standpoint of initial cleanliness, and migration of element

material is severe. The interaction of the cloth with the sintered granular material will release large numbers of particles under mechanical vibration and operating stresses. This medium should not be used for critical airborne pneumatic, hydraulic, or propellant feed applications; however, it may be a good material for eliminating gross contaminants from non-critical fixed systems.

Etched Disc (Figure XI-5-7)

This filter consists of a stack of segments resembling thin washers, each of which has one face chemically etched to provide a predetermined intricate flow path. Each segment can be cleaned separately, thus the initial cleanliness can be reduced to the degree attainable in the assembly room environment for the filter. Since there are no welds, wires, chips, or machined surfaces on the element, migration of media is essentially zero. The depth property of the element is achieved since the contaminants must cross the surface of each segment through a tortuous path. The absolute and nominal ratings of the element are essentially the same, since particles and fibers larger than the pore size will not pass through the element. Dirt holding capacity is good. The element is easily cleaned by releasing the compression on the segments and backflushing. This type of element is suitable for critical hydraulic, pneumatic, and propellant feed applications; however, size and weight may be excessive for airborn propellant feed applications.

Pressed Paper (Figure XI-5-8)

This type of element may be suitable for removal of gross contamination from non-critical fixed systems, but it should not be used in critical airborne hydraulic, pneumatic, or propellant feed systems.

Matted Fibers (Figure XI-5-9)

This type of element may be suitable for removal of gross contamination from non-critical fixed systems, but it should not be used in critical airborne hydraulic, pneumatic, or propellant feed systems.

Comparison Factors for Filters

It is difficult to establish levels for contaminant removal since the level must be related to the functional operation of a fluid component such as a valve. The level of acceptability must be established by experiment or from past experience. However, a review of filter performance obtained from Reference 6 and other literature sources show that some lower limits are imposed by the filter elements. Realistic absolute values appear to be in the size of three microns or larger in size. The filters capable of removing even smaller particles are limited by media migration which is the tearing loose of particles of filter material often greater in size than the majority of particles retained.

The most promising filter element appears to be the etched disc element. Recent innovations in this design have improved its dirt handling capacity by the etching of labyrinth passages on the discs. A comparison chart summarizing filter performance is shown in Table XI-5-1 (Reference 6).

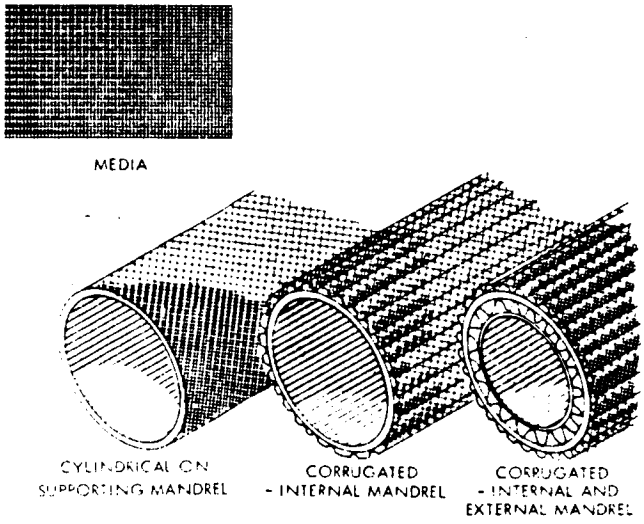

Fig. XI-5-1 Woven Wire Mesh (Ref. 6)

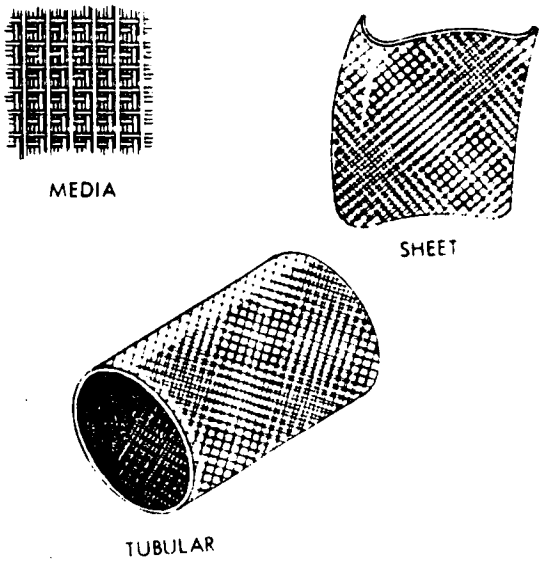

Fig. XI-5-2 Woundwire Mesh (Ref. 6)

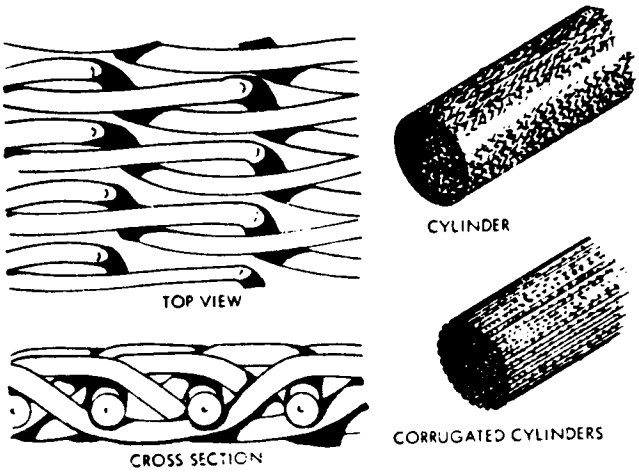

Fig. XI-5-3 Dutch Twill Weave Wire Mesh (Ref. 6)

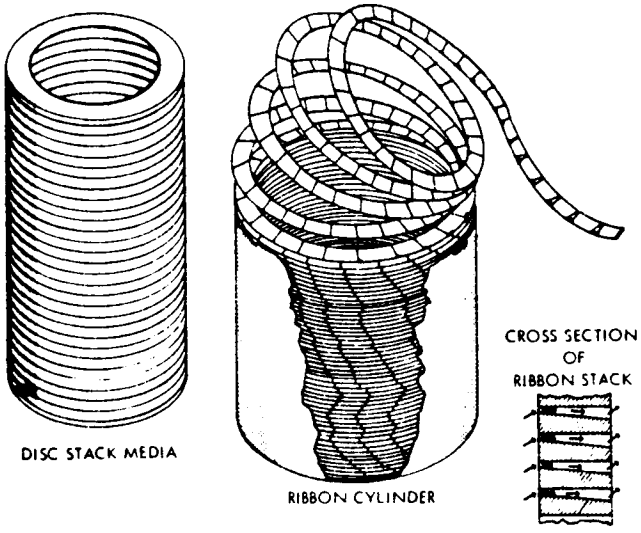

Fig. XI-5-4 Ribbon Edge Filter (Ref. 6)

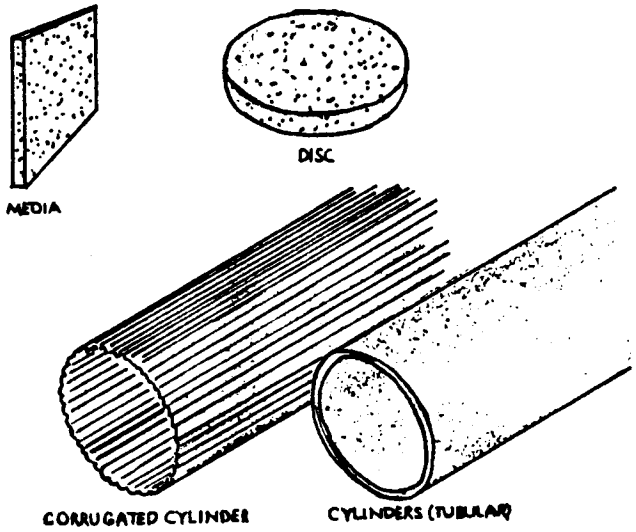

Fig. XI-5-5 Sintered Porous Metal Filter (Ref. 6)

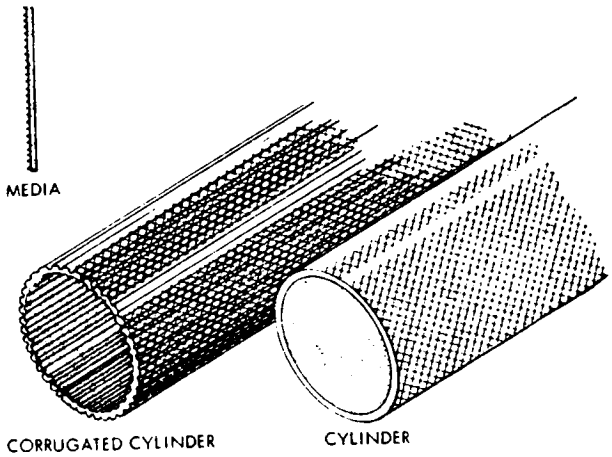

Fig. XI-5-6 Composite Sintered Porous Metal with Wire Mesh (Ref. 6)

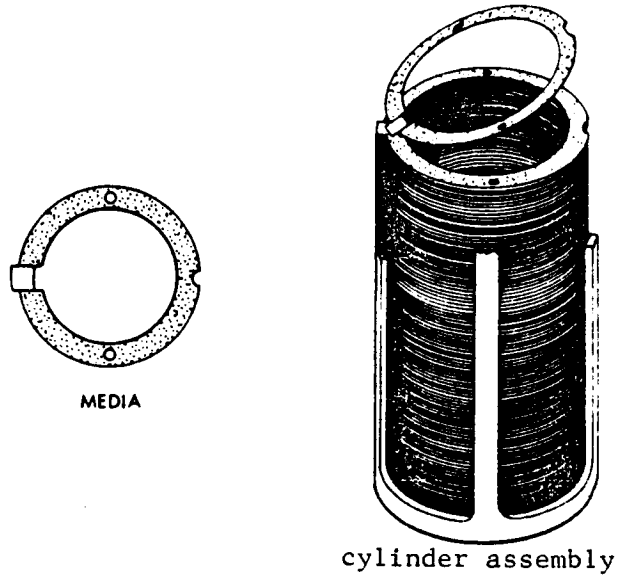

Fig. XI-5-7 Etched Disc Filter (Ref. 6)

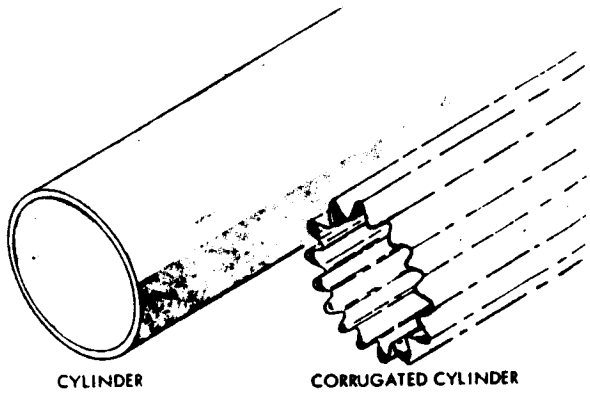

Fig. XI-5-8 Pressed Paper Filter (Ref. 6)

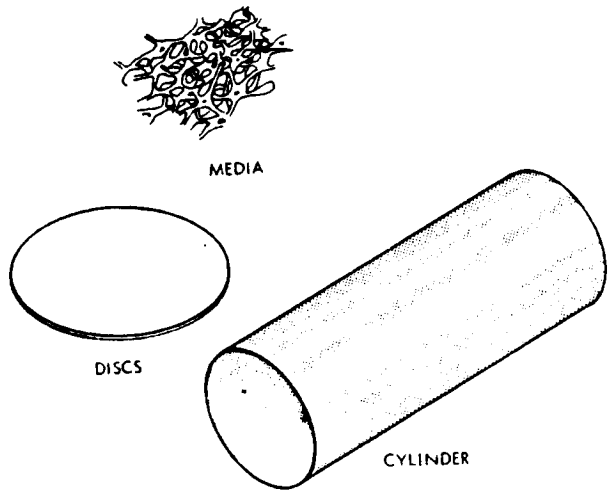

Fig. XI-5-9 Membrane Filter (Ref. 6)

Table XI-5-1

MECHANICAL FILTER COMPARISON CHART (REF. 6)

FILTER TYPE	FILTRATION TYPE	NOMINAL MICRON RANGE AVAILABLE	TEMP*** RANGE (°F)	ABILITY FOR ABSOLUTE CUT-OFF RATING	FILTERING ABILITY: PARTICLES	FILTERING ABILITY: FIBERS	CLEAN-ABILITY	MECHANICAL STRENGTH	PRESSURE DROP PER UNIT AREA	DIRT HOLDING CAPACITY	ABSENCE OF MEDIA MIGRATION	INITIAL CLEANLINESS	SHOCK AND VIBRATION RESISTANCE	WEIGHT
Woven wire mesh	Surface	2 and above	Cryogenic to +1000	Fair	Good	Poor	Fair	Good*	Low	Poor**	Fair	Fair	Fair	Medium
Sintered wire mesh	Surface	2 and above	Cryogenic to +1000	Fair	Good	Fair	Fair	Good*	Low	Poor**	Fair	Fair	Fair	Medium
Wound wire mesh	Depth	2 and above	Cryogenic to +1000	Good	Good	Good	Fair	Good	Low	Good	Fair	Fair	Good	Medium
Dutch weave wire mesh	Surface	2 and above	Cryogenic to +1000	Fair	Good	Fair	Fair	Good*	Low	Poor**	Fair	Fair	Fair	Medium
Sintered porous metal	Depth	2 to 60	Cryogenic to +1000	Fair	Good	Good	Fair	Fair	High	Fair	Poor	Poor	Fair	Medium
Composite sintered porous metal and mesh	Depth	2 to 60	Cryogenic to +1000	Fair	Good	Good	Fair	Fair	High	Fair	Poor	Poor	Poor	Medium
Etched disc	Depth	5 to 75	Cryogenic to +1000	Good	Good	Good	Good	Good	Medium	Good	Good	Good	Good	High
Disc ribbon	Edge	40 to 125 25 to 500	Cryogenic to +1000	Fair	Good	Fair	Fair	Good	Medium	Poor	Good	Good	Good	High
Pressed paper	Depth	5 to 100	Normal ambient to 275	Poor	Poor	Fair	Nil	Poor	Medium	Fair	Poor	Poor	Poor	Low
Matted fibers	Depth	5 to 100 (felted) 10 and over (non-felted)	Normal ambient to 275	Poor	Fair	Good	Nil	Poor	Medium	Good	Poor	Poor	Poor	Low
Membranes	Surface	0.1 to 12	Normal ambient to 260	Good	Good	Good	Nil	Poor	High	Poor	Good	Good	Poor	Low
Class fibers	Depth	5 (matted) to 100	-100 to +1000	Poor	Good	Good	Poor	Poor	Medium	Good	Poor	Poor	Fair	Low
Fretted glass	Surface	0.1 to 125	-100 to +1000	Fair	Good	Good	Fair	Fair	High	Good	Poor	Poor	Poor	Medium
Sintered plastic	Surface	3 to 15	Normal ambient to +300	Fair	Good	Good	Fair	Fair	High	Good	Poor	Poor	Fair	Low
Fired porcelain	Surface	0.2 to 25	2000°F maximum	Fair	Good	Good	Fair	Fair	High	Good	Poor	Poor	Poor	Medium
Bonded carbon	Surface	10 to 70	650°F maximum	Fair	Good	Good	Fair	Fair	High	Good	Poor	Poor	Poor	Medium
Bonded stone	Surface	5 to 100	2500°F maximum	Fair	Good	Good	Fair	Fair	High	Good	Poor	Poor	Poor	Medium

*Dirt holding capacity is low for mesh filters; however, it can be improved by pleating the element within a given filter case size.
**Mechanical strength of cloth filters can be good if the cloth is adequately supported; however, the supporting structure often makes it impossible to reclean a filter element and may seriously affect initial cleanliness.
***Temperature ranges for metal elements are based on 300 series stainless steel, monel and Hastelloy C. (Silver and bronze elements have a maximum temperature of 400°F. and Inconel elements have a maximum temperature of 1200°F. Carbon steel elements have a minimum temperature of -100°F.

XI-6 GENERAL PURPOSE SEALS

Introduction

The seals described in this Part pertain to the general applications of static, sliding or rotating shaft seals in pressurization systems. These seals, for example, may be applied to component housing covers or dynamic applications on a valve control element. The important aspect of these seals is that they are composed of a structural element which form one or more sealing interfaces. A brief description of the various types of seals follows.

Static Seals

A static seal, as commonly envisioned, contains one or more sealing interfaces formed by a structure. These seals can be found in connectors and components within pressurization systems. Aside from the formation of the interface, the static seal can be further subclassed by the shape and function of the seal structure.

Static seals have been classified into the following categories:

(1) Metallic Pressure-Energized Seals
(2) Metallic Non-Pressure-Energized Seals
(3) Combination Pressure-Energized Seals
(4) Combination Non-Pressure-Energized Seals
(5) Nonmetallic Pressure-Energized Seals
(6) Nonmetallic Non-Pressure-Energized Seals

Metallic pressure-energized seals usually have a relatively flexible member that is deformed elastically in a cantilever-type deflection by the flange or housing. The entire bending force is usually exerted at the contact area of the seal. By having a small contact area, a high contact stress may be attained even though the total bending force is relatively small. Usually the amount of initial deflection of the flexible member of the seal is limited by either the seal design or the housing. The force due to fluid pressure acting on the flexible member of the seal is balanced by the contact stress acting on the seal contact area. Since the contact

area is usually much smaller than the surface area of the flexible member which is exposed to the fluid pressure, the reaction to the fluid pressure force produces a contact stress at the seal contact interface which may be larger than the fluid pressure. In this way the fluid pressure itself contributes to the contact stress at the seal contact interface. Because of the action of the fluid pressure and the flexible nature of the seal, these seals are not susceptible to failure because of slight housing or flange deformations. Thus the housing design need not be as rigid as with other seal types. This can result in a considerable saving in housing weights.

The leakage rate depends on many factors. The most influential are contact stress and surface topography. Both factors vary widely with seal design, housing design and surface conditions, the leakage rates for these seals vary widely also. Since these seals are completely metallic, they perform well at extreme temperatures. Since much of the contact stress is due to the reaction at the contact area resulting from cantilever type bending of the flexible member of the seal, loss of stiffness of the seal material at high temperature becomes one of the major high temperature limitations. Brittleness at extremely low (cryogenic) temperatures sets the low temperature limit for these seals, thus the temperature limits for these seals depend on the seal material.

Because of their complicated shapes, most of the seals in this category are relatively high in cost. The surface finish requirement for most of these seals is 16 microinches rms. Since the contact area of most of these seals is very small, these seals are susceptible to failure because of scratches due to contaminants or rough handling. Therefore, cleanliness and careful handling are required for these seals. To further reduce the contact stress necessary for sealing, many of the seals in this category are plated with a soft metal such as silver. Thus, the structural loading of the seal is taken by the base material, and sealing is accomplished by plastic flow of the soft plating material at the seal interface. Because of this plating, many of the seals in this class may be marginally re-used.

Typical seal configurations are shown in Figures XI-6-1 and XI-6-2.

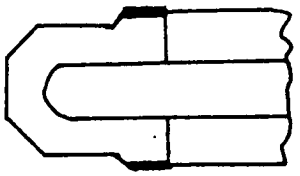

Fig. XI-6-1 Metallic Seal Structure with Plated Sealing Surfaces

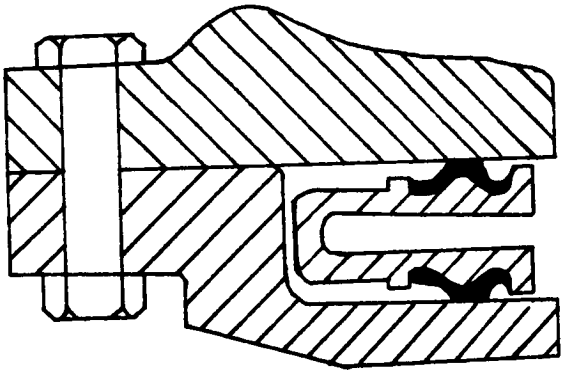

Fig. XI-6-2 Metallic Structure with Plastic Sealing Surface in a Separable Flange

Metallic non-pressure-energized seals must have an externally applied contact load to attain proper contact stress for sealing. Because the contact stress necessary for sealing with metal-to-metal contact is quite high, an attempt is made with some of the seal designs in this category to maintain line contact. In this way, since the entire contact load must be supplied by the seal housing, high interface contact stresses can be attained with relatively low contact loads. Since there is no appreciable pressure actuation and little or no flexibility in the seal itself, these seals are susceptible to increased leakage due to housing deformation, such as flange separation under the action of fluid pressure. Thus, a rigid housing design is necessary to ensure good performance of the seal throughout the range of operating pressure.

Since the sealing action for these seals is metal-to-metal contact, the relations between contact stress, surface finish and leakage are the same as for metallic pressure-energized seals. The only difference is that in this case the entire contact load must be provided by the housing. A decrease in leakage rate can be attained with a given seal only by increasing the contact load and, hence, the contact stress.

Creep, which causes a reduction in contact stress and is usually accelerated at high temperatures, is the principal high temperature limitation on this type of seal. This type of seal has a simple geometrical shape and, therefore, should be lower in cost than the more complicated

seal shapes. If high contact loads are available, this type of seal will perform well providing the proper contact stress can be maintained. Because of their simplicity, the handling and cleanliness requirements for this type of seal are not as severe as for pressure-energized metallic seals. The surface finish requirements are the same as with metallic pressure-energized seals. Typical seals are shown in Figures XI-6-3 and XI-6-4.

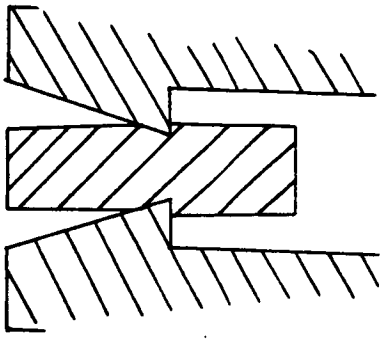

Fig. XI-6-3 Wedge Shaped Flange Soft Flat Gasket

Fig. XI-6-4 Solid Metal Profiled

Combination pressure-energized seals are plastic or rubber materials which have a metallic base that urge the nonmetallic materials into contact with the mating surfaces. The metallic structure provides sufficient loading to achieve deformation of the nonmetallic material at the interface. This loading is maintained even at low temperature when the nonmetallic materials become brittle. In addition, the metallic structure compensates for creep and volume change in the nonmetallic material. Figure XI-6-5 shows various types of these seals.

All combination non-pressure-energized seals must have an externally applied contact load to function. Their geometric configuration is such that the applied fluid pressure does little or nothing to aid in the application of the required contact stress for sealing. The application and maintenance of proper contact load is performed by the seal housing. Spiral wound gaskets are made up of alternate layers of metallic and nonmetallic materials. The metallic layers provide a degree of resilience. The sealing

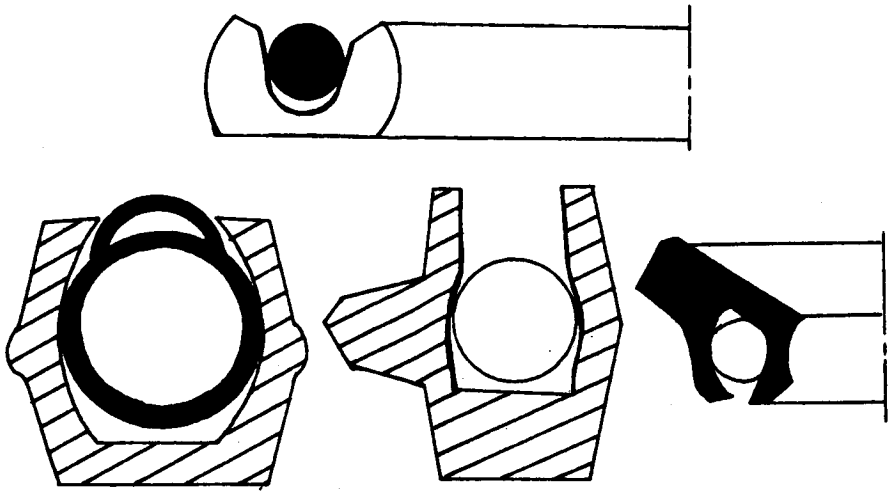

Fig. XI-6-5 Molded Elastomer Seal Metal Loading Spring

is accomplished by the nonmetallic material, usually asbestos. The resilience of the metallic layers makes it possible to re-use the gaskets. The metal jacketed type consists of a thin metal jacket completely enclosing a soft filler material. The filler may be a polymer, asbestos, or a soft metal. The thin metal jacket deforms easily and mates with the flange to form a sealing interface. The filler material acts as a support for the jacket and helps to maintain resilience. This type of seal may be used in applications where the sealed fluid is corrosive to the filler material but compatible with the jacket material.

The nonmetal coated gasket provides good conformability with the mating surface and, therefore, may be used with rough or warped surfaces. The nonmetallic layer is usually thick and is cemented to the metallic core. The metallic part of the seal supports the nonmetallic surface layer and provides resilience.

All the seals in these three subclassifications usually require less contact load than all metal seals, hence flanges and bolts, and similar housing configurations may be made lighter.

The leakage rate of static seals is usually not a straightforward point for discussion. As shown, leakage past an interface is a function of contact stress. Thus, the leakage rate could be decreased by increasing the contact stress. The allowable contact stress may be limited by other considerations such as maximum allowable bolt load and housing design considerations. Figure XI-6-6 shows a typical seal in this category.

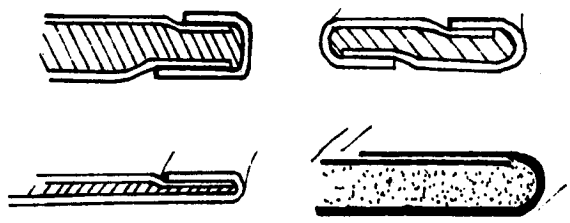

Fig. XI-6-6 General-Purpose Flange (Soft Metal), Gasket (Elastomer) and Metal Jacket Filler (Asbestos)

Nonmetallic pressure-energized seals generally have a flexible member that deflects under the action of the contact load and the pressure force. Because of the inherent flexibility of most nonmetallic seal materials, particularly polymers, the contact force due to deflection of the seal by the housing is usually small. In some designs, the deflection of the seal by the housing contributes a significant portion of the contact stress necessary for sealing. This type of seal is usually made of a polymer material. The natural resilience, the effect of pressure actuation, and the initial deflection, which is usually 10 to 20 per cent of the cross section width, act to reduce the problem of increased leakage due to flange or housing deformation. The leakage rates for polymer seals of this type are usually close to the leakage rates for the mechanically preloaded polymer seals. In many cases, however, the leakage rates for the pressure-actuated polymer seals may be higher than for the mechanically preloaded type because the contact stress may be lower.

The seals of this category have the same temperature limitations as nonmetallic non-pressure-energized seals. These seals are relatively low

in cost because of high volume production. Their natural resilience and ability to conform to the mating surface allows less stringent surface requirements. A surface finish of 16 to 32 microinches rms is usually recommended. Typical seals are shown in Figure XI-6-7.

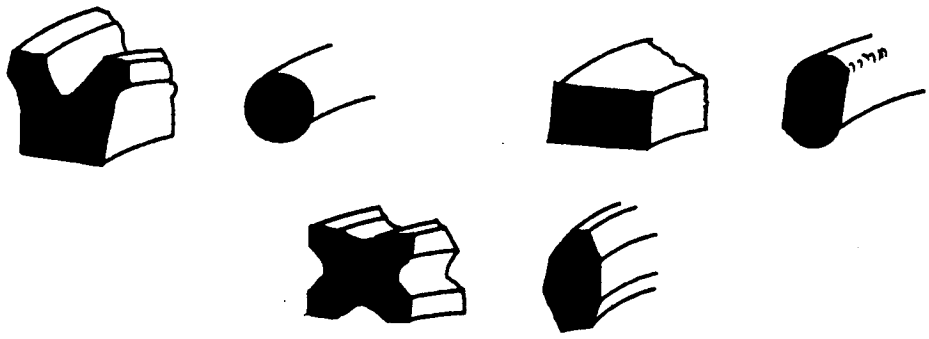

Fig. XI-6-7 Ring-Type Solid Elastomer

For nonmetallic non-pressure-energized seals, as with the other types of of mechanically preloaded seals, the entire contact load must be supplied by the seal housing. However, the contact stress necessary to attain good sealing is lower for nonmetallic seals. The resilient nature of polymers reduces the problem of increased leakage due to housing deformation. However, such materials as cork and asbestos have little natural resilience. The problem of increased leakage due to housing deformation with seals made of these materials could become serious. Therefore, rigid housing designs are necessary for seals made of nonresilient seal material. Because of their generally good performance and versatility, the remainder of this discussion will be devoted mainly to polymer seals.

Probably the best sealing short of welding mating parts can be obtained with resilient polymer seals. Experiments with O-rings and flat rubber gaskets have shown leakage rates of 10^{-6} STD cc per sec of helium and lower. The contact stress necessary to attain such sealing is substantially less than that required to attain minimum leakage with metal seals.

The chief operational limitations of the nonmetallic seals is extreme temperature. Hardening and loss of compression at high temperatures exhibited by polymers is the major limitations of the use of rubber-like

materials. Certain rubber compounds are available for use at temperatures as high as 450°F for continuous operation and even higher temperatures for short periods of time. The Viton compounds are used in this range. Brittleness at low temperatures sets the low temperature limit for polymer-type seals.

Because of their extremely wide usage and well developed manufacturing sources, the polymer seals are generally low in cost. Their natural resilience allows them to be re-used, although as a general rule seals are usually replaced when an installation is disassembled for repair because of their low cost. Since rubber-like materials conform readily to the contact surface under compressive stress the surface finish requirements for rubber static seals are not as stringent as for metallic seals. A surface finish of 16 to 32 microinches rms is usually recommended.

Sliding Seals

Sliding seals can be broadly classed on the basis of materials of construction and use. A distinction is made between metals and nonmetals, but no further differentiation is attempted. The sealing elements are most commonly circular, and seal dynamically at an inner or outer surface as typically described by a rod and piston seal. No distinction is made between uses since most seals can be used in either application.

Conforming seals are continuous elements such as uninterrupted circular rings in which sealing surfaces are urged into contact by resistance of the seal structure to deformation or externally applied forces. Precision mating seals are discontinuous elements with sealing interfaces brought into contact largely by precise geometrical mating of surfaces. Bellows and diaphragm seals are formed by elastically deforming a material. This type seal does not possess a rubbing interface but certain designs do include one or more static interfaces. Labyrinth and bushings are interstitial seals implying no contact of the sealing surfaces as opposed to the interfacial conforming and precision fit seals.

A subclassification of interfacial sliding seals can be made based on the relative influence of fluid pressure on the sealing element. Seal

structures which transmit substantial variations in interface forces when subjected to fluid pressure are classes as pressure-energized seals. Seal structures which transmit nominal variations in interface forces are classed as non-pressure-energized seals.

Interface contact loads are produced by the applied pressure and any radial and axial mechanical preload induced by interference of the seal with surrounding parts or by such external means as adjustment nuts. Seals which rely solely on radial interference are classed as radially preloaded seals. Other seals subjected to axial loads usually transfer part of the axial load to the radial contact surface. These seals are classed as radial and axial preload seals. To make the identification of seals, typical seals conforming to each class and subclass are described in Figures XI-6-8 through XI-6-13.

Rotating Shaft Seals

The subclassification of rotating shaft interfacial seals is based on the construction features of the seals. Two subclassifications are axial and radial seals depending upon the orientation of the interface subjected to relative motion. Axial seals are commonly called face or mechanical seals. Figure XI-6-14 shows a typical face seal. Detailed descriptions of face seals and theory of operation are found in Reference 10. Radial seals can be further classified as lip, packing and circumferential split ring seals. Lip seals, as typically shown in Figure XI-6-15, are commonly made from plastics or rubber materials. A typical identification of these seals is the relatively flexible leg which is urged radially against a rotating shaft. In addition, pressure-energized sliding seals as presented on page XI-6.10 may also serve as rotating shaft seals. Another class of sliding seals identified as precision mating seals may be used as rotating seals. Quite often, however, these seals, when used in rotary applications, are called circumferential split ring seals. Figure XI-6-16 shows a typical seal in this classification. The last type of interfacial seal is the stuffing box or packing seal shown in Figure XI-6-17. Packings can be described as deformable materials such as asbestos, metal foils, or cork

which are compressed in a groove surrounding the shaft. An external loading mechanism is necessary to maintain the material in contact with the shaft.

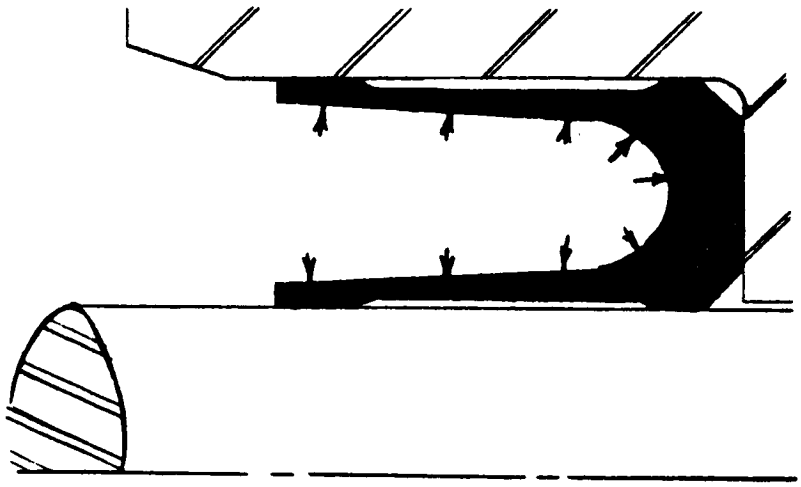

Fig. XI-6-8 Metallic Pressure Energized Seal

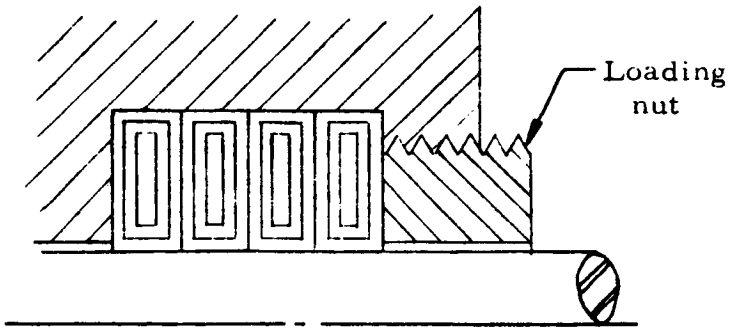

Fig. XI-6-9 Nonmetallic - Nonpressure Energized Seal

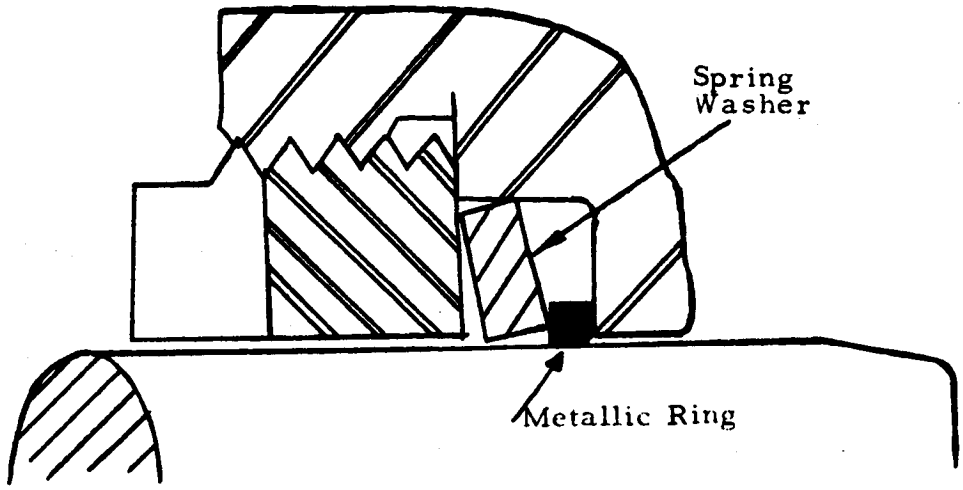

Fig. XI-6-10 Metallic Nonpressure Energized Seal

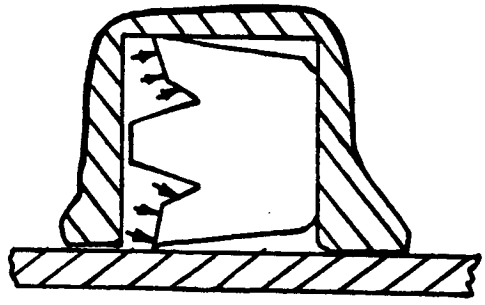

Fig. XI-6-11 Nonmetallic - Pressure Energized Seal

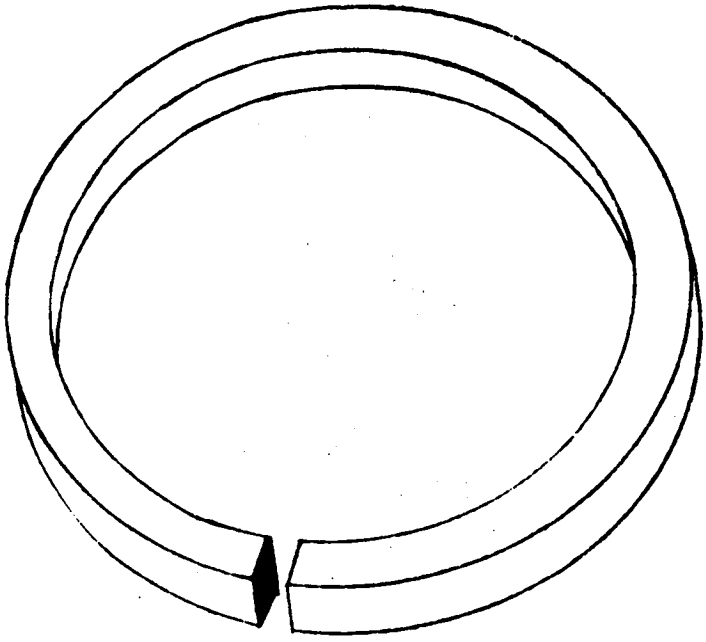

Fig.XI-6-12 Metallic Split Piston Ring Seal

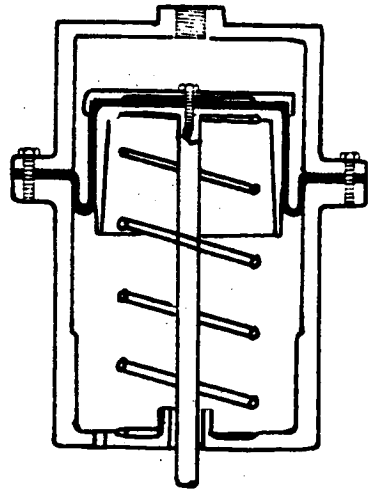

Fig. XI-6-13 Rolling Diaphragm Seal

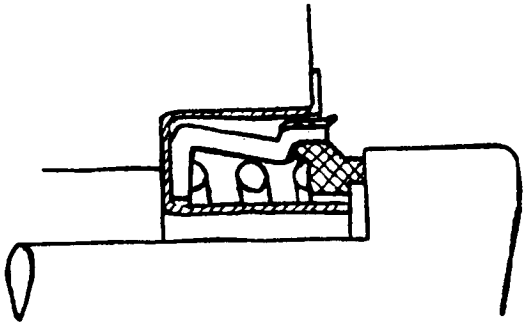

Fig. XI-6-14 Face-Type Seal

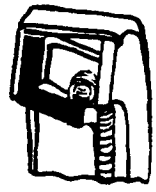

Fig. XI-6-15 Lip-Type Seal

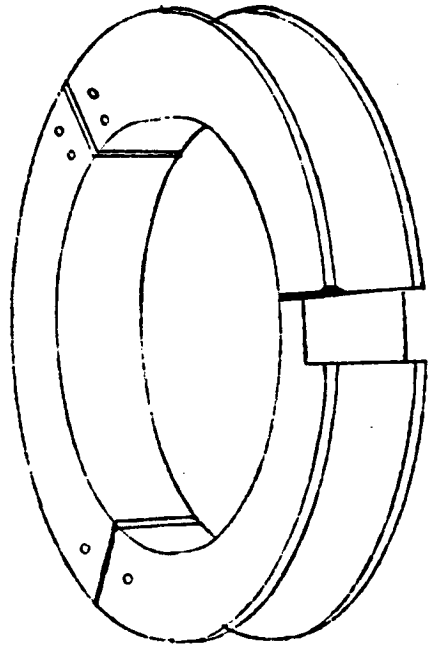

Fig. XI-6-16 Circumferential Split-Ring Seal

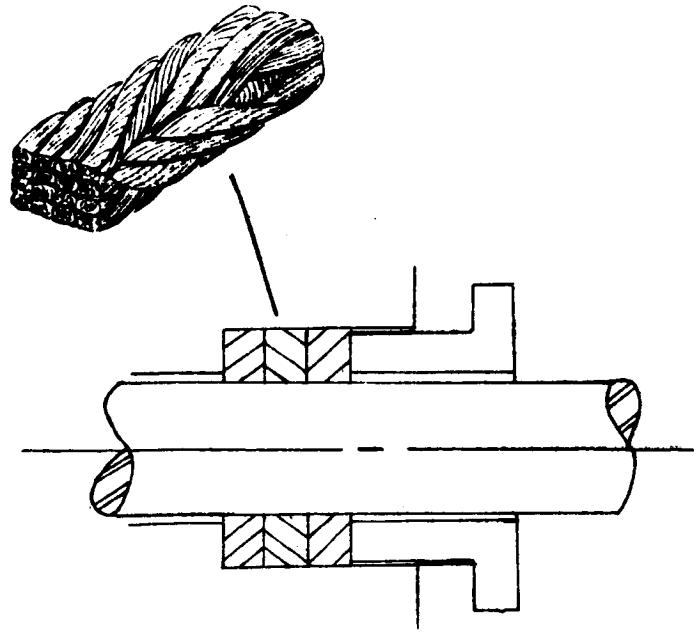

Fig. XI-6-17 Packing or Stuffing Box Seal

XI-7 SEAL DESIGN AND SELECTION METHODS

Introduction

The most important factors governing the leakage performance of a seal are the conditions existing at the sealing interface which include contact loading, material properties, and surface finish. These factors serve as input criteria in the selection of any seal configuration. If any of the general types of seals previously considered can meet and maintain the prescribed interface conditions, the seal can be suitable for a specific application providing it meets the following environmental criteria:

(1) Material-fluid compatibility
(2) Temperature
(3) Pressure
(4) Acceleration and shock loading

The requirements for sealing interfaces are described in Section X and should be reviewed in order to establish the input criteria. The material properties and surface finish are relatively fixed operational properties of a seal. The interface loading, however, is a function of the seal structure geometry and the cavity or housing which contains the seal. Additionally, the interface loading is dependent upon pressure and thermal deformation of both the seal structure and cavity.

Seal Housing

In general, seal housings can be divided into at least the following functional groups: fluid conduit connections, pressure vessel covers, dynamic seals, and for general bulk head applications. The aspects of each seal housing must be considered separately because of differences in configuration and manner in which housing structural loads are applied.

A large number of the seals in pressurization systems are duct and tube connector seals. The structural loads applied to this type of housing

include:

(1) Separation forces due to fluid pressure changes in flow momentum, and dynamic loading

(2) Torsion and bending due to tubing misalignment and thermal expansion

(3) Hoop stresses due to the fluid pressure

In addition to the structural forces applied to the connector assembly, the effects of variable thermal environment must be considered. The major effects on a connector assembly are:

(1) Reduction in contact stress at the seal as a result of creep or relaxation in the support housing

(2) Reduction in strength and modulus of the materials as a result of elevated temperatures

(3) Increased brittleness of some materials at cryogenic temperatures

(4) Differential thermal expansion resulting from differences in the thermal expansion properties of the materials in the seal and housing assembly, and from temperature gradients in the seal and housing assembly

Considering each of the preceding factors, the problem of connector housing design is indeed complex. The final design may often be a compromise between the opposing limitations of strength and weight. Extensive connector design criteria have been developed and are discussed in Section XI-9.

A second category of seal housings is pressure vessel covers. This general category includes such items as end caps of control valves, and flange-type covers on fluid storage tanks. In general, a pressure vessel cover can be considered to be any removable part that closes an opening in a vessel containing fluid, and whose primary purpose is not in the conduction of fluid from one region to another.

Since the cover is usually not a part of the fluid conduit system, it is not subjected to the torques, bending moments, and forces usually associated with the fluid conduit. The main structural loading on a cover comes from the pressure force due to the sealed fluid, the reaction loads due to contact with the seal, the loads imposed during installation, and gravitational effects.

The main function of the cover and its fastening mechanism is to provide the proper seal interface contact load. The interface load is intimately related to the deflections and distortions that take place in the cover and the seal. These distortions are mainly functions of:

(1) The fluid pressure force

(2) The seal reaction loads

(3) Installation loads

(4) Thermal phenomena such as differential thermal expansion and changes in material properties resulting from changes in environmental temperature.

The treatment of the problem including, simultaneous consideration of thermal and structural loads, is complex. Consequently, these effects are treated separately, and the effects of each can be superimposed.

Structural Loads can be analyzed using a generalized approach based on existing plate and shell theory and establishing relationships for the elastic displacement of the seal housing in the vicinity of the seal interface. Consider a cover geometry as shown in Figure XI-7-1 having cylindrical symmetry.

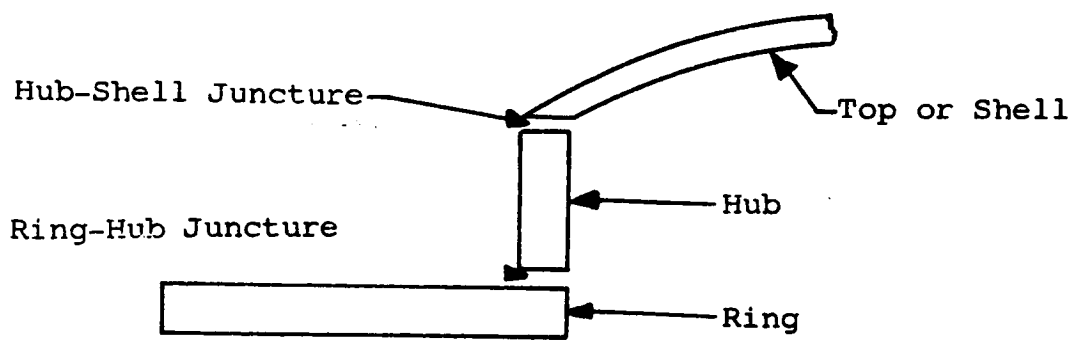

Fig. XI-7-1 General Cover Geometry

When fluid pressure, initial clamping load and seal reaction load are applied to the cover, elastic deformation takes place in each member of the cover. The deformation of each member is treated separately. The internal

stresses at these junctures are replaced by undetermined forces and moments and these, in turn, are treated as external forces in each independent analysis. Thus, a set of simultaneous deflection equations is developed. The solution of these equations is accomplished by the use of common boundary conditions, displacement and rotation, at the junctures.

The derivation of the deflection relations, the application of the boundary conditions, and a detailed discussion of the entire analysis process is contained in Reference 13 and 14. Because of the complex nature of the equations and the iterative process necessary for their solution, a digital computer solution is necessary. The type of computer routine, and the general solution of the problem is also discussed in these References.

In its completed form the results can be optimized and presented in graphical or tabular form to enable a designer to determine the elastic displacements in the vicinity of the seal for any geometry of cover meeting the restriction of cylindrical symmetry, and for the various modes of seal contact:

(1) Total contact (i.e., flat gasket with bolt holes)

(2) Contact within the bolt circle

(3) Contact outside the bolt circle

(4) Contact both within the outside the bolt circle but not total contact.

These force and deflection results can be combined with the seal structural design criteria to yield a complete structural, and leakage performance analysis for the entire seal assembly.

A simplified strength of materials analysis can often be made when the seal housing parts are less complicated. For example, consider a seal housing as shown in Figure XI-7-2 consisting of a flat cover bolted in place. Classical solutions for small elastic deformation of thin plates are contained in Reference 15 for cover geometries assumed equivalent to that shown in Figure XI-7-3. Essentially, the solution yeilds the plate deflection and corresponding load at the seal interface radius shown as r_o.

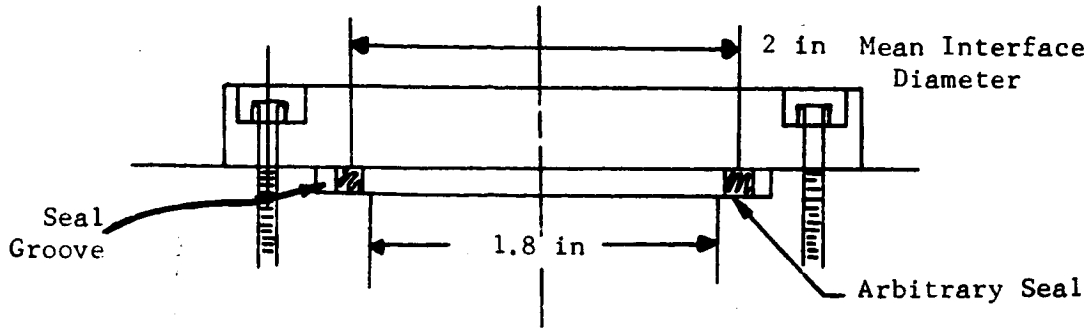

Fig. XI-7-2 Flat Cover Geometry

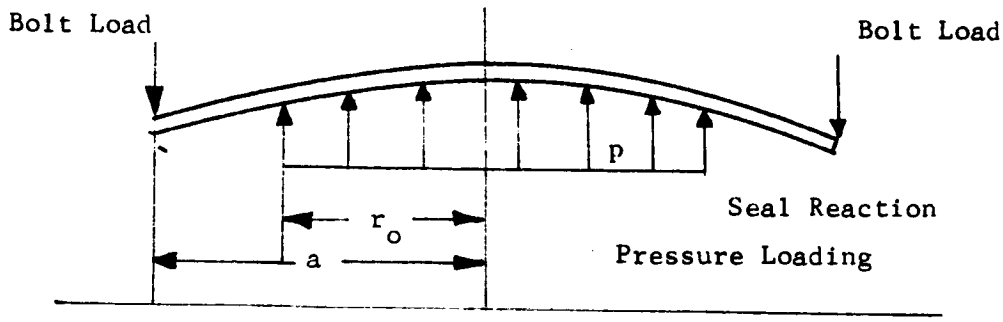

Fig. XI-7-3 Flat Cover Plate Geometry

The preceding discussion describes methods of estimating flange deflection resulting from the influence of fluid pressure. The next important criterion is the means by which the cover plate is fastened to the pressure vessel. The most common type of fastener used in this type of application is the bolt. A great deal of information exists on bolt loading, preload, torque to load relationship for bolt-type fasteners. In the case of bolted pressure vessel covers using the types of seal discussed thus far, certain particular requirements are present which can be stated:

(1) The bolts must be capable of providing the initial contact load at the sealing interface. The load is determined by the seal structural design.

(2) The bolts must be capable of withstanding the full fluid pressure force with tolerable elongation.

(3) The bolts and other members of the seal and housing assembly must have carefully mated thermal properties.

To analyze the cover, we proceed as follows:

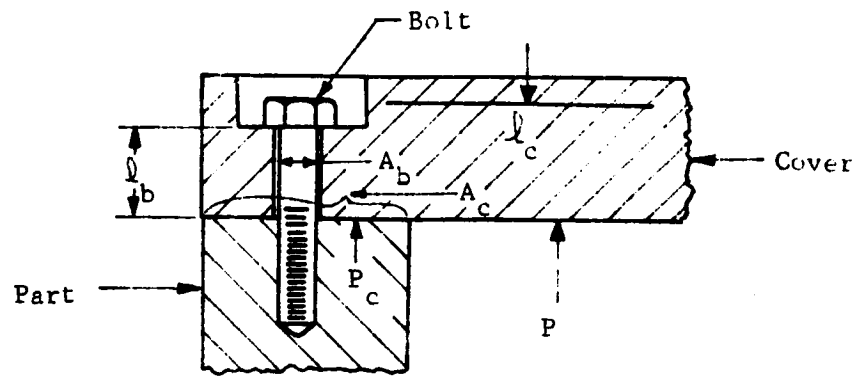

Fig. XI-7-4 Bolted Cover

If a part is bolted in place and an initial tensile force P_o is applied to the bolt, a corresponding compressive load is induced in the part. If no other forces are applied to the system, the load on the cover P_p and the P_b are given by:

$$P_b = P_o \tag{16}$$

$$P_c = P_o \tag{17}$$

If a load P is also applied to the cover, the relationship can now be expressed as

$$\left|P_b\right| = \frac{k_b}{k_b+k_c} P + P_o \tag{18}$$

$$\left|P_c\right| = \frac{k_p}{k_b+k_c} P - P_o \tag{19}$$

where k_b and k_c are the elastic constants of the bolt and cover.

$$k_b = \frac{A_b E_b}{\ell_b} \tag{20}$$

$$k_c = \frac{A_c E_p}{\ell_c} \tag{21}$$

where

A = effective area (in^2)

E = modulus of elasticity (psi)

ℓ = effective length (in.)

Figure XI-7-4 shows that the effective contact area of the cover is much larger than that of the bolt. Thus, as long as compression is maintained on the cover, changes in load, P, will have a small effect on the bolt load, P_b.

In practice, the initial load, P_o, is usually made sufficiently large so that when the load, P, is applied to the part, a compressive load, P_p, is still maintained. Maintaining a compressive load by application of the proper initial bolt load is extremely important in the use of flat gaskets for sealing. This subject has been under study in many fields and by many investigators (References 16 and 17).

The use of a sufficient initial bolt load is advantageous in reducing the effects of fatigue if the load, P, is fluctuating as in the case of varying pressure. In the case of varying load, P, the maximum and minimum bolt loads are found from Equation (18) by substitution of the maximum and minimum values of P. From this relationship it can be seen that the maximum bolt load is increased because of the initial load. However, the minimum bolt load is considerably larger because of the presence of the initial load than it would be if there were no initial load present. The resultant effect is to reduce the range of load fluctuation in the bolt. Since they depend on the magnitude of the range of stress variation, the fatigue effects are also reduced.

When the cover plate bolt and seal reaction loads are considered together, the relationship becomes more complex. Consider the following:

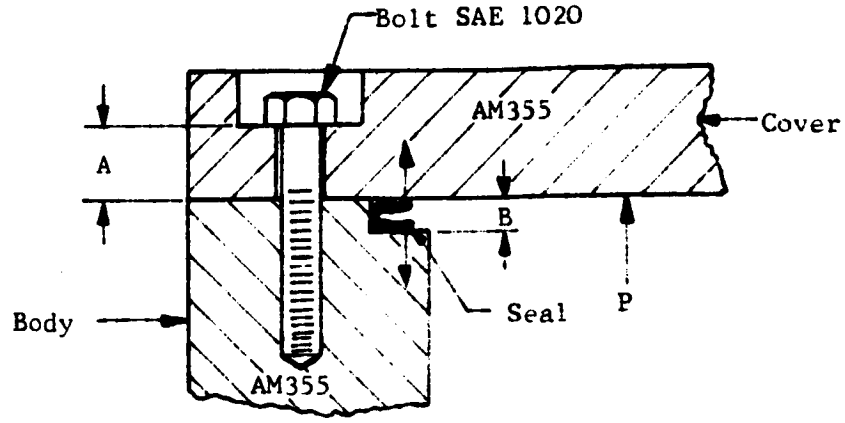

Fig. XI-7-5 Bolt Cover with Seal

When the bolt is torqued so that the cover just barely touches the body, the entire seal contact load, P_s, is taken by the bolts and the corresponding bolt load is given by:

$$P_b = P_s \tag{22}$$

All loads are expressed as forces on each bolt. Any additional load P, such as that due to fluid pressure, is also taken directly by the bolt. In the presence of a load P, the bolt load is now given as:

$$P_b = P + P_s \tag{23}$$

The total bold load variation will now be exactly the same as the variation in force P_s. The range of variation of the bolt force can be reduced if an initial compression is induced in the cover plate by increasing the bolt preload. Since the cover and body are usually much more massive than the seal, the compressive load induced in the cover by the additional bolt preload may not cause sufficient deflection to have a significant effect on the seal interface load P_s.

If the magnitude of the structural load P, due to fluid pressure or other causes, is known, the additional bolt preload, P_o, necessary to keep the cover in compression can be found from Equation (26). Since a load P_s has already been applied to the bolt to deflect the seal, the total bolt

load in the presence of load P can now be expressed as:

$$P_b = \frac{k_b}{k_b+k_c} P + P_o + P_s \tag{24}$$

The maximum, minimum and average bolt loads can now be calculated and plotted on a working stress diagram or Goodman diagram to determine if these stresses are within the fatigue limits of the bolt material.

There may be cases where it is not possible to apply sufficient bolt preload, P_o, such that the cover remains in compression, because an excessive bolt load, as given by Equation (32), would occur. In these cases, the maximum allowable preload, P_o, can be determined from the relation $P_b = P + P_s + P_o$. In this relationship, P_b will be the maximum allowable bolt load determined from working stress considerations.

In addition to the consideration of bolt loading, the deflection or elongation of the bolts under load must also be considered. This elongation must be added to the cover deflection at the seal contact point to determine the total housing deflection at the sealing contact point. The allowable deflection at the sealing contact point is determined by the seal structure and the seal interface criteria. Thus, either the seal structure or the housing design or both may have to be modified until an allowable deflection at the sealing interface point is achieved. The elongation of a bolt is given as:

$$\delta = \frac{F_b \ell_b}{A_b E_b} \tag{25}$$

To minimize bolt elongation the free length of the bolt should be kept as small as possible. Also a short bolt length minimizes the effects of thermal expansion. Thus, bolt load, fatigue considerations, bolt elongation and bolt length must be carefully considered as part of the housing design.

Thermal Expansion

The dimensional changes in the components comprising a housing and

seal structure assembly due to changes in temperature of the assembly can exert a significant influence on the performance of a seal. The differences in expansion or contraction of the parts can often cause displacement equal to or larger than the permissible deflection of the seal structure.

The problem is even more complicated when large temperature fluctuations are expected. This occurs because the expansion characteristics of material change with magnitude of temperature. To minimize the problem of thermal expansion in a seal housing assembly, it is necessary to match the thermal expansion properties of the parts as closely as possible. This will minimize the effects of differential thermal expansion. Even if all of the parts were of identical material, the problem of differential thermal expansion would still exist because of the presence of temperature gradients in the seal and housing assembly.

To illustrate the effects of thermal expansion, the following example is presented. (See Figure XI-7-5 for illustration)

Dimension	Material	Thermal Expansion at 1000°F
Bolt Free length A = 0.375	1020 Stl	0.75%
Groove height B = 0.25	AM355SS	7.2×10^{-6} from manufacturer literature
Seal height B = 0.25	17-7PH	

The thermal expansion under these conditions is given as:

Part	Expansion (in)
Bolt	0.00271
Groove height	0.0018
Seal height	0.0025

The total differential expansion in this case is (0.0027 + 0.0018) - 0.0025 = 0.002 in. This represents a considerable improvement. The differential expansion can possibly be compensated in the design of the seal structure. Sufficient initial elastic deformation of the seal structure can be provided so that after the thermal expansion takes place there will still remain sufficient elastic deflection in the seal structure to maintain an

adequate contact load at the sealing interface. In the case of pressure-actuated seals, the fluid pressure acting on the seal structure tends to increase the contact force.

The same type of procedure is necessary when the seal assembly is to be operated at extremely low temperatures. If the seal contracts at a greater rate than the groove or the bolts, interface separation could occur. If the flange or cover material contracts at a greater rate than the seal, the decrease in groove height may counteract the shrinkage of the flange at the bolt which tends to decrease the bolt clamping load.

The effect of pressure gradients must also be considered. If the seal temperature suddenly increases because of contact with a hot gas, a large temperature gradient can be created between the seal and the bolts. In this case there is a tendency for the seal to expand at a much greater rate than the bolt. However, the seal is in contact with the cover and the expansion of the seal structure is restrained. This restraint against the expansion of the seal induces an additional load on the bolts. It is possible that this induced load can deform the bolts plastically. Thus, when the gradient decreases there may be a substantial decrease in contact force at the sealing interfaces. If large thermal transients and large temperature gradients are expected in the seal and housing assembly, the thermally induced stresses on the bolts should be estimated. The results of this estimation may indicate that, because of effects of the temperature gradient, higher strength bolts are necessary. This would be indicated by an analysis in which temperature gradients are neglected. This estimation can be accomplished using the standard strength of materials approach using elastic theory or the increase in load can be estimated from empirical load deformation data. In the use of empirical data, the change in the seal dimension that is due strictly to thermal expansion can be estimated. The additional bolt load required to restrain this expansion is then assumed to be equal to the load required to produce the same change in seal dimension by deformation of the seal, and is obtained from the load versus deformation data.

A treatment of the problem by elastic theory is illustrated in the following example.

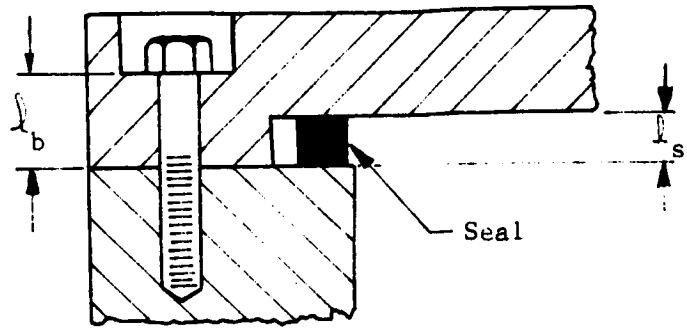

Fig. XI-7-6 Simplified Cover and Seal Geometry

If the temperature of the entire assembly is raised by an amount ΔT, and the seal has a greater rate of expansion than the bolt, the restraint on the seal will induce an additional load on the bolt. From static equilibrium conditions the following conditions must hold:

(1) The total compressive force on the seal must be equal in magnitude to the total additional tensile load on the bolts.

(2) The elongation of the bolt due to the rise in temperature plus the stretching of the bolt due to the additional force must equal the expansion of the seal due to the rise in temperature minus the compression of the seal due to the additional load on the seal interface.

These relations may be expressed as follows.

Load relation:

$$F_b = F_s \tag{26}$$

Elongation relation:

$$\delta_{Tb} + \delta_{Fb} = \delta_{Ts} - \delta_{Fs} \tag{27}$$

The temperature expansion of the seal and the bolt can be expressed as:

$$\delta_{Ts} = a_s \ell_s \Delta T_s \tag{28}$$

$$\delta_{Tb} = a_b \ell_b \Delta T_b \tag{29}$$

The deflection of the bolt and seal due to the forces are given by:

$$\delta_{Fb} = \frac{F_b \ell_b}{A_b E_b} \tag{30}$$

$$\delta_{Fs} = \frac{F_s \ell_s}{A_s E_s} \tag{31}$$

Substituting relations (36) and (38) in (35) yields:

$$a_b \ell_b \Delta T_b + \frac{F_b \ell_b}{A_b E_b} = a_s \ell_s \Delta T_s - \frac{F_s \ell_s}{A_s E_s} \tag{32}$$

Equation (32) shows the general relationship between the loads and deflections of the seal and bolts. In cases where no gradients exist in the assembly but a temperature change of the entire assembly is taking place $\Delta T_b = \Delta T_s$. During a thermal transient, in general $\Delta T_b \neq \Delta T_s$. In the most extreme case of a thermal shock either ΔT_b or ΔT_s can be assumed to be equal to zero while the other assumes some finite value. In all cases the total forces must be equal. Thus, if the geometry and thermal expansion coefficients are known, the additional force that is due to any assumed temperature gradient condition can be calculated from Equation (32). This thermally induced load must be added to the total bolt load including the preload, seal reaction, and pressure load. If the bolt yields, then larger bolts or higher strength bolts are required to withstand the thermally induced forces.

Other Thermal Effects

In addition to the direct effects of thermal expansion, temperature changes exert more subtle influence on the seal and housing assembly be-

cause of the changes in physical properties caused by temperature changes. Tables XI-7-1 and XI-7-2 show the variation of modulus of elasticity and yield strength with temperature for several metals.

As the temperature increases, the modulus of elasticity decreases; thus, more deflection can be produced with a given force. Therefore, structures at high temperature are less rigid under the same loading as structures at lower temperatures. The decrease in yield strength at high temperatures must be carefully considered when designing a seal structure for high temperature applications. The yield strength and modulus of elasticity at the maximum operating temperature are suggested for use at design calculations.

Creep occurs when long periods of operation at elevated temperatures are encountered. Creep is the slow steady continuous plastic deformation that occurs in most metals at elevated temperatures at stress levels far below the yield strength of the material. Quantitative data on creep are extremely limited, and little is known about the theoretical basis of the phenomenon.

Seal Structure

An objective in the analysis of any interfacial seal is to relate the deformation of the seal structure to the load acting at the sealing interface. Among the factors governing deformation, the structural shape is the most significant variable. Aside from strength requirements, the shape of a seal is most often determined by the designer's conception of a seal. It is usually an individualistic design approach since there is often little agreement on the criteria for effective sealing. This is demonstrated by the vast array of commercially available seals, many of which are intended for the same functions. To show general techniques for metallic seal structure analysis, the case of a cantilever leg seal of constant thickness is considered. The analysis of other shapes can be found in References 13 and 14.

The subsequent analytical criteria for the seal shown in Figure XI-7-7 were originally developed by General Electric Company (Reference 14). The

general configuration of the seal is typical of many commercial seals. By maintaining a small contact area, fairly high contact stresses may be achieved without resorting to high total contact loads. This type of seal is usually designed so that the bending stresses in the seal legs remain elastic and the legs thus retain their resilience. A configuration of this type is particularly useful when the sealing contact area can be coated or plated with a soft material. If the seal is not coated or plated, it may be difficult to achieve the proper contact stress at the sealing contact area.

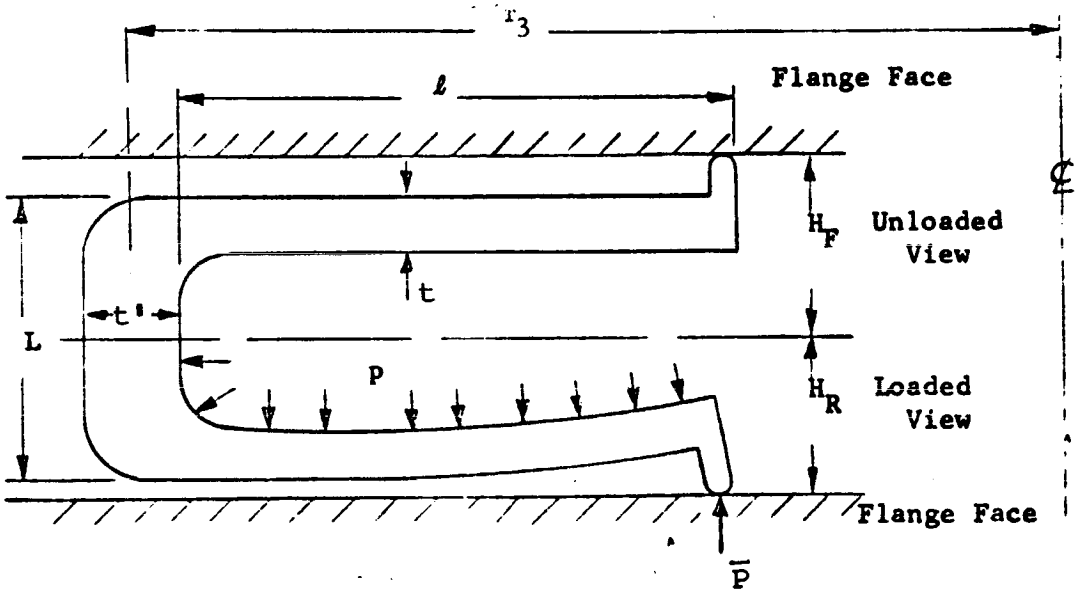

Fig. XI-7-7 Seal with Cantilever Leg of Constant Thickness

As discussed in Section X-2, the contact stress required to achieve adequate sealing with most structural metallic materials such as steel and aluminum is quite high. To attain a sufficient initial interface contact stress and stay within the elastic limits on the bending stress, σ_b, of the seal legs, the stiffness of the seal leg must be large. Large stiffness of the seal legs, however, reduces their ability to deflect under the pressure loading, thereby reducing the effectiveness of the pressure actuation. In any event the procedures developed by General Electric (Reference 14)

simplify the design calculation for these particular seal configurations and should prove useful in cases where the required sealing contact stress is relatively low, i.e., plated or coated contact surfaces. Because the contact load is usually high, these seals are seldom used in dynamic applications. Thus, this type of seal configuration is more suitable for static seal application.

Application of Analytical Methods

An example of the application of analytical techniques to a seal is presented for a Naflex (Reference 13) seal installed in a cover configuration shown in Figure XI-7-13. The materials of construction are shown in Figure XI-7-5.

Following the procedures outlined in this Part, the deformation can be approximated using the simplified flat cover criteria. Since the diameter of the seal contact area is given, a bolt circle radius can now be assumed. Thus, the ratio r_o/a is established where r_o is the contact area radius and a is the bolt circle radius. The flange or cover plate deflection parameter at the contact point can be obtained as a function of the ratio r_o/a. The following relationships are used in the analysis. Assume a maximum deflection at the seal interface, of $y_o = 0.001''$ and $\frac{r_o}{a} = 0.5$. The maximum stress is calculated as 14,940 psi and the cover thickness is 0.61 inches.

A 2 inch nominal diameter Naflex groove flange seal was composed of a 4340 steel structure covered with a 0.004-inch coating of Teflon. The geometry of the metallic structure is shown in Figure XI-7-13. The manufacturer's identification of this seal is VD261-0030-0036 (Reference 13), and it was recommended for the following applications:

Temperature:	-425 to 300°F
Pressure:	5000 psi
Fluid:	Liquid oxygen, nitrogen, hydrogen, air; gaseous oxygen, nitrogen, hydrogen, helium, air; water and corrosive liquids.

The seal was assumed to be installed in a cavity having a depth of 0.148 inches as recommended by the manufacturer. From the free dimensional height of the seal, as shown in Figure XI-7-13, the initial axial seat deformation is 0.1697 - 0.1480 inches or approximately 0.022 inches, neglecting any effects of the Teflon coating.

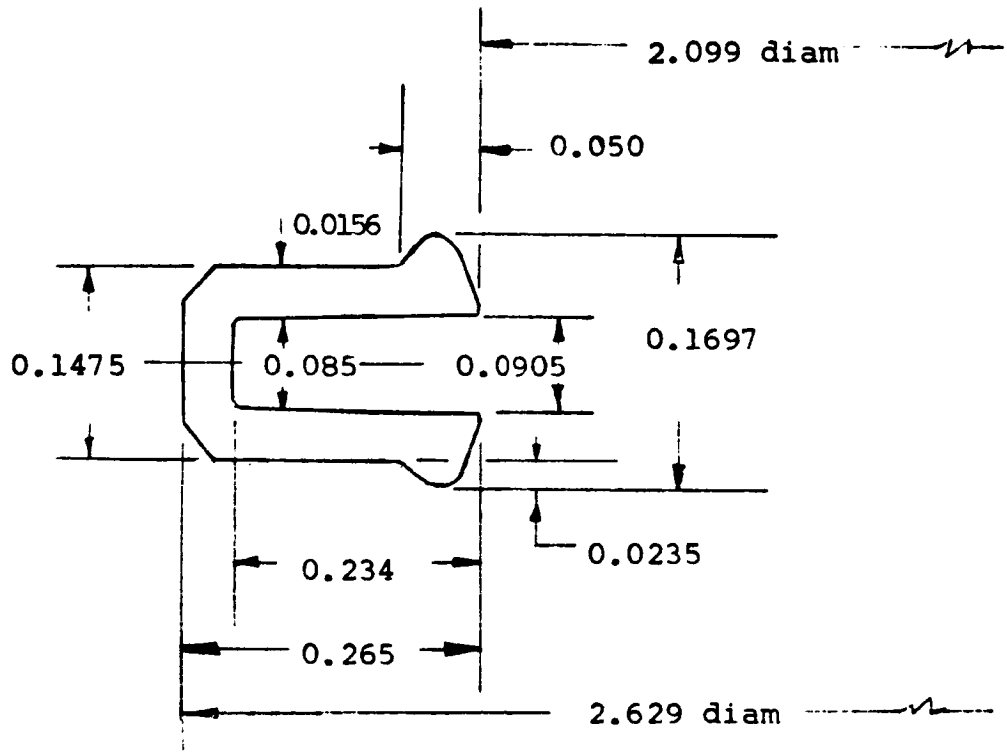

Fig. XI-7-8 Two-inch Diameter Navan Seal (Part No. VD261-0030-0036)(Ref.13)

The deformation of the seal structure is assumed to be elastic and the influence of the Teflon coating is neglected. The analysis is accomplished using equations 33 and 34.

From Figure XI-7-13

$L = 0.1425$ in.

$\ell = 0.234$

$2H_F = 0.1697$

Groove depth = 0.148

$2h = 0.1475 - 0.0850 = 0.0625$

$h = 0.0312$ in.

Then:

$$\frac{\ell}{h} = \frac{0.234}{0.0312} = 7.5$$

The initial deflection is given by

$$2Y_e = 2H_F - 0.148$$
$$2Y_e = 0.1697 - 0.148 = 0.0217$$
$$Y_e = 0.0108 \text{ in}$$

Since all the geometric properties of the seal are known, equation 33 can be used to determine the contact load.

First calculate the deflection parameter:

$$\frac{y_e E}{1-\upsilon^2}$$

where

$E = 30 \times 10^6$

υ = Poisson's ratio = 0.3

$$\text{Deflection parameter} = \frac{(0.0108)\ (30)\ (10^6)}{1 - 0.3^2} = 35.6 \times 10^4$$

The contact load per unit circumference can be determined by dividing the deflection parameter by the known (ℓ/h) ratio. This operation yields a loak:

$$R_s = 210 \text{ lb/in}$$

The results of the load-deflection experiment performance on a Teflon-coated seal are shown in Figure XI-7-14. The maximum load applied at the

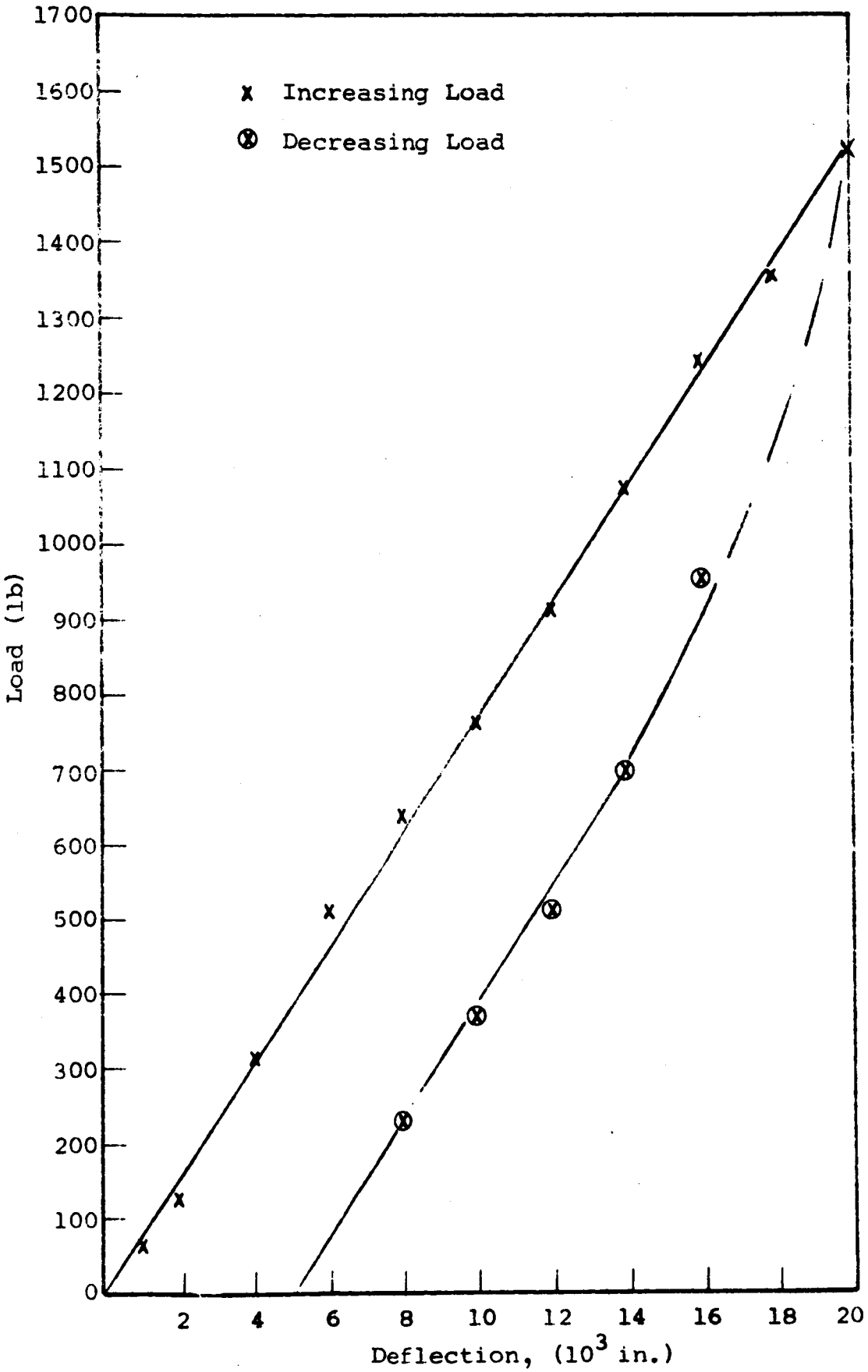

Fig. XI-7-9 Load Deflection Characteristics of a Naflex Seal

maximum deflection of 0.020 inch is 1525 pounds. Thus, the reaction on contact load per inch of interface contact is given as:

$$R_s = \frac{1525}{\pi_3 D_i} = 242 \text{ lb/in}$$

where

$$D_i \approx 2.0 \text{ in}$$

This value is in fair agreement with the theoretical contact load of 210 lb per in predicted in the design analysis. The straight-line loading curve indicates that most of the deflection of the seal legs is an elastic process. This is further substantiated by the fact that only 0.005 inch permanent set was exhibited by the seal after complete release of the load. Part of this is attributed to plastic deformation of the Teflon coating. The preceding results are in close agreement with the manufacturer's literature.

Teflon is fairly deformable under compression. However, because of the spherical interface contact surface it is difficult to estimate the contact area that will result from plastic flow of the Teflon under the compressed contact load.

The design curves of Section X-2 show that for unconfined materials the corrected stress ratio approaches asymtotically a value less than 0.4. This means that as the load increases, the material flows plastically until the apparent contact area is large enough to support the load. Since Teflon is rather easily deformed under a compressive load, a stress ratio will be assumed and the leakage will be calculated. This leakage will be compared with the experimental results and the comparison will serve as a check on the validity of the initial assumption.

Assume the corrected stress-ratio is given by:

$$\frac{W^{2/n'}}{A_A} / \sigma_m = 0.30 \qquad (51)$$

where

σ_m = 3870 psi

n' = 2.8

A_A = apparent area of contact

W = total applied load = $R_s D$

R_s = 210 lb/in. of circumference

D = 2 in.

Then, $A_A = 0.1465 \text{ in}^2$ and the width of contact is:

$$\bar{A} = \frac{A}{\pi D} = 0.0234 \text{ in} \tag{52}$$

Leakage Prediction

The design curves of Section X-2 indicate a conductance parameter of $h^3 = 1 \times 10^{-22}$ in the neighborhood of a stress ratio equal to 0.3.

The helium leakage can now be predicted from the flow equation:

$$Q_o = \frac{(D_o+D_i)(P_{in}^2-P_{out}^2)}{12\mu(D_o-D_i)p_o} h^3 + \frac{0.958\,\lambda_o(P_{in}+P_{out})(D_o+D_i)}{\mu(D_o - D_i)} \tag{53}$$

where

$$D_o = 2 \text{ in.} + \bar{A}$$
$$D_i = 2 \text{ in.} - \bar{A}$$

The leakage predictions as a function of temperature and pressure are shown in Table XI-7-1.

The preceding calculations were based on the assumption that the contact load remains constant and equivalent to the initial seal deformation. In an actual application, the load does vary due to pressure and thermal deformation of the housing and seal structure. The critical effects occur at the higher temperature limit of 300°F, assuming that the seal is installed at normal temperatures. To estimate the effects of load variations, the characteristics of the experimental apparatus, described in Reference 13 are used as guidelines.

Table XI-7-1

LEAKAGE PREDICTION OF A NAFLEX SEAL

PRESSURE	HELIUM LEAKAGE RATE (cc/sec,STP)		
(psia)	@ 80°F	@ -320°F	@ 300°F
114.7	8.85×10^{-7}	2.5×10^{-6}	6.77×10^{-7}
214.7	1.77×10^{-6}	5.0×10^{-6}	1.35×10^{-6}
414.7	3.58×10^{-6}	1.01×10^{-5}	2.74×10^{-6}
514.7	4.44×10^{-6}	1.25×10^{-5}	3.39×10^{-6}
614.7	5.49×10^{-6}	1.55×10^{-5}	4.19×10^{-6}
814.7	7.46×10^{-6}	2.11×10^{-5}	5.71×10^{-6}
1014.7	9.44×10^{-6}	2.67×10^{-5}	7.22×10^{-6}
1214.7	1.16×10^{-5}	3.28×10^{-5}	8.87×10^{-6}
1414.7	1.38×10^{-5}	3.90×10^{-5}	1.05×10^{-5}
1614.7	1.60×10^{-5}	4.52×10^{-5}	1.22×10^{-5}
1714.7	1.72×10^{-5}	4.86×10^{-5}	1.31×10^{-5}
1814.7	1.84×10^{-5}	5.21×10^{-5}	1.41×10^{-5}
2014.7	2.04×10^{-5}	5.77×10^{-5}	1.56×10^{-5}

The experimental flange or cover plate was designed for a 0.001 inch deflection under pressure. Since the seal structure deflection was 0.020 inch, the effects of pressure on the load reduction due to flange separation is negligible. This corresponds to a load reduction of 7 per cent and is well within the 50 per cent limits of hysteresis stress relaxation.

Figures XI-7-15 and XI-7-16 show the results of leakage evaluation of the Naflex seal. Room temperature results, shown in Figure XI-7-15, and the low temperature results, shown in Figure XI-7-16, are in close agreement with the predicted leakage rates. The actual results are within the one order of magnitude deviation that is expected from the predicted leakage rates.

Summary of Seal Structure Requirements

While it was not feasible to consider all of the possible seal structures and applications, the general techniques for seal evaluation have been briefly outlined. Additional details can be found in References 13 and 14. The case of sliding seals was not directly considered but a review of the general class of seals shows that similar analytical techniques

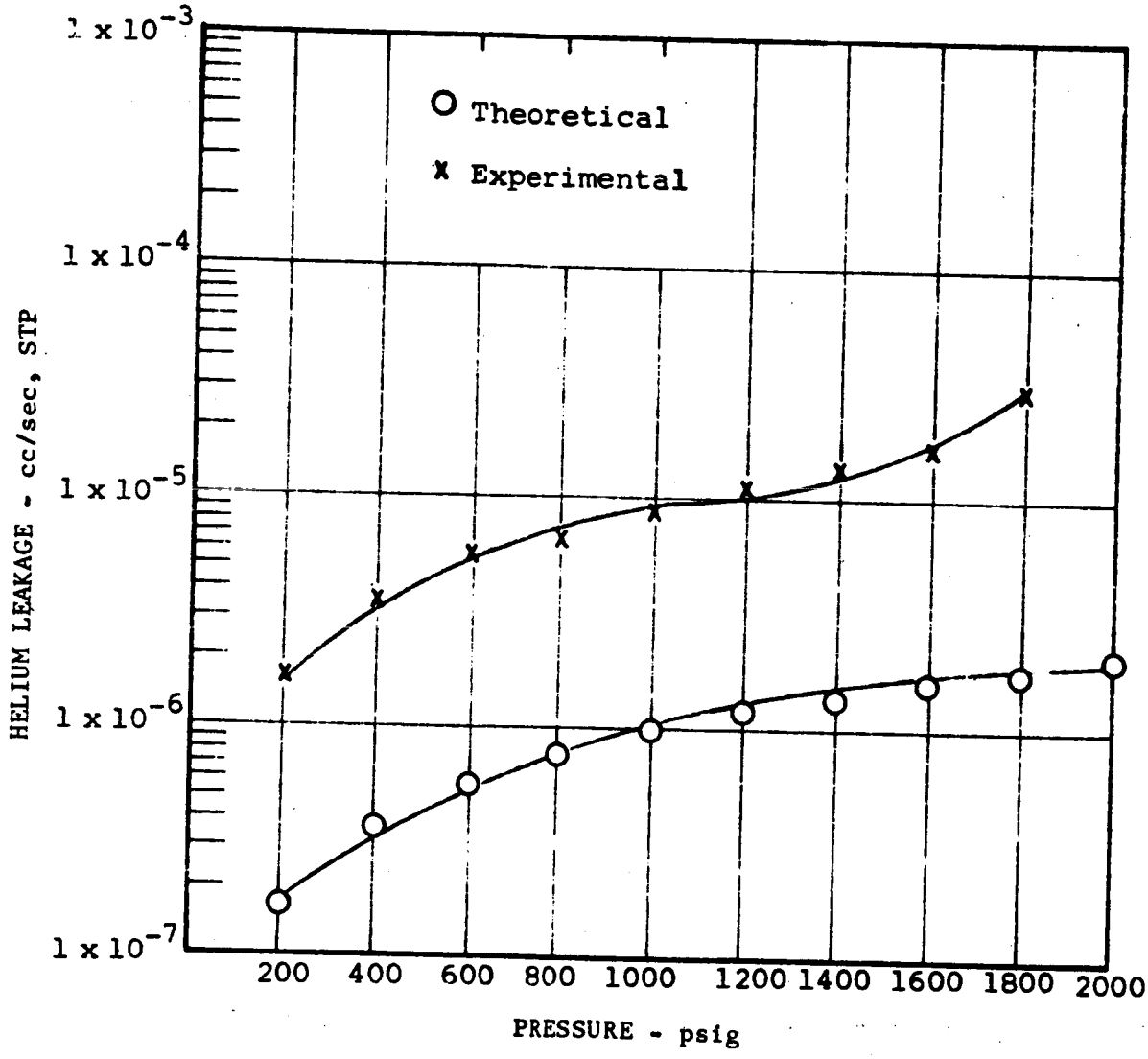

Fig. XI-7-10 Leakage of a Two-inch Naflex Seal at 80°F

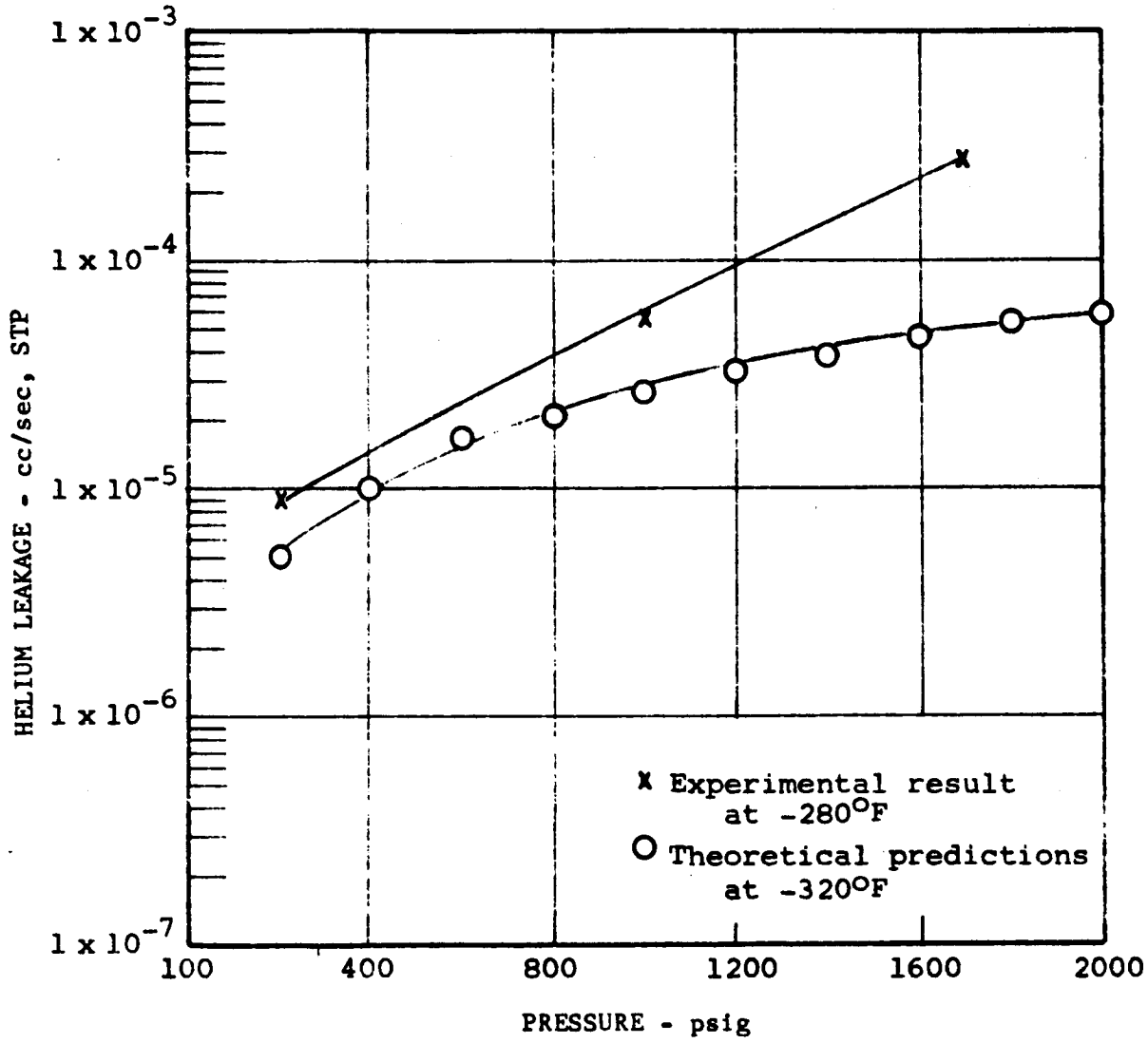

Fig. XI-7-11 Leakage of a Naflex Seal at Low Temperatures

as outlined can be readily applied. Similarly, elastomeric seals were not considered. However, the procedures outlined in Section X-2, can be applied to elastomeric seals if the assumption is made that the forces acting on the seal structure are transmitted hydrostatically through the material.

The general seal structure must be resilient to compensate for thermal and pressure deformations of the seal and seal-related housing. Many commercial seals are pressure-energized to produce this effect, although the philosophy behind it is usually one of attempting to increase the deformation at the interface. The influence of additional pressure loading in commercial seals is almost negligible. To clarify the requirements for a seal structure, the following can be stated:

(1) The structure must be capable of imposing the initial interface load required for minimum leakage under all operating conditions.

(2) The structure must maintain approximately 50 per cent of the initial load when the interface is plastically deformed

$$\frac{W^{2/n'}}{A_A} \sigma_m > 0.1 \quad \text{(Refer to Section X-2)}$$

This effect is defined as a hysteresis phenomenon attributed to the relative influence of elastic structure to plastic interface deformation. Thus, the seal structure must provide a minimum load when deformations occur as the result of individual thermal or pressure effects or combined effects.

(3) No relative transverse displacement of the sealing interfaces should occur due to thermal or pressure deformations. This results in wear debris generation and a deterioration of the minimum leakage paths in the interface.

(4) Thermal effects are difficult to estimate theoretically and, hence, some experimental development is necessary for those seal applications where large temperature variations occur. A selection of materials offering thermal compensation effects can overcome this problem.

(5) The deformation of a metallic structure due to pressure and thermal deformations of the structure plus the housing should remain within the elastic range of the materials. Preferably, maximum stresses should be within the fatigue limits under the most adverse operating conditions.

XI-8 EXPULSION DEVICES

Introduction

The functional requirements of spacecraft subsystems may impose conditions on the pressurization system such that

(1) the pressurant gas must be stored initially in its liquid state in the pressure vessel

(2) the pressurant gas is stored in the same vessel with a different gas or liquid such as a propellant

In both cases, it is functionally necessary to prevent mixing of the fluids where mixing can be produced by sloshing, zero gravity, or normal diffusion. Two methods can be used to produce separation of the fluids. One method employs positive expulsion devices which are characteristically described as a mechanical separation produced by an impermeable membrane. The method is used when the two fluids cannot contact one another without reaction or when sloshing is to be completely eliminated. The second method utilizes other principles of separation and is defined as non-positive expulsion techniques. This latter method is employed when minimum sloshing can be tolerated and when the fluids can form a common interface without reaction. The separation can be achieved on a continuous basis within the pressure vessel or just prior to exhaust from the vessel. Both techniques have common reliability limitations arising from insufficient technological development.

Positive Expulsion Devices

The conception of a positive expulsion device hinges upon the geometry of the pressurized tank and the degree of leakage which can be tolerated. Two forms of devices are the piston and bladder. The piston device shown in Figure XI-8-1 requires sliding seals which can be interchanged with bellows seals. The tank configuration must be relatively cylindrical. The choice of sliding seals suggests significant leakage while the bellows limits the volume which can be expelled to that permitted by its geometry,

volume and deformation characteristics. The design, fabrication, and deformation characteristics of bellows is in a somewhat undeveloped technology status. Several configurations for convolute bellows are available, each differing in the fabrication process employed. In turn, the fabrication and configuration concepts influence the deformation and reliability characteristics. A theoretical insight into the deformation problem is necessary before each aspect can be related together. At the present time no comprehensive analysis of bellows deformation has been advanced. Most of the existing information is based on gross simplifications of the problem or on trial and error.

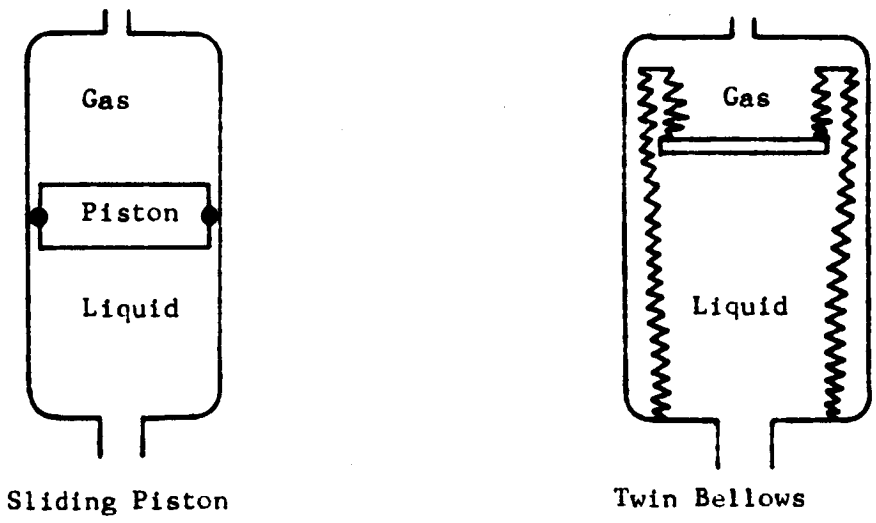

Fig. XI-8-1 Piston Like Positive Expulsion Devices

Generally, the flexible bladder type of expulsion device is more reliable and offers adaptability to spherical tanks with a maximum amount of expulsion efficiency. The bladder materials must be impermeable and compatible with both the liquid and gas.

When a propellant such as hydrazine is to be stored alone in a tank, a number of elastomers serve adequately, i.e., butyl or ethylene propylene rubber. These materials are fairly inert and impermeable to hydrazine. Storing the oxides of nitrogen is another matter, however. In the storage

of nitrogen tetroxide, three materials problems are controlling chemical attack, damage from creases, and permeability. Essentially no elastomers are inert to N_2O_4. Inert polymers, such as Teflon, are permeable. Metals alone seem to be reasonably inert and impermeable to N_2O_4, but metals are easily damaged when tight folding causes creases. Creasing is inevitable unless some form of controlled bladder folding is induced, since most surface shapes will collapse with a multitude of random folds which cause creases. Two typical bladder configurations are shown in Figure XI-8-2.

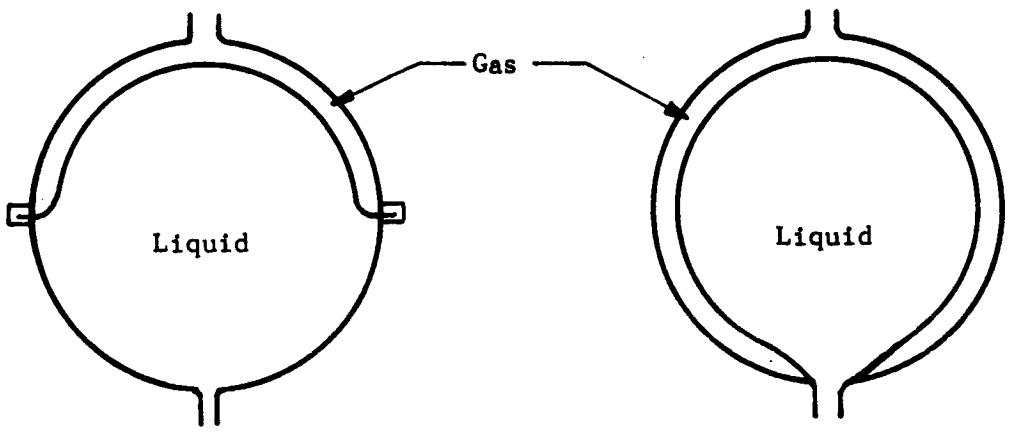

Fig. XI-8-2 Typical Bladder Type Expulsion Devices

When cryogenic liquids are stored, the bladder materials which can be considered are metals and inert polymers. Materials such as Teflon in composite layered form or metals as foils or plated layers appear most promising.

Because bladder technology is also somewhat undeveloped, considerable test and evaluation is necessary to assure reliability. Among these tests are permeation, crease resistance, slosh loading, and long term storage.

JPL (Ref. 11) has investigated all metal convoluted diaphragms. These diaphragms were fabricated by industrial concerns using several methods. The basic drawback of these devices is that they cannot be recycled. Figure XI-8-3 shows a convoluted diaphragm before and after expulsion as well as the typical results of a recycling attempt. Further efforts are

being made by JPL subcontractors to achieve recycle capability with specially modified convoluted diaphragms and reversing metal hemispheres. Despite the limitation on cycling, these diaphragms are the only devices tested thus far which provide completely impermeable barriers to propellants and to pressurizing gases.

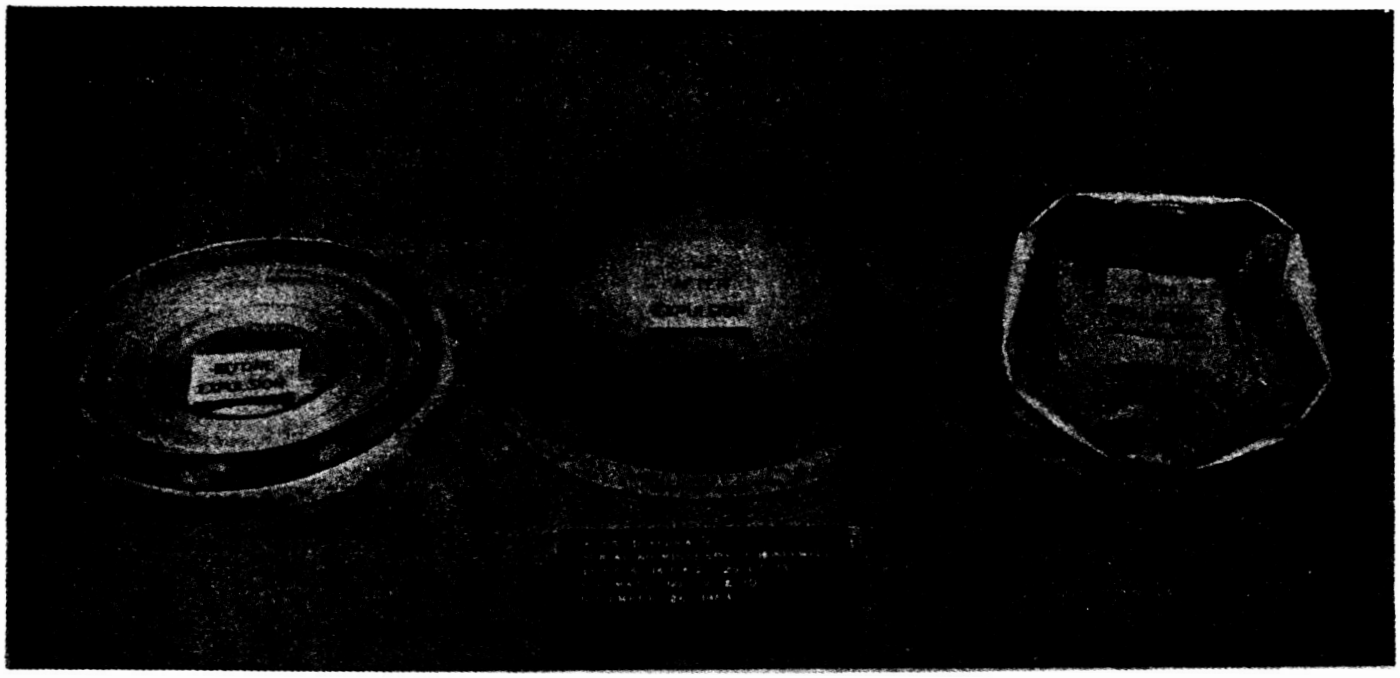

Fig. XI-8-3 Life Cycle of a Convoluted Metal Diaphragm

(a) Diaphragm properly convoluted and ready for installation.
(b) Diaphragm after use in expulsion of fluid from a hemispherical tank.
(c) Diaphragm after an attempt to restore the original convolutions by pumping fluid back into the tank.

(Courtesy of JPL)

Non-Positive Expulsion Devices

Heat leakage to a cryogenic propellant storage tank results in an increase in tank pressure and eventually causes over-pressurization which may be decreased by venting a portion of the stored fluid from the tank. Under zero-gravity conditions the orientation of the liquid or vapor phase is unpredictable resulting in the possible loss of liquid during venting.

ORIGINAL PAGE IS
OF POOR QUALITY

ORIGINAL PAGE
BLACK AND WHITE PHOTOGRAPH

The problem can be approached by:

(1) Applying surface forces such as centrifugal effects and surface tension

(2) Electric field effects such as dielectrophoresis, electric and magnetic field interactions

(3) Magnetic fields

(4) Acoustical fields

(5) The addition of heat in the case of liquid venting by reducing the flow to a lower temperature saturation state and transferring the heat of vaporization to the liquid from the tankage system

During rocket firings using hydrogen fuel, a high propellant feed rate may be required. In such a case it is necessary to pressure feed the propellant by pressurizing the system with the inert helium. For such applications it appears that it is desirable to remove the liquid hydrogen and pass it through a heat exchanger, thus venting it in a vapor form. Such indications are based on systems studies which have showed that there is a greater weight penalty associated with random venting of the denser helium than with venting of the hydrogen vapor. It then becomes necessary to locate the liquid under conditions of weightlessness to insure its removal prior to venture.

There are several means of locating liquids under conditions of weightlessness. TRW systems (Ref. 1) and Bell (Ref. 12) studied several devices that may be used for orienting liquids. Their study was aimed at developing applicable methods of analysis for each device so as to enable one to perform a trade-off analysis for a particular mission requirement. Among the items under study are the stability of the device to disturbances such as accelerations imparted from various sources, the time constant required to orient the liquid following a disturbance, weight penalty associated with the device, compatibility with the attitude control system used for the mission and the reliability and the hazards associated with the use of the device. The reader is referred to the two references for further detailed information.

XI-9 FLUID CONNECTORS

Introduction

The joining of fluid conduits can be accomplished by separable, semi-separable, and non-separable means. The distinction between each method is as follows:

(1) Separable tube connections are mechanically formed by threaded or bolted devices which, when the retaining elements are loosened, the parts can be dismantled with common tools.

(2) Semi-separable tube connections are formed in a manner whereby special tools are required for assembly and dismantling. The reusability of the connection is questionable.

(3) Non-separable tube connectors implies that the parts are joined together by brazing or welding techniques. Although a separation can be effected, considerable effort is required along with special tools. The connection parts are generally non-reusable.

Each of the preceding tube connection elements is considered independently. Non-separable connectors are considered in Section VIII under "Materials and Fabrication" and separable and semi-separable connection in this Section.

Separable Connectors

Separable connectors can be more explicitly described as devices which force together one or more surfaces to form sealing interface(s). The mechanism forcing the surfaces together is either a threaded nut or a number of bolts. This distinction forms the general subclassification of separable connectors into threaded and bolted flange configurations as shown typically in Figures XI-9-1 and XI-9-2.

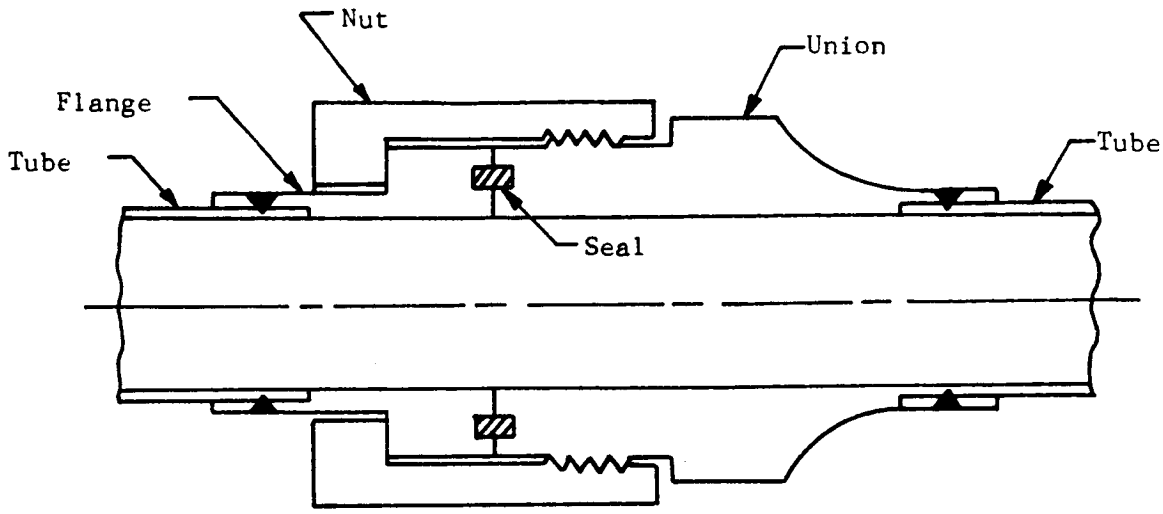

XI-9-1 Typical Threaded Connector Configuration

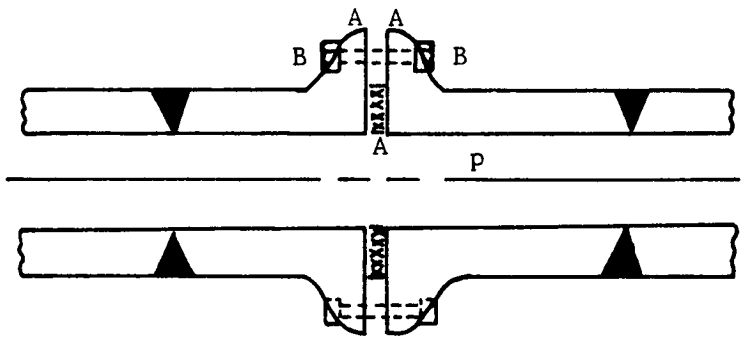

Fig. XI-9-2 Simple Bolted Flange

The criteria governing the selection of the configuration is based on the size of the tube or piping being joined together. The threaded connector is chosen when the tubing outside diameter is one inch or less and where high assembly torque on the nut is not excessively large (under 2400 inch-pounds). When larger diameter tubes and pipes are encountered, the forces required to maintain sealing become quite large thus requiring large threaded nuts and joining tools. To overcome this problem, a series of equally spaced nuts and bolts are employed to join together two flanges where each bolt transmits only a portion of the total force to produce

sealing. Consequently, the bolt torque and tool size are kept within reasonable limits.

Although the threaded and bolted flange connectors differ in basic construction features, the problems in their design and selection are similar. Therefore, the common problems can be considered first followed by an individual treatment of the threaded and bolted connector including specificities in construction features and selection methods.

General Design and Selection Factors

The designer of a pressurized gas storage system can choose a separable connector from a broad group of commercially available items. However, the actual operating conditions imposed on a connector are often such that the manufacturer cannot reliably guarantee the performance of his product. This is attributed to the wide variations in operating conditions which are associated with specific applications. Consequently, the systems designer is faced with the task of analyzing the connector if he is to ensure reliable performance. His selection procedure must be based on a design analysis. With a knowledge of connector design, the systems designer is also in a position to custom design a connector in cases where commercial connectors do not meet design or operating requirements.

The basic problems in designing or selecting a separable connector are:

(1) Selecting fluid compatible materials to effect a seal.

(2) Design a seal supporting structure which is fluid compatible, can be attached to the tube, and will force the sealing surfaces together under all operating conditions.

(3) Optimize the connector from the standpoint of size and weight.

(4) Insure reliability of the connector in maintaining its integrity and initial sealing characteristics throughout its operational life.

(5) Provide a maximum fluid leakage rate based on tolerable considerations for its entire operational life.

Materials for use in connectors must primarily be selected on the basis of their compatibility with the fluids being transferred. Secondly, they must have adequate material properties at the temperatures and other environmental conditions to which they will be subjected. Finally, weight,

weldability, low thermal expansion coefficient, low creep, ease of machining, etc. may be important material considerations in a particular application.

The design of a seal supporting structure is a complex task requiring a detailed theoretical analysis. The details and procedures for such an analysis are not presented in this Section and the reader is urged to obtain these details from the reported efforts of General Electric (Ref. 14) and Battelle (Ref. 18). These references outline analytical techniques based on elastic theory which yield principle stresses and deformations within the connector structure for the following steady state and transient input requirements:

(a) Tubing
  - Material
  - Outside diameter
  - Inside diameter

(b) Fluid contained in the tubing
  - Operating pressure
  - Constant pressure
  - Cyclical pressure
  - Number of cycles of pressure
  - Temperature

(c) Environmental conditions
  - Ambient pressure
  - Ambient temperature

(d) External loads
  - Constant force and moments
  - Cyclical force and moments
  - Number of cycles of force and moments

Following the referenced procedures, most commercially available connectors can be analytically evaluated. Whenever a standard connector meets all the design requirements it should be used. In the event that commercial designs do not meet the requirements, the techniques described in References 14 and 18 can be employed to design a new connector particularly when optimization is required. The references contain an outline for computer programs yielding such information as optimum nut size, thread size, flange configuration, bolt size, bolt spacing, and other geometrical factors of threaded and flanged connectors. It must be noted that the selection of the correct connector for a given application is not only a question

of choosing a connector to meet all of the technical design requirements, but also a question of the time and economics in making an analysis.

The attachment of the connector to the tube must be structurally sound, leakproof, and compatible with the fluid contained. The methods which have been used are welding, brazing, swaging, and high energy rate forming. Welding is preferable followed by brazing. The connector related aspects of importance are the generation of contaminants and the possibility of permanent distortion of the connector due to thermal effects.

The sealing or leakage performance of connectors is related to the operating conditions and the specific configuration. The basic principles of sealing and analytical techniques for leakage prediction contained in Section X-5 should be employed in the design and selection of a connector. Other details of seals are included under the specific topics of threaded and flange connectors.

To illustrate the occurrence of the preceding design and selection problems, an arbitrary connector can be considered. The first step in the design is to select the type of seal and materials. For minimum leakage, the sealing interface loads can be derived as described in Section X-2. For example, where sealing is the result of plastic flow, a sealing stress of about 2.75 times the yield stress is required. Where sealing is achieved by mating surfaces whose finish is in the microinch range, the material selection should emphasize wear resistance. Thus the loss in finish, with repeated use and with the "working" which accompanies assembly as well as temperature and pressure changes, will be minimized.

Ordinarily once a "seal" has been made, the sealing force may be reduced up to about half (the exact value of the reduction will depend on the sealing mechanism and is best determined by test) before its ability to maintain "zero leakage" is lost. This consideration governs the seal width since the initial gasket force must be large enough so proof and operating loads do not reduce it below the minimum value permitted.

Internal pressure has a major effect on connectors. In many designs, it causes a reduction in sealing force and, when below a minimum value, results in increased leakage. A typical example is the conventional flange

coupling shown in Figure XI-9-2. With increasing pressure, p, gasket compression at A decreases. At a sufficiently high pressure, the gasket compression has decreased to be equal in magnitude to the internal pressure. Further increases in internal pressure find the gasket acting as a pressure relief valve with corresponding large-scale leakage. Recognition of the effect of internal pressure on gasket compression has let to many "pressure energized" seals; a typical example of which is shown in Figure XI-9-3. By allowing the internal pressure to "bulge" the U-shaped seal ring, it is possible to have the seal pressure (at A for example) increase with internal pressure, p, rather than decrease.

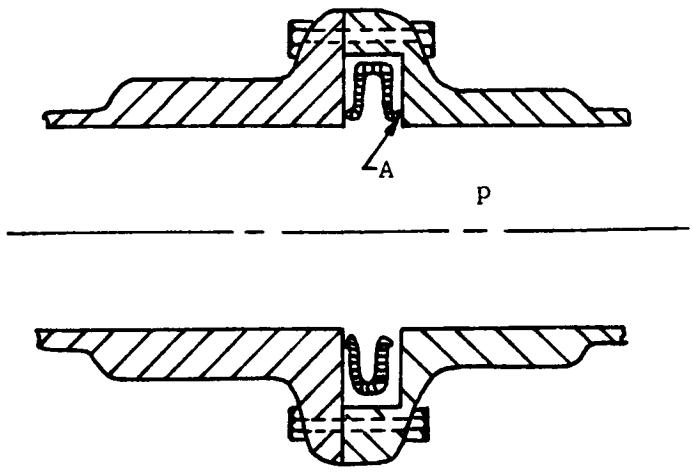

Fig. XI-9-3 Flange with Pressure Energized Seal

Temperature changes and temperature transients also have a major effect on connectors. An example of an AN fitting is shown in Figure XI-9-4. A cold fluid starting to flow through the pipe will cool the inside much more rapidly than the sleeve, A, or nut, B. As a result, the contraction of the sleeve and nut will be slower. The sealing stress will thereby be lowered with increased possibility of leakage. Another example is the flanged connector shown in Figure XI-9-2. Here the flange, A, could cool more rapidly than the bolts, B. As a result, the gasket load will be reduced and leakage made more likely. Again, recognition of the effect of temperature change in causing contraction or expansion has resulted in the

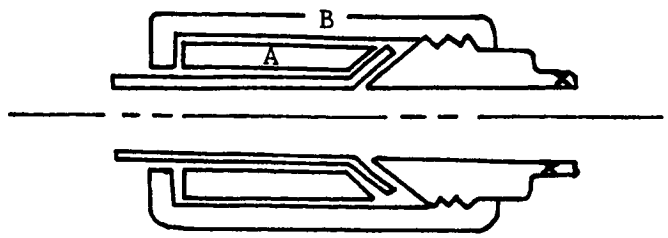

Fig. XI-9-4 Schematic of an AN Flared Fitting

design of "temperature-compensated" connectors. Figure XI-9-5 shows a flange connector with a sealant material confined between the flange and an invar ring. During cooling the sealant contracts proportionally more than the flange material. The invar ring, since it contracts less, tends to compensate for this excess and keeps the joint tight. Since the coefficients of expansion may vary substantially with temperature, true compensation is seldom achieved. Bending forces due to vibration or otherwise, tend to open one side of the connector and close more tightly the other side.

Other environmental effects include radiation, erosion by the fluid flow, water-hammer, high vacuum, etc.

A successful connector in a given environment must, therefore, be capable of withstanding the environment and simultaneously produce sufficient sealing interface contact loads without detrimental stresses or deformations. The preceding conditions can only be achieved through a systematic theoretical analysis of the connector to determine such factors as thread size, wall thickness, bolt sizes, etc.

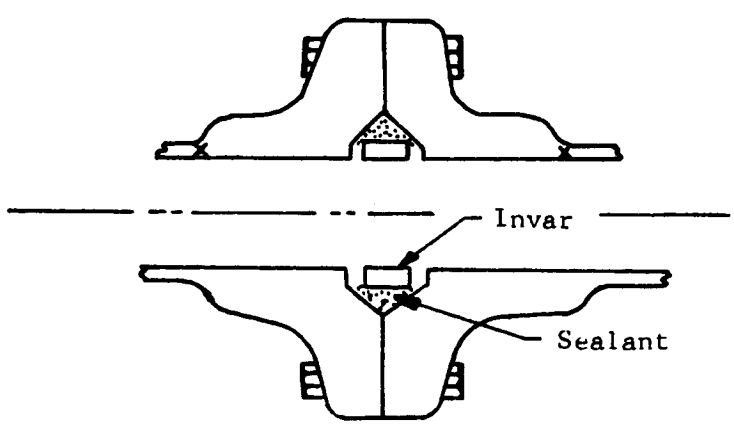

Fig. XI-9-5 Temperature-Compensated Flange Design

Threaded Connectors

The current commercial threaded connectors can usually be grouped as flared-tube, swaged-tube, or flanged-tube connectors.

The flared-tube connector, such as the AN variety shown in Figure XI-9-4, is subject to: high leakage rates unless a soft gasket is used, gross deformation due to excessive hoop stress in the union when it is overtorqued, and fatigue failure at the root of the flare.

To overcome some of these problems, NASA Marshall Space Flight Center developed the "MC" fitting. Basically the "MC" fitting, as shown in Figure XI-9-6 is a high-quality version of the conventional AN fitting. The surface finish, roughness and degree of ovality are rigidly controlled by the "MC" specification, MSFC-SPEC-143. In particular, the union fitting must meet the following limits:

(1) The conical sealing surface must be round within the following tolerances:

a. In 360 degrees the maximum deviation must not exceed 0.0003 inch.

b. The maximum rate of deviation shall not exceed 0.00010 in/15 degrees of the arc.

(2) The conical sealing surface shall not exhibit concave areas but may exhibit a convex configuration of a concentric nature, but not to exceed 0.0005 inch.

(3) The final sealing-surface finish shall have a maximum crest-to-valley profile of 10 to 14 microinches for steel and 22 to 30 microinches for aluminum alloy.

The sealing surfaces are inspected for freedom from such defects as tool chatter marks, scratches, handling marks and ridges.

The rated torques for each size fitting are also specified. There is given a minimum and maximum rated value with provisions for increasing the torque to 150 percent of the maximum rated value in order to improve leak-tightness during test. In addition to the preceding specifications, a special flaring tool was developed at MSFC to control tolerance even closer.

A series of tests on 1/2", 3/4", and 1" fittings using this tool were conducted by General Electric (Ref. 20) and led to the following conclusions:

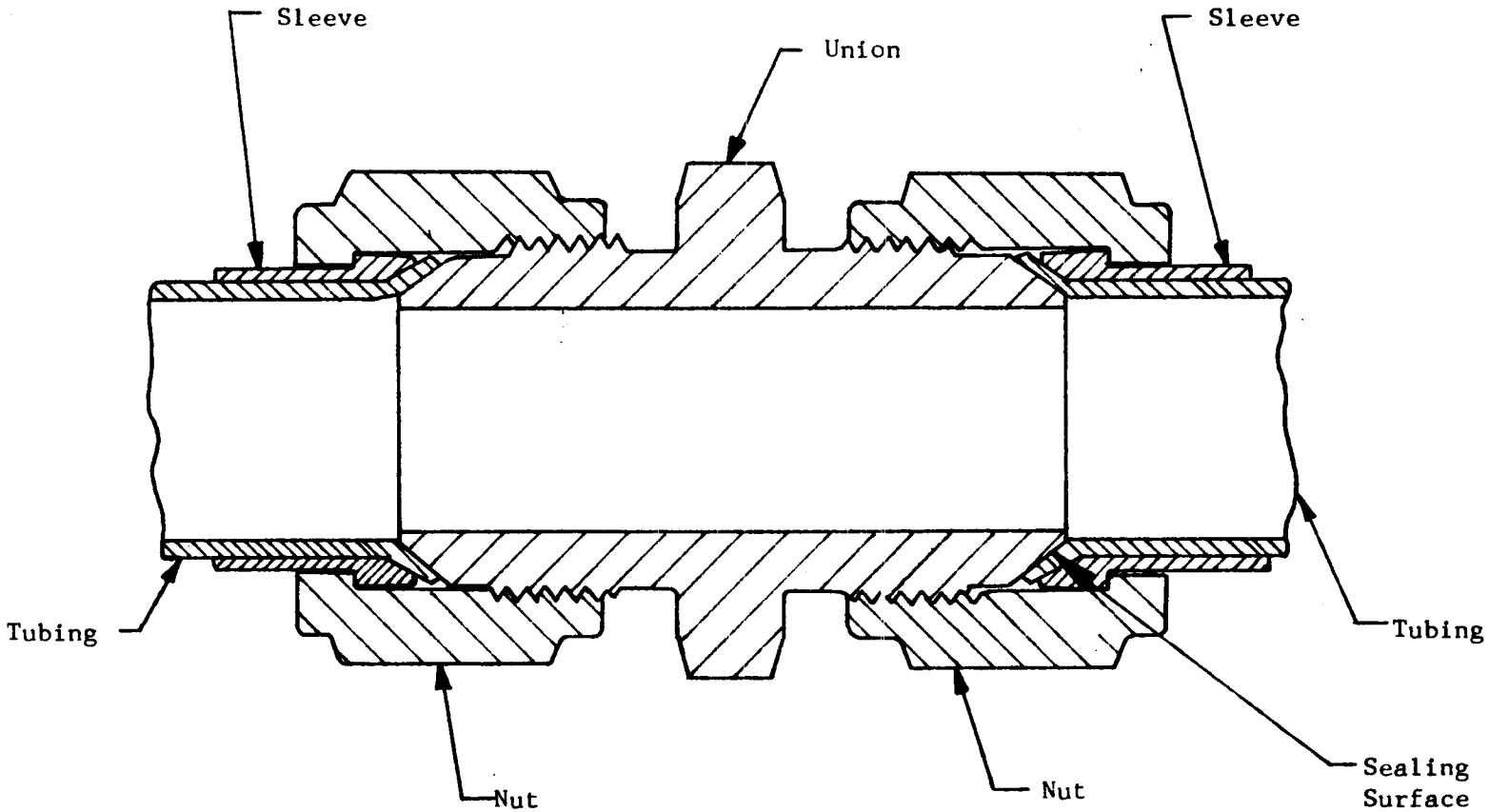

Fig. XI-9-6 "MC" Tube Connector

(1) Leak-tight connections were obtained only in a few cases when gross deformations of the union resulted in a new sealing surface geometry featuring uniform contact with a small contact area. This new sealing geometry and high sealing pressure could be obtained only for stainless steel connectors with high strength sleeves.

(2) Connections not showing gross deformations of the union leaked due to non-uniform sealing pressure. Also the magnitude of the sealing stress when distributed over the whole union sealing area is below the yield stress of the connector materials.

(3) The general leakage level of the "MC" flared connector, when pressurized with helium to 1500 psi, is 10^{-4} to 10^{-2} cc/sec.

(4) The high-quality, smooth sealing-surface finish is an aid in reducing the leakage area but, high sealing stresses are necessary to obtain leak-tightness.

(5) The "MC" specification for union surface flatness is not necessary since the union becomes concave on the first torquing operation due to yielding in the hoop direction.

(6) The special flare process gives a circumferential directional surface finish, but no improvement in crest-to-valley roughness or leakage was evident.

(7) The sealing pressure was not uniform around the fitting. Each time a flared connector is assembled, leakage paths are produced by the ovality of the mating parts.

(8) The leakage level increased with connect-disconnect tests of aluminum fittings, and the sealing surfaces became very rough. When the stainless steel fittings were reassembled with the same parts, the leakage level and the local surface roughness did not increase, although the sealing surfaces of the unions were grossly deformed.

(9) Plating the union sealing surfaces decreased leakage, but did not seal in many cases since the sealing pressure was not uniform.

(10) The leakage-pressure relation was linear.

(11) Torque relaxation was not a problem.

(12) Antifriction bearings on the shoulder of the nut prevented burring.

Insertion of Voi-Shan crush washers, as shown in Figure XI-9-7, improved the leak-tightness of flared connectors. The Voi-Shan washer was developed to patch leaking flared connectors. Since the sealing pressure is often below the yield stress of the fitting materials, the use of a gasket with a low yield stress should provide some improvement.

Another method of improving the AN fitting has been to incorporate an elastomeric "O"-ring in the flared surface as shown in Figure XI-9-8.

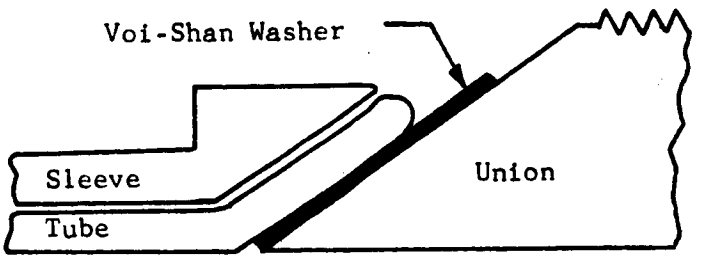

Fig. XI-9-7 "MC" Fitting with Voi-Shan Washer

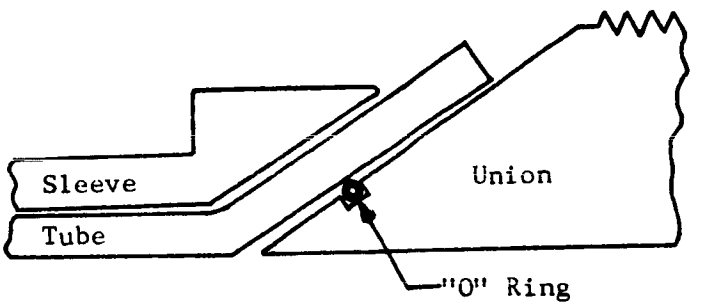

Fig. XI-9-8 AN Fitting with "O"-Ring

The swaged-tube, like the flared tube connector, is subject to leakage unless a gasket is used and to fatigue failure in the swage. The flanged-tube connector is subject to leakage unless a gasket is used and to fatigue failure where the flanged section is attached to the tubing. An example of a flanged tube connection is shown in Figure XI-9-9. This connector is the AFRPL fitting developed by Battelle (Ref. 18) for the Air Force. Detail designs and preliminary MS standards have been prepared for the connector although it is not commercially available. Reference 18 also contains a systematic performance analysis used in the connector design.

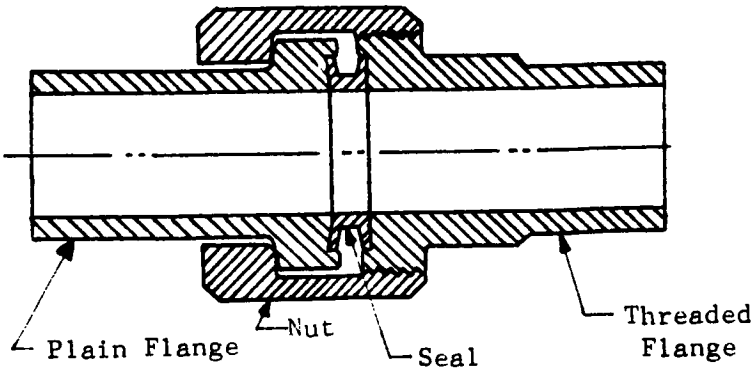

Fig. XI-9-9 AFRPL Flanged Tube Connector

General Electric (Ref. 21) is in the process of designing, manufacturing and evaluating a threaded connector for 3/4 inch tubing utilizing the super-finished surface sealing principle (see Section X-4). The connector, shown in Figure XI-9-10 is being designed for 6000 psi internal pressure. The connector material is fully hardened A-286 which is electron beam welded to the tubing.

Other types of threaded connectors are those employing a bite type of ferrule which is impressed into the tube to form a seal and simultaneously axially retain the tube. To completely assess the merits of these connectors is difficult. Because the ferrule plastically deforms the tube to provide a seal and attachment of the tube to the fitting; it is felt that the performance is equal or less than the AN fitting.

Bolted Flange Connectors

Flanged connectors are used for joining larger sizes of pipes while threaded connectors are used for smaller sizes. Ordinarily the change over from one type to the other occurs at a diameter of about one inch. The transition is dictated by torque requirements on the bolts. If flanged connectors are used for very small pipes, the bolts become too small for reliable torquing. On the other hand, if a threaded connector were used for very large pipes, the wrenches would need to be unreasonably large. In very high-pressure systems the axial loads are so high that the transition from tube to flange connectors might occur at sizes below one inch; while, with very low pressures the size could be somewhat greater than one inch.

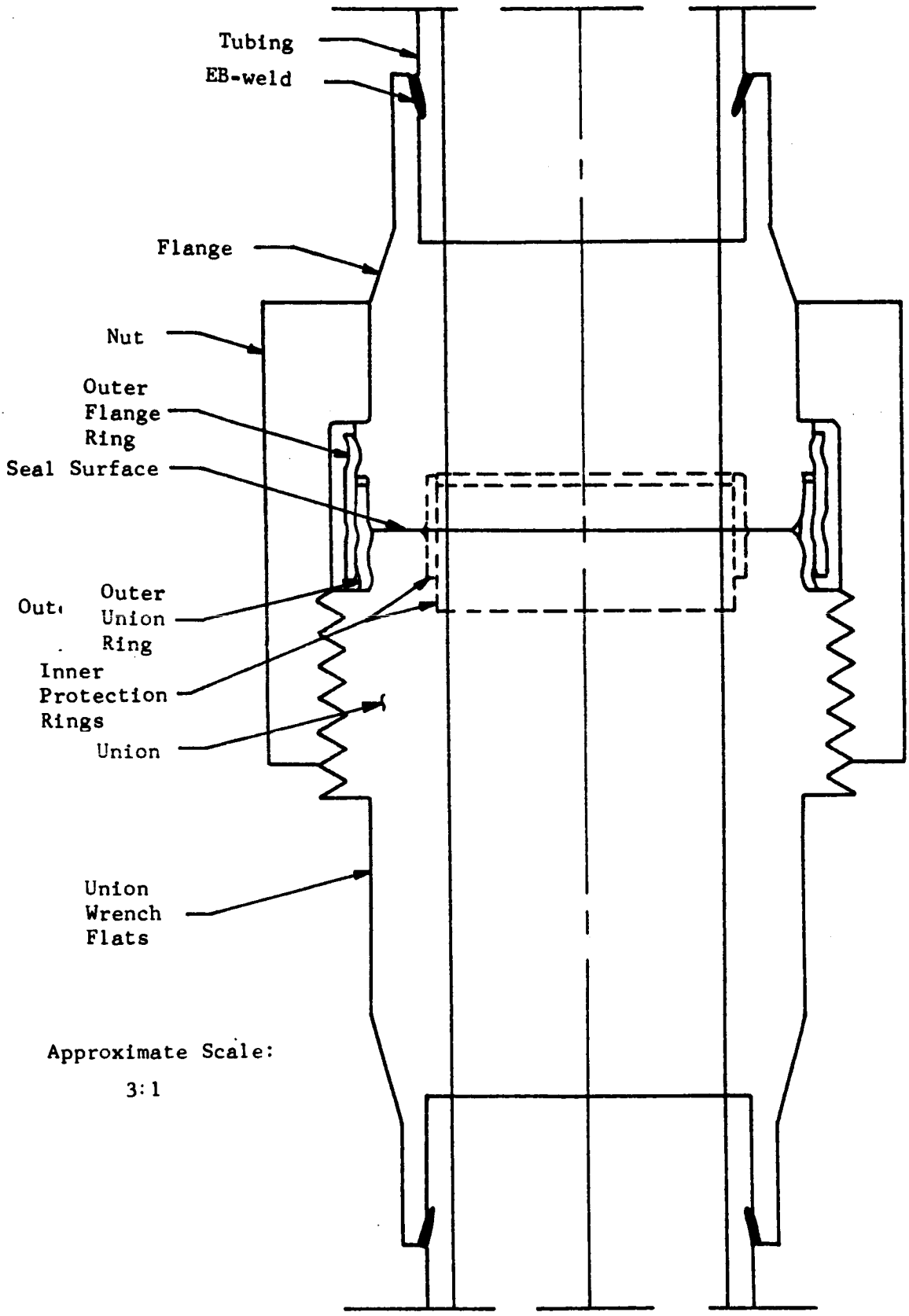

Fig. XI-9-10 Tube Connector Utilizing Superfinished Surface Sealing Principle (Ref. 21)

Most flange connectors retain a separable sealing element which is pressed by tightening of the bolts. The simplest case is shown in Figure XI-9-2 where the seal is a flat gasket. As mentioned earlier in this Section, the gasket transmits all of the loads produced by the bolts, external forces and tube restraints. Consequently, deformations due to pressure and thermal effects tend to reduce the seal contact loads and, hence, leakage. To overcome this problem, a connector is usually designed in a manner so that only a fraction of the total loading due to bolts and external forces is transmitted through the sealing element. This is accomplished by providing flange contact in addition to the seal contact. Two locations of contact are shown in Figures XI-9-11 and XI-9-12. The ASME code contains design criteria for flanges with contact inside the bolt circle. However, this code is not suggested for use in aerospace flange design. It is suggested that Reference 14 be reviewed before a selection of connector geometry is decided upon.

The choice of a seal often determines the assembly preload and the load to be maintained under various operating conditions. Non-pressure energized seals are usually employed when the flanges do not contact. Pressure energized seals are used when flange contact is permissible. The choice of a seal depends upon the leakage requirements and the seal load matching with the structural design of the flanges. Many of the seals described in Section XI-6 can be used as connector seals. For flange reusability it is important that the seal material be softer than the flange material.

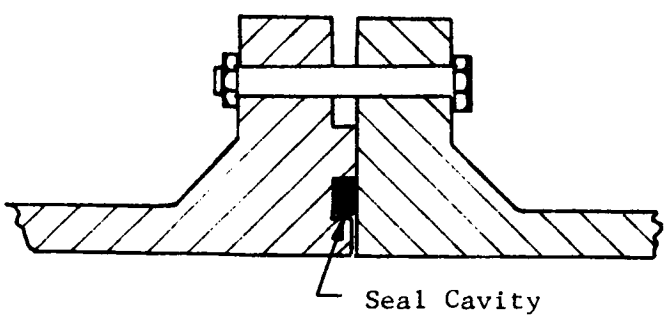

Fig. XI-9-11 Flange Contact Inside the Bolt Circle

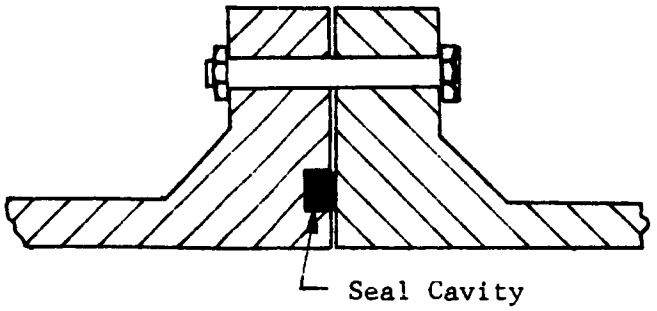

Fig. XI-9-12 Flange Contact Outside the Bolt Circle

Semi-Separable Connectors

In separable fluid connector design, one of the major problems is that of maintaining the necessary sealing stresses on the mating components throughout the life of the connector. The compressive load which effects the seal, whether it be imposed on a metal gasket, a seal having its own geometric flexibility, or a composite material seal such as a spiral wound gasket, is of such a magnitude as to cause plasticity in the sealing area so that the true flexibility of the seal is often not known and in all cases is quite slight. Because of this, loss in bolt load due to relaxation, the vibration environment, and the temperature extremes or transients, often causes loss of sealing. Thus, interest is aroused in fluid connectors having the attribute of being truly zero leakage connectors possessing the characteristic of being insensitive to bolt load reduction. However, with these advantages come the disadvantages of more effort being required in assembly and disassembly. For connections which need be opened only a small number of times, or not at all except for repair functions, such advantages outweigh the disadvantages.

When the idea of semi-permanence is opened to the fluid connector designer, many new concepts become available. Explosive welding, magnetic forming, pressure welding, and many other techniques are at least possible for forming the seals, the structural junction, or in some cases, both. Two flanged fluid connector designs having the intended capability of being insensitive to bolt load reduction during their operational lives are described herein. Other than this design goal, the designs have little in

common. One design, that of the omega seal, is not new. It has been used for applications other than aerospace for some time. The second design uses a diffusion bond, which is not new to the aerospace industry, but is new in connector design. Each design has its own area of application in the aerospace field, each has its advantages, each certainly has disadvantages. In order to be made ready for utilization in any given fluid system, these connectors would have to be developed beyond their present stage of design shown herein.

Each of the designs described in this Section has been brought to its present design state under the sponsorship of the National Aeronautics and Space Administration, References 21 and 22. Neither the configurations nor the specific dimensions are considered optimum. By design techniques now available (Page XI-9.9) they can be improved.

Four semi-separable connectors considered in this Section are the omega, diffusion bonded, the Parker "X" and the cold weld flange seal.

The omega seal, shown in Figures XI-9-13 and XI-9-14, incorporates a hermetic seal by the fusion welding of two segments of a thin toroidal shell about the periphery of the connector. In order to make and break the seal, special welding and cutting equipment is required. Since an alternate load path exists for the compressive loading across the connector and that the toroidal omega seal has flexbility, the system has the ability to withstand flange displacements and rotations. Detailed features of the seal can be found in Reference 21.

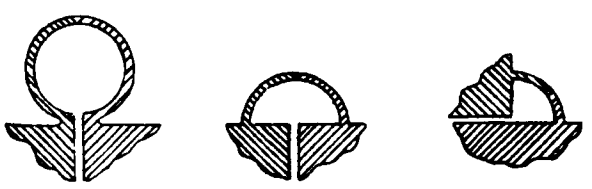

Fig. XI-9-13 Typical Omega Seal Configurations (Ref. 21)

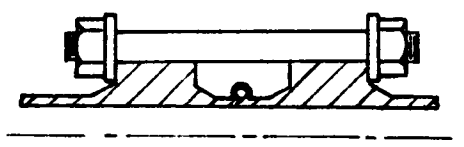

Fig. XI-9-14 Omega Seal Connector Schematic (Ref. 21)

The second design, that of using a diffusion bond as the hermetic seal, allows the seal to be made in the field by the application of moderate heat and bolt stress. Reference 22 describes a bonded flange connector, shown in Figure XI-9-15, in greater detail. It was designed for 6000 psi service at temperatures ranging between -450° and +100°F.

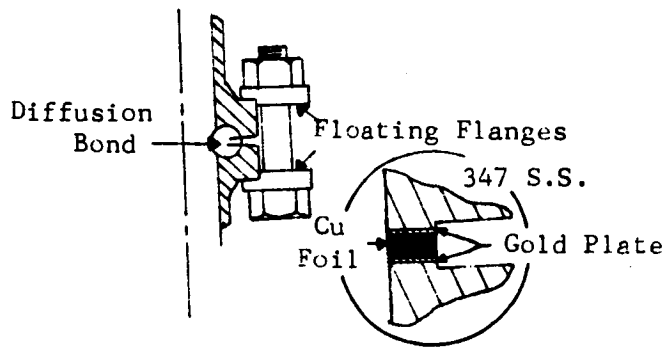

Fig. XI-9-15 Diffusion-bonded Connector Schematic (Ref. 22)

The third device is a swaged connector union described in Reference 21. This Parker Aircraft Co. connector concept is adaptable to all of the typical fitting shapes: unions, tees, bulkhead, boss, etc. and to all sizes of lines from 1/4 inch to the largest diameter duct currently visualized in vehicle design. As a union for tubing, the connector parts consist of two identical sleeves and a collar as shown in Figures XI-9-16 and XI-9-17.

The collar contains the seal and also forms the semi-permanent connection by swaging the outer surface of the collar. The connector can be disassembled by a special cutting tool.

A cold welded sealing interface connector, shown in Figure XI-9-18 is presently being developed by General Electric Co. (Ref. 21). The connector is composed of flange retaining members to provide a minimum transmission of load between tube sections. The seal is formed by two thin 2S aluminum plates welded to the flanges. Two dies, as shown in Figure XI-9-19, are inserted between the flanges and the plates are pressed together forming a leak-proof cold weld seal. The dies are then removed and the flanges are bolted together to complete the assembly. Because the seal is not load

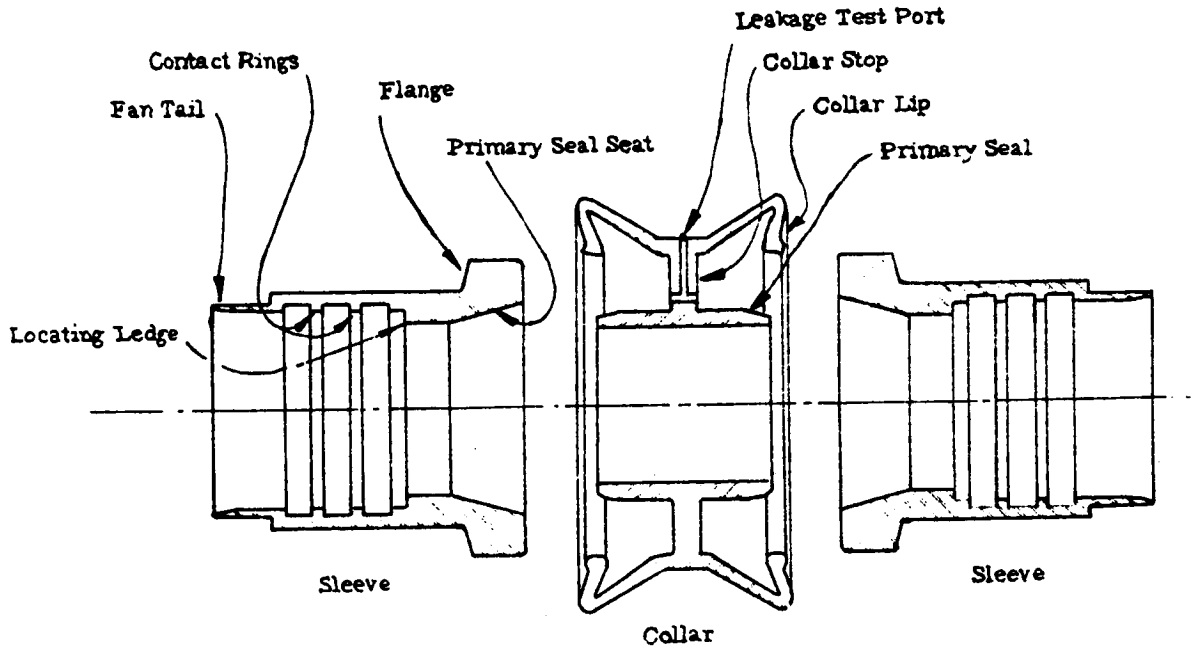

Fig. XI-9-16 Swaged Connector Union, Unassembled (Ref. 21)

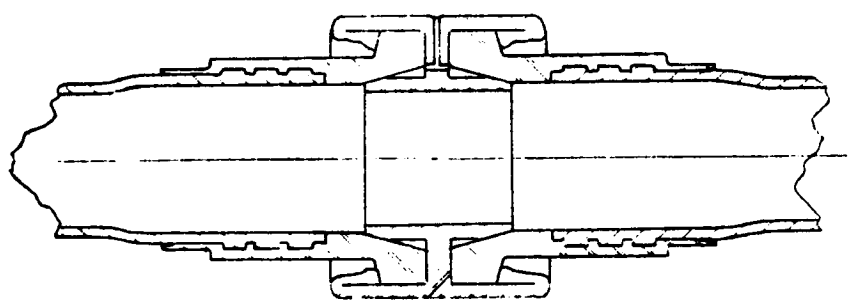

Fig. XI-9-17 Swaged X-fitting (Ref. 21)

dependent, the maximum bolt loads need only be sufficient for structural and pressure loading. Because few materials which cold weld in normal environments have been investigated, the concept requires further development work. The connector can be disassembled with a special cutting tool.

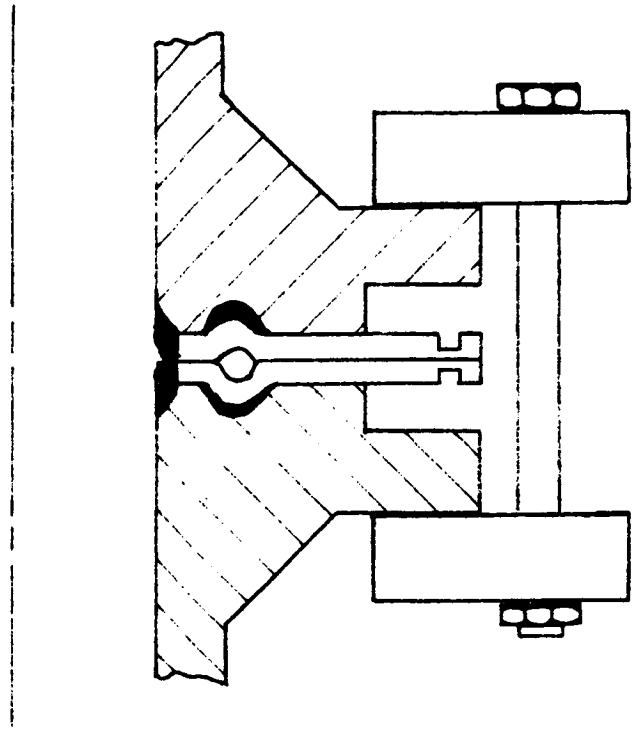

Fig. XI-9-18 General Electric Cold Welded Connector Seal

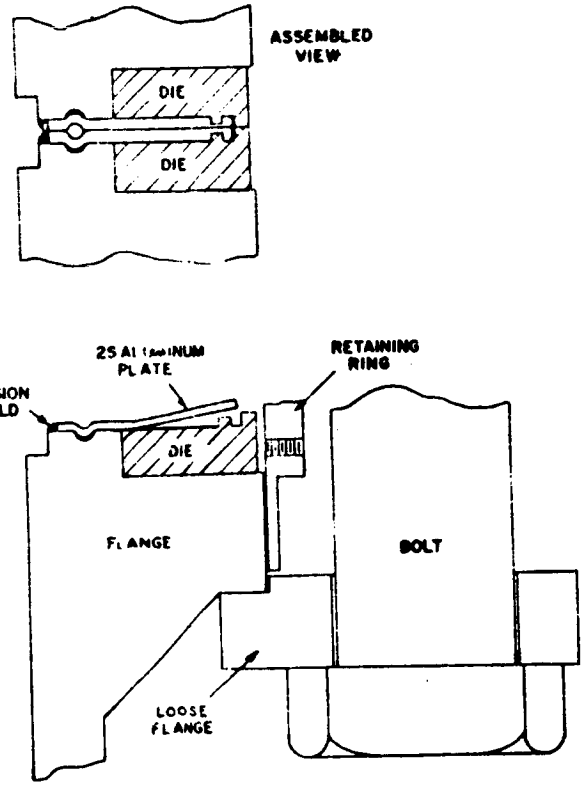

Fig. XI-9-19 Formation of Cold Weld Seal (Ref. 21)

XI-10 REFERENCES

1. Anon. (TRW Systems, Redondo Beach, Calif.) Advanced Valve Technology for Spacecraft Engines. NAS7-107, Rept. no. 8651-6042-SU-000, Final Rept., Washington, D.C., Aug. 1965.

2. Anon. (TRW Systems, Redondo Beach, Calif.) Advanced Valve Technology for Spacecraft Engines, Vol. I and II. NAS7-107, Rept. no. 8651-6033-SC-000, Washington, D.C., July 1964.

3. Anon. (Bell Aerosystems Co., Buffalo, N.Y.) Study, Design and Test of Functionally Integrated Pneumatic Components for Rocket Propulsion Systems. AF04(611)-9077, AFRPL-TR-65-93, AF Systems Command, Rocket Propulsion Lab., Res. and Technol. Div., Edwards AFB, Calif., June 1965.

4. Stone, J.A. (MIT, Dept. of Mech. Eng.) Investigation of Discharge Coefficients and Steady-State Flow Forces for Poppet-Type Valves. SM Thesis, Jan. 1957.

5. Tellier, G.F. (North American Aviation, Rocketdyne Div.) Rocket Engine Valve Poppet and Seat Design Data. AF04(611)-8392, RPL-TDR-64-68, AF Systems Command, Rocket Propulsion Lab., Res. and Technol. Div., Edwards AFB, Calif., May 1964.

6. Anon. (TRW Systems, Redondo Beach, Calif.) Aerospace Fluid Component Designers Handbook, Vol. I. AF04(611)-8385, RPL-TDR-64-25, AF Systems Command, Rocket Propulsion Lab., Res. and Technol. Div., Edwards AFB, Calif., May 1964.

7. Roters, H.C. Electromagnetic Devices. John Wiley and Sons, Inc., New York, 1941.

8. Shapiro, A.H. The Dynamics and Thermodynamics of Compressible Fluid Flow, Vol. I. Ronald Press Co., New York, 1953.

9. Anon. (Parker Aircraft Co.) Solenoid valves. Tech. Note no. 129, March 13, 1964.

10. Anon. (IIT Research Institute) Analytical Techniques for the Design of Seals for Use in Rocket Propulsion Systems, Vol. I and II. AFRPL-TR-65-61, AF Systems Command, Rocket Propulsion Lab., Res. and Technol. Div., Edwards AFB, Calif., May 1965.

11. Anon. (Jet Propulsion Lab., Pasadena, Calif.) On the evolution of advanced propulsion systems for spacecraft. Tech. Rept. no. 32-735, July 15, 1965.

12. Anon. (Bell Aerosystems Co., Buffalo, N.Y.) Development of Expulsion and Orientation Systems for Advanced Liquid Rocket Propulsion Systems. AF04(611)-8200, RTD-TDR-63-1048, Final Rept., AF Systems Command, Rocket Propulsion Lab., Res. and Technol. Div., Edwards AFB, Calif., July 1963.

13. Bauer, P. (IIT Research Institute) Investigation of Leakage and Sealing Parameters. AF04(611)-9704, AFRPL-TR-65-153, AF Systems Command, Rocket Propulsion Lab., Res. and Technol. Div., Edwards AFB, Calif., Aug. 1965.

14. Rathbun, F.O., Jr. (General Electric Co.) Design Criteria for Zero Leakage Connectors for Launch Vehicles. NAS8-4012, Rept. no. 64 GL202, Dec. 1, 1964.

15. Roark, R.J. Formulas for Stress and Strain. McGraw Hill Book Co., New York, 1954.

16. Anon. Pressure Vessel and Piping Design. ASME, Collected Papers, 1927-59.

17. Baumgartner, T.C. High temperature joints. Machine Design 37, no. 2, Jan. 21, 1965.

18. Anon. (Battelle Memorial Inst.) Development of AFRPL Threaded Fittings for Rocket Fluid Systems. AF04(611)-9578, AFRPL-TR-65-162, AF Systems Command, Rocket Propulsion Lab., Res. and Technol. Div., Edwards AFB, Calif., Nov. 1965.

19. Anon. (Battelle Memorial Inst.) Development of Mechanical Fittings, Phase I and II. AF04(611)-8176, RTD-TDR-63-1115, AF Systems Command, Rocket Propulsion Lab., Res. and Technol. Div., Edwards AFB, Calif., Dec. 1963.

20. Anon. (General Electric Co.) Design Criteria for Zero Leakage Connectors for Launch Vehicles. NAS8-4012, Final Rept. Marshall Space Flight Center, Redstone Arsenal, Huntsville, Ala., June 1, 1964.

21. Anon. Proceedings of the Conference on the Design of Leak-Tight Fluid Connectors. NASA-SAE Conf. p. 161-98, Huntsville, Ala., Aug. 4-5, 1965.

22. Anon. (General Electric Co.) Design Criteria for Zero-Leakage Connectors for Launch Vehicles. NAS8-4012, Quarterly Progress Rept. nos. 7,8,9 and 10, Marshall Space Flight Center, Redstone Arsenal, Huntsville, Ala.

XII STORAGE EFFICIENCY

Table of Contents

Section-Part	Title	Section-Part.Page
XII-0	List of Tables	XII-0.3
XII-0	List of Figures	XII-0.4
XII-1	Introduction	XII-1.1
XII-2	Storage Efficiency	XII-2.1
	Definitions	XII-2.1
	Weight Efficiency	XII-2.3
XII-3	Thermodynamics of Pressure Vessel Blowdown	XII-3.1
	General Equations	XII-3.1
	Numerical Examples	XII-3.3
	Blowdown with Heat Transfer	XII-3.4
	Solutions of the Blowdown Equations for constant Mass Flow Rate and constant Heat Transfer Resistance	XII-3.9
	Solutions for Limiting Cases	XII-3.11
	Isothermal Blowdown	XII-3.11
	Adiabatic Blowdown	XII-3.12
	Blowdown at constant Mass Flow with Heat Transfer from an Isothermal Source	XII-3.14
	Blowdown at constant Mass Flow with Inside Resistance Negligible	XII-3.18
	Blowdown through a Critical Flow Nozzle with Heat Transfer from an Isothermal Source	XII-3.21
	Criteria for Limiting Cases of Blowdown	XII-3.23

ORIGINAL PAGE IS
OF POOR QUALITY

Table of Contents

Section-Part	Title	Section-Part.Page
XII-4	More Exact Equations for Blowdown	XII-4.1
	Deviation from Ideality	XII-4.1
	Heat Capacity	XII-4.4
	Estimation of Heat Transfer Rates	XII-4.6
	Free Convection	XII-4.6
	Forced Convection	XII-4.8
	Conduction	XII-4.10
	Relative Importance of each Mechanism	XII-4.11
	Stratification	XII-4.13
	Numerical Method of Solution of Blowdown Equations	XII-4.15
XII-5	Work of Expansion	XII-5.1
	General Equations	XII-5.1
	Isothermal Expansion, Ideal Gas	XII-5.3
	Adiabatic Expansion , Ideal Gas	XII-5.4
	Estimation of γ'	XII-5.5
XII-6	References	XII-6.1
XII-A	Nomenclature	XII-A.1

XII-0 LIST OF TABLES

Section-Part-Table	Title	Section-Part.Page
XII-2-1	Weight Storage Efficiencies	XII-2.4
XII-4-1	Critical Conditions for some Gases	XII-4.2
XII-4-2	Constants of the Beattie-Bridgeman Equation of State (Ref. 4)	XII-4.3
XII-4-3	Molar Heat Capacities (BTU/lb - mol - ^{o}R) (Ref. 8 and 9)	XII-4.5
XII-4-4	Coefficient and Exponent in Correlation for Free Convection Heat Transfer (Ref. 2)	XII-4.7

XII-O LIST OF FIGURES

Section-Part-Figure	Title	Section-Part.Page
XII-1-1	Pressure Vessel and Associated Systems	XII-1.2
XII-3-1	Gas Receiver Model	XII-3.5
XII-3-2	The General Solution for a Few Cases of Blowdown at constant Mass Flow (Ref. 3)	XII-3.10
XII-3-3	Simple Gas Received Models, Case 1 - Large Thermal Capacitance and High Valve of (hA), Case 2 - Extremely Slow Mass Flow (Ref. 3)	XII-3.12
XII-3-4	Isothermal Blowdown (Ref. 3)	XII-3.13
XII-3-5	Adiabatic Blowdown (Ref. 3)	XII-3.13
XII-3-6	Simple Receiver Model for Adiabatic Blowdown (Ref. 3)	XII-3.14
XII-3-7	Simple Gas Receiver Models for, Case 1 - Thermal Capacitance of the Metal Receiver Wall Greatly Exceeds that of the Gas. And Case 2 - Small Heat Capacitance of Receiver Wall (Ref. 3)	XII-3.15
XII-3-8	Simple Gas Receiver Model for Blowdown at constant Mass Flow with Heat Transfer from an Isothermal Source (Ref. 3)	XII-3.15
XII-3-9	Blowdown at constant Mass Flow with Heat Transfer from an Isothermal Source	XII-3.17
XII-3-10	Effect of T_c^* on Blowdown at constant Mass Flow with Heat Transfer from an Isothermal Source	XII-3.17
XII-3-11	Simple Gas Received Model with Negligible Inside Resistance (Ref. 3)	XII-3.19
XII-3-12	Blowdown at constant Mass Flow with Inside Resistance Negligible	XII-3.20
XII-3-13	Effect of External Heat Transfer on Blowdown at constant Mass Flow with Inside Resistance Negligible	XII-3.20
XII-3-14	Infinite Capacitance Gas Receiver Model for Blowdown through a Critical Flow Nozzle with Heat Transfer (Ref. 3)	XII-3.21

Figures

Section-Part-Figure	Title	Section-Part.Page
XII-3-15	Blowdown through a Critical Flow Nozzle with Heat Transfer from an Isothermal Source (Ref. 3)	XII-3.22
XII-3-16	Effect of T_c^* on Blowdown through a Critical Flow Nozzle with Heat Transfer from an Isothermal Source - NTU = 2, K = 1.4 (Ref. 3)	XII-3.22
XII-4-1	Forced Convection	XII-4.9
XII-4-2	Stratification in Pressure Vessel	XII-4.14
XII-5-1	Diagram Illustrating Work of Expansion	XII-5.1
XII-5-2	Blowdown of a Pressure Vessel to the Atmosphere	XII-5.2
XII-5-3	Propellant Expelled from a Tank by a Pressurized Gas	XII-5.6

XII-1 INTRODUCTION

Gas may be stored in a pressure vessel to provide a media to perform such functions as attitude control, the pressurization of a propellant tank, to aid in restart capabilities, or the actuation of systems by operating a piston in a cylinder or a turbine. When the internal gas pressure falls below some minimum, the residual gas is not useful. The amount wasted in this way depends on the temperature of the residual gas, which in turn depends on the thermodynamic and heat transfer conditions of the pressure vessel. For some purposes the pressure during the whole delivery cycle should be maximized. A design objective is to obtain the desired performance at the minimum cost or the minimum weight.

The following presentation begins with calculations of performance for some simplified cases, showing the nature of causes of inefficiencies. Some efficiencies are then defined. More detailed performance calculation methods are then presented.

A pressure vessel must be designed in conjunction with the design of the system in which the gas is to be used, and the expansion device which connects it to the receiver. The arrangement of these parts of the system is shown in Figure XII-1-1. The gas receiving system may consist of a propellant tank, the atmosphere, or the space vacuum. The expansion device may include a pressure regulator, throttling valve, orifice, nozzle, on-off valve, turbine, piston-cylinder, pipe, and heat exchanger, or any combination of these elements. The equations governing each element may differ depending on the regime of operation so that a complete presentation of all possible combinations is beyond the scope of this Section. Some examples are given, and the general design priciples governing the performance of a pressure vessel are presented.

One way to separate the effects due to each part of the system is to define the requirements of the gas receiving system in terms of a duty cycle. A primary independent variable for design of the pressure vessel is the quantity of gas removed. The duty cycle must specify the quantity of gas required over a given time schedule and it may include upper and

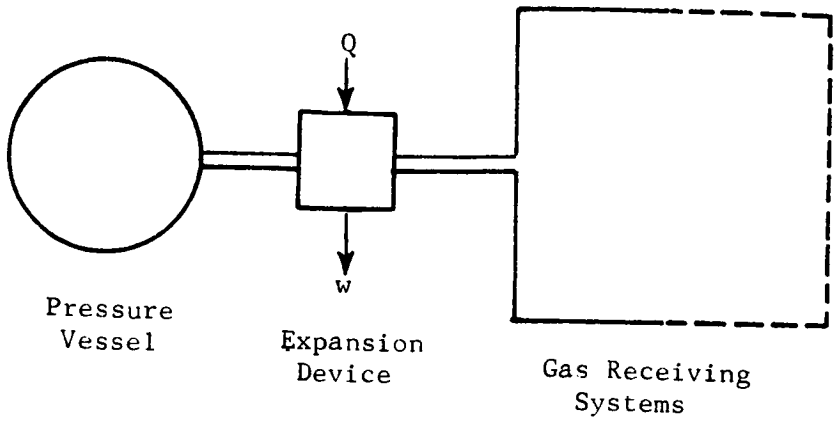

Fig. XII-1-1 Pressure Vessel and Associated System.

lower pressure limits. Usually the duty cycle may be calculated from the equations governing the gas receiving system and the desired performance of that system. Examples of such calculations will be given here only for the simplest gas receiving systems.

The two remaining parts, the pressure vessel and the expansion device, may be considered together as a system if it is desired to calculate conditions of the deliverable gas and associated heat and work. The pressure vessel or its contained gas may be considered as a separate system if conditions of the residual gas are to be calculated. We begin with this simplest system.

In some cases the rate of withdrawal of gas is unimportant, and only the amount withdrawn determines the gas conditions. This is true if heat transfer through the wall of the bottle keeps the internal gas at constant temperature. Then by Dalton's Law the pressure of the gas is proportional to the amount of gas remaining. If half of the gas is withdrawn, the pressure is halved. Such isothermal expansion is observed only when the gas is withdrawn slowly over a long period.

Another simple situation occurs when heat transfer through the tank wall is negligible. In this case the expansion of gas in the tank is adiabatic. The temperature of the residual gas is less than the initial gas temperature because the residual gas does work to push gas out of the tank.

The condition of the residual gas can be calculated by defining the residual gas as a system. For example, the residual gas could have been placed within a balloon inside the tank, so that during venting it expands to just fill the tank. Because the gas in the balloon expands against its own pressure it does the maximum work possible in the sense that there are no dissipative effects or friction. Then when the gas expands adiabatically the expansion is also isentropic. Tribus[1] presented a detailed analysis of a simple problem of this type, which may be consulted for a thorough understanding of the basic principles involved.

XII-2 STORAGE EFFICIENCY

An efficiency can be defined corresponding to each use or objective. The efficiency is a rating of the performance of the gas stored in the pressure vessel compared to the performance of some ideal system, and is useful as a guide to further design improvements. Efficiencies also provide a convenient representation of performance data. When several alternative system designs are being considered, an efficiency may be the only common basis for comparison. In some cases efficiency may be estimated, thus providing an indirect way to estimate performance. A more precise prediction of performance requires the inclusion of addition effects (i.e. heat transfer, stratification, nonideality) in the calculation, and then it is just as convenient to focus attention on the calculation of performance rather than efficiency.

Definitions

There are several ways to define storage efficiency that have meaning for space applications. A weight storage efficiency may be defined as:

$$\frac{\text{Mass of recoverable gas}}{\text{Mass of filled pressure bottle}}$$

A recovery storage efficiency may be defined as:

$$\frac{\text{Mass of gas recoverable above a useful pressure}}{\text{Mass of gas originally in the bottle}}$$

A work storage efficiency may be defined as:

$$\frac{\text{Work produced by the gas in a real expansion device}}{\text{Reversible work which the gas can do under ideal conditions}}$$

A thrust efficiency can be defined as:

$$\frac{\text{Impulse produced by the gas in a real nozzle}}{\text{Impulse produced under ideal conditions}}$$

The thrust efficiency times the weight efficiency is the thrust-weight efficiency. A pumping efficiency, , discussed in Part 5, is defined as

$$= \frac{V_1(P_o - P_f)}{V_p P_2}$$

where

V_1 = volume of the pressure vessel
P_o = initial pressure in gas tank
P_f = final pressure in gas tank
V_p = volume of liquid propellant expelled
P_2 = pressure in the propellant tank, usually regulated to a constant value

These definitions relate actual performance to ideal performance. In some instances it is still necessary to define this ideal. The ideal should be a limiting case which can only be approached in practice.

The isothermal process for an ideal gas is usually the best performance that can be achieved. We propose to use this process as the datum for calculating efficiencies. Then, for example, the work storage efficiency is:

$$\frac{\text{Work done by vented gas}}{\text{Work done by vented gas in an isothermal process}}$$

Examples of efficiency calculations are given on page XII-2.3, and other values may be deduced from Figures XII-3-1 to XII-3-9.

Weight Efficiency

The determination of weight efficiency requires knowledge of the mass of the gas and the mass of the pressure vessel itself. The mass of the gas is given by

$$M = V_1 \rho_1 \tag{1}$$

where

V_1 = volume of pressure vessel, cu-ft
ρ_1 = density of gas at initial pressure, lb/cu-ft

ρ_1 may be determined from the graphs in Section XV.

The mass of a spherical pressure vessel may be roughly computed from the following formula derived by Ring[2]

$$M_s = \frac{3}{2} \frac{\rho_s}{\sigma_s} P_1 V_1 \tag{2}$$

where

ρ_s = density of sphere wall material
σ_s = allowable stress of wall material

The weight efficiency may then be calculated from:

$$\text{Weight efficiency} = \frac{M}{M + M_s} \tag{3}$$

Substituting equations (1), (2) and the ideal gas law into Equation (3) gives:

$$\text{Weight efficiency} = \frac{1}{1 + \frac{3 \rho_s RT}{\sigma_s m}}$$

This equation clearly shows the effect of several parameters on weight efficiency. It should be kept in mind that other efficiencies such as work efficiency are important too. The effects of some of these parameters on efficiencies were discussed by Ring[2]. Some numerical examples given in

Table XII-2-1 show the greater weight storage efficiencies of liquified gases over noncondensable gases.

Table XII-2-1

WEIGHT STORAGE EFFICIENCIES

"NON-CONDENSABLE" GASES 1500 psia, 12" Ti TANK, 4.0 lb		"CONDENSABLE" GASES 500 psia max. 12" Ti TANK, 2.0 lb	
GAS	W.S.E.	GAS	W.S.E.
Hydrogen	0.06	Propane	0.89
Helium	0.13	Ammonia	0.91
Nitrogen	0.49	Water	0.94

XII-3 THERMODYNAMICS OF PRESSURE VESSEL BLOWDOWN

General Equations

The general equations for blowdown can be derived if we focus attention on the gas in the tank at any time. The definition of entropy for a pound of this gas is

$$Tds = \frac{dQ}{M} \tag{4}$$

where

T = temperature, ^{o}R

s = entropy, Btu/lb-^{o}R

Q = heat flux from the wall of the tank to the gas, Btu

M = number of lbs of gas in the tank

It is assumed that all of the heat transferred is distributed uniformly so that all portions of the gas have the same temperature.

We can expand ds

$$ds = \left(\frac{\partial s}{\partial v}\right)_T dv + \left(\frac{\partial s}{\partial T}\right)_v dT \tag{5}$$

where

v = specific volume, cu-ft/lb

The first term reflects the change in internal energy due to the work which the gas does in pushing other gas out of the vessel. The second term reflects the change in energy due to change in temperature.

Using the Maxwell relation

$$\left(\frac{\partial s}{\partial v}\right)_T = \left(\frac{\partial P}{\partial T}\right)_v \tag{6}$$

and the ideal gas law

$$Pv = \frac{RT}{m} \tag{7}$$

where

m = molecular weight of gas

R = gas constant

we obtain

$$\left(\frac{\partial P}{\partial T}\right)_v = \frac{R}{mv} \tag{8}$$

From the definition of heat capacity at constant volume

$$dQ = Mc_v dT \tag{9}$$

where

c_v = heat capacity at constant volume, Btu/lb-^oR

Equation (1) becomes

$$\left(\frac{\partial s}{\partial T}\right)_v = \frac{c_v}{T} \tag{10}$$

By substituting Equations (8) and (10) into Equation (5):

$$ds = \frac{R}{mv}\, dv - \frac{c_v}{T} dT \tag{11}$$

Equation (3) then becomes

$$MT\,\frac{ds}{d\theta} = MT\left[\frac{R}{mv}\,\frac{dv}{d\theta} - \frac{c_v}{T}\,\frac{dT}{d\theta}\right] = \frac{dQ}{d\theta} \tag{12}$$

where

θ = time, hrs

Let the volume of the vessel be V cu-ft. Then

$$v = \frac{V}{M} \tag{13}$$

$$\frac{1}{v}\,\frac{dv}{d\theta} = \frac{1}{M}\,\frac{dM}{d\theta} \tag{14}$$

and Equation (12) becomes

$$-\frac{RT}{m}\frac{dM}{d\theta} + Mc_v\frac{dT}{d\theta} = \frac{dQ}{d\theta} \tag{15}$$

This is the differential equation giving the temperature of the gas in a container when gas is withdrawn and there is heat transfer. A similar equation can be derived for the pressure change

$$-c_p\frac{dM}{d\theta} + \frac{Mc_v}{P}\frac{dP}{d\theta} = \frac{1}{T}\frac{dQ}{d\theta} \tag{16}$$

where

c_p = heat capacity at constant pressure, Btu/lb-^oR

In the adiabatic case dQ = 0. Equation (16) then integrates to the well-known equation:

$$Pv^{\gamma} = \text{constant} = P\left(\frac{V}{M}\right)^{\gamma} \tag{17}$$

or

$$PM^{-\gamma} = \text{constant} \tag{18}$$

where

$$\gamma = c_p/c_v \tag{19}$$

Equation (15) integrates to

$$\log\frac{T_2}{T_1} = \frac{R}{mc_v}\log\frac{M_2}{M_1} \tag{20}$$

Numerical Examples

Helium is withdrawn from a pressure vessel without heat transfer from the walls to the gas. The initial pressure is 3000 psi and the final pressure is 30 psi. The initial temperature is 530^oR. Represent initial conditions by subscript o and final conditions by subscript f. The quantity of gas remaining is deduced by putting Equation (18) in the following form:

$$\frac{P_o}{P_f} = \left(\frac{M_o}{M_f}\right)^{\gamma} \tag{21}$$

For helium $\gamma = 1.67$, $\frac{P_o}{P_f} = 100$, so $\frac{M_o}{M_f} = 15.9$

The fraction of gas remaining is 6.3%, so the recovery efficiency is 93.7%. The final temperature is calculated from Equation

$$\log \frac{T_1}{T_2} = \frac{2}{3} \log 15.9$$

$$T_1 = 6.4T_2$$

$$T_2 = 83^{\circ}R$$

As another example consider the same problem assuming isothermal conditions. Then the fraction of gas remaining is proportional to the pressures. The ideal gas law can also be written as

$$PV = \frac{MRT}{m} \tag{22}$$

Since V and T are constant,

$$\frac{P_1}{P_2} = \frac{M_2}{M_1} = 0.01$$

and

$$M_2 = 0.01M_1$$

Therefore the recovery efficiency is 99%.

The ideal gas law is not valid under the conditions of this problem. For many tank blowdown problems the assumption of constant heat capacity during integration of Equations (15) and (16) is not valid either. A more general presentation is given in Part 4. In the next Part the effect of heat transfer is analyzed, retaining these simplifying assumptions.

Blowdown with Heat Transfer

The analysis and results presented in this Section are taken from a report by Reynolds and Kays[3].

In this presentation the following simplified model of the gas receiver is employed:

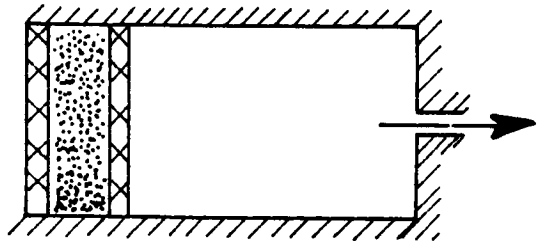

Fig. XII-3-1 Gas Receiver Model

The thermal capacitance of the receiver walls and any interior structure is "lumped" into a single capacitance indicated by , thermal resistances are indicated by , and adiabatic surfaces are indicated by . The general differential equations governing the thermodynamic behavior of blowdown and charging systems, as represented by this model receiver, are developed in detail. These equations are solved generally for the case of constant mass flow. The solutions obtained are in series form, and are rather difficult to use for engineering design purposes. However, more useful closed form solutions can be obtained for certain limiting cases. Solutions are presented for both blowdown and charging at constant mass flow for the following special cases:

1. Isothermal (slow flow rate or low heat transfer resistances)
2. Adiabatic (high flow rate or high inside heat transfer resistances)
3. Heat transfer from an isothermal source (infinite capacitance of receiver walls)
4. Inside resistance negligible

In addition to these closed form solutions, a solution obtained by numerical methods for blowdown through a critical flow nozzle with heat transfer from an isothermal source is presented. Criteria for the application of each of the special solutions are developed; these criteria give the magnitudes of the various system parameters necessary to closely approach the idealized behavior. All solutions are presented both algebraically and graphically in nondimensional form, and give the temperature and pressure of the gas in the receiver as functions of the mass contained therein.

The heat flux from the vessel wall to the gas may be expressed in

terms of the temperature difference:

$$\frac{dQ}{d\theta} = q_i = \frac{T_c - T}{R_i} \tag{23}$$

where

q_i = heat flux at inside of vessel wall, Btu/hr

R_i = inside resistance to heat transfer, hr-^{o}R/Btu

For an ideal gas the two heat capacities are related by

$$c_p - c_v = \frac{R}{m} \tag{24}$$

Substituting Equation (24) into Equation (19):

$$\frac{R}{mc_v} = \gamma - 1 \tag{25}$$

Substituting these expressions in Equation (15) gives

$$M\frac{dT}{d\theta} = (\gamma - 1)T\frac{dM}{d\theta} + \frac{T_c - T}{R_i c_v} \tag{26}$$

The heat transfer between the gas and the vessel walls must also be considered. An energy balance on the vessel walls gives

$$\frac{dE_c}{d\theta} = C_c\frac{dT_c}{d\theta} = q_\infty - q_i \tag{27}$$

where

E_c = energy content of vessel wall, Btu

C_c = heat capacity of vessel wall, Btu/^{o}R, assumed constant

T_c = temperature of vessel wall, ^{o}R

q_∞ = heat flux on outside of vessel wall, Btu/hr

$$q_\infty = \frac{T_\infty - T_c}{R_\infty} \tag{28}$$

where

T_∞ = temperature of environment, ^{o}R

R_∞ = outside resistance to heat transfer, hr-^{o}R/Btu

Substututing Equations (23) and (28) into Equation (27) gives

$$\frac{dT_c}{d\theta} = \frac{T}{R_i C_c} - \left[\frac{1}{R_\infty C_c} + \frac{1}{R_i C_c}\right] T_c - \frac{T_\infty}{R_\infty C_c} \tag{29}$$

Now since

$$w = -\frac{dM}{d\theta}$$

where

w = flow rate, lb/hr

$$\frac{dT}{d} = \frac{dT}{dM}\frac{dM}{d} = -w\frac{dT}{dM}$$

and

$$\frac{dT_c}{d\theta} = \frac{dT_c}{dM}\frac{dM}{d\theta} = -w\frac{dT_c}{dM}$$

Thus Equations (26) and (29) may be written as

$$M\frac{dT}{dM} - \left[(\gamma - 1) + \frac{1}{R_i c_v w}\right]T - \frac{1}{R_i c_v w} T_c = 0 \tag{30}$$

$$\frac{dT_c}{dM} - \frac{1}{C_c}\left[\frac{1}{R_\infty w} + \frac{1}{R_i w}\right] T_c + \frac{T}{R_i C_c w} + \frac{T_\infty}{R_\infty C_c w} = 0 \tag{31}$$

Equations (30) and (31) form a pair of differential equations coupled in zero derivatives, with T and T_c as dependent variables and M as the single independent variable. The instantaneous flow rate, w, is presumed to be describable as a function of temperature and mass. Expressing these equations in nondimensional form allows certain simplifications. The following dimensionless groupings are chosen.

$T^* = T/T_o$ (first dependent variable)

$T_c^* = T_c/T_o$ (second dependent variable)

$M^* = M/M_o$ (independent variable)

$w^* = w/w_o$ (known function of T^*, M^*)

$T_\infty^* = T_\infty/T_o$ (system parameter)

$$\left.\begin{aligned} NTU &= \frac{1}{R_i c_v w_o} = \frac{(\mathcal{H}A)_i}{w_o c_v} \\ NTU_\infty &= \frac{1}{R_\infty c_v w_o} = \frac{(\mathcal{H}A)_\infty}{w_o c_v} \\ C_o^* &= \frac{C_c}{M_o c_v} \end{aligned}\right\} \text{(system parameters)}$$

The physical significance of the first 5 of these terms is readily apparent. The NTU groupings represent dimensionless conductances (reciprocal of resistance) and also serve as a measure of the rate of the process. The symbol NTU represents the "number of transfer units" of a particular heat transfer surface. The C_o^* parameter represents the ratio of the capacitance of the receiver wall, structure, etc., to the initial capacitance of the gas. Note that the choice of parameters is such that the resistive and capacitive elements of heat transfer are separated.

Equations (30) and (31) may be expressed in terms of the dimensionless quantities as follows:

$$w^* M^* \frac{dT^*}{dM^*} - \left[(\gamma - 1) w^* + NTU \right] T^* + NTU\, T_c^* = 0 \tag{32}$$

$$w^* \frac{dT_c^*}{dM^*} - \frac{1}{C_c^*} \left[NTU_\infty + NTU \right] T_c^* + \frac{1}{C_o^*} NTU\, T^* + \frac{1}{C_o^*} NTU_\infty T_\infty^* = 0 \tag{33}$$

Differentiation of Equation (32) with respect to M^*, followed by suitable algebraic manipulation, allows Equations (32) and (33) to be combined to yield a single equation in $T^* = T^*(M^*)$. This equation, which represents the general differential equation for blowdown, may be expressed as follows:

$$w^{*2} M^* \frac{d^2 T^*}{dM^{*2}} + M^* \left[\frac{dw^*}{dM^*} + w^*(2 - \gamma) - NTU - \frac{M^*}{C_o^*} (NTU + NTU_\infty) \right] w^* \frac{dT^*}{dM^*}$$

$$+ \frac{1}{C_o^*} \left[(\gamma - 1) w^* (NTU + NTU_\infty) + NTU\, NTU_\infty - w^*(\gamma - 1) \frac{dw^*}{dM^*} \right] T^*$$

$$- \frac{NTU\, NTU_\infty}{C_o^*} T_\infty^* = 0 \tag{34}$$

The initial conditions to be employed in the integration are as follows: at $M^* = 1$

a) from the definition of the dimensionless variables,

$$T^* = 1$$

b) from Equation (32),

$$\frac{dT^*}{dM^*} = \gamma - 1 + NTU - NTU\, T^*_{c_o}$$

where $T^*_{c_o}$ denotes the initial temperature of the capacitance.

In a similar manner Eqs. (32) and (33) may be combined to give a single second-order equation in T^*_c. This is not presented here because it is felt that T^* is the dependent variable of primary interest.

As stated previously (p. XII-3.4) the ideal gas law can also be written as

$$PV = \frac{M}{m} RT \tag{22}$$

both for initial and instantaneous conditions, from which it can be shown that

$$P^* = M^* T^* \tag{35}$$

Once T^* is known the pressure may be calculated from Equation (35) without the use of Equation (16).

Solutions of the Blowdown Equations for Constant Mass Flow Rate and Constant Heat Transfer Resistance

Reynolds and Kays (Ref. 3) showed that Equation (34) could be solved analytically for the case of constant mass flow rate. The results were given in terms of the confluent hypergeometric functions. For details the original report should be consulted. Some results are given in Figure XII-3-2.

It is unfortunate that for certain ratios of transfer unit to capacitance the solution in series form converges slowly or diverges. Another difficulty is that for integer values of the parameter $2 - \gamma - NTU$ singularities occur, making the series solution invalid. Because of these difficulties in applying the general solution, and because of unrealistic assumptions

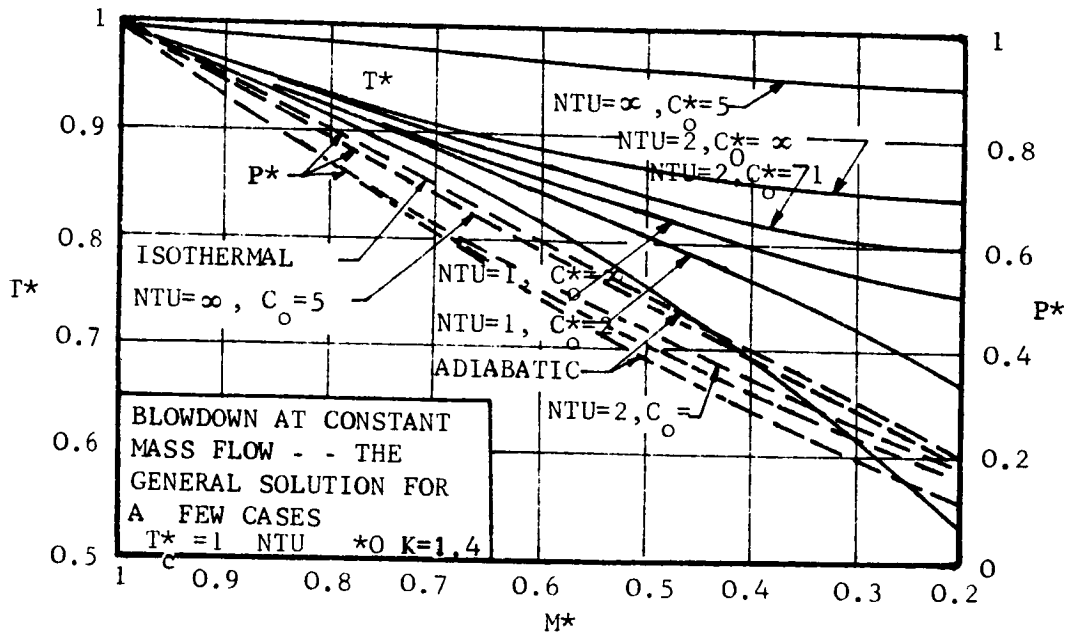

Fig. XII-3-2 The General Solution for a Few Cases of Blowdown at Constant Mass Flow (Ref. 3)

made in its derivation, calculation of further results beyond those presented by Reynolds and Kays is not recommended. Instead, a numerical approach suitable for a computer is presented in Part 4.

Solutions For Limiting Cases

> In many systems of technical interest the magnitudes of the system parameters NTU, NTU_∞, and C_o^* are such that approximate closed form solutions may be employed without introducing any serious error. For example, if the capacitance is large and the process occurs at a fairly rapid rate the temperature change of the capacitance might be negligible, in which case considerable simplification is obtained. On the other hand, if the process is very rapid the amount of heat transfer might be sufficiently small that the process could be called adiabatic.
>
> In this section solutions are presented for a number of special cases of blowdown. These solutions may be obtained by simplification and integration of Eq. (34), and the constant flow solutions by direct reduction of the series solution.

Reynolds and Kays also developed these special solutions from basic principles.

> Criteria are established for determining what values of the parameters give essentially "limiting value" behavior. Typical numerical magnitudes of the various parameters as they might be found in systems of technical interest are presented, and in some of the solutions are compared with experimental data recorded during the blowdown of a gas receiver. While it is not necessarily true that all engineering systems involving blowdown processes may be treated with these special solutions, a good many systems can.

Isothermal Blowdown

> Isothermal behavior is obtained if $C_o^* = \infty$ and $NTU = \infty$, or if $NTU = \infty$ and $NTU_\infty = \infty$. The first obtains in receivers having large thermal capacitance (C_o) accompanied by a high value of inside ($\bar{h}A$), and the latter in systems where the mass flow is extremely slow. The first might be the case of the receiver for a blowdown wind tunnel, where the receiver is partially filled with material having large thermal capacity and heat transfer area for the purpose of obtaining a near-isothermal blowdown. The latter would be the case of the discharge

of an oxygen storage tank for use by oxy-hydrogen flame cutting apparatus. These two cases may be represented by the simple receiver models shown below.

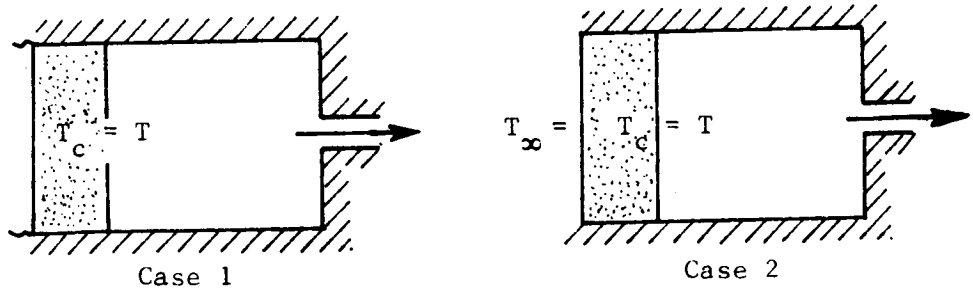

Fig. XII-3-3 Simple Gas Received Models, Case 1- Large Thermal Capacitance and High Valve of hA), Case 2 - Extremely Slow Mass Flow (Ref. 3)

For isothermal blowdown the temperature-mass and the pressure-mass functions come directly from the perfect gas equation of state, $pV = M(R/m)T$, and are simply

$$T^* = 1 \tag{36}$$

$$P^* = M^* \tag{37}$$

Equations (36) and (37) are shown by Fig. XII-3-4. The magnitudes of NTU and C_o^* necessary to obtain essentially isothermal blowdown are discussed in a later part of this section.

Adiabatic Blowdown

The common method of analysis of blowdown systems is to assume that the process is adiabatic. Adiabatic behavior is usually obtained in systems in which the blowdown is extremely rapid, such as the cylinder of an internal combustion engine during the early stages of the exhaust process. However, if the inside of the receiver wall is lined with an insulator such that the gas is insulated from the thermal effects of the wall capacitance, a blowdown approaching adiabatic blowdown may be obtained at relatively slow mass discharge rates. In either case the effect is to make NTU small. Thus the simple receiver model for adiabatic blowdown may be represented as shown:

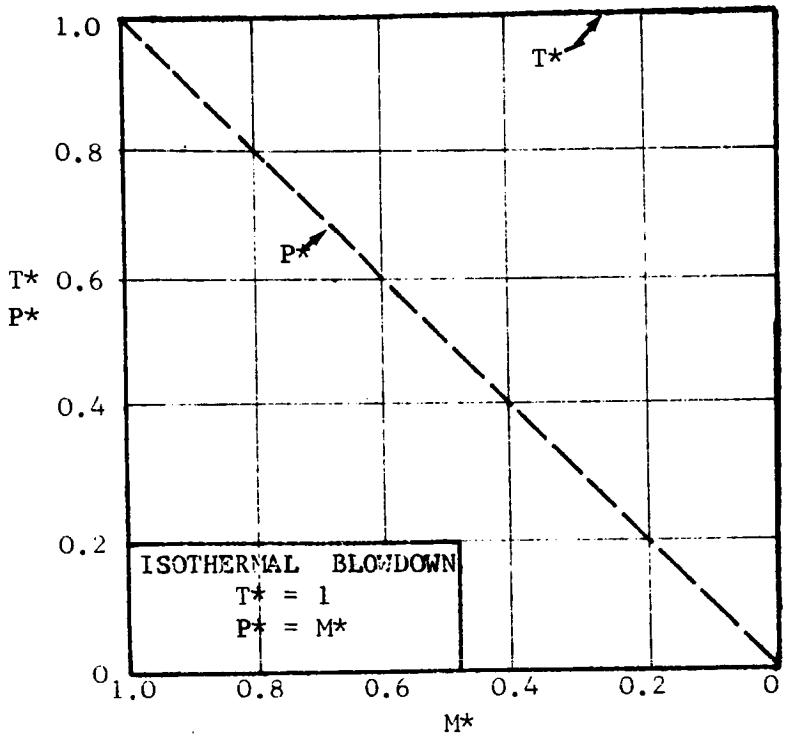

Fig. XII-3-4 Isothermal Blowdown (Ref. 3)

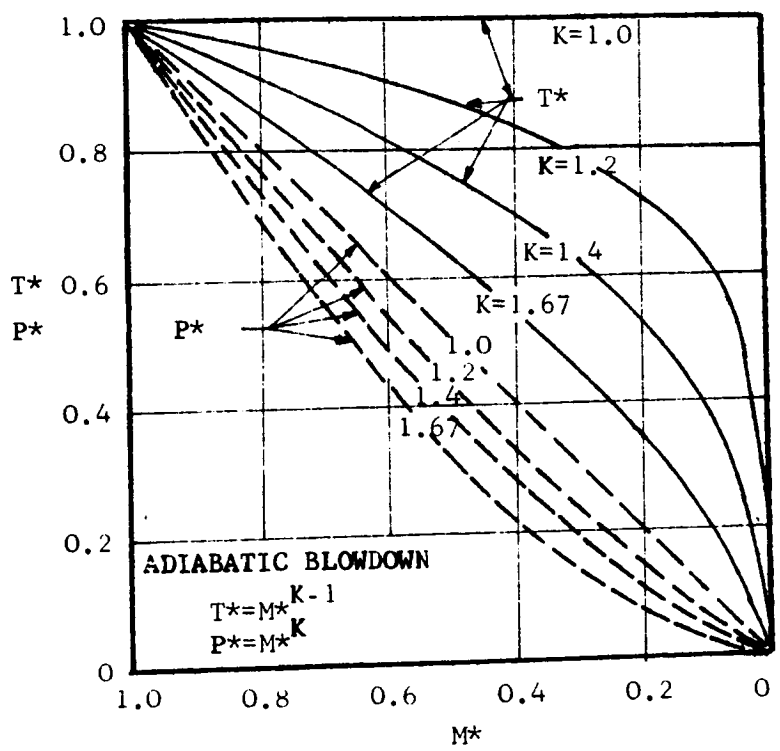

Fig. XII-3-5 Adiabatic Blowdown (Ref. 3)

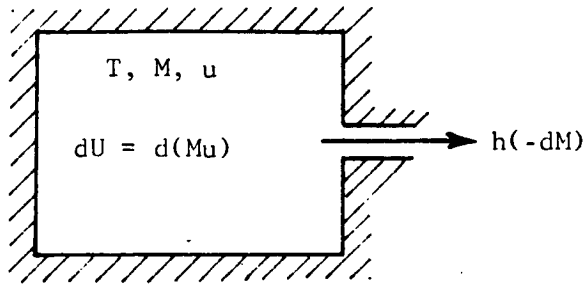

Fig. XII-3-6 Simple Receiver Model for Adiabatic Blowdown (Ref. 3)

Since there are no heat transfer rates to consider it is not necessary to specify mass flow rate.

The equations for the adiabatic case have already been given as an example, page XII-3.3.

The temperature-mass and pressure-mass functions are shown in Fig. XII-3-5 for a wide range of values of γ. Note the significant dependency of T^* on γ, and the relative independence of P^* on γ. For the purpose of plotting the more complicated solutions, γ will be taken as 1.4, but it is well to bear in mind that γ is a parameter of significant importance.

Blowdown At Constant Mass Flow With Heat Transfer From An Isothermal Source

In many systems the thermal capacitance of the metal receiver walls far exceeds the thermal capacitance of the gas. In this case the temperature change of the walls is much less than that of the gas, and it might be expected that a solution for the limiting case of $C_o^* = \infty$, i.e., where the sole heat transfer occurs between the gas and an isothermal source, would be applicable. This is, in fact, an extremely useful solution. A less important situation occurs when the capacitance is very small, such that the heat transfer occurs directly between the gas and the receiver environment. In this case also, the heat transfer occurs effectively between the gas and an isothermal source.

Because a heat transfer rate is involved it is necessary to specify the mass-time variation. The infinite capacitance solution is developed here for the case of constant mass flow rate, and in a following sub-section for blowdown through a critical flow nozzle.

Simple models for blowdown receivers discharging at constant flow under the two conditions are shown below:

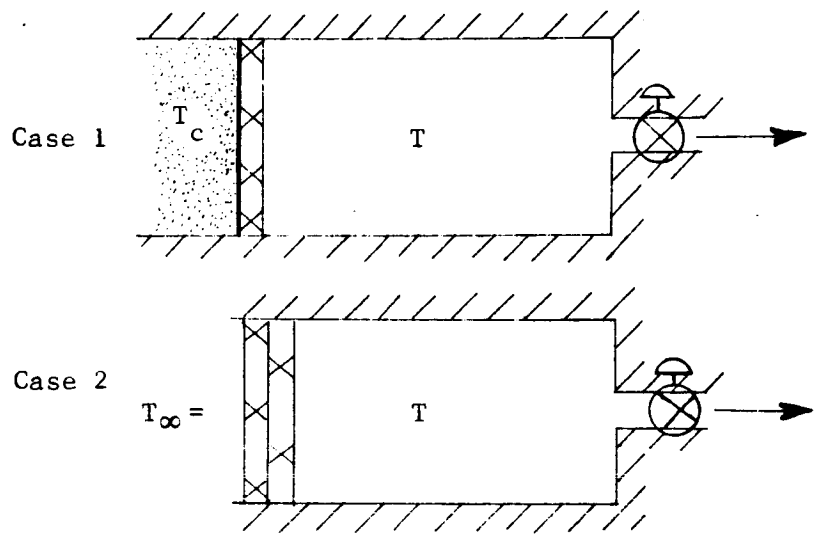

Fig. XII-3-7 Simple Gas Receiver Models for, Case 1 - Thermal Capacitance of the Metal Receiver Wall greatly exceeds that of the Gas. And Case 2 - Small Heat Capacitance of Receiver Wall (Ref. 3)

The solution was developed in terms of the first of these cases, and may readily be extended to the nomenclature of the second. The model is shown below:

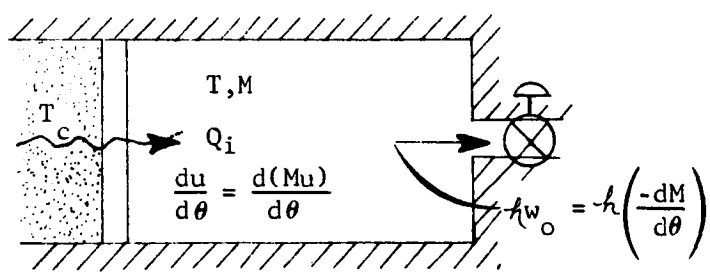

Fig. XII-3-8 Simple Gas Receiver Model for Blowdown at Constant Mass Flow with Heat Transfer from an Isothermal Source (Ref. 3)

The result is given in terms of dimensionless parameters:

$$T^* = \frac{(\gamma - 1 + NTU - T^*_c NTU) M^{*\gamma - 1 + NTU} + T^*_c NTU}{\gamma - 1 + NTU} \tag{38}$$

and

$$P^* = T^* \left[\frac{T^*_c NTU - (\gamma - 1 + NTU) T^*}{T^*_c NTU - (\gamma - 1 + NTU)} \right]^{\frac{1}{\gamma - 1 + NTU}} \tag{39}$$

Note that for NTU = 0 Eqs. (38) and (39) reduce to the adiabatic expressions. For NTU = ∞ use of L'Hopital's rule for indeterminant forms reduces Eqs. (38) and (39) to the isothermal relationships of Eqs. (36) and (37).

It should be noted that even for this simple case where the source is isothermal, the relationships between the temperature and mass and between the temperature and pressure of the gas remaining in the vessel do not correspond to expressions involving a polytropic expansion coefficient k except when the number of transfer units is zero or infinite. Values for the exponent, k, in expression of the sort shown below cannot be found which correctly describe the PVT behavior of the gas remaining in the tank.

$$P/\rho^k,\ P/M^k \text{ or } T/M^{k-1} = \text{constant.}$$

The temperature-mass and pressure-mass relationships are plotted in Fig. XII-3-9 for $T^*_c = 1$. Note that the temperature function is asymptotic and shows a considerable effect of heat transfer. The solutions for NTU = 1 and 2 are compared with solutions for similar values of NTU but finite values of the C^*_o parameter in Fig. XII-3-2. The values of C^*_o used for this comparison are evidently not sufficient to give infinite capacitance behavior. The criteria for infinite capacitance behavior are presented on page XII-3.21.

The influence of the temperature of the isothermal source, T^*_c, on blowdown at constant mass flow is shown by Fig. XII-3-10. Note for $T^*_c = (\gamma - 1 + NTU)/NTU$ the temperature is <u>independent</u> of mass, and an <u>isothermal</u>

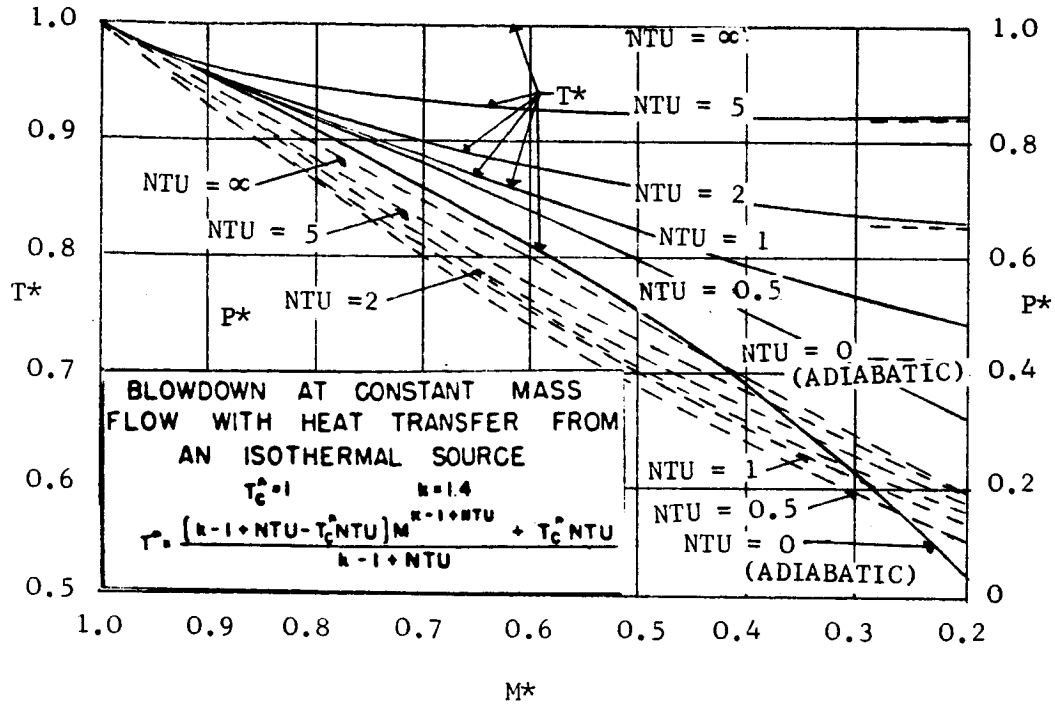

Fig. XII-3-9

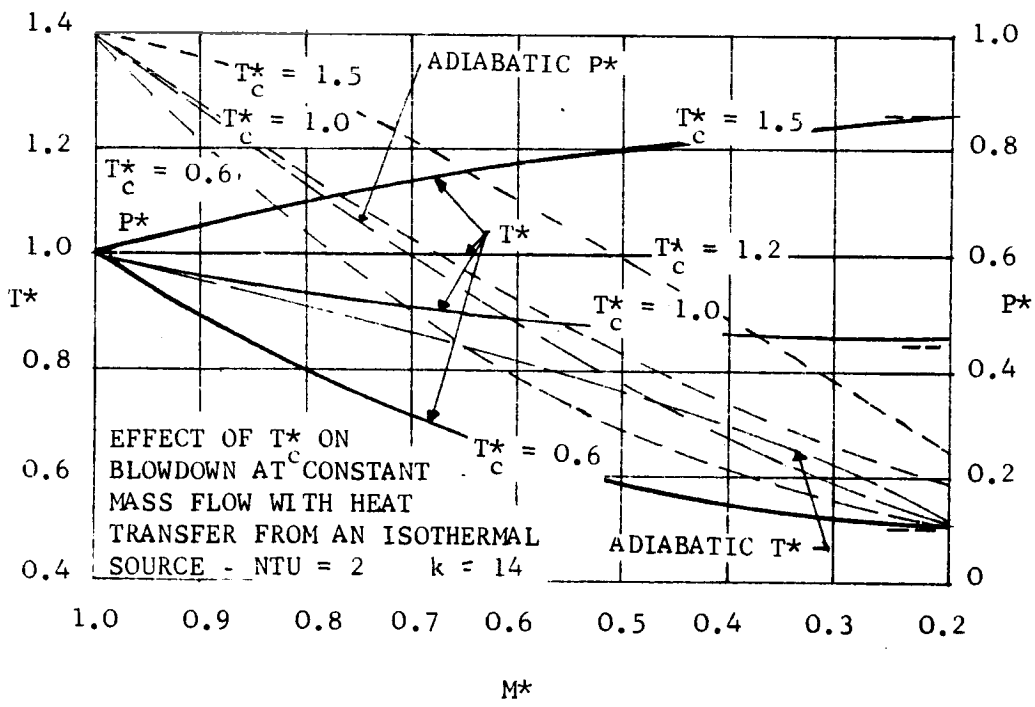

Fig. XII-3-10

blowdown results. For large values of T_c^* it is even possible to experience a rise in temperature during blowdown. It might be suspected that the asymptote of the temperature function is the capacitance temperature, but such is not the case for constant flow blowdown. However, for blowdown through a critical flow nozzle, i.e., at a constantly reduced rate, the asymptote is the capacitance temperature as would be expected from physical reasoning. From this point of view, the critical flow solution would be more desirable for many systems where the flow is not constant; however, the integration must be handled by numerical methods.

Blowdown At Constant Mass Flow With Inside Resistance Negligible

The assumption of NTU = ∞ allows a closed form solution to be obtained. Large values of NTU are obtained in the following three ways;

1. The inside heat transfer area is large
2. The inside heat transfer conductance is high
3. The flow rate is relatively low

The first possibility might arise in the receiver for a blowdown wind tunnel where the receiver is partially filled with a metal matrix having high thermal capacitance for the purpose of obtaining near-isothermal blowdown. It is evident that systems of this nature obtain a high NTU while simultaneously obtaining a high C_o^*, and this tends to give isothermal blowdown. The second case might arise in a high temperature system, where the interior convective conductance is large relative to that on the outside. The possibility of the third is self-evident. However, if high values of NTU are obtained by low flow rates, then most likely NTU_∞ would also be large, in which case the blowdown process would be essentially isothermal. It appears, then, that the only nontrivial possibility for NTU = ∞ lies in having a high inside conductance, i.e., the inside heat transfer resistance negligible

The condition of negligible inside resistance implies that the capacitance temperature is identical with the gas temperature. Because a finite heat transfer rate is involved in heat transfer between

the capacitance and the receiver environment it is necessary to specify a particular mass-time relationship; constant mass flow is assumed for this analysis. From consideration of the energy equation it is evident that for $NTU_{\infty} = 0$ the system is independent of the mass-time relationship and the solution need not be restricted to constant flow. As yet this problem has not been treated for blowdown through a critical flow nozzle.

The simple receiver model with inside resistance negligible is shown below. Significant energy terms are noted.

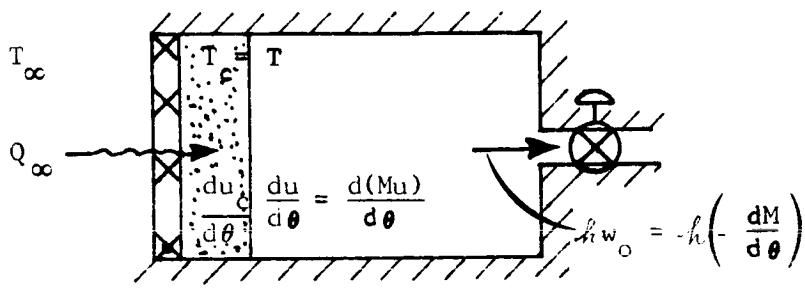

Fig. XII-3-11 Simple Gas Received Model with negligible inside resistance (Ref. 3)

The results were presented in equation form and some numerical results are summarized in Figures XII-3-12 and XII-3-13.

Note the strong effect that a relatively small amount of capacitance has on the blowdown process. In Fig. XII-3-13 the effect of external heat transfer is shown for a moderate value of capacitance. For C_o^* larger than shown the effect of external heat transfer is less, and for C_o^* less than shown the effect is stronger. Note that for $T_\infty^* = (\gamma - 1 + NTU_\infty)/NTU_\infty$ the temperature function is independent of mass, and an isothermal blowdown occurs. If the external heat transfer is great enough it is actually possible to obtain a rise in the temperature of the gas in the receiver during blowdown.

In this analysis constant flow was assumed, and the inside heat transfer resistance was considered

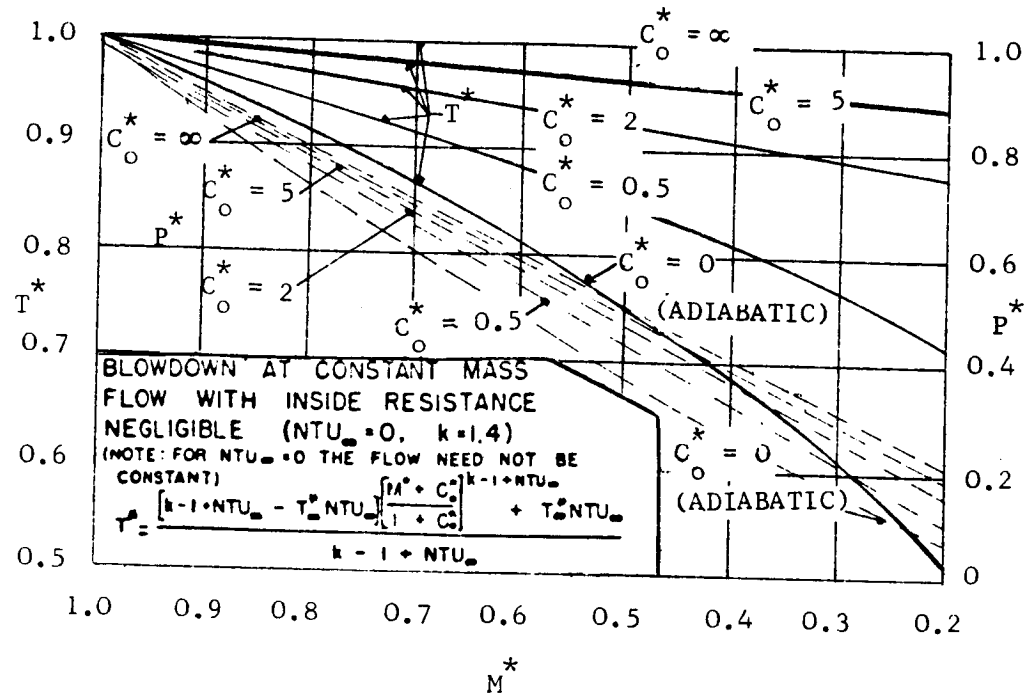

Fig. XII-3-12

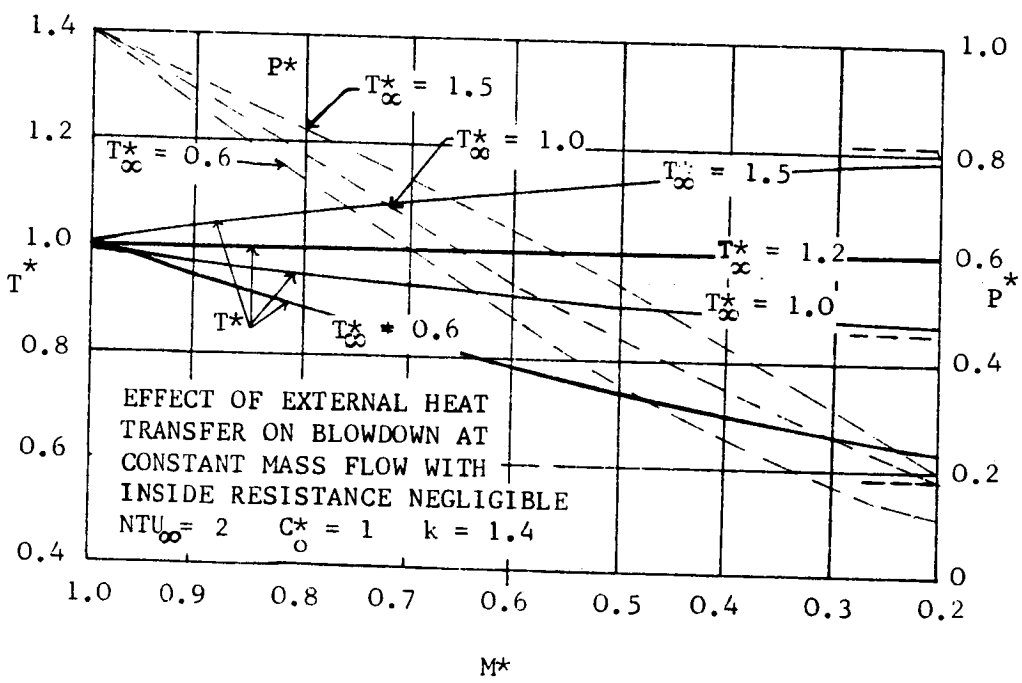

Fig. XII-3-13

to be zero. It may not appear that the assumptions could lead to a solution of technical interest, but the real value of this solution is that it supplies definite information for determining the effects of capactitance upon the thermodynamic behavior of blowdown systems.

Blowdown Through A Critical Flow Nozzle With Heat Transfer From An Isothermal Source

In systems when regulators are not provided to maintain constant flow blowdown, the flow variation is not easily described analytically. However, if the discharge occurs through a valve or other constriction the flow will somewhat resemble flow through a critical flow nozzle. Unfortunately, the governing differential equation for blowdown with critical flow cannot be integrated in closed form, and so numerical methods must be employed. This limits the usefulness of the critical flow solutions considerably, as a separate numerical integration must be performed for each set of system parameters. Nevertheless, the critical flow solution serves as an indication of the effects of variations in mass flow rate.

As in the case of constant flow blowdown considered previously, the same two models of the receiver are possible. The "infinite capacitance" model is used in this development, and is shown below with significant energy terms.

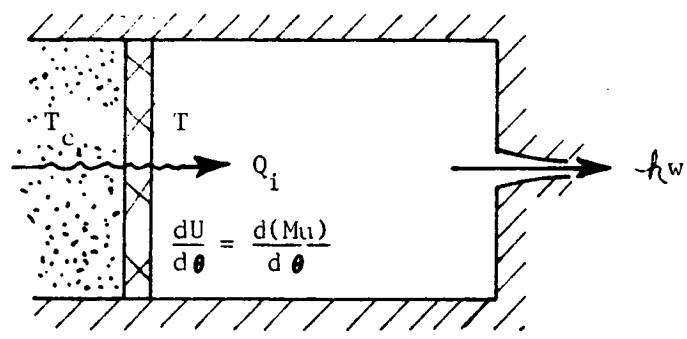

Fig. XII-3-14 Infinite Capacitance Gas Receiver Model for Blowdown through a Critical Flow Nozzle with Heat Transfer (Ref. 3)

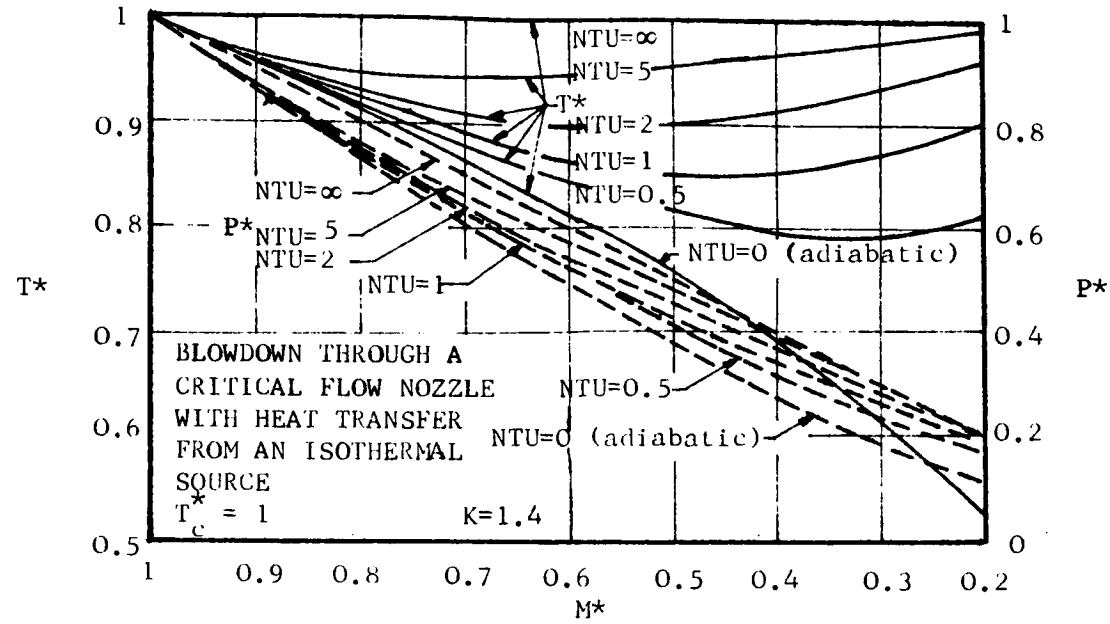

Fig. XII-3-15 Blowdown Through a Critical Flow Nozzle with Heat Transfer from an Isothermal Source (Ref. 3)

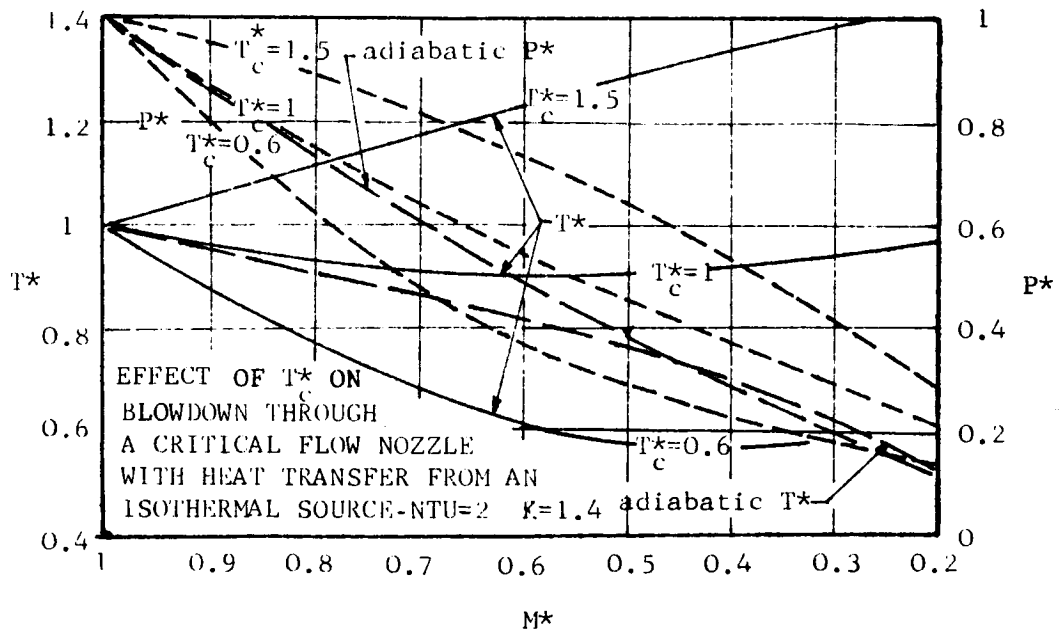

Fig. XII-3-16 Effect of T_c^* on Blowdown through a Critical Flow Nozzle with Heat Transfer from an Isothermal Source - NTU-2, K=1.4 (Ref. 3)

The mass flow rate through a critical flow nozzle is described by

$$w = B_1 \frac{p}{\sqrt{T}} = \left(- \frac{dM}{d\theta}\right) \tag{40}$$

The result is given in dimensionless form:

$$M^* \frac{dT^*}{dM^*} - (\gamma - 1)T^* + \frac{(T_c^* - T^*)NTU}{M^*\sqrt{T^*}} = 0 \tag{41}$$

Note that NTU is characterized by w_o, the <u>initial</u> flow rate.

Equation (41) has been integrated numerically from the initial values for constant values of NTU, and the results of the integrations are shown in Figs. XII-3-15 and XII-3-16. Note that as the flow rate decreases the "cooling" effect of the gas expansion loses its controlling influence to the "heating" effects of the capacitance, and thus the temperature tends to return to the capacitance temperature T_c^*. It must be remembered that the solution is only exact as long as critical flow exists in the exit. Nevertheless, this solution may in many cases be better than the constant flow solution, even in the very last stages of blowdown when critical flow no longer exists.

<u>Criteria For Limiting Cases Of Blowdown</u>

Reynolds and Kays (Ref. 3) developed some rules to indicate the errors which would result from using their limiting cases. These rules were deduced by comparison of graphical results and are summarized below.

1) Adiabatic Limit

The error in assuming adiabatic behavior is less than 5% down to a value of $M^* > 0.2$ if

$NTU < 0.08$ for all C_o^*

(little heat is transferred from wall to gas)

or

$C_o^* < 0.04$, NTU is reasonably low for all NTU

(wall has low capacity and is not heated much by environment)

For smaller values of M^* the limits are much more stringent.

2) Isothermal Limit

The error in assuming isothermal behavior is less than 5% for all values of M^* if

$$C_o^* > 6.5 \text{ and } NTU > 8$$

or

$$NTU > 8 \text{ and } NTU_\infty > 8$$

For lower values of these parameters the error increases markedly, especially at low values of M^*.

3) Negligible Inside Resistance

The error in assuming negligible inside resistance is less than 5% for values of $M^* > 0.2$ for all values of capacitance if $NTU > 8$.

4) Constant Temperature Capacitance

The error in assuming that the wall temperature is constant is less than 7% for all values of M^* if $C_o^* > 6.5$ for all values of NTU or for $NTU_\infty > 8$.

Beyond the limits of these conditions the error increases markedly for small values of M^*. Reduced gravity would affect the value of NTU, but would not affect the numerical limits given above.

XII-4 MORE EXACT EQUATIONS FOR BLOWDOWN

The equations given by Reynolds and Kays are based on several simplifying assumptions; a) the gas is ideal, b) the heat capacity is constant, c) the heat transfer resistances are constant, d) there is no stratification of the gas. Furthermore Reynolds and Kays gave few results for flow conditions other than constant flow because of difficulties in solving even the simplified equations. In practical problems the flow is seldom constant.

Deviation from Ideality

The ideal gas law is not obeyed exactly by a gas under usual pressure tank conditions. For helium or nitrogen at 2000 psi the deviation in density from the ideal value is about 5%. At 15000 psi the deviation for nitrogen is almost a factor of 2. The deviation is usually great for a gas near its critical temperature and pressure. Critical conditions are listed in Table XII-4-1. See Section XV for additional gas property data.

Whether a gas can be considered ideal can be determined by looking up its compressibility factor at the temperature and pressure in question. Table XII-4-2 is a reduced compressibility correlation that may be used for all gases for this purpose. The reduced temperature and pressure are the ratios of actual temperature and pressure to the critical temperature and pressure given in Table XII-4-1.

If any of these assumptions are correct then the resulting equations must be solved numerically. If this is done, then it is well to include the most realistic available formulation of these conditions, since this will not make the problem much more difficult to solve with a computer.

Table XII-4-1

CRITICAL CONDITIONS FOR SOME GASES

GAS	CRITICAL TEMPERATURE ^{o}R	CRITICAL PRESSURE psi
Air	238	546
Ammonia	730	1638
Argon	274	705
Carbon Monoxide	242	508
Helium	9.4	34
Hydrogen	59.7	188
Neon	80	381
Nitrogen	227	492
Oxygen	278	227
Propane	666	632
Water	1165	3210

The real gas behavior enters into the calculation through the term in Equation (6) involving $\left(\frac{\partial P}{\partial T}\right)_v$. One way to account for real gas behavior is to use a more accurate equation of state than the ideal gas law. For example the Beattie-Briggeman equation may be used:

$$P = \frac{RT(1 - \frac{c}{vT^3})}{v^2} \left[v + B_o(1 - \frac{b}{v}) \right] - \frac{A_o}{v^2}(1 - \frac{a}{v}) \tag{42}$$

where a, A_o, b, B_o and c are arbitrary constants to be evaluated from experimental data. The derivative is then:

$$\left(\frac{\partial P}{\partial T}\right)_v = \frac{R}{v^3}\left[v + B_o(1 + \frac{b}{v}) \right]\left(\frac{3c}{T^3}\right)\left(1 - \frac{c}{vT^3}\right) \tag{43}$$

Dodge[4] summarized numerical values of the constants for 19 gases in cgs units. The equation is valid for nitrogen and hydrogen up to 15000 psi, and for other gases up to 1500 psi. The equation gives serious error near the critical point, although it is better than the ideal gas law.

Table XII-4-2

CONSTANTS OF THE BEATTIE-BRIDGEMAN EQUATION OF STATE

(Units: atm., liters, g.-moles, ^{o}K. R=0.08206) (Ref. 4)

Gas	A_0	a	B_0	b	$c \times 10^{-4}$	Temp. range, ^{o}C	Maximum pressure, atm.	Minimum volume, cc./g.-mole	Ref.
He	0.0216	0.05984	0.01400	0.0	0.0040	400 to -252	102	100	1
Ne	0.2125	0.02196	0.02060	0.0	0.101	400 to -217	106	118	1
A	1.2907	0.02328	0.03931	0.0	5.99	400 to -150	114	167	1
H_2	0.1975	-0.00506	0.02096	-0.04359	0.0504	200 to -244	103	100	1
H_2(below critical density)	0.12404	0.05618	0.02022	-0.00722	2.00	300 to - 70	1,000	65	6
H_2(above critical density)	0.12404	0.05618	0.01750	-0.01968	2.00	300 to - 70	1,000	37	6
N_2	1.3445	0.02617	0.05046	-0.00691	4.20	400 to -149	134	182	1
N_2	1.2317	0.01866	0.04603	-0.02587	6.16	400 to - 70	1,000	84	5
O_2	1.4911	0.02562	0.04624	0.004208	4.80	100 to -117	103	111	1
Air	1.3012	0.01931	0.04611	-0.01101	4.34	200 to -145	177	125	1
CO_2	5.0065	0.07132	0.10476	0.07235	66.00	100 to 0	111	182	1
CH_4	2.2769	0.01855	0.05587	-0.01587	12.83	200 to 0	243	167	
$(C_2H_5)_2O$	31.278	0.12426	0.45446	0.11954	33.33	325 to 150	90	370	1
C_2H_4	6.1520	0.04964	0.12156	0.03597	22.68	200 to 0	286	125	2
NH_3	2.3930	0.17031	0.03415	0.19112	476.87	325 to - 35	130	340	3
CCl_2F_2	23.7	0.305	0.59	0.622	0	126 to 30	18.5	1,430	4
C_2H_6	5.8800	0.05861	0.09400	0.01915	90.00	25 to 250	153	200	7
C_3H_8	11.9200	0.07321	0.18100	0.04293	120.00	97 to 275	305	100	8
n-C_4H_{10}	17.7940	0.12161	0.24620	0.09423	350.00	150 to 300	118	280	9
n-C_7H_{16}	54.520	0.20066	0.70816	0.19179	400.00	275 to 350	315	200	10
Iso-C_4H_8	16.9600	0.10860	0.24200	0.08750	250.00	150 to 250	250	111	11
CH_3OH	33.309	0.09246	0.60362	0.09929	32.031				12

Note: The constants for N_2 can be used for CO and the CO_2 constants for N_2O at moderate pressures and temperatures not too near the critical ones.

*Somewhat better agreement was obtained by adding a sixth constant a', making the last term of Eq. (V.77): $1 - (a/v) - (a'/v)$. The difference does not seem great enough to warrant the additional complication.

1. Beattie, J. A., and Bridgeman, O. C., Proc. Am. Acad. Arts Sci., 63, p.229-308, 1928.
2. Gillespie, L. J., J. Phys. Chem. 33, p.354-360, 1929.
3. Beattie, J. A., and Lawrence, C. K., J. Am. Chem. Soc., 52, p.6-14, 1930.
4. Buffington, R. M., and Gilkey, W. K., Ind. Eng. Chem., 23, p. 254, 1931.
5. Deming, W. E., and Shupe, L. E., J. Am. Chem. Soc., 52, p. 1382-1389, 1930.
6. Deming, W. E., and Shupe, L. E., J. Am. Chem. Soc., 53, p.843-849, 1931.
7. Beattie, J. A., Hadlock, C., and Poffenberger, N., J. Chem. Phys., 3, p.93-96, 1935.
8. Beattie, J. A., Kay, W. C., and Kaminsky, J., J. Am. Chem. Soc., 59, p.1589-1590, 1937.
9. Beattie, J. A., Simard, G. L., and Su, G., J. Am. Chem. Soc., 61, p.26-27, 1939.
10. Smith, L. B., Beattie, J. A., and Kay, W. C., J. Am. Chem. Soc., 59, p.1587-1589, 1937.
11. Beattie, J. A., Ingersoll, H. G., and Stockmayer, W. H., J. Am. Chem. Soc., 64, p. 548, 1942
12. Beattie, J. A., and Stockmayer, W. H., Reports on Progress in Physics, 7, p. 195, 1940.

ORIGINAL PAGE IS
OF POOR QUALITY

The graphs of constant density given in Section XV of this handbook could be used to evaluate $\left(\frac{\partial P}{\partial T}\right)_v$, since this derivative is just the slope of the line of constant density at any given P and T. Because the lines are nearly straight, it should be possible to fit these lines to equations involving P and T for computer use.

Heat Capacity, C_v

Heat capacity varies with pressure and temperature. The heat capacity at constant volume, C_v, is much less affected by pressure than the heat capacity at constant pressure, C_p. In most of the above equations C_v, rather than C_p, is involved, and the following discussion refers to C_v. Equations relating C_p to C_v are given in thermodynamic texts.

In practical conditions the error due to assuming constant heat capacity is seldom greater than 10%. Larger errors can occur when the gas is under high pressure at low temperature. Some values are given in Table XII-4-3. Heat capacities for monatomic gases are constant above some low temperature and equal to 2.98 BTU/lb-mol-$^{\circ}$R. The value for diatomic gases is about 4.97 at room temperature. It drops off at very low temperatures, and at high temperatures it approaches 7.0. The values for polyatomic gases vary more widely. Examination of the table shows that in many cases the effect of temperature on C_v can be ignored. The effect can be taken into account by fitting data for C_v to a quadratic or cubic polynomial in temperature.

Experimental data show that C_v is little affected by pressures up to 6000 psi at room temperature. At low temperatures, high pressure raises C_v. For diatomic gases a pressure of 1500 psi increases C_v by 1 to 5% at room temperature, or 5 to 20% at 360°R. Fortunately, in tank blowdown the temperature decreases only as pressure decreases, so the effect of pressure on C_v may usually be neglected. At very low temperatures the pressure effect is pronounced and irregular.

Table XII-4-3

MOLAR HEAT CAPACITIES (BTU/lb-mol-^{o}R) (Refs. 8 and 9)

TEMPERATURE ^{o}K	^{o}R	He, Ar, Ne, METAL VAPORS	H_2	N_2	O_2	CO	AIR	CH_4	NH_3	CO_2
50	90	2.98	2.98							
100	180	2.98	3.38		5.02	4.97	4.97	5.45		5.00
150	270	2.98	4.05		5.00	4.97	4.97	5.60		5.74
200	360	2.98	4.50	4.97	5.00	4.97	4.97	5.76		6.90
250	450	2.98	4.75	4.97	5.00	4.97	4.97	6.08		7.88
300	540	2.98	4.86	4.97	5.06	4.97	4.97	7.20		8.67
400	720	2.98	4.98	5.00	5.20	5.02				9.30
500	900	2.98	4.99	5.10	5.45	5.14				9.80
600	1080	2.98	5.00	5.20	5.70	5.29				
700	1260	2.98	5.04	5.40	5.90	5.46				
				EFFECT OF PRESSURE						
		He, little effect above 25°K		+10% @400 atm 300°K	+5% @100 atm 300°K +12% @100 atm 200°K	+ 1% @400 atm 300°K +10% @400 atm 250°K	+ 7% @30 atm 200°K			

Estimation Of Heat Transfer Rates

The detailed analysis of the effects of heat transfer on the PVT behavior of the fluid left in the pressure vessel while fluid is being discharged is discussed in Part 3. To apply that analysis to particular problems, heat transfer rates at both the internal and external surfaces of the pressure vessel are required. The important heat transfer parameter in that analysis is the number of transfer units, NTU.

$$NTU = \frac{\mathcal{h} A}{c_v w}$$

where

A = area for heat transfer
c_v = specific heat of the fluid in the vessel at constant volume
$\mathcal{h}$ = heat transfer coefficient
w = discharge rate

This quantity represents the ratio of the temperature change experienced by a quantity of fluid passing through a system and the mean temperature difference between the fluid and the surface from which heat is transferred. To estimate the rate of heat transfer that results from the difference between the temperatures of the pressure vessel and its contents, the various mechanisms by which heat can be transferred need to be considered.

Free Convection

Because the density of the fluid next to the vessel wall is different from the density in the interior, the fluid next to the wall experiences a buoyancy force which produces a circulating flow upward along the vessel walls and downward in the interior when the wall is warmer than the contents of the tank. Heat transfer rates due to this free convection mechanism can be estimated from the correlation shown below.

$$\frac{\mathcal{h} L}{k_f} = c\left[\frac{L^3 \rho_f^2 g \beta_f \Delta T}{\mu_f^2}\left(\frac{c_p \mu}{k}\right)_f\right]^n \qquad (44)$$

where

c_p = specific heat at constant pressure
g = gravitational constant
h = heat transfer coefficient
k = thermal conductivity
L = vertical dimension of pressure vessel
ΔT = temperature difference between pressure vessel and contents
β = coefficient of volumetric expansion
μ = viscosity
ρ = density

In this section the subscript f denotes that the fluid property is to be evaluated at a temperature which is midway between the temperature of the wall and the bulk of the fluid.

The exponent, n, depends on whether the fluid motion is laminar or turbulent and the coefficient, c, depends on both the value of n and the configuration of the surface at which heat is transferred. For cylindrical pressure vessels standing vertically or placed horizontally the coefficient and exponent may be obtained from Table XII-4-4. The proper vertical length dimension, L, in the case of horizontal cylinders is the inside diameter of the vessel.

Table XII-4-4

COEFFICIENT AND EXPONENT IN CORRELATION FOR FREE CONVECTION HEAT TRANSFER (Ref. 2)

$\frac{L^3\rho_f^2 g\beta_f \Delta T}{\mu_f^2}\left(\frac{c_p\mu}{k}\right)_f$	LAMINAR 10^4 to 10^9		TURBULENT 10^9 to 10^{12}	
	n	c	n	c
Vertical cylinders	1/4	0.59	1/3	0.13
Horizontal cylinders	1/4	0.53	1/3	0.12

The values shown in Table XII-4-4 for vertical cylinders were obtained from experiments with plane vertical surfaces. Some data for free convection heat transfer inside vertical cylinders are discussed in McAdams[5] and are shown to be almost identical with that for plane vertical surfaces. Correlations given here for horizontal cylinders are based on measurements of heat transfer from the outside surface of cylinders because few data pertaining to free convection inside horizontal cylinders are available. What data are available are discussed in Ref. 4 and are different from the correlations given here by about 12 per cent. This small difference can probably be attributed to experimental error just as well as to the difference in the physical problem. The values given in Table XII-4-4 are, therefore, suitable for estimating heat transfer coefficients for both the internal and external surfaces of cylindrical pressure vessels.

Data for heat transfer from surfaces having shapes different from cylinders, such as spheres, seem to be unavailable. However, the small difference in the coefficient for horizontal and vertical cylinders given in Table XII-4-4 indicates that the heat transfer rate is not very sensitive to the exact shape of the surface and that the correlation for horizontal cylinders could be used for vessels having different shapes with relatively little error.

Forced Convection

In an environment where gravity and acceleration approach zero, the heat transfer from the free convection mechanism will approach zero and other heat transfer mechanisms will be predominant. While fluid is being taken from a pressure vessel, the resulting flow in the vessel can produce significant forced convection effects. An approach for estimating the heat transfer rate for this effect in cylindrical vessels is discussed in the following.

As fluid is discharged from a cylindrical vessel, the fluid remaining expands very nearly equally in all parts of the vessel and gives rise to a velocity which increases linearly with distance along the axis of the tank.

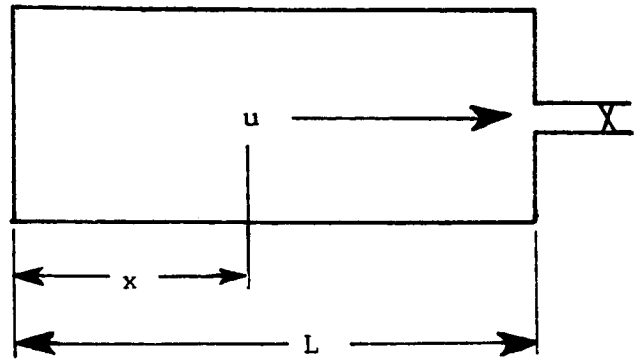

$$\frac{du}{dx} = \frac{U_o}{L} = \frac{4w}{\pi\rho D^2 L} \tag{45}$$

Fig. XII-4-1 Forced Convection

w = discharge rate
D = diameter of cylinder
L = length of cylinder
u = local velocity
U_o = velocity as outlet is approached
ρ = density of fluid

A boundary layer is formed along the cylindrical surface which originates at x = 0. Heat transfer rates from a boundary layer over which the free stream velocity is proportional to distance from the leading edge are given by Goldstein[4] and have the form shown below.

$$h = 0.57\left(\frac{c_p\mu}{k}\right)^{0.4} k\sqrt{\frac{\rho}{\mu}\frac{du}{dx}} \tag{46}$$

By substitution with Eq. (45), Eq. (46) can be expressed as

$$\frac{hD}{k} = 0.66\sqrt{\frac{w}{\mu L}}\left(\frac{c_p\mu}{k}\right)^{0.4} \tag{47}$$

This equation pertains only to laminar flow. However, for the case of a boundary layer where the velocity of the external fluid increases linearly with distance along the surface, transition to turbulence does not occur until the Reynolds Number, $\frac{4}{\pi}\frac{Lw}{\mu D^2}$, exceeds 10^8. The discharge

rate corresponding to this is extremely large even for low viscosity fluids such as compressed air. It seems, therefore, that turbulent flow would be encountered only in very rare instances.

The method for estimating heat transfer rates due to the forced convection mechanism applies only to cylindrical vessels. In vessels having a different shape the flow in the interior could be much more complex and it does not seem possible to estimate rates of heat transfer due to the forced convection mechanism for such vessels at the present time.

Conduction

When no fluid is being discharged from the pressure vessel and all residual motion in the stored fluid has been dissipated and gravity effects are negligible, heat will be transferred only by conduction. Solutions for heat transfer by this mechanism are obtained from the differential equation of heat conduction,

$$\frac{\partial T}{\partial t} = \frac{1}{\rho c_p} \nabla(k \nabla T) \tag{48}$$

a precise description of the initial temperature distribution, and the conditions existing at the vessel boundaries.

Heat transfer by this mechanism is not ordinarily approached in terms of a heat transfer coefficient. Although a coefficient could be defined in terms of the ratio of the heat flux at the vessel walls and a difference between the temperature of the wall and the mean fluid temperature,

$$q = h(T_w - T_m) \tag{49}$$

the coefficient would depend upon the initial temperature distribution, all of the boundary conditions, and would vary with time as the temperature distribution in the fluid changes. Hence, the heat transfer coefficient concept offers no advantages for dealing with the problem and one must resort to solutions of the heat conduction equation.

Solutions are presented in graphical form by Jakob[6] for objects having simple shapes such as flat slabs infinite in extent, cylinders of

infinite length, and for spheres. The initial condition is that of uniform temperature and the heat flow across the boundaries of the material is represented by,

$$h(T_s - T_a) = k \frac{\partial T}{\partial n} \tag{50}$$

where

h = external heat transfer coefficient
n = normal distance from the surface
T_a = ambient temperature
T_s = temperature at surface of the material

When a pressure vessel is considered in which the heat capacity of the vessel walls is large with respect to that of the stored fluid, the temperature of the fluid at the vessel walls will be nearly constant. For this case the solutions presented by Jakob[6] for $h = \infty$ would be applicable. When the heat capacity of the vessel walls is not large, the wall temperature will change as heat flows into the fluid. For this case the boundary conditions given below would be appropriate.

$$C_c \frac{dT_c}{d\theta} = A_i k_i \frac{\partial T_i}{\partial n} + \frac{T_\infty - T_c}{R_\infty} \tag{51}$$

A_i = area for heat transfer inside vessel
C_c = heat storage capacity of vessel walls
k_i = thermal conductivity of fluid inside vessel
n = normal distance from wall
R_∞ = resistance for heat transfer between environment and vessel
T_c = temperature of vessel wall
T_∞ = equilibrium environment temperature

Solutions for the heat conduction equation with this boundary condition do not appear to be available for cylindrical or spherical configurations.

Relative Importance of Each Mechanism

It seems worthwhile to stress that heat transfer by conduction is slow when compared with the mechanisms of forced or free convection. If gas is drawn from a spherical vessel and the temperature of the gas

inside is reduced by some amount, the time required for the gas to return to thermal equilibrium can readily be determined for the case where the walls of the vessel have enough heat capacity to remain at a constant temperature.[5] The time required for the center temperature to accomplish 90 per cent of its temperature change is

$$\theta = 0.075 \frac{D^2 \rho_i c_{pi}}{k_i} \tag{52}$$

where

D = inside diameter of vessel

For compressed air at 60°F and 2200 psi one has

$$\theta = 16.5 \, D^2$$

where θ = time in hours.

As a result even a small vessel would require a long time to return to thermal equilibrium by conduction.

The mechanism of free convection, which under atmospheric conditions produces only moderate heat transfer coefficients, would produce the rather substantial value of 30 Btu/hr-sq ft°F in air at 2200 psi with a temperature difference of 100°F. By the mechanism of forced convection, a coefficient of only one Btu/hr-sq ft°F would be produced by air at the same conditions in a cylindrical vessel of one foot in diameter and four feet in length having a discharge rate of one pound per second. To summarize, the mechanism of free convection would be most important when gravity is present. In the complete absence of gravity, forced convection would be most important while fluid is being removed from the vessel. Only when gravity is completely absent and all residual motion in the pressure vessel has stopped would the conductive mechanism be significant.

One should not assume that the free convection mechanism can be neglected in the case of a vehicle moving in space even while no thrust is being developed. Most vehicles have some spin and a typical low rate is about ten revolutions per hour. A pressure vessel 5 feet away from the axis of rotation would experience an acceleration of 0.0015 ft/sec^2. This magnitude of acceleration would give rise to a free convection heat transfer coefficient of one Btu/hr-sq ft°F for the same case discussed above

where the heat transfer coefficient was 30 Btu/hr-sq ft^{o}F in a one g environment. This low value is roughly the same as that obtained by forced convection for a comparatively high rate of discharge.

The magnitude of the residual fluid motion occurring in a pressure vessel some time after fluid has been discharged is difficult to ascertain. It is possible to make approximate estimates of the time required for the decay of residual motion by the analogy that exists between momentum and heat transfer. By analogy with the dimensionless correlation for the transient temperature distribution shown in Ref. 6, the decay of fluid motion depends on the ratio

$$\mu t/\rho L^2$$

in roughly the same way that the temperature distribution depends on the ratio

$$\alpha t/L^2$$

In the case of gases, the kinematic viscosity μ/ρ is not very different from the thermal diffusivity, α, and the time required for the decay of fluid motion is roughly the same as the time required for the temperature distribution to approach that of thermal equilibrium by the mechanism of conduction. As shown in the estimate of the time required for the return to thermal equilibrium by conduction, several hours would be required for the decay of residual motion in some cases. In conclusion, the heat transfer coefficient should be estimated by considering both free and forced convection mechanisms and then selecting the largest value. Only when gravity, thrust and spin are completely absent and all residual motion has stopped should the conductive mechanism be considered.

Stratification

Due to the effect of gravity, the fluid at the wall of a pressure vessel is buoyant when heat is being transferred from the wall to the fluid. A stratified temperature distribution consisting of a layer of heated fluid at the top of the tank is produced by the buoyancy of the heated fluid. The rate of growth of the layer and its temperature excess above the rest of the fluid can be estimated from the analysis of Bailey, Vandekoppel, and Skartvedt.[7]

The heat added to the fluid in a vessel by the free convection mechanism is discussed on Page XII-4.6. All of the heat added at the walls is in the fluid flowing upward along the tank vessel walls as indicated in the sketch below.

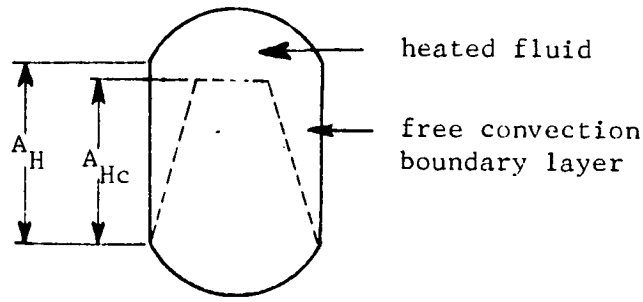

Fig. 4-2 Stratification in Pressure Vessel

Because the distribution of velocity and temperature in the boundary layer is known, the upward flow can readily be determined.

$$\frac{dm_H}{d\theta} = \frac{4hA_{Hc}}{c_p} \tag{53}$$

where

A_{Hc} = the area for heat transfer to the unheated fluid

m_H = mass of heated layer

The heat added to the fluid is given by

$$\frac{dQ}{d\theta} = hA_H(T_w - T) \tag{54}$$

where

A_H = total area for heat transfer

T_m = mean temperature of fluid in tank

The mean temperature excess of the heated fluid is obtained by integrating the rate of heat addition and rate of mass addition over time because both of these quantities can vary with time.

$$\Delta T = \frac{\int_0^{\theta} \frac{dQ}{d\theta}\, d\theta}{c_p \int_0^{t} \frac{dm_H}{d\theta}\, d\theta} \tag{55}$$

where

ΔT = temperature excess

The problem is further complicated if the vessel outlet is at the top and fluid is being withdrawn as the stratification process is going on. Values used for $dQ/d\theta$ and $dm_H/d\theta$ would be net values based on differences between values given by Equations (53) and (54) and the flow of mass and heat out of the tank. Two situations could arise in this case. If the rate of discharge, w, were greater than the growth rate of mass in the heated layer, as given by Equation (53), no heat would be added to the fluid left in the vessel. As a consequence the fluid remaining in the vessel expands isoentropically. The fluid leaving the tank would have an enthalpy which is a mean value weighted in accordance with the amount of fluid flowing from the boundary layer and that from the rest of the tank. When the rate of discharge is not greater than the heated layer growth rate, heated fluid accumulates at the top of the tank.

Numerical Method of Solution of Blowdown Equations

The two differential equations (32) and (33) are in proper form for application of the Runge-Kutta method, for which standard computer algorithms are available.* The corrections for non-ideality, variable heat transfer, etc. discussed above can be included in the equations by carrying their formulation through the derivation leading to Equations (32) and (33).

* Share Fortran Program, or Algol Algorithm 9, Proc. Assn. Comp. Mach. 5, p. 312, 1960.

XII-5 WORK OF EXPANSION

General Equations

Gas from a pressure vessel may be expanded through a turbine or piston. If the purpose of storing the gas is to obtain useful mechanical work, then it is of interest to calculate the work produced and a work storage efficiency.

There are three terms in the expression for work done. These may be identified by considering the flow process occurring in the expansion device. In the diagram below consider that the system, bounded by the dotted lines, contains an expansion device.

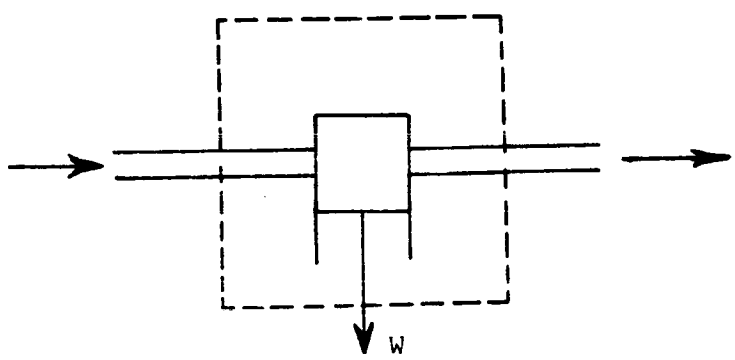

Fig. XII-5-1 Diagram Illustrating Work of Expansion

The work produced is

$$W = MP_1v_1 - M\int_{P_1}^{P_2} P\,dv - MP_2v_2 \qquad (56)$$

where

W = work produced, ft-lb/hr
M = mass of gas flowing, lb
P = pressure, psi
v = specific volume, cu ft/ lb gas
subscript 1 refers to upstream conditions
subscript 2 refers to downstream conditions

The first term in Equation (56) is the work which the remaining gas in the pressure vessel does on the gas which is expelled; the second term is the work of expansion occurring within the device, and the last term is the work which the vented gas does on the ambient atmosphere.

Because of the identity

$$\int_{P_1 v_1}^{P_2 v_2} d(Pv) = \int_{v_1}^{v_2} P\, dv + \int_{P_1}^{P_2} v\, dP \tag{57}$$

Equation (56) simplifies to

$$W = -M \int_{P_1}^{P_2} v\, dP \tag{58}$$

There are several situations of interest:

1) Venting a pressure bottle to the atmosphere or to space
2) Venting a pressure bottle to pressurize a tank
3) Charging a pressure bottle

For example, consider the blowdown of a pressure vessel to the atmosphere, or to another tank regulated at constant pressure, according to the following diagram:

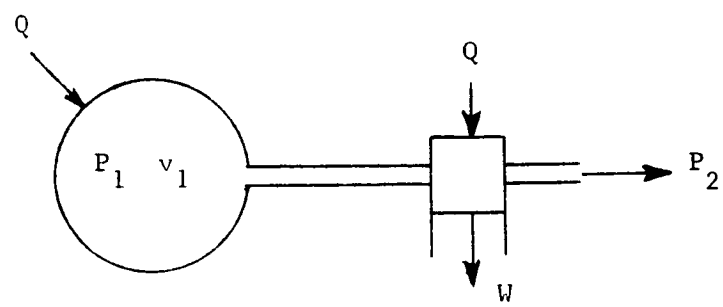

Fig. XII-5-2 Blowdown of a Pressure Vessel to the Atmosphere

Since P_1 varies, Equation (58) can be applied only for an increment of flowing gas.

$$dW = -dM \int_{P_1}^{P_2} v \, dP \tag{59}$$

The total work can be found by integrating Equation (59)

$$W = -\int_{M_o}^{M_f} dM \int_{P_1}^{P_2} v \, dP \tag{60}$$

To carry out the integration, equations are needed relating dM, dP, v and P_1. The form of these equations depends on whether the processes in the expansion device and the pressure vessel are isothermal, adiabatic, or occur with arbitrary heat transfer. Furthermore, the expansion device may be a combination of an engine with a throttling valve or a nozzle. Since so many combinations are possible, only examples which show the basic equations to be applied to each part of the process can be given.

Isothermal Expansion, Ideal Gas

This case is of particular importance since it is the basis for calculation of work efficiency. The work efficiency was defined above as the actual work divided by the reversible work obtained under isothermal conditions.

If all parts of the process are isothermal and the gas behaves ideally, then, from the ideal gas law

$$dM = -\frac{V_1 dP_1}{(R/m)\ T} \tag{61}$$

$$v = \frac{RT}{mP} \tag{62}$$

where V_1 = volume of pressure vessel, cu ft.

Substituting Equations (61) and (62) into Equation (60) the total work is

$$W = \int_{P_o}^{P_f} \frac{mV_1 dP_1}{RT} \int_{P_1}^{P_2} \frac{RT\ dP}{mP} \tag{63}$$

where

P_o = initial value of P_1

P_f = final value of P_1

$$W = V_1 \int_{P_o}^{P_f} \left[\ln P_2 - \ln P_1\right] dP_1 \tag{64}$$

$$= V_1 \left[(P_f - P_o)\ln P_2 - P_f \ln P_f + P_o \ln P_o - P_o + P_f\right] \tag{65}$$

In case $P_f = P_2$, then

$$W = V_1 \left[P_o \ln \frac{P_o}{P_2} + P_2 - P_o\right] \tag{66}$$

As a numerical example, suppose that V_1 = 0.1 cu ft, P_1 = 3000 psi, and P_2 = 300 psi. Then

$$W = 0.1 \times 144 \left[3000 \times 2.3 \log 10 + 300 - 3000\right]$$
$$= 60{,}500 \text{ ft-lb}$$

As a further example suppose that the problem is the same, except that the gas is vented to space. The gas cannot be expanded to zero pressure in an engine of finite size. Therefore Equation (66) applies when P_2 is put equal to the pressure at which the gas leave: he engine.

Adiabatic Expansion, Ideal Gas

If all parts of the process are adiabatic, then the adiabatic law, Equation (67), applies

$$v = v_1 \left(\frac{P_1}{P}\right)^{1/\gamma} \tag{67}$$

$$W = V_1 \int_{P_o}^{P_f} P^{1/\gamma - 1}\, dP_1 \int_{P_1}^{P_2} P^{-1/\gamma}\, dP \tag{68}$$

$$= \frac{V_1}{1 - \frac{1}{\gamma}} \int_{P_o}^{P_f} \left[P_2^{1-1/\gamma} P_1^{1/\gamma - 1} - 1\right] dP_1 \tag{69}$$

$$W = \frac{V_1}{1 - \frac{1}{\gamma}} \left[\gamma P_2^{1-1/\gamma}\left(P_f^{1/\gamma} - P_o^{1/\gamma}\right) + P_o - P_f\right] \tag{70}$$

If $P_f = P_2$ then

$$W = \frac{V_1}{1 - \frac{1}{\gamma}} \left[\gamma\left(P_2 - P_2^{1-1/\gamma} P_o^{1/\gamma}\right) + P_o - P_2\right] \tag{71}$$

Consider the same example as for the isothermal case, with $\gamma = 1.4$. Then

$$W = \frac{0.1 \times 144}{0.286} \left[1.4\left(300 - 300^{0.286} \times 3000^{0.714}\right) + 3000 - 300\right]$$
$$= 48{,}400 \text{ ft-lb}$$

The work efficiency for this case is 48,400/60,500 = 80%. As the expansion ratio increases the work efficiency falls, so that if P_2 = 30 psi in the above example, the work efficiency is only 6.1%.

In the case where the expansion in the engine is adiabatic, but the process in the pressure vessel includes heat transfer from the walls, then Q_e is zero, letting Q_e = total heat transferred in the expansion device Btu.

Estimation of γ'

It has been the practice at some laboratories to present the results of pressure vessel behavior in terms of a dimensionless parameter γ', at least for the application where propellant is to be expelled from a tank by means of the gas from a pressure vessel, as in the arrangement shown in Fig. XII-5-3. As defined in Part 2

$$\gamma' = \frac{V_1(P_o - P_f)}{V_p P_2} \tag{72}$$

The denominator of this expression is the work done to expel the propellant from the tank. The numerator is derived from Equation (58), which gives the maximum work available from the gas in the pressure vessel, although in Equation (58), v is a variable which depends on pressure. If a mean value of v can be found, it can be taken outside the integral. Final-

ly, if v is used as an approximation to the unknown mean value of Mv, the result is Equation (72).

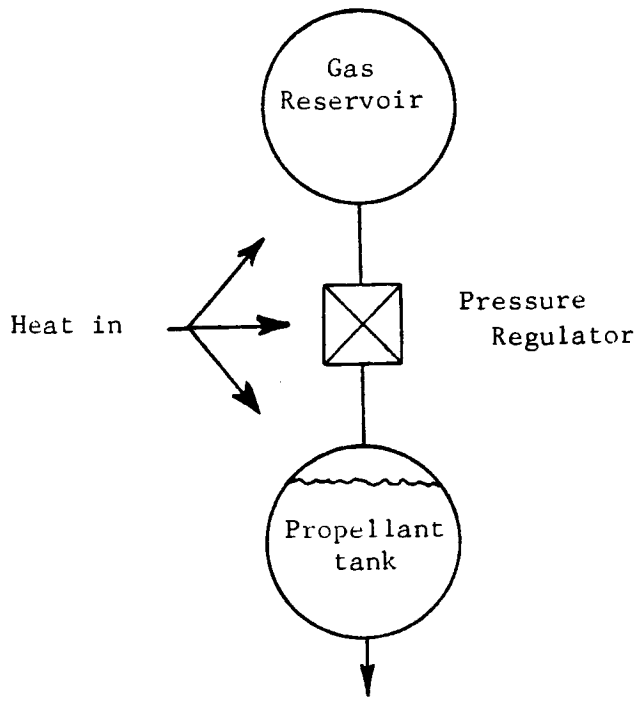

Fig. XII-5-3 Propellant Expelled from a Tank by a Pressurized Gas

For an ideal gas without heat transfer, it can be shown that $\gamma' = c_p/c_v$, and for an isothermal expansion $\gamma' = 1$. In this respect γ' behaves similar to the polytropic expansion coefficient γ, which is well known in the thermodynamics of gas compressors. However, γ' is not equal to γ except at these two limiting conditions. Because the value of γ' is bracketed by these two values, it is easy to estimate values of γ' for intermediate cases where there is some heat transfer, but not enough to result in isothermal expansion. Thus a design engineer may aquire a feel for estimating γ' based on experimental data for similar systems. An estimate of this single parameter then serves to predict the performance of the pressure vessel under a variety of conditions.

The propellant tank usually contains an ullage volume at the start of pressurization. The gas in this space is often at a pressure different than the regulated pressure, and therefore some of the pressurizing gas must be used to bring the tank up to the regulated pressure. In order to compare measured values of γ' in experiments with different ullages, a correction is needed. The effect of ullage can be eliminated by defining a new function, γ'':

$$\gamma'' = \gamma' - \frac{V_x\left(1 - \frac{P_x}{P_2}\right)}{V_p} \tag{73}$$

where

V_p = volume of propellant displaced
V_x = ullage volume
P_x = initial pressure in propellant tank
P_2 = regulated pressure in propellant tank

γ' has also been used to correlate experimental data on heat transfer effects during pressurizing of propellant tanks.

We have considered the possibility that the approach based on the use of γ' could be made more exact by investigating the relation between γ' and the conditions which determine heat transfer in the pressure vessel. For the case of an isothermal source and constant mass flow an expression for γ' can be derived

$$\gamma' = \frac{1 - \frac{NTU}{\gamma - 1 + NTU}M^* - \frac{\gamma - 1}{(\gamma - 1 + NTU)}M^{*\gamma+NTU}}{\frac{1}{\gamma + NTU} - \frac{NTU}{\gamma - 1 + NTU}M^* - \frac{\gamma - 1}{(\gamma - 1 + NTU)(\gamma + NTU)}M^{*\gamma+NTU}} \tag{74}$$

Since γ' depends on M^* it cannot be correlated with NTU alone. The expression for γ' therefore does not simplify calculations of the efficiency, and the method of Reynolds and Kays is preferable.

XII-6 REFERENCES

1. Tribus, M. (Thayer School of Eng., Dartmouth College, N.H.) Thermostatics and Thermodynamics. D. Van Nostrand Co., Inc., Princeton, N.J. 1961.

2. Ring, E. (Ed.) Rocket Propellant and Pressurization Systems. Prentice-Hall, Inc., Englewood Cliffs, N.J., 310 pp., 1964.

3. Reynolds, W.C. and Kays, W.M. (Dept. of Mech. Eng., Stanford Univ., Stanford, Calif.) An analytical investigation of the blowdown and charging processes in a single gas receiver including effects of heat transfer. NR - 065 - 104, Tech. rept. no. T-1, Oct. 1, 1955.

4. Dodge, B.F. (Dept. Chem. Eng., Yale Univ.) Chemical Engineering Thermodynamics. McGraw-Hill Book Co., Inc., New York, 680 pp., 1944.

5. McAdams, W.H. (Dept. Chem. Eng., MIT) Heat Transmission. McGraw-Hill Book Co., Inc., 2nd edn., 9th impression, New York, 1942.

6. Jakob, M. Heat Transfer, Vol. 1. John Wiley and Sons, 1949.

7. Bailey, T., Vandekoppel, R. and Skartvedt, G. Cryogenic propellant stratification analysis and test data correlation. AIAA J. 7, p. 1657, July 1963.

8. Johnson, V.J. (Ed.) A compendium of the properties of materials at low temperatures, Pt. 1, WADD Tech. rept. 60-56, July 1960.

9. Stull, D.R., et al. JANAF Thermochemical Data Tables. AF 33 (616) 6149, Dow Chem. Co.

XII-A NOMENCLATURE

English Letter Symbols

A	Area, ft^2
A_1, A_2	Constants, dimensionless
A_H	Total area for heat transfer
A_{Hc}	Area for heat transfer to the unheated fluid
B_1	Constant
B_2	Constant
C_c	Heat capacity of vessel wall, Btu/^oR, assumed constant
c_p	Specific heat at constant pressure, Btu/(lb-^oR)
c_v	Specific heat at constant volume, Btu/(lb-^oR)
C_p	Heat capacity at constant pressure, Btu/lb-^oR
C_v	Heat capacity at constant volume, Btu/lb-^oR
E	Total Energy, Btu
E_c	Energy content of vessel wall, Btu
g	Acceleration due to gravity, $g = 32.2$ ft/sec^2 at sea level
h	Specific enthalpy, Btu/lb
$\mathcal{h}$	Unit heat transfer convective conductance, Btu/hr-ft^2-^oR
$\mathcal{k}$	Thermal conductivity, Btu/(hr-ft^2-^oR/ft)
L	Length dimension, ft
M	Mass of a gas
M_h	Mass of heated layer
M_s	Mass of a sperical pressure vessel
m	Molecular weight of gas
p	Pressure, #/ft^2
P	Pressure, psi

NOMENCLATURE (contd)

P_2	Regulated pressure in propellant tank
P_x	Initial pressure in propellant tank
Q	Heat flux from the wall of the tank to the gas, Btu
q	Heat transfer rate, Btu/hr
q_i	Heat flux at inside vessel wall, Btu/hr
R_t	Total heat transfer resistance, hr-^{o}R/Btu
(R/m)	Universal gas constant/molecular mass of gas, ft-#/(lb-^{o}R)
R	Gas constant
R_i	Inside resistance to heat transfer, hr-^{o}R/Btu
s	Specific entropy, Btu/(lb-^{o}R)
T_m	Mean Temperature of fluid in tank
T	Absolute temperature, ^{o}R
T_c	Temperature of vessel wall, ^{o}R
ΔT	Temperature excess
V	Volume, ft^3
V_1	Volume of pressure vessel cu ft.
V_P	Volume of propellant displaced
V_x	Ullage Volume
v	Specific volume cu ft/lb gas
W	Work produced ft-lb/hr
w	Mass flow rate, lb/hr

Greek Letter Symbols

γ	c_p/c_v
ρ	Density, lb/ft^3
ρ_1	Density of gas at initial pressure, lb/cu ft
ρ_2	Density of sphere wall material

NOMENCLATURE (contd)

μ	Viscosity, lb/(hr-ft)
θ	Time, hr
α γ	Parameters defined where used, dimensionless
Δ	Denotes a difference (final minus initial)
σ_s	Allowable stress of wall material

Nondimensional Groupings

C_o^*	$C_c/(M_o c_v)$
γ	c_p/c_v
M^*	M/M_o independent variable
M'^*	M'/M_o
M_β^*	M_β/M_o
NTU	$1/(R_i c_v w_o) = (\ A)_i/c_v w_o$
NTU_∞	$1/(R_\infty c_v w_o) = (\ A)_\infty/c_v w_o$
P^*	p/p_o
q_∞	Heat flux on outside of vessel wall, Btu/hr
R_∞	Outside resistance to heat transfer, hr-^oR/Btu
T^*	T/T_o first dependent variable
T_c^*	T_c/T_o second dependent variable
T_1^*	T_1/T_o
T_{mean}^*	T_{mean}/T_o
$T_{vol.}^*$	T_{vol}/T_o
T_∞^*	T_∞/T_o system parameter
T	Temperature of enrivonment, ^oR
V^*	V'/V_o

w^*	w/w_o known function of T^*, M^*
W^*	w/w
Nu	Nusselt Number, $(\ell L/k)$
Gr	Grashof Number, $(L^e \rho^2 g \beta \Delta T/\mu^2)$
Pr	Prandtl Number, $(\mu c_p/k)$

Subscripts

o	Refers to initial conditions
1	Refers to inlet state
g	Refers to gas
c	Refers to capacitance
α	Refers to initial quantities
β	Refers to gas added during charging
∞	Refers to environmental conditions, or conditions outside the receiver shell
i	Refers to conditions inside the receiver shell
AD.	Refers to adiabatic solution
H.T.	Refers to solution including heat transfer
INF. C_w^*	Refers to solution for $C_w^* = \infty$
FIN. C_w^*	Refers to solution for $C_w^* = \infty$
INF. NTU	Refers to solution for NTU $= \infty$
FIN. NTU	Refers to solution for NTU $= \infty$
CONST.	Refers to constant flow solution
CRIT.	Refers to critical flow solution

XIII HEAT BALANCE

Table of Contents

	Title	Section-Page
Sec. XIII	Heat Balance	XIII-1
Table XIII-1	Free Path of Atmospheric Air at Various Altitudes	XIII-9
Table XIII-2	Equilibrium Temperatures of Spherical Space Probes with Various Coatings	XIII-10
Table XIII-3	Representative Materials for Passive Thermal Control of Space Vehicles	XIII-11
Figure XIII-1	A Typical Spectral Emissive Power Curve for the Thermal Radiation Leaving the Earth	XIII-12
Figure XIII-2	Earth Radiation as a Function of Latitude Under Various Sky Conditions	XIII-13
Figure XIII-3	Albedo as a Function of Latitude Under Various Sky Conditions	XIII-14
Figure XIII-4	Relative Spectral Distributions of Albedo Radiation Under Various Sky Conditions	XIII-14
Figure XIII-5	Space-Time Average Effective Space Temperature as a Function of Surface Finish and Orbit Inclination	XIII-15
Figure XIII-6	Space-Time Average Surface Temperature as a Function of Surface Finish and Internal Power Dissipation	XIII-16
Figure XIII-7	Space-Time Average Surface Temperature as a Function of Surface Finish and Internal Power Dissipation	XIII-17
Figure XIII-8	Space-Time Average Surface Temperature as a Function of Surface Finish and Internal Power Dissipation	XIII-18
Figure XIII-9	Variations with Temperature of Emissivity and Absorptivity and of Their Ratio for Two Metals	XIII-19
Figure XIII-10	Variation of Equilibrium Temperature with Distance from Sun in Case of Aluminum or Silver Sphere having Uniform Temperature	XIII-20

Table of Contents

	Title	Section-Page
Figure XIII-11	Variation of Equilibrium Temperature with Distance from the Sun in Case of a Sphere Having Uniform Temperature	XIII-21
Figure XIII-12	Power Input per Unit Cross-Sectional Area of a Satellite Plotted as a Function of Altitude for the Range 200-3200 Miles	XIII-22
Figure XIII-13	Power Input per Unit Cross-Sectional Area of a Satellite Plotted as a Function of Altitude for the Range 200-32,000 Miles	XIII-23
	References	XIII-25

ORIGINAL PAGE IS
OF POOR QUALITY

XIII HEAT BALANCE

The equations governing the flow of heat between the pressure vessel wall and its fluid contents have already been presented in Section XII-4. For many problems where blowdown is rapid, there is not sufficient time for external heat transfer to have an effect. For slower or cyclic blowdown, heat transfer with the surroundings will affect the temperature of the vessel.

The mechanisms of external heat transfer are free convection, forced convection, radiation and conduction along solid supports. Heat transfer by convection or conduction through a gas decreases rapidly below the pressure at which the mean free path of the gas molecules exceeds the length of the path of heat transfer. Free path lengths in the atmosphere are given for various heights in Table XIII-1. When free or forced convection is an important mode of external heat transfer, the correlations presented in Section XII-4 can be used.

In a vacuum, the primary mode of heat transfer is usually by radiation. The calculation of a heat balance by radiation involves summing the heat contributions from various sources and sinks, including the calculation of the temperatures of other portions of the system which reflect or reradiate heat from source to sink. Detailed proceedures are given in Reference 8, W.H. McAdams' book entitled HEAT TRANSMISSION. Additional information on the solar energy is given in Section 111-5.

Spacecraft systems are subjected to environmental testing and the methods discussed in Section XII-4 may be applied to the calculation of the system heat balance to aid in compensation for the errors incurred from the presence of atmosphere.

The following discussion is quoted from various sections of the SPACE MATERIALS HANDBOOK, published by Lockheed Missiles and Space Company under Air Force Contract AF04(647)-673 (Ref. 1). The selected portions should serve as a guide to illustrate the various factors that need to be considered when a heat balance of any space vehicle or component is to be attempted.

The ensuing discussion is considering an Agena spacecraft and an earth orbit. However, the basis of the heat balance is applicable to any type space vehicle and any orbit.

In the space environment, a spacecraft constitutes a system that exchanges thermal energy with its surrounding exclusively through thermal radiation. The space thermal environment is composed of the following typical sources of energy:

General Case	Specific Case
Emission of radiation from distant bodies	Solar radiation encountered at one astronomical unit from the sun
Emission of radiation from large nearby bodies	Earth emission
Reflection of radiation from distant objects by nearby bodies	Earth albedo radiation

The radiation from the background of space itself can be neglected, since its effective temperature is only a few degrees above absolute zero.

Temperatures encountered by spacecraft are, therefore, determined by its energy exchange with these sources, and may be calculated by solving the appropriate energy balance equations. Through suitable adjustment of thermal design parameters, such as vehicle geometry and thermal properties, one may arrive at a vehicle configuration with the structural and mechanical features necessary to maintain the various component temperatures within the required limits.

There are two fundamental methods for controlling spacecraft temperatures: passive thermal control and active thermal control. Passive thermal control of a system and its components is attained wholly through geometrical design and the selection of materials with requisite thermophysical properties. This method includes the static employment of temperature-induced physical changes in materials. Neither power nor moving parts are employed. Some techniques for passive thermal control follow:

a) Selection of materials with desired thermal radiation properties
b) Geometrical design

c) Selection of materials with desired values of thermal conductivity
d) Employment of the thermal behavior of materials at a change of phase, utilizing the materials as heat sinks
e) Self-thermostatic surfaces

Active thermal control of a system and its components is attained through a feedback control system, with temperature as the controlled variable. This method includes the dynamic employment of temperature-induced physical changes in materials. Generally, either power or moving parts are employed. Techniques for active thermal control include the use of:

a) Thermostats and heaters
b) Bimetallic strips to control shutter system
c) Fluid transport refrigeration systems
d) Variable thermal resistance techniques
e) Thermoelectric cooling

Passive thermal control systems have certain advantages over active systems in regard to reliability. They employ no moving parts or switches, which may malfunction due to such factors as the cold-welding of bearing surfaces in the low pressures of space. Also, the passive solution to a design problem generally results in a minimum weight solution.

Active thermal control systems, on the other hand, can correct for environmentally induced alterations in the thermal behavior of a vehicle. An example of such an alteration is the increase in the solar absorptance of an exterior surface due to the influence of extra-terrestrial solar ultraviolet energy. These systems can also account for changes in the thermal environment, such as the increase in the solar constant experienced by a Venus probe. Extremely accurate knowledge of external thermal radiation characteristics is not mandatory for active systems, as it is for passive. Among other things, this means that successful operation of a given vehicle is less likely to be jeopardized by the various factors of the pre-launch environment. In addition, active control can provide much more precise control of temperature than is possible passively. For this reason, life support systems employ active thermal control.

Passive Thermal Control

The ultimate goal in the thermal design of any spacecraft is to assure that the various components of the vehicle will operate within their respective allowable temperature ranges through all phases of its mission. The problems associated with the thermal design of spacecraft are unique only insofar as the spacecraft environment is unique. The following simplifying assumptions are made to focus attention on the unique aspects of the problem:

a) The thermal (mathematical) model of the spacecraft is known exactly; i.e., for a given set of external temperatures, internal temperatures are known.
b) The geometry of the spacecraft is free of protuberances
c) The spacecraft is an earth satellite which is to be launched into a circular polar orbit of known altitude at a specified time of day on a specified date, and from a specified launch base.
d) The required operating life of the vehicle is sufficiently short that changes in the angle between the orbit plane and the earth-sun line may be neglected and such that there will be no change in the thermophysical properties of the vehicle due to the space environment.

The external thermal analysis for the orbit phase comprises four main steps in which the following are determined:

1) The magnitudes of incident radiation from several sources - this is essentially a geometry problem involving the relationships among the various sources and the vehicle.

2) The magnitudes of absorbed radiation - this step requires a knowledge of the spectral energy distribution of the sources and of the spectral radiation characteristics of the vehicle surface. In some cases, Steps 1 and 2 must be considered simultaneously.

3) The overall heat balance, including internal power, absorbed radiation, and re-radiation to space - this step might be accomplished for the entire vehicle or for separate segments of the vehicle. In such case, Step 4 would be an

integral part.

4) The effect of conduction through vehicle skin and other structures - internal designs will generally be based on temperature boundary conditions which are established in Steps 1 through 4.

In taking these steps, the designer must choose the type of passive control best suited for the given design problem. Generally, passive control will be exercised through the proper selection of geometries and of materials with fixed radiation characteristics. However, other methods are available. .....uutilization of the Curie point transition.

Regardless of the method used, surface temperatures of the earth satellite are determined by the heat balance between the satellite and its environment, which includes the sun, the earth and its atmosphere, and space. Whether aerodynamic heating is an important heat source depends not only on its magnitude but also on the average values of the absorbed insolation, earth reflection, and earth emission. If the latter are large, aerodynamic heating may be negligible in comparison with other heat inputs even as high as 200 miles. However, calculations based on Oppenheim's generalized theory of convective heating in free molecule flow (Ref. 6) and on atmospheric density data show that for mean altitudes greater than 200 miles aerodynamic heating averaged over the entire surface of a three-dimensional solid is small enough in comparison with the other heat sources to be neglected. The external sources of energy for the satellite are, therefore, restricted to direct insolation, albedo radiation consisting of solar radiation reflected and scattered by the earth-atmosphere system, and to earth and atmospheric emission.

The total emissive power of the earth and its atmosphere, called earth emission, is approximately equivalent to that of a blackbody at 250°K(-10°F), which has a peak intensity at 11.6 μ (See fig. XIII-1). This earth emission has an average value of about 71.0 Btu/hr-sq ft(0.32 cal/min-sq cm) and, as a simplification, is usually taken to be uniform over the surface. The earth emission incident on the satellite is a function of vehicle altitude and geometry. The satellite surface absorptance for earth emission is about the same as the room-temperature total hemispherical emittance of the surface.

Both earth reflection and insolation consists of energy given approximately by a blackbody radiation at 6000°K and have peak intensities at about 0.5 μ. The earth

reflection is roughly proportional to the cosine of the zenith angle and has a maximum value of 159 Btu/hr-sq ft (0.80 cal/min-sq cm) if the earth's reflectivity (albedo) is taken to be 36%. This part of the irradiation of the satellite is determined by the altitude, vehicle geometry, and geometric relationship between the satellite and the earth-sun line; it is generally a function of time. Insolation on a plane normal to the earth-sun line at the earth's mean distance from the sun is about 443 Btu/hr-sq ft(2.0 cal/min-sq cm)[7]. The insolation on a given surface is proportional to the cosine of the angle between the normal to the surface and the earth-sun line and is thus also a function of time.

For a prediction of satellite temperatures refer to Reference 1 - pp. 87-106.

Some estimate of the uncertainties and variations of internal heat-balance factors must be made as a step in establishing the amount and kind of control required. Uncertainties arise here because of manufacturing tolerances in material gages, variations in material properties, differences in fabrication, and variations in the final assembly that affect such things as contact resistances in the joints of heat-flow paths. In addition, relatively large uncertainties are introduced in all but the most complicated analyses because of inexact analytical methods and a lack of refinement in the mathematical model. Such uncertainties are difficult to assess in most instances, although a systematic approach could be developed.[2]

Internal spacecraft temperatures are predominantly controlled by the radiation characteristics of the external satellite surfaces. The parameter of greatest importance is the ratio of solar absorptance α_s to infrared emittance ϵ. Additionally, heat transfer interior to satellite vehicles is largely controlled by the emittance of internal surfaces.[3]

Thermal radiation characteristics clearly constitute the material properties most critical to thermal design; they are by no means, however, the only factors to be evaluated before choosing a particular material for a specific spacecraft application. Knowledge of the other thermophysical properties, such as thermal conductivity, specific heat, and thermal diffusivity, is also necessary to thermal control.

The orbital temperature variations experienced by earth-satellite components are directly related to the thermal capacity of the materials employed in satellite construction. Through knowledge of specific heat and proper design, thermal strains, fatigue failures, and other temperature-induced damage may be avoided.

Reliable design requires not only accurate nominal values of thermal parameters, but, even more importantly, a careful assessment of the range of values to be expected owing to variations in composition and accuracy of the measurement techniques employed. Obtaining such information will often entail embarking on an experimental program. Several agencies are attempting to alleviate this situation both by assembling the available thermophysical property data and by publishing annotated bibliographies of the applicable literature. The most notable efforts at present are the memoranda issued by the Defense Metals Information Center at Battelle Memorial Institute, and the compilation of thermophysical properties information by the Armour Research Foundation.[4]

Temperatures of near-earth satellites are determined to a large extent by the thermal radiation interchange between the earth and the satellite and by the surface radiation characteristics of the vehicle. Selection of surface finishes and determination of other thermal design requirements must be based on a knowledge of the total energy leaving the earth's surface, the spectral energy distribution, and the spatial and temporal variations of these quantities. Temperature levels, thermal cycling (temperature oscillations), and ultraviolet degradation of surface materials are all influenced by the thermal radiation from the earth, which occurs in two broad, distinctly different spectral regions. Albedo radiation (reflected solar radiation) consists of ultraviolet, visible, and infrared energy having wavelengths between 0.29 and 4.0μ. The other component, earth emission, consists of infrared energy nearly all at wavelengths longer than 4.0 μ radiated by the earth-atmosphere system. Most of the information required for spacecraft design can be obtained from studies of the albedo(reflectance) and heat budget of the earth.[5]

Figures XIII-2 through -4 present some values of the earth's radiation and albedo.

Figures XIII-5 through XIII-8 present a space-time average effective temperature for various ratios of α/ϵ, solar absorptance to infrared emittance under various surface finish conditions, orbit inclinations and internal power dissipation rates for a vertical cylinder at a 300 mile altitude. Figures XIII-9 through -15 are original SRI figures and present various thermal relationships applicable to heat balance calculations.

Tables XIII-2 and XIII-3 are also original SRI data and give some indication of material behavior with various coatings and for passive thermal control respectively.

Table XIII-2

FREE PATH OF ATMOSPHERIC AIR
AT VARIOUS ALTITUDES (Ref. 18)

ALTITUDE	MEAN FREE PATH
ft	ft
50,000	1.4×10^{-6}
100,000	1.6×10^{-5}
200,000	9.8×10^{-4}
300,000	1.1×10^{-1}
500,000	150
700,000	999
1,000,000	6300

Table XIII-2

EQUILIBRIUM TEMPERATURES OF SPHERICAL SPACE PROBES WITH VARIOUS COATINGS (Ref. 11)

COATING	SOLAR				TEMPERATURE, °F	
	ρ	α	ϵ	α/ϵ	SPHERE	STRIPED SPHERE
White	0.82	0.18	0.95	0.2	-135	-20
White plus carbon black	0.47	0.53	0.95	0.6	-30	32
Aluminum plus clear lacquer				1.0	40	
Flat black	0.03	0.97	0.95	1.0	45	85
Aluminized silicone				1.3	60	
Flat black plus aluminum	0.05	0.95	0.80	1.2	65	120
Stainless steel				2.5	170	
Aluminum				4.0	250	

Table XIII-3

REPRESENTATIVE MATERIALS FOR PASSIVE THERMAL CONTROL OF SPACE VEHICLES

(Ref. 12, 13, 14, 15, 16, 17)

MATERIAL	SUBSTRATE AND/OR TREATMENT	ABSORPTANCE, EMISSIVITY*			EXAMPLES OF USE
		α_s	ϵ_H	α_s/ϵ_H	
Metals					
Stainless Steel	Sand-blasted	0.81	0.42	1.92	Explorers I, III, IV
Aluminum Foil, (sandblasted)	Fiberglass	0.42	0.21	2.0	Explorer VII
6061 Aluminum Alloy	Chemically cleaned				
Sheet		0.26	0.06	4.34	
Forging		0.29	0.09	3.22	
Weld Area		0.26	0.10	2.6	
6061 Aluminum Alloy	Degreased, cleaned, acid rinsed	0.39	0.03	13.0	
2024 Aluminum Alloy	Degreased, cleaned, acid rinsed	0.34	0.06	5.67	
QMV Beryllium	Sintered, machined, chemically polished	0.50	0.10	5.00	
Hanovia Gold 6518	René 42	0.53	0.09	6.00	
Oxides					
Rokide A (Al0)	Sand-blasted stainless and/or fiberglass	0.15	0.77	0.20	Explorers I, III, VII
Rokide C	René 14	0.90	0.85	1.06	
Silicon Oxide	Vacuum deposited on aluminum			1.2	Vanguard
Titanium Oxide	From oxidation of Ti vacuum-deposited on Al	0.77	0.14	5.5	Atlas-Able-IV
Titanium Oxide	Adhesive-backed vinyl film	0.25	0.84	0.3	Atlas-Able-IV
Paints					
Silicone Alkyd Enamel + TiO_2		0.18	0.95	0.19	Journeyman
Grey Alkyd Enamel + Aluminum Flakes		0.95	0.80	1.18	Journeyman
Epoxy Paint + Black Iron Oxide	Plastic	0.97	0.95	1.02	Transit I-B
Polyurethane Lacquer + TiO_2	Plastic	0.18	0.95	0.19	Transit I-B

* 70°F

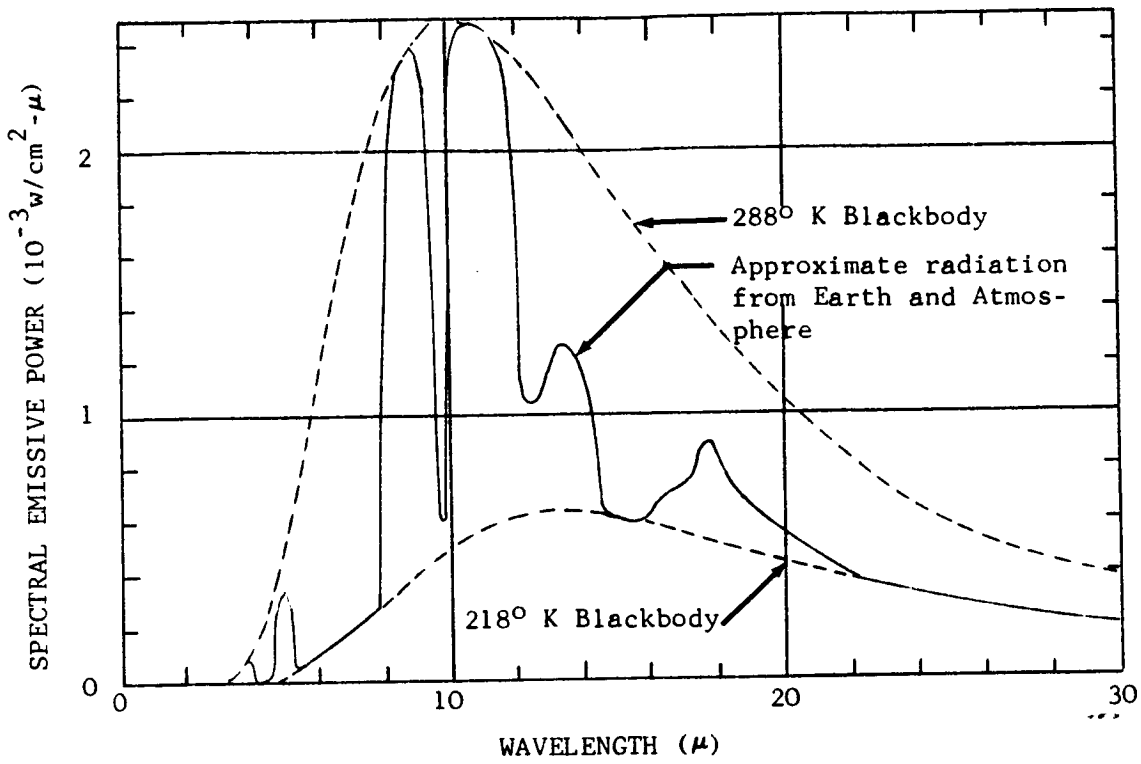

Fig. XIII-1 A Typical Spectral Emissive Power Curve for the Thermal Radiation Leaving the Earth. (The 288° K blackbody curve approximates the radiation from the earth's surface, and the 218° K blackbody curve approximates the radiation from the atmosphere in those spectral regions where the atmosphere is opaque) (Ref. 1)

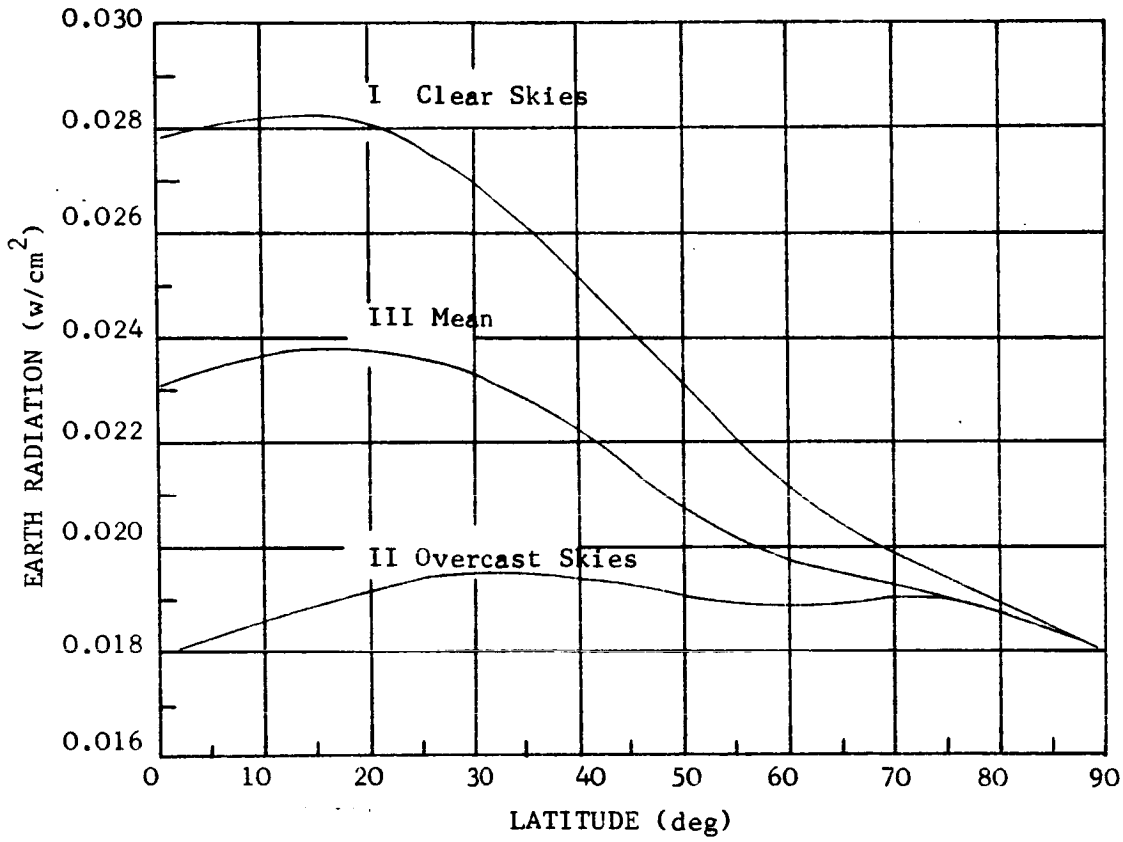

Fig. XIII-2 Earth Radiation as a Function of Latitude Under Various Sky Conditions (Ref. 1)

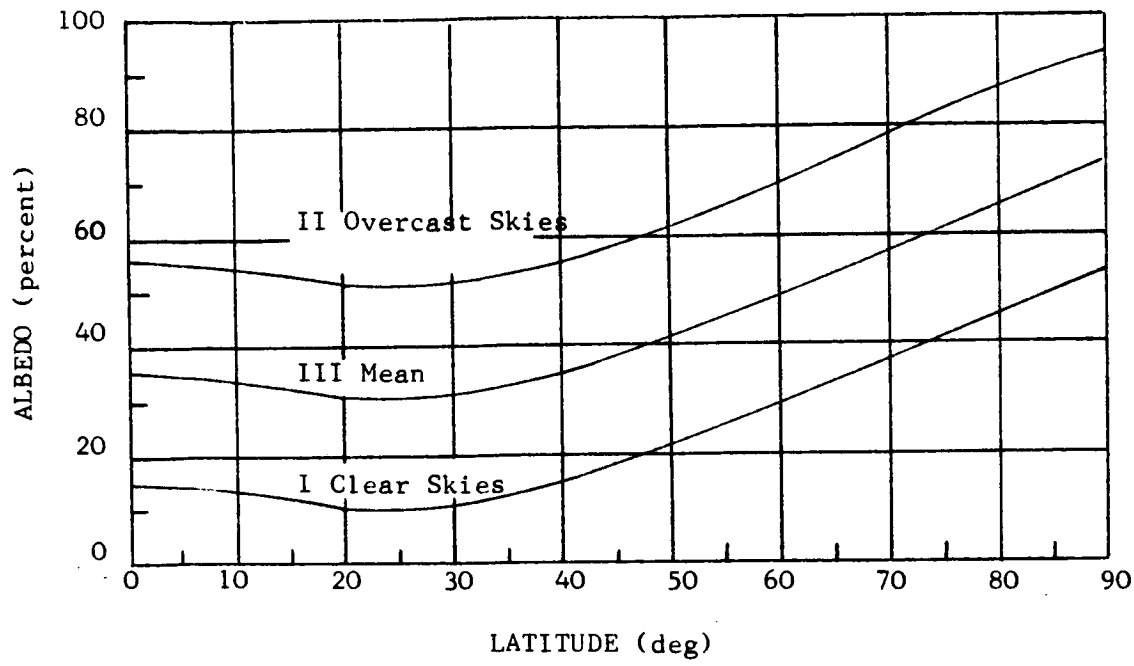

Fig. XIII-3 Albedo as a Function of Latitude Under Various Sky Conditions (Ref. 1)

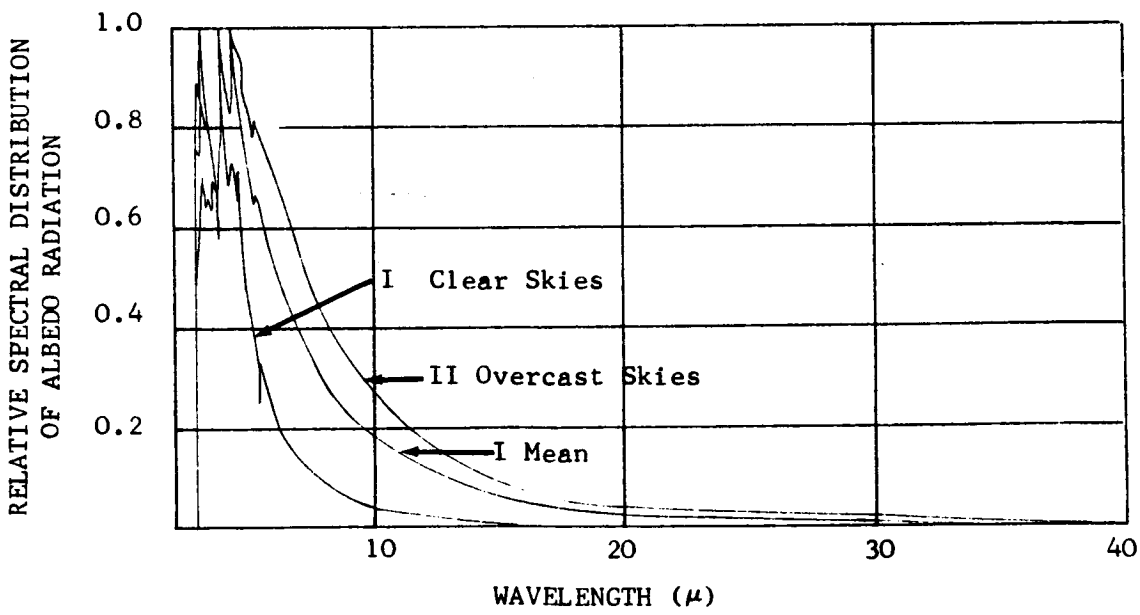

Fig. XIII-4 Relative Spectral Distributions of Albedo Radiation Under Various Sky Conditions (Ref. 1)

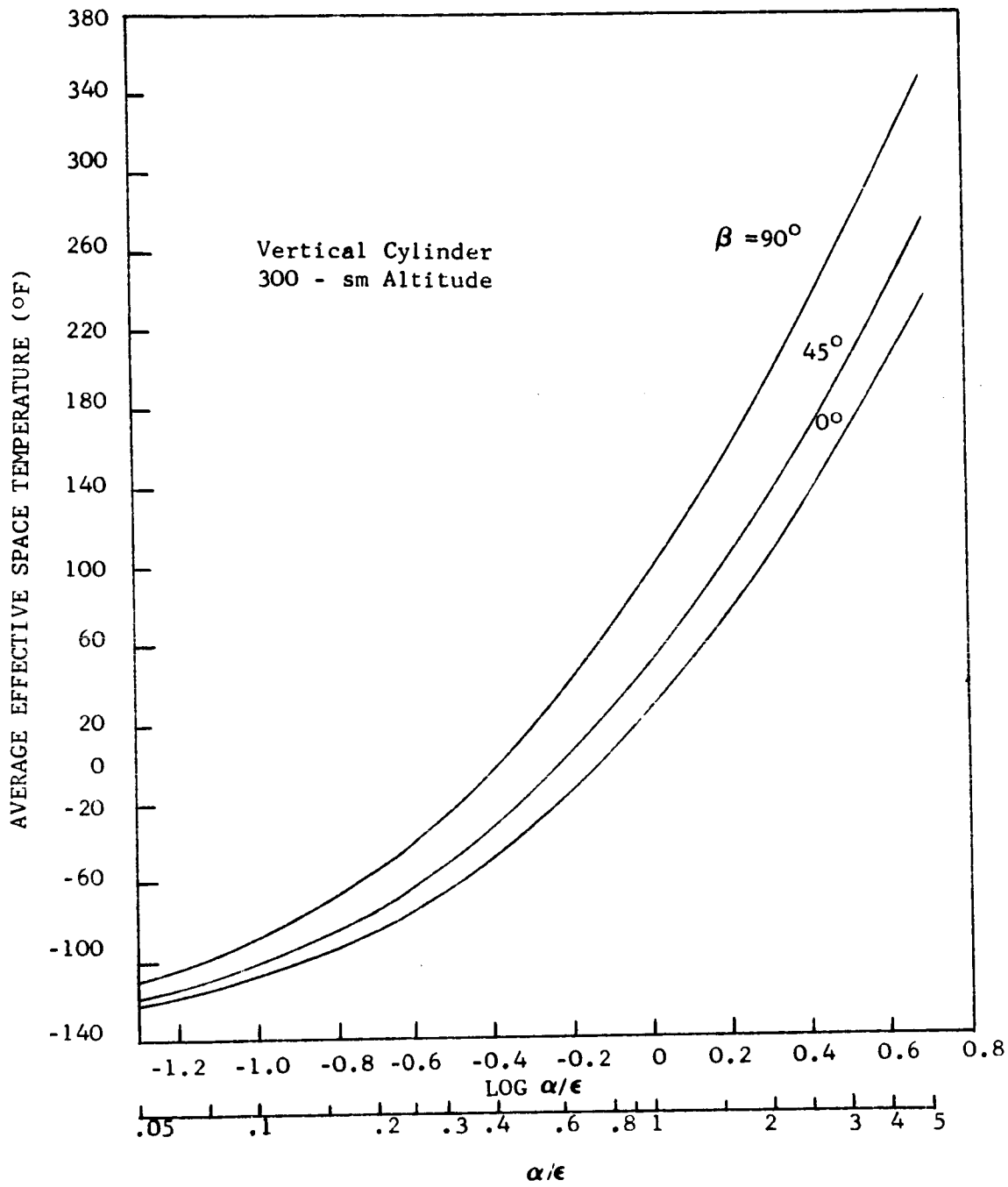

Fig. XIII-5 Space-Time Average Effective Space Temperature as a Function of Surface Finish and Orbit Inclination (Ref. 1)

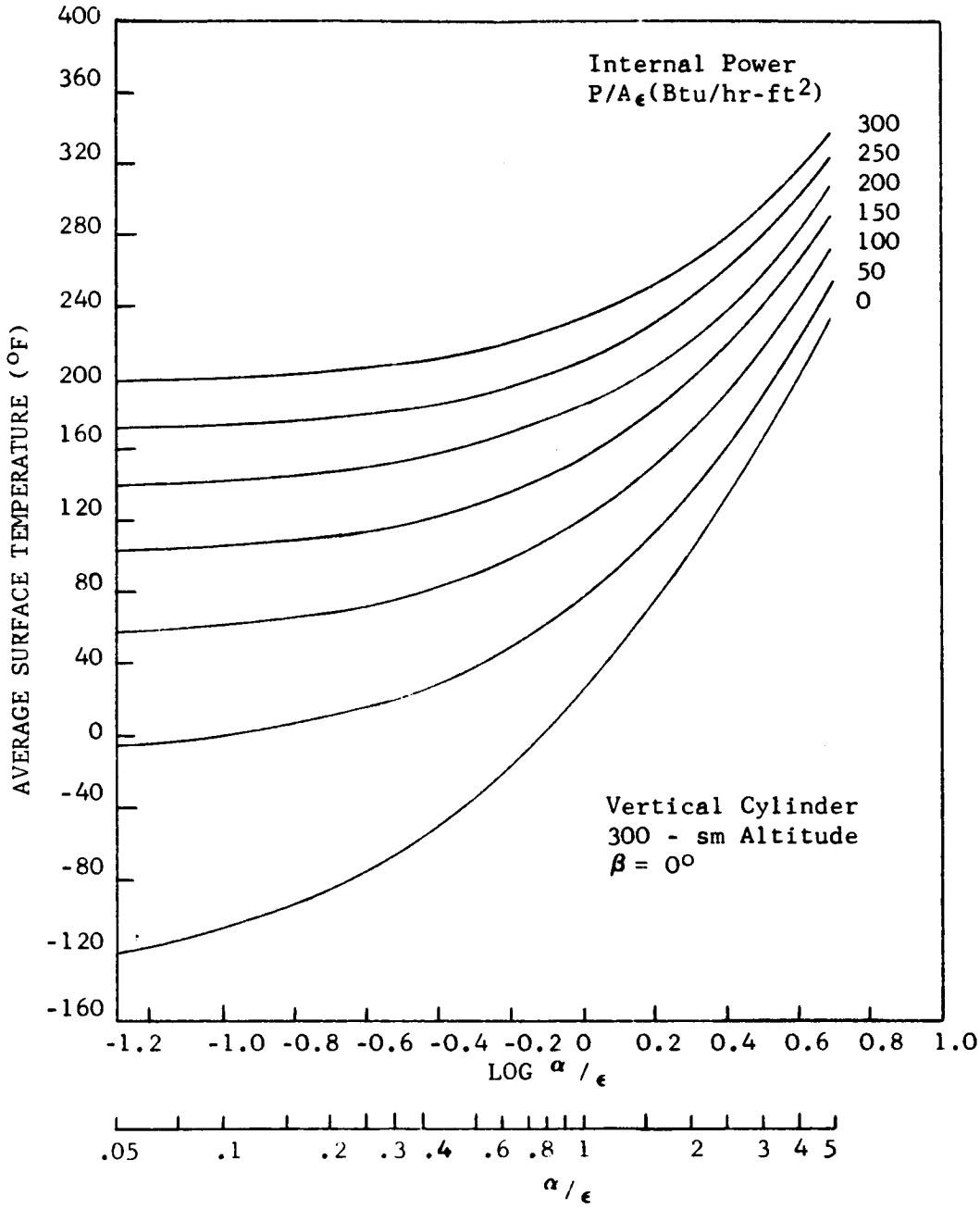

Fig. XIII-6 Space-Time Average Surface Temperature as a Function of Surface Finish and Internal Power Dissipation (Ref. 1)

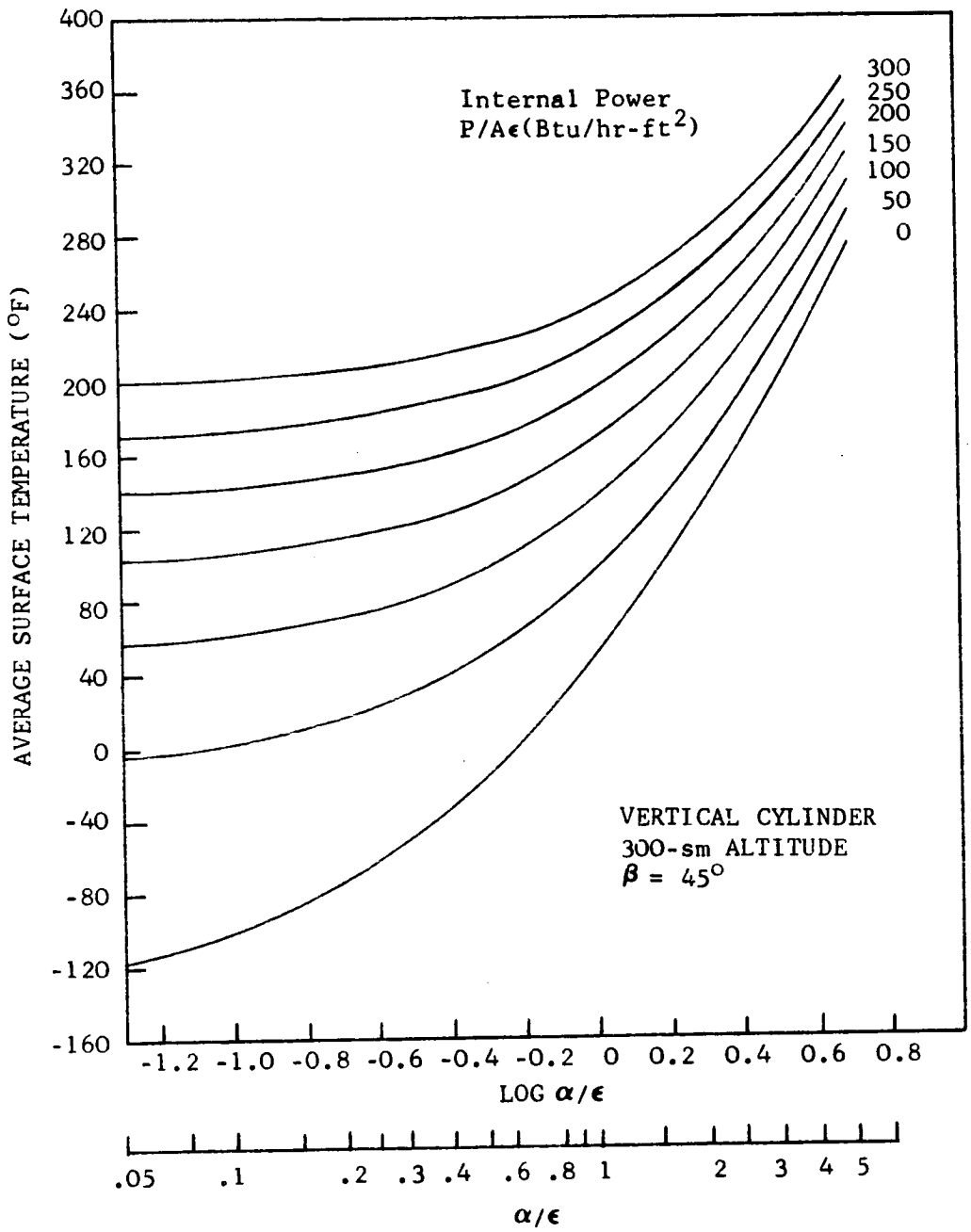

Fig. XIII-7 Space-Time Average Surface Temperature as a Function of Surface Finish and Internal Power Dissipation (Ref. 1)

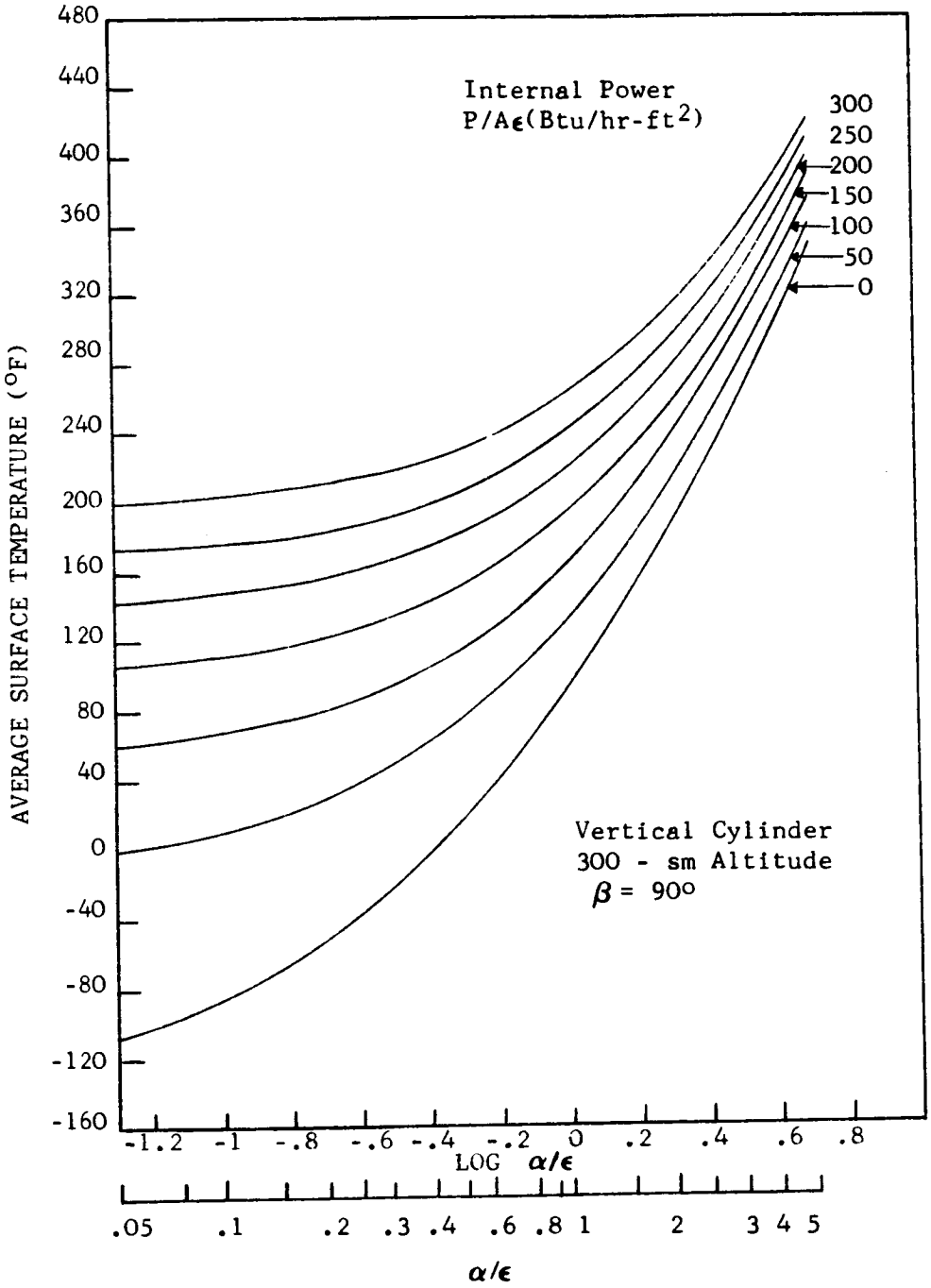

Fig. XIII-8 Space-Time Average Surface Temperature as a Function of Surface Finish and Internal Power Dissipation (Ref. 1)

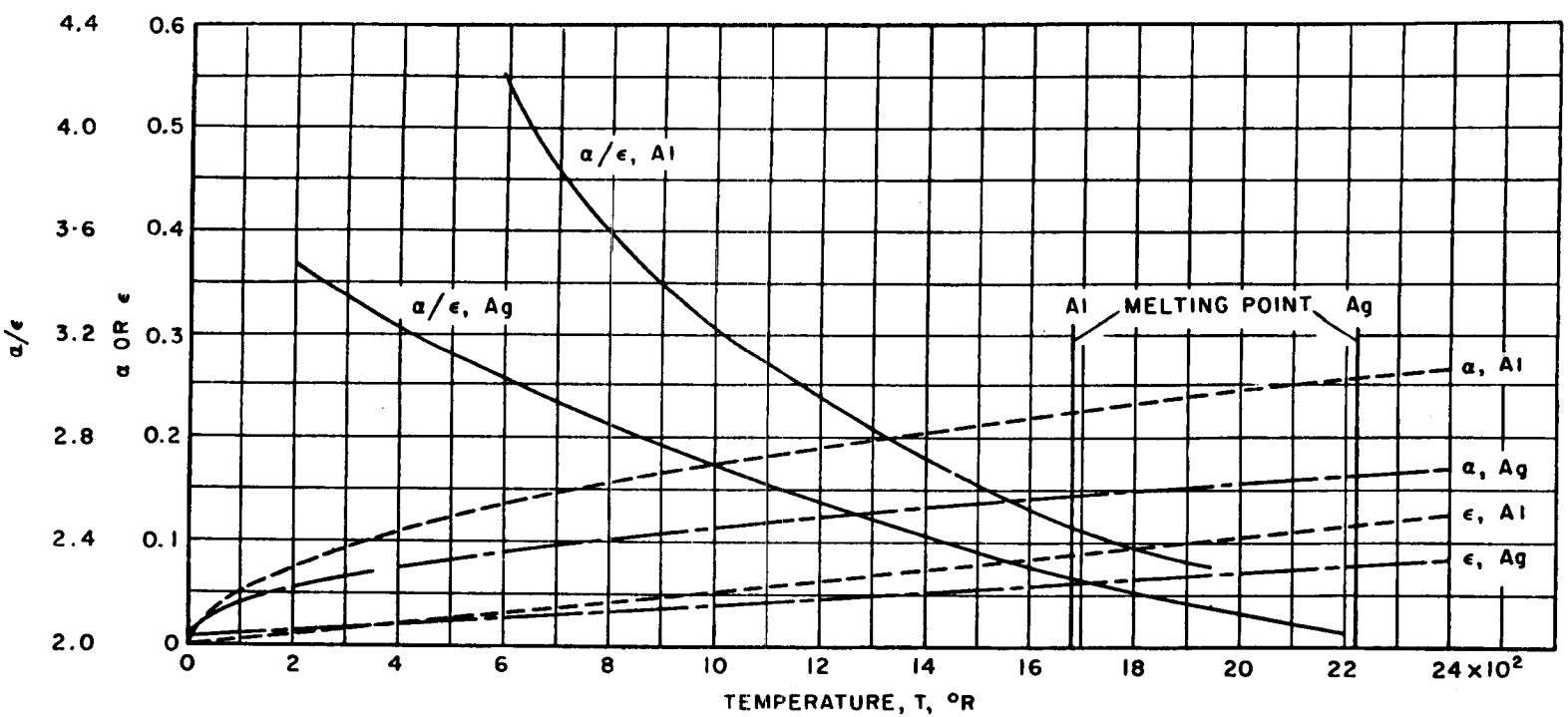

FIG. XIII-9 VARIATIONS WITH TEMPERATURE OF EMISSIVITY AND ABSORPTIVITY AND OF THEIR RATIO FOR TWO METALS (Ref. 9)

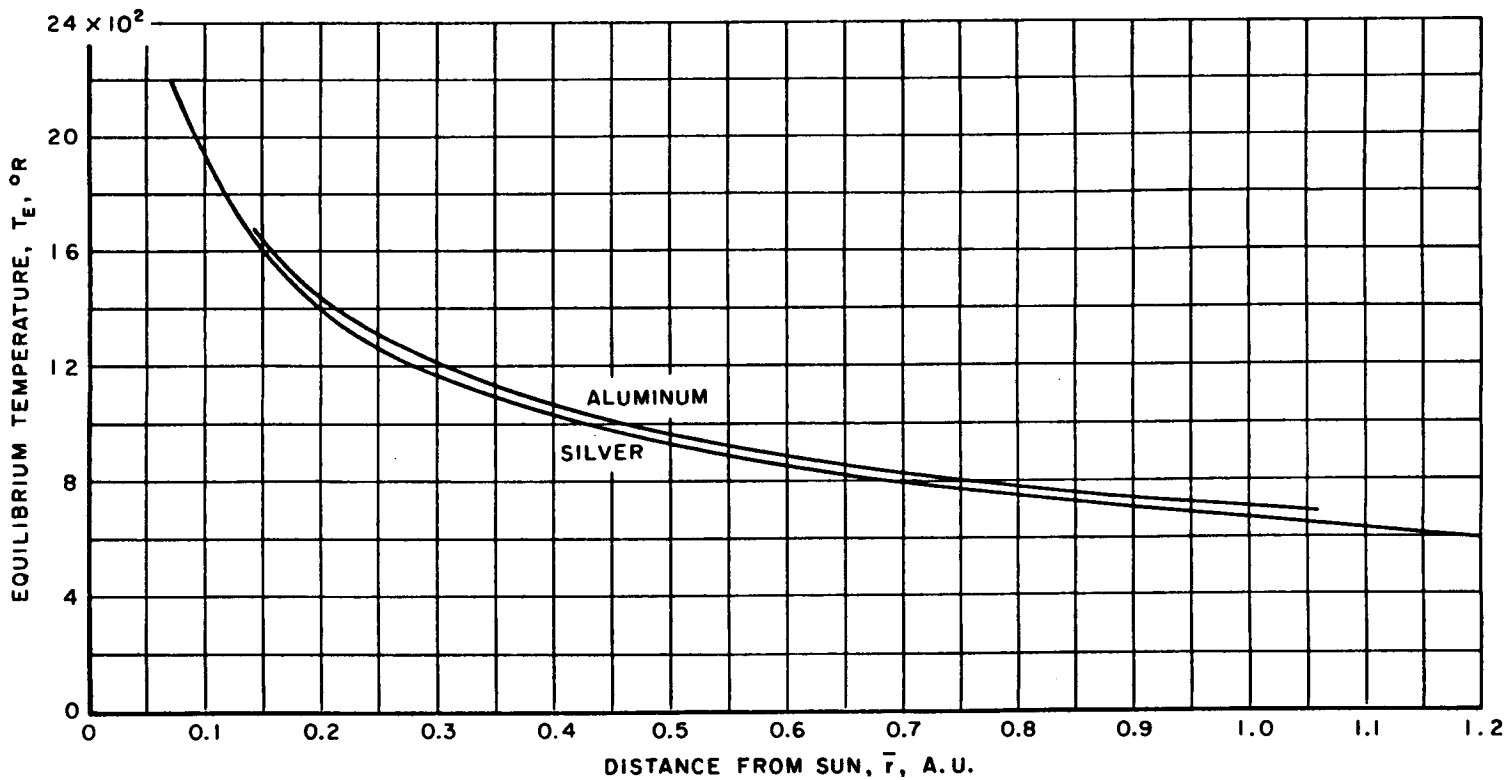

FIG. XIII-10 VARIATION OF EQUILIBRIUM TEMPERATURE WITH DISTANCE FROM SUN IN CASE OF ALUMINUM OR SILVER SPHERE, HAVING UNIFORM TEMPERATURE (Ref. 10)

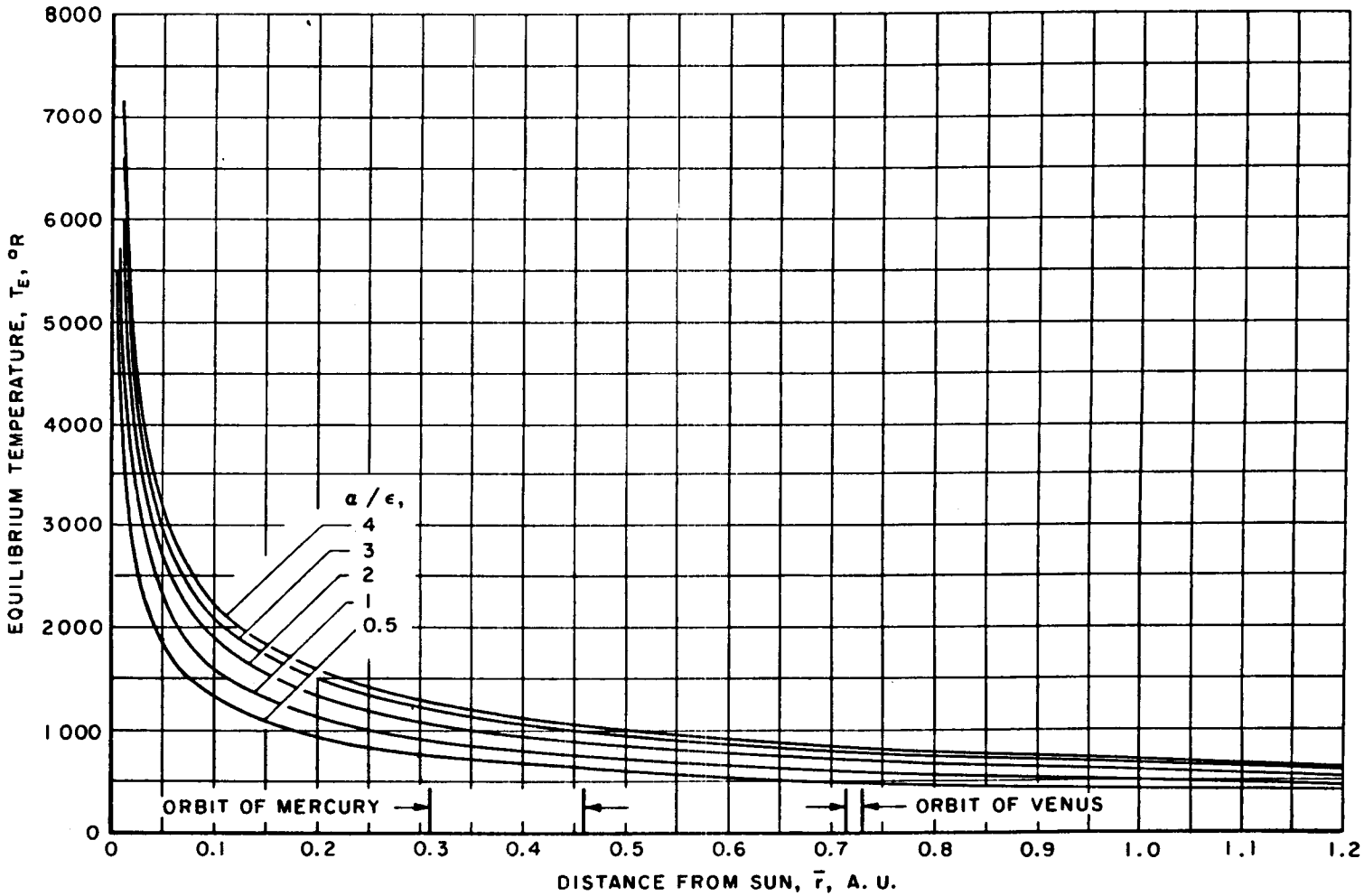

FIG. XIII-11 VARIATION OF EQUILIBRIUM TEMPERATURE WITH DISTANCE FROM THE SUN IN CASE OF A SPHERE HAVING UNIFORM TEMPERATURE (Ref. 9)

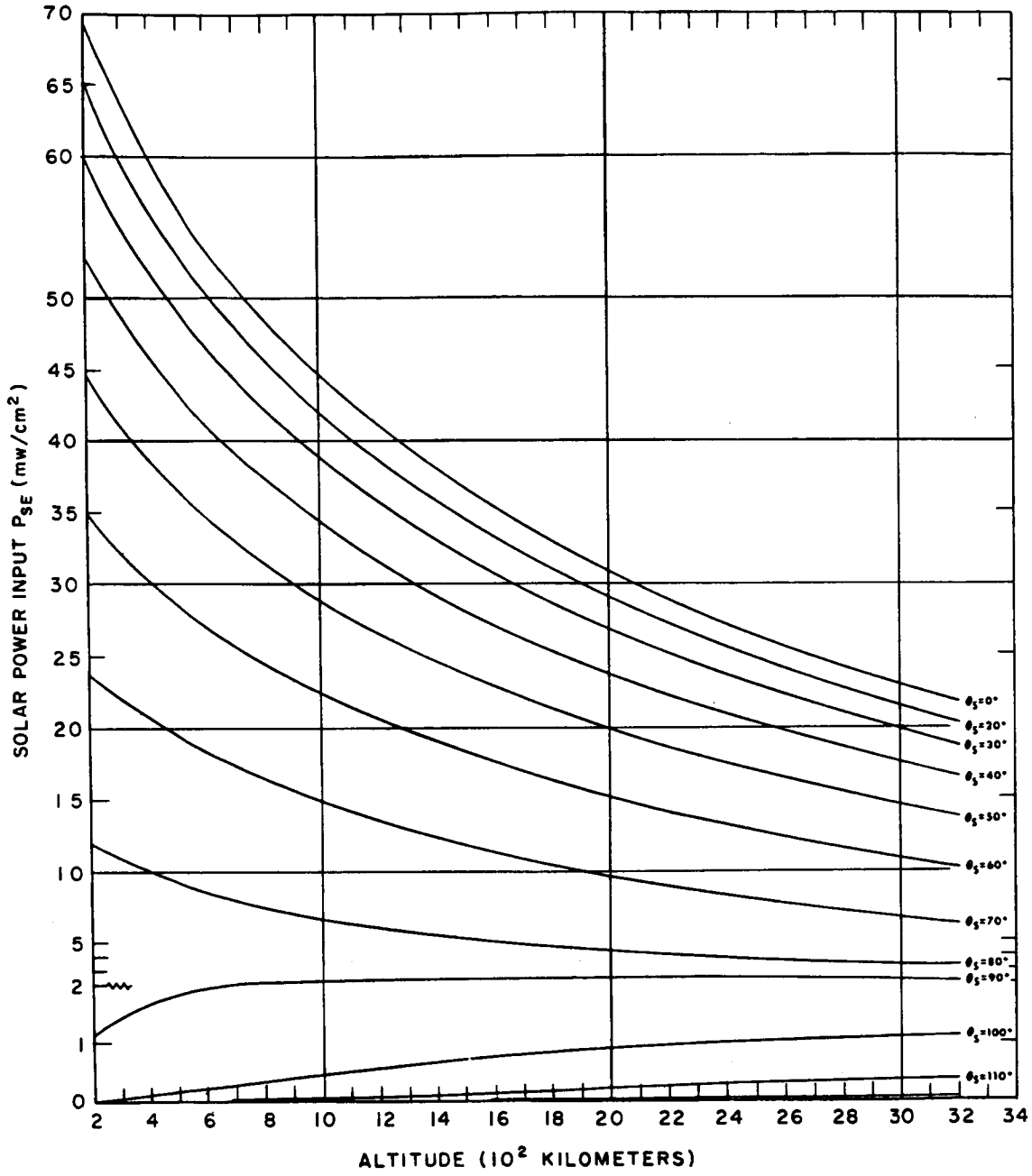

FIG. XIII-12 POWER INPUT PER UNIT CROSS-SECTIONAL AREA OF A SATELLITE PLOTTED AS A FUNCTION OF ALTITUDE FOR THE RANGE 200-32000 MILES (Ref. 10)

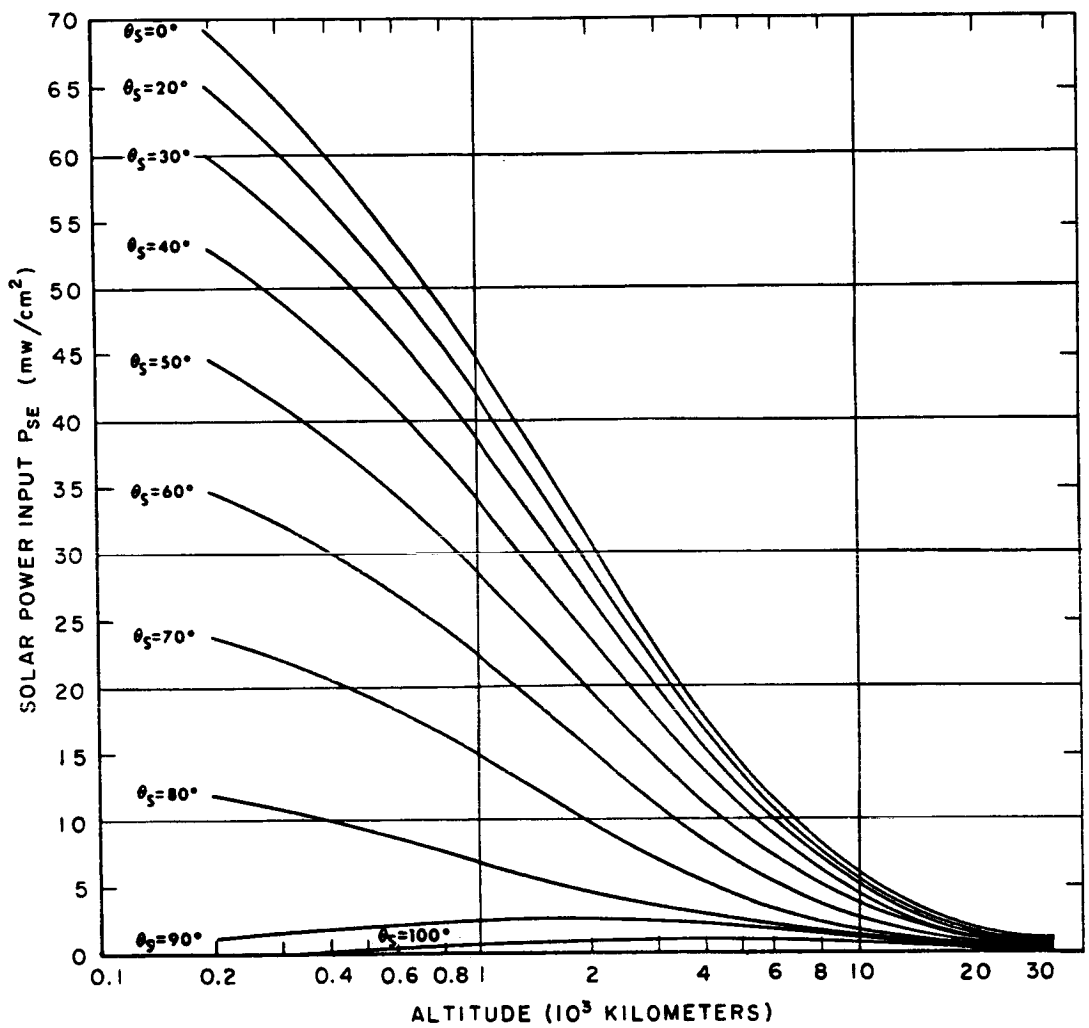

FIG. XIII-13 POWER INPUT PER UNIT CROSS-SECTIONAL AREA OF A SATELLITE PLOTTED AS A FUNCTION OF ALTITUDE FOR THE RANGE 200-32,000 MILES (Ref. 10)

XIII - REFERENCES

1. Goetzel, C.G. and Singletary, J.B. (Eds.) (Lockheed Missiles and Space) Space Materials Handbook. AF04(647)-673, 523 pp. Jan 1962. AD 284 547
2. Ibid. Camack, W.G. and Vajta, T.F. pp. 82-111.
3. Ibid. Gaumer, R.E., Shaw, C.C. and Streed, E.R. p. 143.
4. Ibid. McKellar, L.A. pp. 142-3.
5. Ibid. Camack, W.G. p. 39.
6. Oppenheim, A.K. Generalized theory of convective heat transfer in free-molecule flow. J. Aeronaut. Sci. 20, pp. 49-58, 1953.
7. Johnson, F.S The solar constant. J. Meteorol. 11, pp. 431-9, 1954.
8. McAdams, W.H. Heat transmission. McGraw-Hill Book Co., Inc., 2nd edn 9th impression, New York, 1942.
9. Dugan, D.W., NASA TN D-783, April 1961.
10. Cunningham, F.G. NASA TN D-1099, Oct. 1961.
11. Weaver, J.H., and Jacobs, C. Materials Symposium, Phoenix, Arizona, Sept. 1961, ASD TR 61-322, pp. 456-69
12. Gaumer, R.E., et al. Space Materials Handbook. Lockheed Missiles and Space Co., p. 476, Jan. 1962.
13. Acker, R.M., Lipkins, R.P. and Vehrencamp, J.E. (Space Technol. Lab., Inc.) AFBMD Doc. no. 61-04-6963.
14. Van Vliet, R.M., Mattice, J.J. and Cross, R.A WADD TR 60-386, Oct. 1960.
15. Eckard, L.D., Jr. (Johns Hopkins Univ., Applied Physics Lab.) Rept. no. CM-1001, Sept. 1961. AD 273 555
16. Heller, G. and Jones, B.P. NASA TN D-608, July 1961.
17. Heller, G. ARS J. 30, p. 344, 1960.
18. U.S. Standard Atmosphere, U.S. Government Printing Office, Wash. D.C., 1962.

XIV RELIABILITY

TABLE OF CONTENTS

Section-Part	Title	Section-Part. Page
XIV-0	List of Tables	XIV-0.2
XIV-1	Introduction	XIV-1.1
XIV-2	Reliability Models	XIV-2.1
XIV-3	Probability Distribution	XIV-3.1
XIV-4	Reliability Sampling	XIV-4.1
XIV-5	Design of Experiments	XIV-5.1
XIV-6	Tolerance Limits	XIV-6.1
XIV-7	References	XIV-7.1

XIV-0 LIST OF TABLES

Section-Part-Table	Title	Section-Part. Page
XIV-2-1	Reliability Each Component Must Have To Bring Out Over-all Reliability of a Serially Constructed System of Individual Components	XIV-2.5
XIV-3-1	Operational Probabilities	XIV-3.5
XIV-6-1	Tolerance Factors for Normal Distribution	XIV-6.2

XIV-1 INTRODUCTION

The objective of this section is briefly to mention and illustrate a few techniques of statistical reliability theory in order to make the reader aware of their existence and applicability to the determination of the reliability of pressurized gas systems and components. The fundamental theories of reliability mathematics are discussed in some detail in the Interim Report, issued in August 1963, and several texts are cited at the end of this section as references for the reliability engineer.

Reliability may be defined as the probability that a device will perform a specific function without failure under given environmental conditions for a given period of time. Probability is a mathematical term referring to the chance of occurrence. Failure means any variation in performance beyond allowable limits, not necessarily total failure. Conditioning environmental factors under which the device must operate are such factors as temperature, vibration, shock, pressure, moisture, etc. Time refers to the life span designed for the device under consideration; it might be fifteen years for a household appliance and thirty minutes for a missile.

This section considers some of the pertinent factors and computations involved in the various aspects of reliability which are defined in the above paragraph.

Although the causes of unreliability are many, with reference to space vehicles the primary cause is due to the complexity of the equipment involved. In general, a space vehicle requires that all of its subsystems, components, and parts must operate correctly in order for the flight to be successful. Probability theory determines a vehicle's reliability. The probability of a successful mission is equal to the product of the probabilities that each lesser device within the vehicle will operate successfully. In effect, reliability tends to decrease as the complexity of a device increases.

A reliability program to be successful must be based upon a well-organized and carefully planned system for collecting, analyzing, and following up reliability data. Lloyd and Lipow[6] present an example of an on-line reliability data reporting system which effectively illustrates the dependence of the reliability program upon the adequacy of the reporting system.

XIV-2 RELIABILITY MODELS

Reliability models are concerned first with the relationship between the components of a system and second with the aggregate component effect upon the systems performance. The performance of an individual component must be considered separately, and then the relationship between the components which form the structure of the system are analyzed. The objective in specifying the reliability model is to determine the reliability (R) of a system composed of components with either known or estimated reliabilities.

Consider an attitude control system that is comprised of n components, and let S equal the event that the system is successful, and S_j, $j = 1 \ldots, n$ the events that each of the components are successful. If S can occur only when all the S_j occur, the system is called *serial*, and:

$$R = P(S) = P(S_1 S_2 S_3 \ldots S_n) \quad .$$

If the S_j are mutually independent (the probability of success for each subsystem is independent of the success or failure of all other subsystems) then:

$$R = P(S) = \prod_{j=1}^{n} P(S_j)$$

or

$$R = \prod_{j=1}^{n} \frac{(n_j - f_j)}{n_j}$$

where

n_j = number of tests of component j

f_j = number of failures in n_j test.

If $n = 2$ and $n_1 = 50$; $n_2 = 100$; $f_1 = 2$; and $f_2 = 3$ then

ORIGINAL PAGE IS
OF POOR QUALITY

$$R = \left[\frac{50 - 2}{50}\right] \cdot \left[\frac{100 - 3}{100}\right] = 0.9312 \quad .$$

A parallel system is one consisting of n subsystems such that the system fails only if all subsystems fail. Or conversely, the system is successful if at least one subsystem operates. This property of parallel systems is commonly called redundancy and a frequently used measure of the amount of redundancy in a system is the ratio of the total number of components available for a particular task to the number of components actually necessary. The term stand-by redundancy refers to systems composed of two or more subsystems where the system is first made operational by turning on system one. If system one fails before the required operating time, system two becomes operative and the system fails only if system two fails before the required time of operation has elapsed.

Consider a simple serial system, that is, one with no redundancy, made up of n independent components.

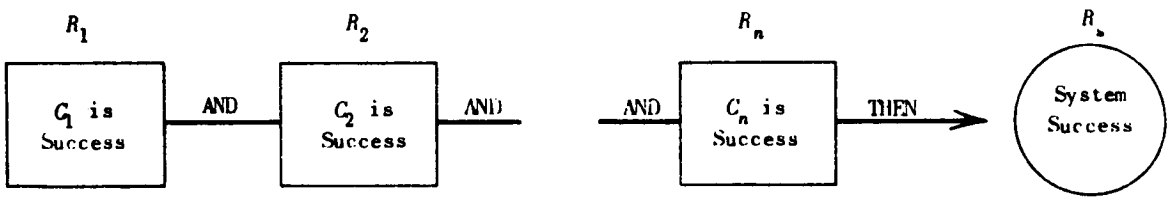

and

$$R_s = P[(C_1 \text{ success}) \cap (C_2 \text{ success}) \cap \ldots \cap (C_n \text{ success})]$$

or

$$R_s = R_1 \cdot R_2 \ldots R_n \quad .$$

Table XIV-2-1 illustrates this relationship between component and system reliability.

For a simple parallel system with $n - 1$ components redundant:

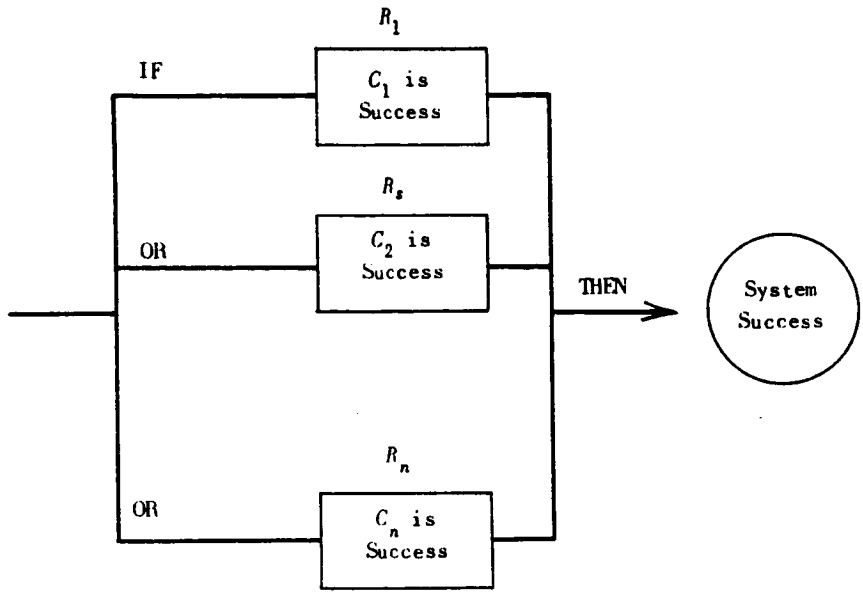

The probability that C_n will fail is $F_n = 1 - R_n$, and $R_s = 1 - (1 - R_1)(1 - R_2) \ldots (1 - R_n)$. Or $R_s = 1 - (1 - R_n)^n$ if $R_1 = R_2 = \ldots R_n$.

For example if a system is composed of three redundant components with $R_1 = 0.5$, $R_2 = 0.6$ and $R_3 = 0.4$ the reliability of the system would be

$$R_s = 1 - (1 - 0.5)(1 - 0.6)(1 - 0.4) = 0.88$$

If each component of the parallel system was replaced with a serial system of components, the reliability structure would be:

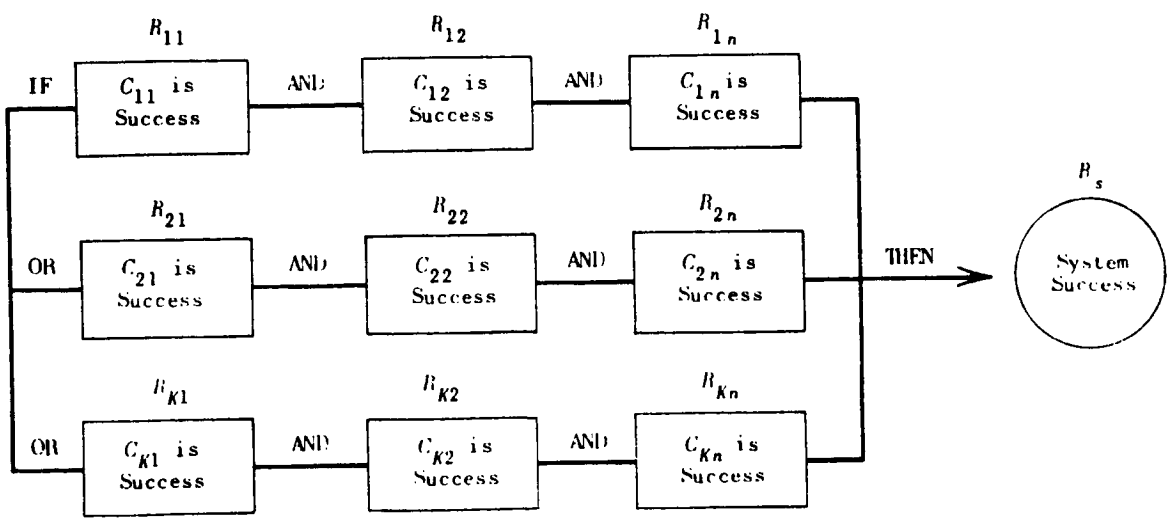

and the system's reliability is:

$$R_s = [1-(1-R_{11}\cdot R_{12}\ldots R_{1n})(1-R_{21}\cdot R_{22}\ldots R_{2n})\ldots(1-R_{K1}\cdot R_{K2}\ldots R_{Kn})] \quad .$$

Parallel-serial systems involve replacing each component of a serial system with a parallel system of components and the reliability structure is:

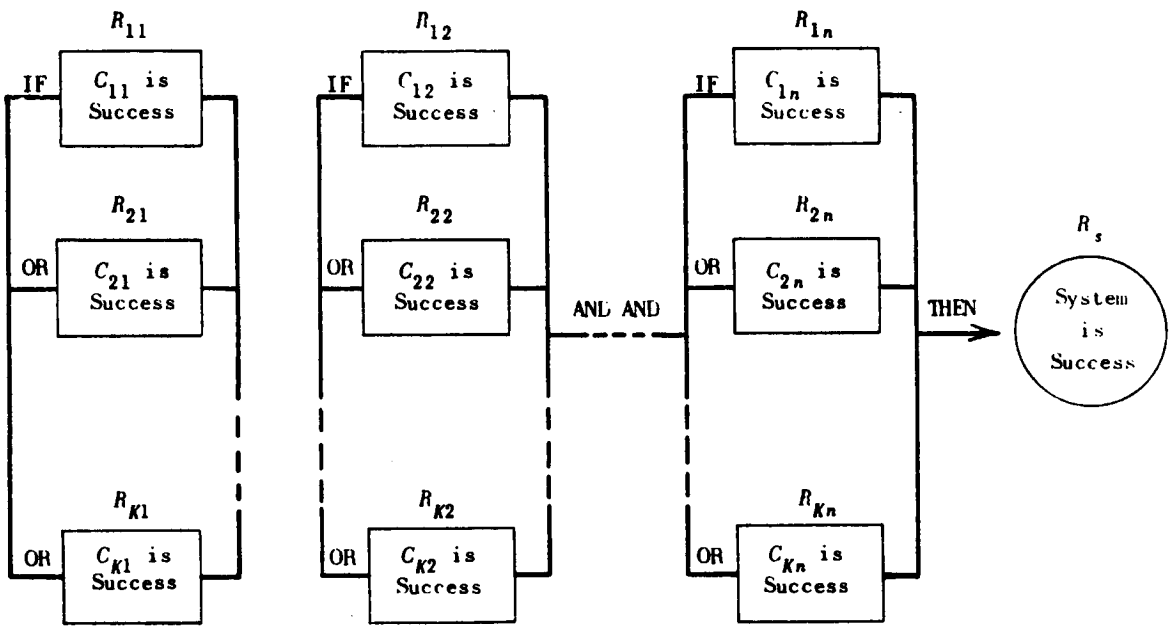

and

$$R_s = [1-(1-R_{11})(1-R_{21})\ldots(1-R_{K1})]\cdot[1-(1-R_{12})(1-R_{22})\ldots(1-R_{K2})]\ldots$$

$$[1-(1-R_{1n})(1-R_{2n})\ldots(1-R_{Kn})] \quad .$$

From the four basic reliability structures it is obvious that the magnitude of R_S can be changed by the number of components and the way in which they are arranged. Additional redundant components of course, add to the physical complexity of the circuitry and to the weight and space requirements.

Table XIV-2-1

RELIABILITY EACH COMPONENT MUST HAVE TO BRING OUT OVER-ALL RELIABILITY OF A SERIALLY CONSTRUCTED SYSTEM OF INDEPENDENT COMPONENTS

NUMBER OF SERIAL COMPONENTS	REQUIRED OVER-ALL RELIABILITY			
	0.95	0.9	0.7	0.5
1	0.95	0.9	0.7	0.5
2	0.9745	0.9486	0.8368	0.7071
3	0.9831	0.9654	0.8880	0.7938
4	0.9872	0.9738	0.9147	0.8409
5	0.9897	0.9790	0.9311	0.8706
6	0.9915	0.9826	0.9423	0.8908
7	0.9926	0.9851	0.9504	0.9057
8	0.9913	0.9870	0.9563	0.9170
9	0.9942	0.9883	0.9612	0.9260
10	0.9949	0.9897	0.9649	0.9330
15	0.9965	0.9928	0.9766	0.9548
20	0.9974	0.9947	0.9824	0.9661
50	0.9991	0.9979	0.9928	0.9863
100	0.9995	0.9988	0.9965	0.9931

Example: It is required to bring out success with 90 percent probability, using 10 serial components. Each must have a reliability of at least 9897.

XIV-3 PROBABILITY DISTRIBUTION

Statements such as "the attitude control system performed as intended," "the time to failure of a pressure valve exceeds 7," "the output of this power supply system is between 112 and 117 volts," etc., could all be expressed as the simple event success. The probability of success occurring is called reliability. Quite frequently the event failure, the ratio of the number of failures to the number of trials, is actually observed while what is really desired is a measure of success. The measure (probability) of success is, of course, simply defined as one minus the measure of failure.

For experiments which can be characterized by the discrete events success or failure, and one wishes to determine the probability of exactly x successes in n trials, the binomial probability distribution applies.

The binomial distribution states that if an experiment consists of N independent trials, each with a probability of success of p and a probability of failure of $q (q = 1 - p)$, then the probability of exactly X successes and $N - X$ failures is:

$$P(X) = \binom{N}{X} p^X q^{N-X}$$

in which the expression

$$\binom{N}{X} = N!/X!(N - X)! \quad .$$

As an example, given that the reliability of an attitude control system is 0.90, *i.e.*, the probability of successful operation on a mission is 0.90. What is the probability that it will work successfully in each of ten consecutive missions?

$$P(X) = \binom{10}{10}(0.90)^{10}(0.10)^0 = (1)(0.349) = 0.349 \quad .$$

ORIGINAL PAGE IS
OF POOR QUALITY

If the question had been, "what is the probability of at least nine successes in ten missions?," then the event X is the union of two events, exactly 9 successes and 10 successes. Since these two events are mutually exclusive, the probability of their union is the sum of their individual probabilities and:

$$P(X) = \binom{10}{9}(0.90)^9(0.10)^1 + \binom{10}{10}(0.90)^{10}(0.10)^0$$

$$= 10(0.387)(0.10) + 0.349 = 0.736 \quad .$$

Another distribution that arises whenever a discrete event may occur randomly over a time period, and one considers as a random variable the number of times this event will occur over the given period of time, is the Poisson distribution:

$$P(X) = \frac{\lambda^X \cdot e^{-\lambda}}{X!}$$

where X is the number of occurrences of the event; λ is the expected number of occurrences; *i.e.*, λ = average of X.

Given that a control system pressure valve-failure rate over a long period of time has been 3.41 per 10,000 cycles, and that a particular mission will require the valve to cycle 1,000 times, what is the probability of no valve failure during the mission?

The expected number of failures per 1,000 cycles is $\lambda = 0.341$, and

$$P(X = 0) = \frac{\lambda^X \cdot e^{-\lambda}}{X!} \quad \text{note } 0! = 1$$

$$= (0.341)^0 \cdot e^{-0.341}$$

$$= 0.71 \quad .$$

Continuous probability distributions are used to measure the probability of events having a time characteristic such as the event "the time-to-failure exceeds T" or events like "the output of this rectifier is within certain limits."

A continuous probability distribution of particular importance in reliability calculations is the exponential distribution of time-to-failure. If reliability R is defined as the probability that a device will operate for a period of time equal to or greater than T, then by the exponential distribution

$$R = \int_T^{\infty} \frac{1}{\theta} \cdot e^{-T/\theta} = e^{-T/\theta}$$

and since T is known, R is a function of θ.

If θ, the mean time-to-failure of a device, is equal to 10 hours then the probability that a device will operate for 3 hours or more would be

$$P = e^{-T/\theta} = 2.718^{-3/10} = 0.74 \quad .$$

Table XIV-3-1 lists R for several values of T and θ.

Many output characteristics exhibit a normal (Gaussian) probability distribution. In fact when non-normality is observed, it often indicates that something is wrong. In order to compute the reliability of an item R when the value of the performance factor has a continuous probability distribution, it is necessary to integrate over a range of values constituting successful performance. The normal distribution is defined as

$$R = \int_{X_1}^{X_2} \frac{1}{S\sqrt{2\pi}} \cdot \exp -\left[\frac{(X - M)^2}{2S^2}\right] dx$$

R is a function of X_1, X_2, M and S. Since X_1 and X_2 are usually given but M and S (the populations mean and standard deviation) are usually not known, it is first necessary to estimate these parameters and then solve for R.

To obtain estimates of the means and standard deviations of probability distributions, the method of maximum likelihood is usually used. it is easy to apply, yields the best estimates according to widely used criteria, and has the property that as the size of the sample grows larger, the distribution of the estimates approaches the normal distribution regardless of the probability distribution originally considered. This

ORIGINAL PAGE IS
OF POOR QUALITY

fact makes it possible to state confidence limits for the estimated probability distribution parameters. Although widely used in reliability work, a discussion of confidence limits is beyond the scope of this discussion and the reader is referred to any of the several referenced statistical texts.

Table XIV-3-1

OPERATIONAL PROBABILITIES

Mean time to failure	Probability of Operational Time														
	1/2 sec	1 sec	2 sec	3 sec	10 sec	1 min	2 min	3 min	10 min	1 hr	2 hr	3 hr	10 hr	1 day	etc.
1 sec	0.61	0.37	0.14	0.05	0	0									
2 sec	0.78	0.61	0.37	0.22	0.01	0									
3 sec	0.85	0.72	0.51	0.37	0.04	0									
10 sec	0.95	0.90	0.82	0.74	0.37	0	0	0	0						
1 min	0.99	0.99	0.97	0.95	0.85	0.37	0.14	0.05	0						
2 min	1.	1.	0.99	0.98	0.92	0.61	0.37	0.22	0.01	0					
3 min	1.	1.	1.	0.99	0.95	0.72	0.51	0.37	0.04	0					
10 min	1.	1.	1.	1.	0.99	0.90	0.82	0.74	0.37	0	0	0	0		
1 hr	1.	1.	1.	1.	1.	0.99	0.97	0.95	0.85	0.37	0.14	0.05	0		
2 hr	1.	1.	1.	1.	1.	1.	1.	1.	1.	0.61	0.37	0.22	0.01	0	
3 hr	1.	1.	1.	1.	1.	1.	1.	1.	1.	0.72	0.51	0.37	0.04	0	
10 hr	1.	1.	1.	1.	1.	1.	1.	1.	1.	0.90	0.82	0.74	0.37	0	
1 day	1.	1.	1.	1.	1.	1.	1.	1.	1.	0.99	0.97	0.95	0.85	0.37	
etc.															

Examples (1) If the mean time to failure is 10 min, the probability of remaining operational for at least 2 min is 0.82

(2) If the mean time to failure is θ , the probability of remaining operational for at least T is $e^{-T/\theta}$

XIV-4 RELIABILITY SAMPLING

Reliability sampling refers to sampling plan techniques used in order to determine if reliability requirements are met. In general, these techniques involve random sampling from populations with only success or failure attributes or from continuous populations such as time-to-failure distributions. In either case the problem is to estimate a function of the parameters of the population which can be defined as the reliability R of the system.

A binomial sampling plan consists of testing a group of items one by one and recording either a success or a failure on each trial. The result of each trial is independent of the result of any other trial and the objective of the testing is to determine if the item is sufficiently reliable for its intended purpose.

It is, of course, first necessary to specify the maximum value of unreliability P that will be tolerated. Then if the devices unreliability P' is less than this value, it is accepted as meeting the reliability standard, and conversely, if greater, the device is rejected as not meeting the reliability standard. Since no sampling plan is 100 percent efficient, any plan can at times result in rejecting a device because the estimated value of P' exceeds the value of P when in actuality the true value of the populations unreliability P' is less than P. Alternately a sampling plan due to these sampling errors in estimating P' can lead to the acceptance of the item when it would be rejected if the true value of P' were known.

Instead of estimating a single value of P', the usual procedure is to determine two values A and B such that there is given probability α that the true value of P' lies outside the interval A and B. The probability that the interval A and B contains the true value of P' is then, of course, $1 - \alpha$. The values A and B are called the 100 $(1 - \alpha)$ percent confidence limits for the parameter P' and the interval between them a 100 $(1 - \alpha)$ confidence interval.

The specification of P and α enables one to determine the maximum number of failures permissible (F) in N trials in order to reach an

ORIGINAL PAGE IS
OF POOR QUALITY

acceptance decision. For any explanation of the theory of and the techniques used for determining these values, see Ref. 3, Ch. 10 and Ref. 5, p. 140ff. For use in reliability work, extensive tables and graphs have been constructed relating the reliability specifications P, α, N, and F.

Wald sequential sampling plans[12] are based on the fact that the acceptance and rejection boundaries in a failures versus life (time) plane can be approximated by two parallel straight lines. The lines are functions of the reliability specifications only and are plotted in a failure-life graph before testing starts. Testing then continues until a plot of the observed life versus failures first crosses or touches one of the boundaries at which time the appropriate decision is made.

XIV-5 DESIGN OF EXPERIMENTS

In testing components or systems, the objective is to subject them to conditions such that the real characteristics of the items tested can be observed.

Time or life testing is important for considerations other than estimating and demonstrating numerical reliability. Which part in a component or which component in the system failed and the types of and the reasons for the failures must be specified and analyzed. Time-to-failure testing by generating failures helps to answer these questions when time is the critical parameter of the item.

In event testing, samples are cycled repeatedly until failure; it is used when starting and stopping operations are more destructive than the accumulation of time. In this type of testing, the mean cycles to failure becomes the principal parameter.

Environmental testing is undertaken to determine the reactions of the item tested to ambient conditions resembling as closely as possible the environment in which the item is expected to operate.

The design and analysis of experiments, statistical experimentation, differs from the traditional method in that more than one factor at a time is allowed to vary. Varying only one factor at a time is not only inefficient but can produce wrong results as well as obscuring factor interaction. The fundamental basis of statistical experimentation is to apply the factors in such a manner that their effects can be factored out and the variations caused by the factors on performance can be measured and compared. This type of test is called a factorial experiment.

Assume a rocket engine is to be tested to determine the chamber pressure under three environmental conditions (factors) and at two levels for each condition. This represents a factorial design involving a total of 8 treatment combinations (an experiment involving K factors at X levels and XK combinations). The data from such a test could be shown in the following way.

ORIGINAL PAGE IS
OF POOR QUALITY

Environment

Environment	level							
A. Temp.	a_1				a_2			
B. Vibration	b_1		b_2		b_1		b_2	
C. Humidity	c_1	c_2	c_1	c_2	c_1	c_2	c_1	c_2
Pressure	11.8	20.9	8.5	16.2	9.9	18.3	8.1	16.0

An estimate of the total effect of factor A upon the pressure is given by the sum of all pressures observed at level a_2 minus the sum of those at level a_1.

$$A = (9.9 + 18.3 + 8.1 + 16.0) - (11.8 + 20.9 + 8.5 + 16.2) = -5.1$$

and

$$B = (8.5 + 16.2 + 8.1 + 16.0) - (11.8 + 20.9 + 9.9 + 18.3) = -12.1$$

$$C = (20.9 + 16.2 + 18.3 + 16.0) - (11.8 + 8.5 + 9.9 + 8.1) = 33.1 .$$

The interaction effect of A and B is the difference between the effect of A at the upper level of B and the effect of A at the lower level of B.

$$AB = [(16.0 - 16.2) + (8.1 - 8.5)]$$

$$- [(18.3 - 20.9) + 9.9 - 11.8)] = 3.9$$

and

$$AC = [(16.0 - 16.2) + (18.3 + 20.9)]$$

$$- [(8.1 - 8.5) + (9.9 - 11.8)] = -0.5$$

$$BC = [(16.0 - 18.3) + (16.2 - 20.9)]$$

$$- [(8.1 - 9.9) + (8.5 - 11.8)] = -1.9 .$$

The AB interaction for the two levels of C are

$$[(16.0 - 16.2) - (18.3 - 20.9)] \quad \text{and} \quad [(8.1 - 8.5) - (9.9 - 11.8)]$$

and the difference between these two expressions represents the effects of C upon the AB interaction; *i.e.*,

$$ABC = (2.4) - (1.5) = 0.9 \quad .$$

These factor effects are summarized in the table below:

FACTOR	EFFECT	$(\text{Effect})^2/8$*
A	-5.1	3.251
B	-21.1	18.301
C	33.1	136.951
AB	3.9	1.901
AC	-0.5	0.031
BC	-1.9	0.451
ABC	0.9	0.101

* This column represents the contribution to the sum of the squares of each chamber pressure observation that is made by each factor. To obtain this, the effect is squared and then divided by 8 (the total number of combinations; *i.e.*, 2^3).

In order to determine the significance of the factors upon performance a formal analysis of variance shows that factors B and C are significant at the 99 percent level. That is, the odds are 99 to 1 that the improved performance due to a decrease in vibration and an increase in humidity is not due to chance alone. For an explanation of analysis of variance theory and techniques, see Bennett and Franklin (Ref. 2, Ch. 7, pp. 319-477).

XIV-6 TOLERANCE LIMITS

Whenever parameters, such as permeability rates, are experimentally determined, it is preferable for design and reliability evaluation to specify tolerance limits such that a certain percentage of future measurements may be expected to fall between the limits. Experience has shown that the majority of experimental data are approximately normally distributed; moreover, moderate departures from normality do not seriously affect the tolerance limits computed on the basis of normal distribution. Assuming normality, if the true mean and standard deviation of the population were known, tolerance limits would be formed by adding to and subtracting from the mean a certain multiple K of the standard deviation. For example, if the mean μ and standard deviation of the population σ are known, then the limits $\mu \pm 1.6456\sigma$ will include 90 percent of the distribution of the mean. However, the same assertion cannot be made about the limits $\overline{X} \pm 1.6456 \cdot S$ where $\overline{X}$ is the mean and S is the standard deviation of a sample of N observations. In fact, if K is fixed, no two samples from a given population will yield identical tolerance limits as both the sample means and standard deviations will vary from sample to sample. Therefore, the proportion of the population that is included between the limits $\overline{X} \pm K \cdot S$ is a random variable and it is impossible to determine so that the limits will always contain a specific proportion of the population. It is, however, possible to determine K so that a certain proportion γ (called the confidence coefficient) of the tolerance limits $\overline{X} \pm K \cdot S$ will contain a fixed percentage of the population P.

Table XIV-6-1 presents values of K associated with a specified coefficient γ, sample size N, and population proportion P assuming a normal distribution. Confidence limits $\gamma = 0.95$ or 0.99 are most frequently used in practice.

It is occasionally appropriate to specify a single tolerance limit $\overline{X} - K \cdot S$ such that a fixed proportion of the population lies above this limit, or a limit $\overline{X} + K \cdot S$ such that a fixed proportion lies below the limit. These single limits are called one-sided tolerance limits. [See Bowker and Lieberman (Ref. 3, p. 230-1) for a table of K values to use in computing one-sided tolerance limits.]

ORIGINAL PAGE IS
OF POOR QUALITY

Table XIV-6-1

TOLERANCE FACTORS FOR NORMAL DISTRIBUTIONS*

Factors K such that the probability is that at least the proportion P of the distribution lies between the interval $\bar{X} \pm Ks$, where $\bar{X}$ and s are the mean and standard deviation computed from a sample of size N

	$\gamma = 0.90$				$\gamma = 0.95$				$\gamma = 0.99$			
N \ P	0.75	0.90	0.95	0.99	0.75	0.90	0.95	0.99	0.75	0.90	0.95	0.99
2	11.407	15.978	18.800	24.167	22.858	32.019	37.674	48.430	114.363	160.193	188.491	242.300
3	4.132	5.847	6.919	8.974	5.922	8.380	9.916	12.861	13.378	18.930	22.401	29.055
4	2.932	4.166	4.943	6.410	3.779	5.369	6.370	8.299	6.614	9.398	11.150	14.527
5	2.454	3.494	4.152	5.423	3.002	4.275	5.079	6.634	4.643	6.612	7.855	10.260
6	2.196	3.131	3.723	4.870	2.604	3.712	4.414	5.775	3.743	5.337	6.345	8.301
7	2.034	2.902	3.452	4.521	2.361	3.369	4.007	5.248	3.233	4.613	5.488	7.187
8	1.921	2.743	3.264	4.278	2.197	3.136	3.732	4.891	2.905	4.147	4.936	6.468
9	1.839	2.626	3.125	4.098	2.078	2.967	3.532	4.631	2.677	3.822	4.550	5.966
10	1.775	2.535	3.018	3.959	1.987	2.839	3.379	4.433	2.508	3.582	4.265	5.594
11	1.724	2.463	2.933	3.849	1.916	2.737	3.259	4.277	2.378	3.397	4.045	5.308
12	1.683	2.404	2.863	3.758	1.858	2.655	3.162	4.150	2.274	3.250	3.870	5.079
13	1.648	2.355	2.805	3.682	1.810	2.587	3.081	4.044	2.190	3.130	3.727	4.893
14	1.619	2.314	2.756	3.618	1.770	2.529	3.012	3.955	2.120	3.029	3.608	4.737
15	1.594	2.278	2.713	3.562	1.735	2.480	2.954	3.878	2.060	2.945	3.507	4.605
16	1.572	2.246	2.676	3.514	1.705	2.437	2.903	3.812	2.009	2.872	3.421	4.492
17	1.552	2.219	2.643	3.471	1.679	2.400	2.858	3.754	1.965	2.808	3.345	4.393
18	1.535	2.194	2.614	3.433	1.655	2.366	2.819	3.702	1.926	2.753	3.279	4.307
19	1.520	2.172	2.588	3.399	1.635	2.337	2.784	3.656	1.891	2.703	3.221	4.230
20	1.506	2.152	2.564	3.368	1.616	2.310	2.752	3.615	1.860	2.659	3.168	4.161
21	1.493	2.135	2.543	3.340	1.599	2.286	2.723	3.577	1.833	2.620	3.121	4.100
22	1.482	2.118	2.524	3.315	1.584	2.264	2.697	3.543	1.808	2.584	3.078	4.044
23	1.471	2.103	2.506	3.292	1.570	2.244	2.673	3.512	1.785	2.551	3.040	3.993
24	1.462	2.089	2.489	3.270	1.557	2.225	2.651	3.483	1.764	2.522	3.004	3.947
25	1.453	2.077	2.474	3.251	1.545	2.208	2.631	3.457	1.745	2.494	2.972	3.904
28	1.430	2.044	2.435	3.199	1.514	2.164	2.579	3.388	1.695	2.424	2.888	3.794
30	1.417	2.025	2.413	3.170	1.497	2.140	2.549	3.350	1.668	2.385	2.841	3.733
32	1.405	2.009	2.393	3.145	1.481	2.118	2.524	3.318	1.644	2.351	2.801	3.680
34	1.395	1.994	2.376	3.122	1.468	2.099	2.501	3.286	1.623	2.320	2.764	3.632
36	1.386	1.981	2.361	3.102	1.455	2.081	2.479	3.258	1.604	2.293	2.732	3.590
38	1.377	1.969	2.346	3.083	1.446	2.068	2.464	3.237	1.587	2.269	2.703	3.552
40	1.370	1.959	2.334	3.066	1.435	2.052	2.445	3.213	1.571	2.247	2.677	3.518
45	1.354	1.935	2.306	3.030	1.414	2.021	2.408	3.165	1.539	2.200	2.621	3.444
50	1.340	1.916	2.284	3.001	1.396	1.996	2.379	3.126	1.512	2.162	2.576	3.385

* K values taken from Eisenhart, Hastay, and Wallis, "Techniques of Statistical Analysis," McGraw-Hill Book Co., Inc. 1947.

ORIGINAL PAGE IS
OF POOR QUALITY